A geoscientific framework for the proposed site of South Africa's second nuclear power plant - Thyspunt, Eastern Cape.

By

Debbie Claassen

Submitted in fulfilment of the requirements for the degree of Magister Scientiae in the Faculty of Science of the Nelson Mandela Metropolitan University, Port Elizabeth

Supervisor: Prof. M. de Wit (AEON-Africa Earth Observatory Network, Nelson Mandela Metropolitan University)

Declaration of own work

I, Debbie Claassen (maiden name Kilian), student number 203003632, hereby declare that this thesis: 'A geoscientific framework for the proposed site of South Africa's second nuclear power plant' for Master in Geology, is my own work unless otherwise stated and that it has not previously been submitted for assessment or completion of any postgraduate qualification to another university or for another qualification.

Sign and date...

Acknowledgments

I would like to thank my supervisor, Prof. Maarten de Wit for his support and assistance during the writing of this dissertation. His guidance has been invaluable.

I would like to thank Eskom for permitting me to undertake this study. Without their willingness to further scientific endeavors this thesis would not have been possible. Special reference must be made to Andre Nel, Eskom's Nuclear Sites Programme Manager who approved access to and use of confidential data.

I would like to thank the Council for Geoscience for funding the cost of my studies at the Nelson Mandela Metropolitan University. To Dr. Greg Botha, my previous manager at the Council for Geoscience; thank you for supporting the dissertation and getting it approved.

The technical and moral support of collages from Council for Geoscience is greatly appreciated. In particular I would like to thank, Dawn Black. She has, in the last few years, become a good friend. Her door was always open and she always assisted me with eagerness. Thank you for motivating me.

I express my greatest gratitude to Dr. Johann Neveling at the Council for Geoscience for not only the technical support and advice on topics covered in this thesis, but also for being the middleman between me and Eskom. I would like to thank him from the bottom of heart for all the moral support and interest he showed in the thesis.

To Coenie De Beer from the Council for Geoscience, thank you for editing the first chapter of this dissertation.

I would like to express my gratitude to Andre Gerber, manager at the St. Francis Links Golf Course, for allowing me to use their on-site borehole information.

I am indebted to my husband, Marcel Claassen and my 4 year old daughter, Lilly Gabriella Claassen. They understood all the late nights and weekends mommy had to work and supported me always. I'm fortunate to have such a great family where love is unconditional even in those very tough times.

To my parents who always believed in me and provided much needed words of encouragement when times were difficult. To my mother, Yvonne Kilian, thank you for giving me the mantra; "meisie, jy kan dit doen!" And thank you for all the weekends you looked after Gabby when I had to work.

Thank you to every person who said a kind word of support, gave a hug at that moment I needed it or sent an email or message to ask how things were going – thank you, thank you, thank you.

"The good thing about science is that it's true whether or not you believe in it."

-Neil deGrasse Tyson

Abstract

This study describes the bedrock lithologies and structure of the Ordovician to early Devonian (485-419 Ma) Table Mountain Group (TMG), the Devonian (419-358 Ma) lower Bokkeveld Group, and the Miocene to Holocene (<23 Ma) overburden sediments of the Algoa Group within an area identified by Eskom for the potential construction of South Africa's second proposed nuclear power plant (NPP), 'Nuclear-1'. The study area is located along the southern coastal margin of the Eastern Cape Province, South Africa, between Oyster Bay and St. Francis (approximately 88 km west of Port Elizabeth), and encompasses the Thyspunt site where the proposed NPP will be built. The study aims to supplement existing information about the Thyspunt area, related to the geoscientific topic 'Geological Setting', as outlined in section 2.5.1.1 of the US Nuclear Regulatory Commission (USNRC) Standard Review Plan NUREG-800, which details the geological information required for review of a proposed NPP. The results obtained from geoscientific studies are used to determine geological factors that may potentially affect site specific design. Factors considered include: bedrock lithology, stratigraphic bedrock contacts, bedrock palaeotopography, thickness of overburden sediments and structural geology. Work by previous authors is combined with new data to create a GIS based 2½D model of the study area's geology (geomodel) and on which future research or interpretations can be based.

Field mapping and petrographic analyses of the TMG, comprising the Peninsula, Cedarberg, Goudini, Skurweberg and Baviaanskloof Formations as well as the lower undifferentiated Bokkeveld Group were undertaken to define the study area's lithologies and structure. Interpretation of geophysical results and the integration of existing borehole data aided in defining the variability in overburden sediments, the identification of contacts between TMG formations beneath overburden, and the palaeotopography of bedrock. Borehole data indicates a clear N-S trend in the thickness distribution of Algoa Group aeolian and marine related sediments. Four coast-parallel trending thickness zones (zones A – D) are recognized within the study area. At Thyspunt overburden thickness reaches a maximum of 61 m, approximately 1200 m from the coastline, in areas underlain by the argillaceous Goudini and Cedarberg Formations. Overburden thickness is influenced by a combination of dune relief, bedrock lithology, palaeotopography and the area's sediment supply. Interpolation of bedrock elevation points and detailed cross sections across bedrock reveals four NW-SE trending palaeovalleys at Thyspunt, Tony's Bay, Cape St. Francis and St. Francis, where bedrock relief (beneath overburden) is formed to be below present day sea-level. Approximately 450 m NW of Thys Bay, a 1050 m^2 (area below sea-level) palaeovalley, gently sloping SE to a depth of -15.5 m asl, is cut into strata of the Goudini Formation resulting in thicker overburden fill in that area.

Structural analysis of the TMG confirms that NE-SW striking strata form part of the regional SE plunging, north verging Cape St. Francis anticline. Bedding inclination is controlled by the distance away from the fold axis, varying from a 5° SE dip along the broad fold hinge to 65° along its moderately steeper SE limb. Folds within the study area plunge gently southeastward at shallow angles, with axial planes dipping steeply SW or NE. Fold axes orientated perpendicular to the fold axis of the Cape St. Francis anticline indicate a secondary stress orientation oblique to the main palaeostress direction. The previously identified 40 km long, NW-SE trending Cape St. Francis fault occurring offshore within 17.5 km of Thyspunt show no onshore continuation within the bounds of the study area. Late jointing is pervasive within the study area and four joint systems are identified. The dominant joint set J1, trends N-S to NNE - SSW; perpendicular to bedding and has a subvertical dip. Normal right-lateral and left-lateral micro-faults dip subvertically, with a displacement that ranges from a few centimetres to <3 m. Micro-faults trend parallel to joints sets J1 and J4 (ESE-WSW). Inferred faults, identified by the Atomic Energy Co-operation (AEC), are interpreted as zones of closely spaced jointing (shatter zones), and show little to no recognizable displacement. Faults and joints do not extend into the younger cover deposits of the Algoa Group and are therefore older than 23 Ma years.

List of Abbreviations

3D – Three dimensional

AEC – Atomic Energy Corporation

BH – Borehole

CFB – Cape Fold Belt

CGS – Council for Geoscience

CSF – Cape St. Francis

DoE – Department of Energy

FDEM – Frequency domain electromagnetic

GIS – Geographical information system

IAEA – International Atomic Energy Agency

INEP – Integrated National Electrification Programme

IPCC – Intergovernmental Panel on Climate Change

IRP – Integrated Electricity Resource Plan

Necsa – Nuclear Energy Cooperation of South Africa

Niasa – Nuclear Industry Association of South Africa

NNR – National Nuclear Regulator

NPP – Nuclear power plant

NSIP – Nuclear Siting Investigation Programme

PBMR – Pebble Bed Modular Reactor

PPL – Plane polarised light

PWR – Pressurised water reactors

SACS – South African Committee of Stratigraphy

SSR – Site safety report

TDEM – Time domain electromagnetic

TIN – Triangulated irregular network

TMG – Table Mountain Group

USC – Uniaxial compressive strength

UNFCCC – United Nations Framework Convention on Climate Change

USNRC – US Nuclear Regulatory Commission

XPL – Cross polarised light

Table of contents

<u>**Appendices**</u>

Appendix A – Journal article and reports

List of Figures

List of Tables

1. Introduction

1.1 Nuclear power in South Africa

1.1.1 A need for energy

The global consumption of energy has increased significantly within the late twentieth and early twenty first century. The increased demand for energy is mainly driven by rapid population growth and industrialisation. South Africa is not immune to this global trend (Figure 1.1 a & b). As part of BRICS (Brazil, Russia, India, China, South Africa), a group of countries regarded as emerging and fast growing economies with global influence (www.brics.co.za), South Africa is expected to place even greater emphasis on its energy generating capacity to attain socio-economic growth through infrastructure development and industrialisation (Van Wyk, 2013). When coupled with South Africa's rapid population growth and governmental initiatives such as the Integrated National Electrification Programme (INEP), aimed at addressing access to electricity in the 4.3 million un-electrified households, a sharp increase in the demand for electricity could be expected (www.energy.gov.za[1]).
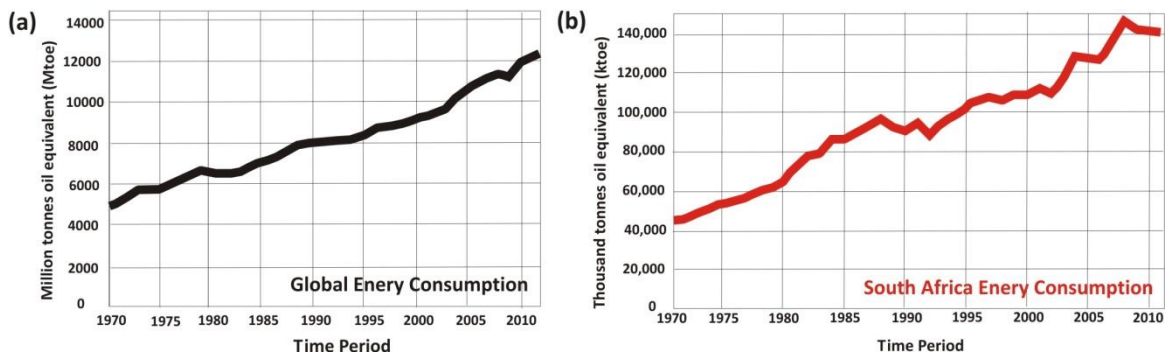
Figure 1.1: (a) Global energy consumption since 1970. (b) South Africa's energy consumption since 1970 (Data from data.worldbank.org).

An urgent focus on meeting future energy demands is therefor needed. Since 2008, South Africa has been plagued by large power outages (load shedding) and an overall unstable power supply grid. It is clear that South Africa's state owned electricity utility, Eskom, is currently unable to fully meet the growing national energy demands through its aging energy infrastructure. Some of South Africa's operating coal-fired power stations was constructed in the 1950's, while Koeberg Nuclear Power Station has been generating electricity for more than 30 of its already extended 40 year lifespan (Van Wyk, 2013; Mfundisi, 2013). Excluding the 4000 megawatt Majuba Power Station in Mpumalanga, no new power stations have been built since the 1980's. Simultaneously a backlog in the maintenance of existing power plants, transmission grids and municipal infrastructure has aggravated the ability to supply electrical energy even further (Steyn, 2003).

1.1.2 A need for nuclear energy

Past global electricity generation primarily used fossil fuels as a source of energy. Historically this has also been the case in South Africa where enormous reserves of easily accessible coal made it the main energy source utilized in electricity generation (Fawkes, 2005). In 2013 South Africa's 13 coal power plants generated approximately 85% of South Africa's electricity (Figure 1.2 a). The country is the world's sixth largest producer of coal and through this is a major contributor to greenhouse gas emissions. The predominant use of coal and other fossil fuels within South Africa has led to the emission of more than 10 metric tons of carbon dioxide per year within the atmosphere since 2009 (www.dataworldbank.org[2]). With the construction of two new (delayed) coal-fired power stations (set to have a combined 9000 megawatt generating capacity by 2015/16), underway at Medupi and Kusile at a cost of R200 billion, this reliance on coal is unlikely to change in the near future (www.engineeringnews.co.za). However, with growing scientific evidence for global warming resulting from the use of fossil fuels, the transition to clean renewable and environmentally 'friendly' energy sources has become critical. The Intergovernmental Panel on Climate Change (IPCC) states that the global temperature increase should remain below 2 degrees Celsius in order to prevent potentially dangerous anthropogenic interference with the climate system. The Kyoto Protocol to the United Nations Framework Convention on Climate Change (UNFCCC) is an international treaty that outlines legally binding limitations or reductions in the emissions of greenhouse gases. South Africa, along with many other developed countries signed the Kyoto Protocol in 2012 to limit or reduce carbon emissions during the commitment period 2013-2020 (https://unfccc.int). In 2013 the South African government announced its commitment to a 34% reduction in carbon emissions by 2020 and 42% by 2025 (www.energy.gov.za[2]). In order to achieve this reduction, the country's over dependence on coal as the main source of energy for electricity production, needs to be weaned by investing in renewable energy or non-carbon emitting power generation. South Africa's only non-carbon emitting power station currently is Koeberg Nuclear Power station situated 30 km outside Cape Town, which generates approximately 5% of South Africa's electricity from two nuclear reactors (www.eskom.co.za[1]).

At the 2013 conference of the Nuclear Industry Association of South Africa (NIASA) held in Port Elizabeth, the Department of Energy (DoE) Director General Nelisiwe Magubane, affirmed the government's commitment to the development of alternative energy sources such as nuclear energy through its Integrated Electricity Resource Plan (IRP) for 2010-2030; stating: *"Preliminary results indicate that if we intend to reduce our carbon footprint and also have a vibrant economic growth, nuclear energy will be part of the solution"* She went on to say: *"It is a known fact that nuclear power will be the most affordable baseload option after coal. Given our climate change commitments, and the fact that some of the coal-fired power stations will retire around 2022 and require replacement, nuclear power is becoming more of a necessity than an option."* (Magubane, 2013). The IRP dictates that South Africa's electricity generation mix by 2030 should include: 48.2% coal; 13.4% nuclear; 13.8% wind; 13% open and combined cycle gas turbine; 6.5% hydro-electricity; 3.4% pumped storage and 0.8% other sources (www.energy.gov.za[2]) (Figure 1.2 b).

Eskom is committed to the IRP through the development of large scale clean and renewable energy projects. The R2.4 billion, 100 megawatt Sere Wind Farm project is currently underway in the Matzikama Municipality (www.eskom.co.za[2]), Western Cape and construction of the planned R1.3 billion 100 megawatt Concentrating Solar demonstration project near Upington in the Northern Cape is set to start in 2014/15 (www.eskom.co.za[3]) (Figure 1.3). Eskom's firm commitment to the development of nuclear power in South Africa was reasserted by the confirmation of Duynefontein, Bantamsklip and Thyspunt, as the next three possible sites for the construction of Nuclear-1, South Africa's second nuclear power plant (NNP) (Figure 1.3). These sites were identified after a lengthy Nuclear Siting Investigation Programme (NSIP). The Thyspunt site located 88 km west of Port Elizabeth and 14 km west of Cape St. Francis is set to be the first of these 3 sites to be utilised for the construction of a proposed 4000 megawatt NNP (www.eskom.co.za[4]).
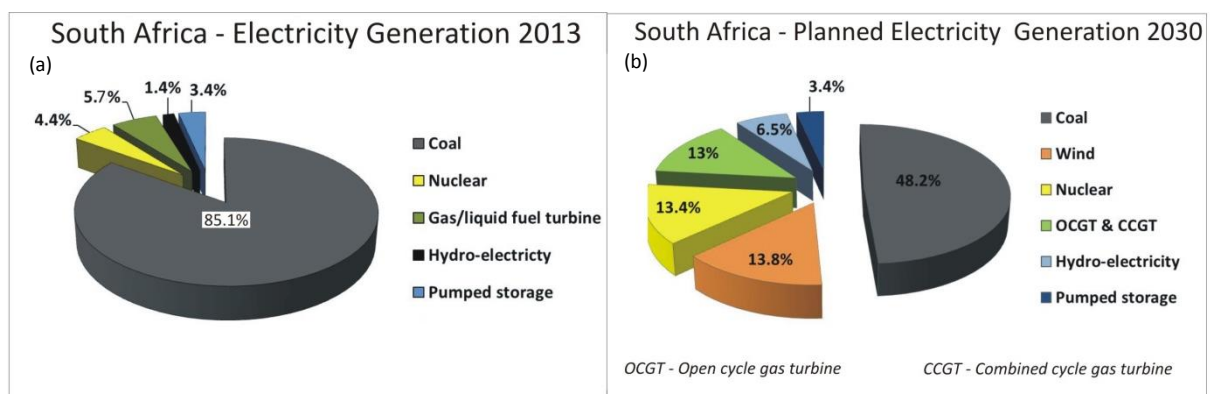
Figure 1.2: (a) Percentage of South African electricity generation per source in 2013 (Eskom, 2014) and (b) planned percentage electricity generation by 2030 per source as indicated by the IRP (data from www.energy.gov.za[2])
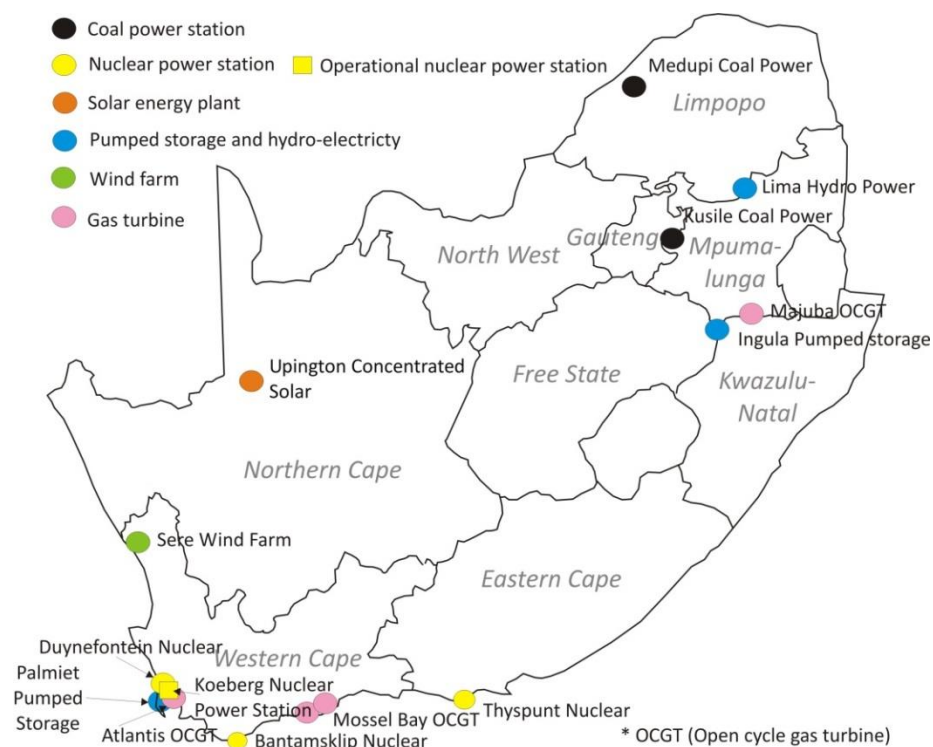
Figure 1.3: Future electricity generating sources / projects in South Africa.

1.1.3 The future of nuclear power in South Africa

Between 1993 and 2010, Eskom in collaboration with the South African government, Westinghouse, and the Industrial Development Corporation of South Africa were engaged in the development of a Pebble Bed Modular Reactor (PBMR) for possible future use in its proposed Nuclear-1 programme. The South African company PBMR (Pty) Ltd was started in 1994 to aid in the development of this Generation IV technology, a mainly theoretical nuclear power generating reactor technology (Van Wyk, 2013). Over a ten year period stretching from 1999-2009, an investment of R9.2 billion in the development of PBMR was made by these stakeholders (www.world-nuclear.org). However in 2010, the then Public Enterprises Minister, Barbara Hogan announced that the government would cease investment in the PBMR programme (Van Wyk, 2013). Conjointly Eskom announced that it does not plan to order any reactor units of this design (Thomas, 2010). Eskom conceded that the duration and cost of this project had become excessive. The problem with PBMR technology started when no investor or client for the PBMR could be secured after major unresolved technical problems in the operation of a German PBMR were reported by the Forschungszentrum Jülich Nuclear Research Centre (Moormann, 2008). Consequently, international banks refused to grant loans to PBMR programmes. In addition, it was estimated a further R30 billion would be needed to sustain research in South Africa at a time when the PBMR programme had not produced favourable results and consistently missed deadlines (www.world-nuclear.org). By 2006 Eskom already attempted to seek alternatives to the failing PBMR programme. The South African government and Eskom began considering more conventional and proven Generation II or III reactor technologies (Figure 1.4). In 2007 Eskom launched a tender calling for 3200 to 3400 megawatt of new nuclear capacity to be built in the near future and up to 20,000 megawatt by 2025. Areva, a consortium consisting of the South African engineering group Aveng; Bouygues, a French construction group and EDF Energy, a United Kingdom based electricity producer, submitted a bid to provide two 1600 megawatt third generation pressurised water reactors (PWR). A second bid was submitted by Westinghouse and included the Shaw Group and the South African engineering firm Murray & Roberts. The bid provided for three 1134 megawatt PWRs. Both bids provided for a further 20 gigawatt capacity in future (www.world-nuclear.org). Upon review Eskom in 2008 decided to abandon the tender process, siting difficulty carrying the financial "*magnitude of the investment*" (Thomas, 2010; Van Wyk, 2013).
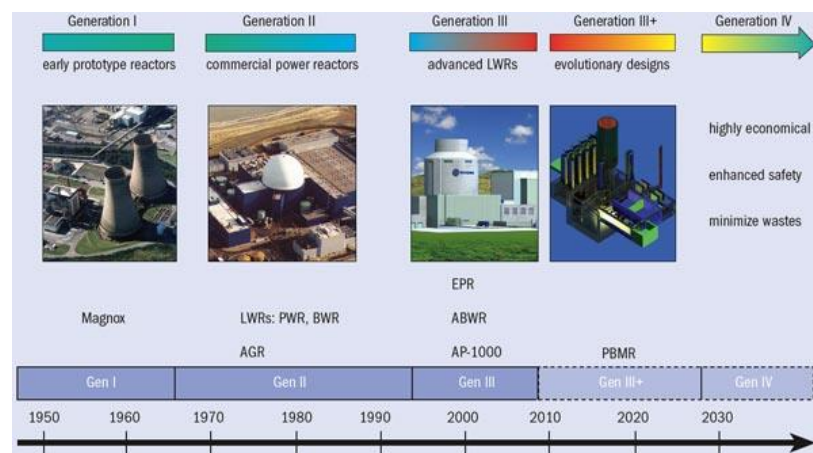
Figure 1.4: Figure indicating the technological development of nuclear reactors over time categorized as 'generations' (http://environmentalresearchweb.org).

More recently, in September 2014, the South African Government signed a strategic partnership to the value of $50-billion with the Russian based Rosatom State Atomic Energy Corporation to advance extensive nuclear research and gain access to Russian technologies, funding and infrastructure. South Africa's Energy Minister Tina Joemat-Pettersson stated that *"This agreement opens up the door for South Africa to access Russian technologies, funding, infrastructure, and provides proper and solid platform for future extensive collaboration."* The Rosatom State Atomic Energy Corporation stated that it would be able to provide up to eight nuclear reactors with a combined capacity of 9.6 gigawatt to South Africa by 2023 as part of the $50-billion partnership. However, Nuclear Energy Cooperation of South Africa (Necsa) stated that the partnership *"initiates a preparatory phase for the procurement process for the new nuclear build in South Africa. Similar agreements will be signed with other vendor countries that have expressed an interest in assisting South Africa with the build program...No vendor country has been chosen yet and no technology has been decided. The agreement refers only to what Russia could provide if chosen." (www.world-nuclear.org).* One month later in October 2014, a similar agreement was signed with France (www.world-nuclear-news.org). Minister Tina Joemat-Pettersson described the agreement as paving the way *"for establishing a nuclear procurement process".* The agreement also aims to further research and development of skills related to the nuclear industry. More recently an agreement was also signed with China (www.world-nuclear.org).

1.1.4 The nuclear 'climate'

Although the energy generated by NPP is regarded as clean; emitting virtually no greenhouse gasses or conventional pollutants such as sulphur dioxide (associated with acid rain), hydrocarbons, nitrogen oxides (associated with smog), and heavy minerals (associated with health conditions) traditionally generated by coal power plants, it still remains controversial. This is in part due to the significant environmental costs associated with industries affiliated with nuclear power. Uranium mining, the refining and enriching of fuel, the management of radioactive spent nuclear reactor fuel, high level radioactive nuclear waste disposal, and the building, maintaining and decommissioning of a NPP are some of the major concerns. The issue of high level radioactive waste disposal in deep and stable geological depository facilities for a period of 10,000 years to ensure safe radioactive decay is particularly controversial. Very few countries (Finland, the United States and Sweden) are actively using or building sites for long term waste disposal of high risk contaminant (Van Wyk, 2013) with sites like the well-known Yucca Mountain high level nuclear waste repository in the United states being closed due to opposition from scientists and local residents who protest its potentially harmful environmental effects. The negative perception of the nuclear industry is further fueled by the risk nuclear power plants can pose through the release of radioactivity due to natural or human induced events that may cause a breach at NPP facilities housing radioactive material. Large scale nuclear power plant disasters like those at Chernobyl in Ukraine (1986), Three Mile Island and SL-1, (Stationary Low-Power Reactor Number One) (1961) in the United States, and the Fukushima Daiichi NPP in Japan (2011) caused deep public anxiety and raised fundamental questions about the future of nuclear power around the world. The enormous capital costs and time associated with the construction of a nuclear power plant facility is also a major problem. Within the past decade construction costs of a new nuclear power generating facility has increased five-fold (Thomas, 2010).

These factors have led countries like Germany, Switzerland and Belgium to either initiate programmes to phase out nuclear power or express interest in doing so by providing subsidised support to the development of renewable energy sources. Alternatively, countries like China, India, Korea and Russia have chosen to expand their nuclear programmes. Russia and China have a combined 38 new nuclear power stations under construction (Van Wyk, 2013), while countries like France generate 73% of its electricity from 58 nuclear reactors (www.iaea.org).

1.1.5 Regulation for nuclear studies

In South Africa the construction and functioning of nuclear power plants is regulated by the National Nuclear Regulator (NNR) Act, 1999 (Act No. 47 of 1999). The state-owned nuclear enterprise, Necsa undertakes and promotes research and development in the field of nuclear energy and radiation sciences and technology in terms of the Act of 1999. It also ensures that nuclear safety standards are adhered to during the operation of nuclear facilities. It does not oversee regulatory investigations nor provide guidelines on the siting of new nuclear facilities. All geoscientific investigations for the siting of a new nuclear power plant are subject to international regulatory requirements. South Africa currently has no specific regulations for geoscientific studies relating to the siting and licensing of nuclear power plant sites. Consequently Eskom has adopted regulations set out in the US Nuclear Regulatory Commission (USNRC) Standard Review Plan NUREG-800, the most conservative and most readily interpreted. The US nuclear industry is well developed and their methodology on geoscientific studies are tried and tested.

USNRC Standard Review Plan specifications defined in chapters 2.5.1 (Geological Characterization Information) outline the responsibilities of the applicant (in this case Eskom) to investigate the geological characteristics of the proposed nuclear site and its environs. Investigations must be undertaken in sufficient scope and scale to evaluate the suitability of the site for the proposed power plant. Geological information should consider natural phenomena historically reported for the site and surrounding areas. New and relevant information must also be collected. The results obtained from these geoscientific studies are utilized to determine geological factors that may affect location, design and operation of a proposed site and its associated infrastructure, likely to include: nuclear reactors and auxiliaries, a turbine complex, spent fuel, nuclear fuel storage and waste handling facilities, intake, outfall structures and various other auxiliary service buildings similar to those currently erected at the Koeberg NPP in the Western Cape.

Furthermore results also aid other investigations outlined in section 2.5.2 (site-specific ground motion response spectrum and probabilistic seismic hazard analysis) of the USNRC Standard Review Plan. Section 2.5.1 outlines three specific geoscientific topics that need consideration. They are: geological setting (section 2.5.1.1), tectonic framework (2.5.1.2) and conditions caused by human activities (2.5.1.3).

1.1.5.1 Regulation as it applies to this dissertation

This thesis aims to supplement information to the geoscientific topic 'Geological Setting' as outlined in section 2.5.1.1 of the USNRC Standard Review Plan NUREG-800, which details the geological information required for review. Information required relate to physiography, stratigraphy, lithology, geomorphology, tectonic setting, faulting and folding characteristics of the region encompassing the site with associated

geological history. Four regulatory areas are defined for investigation. These areas are expressed as radii around the proposed nuclear power plant and reflect the scale of geoscientific investigation and are defined by radii of 320 km around the site (site region), 40 km around the site (site vicinity), 8 km (site area) and 1 km (site locality). However, investigations relating to the proposed site of the NPP may be conducted at any scale benefitting site safety.

1.1.5.2 Confidentiality, data distribution and scope

Geoscientific work conducted by previous authors under the direction of Eskom for direct or indirect usage in establishing a geoscientific framework for the proposed NPP at Thyspunt are confidential and remain the property of Eskom. This includes any data gathered, interpreted and summarized in report or other format by companies, consultancies (e.g. Council for Geoscience, SRK, AMEC & Geomatrix) or individuals. The data and associated reports can only be obtained and used with the written consent of Eskom. The confidentiality status of reports and data are highlighted in chapter 8 within the references list. The use of confidential data within this dissertation has been approved by Eskom's Nuclear Sites Programme Manager, Andre Nel. The author undertook signing of a confidentially agreement.

Authors from a variety of scientific spheres are involved in ongoing investigations surrounding the construction of the proposed NPP at Thyspunt. Consequently results contained within this dissertation have been shared with Eskom to further investigations by other authors. In addition, certain results presented in this dissertation have been published by the author as part of a bursary condition set out by the Council for Geoscience. Appendix A1 makes provision for the inclusion of the published data.

This dissertation does not aim to comment on the seismicity of the area or seismic hazard risk geological features may pose to site safety. This task is assigned to the probabilistic seismic hazard analysis (PSHA) team and involves the seismic characterisation of the site in terms of vibratory ground motions due to natural earthquakes. These studies are governed by a different set of criteria: the Regulatory Guide 1.208, '*A Performance-Based Approach to Define the Site-Specific Earthquake Ground Motion*' (USNRC, 2007) and ASCE/SEI 43-05 '*Seismic Design Criteria for Structures, Systems, and Components in Nuclear Facilities'* (ASCE, 2005).

1.2 The study area

1.2.1 Location of study area

The study area is located onshore between the villages of Oyster Bay and Cape St. Francis (approximately 88 km west of Port Elizabeth) along the southern coastal margin of the Eastern Cape Province, South Africa (Figure 1.5). It includes the locality of Thyspunt, one of three sites identified by Eskom for the construction of South Africa's second proposed nuclear power plant – *'Nuclear-1'.* The 105 km^2 study area is covered by 1:10,000-scale topographical sheets of 3424BA19, 3424BA20, 3424BB16, 3424BB17, 3424BB21 and 3424BB22 (Figure 3.1).

1.2.2 The choice of study area

The study area encompasses the onshore area of the site locality (1 km radius around Thyspunt) and was expanded westward to include the region of St. Francis and northeastward to include the village of Oyster Bay. This was done to ensure that areas that exhibit geological features possibly affecting design and operation of the proposed site are not omitted and strongly aid geological description and interpretation. The study area will therefore partially include the geological setting of the site area (8 km radius around Thyspunt) and site vicinity (40 km radius) areas. Among the geological features considered in defining the outline of the study area, are the possible landward continuation of the Cape St. Francis fault along the coastline between Cape St. Francis and Oyster Bay (Stettler *et al.*, 2008) and the occurrence of inferred faults in the area by the Atomic Energy Commission (AEC) (Muller *et al.*, 1986; Anderson *et al.*, 1986 b; Van Wyk, 1987; Norman *et al.*, 1987a & b).

The dense distribution of data in the site locality also provides a good location for the creation of a geomodel. Such a model would serve as an interactive source of information upon which future geoscientific studies can be based. The model should succeed in integrating a large amount of data from a variety of sources into a singular location with a multi-dimensional perspective.
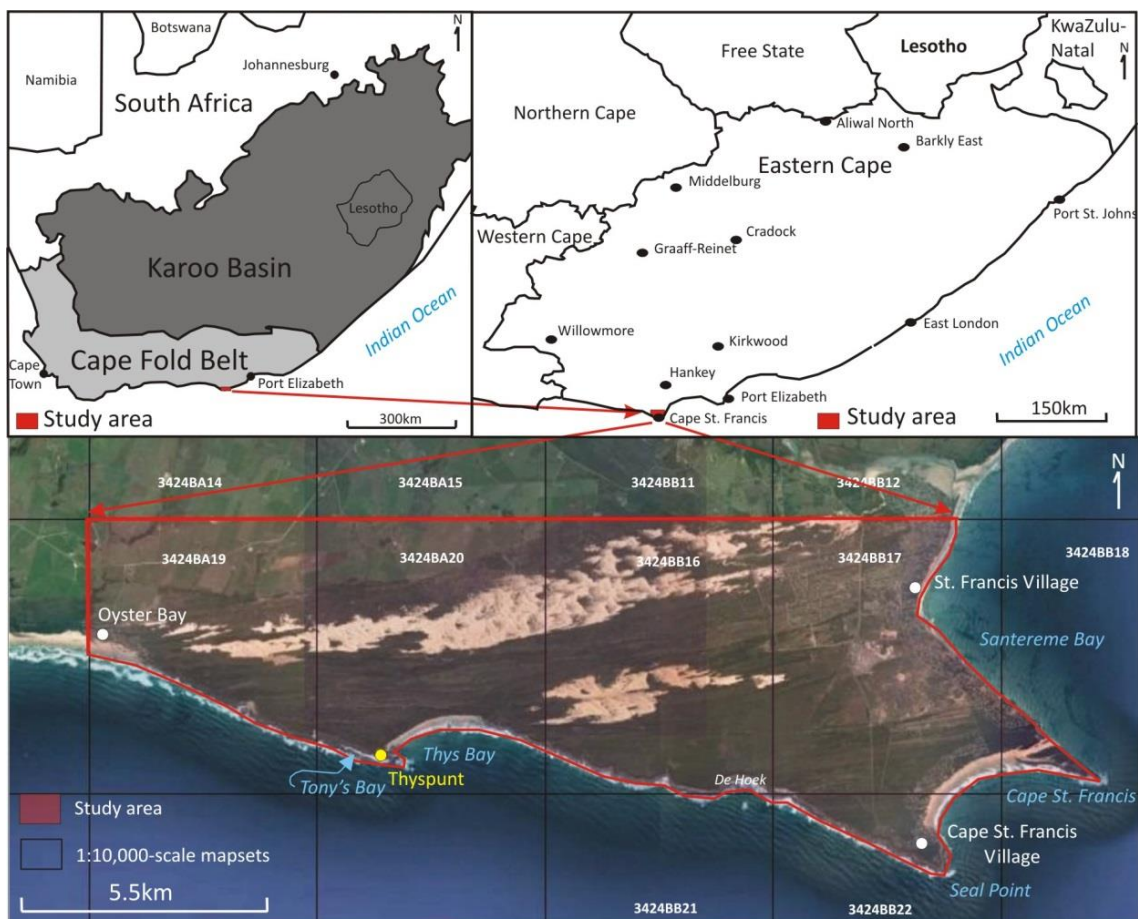
Figure 1.5: Location of the study area.

1.2.3 Physiography of the study area

The geomorphology of the region surrounding the study area is that of a relatively broad, flat lying to gently seaward-sloping coastal platform. The Kareedouw and Suuranys Mountains (located outside the study area) (Figure 1.6) rise above this coastal plain. The landward extent of the transgressive Miocene marine planation (Illenberger *et al*, 2005) event which created the platform terminates against the palaeo-sea cliff (insert of Figure 1.6), marked by a sharp break in slope situated at the southern foot (~300 m asl) of the mountainous interior, NW of Humansdorp near the town of Kruisfontein (insert, Figure 1.6). These mountains (Kareedouw, Suuranys, and also Kareedouw Mountains) reach elevations more than 1800 m above sea level. The marine-planed surface is incised by post-planation rivers that expose inclined bedrock layers. Two rivers provide drainage to the Indian Ocean within the study area. The largest of them, the perennial Kromme River, drains the northern perimeter of the study area and cuts into argillaceous bedrock of the Bokkeveld Group to the north and east. The ephemeral Slang River flows through Oyster Bay into the Indian Ocean (Figure 1.7).
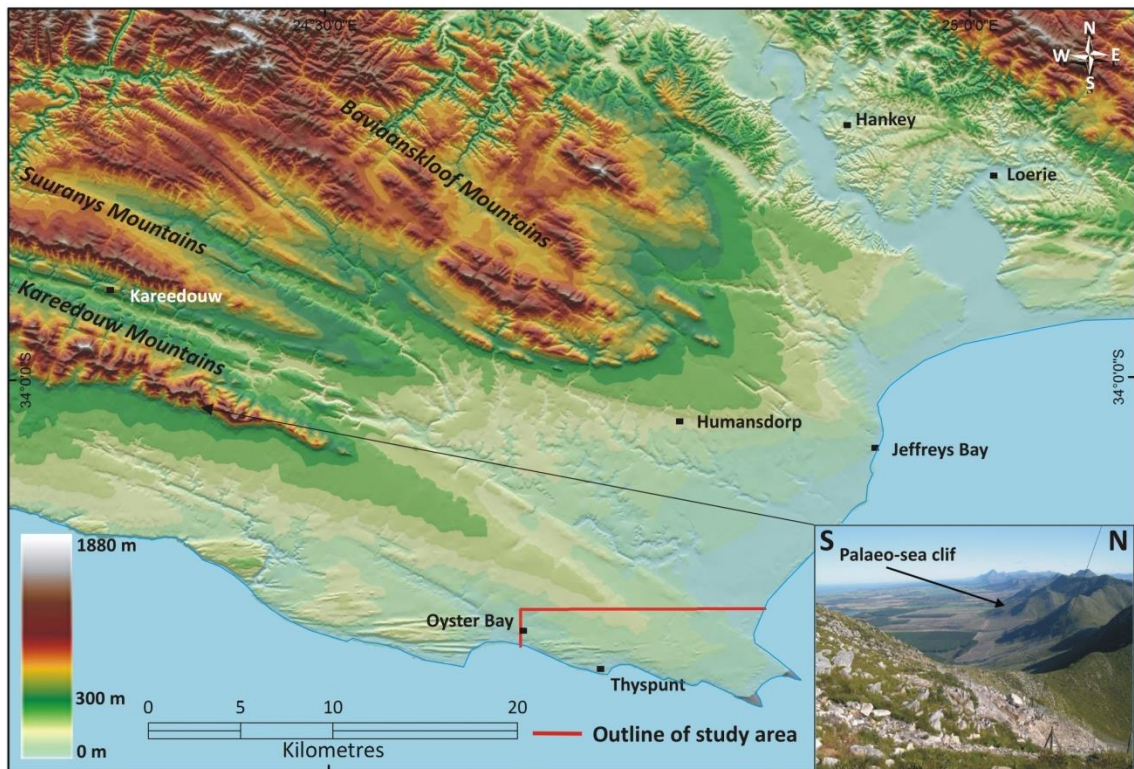
Figure 1.6: A digital elevation model of the study area and surroundings.

Along the coastal margin, the platform is overlain by Cenozoic aeolian and marine deposits (Figure 1.8). Within the study area older Cenozoic deposits are buried by modern linear E-W trending dunes that form part of the Oyster Bay–St. Francis headland bypass dune field. On the Cape St. Francis headland, two active large-scale headland-bypass dune corridors are recognised; namely the Oyster Bay and Thys Bay dunefields (Figure 1.8). The Oyster Bay dunefield, which varies in width from about 500 to 1,200 m, is currently active over a length of about 13–14 km. Transverse dune height varies from 22 m in the upwind (western) end of the dunefield to 5 m at the downwind (eastern) end. The smaller Thys Bay dunefield has a maximum length of about 6 km, a maximum width of about 1,000 m, and average transverse dune

height within the field is about 11 m (Burkinshaw, 1998). A third dunefield, the Santareme dunefield, which occurred along the downwind (eastern) seaboard of the headland (Figure 1.8), was stabilised during the 1970s and 1980s to enable development of a holiday resort suburb in the area. A small headland-bypass system, about 200 m wide and 700–800 m long, crosses the easternmost cape (Cape St. Francis) (McLachlan *et al*. 1994; La Cock & Burkinshaw 1996; Illenberger & Burkinshaw 2007). These deposits extend approximately 4 km into the hinterland near Thyspunt and 10 km inland near Cape St. Francis.
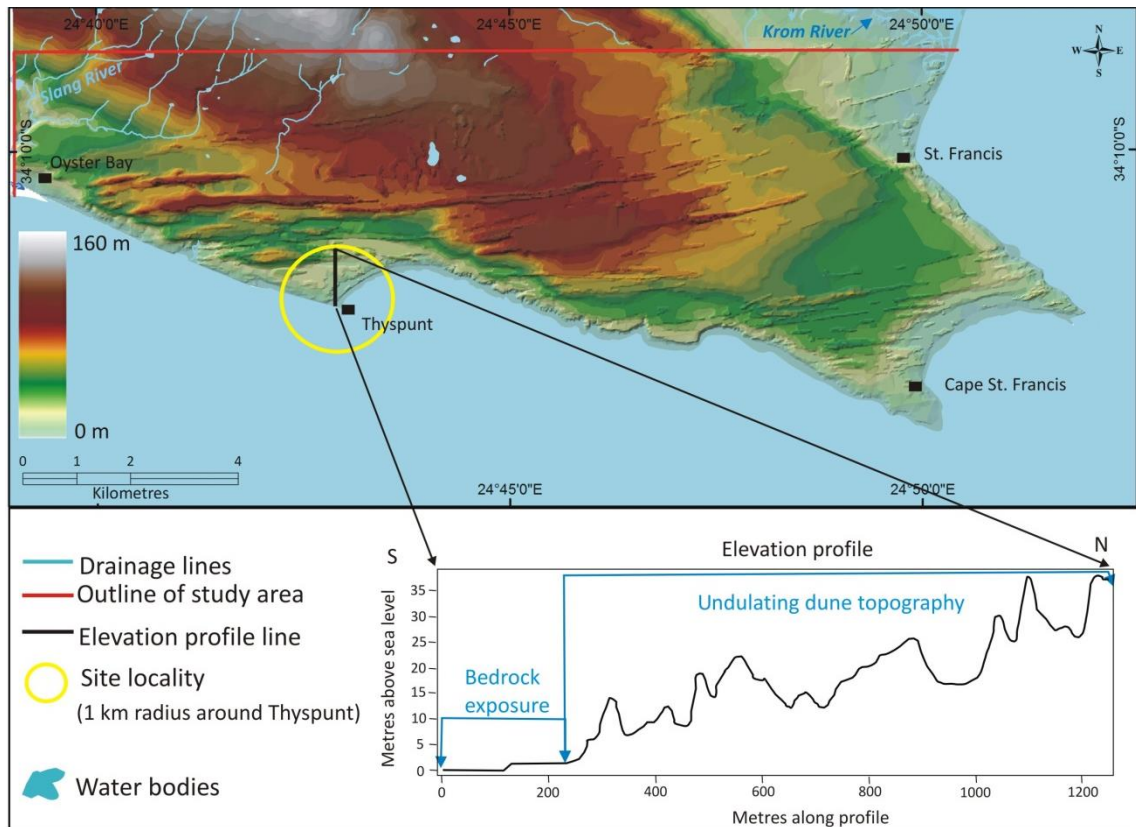
Figure 1.7: Digital elevation model of the study area showing N-S trending elevation profile across the site locality (1 km radius around Thyspunt). Note the undulating dune ridges and troughs.
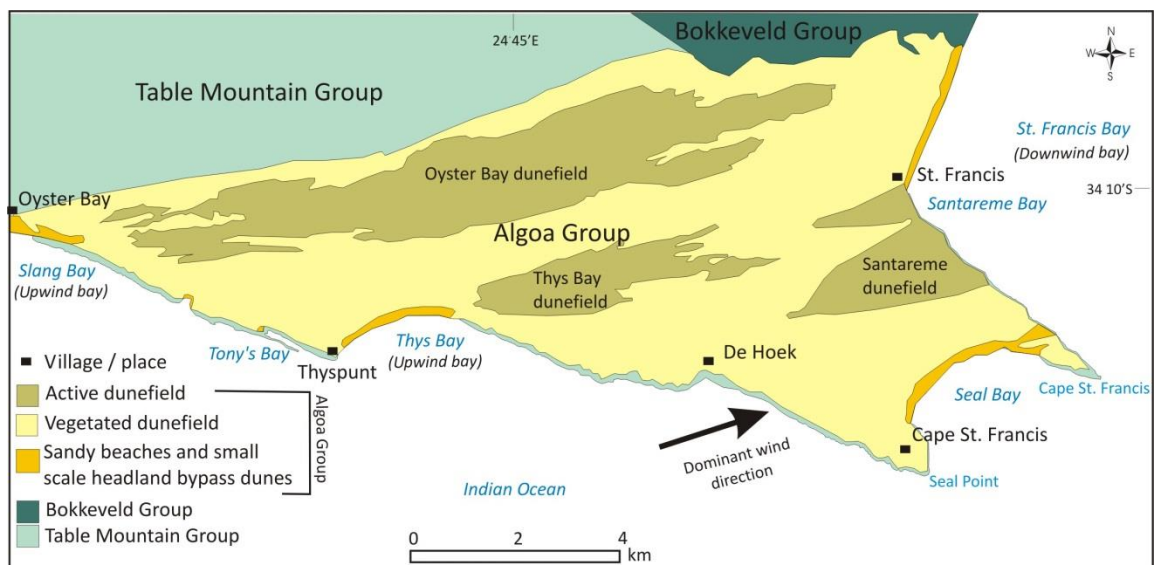
Figure 1.8: Occurrence of dune fields within the study area.

Bedrock is exposed on a narrow (30-250 m wide) NW-SE trending, south-facing, relatively straight and rocky coastline (Figure 1.8) that reflects the strike of bedding in the underlying folded Palaeozoic rocks of the Table Mountain Group (TMG) from Oyster Bay to Cape St. Francis. North of Cape St. Francis the coastline exhibits a SW-NE trending, SE facing undulating coastline underlain by Devonian-aged rocks of the Bokkeveld Group. Intermittent steep narrow inlets or gullies cross-cut perpendicular, parallel and oblique through the rugged coastline. The coastline also exhibits several bays with sandy beaches like the Cape St. Francis Bay, Seal Bay, Thys Bay and Oyster Bay (part of larger Slang Bay). Smaller localised embayments such as Tony's Bay, located approximately 1.5 km NW of Thyspunt also occur. Bays are typically bounded by headlands of more erosion resistant units of the TMG as is the case with Thyspunt, Seal Point and Cape St. Francis (Figure 1.8).

A steady progression of increasing surface elevation is observed from the coast toward the interior. The portion of the study area blanketed by dune cover is characterized by undulating topography; a consequence of alternating E-W trending dune ridges and troughs (Figure 1.7). Topographic highs are associated with the occurrence of the Peninsula Formation quartzite which occurs within the apex of the Cape St. Francis anticline and is expressed in the landscape as a linear NW-SE trending convex ridge. The maximum elevation of 120 m in the study area is reached approximately 7 km west of Cape St. Francis.

1.2.4 Geomorphology of study area

The Cenozoic coastal littoral marine, estuarine, fluvial, lacustrine and aeolian deposits denoted above (Figure 1.8) reflect not only the relative rates of sediment supply and local subsidence, but also the major eustatic sea level movements (Roberts *et al.*, 2006). There is currently much controversy surrounding the Cenozoic land-level change or evolution of southern Africa. Contrasting models are proposed. Partridge and Maud (1987) proposed an episodic uplift model that invoked periods of rapid uplift resulting in the development of pediplains and large-scale erosion and termed these resultant geomorphological features '*African erosion surfaces*' (Partridge & Maud, 2000; Partridge *et al.*, 2006). Their model is based largely on field observations and interpretation since no analytical tools were available at that time. Criticism of their model is driven by lack of reliable age-constraints on erosional surfaces and uncertainty in correlating these surfaces over broad regions of the sub-continent. Doubts were also raised as to whether discrete uplift events would result in regional erosion surfaces (Brown *et al.*, 2000; Summerfield, 1996).

More recent studies have a contrasting view of the episodic uplift model presented by Partridge and Maud (1987). Authors present evidence of slow and uniform low rates of erosion and thus low rates of isostatic uplift during the Cenozoic from dating of surfaces using cosmogenic nuclides and by determining the cooling rates associated with uplift and denudation using fission track analysis (Tinker *et al.*, 2008; Brown *et al.*, 2002, Fleming *et al.*, 1999). A reconstruction of the palaeotopography of the African continent also indicates that the topography had already been high in the Cretaceous and that modern topography did not require high uplift rates during the Cenozoic (Doucouré & de Wit, 2003). Along the southern Cape, Tinker *et al.*, (2008) calculated denudation of <1000 m during the Cenozoic. Very slow land erosion rates of 5.4m/Myr (4.4 m My^{-1} rock uplift rate) are calculated based on ^{10}Be content of sand samples collected from 6 different river systems along southern South Africa (Bierman, 2012). Erlanger *et*

al. (2012) inferred incision rates of less than <20m/Ma (9 to 16 m My^{-1} rock uplift rate). Mantle convection (Burke, 1996; Simmons *et al.*, 2007), igneous activity (Conrad & Gurnis, 2003), and flexural isostatic response (Gilchrist & Summerfield, 1990) are regarded as some of the mechanism for uplift currently being debated (de Wit, 2007).

1.2.5 Geology of the study area

This section aims only to provide a brief introduction to the geology of the study area. Refer to § 2 (Geological Setting) and § 3 (Previous work at Thyspunt) for more detailed geological descriptions on a regional and site specific scale.

Regionally outcrop of the TMG and Bokkeveld Groups were mapped by the (Council for Geoscience) CGS on a 1:250,000-scale. Locally, the geology of the study area and surrounding areas within a 40 km radius (site vicinity) around Thyspunt were mapped as part of a CGS study aimed at producing an initial site safety report (SSR) for the proposed building of a nuclear power plant at Thyspunt (Goedhart *et al.*, 2008). The investigation produced seven 1:50,000-scale maps, fifthteen 1:10,000-scale and eight 1:5000-scale geological maps (Figure 1.10) with a map explanation (Goedhart *et al.*, 2008). Map sheets of a 1:5000-, 1:10,000- and 1:50,000-scale cover the study area in its entirety at a 1:50,000-scale or partially at a 1:5000 and 1:10,000-scale along coastal areas. These map sets include geological data from the published 1:250,000-scale Port Elizabeth map set (Council for Geoscience, 1991), the unpublished 1:50,000-scale maps produced by Toerien (1973), the 1987 unpublished AEC 1:50,000-scale map and the 1:2500-scale coastal maps produced by Raubenheimer *et al.* (1988 a & b). The most recently mapped geology as it pertains to the study area is presented in Figure 1.11 (after Goedhart *et al.*, 2008).
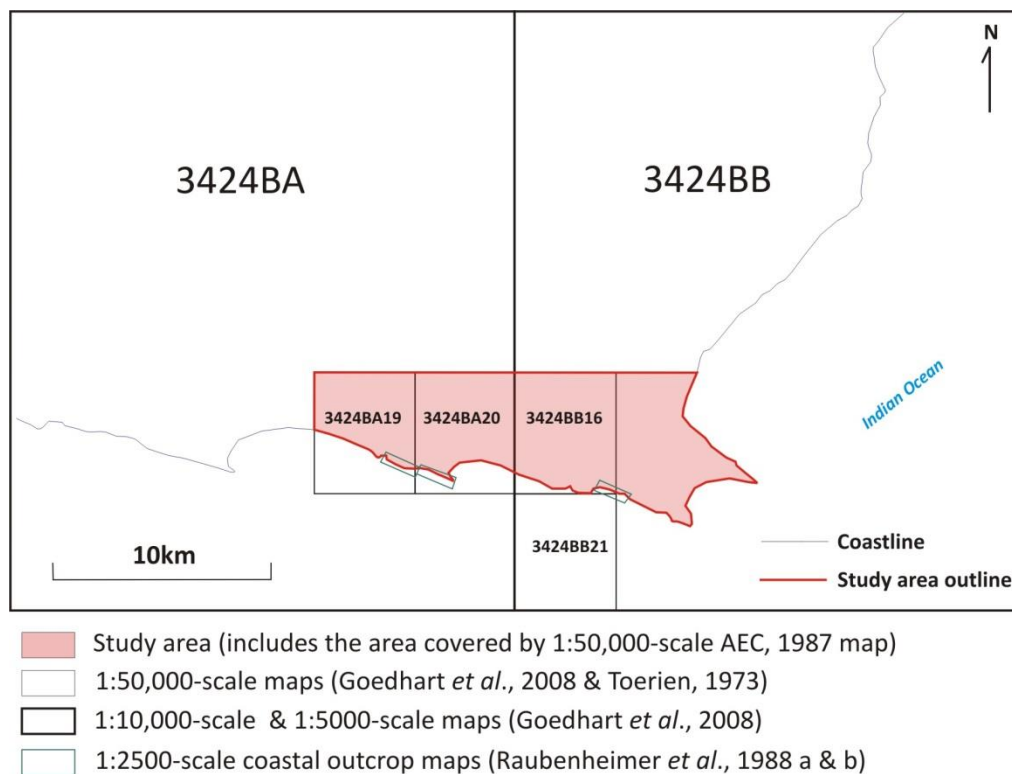
Figure 1.9: Scale of existing geological maps.
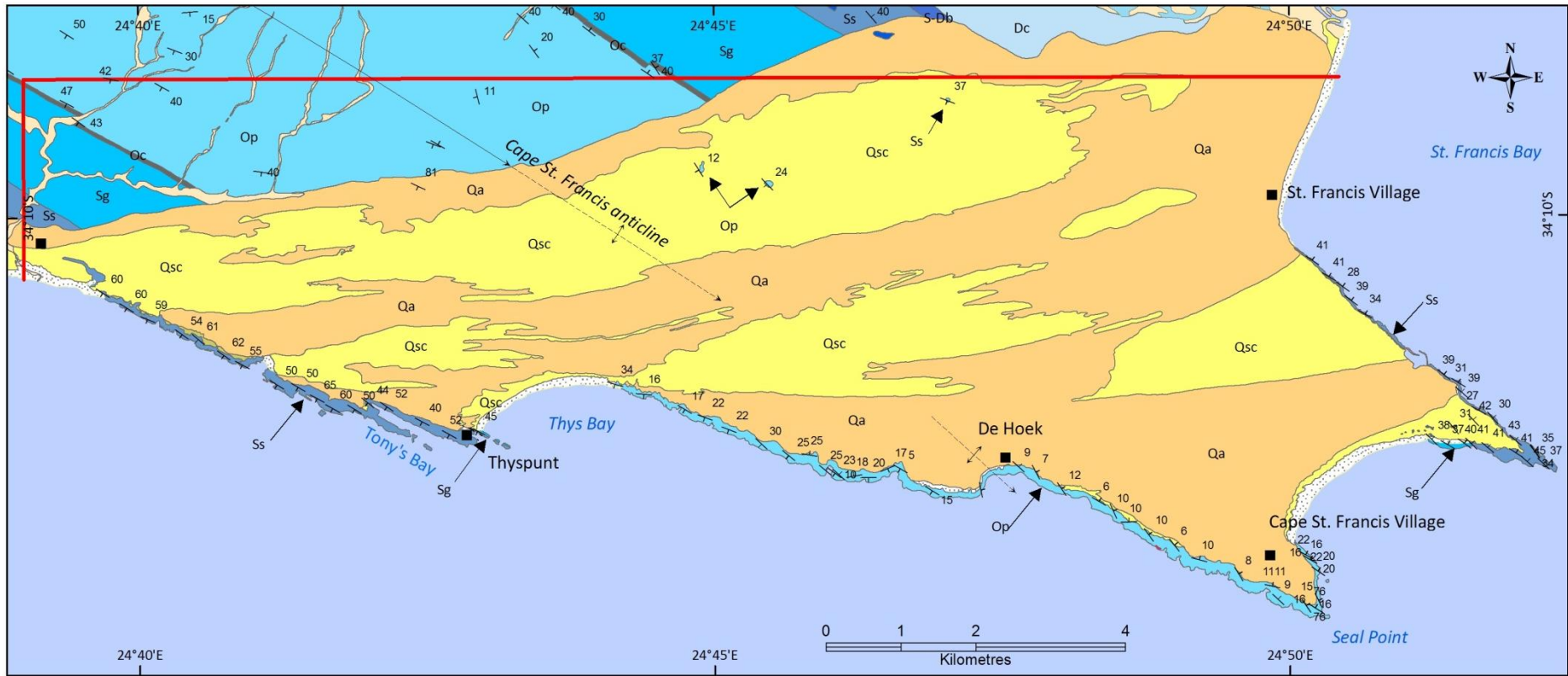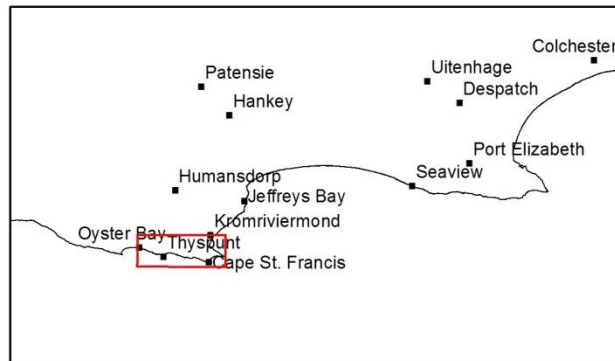
Figure 1.10: Geology of the study area (after Goedhart et al., 2008).

1.3 Study aims

In aid of supplementing geoscientific information to the topic 'Geological Setting' as outlined in section 2.5.1.1 of the USNRC Standard Review Plan NUREG-800, the following investigations or tasks are undertaken:

• Focused mapping of the TMG, lower Bokkeveld Group and Algoa Group within the study area. Lithological descriptions of formations are provided. Particular focus is placed on identifying stratigraphic contacts beneath overburden cover.

• Structural characteristics of the study area including folding, faulting and jointing are detailed.

• Petrographic analysis of lithostratigraphic units within the study area.

• Geological re-interpretation of multi-electrode resistivity and time domain electromagnetic (TDEM) surveys to determine stratigraphic contacts between Palaeozoic units and to identify the possible occurrence of bedrock faults.

 • A holistic overview of borehole datasets as it relates to subsurface characteristics of the study area. Borehole data is utilized to determine the thickness distribution of overburden cover (Algoa Group), bedrock topography (palaeotopography) and contacts between stratigraphic units. Specific focus is placed on determining the thickness distribution of overburden material as construction of the NPP will be done on bedrock requiring major excavation of cover deposits (Eskom, 2009).

• Creation of a geomodel that incorporates mapping results, geophysical results and borehole data using primarily Google SketchUp software.

A description of the chapters within this dissertation is outlined below:

→ Chapter 2: A literature review of the geological history of the CFB that includes lithological descriptions of the Table Mountain and lower Bokkeveld Groups of the Cape Supergroup comprising bedrock in the study area. Strata of the Algoa Group (overburden cover) are also reviewed.

→ Chapter 3: A review of previous work undertaken at Thyspunt as it relates to this dissertation.

→ Chapter 4: Methodologies used throughout the dissertation. This chapter outlines the field mapping process, petrographic analysis, the various geophysical survey methods utilized and geomodelling process.

→ Chapter 5: Results as they relate to study aims are presented in this chapter.

→ Chapter 6: The analysis and interpretation of results obtained in Chapter 5 are interpreted in conjunction with results obtained by previous authors and presented in a discussion format.

→ Chapter 7: A conclusion to the dissertation

2. Geological setting

This chapter provides a literature review of the geological setting of the study area from a regional and local perspective and aims to cover the following topics:

- Regional tectonics, Cape Basin development and subsequent deposition and deformation of the Cape Supergroup;

- A lithostratigraphic and structural description of the TMG and lower Bokkeveld Group within the CFB;

- Deposition of Cenozoic material and lithostratigraphy of the Algoa Group.

2.1 Regional tectonic framework

The Cape Basin formed along the southern margin part of the supercontinent Gondwana. This supercontinental landmass was amassed in the Late Neoproterozoic and Cambrian by Pan-African - Brasiliano orogenic belts that sutured the cratons of West Gondwana; and by collision with the East Gondwana along the Mozambique belt during the late-stage East-African – Ross orogeny (Grunow *et al*., 1996). The southern portion of Gondwana was an assemblage of southern Africa, southern South America, East Antarctica, Falkland Islands and Falkland Plateau (now submerged) and the microplates of West Antarctica (Figure 2.1) (Tankard *et al*., 2012).

Four major compressional and extensional events occurred along the southern margins of Gondwana which contributed to the creation of the Cape Basin, deposition of the Cape Supergroup and subsequent deformation (de Wit & Ransome, 1992 b; Newton *et al*, 2006; Linol *et. al*., in press). These four events are:

1) The Pan-Gondwanean convergence (650 ±100 Ma).

2) The late Proterozoic to early Palaeozoic extension (500 ±100 Ma), which resulted in the extension and thinning of the Pan-African belts of southern Gondwana, ultimately leading to the development of a rift-subsidence (Atlantic-type passive margin) along southern Gondwana (Johnson, 1991) and Cape Supergroup sedimentation.

3) Late Palaeozoic convergence (300±100 Ma) culminating in the development of the CFB. Deformation in the CFB has been dated between ~245 and ~278 Ma (Fitch & Miller, 1984; Tankard *et al*., 2012; Hansma *et al*., in press). The Permian-Triassic CFB is linked to the La Ventia Fold Belt in Argentina through to Antarctica and to Australia in what is known as the Gondwanide Orogenic Belt (Figure 2.2).

4) The early-mid Mesozoic extension (180-170 Ma) resulting in the break-up of Gondwana and the opening of the southern oceans. Buoyancy associated with mantle upwelling during the Mesozoic extension is regarded as a possible factor in the initiation of rifting and the break-up of Gondwana (Reeves, 1999; Conrad & Gurnis, 2003; Brown *et al*., 2014). Reactivation of old CFB fault lines as extensional faults are associated with rifting and the right-lateral rifting of the Agulhas-Falkland Fracture Zone, located offshore along the southeastern margin of South Africa (Broad *et al*., 2012) (Figure 2.1 & Figure 2.3).
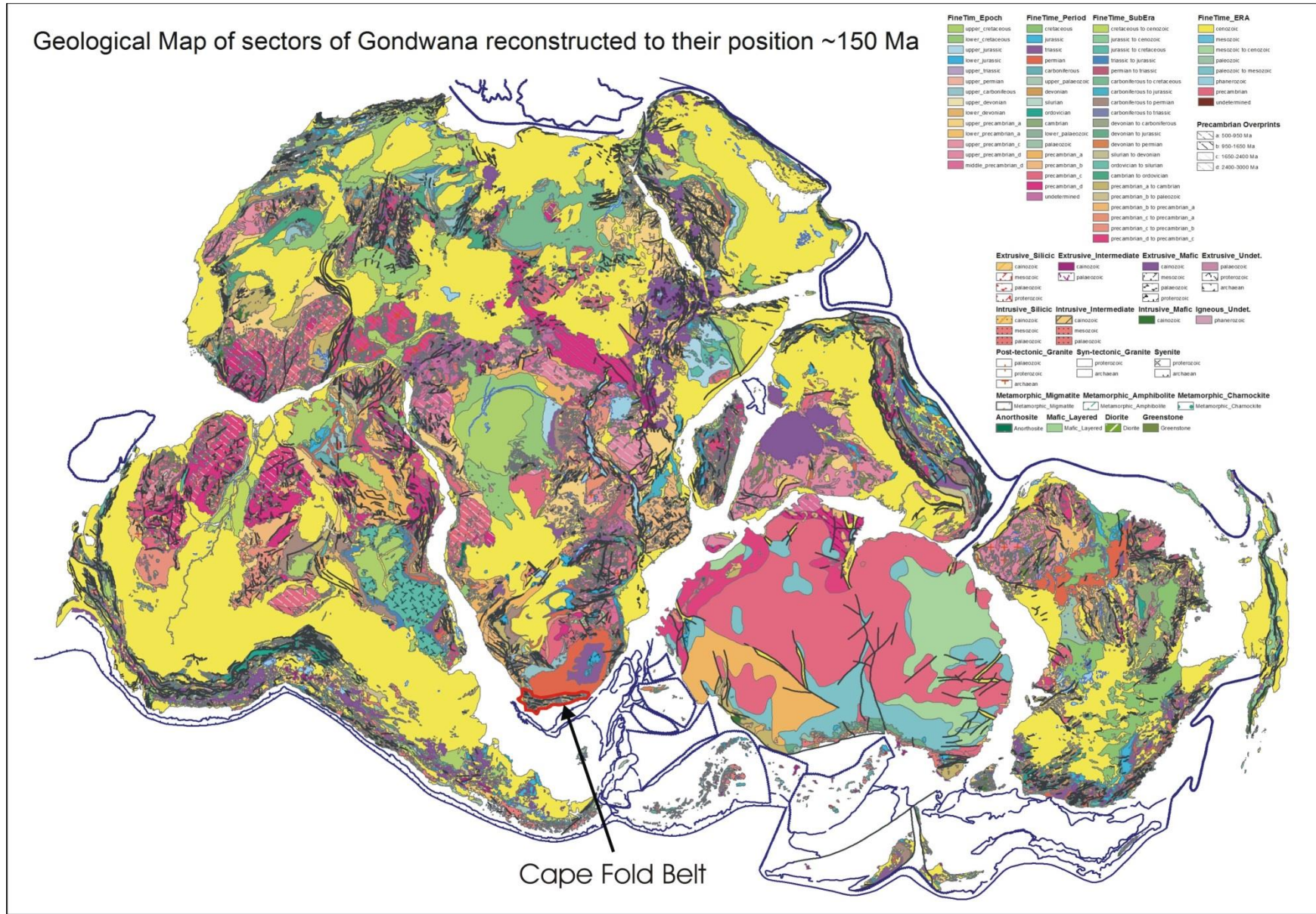
Figure 2.1: Geological map of Gondwana by Gondwana GIS database based on de Wit & Ransome (1992b), indicating the Cape Supergroup sequences (Early Ordovician to Early Carboniferous) within the Cape Fold Belt.
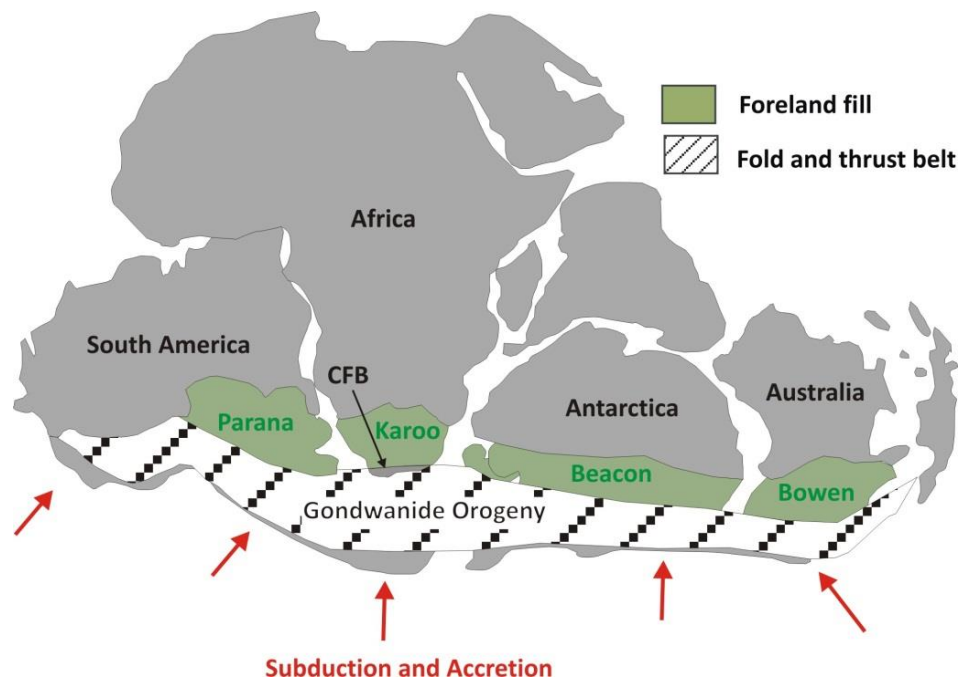
Figure 2.2: The Cape Fold Belt in South Africa is linked to the La Venetia Fold Belt in Argentina through Antarctica and to Australia in what is known as the Gondwanide Orogenic Belt (adapted from de Wit and Ransome (1992 b)).
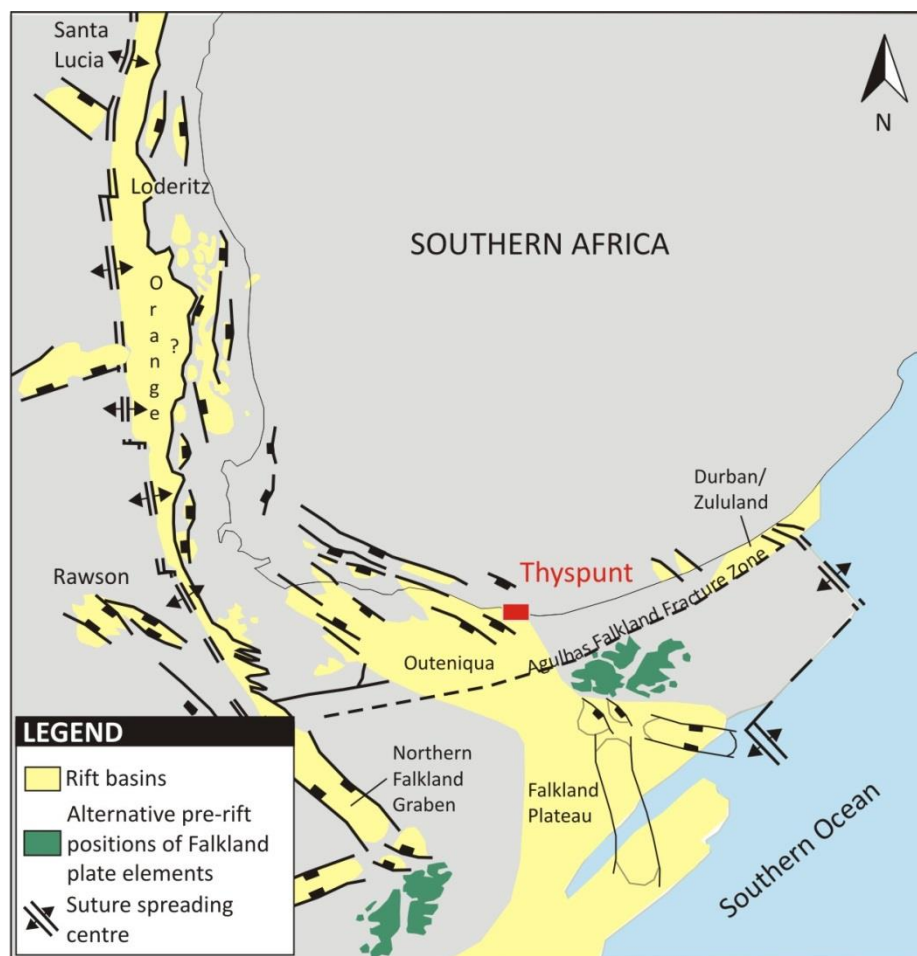
Figure 2.3: Reconstruction of the likely plate tectonic configuration of southern Gondwana during Late Jurassic to Early Cretaceous pre-Gondwana breakup. Note the presence of the Agulhas Falkland Fracture Zone (after Broad et al., 2012).

2.2 Tectono-sedimentary environment of the Cape Supergroup

The siliclastic Cape Supergroup was deposited after the late Precambrian to Early Cambrian Saldanian Orogeny (part of the Late Neoproterozoic to mid-Cambrian East-African - Ross orogeny) and Pan-African depositional cycles ended (Tankard *et al*., 2012). Sediments were deposited on the Precambrian-Cambrian basement (pre-Cape rocks) that includes late Namibian and Cambrian granitic intrusions (Cape Granite suite, ~136 Ma) and metasediments of the Vanrhynsdorp, Gifberg, Malmesbury, Cango Caves, Kansa, Kaaimans and Gamtoos Groups. Deposition of the Cape Supergroup strata occurred from Early Ordovician (~485 Ma) to Early Carboniferous (~300 Ma) along a passive continental margin in a single main sedimentary basin, the Cape Basin (Thamm & Johnson, 2006; Shone & Booth, 2005) thought to have formed by extensional processes in an episutural (rifted) basin setting (Tankard *et al*., 2012).

The onland extent of the Cape Basin measures 200,000 km^2. Downward flexure of the continental margin in response to sediment loading attributed to the substantial 8 km thickness of the Cape Supergroup strata (Johnson, 1991). Sediments of the Cape Supergroup are subdivided into three groups, all of which are lithologically distinct and show great lateral continuity across the length of the Cape Basin. From oldest to youngest they are the Table Mountain Group, Bokkeveld Group and Witteberg Group (Figure 2.5 & Table 2.1). The Ordovician – Devonian Msikaba Formation is also regarded as part of the Cape Supergroup (Thomas *et al*., 1992; Marshall & von Brunn, 1999) and outcrops along the northeastern margins of the Eastern Cape and southern portions of the KwaZulu Natal coast (Thomas *et al*., 1992; Marshall & von Brunn, 1999) (Figure 2.4).

Figure 2.4: Present day distribution of the Cape Supergroup (after Thamm & Johnson, 2006).Note the location of Thyspunt within both the Table Mountain and Bokkeveld Group.

During the Early Ordovician (490-470 Ma) initial rifting towards southern Gondwana occurred along listric faults that exploited pre-existing lines of crustal weakness (Tankard *et al*., 2012) leading to deposition of coarse clastic sediments of Piekenierskloof Formation (comprised of predominantly conglomerate and sandstone) into fault-bounded graben and half-graben basins. The Piekenierskloof Formation forming the basal strata of the Cape Supergroup along the western portions of the Cape basin (Table 2.1 & Figure 2.5).

Table 2.1: Lithostratigraphy and palaeoenvironments of the Cape Supergroup (after Cloetingh et al., 1992; Thamm & Johnson, 2006). Subgroups & formations occurring within the study area are highlighted in grey. (cgl=conglomerate; d=diamictite; m=mudstone; s=shale; sl=siltstone; ss=sandstone; r=rhymatite)

		PERIOD	SUB-GROUP	WEST OF ~21° E FORMATION	SUB-GROUP	EAST OF ~21° E FORMATION	PALAEOENVIROMENTS
CAPE SUPERGROUP	WITTEBERG	CARBONIFEROUS (361-299 Ma)			KOMMA-DAGGA	Dirkskraal (ss)	Beach / shoreface /delta-front
						Soutkloof (s, r)	Lacustrine (proglacial?)/offshore shelf/prodelta slope
						Swartwaterspoort (ss)	Beach / fluvioglacial
						Miller (d)	Glacial
			LAKE MENTZ	Waaipoort (m, ss)	LAKE MENTZ	Waaipoort (m, ss)	Shelf, lagoon, distal delta front, interdistributary bay
				Floriskraal (s, ss)		Floriskraal (s, ss)	Shelf transition zone, shallow marine
				Kweekvlei (s)		Kweekvlei (s)	Offshore shelf, shelf transition zone
	BOKKEVED	DEVONIAN (416-361 Ma)		Witpoort (ss)		Witpoort (ss)	Shallow marine, distributary channel/fluvial
			WELTE-VREDE	Swartruggens (s, sl, ss)		Weltevrede (s, sl, ss)	Tidal flat, shallow marine delta
				Blinkberg (ss, sl)			Distributary, delta-front, barrier
				Wagen Drift (s, sl, ss)			Shelf, shallow marine, delta
			BI-DOUW	Karoopoort (m, sl, ss)	TRAKA	Sandpoort (m, sl, ss)	Tidal flat, delta front, prodelta slope, shelf
				Osberg (ss)		Adolphspoort (ss, sl)	Distributary channel, shallow marine
				Klipbokkop (m, sl, ss)		Karies (m, r)	Tidal flat, delta front prodelta slope, shelf
				Wuppertal (ss, sl)		*(deep marine)*	Tidal flat, delta front, shallow marine
				Waboomberg (m, sl, ss)			Offshore shelf, prodelta slope
			CERES	Boplaas (ss)	CERES	Boplaas (ss)	Delta front, shallow marine
				Tra-Tra (m, sl)		Tra-Tra (m, sl)	Offshore shelf, prodelta slope
				Hex River (ss)		Hex River (ss)	Delta front, shallow marine
				Voorstehoek (m, sl)		Voorstehoek)m, sl)	Offshore shelf, prodelta slope
				Gamka (ss)		Gamka (ss)	Delta front, shallow marine
				Gydo (m, sl)		Gydo (m, sl)	Delta front, shallow marine
	TABLE MOUNTAIN GROUP	SILURIAN (444-416 Ma)	NAR-DOUW	Rietvlei (ss)	NAR-DOUW	Baviaanskloof (ss, s)	Shallow marine and offshore shelf in the east
				Skurweberg (ss)		Skurweberg (ss)	Fluvial braid-plain in west, shallow marine
				Goudini (ss)		Goudini (ss, s)	Shallow marine, fluvial braid-plain
		ORDOVICIAN (488-444 Ma)		Cedarberg (s, sl)		Cedarberg (s)	Offshore shelf
				Pakhuis (d, ss)			Glacial
				Peninsula (ss)		Peninsula (ss)	Fluvial braid-plain, shallow marine
				Graafwater (ss, sl, s)		Sardinia Bay (cgl, t)	Distal fluvial, tidal flat, shallow marine
				Piekenierskloof (ss, cgl)			Fluvial braid-plain

Figure 2.5: The stratigraphic and tectonic progression of the Cape and Karoo Basins (Tankard et al., 2012).

The Piekenierskloof Formation's contact with the underlying pre-Cape rocks is marked by an angular unconformity or in some places a disconformity. Deposition of the basal units probably occurred in small narrow NW-SE trending rift embayments, open to the sea at its southeastern extremity (Shone & Booth, 2005; Rust, 1967). In the Eastern Cape, the Sardinia Bay conglomerate (not formally recognized as a formation by SACS) occupies a similar stratigraphic position as the Piekenierskloof Formation (Table 2.1). These two basal units are the result of coarse clastic terrestrial sedimentation on a rocky, freshly eroded pre-Cape landscape. Strata of the Sardinia Bay and Piekenierskloof Formation were deposited in a braided fluvial setting (Tankard *et al*., 1982; Thamm, 1989).

Subsequent (470-405 Ma) thermal subsidence unaided by brittle deformation along the newly formed divergent margin steered deposition from a terrestrial to shallow marine setting where initial deposition of Graafwater (Western Cape only) and the lateral extension and thick (3500 m) Peninsula Formations took place (Table 2.1; Figure 2.5) (Johnson, 1991).

Towards the Late Ordovician much of North Africa was then situated over the South Pole and experienced an extensive but short lived global glacial period (Pakhuis glaciation) during which deposition of the Pakhuis Formation tillites (Western Cape only) took place (Table 2.1) (Thamm & Johnson, 2006). During early Ordovician time (~416-359 Ma) the distal marine/meltwater facies of the Pakhuis Formation and the Cedarberg shale was deposited (Table 2.1). The thin ~150 m Cedarberg Formation was deposited in shallow embayments and glacial lakes. Tankard *et al.*, (1982) suggested that glaciation (Pakhuis Formation) did not involve significant lowering of sea-level, but did interpret the Cedarberg Formation as a marine transgression (Cooper, 1986; Cotter 2000). Shone & Booth (2005) highlighted that regressions and transgressions are not solely the consequence of sea-level change, but that tectonically-induced change in relative sea-level is also expected in the setting of a divergent margin basin. The upper Cedarberg Formation represents the end of large subsidence (Tankard *et al.*, 2012).

Towards the western portion of the basin, the Nardouw Subgroup (Table 2.1) was subsequently deposited on a shallow-marine shelf which, along the northern extremities of the basin, graded into an extensive fluvial coastal plain (Theron & Thamm, 1990, Thamm & Johnson, 2006) associated with a period of lithospheric recovery and basin stability (Tankard *et al.*, 2012). Along the eastern portion of the basin, deposition of the upper Goudini Formation and Skurweberg Formation took place in an environmental setting associated with braided streams. The lower Goudini Formation sediments were deposited by longshore currents in a shallow-marine environment (Table 2.1). The Baviaanskloof Formation, the uppermost formation of the Nardouw Subgroup east of 21° E, was deposited in a low-energy marine shelf (Thamm & Johnson, 2006). The Rietvlei Formation the uppermost formation of the Nardouw Subgroup west of 21° E, was deposited by near-shore processes in a shallow marine shelf setting grading into an extensive fluvial coastal plain near the northern basin edge.

The TMG is overlain by thick successions of the Devonian Bokkeveld and Witteberg Groups. During the early Devonian (405-330 Ma) a second phase of mantle extension and a significant amount of thermal subsisdence, lacking any substantial fault accommodation deepened the Cape Basin (Figure 2.5) (Tankard *et al.*, 2012). This initiated the deposition of deeper-water, fine-grained predominantly muddy marine sediments of the Bokkeveld Group that represents the first major marine incursion along the southern African margin of Gondwana (Milani & de Wit, 2008; Tankard *et al.*, 2012). Subsequent deposition of more sand-rich deposits of the Witteberg Group took place during the Middle to Late Devonian through to Early Carboniferous (Table 2.1). The lower deposits of the Witteberg Group represent a continuation of Bokkeveld Group sedimentary processes resulting in the aggradation of thick delta-front, tidal front, interdistributary bay and fluvial sediments that were subject to marine reworking. Shoaling marine sequences were followed by continental sedimentation and a final progradational offshore to deltaic sequence.

2.3 Lithostratigraphy of TMG and Bokkeveld Group in the Southern Eastern Cape

2.3.1 Table Mountain Group (TMG)

Within the Eastern Cape the TMG comprises 3500 m thick clastic succession predominantly arenaceous supermature sandstone stratigraphically defined by the Peninsula, Cedarberg Goudini, Skurweberg, Baviaanskloof and Sardinia Bay Formations (Figure 2.6 a). The Sardinia Bay Formation does not outcrop in the study area. The TMG is unconformably underlain by the Namibian aged Gamtoos Group that forms the basement in the study area. The Gamtoos Group is comprised of quartzites, conglomerates, phyllite, shale and limestone (Figure 2.6 b).
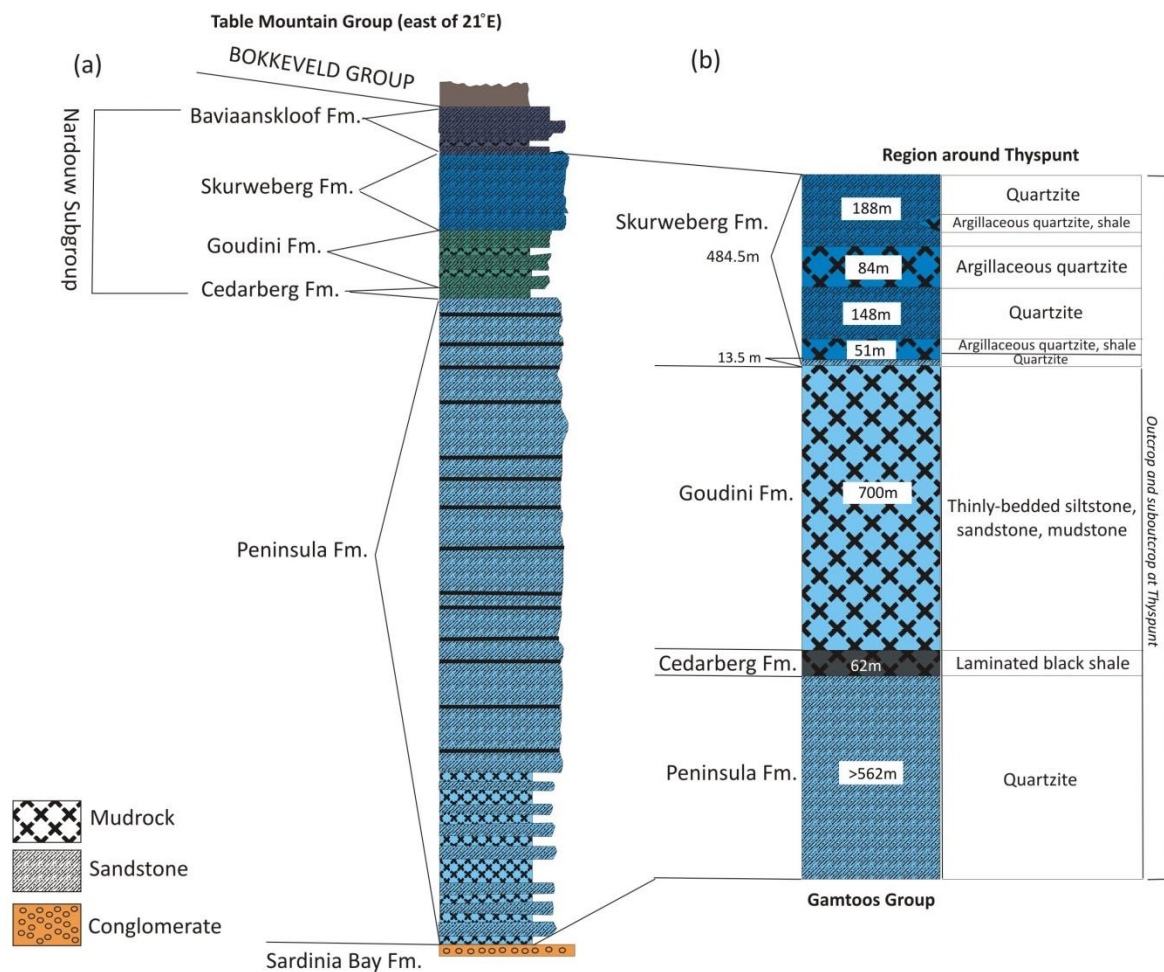
Figure 2.6: (a) A representative cross section though the TMG east of 21° (modified after Thamm & Johnson, 2006). (b) The approximate thicknesses and lithology of TMG formations in regions surrounding the Thyspunt site (after Goedhart et al., 2008).

2.3.1.1 Peninsula Formation

The Ordovician Peninsula Formation consists of pale-grey, medium to coarse-grained, supermature quartzose sandstone with subordinate lenticular black shale horizons generally less than a metre thick. Although strata appear massive, horizontal bedding and low-angle cross-bedding are common (Toerien & Hill, 1989). The formation becomes more coarse-grained and gritty towards the top. Localised lenses of matrix-supported, small-pebble conglomerate occur in places (Le Roux, 2000). In the eastern portion of the Cape Basin, Rust (1967) indicates a maximum thickness of ~2700 m for the Peninsula Formation. The

supermature Peninsula Formation quartzites are envisioned to have been deposited in a shallow marine setting (Rust, 1973; Johnson *et al*, 1999). Authors such as Hobday and Tankard (1978) envisioned a beach foreshore, barrier and back-barrier environment with coast-parallel, lateral migration of tidal inlets. In addition deposits reflect small back-barrier tidal channels. Tidal sand ridges and sand waves have also been identified within the greater Peninsula Formation.

2.3.1.2 Cedarberg Formation

The normally lateral persistent Ordovician Cedarberg Formation outcrops eastward up to ~100 km west of Port Elizabeth (Shone & Booth, 2005). The formation attains a thickness of 50 – 120 m. In the region east of Kareedouw Goedhart *et al*., (2008), calculated the thickness of the Cedarberg Formation as 62 m (Figure 2.13 b). Two members are recognised within the Cedarberg Formation. The basal Soom Shale Member comprises black, carbonaceous, thinly laminated shale which coarsens upward into pale coloured mudrocks, siltstones and sandstones of the Disa Member. Shale appears grey to greenish grey or yellowish in weathered exposures. The lower contact with the Peninsula Formation is sharp, whereas the upper contact with the Goudini Formation is gradational (Johnson *et al*., 1999). Shale units often contain pyrite (Shone & Booth, 2005).

Absence of the Cedarberg Formation may be related to folding and thrusting. Shone and Booth (2005) documented an absence of the formation along fold limbs of large-scale folds. They suggested that the Cedarberg Formation forms a structurally favourable detachment zone, causing the formation to be "*smeared out*" along fold limbs and preserving remnants of the formation in fold noses.

2.3.1.3 Goudini Formation

The basal unit of the Nardouw Subgroup is the Goudini Formation, previously known as the Tchando Formation. The formation comprises supermature medium-grained quartzose sandstones, with thin subordinate shale and siltstone lenses. Sandstone units are medium to thick bedded and intensely bioturbated (Malan *et al*., 1989). Sandstones of the Goudini Formation characteristically weather to a brownish colour. Sedimentary structures include horizontal lamination, planar cross-bedding, trough cross-bedding, subordinate wavy bedding and inclined bedding. Fine to very fine-grained mudrock units are micaceous or carbonaceous and thinly bedded. Mudrock units are generally structureless or show horizontal lamination. The formation has a thickness of 260 m (as measured in the Baviaanskloof). Deposition of the Goudini Formation strata occurred in a shoreline environment on a shallow stable shelf (Toerien & Hill, 1989; Malan *et al*., 1989). Palaeocurrent data indicates a fluvial depositional environment (Johnson, 1976).   The Goudini Formation shows a variation in thickness in the surrounding region of the study area. Near Thyspunt Goedhart *et al*., (2008) indicated an approximate thickness of 700 m (Figure 2.13 b) whilst Malan *et al*., (1989) calculated a thickness of 230 m ± 30 m in the areas NW of Humansdorp (30 km NNE of Thyspunt).

2.3.1.4 Skurweberg Formation

The Skurweberg Formation, previously known as the Kouga Formation, conformably overlies the Goudini Formation and comprises up to 400 m of thick to very thick-bedded (13 – 85 m), medium to coarse-grained, moderately sorted profusely cross-bedded quartzitic sandstone (Theron *et al*., 1989). The

sandstone is medium to very pale grey, orange, orange-pink or pale orange and weathers white. Trough and planar cross-bedding are most prevalent with subordinate wavy and inclined bedding. The formation may appear massive in places. Shale units are subordinate and generally structureless or horizontally laminated. Both the upper boundary with the Baviaanskloof Formation and lower boundary with the Goudini Formation are described as conformable to gradational (Theron *et al.*, 1989). The lower contact is defined as the base of the first quartzitic sandstone unit that indicates a recognisable change in the depositional setting (SACS, 1980). The lower contact is defined as the base of the first quartzitic sandstone unit that indicates a recognisable change in the depositional setting (SACS, 1980; Theron *et al.*, 1989). Goedhart *et al.,* (2008) interpreted the 'first major influx of sand', as a 13.5 m thick, massive quartzitic unit as the basal unit of the Skurweberg Formation, occurring towards the north of Thyspunt (Figure 2.15). Underlying this basal unit are two fine-grained, silty argillaceous quartzite (grey-wacke) and shale units separated by quartzitic units. Deposition of both argillaceous units are interpreted to occur in either a back-barrier stagnant, anoxic, lagoonal setting or a restricted shoreline setting, similar to the Goudini Formation (Goedhart *et al.*, 2008).

2.3.1.5 Baviaanskloof Formation

The Baviaanskloof Formation consists of immature, fine-grained, sandstone (~80%), subordinate dark-grey shale, laminated rhythmite (<5%) and dark grey to black siltstone (<15%). Sandstone appears massive, siliceous, medium dark grey in colour, fine to very fine-grained. Sedimentary structures in sandstone of the formation include horizontal lamination, wavy bedding, micro-cross lamination, rare cross-bedding and ripple marks. Siltstones are often densely bioturbated. Sandstone units range in thickness from 7 - 40 m. The formation attains almost 200 m at the Paul Sauer Dam, north of Humansdorp. A prominent 50 - 80 m thick, pale-grey, medium to coarse-grained, feldspathic sandstone unit, known as the Kareedouw Member occurs roughly halfway through the formation (Hill, 1991). The Kareedouw Member is thickly bedded and cross bedded in places. The formation's lower contact with the Skurweberg Formation is gradational, while the upper contact with the Bokkeveld Group is conformable.

2.3.2 Bokkeveld Group

The predominantly argillaceous Bokkeveld Group conformably overlies the arenaceous strata of the TMG and comprises a cyclic alteration of fine-grained sandstone and mudrock units. The group attains a thickness of 3500 m in the eastern portions of the Cape Basin (Theron & Johnson, 1991). Along the southern Cape Basin, east of 21° E, the Bokkeveld Group is subdivided into lower Ceres and upper Traka Subgroups. Three upward-coarsing cycles are recognised in the lower 1700 m thick Ceres Subgroup. The Gydo and Gamka Formations form the lower cycle, the Voorstehoek and Hex Formations form the middle cycle and the upper cycle is represented by the Tra-Tra and Boplaas Formations. The predominately argillaceous Gydo, Voorstehoek and Tra-Tra Formations are comprised of mudrock, siltstone and very subordinate sandstone. The more arenaceous Gamka, Hex River and Boplaas Formations consist of fine to medium-grained feldspathic wacke and arenite and subordinate mudrock and siltstone.

2.4 Deformation of Cape Supergroup strata

Subsidence and subsequent sedimentation along the Cape Basin margin was followed by a period of deformation and uplift related to shortening in the late Palaeozoic. The Palaeozoic compression (Cape Orogeny) and formation of the CFB occurred between ~245 and ~278 Ma. The Cape Orogeny is described as a single phase; multi-event consisting of four compression phases/events, coupled with a concluding extension phase that affected deposits of both the Cape Supergroup and deposits of the southernmost regions of the Karoo foreland basin (de Wit & Ransome, 1992 a & b; Newton *et al*, 2006; Hansma *et al*., in press). These phases/events are outlined by Hälbich, (1983, 1992):

1) **First deformational event - Swartberg folding 278 ± 2Ma (Early Permian)**

   The first phase of deformation entails flexural-slip folding and is confined predominantly to the present Swartberg mountain range where thrusting and folding formed a mega-anticlinorium exhibiting 35% crustal shortening through mechanisms such as northward overfolding.

2) **Second deformational event - Outeniqua folding 258 ± 2Ma (Mid to Late Permian)**

   The second event occurred further south and resulted in the formation of isoclinal, almost recumbent, structures formed by northward overturning in the Outeniqua Range. The George Anticlinorium formed in this phase, resulting in further horizontal shortening. Substantial thrusting of the basement and near-recumbent folding of overlying strata led to a 70% shortening in places. Temperatures did not exceed 300°C (Hälbich, 1983).

3) **Third deformation event - crenulation cleavage 247 ± 3Ma (Late Permian to Early Triassic)**

   During the third phase, deformation shifted towards the northern portion of the fold belt. The third phase is characterised by the formation of steeply asymmetric megafolds which extend into the lower Beaufort sequence and semi-lithified Ecca beds.

4) **Fourth deformational event - kink banding 230 ± 3 Ma (Mid to Late Triassic)**

   The final phase of north-south compression was associated with kink-banding and shearing, low amplitude and near-upright folds in the Karoo strata formed during this event.

Table 2.2 outlines the resultant type of deformation each of the compressional (shortening) events listed above imprinted onto strata of the Cape Supergroup.

A final phase of relaxation occurred during the Late Triassic (215 ± 5Ma) that facilitated movement along east-west normal faults and so accordingly is closely associated with a set of tensional kinks that developed due to uplift. Deposition continued to occur in the Karoo foreland basin north of the CFB until Upper Jurassic times, and included the Karoo volcanism around 182 Ma, which was then followed by rifting and eventual Gondwana fragmentation during the Cretaceous (Hälbich, (1983; 1992; de Wit & Ransome, 1992 a & b; Newton *et al*, 2006).
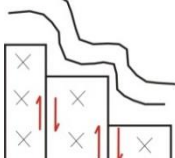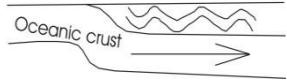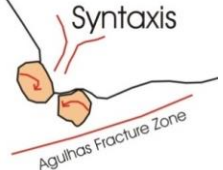
Table 2.2: The four compressional events of the Permo-Triassic Cape Orogeny and their resultant effect on strata (after Hälbich et al., 1983).

Event & Time	Type of Deformation	Resultant Structures
First Paroxysm ± 278 Ma	Folding	● Flexture slip folds ● Asymmetric folds
	Cleavage	● S_1 cleavage
Second Paroxysm ± 258 Ma	Folding	● Isoclinal, almost recumbent folds
	Cleavage	● S_2 Cleavage
Third Paroxysm ± 247 Ma	Folding	● Refolded folds
	Faults	● Thrusts
	Cleavage	● S_3 cleavage
Fourth Paroxysm ± 230 Ma	Folding	●Listric folds ●Kink bands
	Faults	● Listric thrusts ● Minor shears
	Cleavage	● Fanning of axial plane cleavage

2.4.1 Models of deformation

Although the events relating to the Cape Orogeny are well defined, the mode of deformation is in dispute. Many authors have proposed models of deformation taking into account anomalous characteristics of the CFB, including a lack of granitic intrusion, carbonate rock, lavas or pyroclasts, lack of medium to high grade metamorphic rocks, ocean floor derivatives and major shear zones or melanges, along strike or transcurrent, while trying to explain known structural geology. Sequence of the various deformation models proposed are briefly summarized in Table 2.3. The Cape Orogeny is traditionally viewed as a foreland northward-vergent thrust-fold belt that hosts both thick-skinned and thin-skinned deformation with a north dipping subduction zone dipping south of the CFB (De Beer, 1990; Newton *et al*., 2006; Paton *et al*., 2006). This model is problematic due to the large distance between the CFB and the interpreted subduction zone (> 1000 km) and lack of granitic intrusions. Alternative models placed greater importance on strike-slip processes (Johnston, 2000; Tankard *et al*., 2009) (Table 2.3). However, lack of structural features such as persistent and penetrative horizontal lineations in the CFB do not support the strike-slip model (Lindeque *et al*., 2011). Interpretation of borehole data, surface geology, various geophysical datasets and seismic data by Lindeque *et al*., (2011) indicates a collisional tectonic setting formed in response to continent-continent-, arc collision, or suturing south of the CFB, and far-field subduction to the south. The Karoo Basin may have developed in front of a thin-skinned Jura-type fold belt; negating the retro-arc or orogenic foreland basin as previously proposed. Most recently, Tankard *et al*., (2012) interpreted the CFB as a thick skinned sinistral strike-slip orogen linked to oblique reactivation of the southern Namaqua suture (Figure 2.7).

Table 2.3: Summary table indicating proposed models of CFB deformation.

Proposed Deformation Model	Model Description
Gravity model Newton, 1973 	A model based on vertical tectonics instead of conventional orogenic tectonics is proposed. Towards the southern and western portions of the CFB, pre-Cape basement rocks were down-dropped along normal faults that developed parallel to the long axis of the basin as a result of either the weight of the overlying strata or due to uplift cause by a bulge in the mantle. As a result strata were deformed through gravity sliding over step-like fault blocks of pre-Cape basement descending on a palaeoslope towards the north. The Cape syntaxis is envisaged as a convergence between the eastward and northward flowing sedimentary masses.
Conventional subduction model De Beer *et al.*, 1974	This model of conventional plate tectonics explains geophysical anomalies such as the Southern Cape Conductive belt, Beattie magnetic anomaly, and a negative anomaly in the southeastern Cape by suggesting that Gondwana was underthrusted by an oceanic plate and later experienced a continental collision resulting in orogeny.
Alpine model De Swardt & Rowsell., 1974	The model proposes that the CFB was formed by gravity sliding of cover rocks over a more rigid basement. A median zone of uplift is thought to have facilitated this gravitational gradient. Folding and thrusting is seen as verging away from this median zone with basement becoming involved at a later stage. The model is similar to that of an Alpine type deformation.
Flat plate subduction model Lock, 1980 	The Proto-African plate collided and fused with the south-western margin of Gondwana at the position of the present day southern coastline of Africa. The resultant subducted oceanic crust caused major stresses at the leading edge of the proto-African plate. The fused plates continued to converge causing major friction, which resulted in tectonic deformation, shortening, and the eventual formation of the CFB. The subduction zone initiated approximately 1000km south-east of the present day coastline. The fusing of plates explains the lack of any significant volcanic rocks during the development of the CFB.
Ensialic model Hälbich, 1983	The ensialic model proposes extension normal to the basin axis. Multiphase deformation resulting in thinning within the crust and the formations of grabens-type basin. Rising mantle convection currents resulted in the formation of an aulacogen, into which terrigenous sediments were deposited. Tectonic shortening occurred at the northern extent of the graben, where faults show a decreased dip.
Collision model & Andean model De Wit & Ransome, 1992 b 	The collision model describes collision of microplates during the Late Precambrian resulting in the two different branches of the CFB. The model suggests that the syntaxis formed as a result of the rotation of these microplates. Trouw & de Wit (1999) stated that the model needs more evidence to be confirmed. They suggested a model where deformation can be attributed to compression in a back-arc setting of an Andean-type magmatic arc with a dextral strike slip component.
Transpression model (Dextral convergence model) Johnson, 2000 	This model proposes that the CFB forms the east-west trending inboard step in a larger northwest-trending dextral intracontinental transpression belt that includes the South American and Antarctic portions of the Gondwanide Orogeny. The dextral movement explains en-echelon folds and faults as well as suspected flower structures in the Karoo.
Thin skinned Jura-type fold belt (Lindeque *et al.*, 2012)	Lindeque *et al.*, (2011) proposed a collisional tectonic setting formed in response to continent-continent-, arc collision, or suturing south of the CFB, and far-field subduction to the south. The Karoo Basin developed in front of a thin-skinned Jura-type fold belt; negating the retro-arc or orogenic foreland basin as previously proposed.
Sinistral strike-slip model (Tankard *et al.*, 2012)	CFB as a sinistral strike-slip orogen linked to oblique reactivation of the southern Namaqua suture. Thick-skinned interpretation is based on the occurrence en-echelon faults and folds, flower structures, uplift along a restraining the bend on the Worcester fault, and the way in which translation is accommodated. ''Strain was partitioned between the transpressional Worcester–Cango fault system and the northward-vergent thrust-fold belt.''
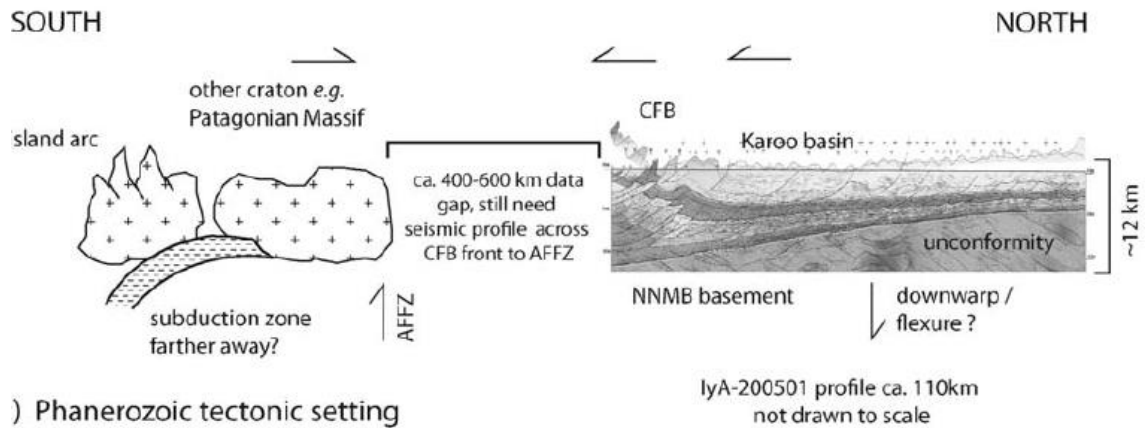
Figure 2.7: Schematic model depicting the proposed Phanerozoic tectonic setting of the Cape- and Karoo Basins and CFB. A collisional tectonic setting formed in response to continent-continent-, arc collision, or suturing south of the CFB, and far-field subduction to the south. A crustal block farther to the south (e.g. Patagonia), now embedded in South America is shown (Lindeque, et al., 2011).

2.4.2 Deformation styles

The CFB is divided into two branches separated by the Cape syntaxis (Figure 2.8). The western branch is characterised by open upright megafolds, monoclines and normal faults striking NW-SE to roughly N-S. The southern branch is characterised by tighter northward verging asymmetric folds (often overfolding) striking roughly east-west. Fold intensity decreases northward (De Villiers, 1944, Shone & Booth, 2005, Söhnge, 1983) into the Karoo Basin. The southern branch extends from the Cape syntaxis to just west of the Fish River mouth (De Villiers, 1944, Johnston, 2000) (Figure 2.8). The following section deals with deformation styles of the southern branch of the Cape Fold Belt. The variation in the style of deformation of folds, faults, cleavage, thrusts and normal faults are discussed as it is documented regionally and locally by previous authors. The syntaxis is characterised by flexural slip interference between folds of the two major branches.
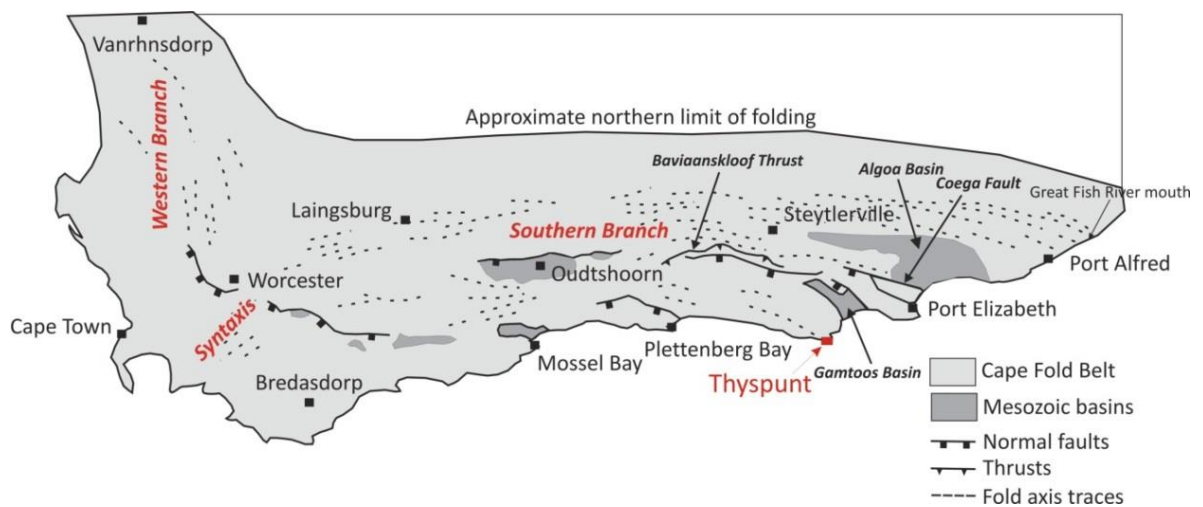
Figure 2.8: The CFB extent. Map shows major faults, fold axial traces and Mesozoic basins (Newton et al., 2006)

2.4.2.1 Folds

In the southern branch of the CFB fold styles are very diverse. Documented fold styles include open folds, tight folds, recumbent folds, box folds, chevron folds and monoclines. Folds plunge gently eastward or westward at shallow angles with fold axes generally dipping steeply south. In the Eastern Cape an area known as the Port Elizabeth antitaxis shows folds that gently plunge to the ESE (Figure 2.9) (Mielke & de Wit, 2009). Northward dipping axial planes are rare and normally associated with conjugate fold structures (e.g. near Touws River) or monoclines in the Karoo. Fold tightness and shortening intensity is greater north of major anticlinoria which are often transected by axial-plane parallel reverse faults or out-of-the-forelimb thrusts (Booth, 2002; Dingle *et al.*, 1983). The southern branch displays first order north verging recumbent folds and abundant more intense second order folds (Hälbich, 1992; de Beer, 1995). These folds appear to be a result of disharmonic folding and decoupling especially within the Nardouw Subgroup, which resulted in superimposed second order recumbent folds on north verging normal limbs of large anticlinoria. Small northward bedding inversions are common in the southern branch of the fold belt (Gresse *et al.*, 1992). A consistent relationship between the wave length of folds, lithological competency and bed thickness is well established in the CFB. Competent formations such as the Peninsula Formation form large megafolds with wavelength of several kilometres and anticlinoria can be spaced more than 20 km apart. Lithologically incompetent layers in the Bokkeveld Group form more numerous folds with smaller wavelengths of on average 1 km (De Beer, 1989, 1990, 1995, Newton *et al.*, 2006, Tankard *et al.*, 2012).
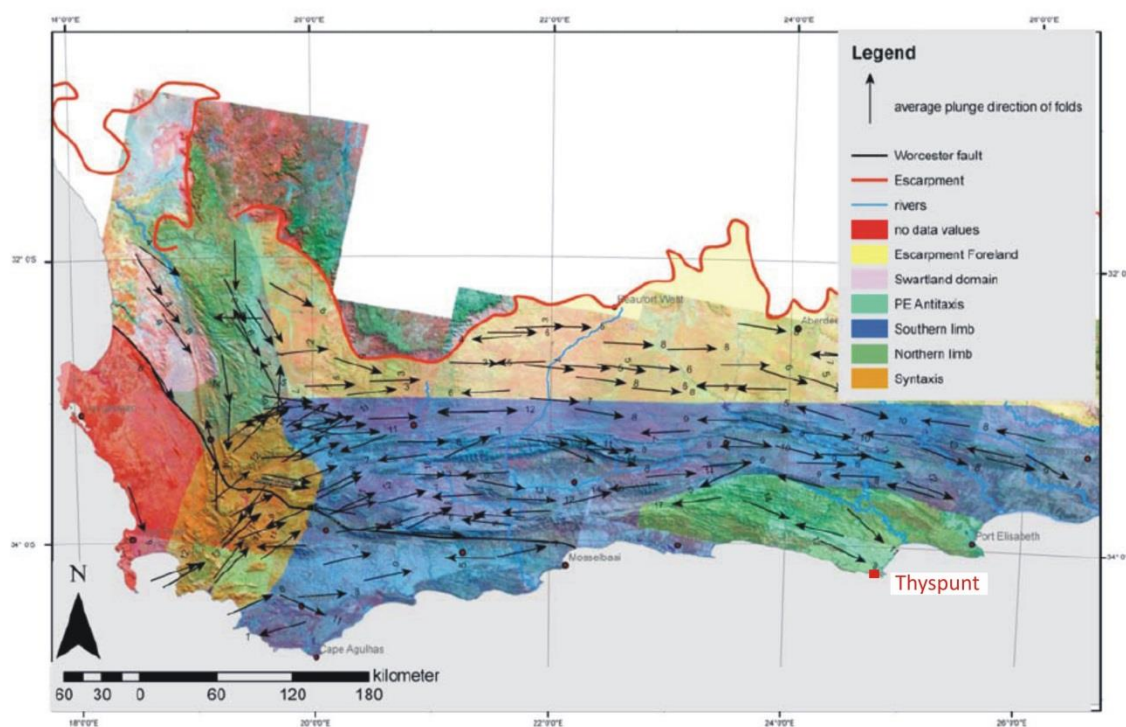
Figure 2.9: Structural domains in the CFB. Black arrows depict the general plunge direction of large scale folds (Mielke & de Wit, 2009).

2.4.2.2 Cleavage

A well-developed slaty axial-plane cleavage occurs in peletic rocks throughout the southern branch of the Cape Fold Belt. Cleavage planes dip steeply south in accordance with north-verging folds. Closely spaced axial plane cleavage is especially pervasive in the Bokkeveld Group, while being less prevalent in the Table Mountain and Witteberg Groups where cleavage tends to refract upon entering quartzitic horizons (Shone & Booth, 1993). Fracture cleavage dominates in arenaceous lithological units like the Peninsula Formation and the Nardouw Subgroup (De Beer, 2000).

2.4.2.3 Thrusts

Thrusting is a major feature in the southern branch of the CFB. Thrusting occurs on a mesoscale and megascale (Booth, 2002, Booth *et al.*, 2004, Booth & Shone, 1992, Booth & Shone, 1999). Thrusts developed as breakthrough structures on steep northward dipping limbs of asymmetrical anticlines and are gently folded. This would suggest a contemporaneous relationship between thrusting and folding. The sequential relationship between thrusting and folding in the Eastern Cape is not always clear and may vary from place to place (Booth, 1996; Booth & Shone, 1992).

In the Eastern Cape, thrusting takes place along bedding, cross-bedding foresets, cleavage planes and fold limbs. Thrust planes dip southward with a northward thrust propagation. Thrust displacement of up to 15 km is documented for the Baviaanskloof thrust (Booth *et al.*, 2004) (Figure 2.8). Along the southern most portion of the CFB thrusts are more frequently closely spaced and displacement is more difficult to ascertain. Thrusts generally display ramp and flat geometries. Ramps are identified by their steep inclination in relation to the relatively gently dipping flat thrust planes (Newton *et al.*, 2006). Booth, (1996, 1998) documented backthrusts and associated pop-up structures in the Witteberg Group where quartzitic rocks associated with these structures are usually highly fractured. In the eastern sector duplexing is seen as the main deformation mechanism in quartz arenites of the CFB with the resultant thrust stacking hampering stratigraphic studies and determination of true bedding thicknesses (Booth *et al.*, 2004). Goedhart *et al.*, (2008) recognized localised NW-SE striking thrust faults generally forming parallel to bedding west of Oyster Bay.

2.4.2.4 Normal faults

In southern branch of the CFB, normal faults are E-W to NE-SW striking with downthrown blocks to the south. Displacement in the order of thousands of metres occurs along major faults including the Coega, Gamtoos and Worcester faults (Figure 2.8). Extensive normal faults result in the development of complex graben and half graben basins (Algoa Basin and Gamtoos Basin) in which Mesozoic strata are preserved (Figure 2.8) (Shone, 1967; Shone *et al.*, 1990). In the region between Kareedouw and Gamtoos mouth, Norman *et al.*, (1987b); Raubenheimer *et al.*, (1988a) and Goedhart *et al.*, (2008) recognized NNE–SSW to NE-SW trending, steeply SE-dipping normal faults and described these faults as '*high-angle cross-faults*'. NW-SE trending faults described as '*strike faults*' are steeply dipping to near-vertical and frequently have a down-to-the-south sense of displacement.

2.4.2.5 Joints

The formation of joints is interpreted as the result of Permo-Triassic deformation and in places Mesozoic extension associated with the breakup of Gondwana. As joint sets formed in response to local compressive stresses during folding of TMG strata that took place during the Cape Orogeny, some joints developed along incipient conjugate shears, some of which may have experienced localized incremental slip at the time (Goedhart *et al.*, 2008).

Jointing systems within the study area and greater surroundings are described by various authors (Norman *et al.*, 1986; Norman *et al.*, 1987 a & b; Raubenheimer *et al.*, 1988 a; De Beer, 2000; Goedhart & Cole, 2007; Goedhart *et al.*, 2008) to varying degrees of detail. Orientations of joint systems vary among authors, owing to the location, size of areas investigated and possibly the volume of joint readings measured. In the area between Kareedouw and Gamtoos mouth, which includes the southern portion of the study area to the south, the dominant joint set direction, J1, is NE-SW perpendicular to bedding trend. J2, the subordinate joint set strikes ENE-WSW. Together, joint sets J1 and J2 form conjugate set X. Joint set J3 has a NW-SE trend, parallel to bedding direction. Joint set J4 strikes WNW and ESE. Joint sets J3 and J4 produce conjugate set Y (Goedhart *et al.*, 2008). Joint and fracture openings of Table Mountain strata are generally empty or filled with either rusty brown iron precipitate or milky white quartz (De Beer, 2000).

2.4.3 Mesozoic extension (Gondwana break-up)

The mid to late Mesozoic extension (180-170 Ma) resulted in the break-up of Gondwana and the opening of the southern oceans (Reeves, 1999). During the Early Jurassic, this event was accompanied by the outpouring of continental Karoo lavas and abundant dykes and sill complexes (178–183 Ma) (Duncan *et al*. 1997; Jones *et al*. 2001; Jourdan *et al*. 2007) in South Africa, Botswana and in Zimbabwe.

Buoyancy associated with mantle upwelling during the Mesozoic extension is regarded as a possible factor in the initiation of rifting and the break-up of Gondwana (Reeves, 1999; Conrad & Gurnis, 2003; Brown *et al*., 2014). The separation of east and west Gondwana and separation of South America and the Falkland Plateau from Southern Africa was facilitated by a process involving continental rifting followed by continental drift (Fouché *et al*., 1992, Watkeys, 2006). Tankard *et al*., (2009) suggested that the graben and half-graben Mesozoic Basins (e.g. Algoa Basin, Gamtoos Basins) along the southeastern margin of South Africa (Broad *et al*., 2012) formed during this time as a result of strike-slip extensional forces initiating dextral movement along the the Agulhas-Falkland Fracture Zone (Figure 2.3) resulting in the reactivation of pre-Cape and Cape faults in the eastern sector of the CFB (Booth *et al*., 2004, Booth, 1996) Reactivated faults show a southerly downthrow (Bate & Malan, 1992; Broad *et al*., 2006, Shone, 2006) (Figure 2.8).

2.5 Sequences post-dating CFB deformation and Mesozoic extension

Onshore Cenozoic deposits (< 66 Ma) of littoral marine, beach, nearshore estuarine, fluvial and aeolian origin, occur intermittently along coastal plains of southern Africa (Figure 2.10). These deposits reflect a passive coastal margin subjected to global eustatic marine transgressions and regressions superimposed on uplift and seaward tilting of the subcontinent during the Cenozoic Era (Roberts *et al.*, 2006). The South African Committee for Stratigraphy (SACS) accepted a lithostratigraphic framework that geographically partitions coastal Cenozoic deposits into five distinct groups: the east coast region (Maputaland Group); the southeastern coast (Algoa Group); the southern coast (Bredasdorp Group); the southwestern coast (Sandveld Group); and the west coast (West Coast Group) (Roberts *et al.*, 2006) (Figure 2.10).

The Algoa Group deposits are restricted to the Eastern Cape; occurring east of Oubosstand (35 km west of Cape St. Francis) to East London and comprises of the Bathurst, Alexandria, Nanaga, Salnova, Nahoon, and Schelm Hoek Formations (SACS, 1980) and that unconformably overlay strata of the Cape Supergroup. The Bathurst Formation does not occur within the study area. Isolated deposits equivalent to those of the Algoa Group, have recently been identified (Reddering *et al.*, 2006) along the Wild Coast, between East London and Port St. Johns, with a new lithostratigraphic terminology (Mount Thesiger Formation) proposed by Reddering *et al.*, (2006), but not yet accepted by SACS, for marine conglomerates in the vicinity of Port St. Johns. If these equivalents are truly part of the Algoa Group it will lead to an extension of the Cenozoic Algoa Group farther along the Eastern Cape coastline. Luminescence ages for dune deposits in the Oyster Bay and Thys Bay dunefields range from Holocene to middle Pleistocene (>490 ka) (Illenberger *et al.*, 2005). Optically stimulated luminescence (OSL) ages form samples of core (Hanson *et al.*, 2012) collected within the Oyster Bay-Cape St. Francis dunefield ranged in age from approximately 25 ka to >130 ka (Forman, 2012).
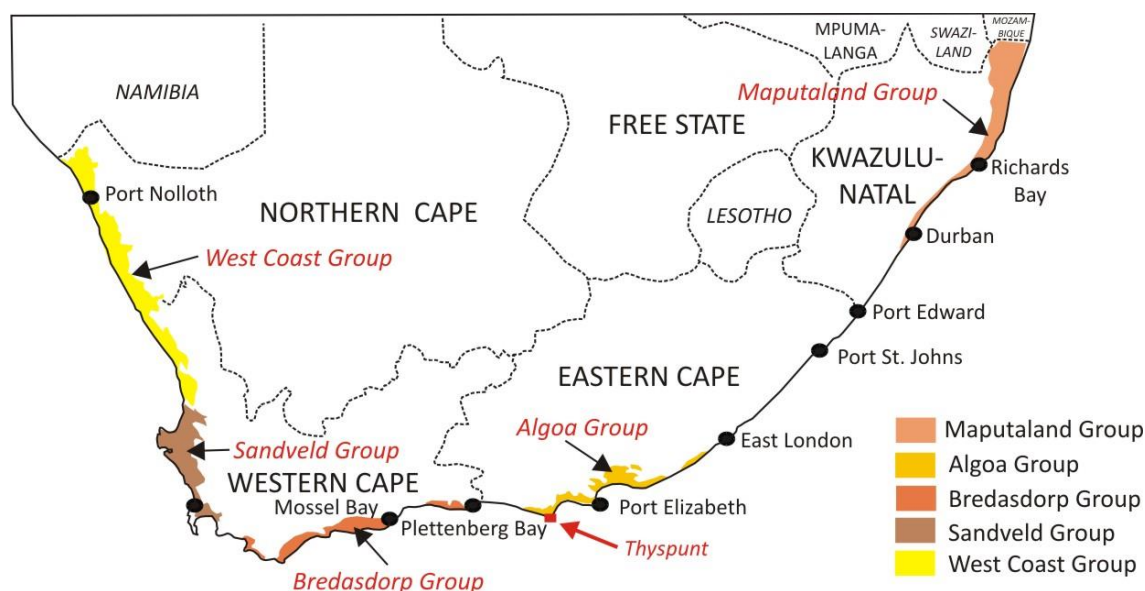
Figure 2.10: The regional distribution of Cenozoic coastal deposits along the coastal margins of South Africa. Note the location of Thyspunt associated with the area of occurrence for the Algoa Group (Roberts et al., 2006).

2.5.1 Lithostratigraphy of the Algoa Group

Lithostratigraphy of the Cenozoic Algoa Group after (SACS, 1980; Roberts *et al*., 2006) is presented in Figure 2.11.
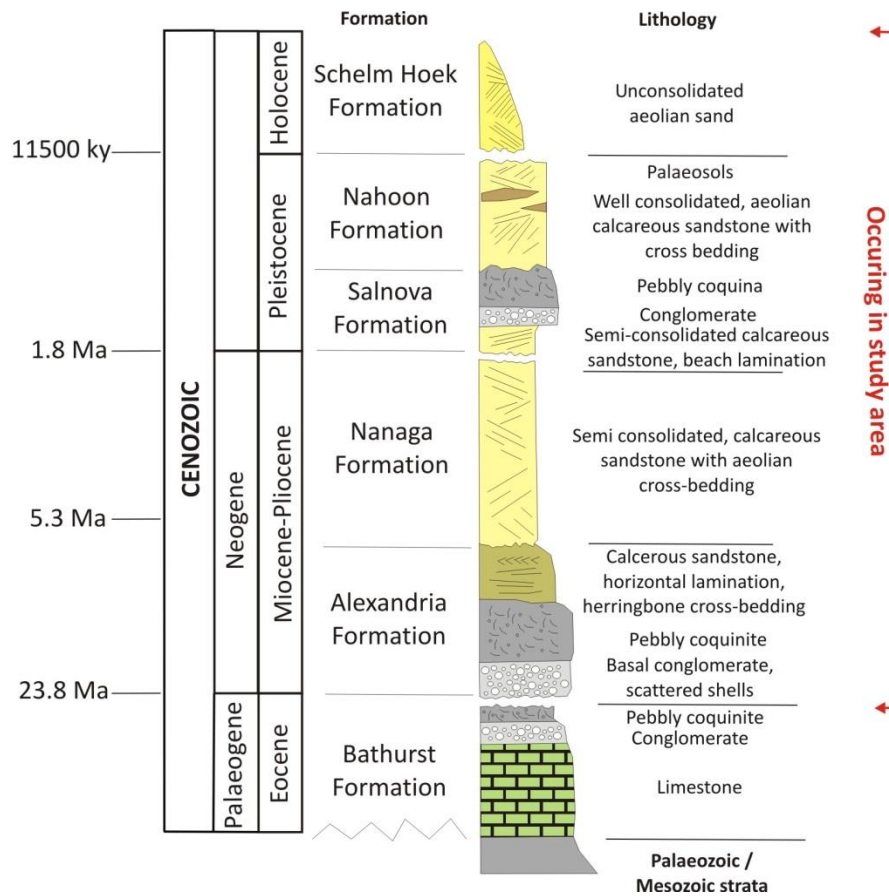
Figure 2.11: Summary diagram of Cenozoic deposits within the Eastern Cape (after Partridge & Maud, 2008; Roberts et al., 2006).

2.5.1.1 Alexandria Formation

The Miocene to Early Pleistocene (7-5 Ma) (Maud & Botha 2000, Roberts *et al*. 2006; Hanson *et al.,* 2012) Alexandria Formation overlie bedrock platforms with elevations of between ≥18–30 m asl (Le Roux, 1987). Sediments rest unconformably on a narrow, planar, seaward sloping marine platform which is cut into older Palaeozoic successions (Roberts, 2006; Goedhart *et al*., 2008; Hanson *et al*., 2012). The Alexandria Formation ranges from 3 to 13 m in thickness, with an average of 9 to 10 m (Le Roux 1987a, Goedhart & Hattingh, 1997). Maud & Botha (2000) measured a maximum thickness of 18 m between the Swartkops and Sundays Rivers (~100 km east of Thyspunt).

The Alexandria Formation consists of three alternating paralic lithologies. A conglomerate layer (often referred to as a basal gravel, clast lag or stone line) forms the lowermost unit of the formation. The conglomerate unit is 1m to 3.5 m thick, thin to medium bedded, horizontal to subhorizontal in attitude. The conglomerate contains imbricated sandstone clasts of TMG, Uitenhage Group sandstone, (intrabasinal derivation), ydianite, tillite, chert, dolomite, silcrete, shale of the Bokkeveld Group, extrabasinal basalt of the Drakensberg Group, and also quartz and intraformational coquinite (Roberts *et*

al., 2006). The clasts range in size from pebbles to cobbles and are contained within a fine- to coarse-grained sandy matrix (Le Roux, 1987a). A tabular, thin to medium bedded, generally pebbly coquinite 1 to <4 m in thickness overlies the basal conglomerate. Isolated horizontal lamination and cross-bedding structures are present. Pebbly coquinite is comprised predominantly of 5 to 15 mm sized recrystallised shell remains (70%) (Smuts, 1987). The upper unit of the Alexandria Formation is a tabular to lenticular pale- to yellow grey glauconitic sandstone (<3.5 m thick) cemented by calcite and comprised of well-rounded, moderately- to well sorted, fine to coarse-grained particles. The units are 3 - 30 cm thick and show internal structures such as horizontal lamination planar cross-bedding and trough cross-bedding (Le Roux, 1987a).

The Alexandria Formation is not laterally persistent and spatially shows great thickness variation (Le Roux, 1989). The formation is generally overlain by coastal dune deposits of the Nanaga- and Schelm Hoek Formations (Le Roux, 1987a; Le Roux, 1989). Depositional environments range from shore face, foreshore, lagoonal and/ or estuarine (Le Roux, 1987a; Le Roux, 1989). Sedimentary structures such as horizontal lamination and low angle bedding, supported by biogenic structures and fossil assemblages within the Alexandria Formation point to a range of depositional environments from shoreface to foreshore to lagoonal and/ or estuarine (Le Roux, 1987a; Le Roux, 1989, Roberts *et al*., 2006). Deposition of the Alexandria Formation occurred during regressive periods where shelly, sand dominated sediments were deposited along the shore face on the coastal platform and during periods of stable seas where gravel dominated sediments were deposited along linear slope breaks along the beach ridge shoreline (Le Roux, 1987a & b). The depositional environment is said to have consisted of a rocky shore face with discontinuous pockets of subordinate sandy beaches. These deposits have been correlated with similar deposits in the Western Cape and Kwa-Zulu Natal (Maud & Botha, 2000).

2.5.1.2 Nanaga Formation

The Nanaga Formation is regarded as a multiple-generation ENE striking palaeodune deposit that forms smooth rounded hills with undulating ridges along the coastal margins of the east coast (Norman *et al*., 1987 a & b; Le Roux, 1989; Le Roux 2000). The formation accumulated in coastal dunefields along Late Miocene to Pleistocene's receding shorelines, and as a result, formation deposits become gradually younger coastward (Le Roux, 1992; Maud & Botha, 2000; Roberts *et al*., 2006). The formation is composed of unconsolidated to semiconsolidated medium-grained, cross-bedded, calcareous dune sand and calcretes. The formation is thickly bedded and has a pale grey to greyish-yellow colour. Occasional thin, dense, and dark brown organic rich silty pedogenic horizons generally <2 m occur throughout the formation (Le Roux, 1992). Le Roux (1992) measured a maximum thickness of ≤ 250 m in the Port Elizabeth area (88 km east of Thyspunt). The formation is generally overlain by the younger active mobile dunes of the Schelm Hoek Formation or represents the uppermost Cenozoic deposits in the area. In addition, the Nanaga Formation may sporadically be overlain by the Nahoon Formation, a well consolidated palaeodune rock. The presence of numerous shell fragments, gives the deposit a calcareous nature (Roberts *et al*., 2006).

2.5.1.3 Salnova Formation

The Late Pleistocene sediments of the Salnova Formation include fine to coarse-grained calcareous sandstone, shelly limestone and coquinite; or unconsolidated fine to coarse-grained calcareous sand, gravel, coquina and conglomerate deposited on wave cut platforms below approximately 18 m amsl across the Cape Supergroup and Karoo Supergroup litho-units (Le Roux, 1991). The thin (1.6 -5.6 m), discontinuous formation is thought to represent highstands of sea level during a series of several Mid to Late Pleistocene transgressions and was deposited in an intertidal zone ranging from the sandy beach environment to a rocky shore environment (Le Roux, 1989; Le Roux, 1991; Hanson *et al*., 2012).

The pale yellow-grey to pale yellow-orange coloured gravel and conglomerate (basal gravel) is comprised of imbricated discoidal to roller-shaped clasts of TMG quartzite, Uitenhage Group sandstone and an intraformational, coarse-grained calcareous sandstone matrix. The units are between 1 and 2 metres thick and contain horizontal beds of between 3 and 30 cm thick. It consists of tabular to lenticular units containing inclined and wavy bedding, planar and tough cross-bedding and weak horizontal lamination. The very pale grey or yellowish coquinite is arranged in tabular units and is composed of moderately to well-sorted, subangular to subrounded shells and shell fragments and pebbles (occasional). These particles range in size from 5 to 60 mm. The coquinite is between 40 and 60 centimetres thick and is usually structureless with indistinct 1 to 10 cm thick horizontal lamination.

The formation is overlain by aeolianite of the Nahoon Formation, unconsolidated windblown sand of the Schelm Hoek Formation or by sand and soil horizons (Le Roux, 1991; 1989). The Salnova Formation is lithologically similar but less cemented or consolidated than the older Alexandria Formation and consists of fossiliferous bioclastic marine sediments deposited in beach and estuarine environments.

2.5.1.4 Nahoon Formation

The Middle to Late Pleistocene Nahoon Formation is a consolidated palaeodune rock (often referred to as beachrock) generally less than 15 m thick and composed of calcareous sandstone, interbedded palaeosols and occasional thin calcrete layers (Le Roux, 1989). The formation is not laterally persistent. The humic palaeosol component of the formation is semi-consolidated and varies in colour from greyish-yellow to pale olive grey. The calcareous component varies in colour from grey-yellow to yellow-brown and is composed of fine to medium-grained structureless or cross bedded dune sand. Ripple marks, disturbed bedding and slumping may be present locally (Le Roux, 1989). The formation is generally underlain by the Salnova or Nanaga Formation.

A glacio-eustatic fall in sea level resulted in the exposure of large tracts of sandy seafloor that were later reworked by prevailing south westerly and south easterly winds that deposited calcareous sand onshore. These coastal dunefields were deposited disconformably on the marine / beach deposit of the Salnova Formation and unconformably on pre-Cenozoic strata deposits later underwent cementation by calcareous recrystallization (Le Roux, 1989; Roberts, 2006).

2.5.1.5 Schelm Hoek Formation

The Holocene (11.7 kya - present) deposits of the Schelm Hoek Formation are composed of unconsolidated calcareous to semi-consolidated fine-grained and well sorted aeolian sands (Illenberger, 1992). The unconsolidated sand is on average 30 m thick and forms both vegetated and unvegetated hummock, parabolic and longitudinal dune ridges. Intercalated calcified lenses, thin palaeosols, organic matter and root casts are also present. Palaeosols make up 3% of the formation and consist mainly of sand and a small amount of silt and organic matter (Illenberger, 1992). The unconsolidated, well-sorted and well-rounded sand particles comprise of 65% quartz, 35% shelly fragments and traces of heavy minerals (predominantly ilmenite) in places. The pale orange coloured sand contains internal structures such as wind ripples and high angled planar aeolian cross-bedding. The latter is arranged in lenticular sets between 1 and 50 m thick (Le Roux, 1989; Illenberger, 1992).

The formation disconformably overlies the Algoa Group formations of the Nahoon or Salnova (Illenberger & Rust, 1988) and Palaeozoic bedrock of the Table Mountain and Bokkeveld Group (Illenberger, 1992).

Sea level during the Holocene interglacial period reached a maximum transgression height of approximately 3 m above present sea level, since the start of the transgression sand has been blown onshore in several pulses, resulting in the deposition of the Schelm Hoek Formation along the southestern coast.

3. Previous studies at Thyspunt

Previous studies predominantly aimed to evaluate the geological suitability of various sites along the Eastern Cape for the potential construction of a new NPP. Siting studies along the Eastern Cape coast were initiated in 1980's by the Atomic Energy Corporation (AEC), under the direction of Eskom (Huskins, 1981; Young *et al.*, 1981; Norman, 1985) and included investigation of the Thyspunt area (Muller *et al.*, 1986; Anderson *et al.*, 1986 a & b; Henop, 1987; Norman *et al.*, 1987a & b; Raubenheimer *et al.*, 1988a; Raubenheimer *et al.*, 1988b). Since then, more focussed studies directed towards Thyspunt as a preferred site for *Nuclear-1*, involved greater collation, collection and review of geological data within the study area and greater surroundings (De Beer, 2000; De Beer 2001; De Beer, 2005). More site specific geological and geophysical investigations followed on from 2007 (Goedhart & Cole, 2007; Cole & Naude, 2007; Raath & Cole, 2007; Goedhart *et al.*, 2008; Stettler *et al.*, 2008; Eskom, 2009; Eskom, 2010a; Eskom, 2010b; Hanson *et al.*, 2012, Engelsman & Constable, 2012). The results of previously studies that bear influence on the study aims (§ 1.3) of this thesis and not reviewed in § 2 (Geological setting) are detailed below in § 3.1, § 3.2, § 3.3 & § 3.4.

3.1 Lithostratigraphic bedrock contacts

Determining the bedrock contacts between TMG formations underlying the Cenozoic cover was initially attempted by Muller *et al.* (1986) and Anderson *et al.*, (1986b) who based interpretations solely on results obtained from a medium-sensitivity aeromagnetic survey (See § 3.4; Figure 3.3 for more information). More recently the location of contacts zones beneath Cenozoic deposits where determined by Eskom (2009). Subsurface transition zones between the Skurweberg and Goudini Formation and between the Goudini and Cedarberg Formation were inferred by extrapolation coastal exposures along strike to coastal exposures (which did not include more recently updated mapping by Goedhart *et al.*, (2008), while conforming to bedrock stratigraphy logged in borehole sets (Eskom, 2010 a, Eskom 2010 b). The subsurface contact zones beneath Cenozoic cover were only determined for the Thyspunt area (Figure 2.16). Results from ground geophysics (Stettler *et al.*, 2008) were not included in the determination of transition zones. A revision of Palaeozoic contact locations beneath overburden that includes results from afore mentioned geophysical surveys and omitted borings (Raubenheimer *et al.*, 1988a; Raubenheimer *et al.*, 1988b; Rosewarne & Lomberg, 1989; Maclear, 2002, Maclear, 2005, Maclear, 2006; Hanson *et al.*, 2012, Engelsman & Constable, 2012) is required to more accurately define contacts not only at Thyspunt, but across the entire study area.

Contacts between lithological units within the lower Skurweberg Formation were determined by Goedhart *et al.,* (2008) who interpreted the first major influx of sand, a 13.5 m thick, massive quartzitic unit as the basal unit of the Skurweberg Formation, occurring towards the north of Thyspunt (Figure 3.1 b). Underlying this basal unit are two fine-grained, silty argillaceous quartzite and shale units separated by quartzitic units. Both argillaceous units occur along the trend of two small NW-SE trending inlets.
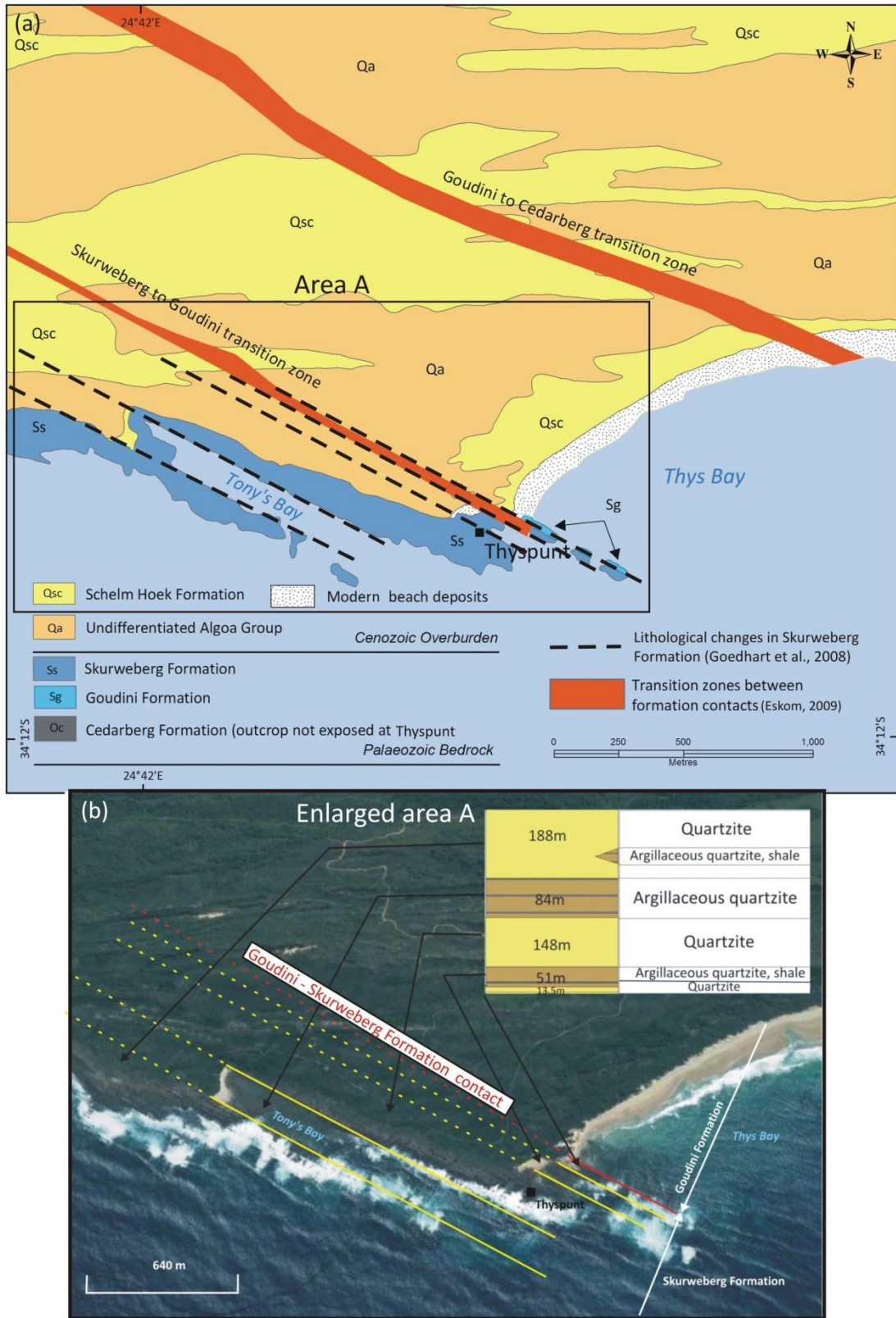
Figure 3.1: (a) The Skurweberg-Goudini formation and the Goudini-Cedarberg transition zones beneath Cenozoic cover deposits at Thyspunt (after Eskom, 2009). (b) Lithological contacts of the Skurweberg Formation at Thyspunt (after Goedhart et al., 2008).

3.2 Thickness of Cenozoic overburden

Construction of the proposed NPP will commence on bedrock, requiring major excavation of cover deposits. The removal of these deposits is viewed as a risk to site safety during construction. Excavations will need to cut back overburden to tolerable angles (<20°) to ensure safe conditions during construction. The thickness of predominantly semi-consolidated and non-cohesive Cenozoic overburden are categorised according to three sensitivity or risk classes by Eskom (2009). The thickness range that defines each risk/sensitivity class is outlined below:

• Low sensitivity areas exhibit <10 m thick vertical overburden cover. These areas pose a low risk to site safety during excavation activities

• Medium sensitivity areas exhibit cover deposits 10 - 20 m in thickness and pose a greater risk to site safety than low sensitivity areas.

• High sensitivity areas pose the greatest risk to site safety during excavation. These areas exhibit cover deposits exceeding 20 m thicknesses.

At Thyspunt, Eskom (2009) categorised overburden thickness according to these risk classes (Figure 3.2). No indications are given as to how the thicknesses of overburden were determined. A crude review of thickness recorded in borings (Raubenheimer *et al*., 1988 a & b), that would have been available to Eskom (2009), indicates that these thickness divisions do not accurately portray the thickness of overburden sediments at Thyspunt. Consequently an updated investigation into the overburden thicknesses at Thyspunt and across the study area is required. Such a review should include borehole data (Raubenheimer *et al*., 1988a; Raubenheimer *et al*., 1988b; Rosewarne & Lomberg, 1989; Maclear, 2002, Maclear, 2005, Maclear, 2006; Eskom, 2010 a, Eskom, 2010 b; Hanson *et al*., 2012; Engelsman & Constable 2012) and geophysical data (Stettler *et al*., 2008).
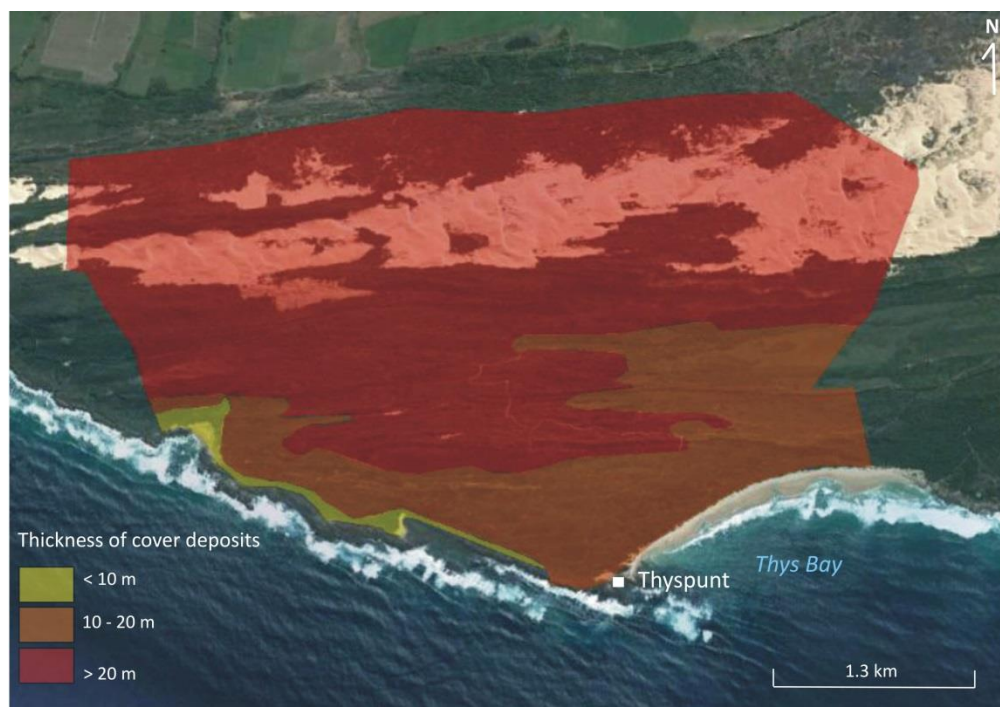
Figure 3.2: Cenozoic overburden thickness categories at Thyspunt (after Eskom, 2009).

3.3 Rock strengths of the TMG

Results from laboratory and field point load tests conducted to determine rock strengths of the Peninsula, Cedarberg, Goudini and Skurweberg Formations at Thyspunt (Eskom, 2009; Engelsman & Constable, 2012) are given in Table 3.1. Minimum, maximum and mean uniaxial compressive strengths (UCS) for each formation are detailed.

Results show that rocks of the Cedarberg Formation exhibit the lowest rock strength. Rocks of the Peninsula Formation show the greatest rock strength. Comparatively rocks of the Skurweberg Formation are stronger than rocks of the Goudini Formation (Table 3.1).

Table 3.1: Minimum, maximum and mean rocks strength values (MPa) derived from laboratory and field load tests on Peninsula, Cedarberg, Goudini and Skurweberg Formation strata at Thyspunt (Eskom, 2009; Engelsman & Constable, 2012).

	Eskom, 2009		Engelsman & Constable, 2012	Rock strength description (MPa min-max values)
	Point load tests	Laboratory tests		
Peninsula Formation				
Mean			157	
Minimum			75.9	STRONG to EXTREMELY STRONG
Maximum			279	
Cedarberg Formation				
Mean			4	
Minimum			1.49	VERY WEAK to WEAK
Maximum			7.61	
Goudini Formation				
Mean	79	35	26	
Minimum		1.7	1.35	VERY WEAK to VERY STRONG
Maximum	350	196	196	
Skurweberg Formation				
Mean	160	120	117	
Minimum	15	3.8	3.82	VERY WEAK to EXTREMELY STRONG
Maximum	427	254	254	

3.4 Geophysics

Muller *et al*., (1986) conducted a broad medium sensitivity aeromagnetic survey with a 300 m flight line spacing, 1200 m spaced tie line and a 100 m mean terrace clearance within the study area and immediate surroundings. From survey results, faults were interpreted in areas where anomalies associated with specific formations appeared displaced (Anderson *et al.*, 1986 b; Van Wyk, 1987). Collectively these faults became known as the '*AEC faults'* (Figure 3.3).
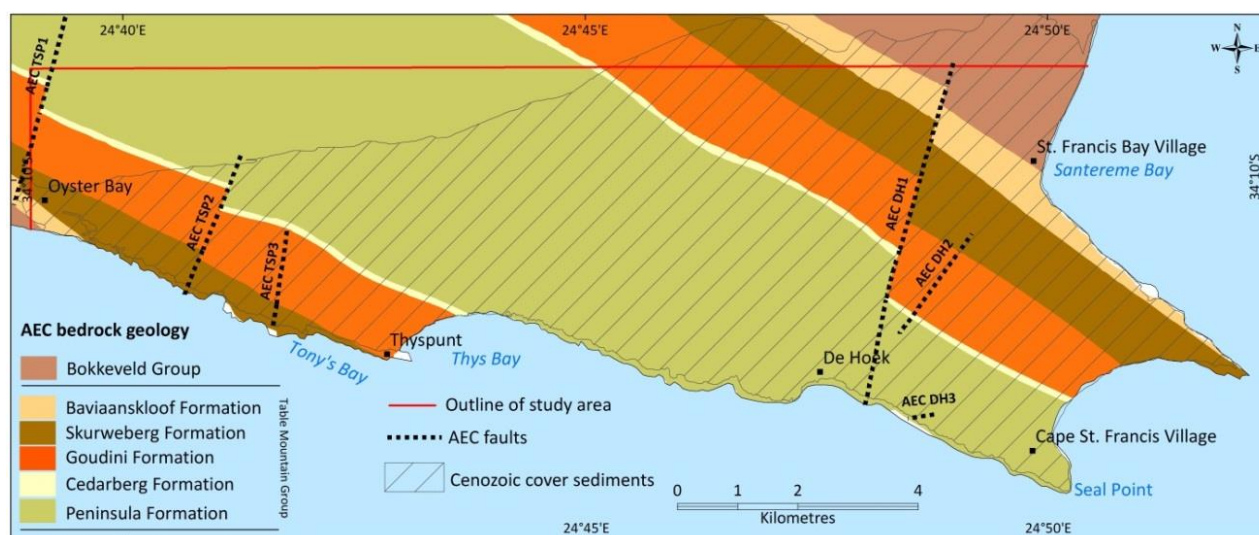
Figure 3.3: Geological map of study area based on aeromagnetics (after Muller et al., 1986; Anderson et al., 1986 b; Van Wyk, 1987).

In the Thyspunt region, subsequent investigations into the possible presence of additional onland faults, other than the AEC faults, were undertaken by Cole and Naude (2007) with the aid of two high resolution aeromagnetic surveys (Figure 3.4 & Figure 3.5). Data was collected at two different resolutions. A 200 m wide flight line spacing was initially conducted with a tie line spacing of 2000 m and a 80 m flying height above terrain. This initial survey (near regional survey) extended 25 km, east, west and north of Thyspunt (Figure 3.4). A second more detailed magnetic survey (site vicinity survey) was conducted thereafter with a 50 m flight line spacing and 1000 m tie line spacing at a 80 m flight height above terrain. This secondary magnetic survey extended 8 km east, west and north of Thyspunt. From survey results authors identified linear features within the data that were categorised as either magnetic lineaments; lineaments, inferred faults and probable faults (Figure 3.4 & Figure 3.5).

The existence of inferred AEC faults and lineaments identified by Cole and Naude (2007) were investigated by Goedhart *et al* (2008). Validity was investigated based on a review of findings by previous authors (Van Wyk, 1987; Norman *et al.*, 1987b; Raubenheimer *et al.*, 1988a, Cole, 2006; Cole & Naude, 2007; Goedhart & Cole, 2007; Raath & Cole, (2007) and field work. No substantial evidence was found that any of the 253 lineaments identified by Cole & Naude, 2007) within the site vicinity (40 km radius around Thyspunt) could be related to faulting. The exception being one lineament denoted the *'SV1 lineament'.* In addition, Goedhart *et al.*, (2008) concluded that uncertainty as to the presence of certain AEC faults still remained, due to a lack of definitive data. Authors did not consider borehole data during the review process nor was an attempt made to correlate the AEC features to coastal exposures.
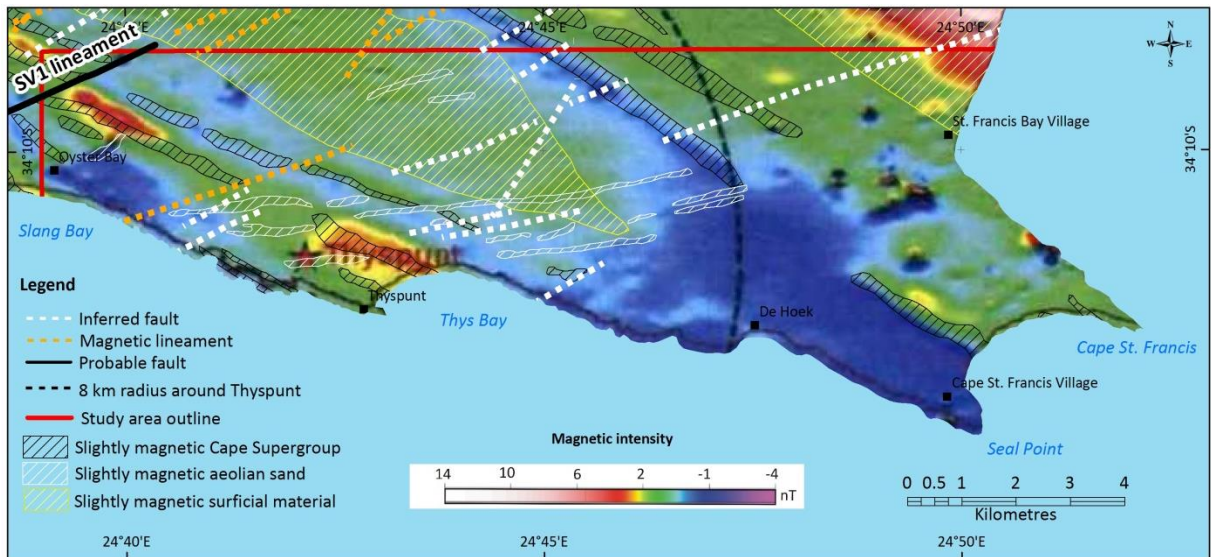
Figure 3.4: Map showing results from the near regional aeromagnetic survey as it relates to the study area. Lineament types interpreted from survey results are also indicated (after Cole & Naude, 2007). Note the SV1 lineament.
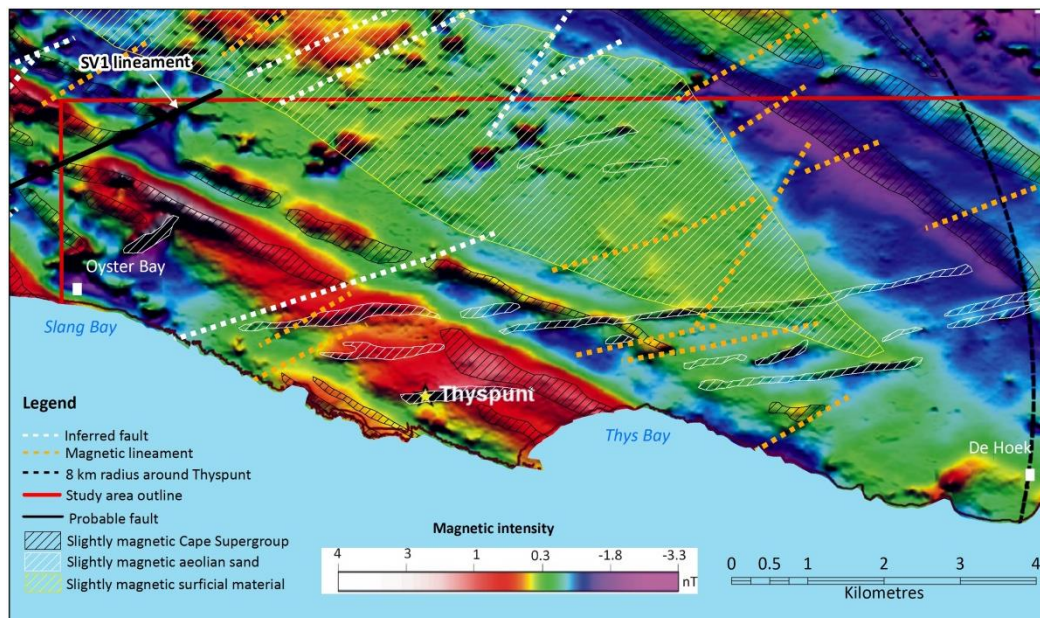
Figure 3.5: Map showing results of the site vicinity aeromagnetic survey. Lineament types interpreted from survey results are also indicated (after Cole & Naude, 2007).

A summary detailing the characteristics of AEC faults and the SV1 lineament are outlined below with reference to the possible onshore continuation of the offshore Cape St. Francis Fault:

Fault AEC TSP1 / SV1 lineament: The NNE-SSW trending AEC TSP1 fault is located 500 m west of Oyster Bay (Figure 3.3) and exhibits an interpreted ~250-500 m right-lateral displacement (Van Wyk, 1987; Norman *et al*., 1987b). The position of the fault was inferred from the discontinuation of a magnetic anomaly interpreted to be the Cedarberg Formation (Anderson *et al*., 1986 b). The validity of fault AEC TSP1 was substantiated by Cole (2006) and Cole and Naude (2007), who interpreted a similar magnetic feature in the results obtained from aeromagnetic surveys conducted in the area. They defined the magnetic feature as a 15.4 km NE-SW trending probable fault showing a 600 m right-lateral displacement of strata and termed it the SV1 lineament.

Subsequent investigation into the validity of the SV1 lineament was undertaken by (Raath & Cole, 2007; Cole & Naude, 2007). Two multi-electrode resistivity traverses A and B; and two magnetic and frequency domain electromagnetic (FDEM) traverses 7.1 and 7.2 were conducted. Surveys trend NW-SE, perpendicular to bedding and were conducted approximately 3.5 km NE of Oyster Bay (Figure 3.6).

Magnetic and FDEM results obtained along traverse 7.1 indicate that a conductive body with consistent magnetic intensity associated with the Cedarberg shale occurs between 240-560 m along the survey line. To the east this conductive body is bordered by an area of lower conductivity / more resistive signal, interpreted to be quartzites of the Peninsula Formation (Raath & Cole, 2007). Furthermore two geophysical anomalies occurring between 180 to 200 m and between 600 m to 630 m along both the magnetic and FDEM surveys were interpreted as either lithological changes or faults (Figure 3.6). The first anomaly coincides with the locality of the probably fault, lineament SV1 (Cole & Naude, 2007) but could also indicate a change in lithology from the Peninsula Formation to the Cedarberg Formation (Raath & Cole, 2007).

The peak in the magnetic intensity occurring within quartzites of the Peninsula Formation at 170 m along survey line 7.2 is interpreted as the location of the SV1 lineament. Results from multi-electrode resistivity traverse A indicate that a conductive body can be associated with the occurrence of the Cedarberg Formation between 190 – 300 m along the survey line (Cole & Naude, 2007).

A multi-electrode traverse B was conducted across the Goudini Formation. Interpretation of results obtained along traverse B did reveal a slightly higher conductivity in the region around the inferred position of the SV1 lineament between 170 - 230 m (Figure 3.6). Raath and Cole (2007) interpreted this zone of slightly higher conductivity as a possible fracture zone.

Raath and Cole (2007) concluded that the SV1 lineament exhibits a 150 m right-lateral displacement of the Cedarberg Formation along its southwestern extent. They could not confirm the validity of the SV1 lineament as it extends further to the northeast. Goedhart & Cole (2007) later suggested that field evidence did not support the assumption that the SV1 lineament is a fault along its entire 15 km length as suggested by Cole and Naude (2007). Towards the northeast the lineament coincides with an area of closely spaced jointing that adheres to the already-documented jointing pattern in the area where minimal movement has occurred along joint planes. The displacement along the southwestern end is attributed to a syn-folding Permo-Triassic compressional joint or fracture that was reactivated by dextral transtension during the Cretaceous (Goedhart & Cole, 2007).
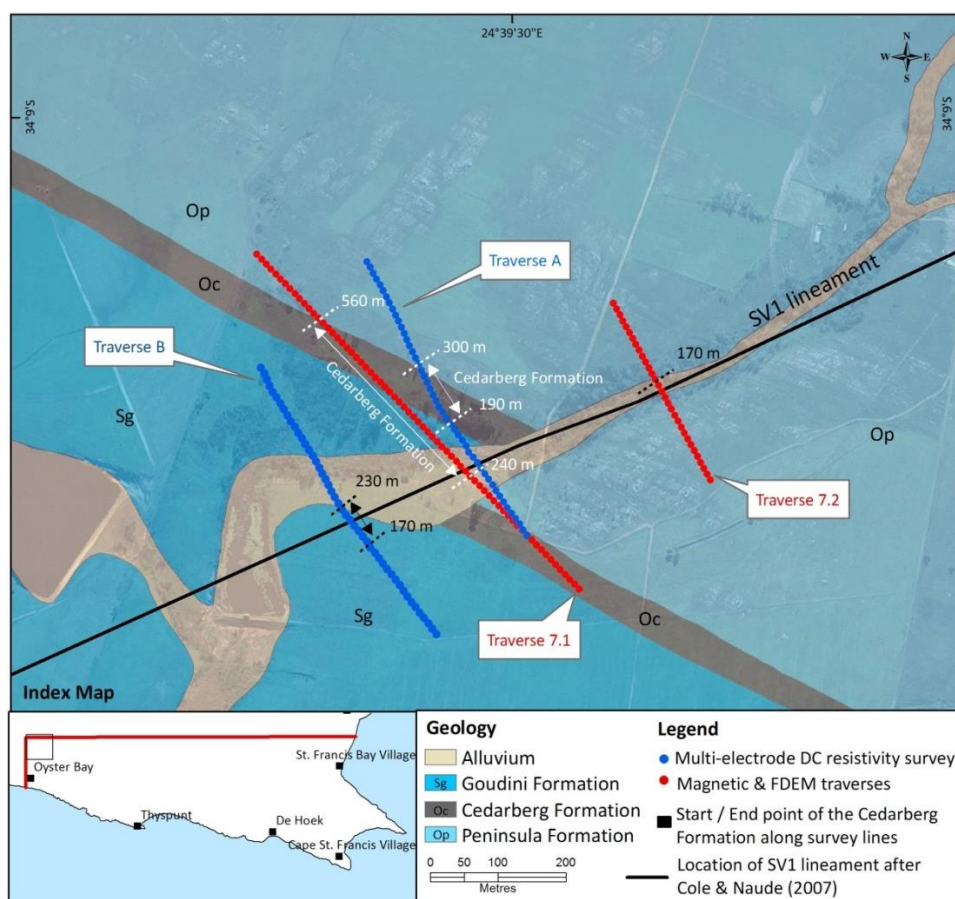
Figure 3.6: *Map showing the location of multi-electrode DC resistivity surveys Traverse A and B and magnetic and FDEM surveys 7.1 and 7.2 across the SV1 lineament (after Raath & Cole, 2007).*

Fault AEC TSP2: The NNE-SSW striking AEC TSP2 fault is located 4 km from Oyster Bay and is 3 km in length. AEC maps (Anderson *et al*., 1986 b; Van Wyk, 1987; Norman *et al*., 1987b) indicate a roughly 500 m right-lateral displacement of the Cedarberg- and Peninsula Formations along fault AEC TSP 2's northern extent and a roughly 100 m displacement of the Peninsula and Goudini Formations along its southern extent (Figure 3.3). The fault is indicated by AEC as extending through coastal exposures west of Tony's Bay.

High resolution aeromagnetics (Cole & Naude, 2007) did not identify a magnetic feature that corresponds to the trend or location of fault AEC TSP2. A 4 km long NE-SW trending lineament simply categorised as an inferred fault was however identified northwest of fault AEC TSP2 (Figure 3.4 & Figure 3.5). No correlation between these features were made.

Fault AEC TSP3: The ~2 km long NNE-SSW trending fault occurring west of Tony's Bay show no displacement. Aeromagnetic surveys (Cole & Naude, 2007) could not substantiate the occurrence of a magnetic feature in the same location and along the same trend that could be interpreted as a fault. A 1.5 km long magnetic lineament with a NE-SW orientation was however identified 2 km west of Tony's Bay (Figure 3.3).

Fault AEC DH1: Fault AEC DH1, is 10.5 km in length with an inferred 250-500m left-lateral displacement (Van Wyk, 1987). Van Wyk (1987) depicts the interpreted northern extent of the fault 2 km west of Sea

Vista, north of Cape St. Francis (Figure 3.4). From here the fault is interpreted to extend beneath the Cenozoic cover deposits, towards the coast, until a portion of the fault is shown (Van Wyk, 1987) to cut through coastal exposures west of De Hoek. The fault is interpreted to continue further offshore along the same trend for 5 km. Goedhart *et al.* (2008) described the presence of fault AEC DH1 as "*problematic*". He noted that although the fault appears on the AEC 1:50,000-scale geology map, it is not included on their 1:2500-scale site location maps. Originally identified by broad scale medium sensitivity aeromagnetic survey (Muller *et al.*, 1986; Anderson *et al.*, 1986 b), a comparison to recent high resolution aeromagnetics (Cole & Naude, 2007; Cole & Cole, 2007) do not support the existence of fault AEC DH1 nor its interpreted displacement (Goedhart *et al.*, 2008).

Faults AEC DH2 & AEC DH3: Interpretation of results obtained from recent high resolution aeromagnetics do not support the presence of faults AEC DH2 or AEC DH3 (Cole & Naude, 2007). Fault AEC DH3 is interpreted as a short NE-SW trending 500 m long fault with a narrow 70 m wide fault zone (Van Wyk, 1987) (Figure 3.3). Authors (Van Wyk, 1987; Raubenheimer *et al.*, 1988; Norman *et al.*, 1987 a & b, Goedhart *et al.*, 2008) acknowledge that faults may be linked to areas associated with high frequency jointing ('*shatter zones*'). There does however appear to be a NE-SW horst-like structure near Cape St. Francis. Fault AEC DH2 coincides with the eastern side of the structure. No mention of this structure was made by Cole and Naude (2007). Its origin remains uncertain.

The NW-SE trending Cape St. Francis fault is located 17 km SE of Thyspunt and is interpreted to occur entirely offshore along its 40 km length (Bate & Malan, 1992; McMillan *et al.,* 1997; Roux, 2011) (Figure 3.7). The Cape St Francis fault and other associated faults in the nearby vicinity and along the Cape St Francis Arch are extensional faults with tectonic age and style similar to that of the major onshore normal faults, such as the Kango-Baviaanskloof-Coega and Kouga Faults (Bate & Malan, 1992; Goedhart, 2007). The fault may possibly extend onshore within the study area. In the offshore Bate & Malan (1992) made interpretations of seismic profiles occurring across faults along the St Francis Arch and concluded no offset of Tertiary units. The mapped horizons from the survey data place the fault trace within Cretaceous strata. Goedhart (2007) identified two possible locations within the study area where the fault may continue onshore (Figure 3.7). The onshore continuation of the Cape St. Francis Fault is interpreted to occur either along the bay north of Seal Point, or along the eastern extend of Thys Bay. Interpretation of results from aeromagnetics did not recognize the presence of a NW-SE striking fault in either of the two possible onshore locations, noting that the Cape St. Francis fault plane could occur along the bedding and therefor may not be detected by airbourne geophysics (Cole & Naude, 2007).
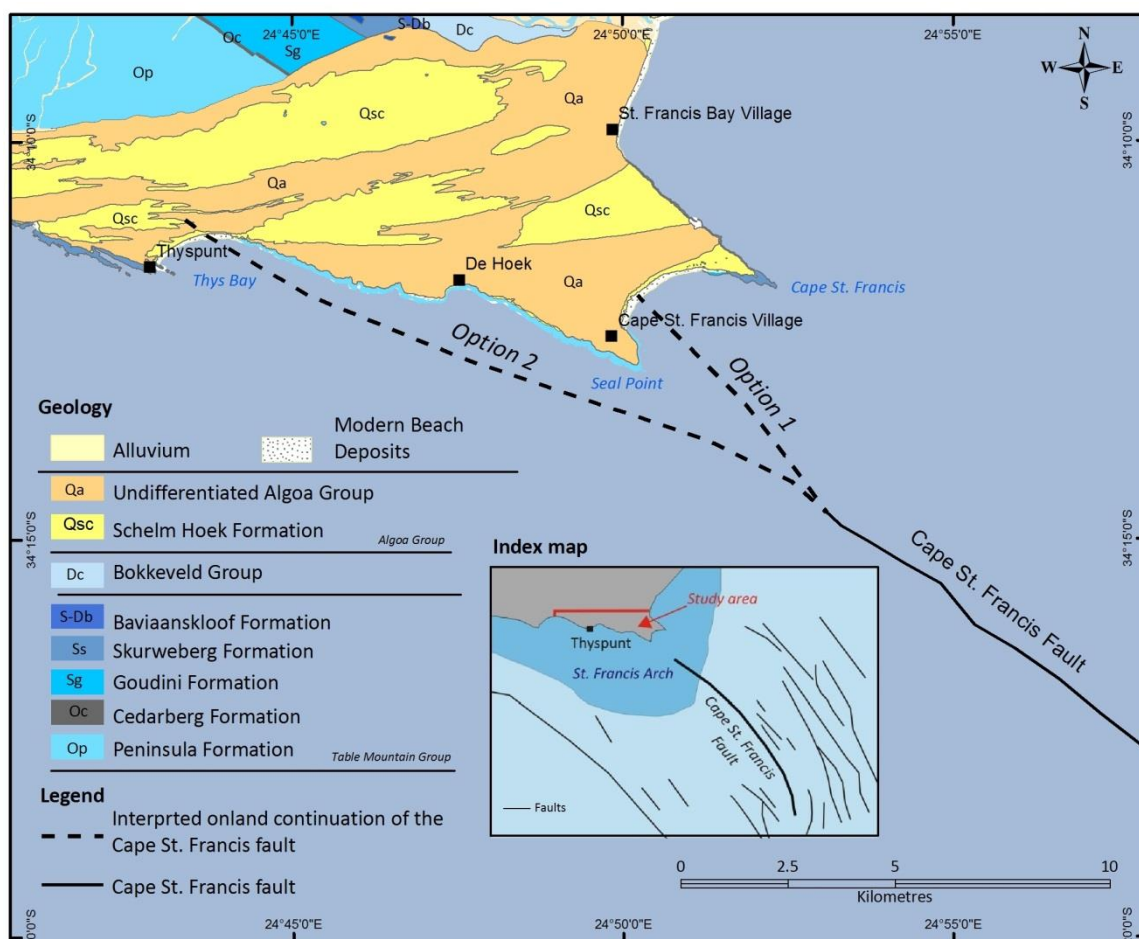
Figure 3.7: Two possible locations where the offshore Cape St. Francis Fault may extend onshore within the study area. (after Goedhart, 2007). Index map after Bate & Malan (1992)

Time domain electromagnetic (TDEM) surveys were conducted at locations where Goedhart (2007) projected the Cape St. Francis Fault to possibly continue onshore. TDEM traverse T was conducted along the eastern portion of the Thys Bay beach (Figure 3.8) perpendicular to bedding (Stettler *et al*., 2008). The roughly 620 m long east-west trending survey line consisted of 13 TDEM soundings, 50 m apart. Results from traverse T show a strong conductive zone interpreted as the Cedarberg Formation, occurring between ~300 – 450 m (sounding points 6 - 9) along the survey line. The formation is interpreted by Stettler *et al*., (2008) to dip SW roughly 30 – 35° and survey results specify a thickness of 60-70 m, with a slight increase or decrease due to interpreted folding and/or shearing. The Cape St. Francis fault was not interpreted to occur at this locality. Stettler *et al* (2008) also conducted a TDEM survey (traverse CSF) along the southern extent of the Cape St. Francis beach between the Seal Point and the Cape St. Francis headlands (Figure 3.9). The NNE trending survey line was conducted from S to N, perpendicular to bedding. Twenty five TDEM soundings were conducted 50 m apart over the 1250 m survey length. Results indicate the presence of the Cedarberg Formation between ~75 – 190 m (sounding points 2 -5) beneath Cenozoic cover along the survey line. The Cedarberg Formation is postulated to be 80 m thick. The formation is bordered by a zone that Stettler *et al.,* (2008) interpreted as fault mélange. An anomaly identified at 450 m along the survey line within possibly the Goudini Formation at -34°12'05.25" 24°50'06.45", is interpreted to be the Cape St. Francis Fault inclined at approximately 60–70° SW (Figure 2.24).

Stettler *et al.,* (2008) considered an alternative geological interpretation to the TDEM results presented in Figure 3.10. A re-interpretation of the geological model from the same TDEM sounding results (Stettler *et al.*, 2008) shows that steeper anticlinal folding could also fit the measured data collected along the length of the TDEM traverse CSF. The alternative geological model suggests a duplication of the Cedarberg Formation along the bay and eliminates the interpreted onland extension of the Cape St. Francis fault and associated zone of fault mélange.
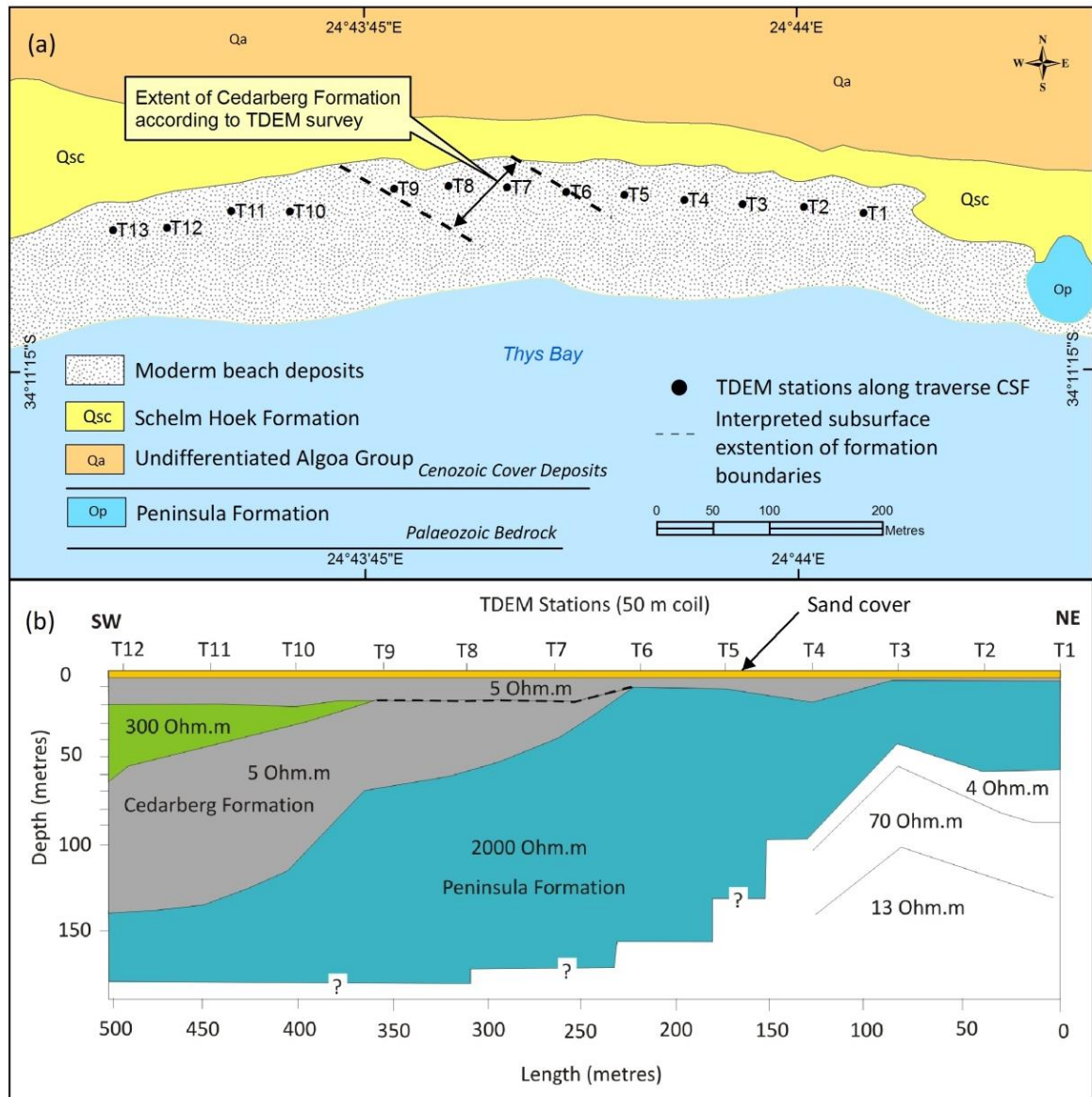
Figure 3.8: (a) Map showing the location of TDEM stations along traverse T. Geological model of survey results, (b), delineates the occurrence of the Cedarberg Formation beneath Cenozoic overburden. A conductive zone, interpreted to be Cedarberg Formation was detected between survey points T6 – T9 (after Stettler et al., 2008).
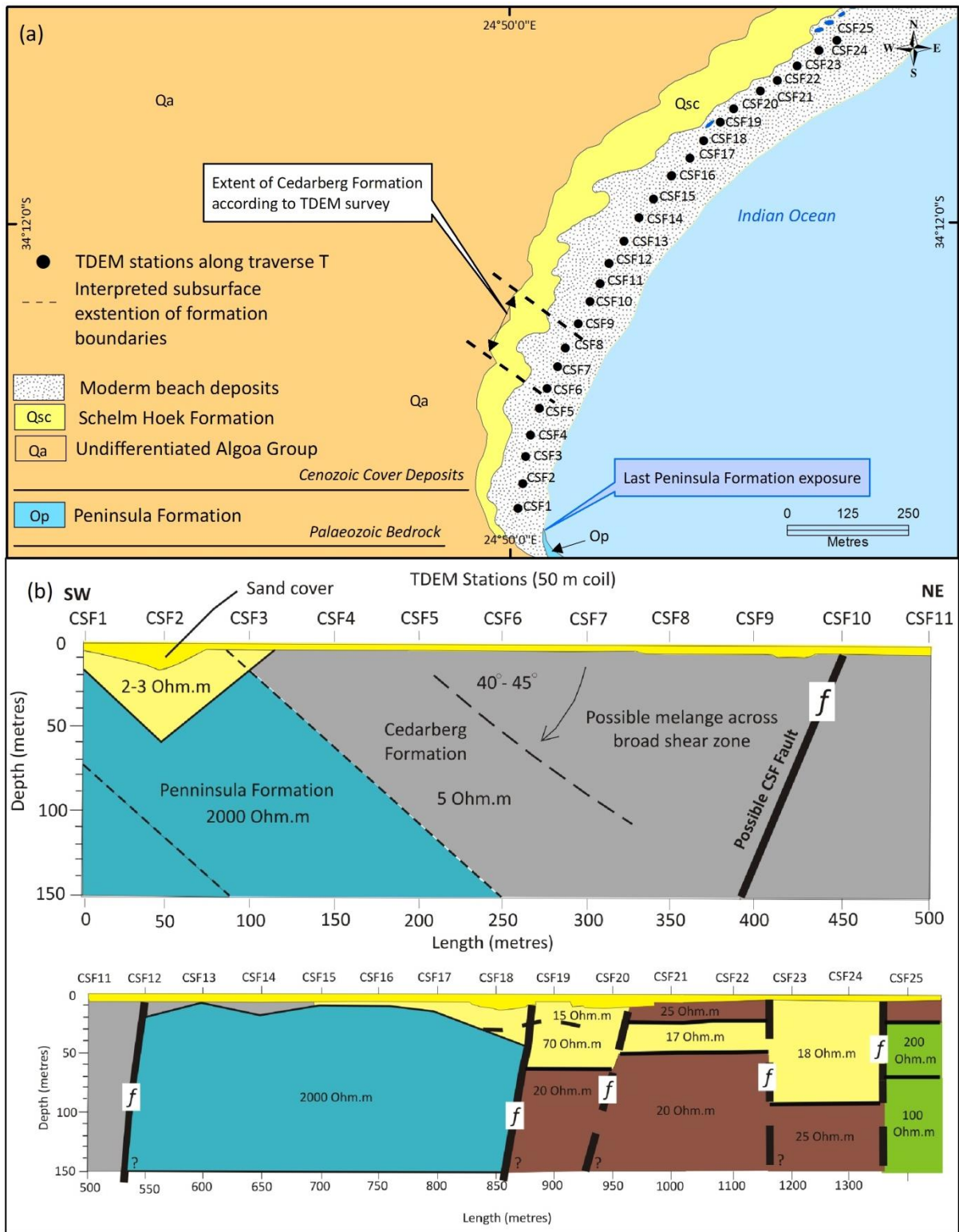
Figure 3.9: (a) Map showing the location of TDEM stations along traverse CSF. (b) A geological model of survey results obtained from traverse CSF. A conductive zone interpreted to the Cedarberg Formation was detected between survey points CSF2 – CSF3 and CSF4 – CSF5 (after Stettler et al., 2008).
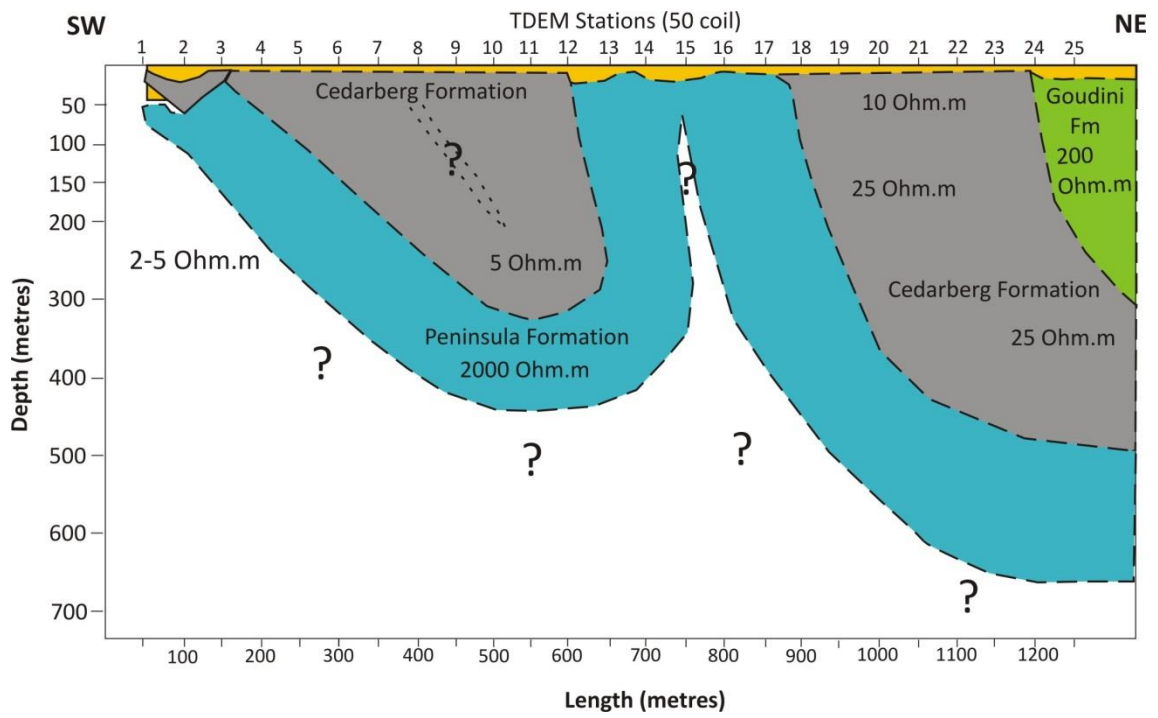
Figure 3.10: An alternative geological interpretation to the TDEM sounding results along Traverse CSF (after Goedhart et al., 2008).

4. Methodology

This chapter details methodologies used throughout the dissertation for field investigation, sample collection, geophysical methods utilized in the re-interpretation of initial survey results, the use of borehole data and modeling processes.

4.1 Field investigation

Focused mapping of the TMG, Bokkeveld Group and Algoa Group between Oyster Bay and Cape St. Francis were undertaken by the author in conjunction with members of the Council for Geoscience (CGS) during 2008 as part of a larger initial site safety report (SSR) study between Kareedouw and the Gamtoos River Mouth for the proposed NPP (Goedhart *et al.*, 2008) that produced geological maps of various scales (Figure 1.10). Subsequent follow-up investigations were conducted by the author in 2009, 2011 and 2014 to acquire additional data relevant to the study area.

Lithological and sedimentological descriptions of the Skurweberg, Goudini and Peninsula Formations are primarily derived from rugged coastal exposures. Inadequate or complete lack of outcrop exposure with an area predominantly blanketed by Cenozoic cover necessitated additional, but limited field work in areas immediately outside the study area to facilitate lithological and sedimentological unit descriptions of the Cedarberg, Baviaanskloof Formations and Bokkeveld Group

Structural readings were obtained using a Brunton compass adjusted to the area's current magnetic declination. The locations of all readings were captured using a Garmin GPS with a ± 4m accuracy. See Appendix B for a list of structural readings captured. The Munsell rock colour chart was used to determine the colour (hue and chroma) of rock exposures. Garmin Mapsource software was used to download GPS co-ordinates. Stereonets and rose diagrams were plot with the aid of Stereo software. ArcGIS software and/or Google Earth were utilized to capture, edit and display spatial data and to create maps.

4.2 Petrographic analyses

Nine samples were collected for thin section analysis; eight samples of the TMG and one from the Bokkeveld Group. Thin sections of these samples were examined for rock textures, grain size, mineral identification, mineral assemblages and sedimentary structures. Minerals were identified according to their optical properties. Thin section analysis was done using a Zeiss Axiophot polarizing microscope. Thin sections were viewed at magnifications of 4x, 10x, 20x and 40x. Sample localities are shown in Figure 4.1 and Table 4.1.
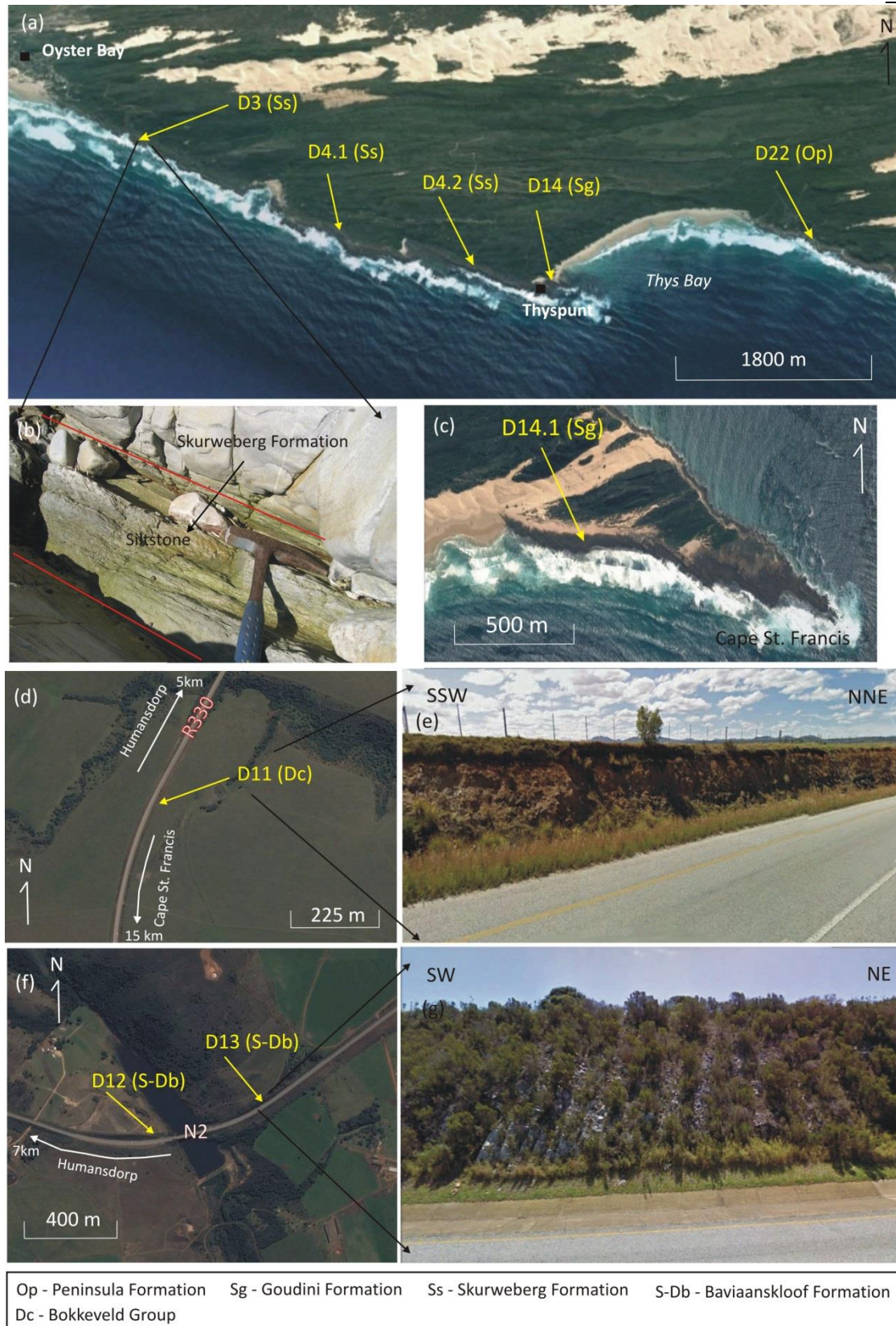
Figure 4.1: (a) Map showing the location of samples taken for petrographic analyses between Thys Bay and Oyster Bay. (b) Argillaceous / grey-wacke layer of the Skurweberg Formation sampled (sample D3). (c) Map showing the locality of sample D14.1 near the Cape St. Francis headland. (d) The locality where shale of the Bokkeveld Group (D11) was sampled. (e) Road cutting (outside study area) where shale of the Bokkeveld Group was sampled (sample D11). (f) Map showing area where shale (sample number D12) and sandstone (sample number D13) of the Baviaanskloof Formation was sampled. (g) Road cutting where sandstone (sample D13) of the Baviaanskloof Formation was sampled.

Table 4.1: The locations and lithostratigraphy of samples taken for petrographic analyses.

Sample	Formation/Group	Lithology	Latitude	Longitude
D3	Skurweberg Formation	Siltstone	34°10'45.47"	24°40'12.85"
D4.1	Skurweberg Formation	Quartzitic sandstone	34°11'16.26"	24°41'33.14"
D4.2	Skurweberg Formation	Quartzitic sandstone	34°11'27.73"	24°42'26.42"
D11	Bokkeveld Group	Mudstone	34°04'20.88"	24°47'54.88"
D12	Baviaanskloof Formation	Mudstone/siltstone	34°01'41.11"	24°51'25.45"
D13	Baviaanskloof Formation	Sandstone	34°01'37.30"	24°51'42.10"
D14	Goudini Formation	Sandstone	34°11'32.51"	24°42'58.09"
D14.1	Goudini Formation	Quartzitic sandstone	34°11'39.18"	24°51'30.45"
D22	Peninsula Formation	Quartzitic sandstone	34°11'14.54"	24°44'15.73"

4.3 Geophysical methods

In addition to previous geophysical surveys outlined in § 3.4 (Geophysics); seven multi-electrode resistivity surveys and one TDEM survey were also conducted within the study area. The author participated in field work, siting of lines, and was the geologist responsible for geological interpretation of survey results. Processing of multi-electrode resistivity results and rendering of geoelectrical profiles were conducted by L. Loots and E.Chirenje (CGS), while geophysical modelling of the TDEM results was undertaken by Dr. V. Zadorozhnaya and D. Eberle (CGS). Surveys were conducted to determine the elevation of bedrock beneath overburden, identify contacts between formations of the TMG and to identify possible faults in the area. Two reports (Loots *et al.*, 2009; Zadorozhnaya *et al.*, 2012) were generated for the client, Eskom (See Appendix A2 & A3). A more detailed re-interpretation of the subsurface geology along these survey lines is required in light of subsequently drilled boreholes (Hanson *et al.*, 2012; Engelsman & Constable, 2012) and a greater understanding of the area's regional and local geological setting and is provided for in § 5.4.

To aid understanding of how geophysical results were obtained and how the geology was ultimately re-interpreted, a brief introduction to the multi-electrode resistivity and TDEM survey techniques is provided in § 4.3.1 and § 4.3.2 below.

4.3.1 Multi-electrode electrical resistivity

4.3.1.1 Introduction

The multi-electrode resistivity technique is an electrical ground survey technique. It makes use of a multi-core cable with numerous electrodes attached to control nodes plugged into the ground through which a man-made electrical current is transmitted. Electrodes are located at a fixed spacing. The electrical current is introduced into the ground through electrodes C1 and C2 and the resulting voltage difference is then measured by electrodes P1 and P2. From the current (I) and the voltage (V) values the apparent resistivity (*pa*) can be calculated [1] (Figure 4.2).

The k value represented in Figure 4.2 represents the geometric factor which depends on the arrangement of the four electrodes (Loke, 1999; Loke, 2001; Milsom, 2003).

$$pa = kV \: / \: I \text{...............}^{(1)}$$
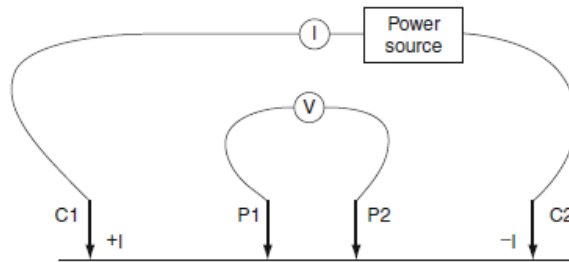
Figure 4.2: Conventional four electrode array for determining resistivity of the subsurface using the multi-electrode resistivity technique (Loke et al., 2011).

Apparent resistivity is however not a true reflection of the subsurface, but rather the resistivity of a homogeneous half-space that will give the same resistive value for the same electrode arrangement. Software programs are generally used to inverse measured apparent resistivity values and generate true subsurface resistivity. The arrangement of electrodes will depend on the type of feature to be mapped, the sensitivity of the meter and background noise level. Eight different array types or configurations are commonly used in resistivity surveys (Loke, 1999; Loke *et al*., 2011). The Dipole-Dipole (Figure 4.3) and Werner-Schlumberger resistivity survey configuration arrays (Figure 4.4) were utilized within the study area. The Dipole-Dipole array was chosen for its sensitivity to vertical structure. This array suites the subsurface identification of fractures and faults and boundaries between steeply dipping lithological contacts. The Werner-Schlumberger configuration array was chosen for its sensitivity to both vertical and horizontal structures, aiding in the determination of overburden thickness. A SYSCAL Pro 72 unit was used with a multi-core cable and stainless steel electrodes with 10 m ground spacing to conduct the multi-electrode surveys at Thyspunt and Cape St. Francis. The position of survey points were recorded using a Garmin ETrex GPS with a ± 4 m accuracy.

$$K = x \: n \: (n + 1) \: (n + 2) \: a$$
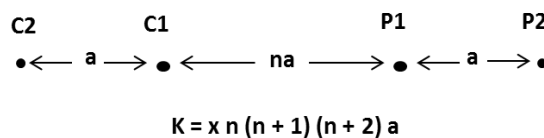
Figure 4.3: Design of Dipole-Dipole array configuration using the multi-electrode resistivity technique. Where a = the dipole length and n= the dipole separation factor (after Loke, 1999).

$$K = x \: n \: (n + 1) \: a$$
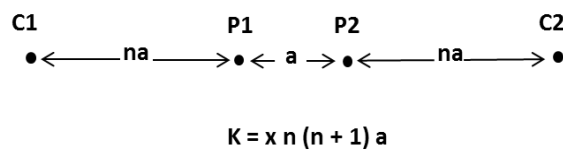
Figure 4.4: Design of Werner-Schlumberger array configuration using the multi-electrode resistivity technique, where a = the dipole length and n= the dipole separation factor (after Loke, 1999).

Prosys II software was utilized to reduce sounding measurements to apparent resistivity and convert to Res2Dinv software file format to allow for inverse modeling and the creation of apparent resistivity sections as a function of depth. The default parameters of the Res2Dinv software were used to guide the inversion process. The issue of non-uniqueness in the inversion process occurs not only in resistivity soundings, but also other geophysical data, allowing for a range of models to arise from the same measured dataset. Thus, to limit the array of feasible models, the nature of the subsurface geology and borehole information was incorporated into the inversion subroutine. Final models were exported to Geosoft Oasis Montaj for gridding.

4.3.1.2 Methodology

Two multi-electrode resistivity survey lines TS 1 (Figure 4.3 a) and TS 3 were completed at Thyspunt and five multi-electrode resistivity survey lines, CSF 1, CSF 2, CSF 3, CSF 4, CSF 5 were conducted NW of Cape St. Francis (Loots *et al.*, 2009). All resistivity survey lines were conducted atop Cenozoic dune deposits. The siting of all survey lines were subject to careful consideration. At Thyspunt the siting of lines were done on the property of Eskom and were subject to on-site approval by Hennie de Beer, Eskom's Thyspunt site manager and environmentalist. No clearing of sensitive vegetation, which includes Milkwood trees (Figure 4.5 b) or siting of lines along archeological sensitive sites were permitted. Such sites included shell middens and any areas that may possibly contain Khoisan tools. Clearing of vegetation was required at Thyspunt along survey line TS3, to ensure survey electrode conductors made contact with the ground surface (Figure 4.5 b). The siting of survey lines also considered boreholes within a ±50 m – 100 m range that could aid in constraining survey results and interpretation of subsurface geology (Figure 4.5 c).
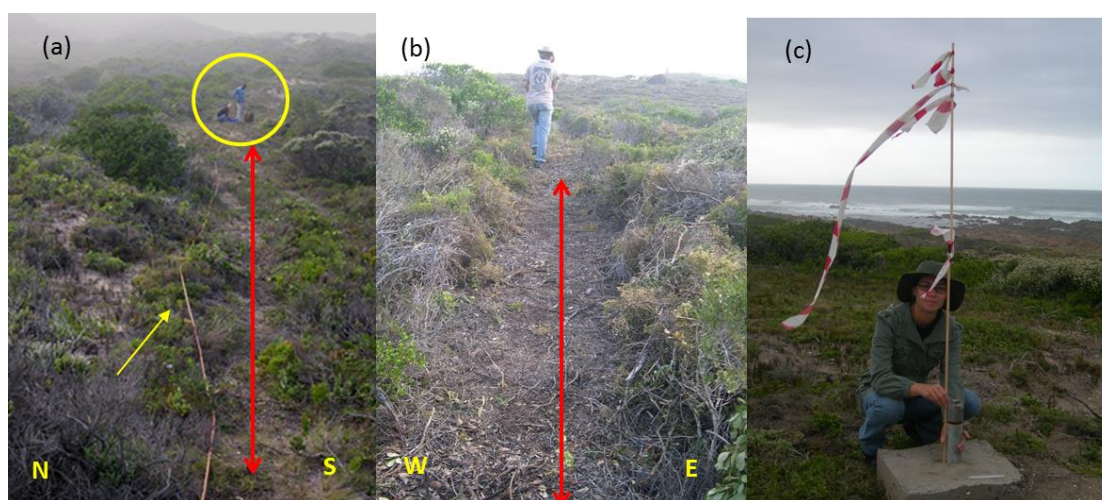
Figure 4.5: (a) Line TS 1 looking east. (b) Looking north along path clearing through non-sensitive vegetation for survey line TS 3. (c) Borehole TB31 (Eskom, 2010 b). Survey line TS 3 was conducted in close proximity to borehole TB31 to aid in constraining survey results.

 At Cape St. Francis an initial field visit with Hendrik Louw, from the local Kouga Municipality aimed at identifying any above ground and subsurface hindrances that may skew survey results. Hindrances identified included transformers, power cables, subsurface Telkom telephone lines and water pipes. Five survey lines were sited to minimize interference with these structures whilst finding easy access roads

along which surveys could be conducted. Along survey line CSF1 a communal power line trends parallel to the line for the last 900 m.

(i) Thyspunt

Two multi-electrode resistivity survey lines, TS1 and TS3, were conducted near Tony's Bay (Figure 4.6 a) (Loots *et al*., 2009). The start and end co-ordinates and associated attributes of survey line TS1 and TS3 are summarised in Table 4.2.

Survey line TS 1 trends E-W and measures 810 m in length. The survey line was conducted in close proximity to boreholes TB16, NEW30, TB21, BHDB6, Tony's Bay BH5, TB14, BHPB5, Tony's Bay 3 and THY-RP10 (Raubenheimer *et al*., 1988 a & b; Eskom, 2010 b) (Figure 4.6 a & b). The survey was conducted oblique to the bedrock bedding strike of the Skurweberg Formation and perpendicular to the inferred NNE striking AEC TSP3 fault (§ 3.4, Figure 3.3, Figure 4.6). Line TS1 was initially conducted to determine bedrock depth below cover sediments, however re-interpretation would also allow investigation into the presence of the AEC TSP3 fault and the more lithologically incompetent fine-grained sandstone and shale units within the Skurweberg Formation responsible for the development of the NW-SE trending Tony's Bay embayment.

Survey line TS3, trends N-S and measures 450 m in length. Surrounding boreholes that aid in constraining survey results include boreholes BHDB5, Thyspunt BH4 & BH3 and TB31, NEWN1, NEWS1, TB37 and TB43. (Raubenheimer *et al*., 1988 a & b; Eskom, 2010 b) (Figure 4.6 c). The survey was conducted oblique to bedrock bedding assumed to be Skurweberg Formation. The location of survey line TS3 was initially chosen to determine bedrock depth below cover sediments, however the results can also be used to possibly identify the contact between the Skurweberg and Goudini Formations.
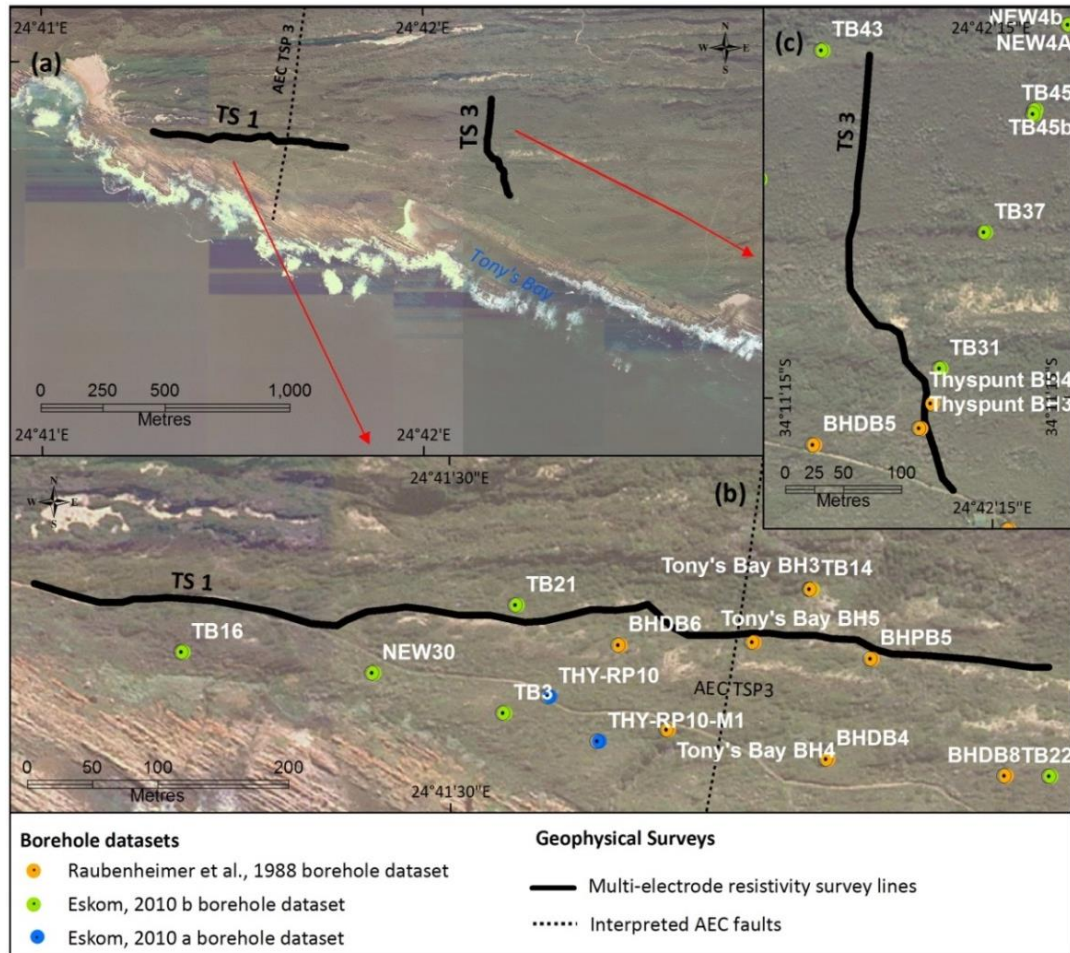
Figure 4.6: (a) Location of multi-electrode resistivity survey lines TS1 and TS3 near Thyspunt. (b) Survey line TS1 and (c) TS3 and surrounding borehole locations at the time surveys were conducted.

Table 4.2: Table summarizing survey attributes of multi-electrode resistivity lines T 1 and T 3, located at Thyspunt.

Line	Line trend	To bedding	Length of line	Presumed bedrock	Co-ordinates (start of line)		Co-ordinates (end of line)	
					South	East	South	East
TS 1	W-E	Oblique	810 m	Skurweberg Formation	34°11'09.24"	24°41'17.52"	34°11'40.40"	24°41'47.76"
TS 3	S-N	Oblique	450 m	Goudini Formation	34°11'04.92"	24°42'27.24"	34°11'17.88"	24°42'14.04"

(ii) Cape St. Francis

Five multi-electrode resistivity survey lines, CSF1, CSF 2, CSF 3, CSF 4 and CSF 5 were conducted near Cape St. Francis (Figure 4.7). The start and end co-ordinates, and associated attributes of survey lines are summarised in Table 4.3. In the initial report produced for Eskom (Loots *et al*., 2009) the position of survey lines CSF3 and CSF5 were mislabeled, this error came to light after co-ordinates taken in the author's field notebook and diagram of line positions prior to field work were cross-examined. The error may have occurred because the length of both survey lines are the same and were not numbered in sequence but rather in order of importance. Results presented here reflect the correction of that error.

Survey line CSF 1 trends NNW-SSE and has a length of 1800 m. The survey trends perpendicular to bedrock bedding. The survey was conducted NW of Cape St. Francis, east of road R330 (Figure 4.7). Line CSF 1 was sited to identify bedrock elevation beneath overburden cover and possible onland extension of the Cape St. Francis fault. The information from survey line CSF1 also aid in the identification of contacts between the Peninsula, Cedarberg and Goudini Formations.

Survey line CSF 2 has a dual trend. The survey line trends W-E for 400 m, after which it changes orientation to a NW-SE trend for the remainder of its 950 m length. Survey lines CSF 3, CSF 4 and CSF 5 all trend W-E and have a length of 450 m. The siting of survey lines CSF 2, CSF 3, CSF 4 and CSF 5 were done with the aim of determining bedrock elevation beneath Cenozoic cover.
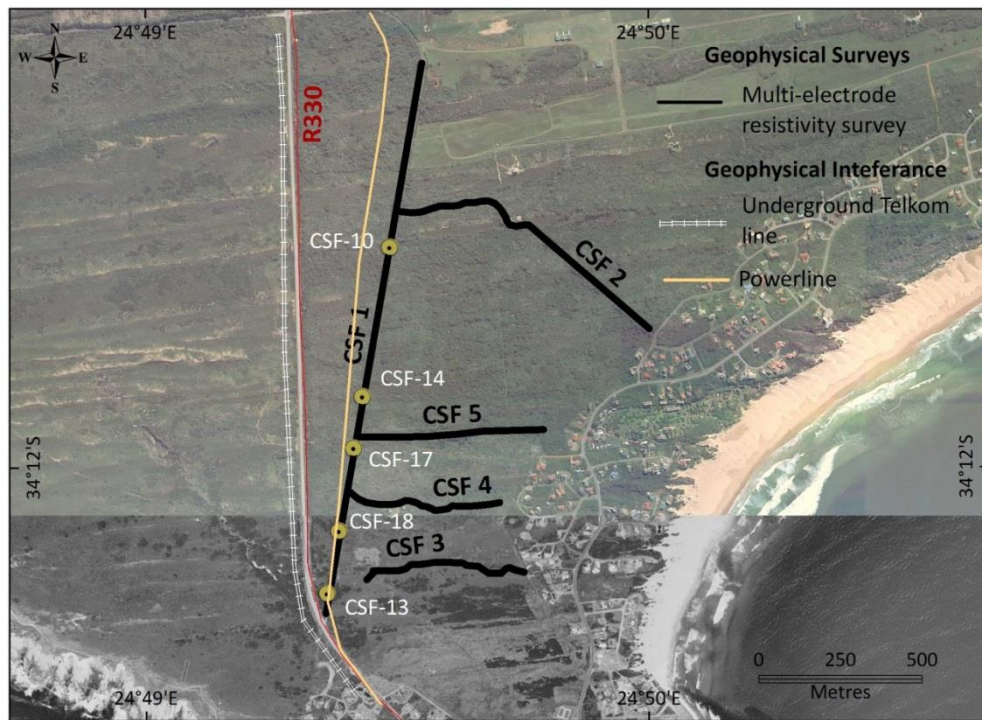
Figure 4.7: Location of the five multi-electrode resistivity survey lines CSF1, CSF 2, CSF 3, CSF 4 and CSF 5 conducted near Cape St. Francis.

Table 4.3: Table summarising survey attributes of multi-electrode resistivity lines CSF1, CSF 2, CSF 3, CSF 4 and CSF 5 located at Cape St. Francis.

Line	Line Trend	To Bedding	Length of line	Presumed bedrock	Co-ordinates (start of line)		Co-ordinates (end of line)	
					South	East	South	East
CSF 1	S-N	Roughly perpen-dicular	1800 m	Peninsula, Cedarberg, & Goudini Formation	34°12'14.76"	24°49'21.36"	34°11'17.88"	24°49'32.16"
CSF 2	W-E /NW-SE	Oblique to sub-parallel	950 m	Goudini Formation	34°11'46.68"	24°50'00.60"	34°11'34.8"	24°49'30.72"
CSF3	W-E	Oblique	540 m	Goudini Formation	34°12'10.44"	24°49'45.12"	34°12'11.52"	24°49'26.04"
CSF 4	W-E	Oblique	540 m	Goudini Formation	34°12'01.80"	24°49'23.52"	34°12'03.60"	24°49'42.60"
CSF 5	W-E	Oblique	540 m	Peninsula, Cedarberg, & Goudini Formation	34°11'57.12"	24°49'25.32"	34°11'59.28"	24°49'45.84"

4.3.2 Time domain electromagnetics (TDEM)

4.3.2.1 Introduction

The TDEM method utilizes a transmitter that sends an alternating current through a square loop insulated electrical cable placed on the ground surface. A receiver coil is placed in the center of this transmitter loop (Figure 3.8 a). An electrical current with base frequencies that can range between 3 – 75 Hz are passed through the transmitter loop to produce an electromagnetic field. The current consists of equal periods of time-on and time-off. Termination of current flow is not instantaneous, but rather decreases over a few milliseconds of time referred to as "ramp time". During ramp time the primary electromagnetic field is time-variant and able to create a secondary electromagnetic field in the ground directly beneath the transmitter loop. As the secondary electromagnetic field starts to decay it inducing additional eddy currents. These eddy currents propagate in a downward and outward series of rings that weaken and expand as they travel down into the subsurface (Figure 4.8 a). The magnitude and rate of secondary currents generally depends on the electrical conductivity of the medium through which it travels and its geometry. The time interval after termination of current will determine the depth of the survey. With a longer time-off period, eddy currents will propagate to progressively deeper depths (Milsom, 2003). The center receiver coil measures the voltage of secondary currents during the time-off period. Measurements of the secondary current are generally recorded and a plot is made of the measured resistivity against the delay time. This plot is referred to as a sounding curve and is today typically generated by computer software that ultimately provides a model showing the thickness and resistivity of the layers. The surveyor inputs preliminary data into this software program, which then calculates the sounding curve for this model. The software applies inversion, the process that adjusts the model and calculates a new sounding curve that better fits the field data. Inversion, is repeated until a satisfactory fit is obtained between the model and the field data (McNeill, 1994).
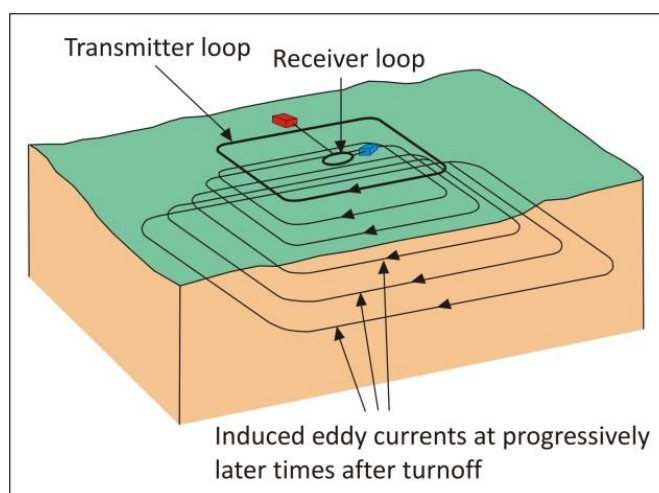
Figure 4.8: (a) A schematic presentation depicting the principles of the geophysical time domain electromagnetic method (after www.ncwater.org).

4.3.2.2 Methodology

One TDEM survey line, TDEM CFS was conducted NW of Cape St. Francis (Zadorozhnaya *et al.,* 2012). The roughly 1675 m long line was conducted perpendicular to the NW-SE bedding strike. The start and end co-ordinates and associated attributes of survey line TDEM-CSF1 are provided in Table 4.4. The TDEM survey was performed in the same location and along the same trend as multi-electrode resistivity line CSF 1. Similar to the purpose of resistivity line CSF-1, the aim of the TDEM survey line was to determine the location of the Peninsula, Cedarberg and Goudini Formations below Cenozoic cover and to detect whether the proposed onland extension of the Cape St. Francis fault in this area could be substantiated. The objective for siting a TDEM survey in the same location as resistivity line CSF 1 was to validate results obtained by the multi-electrode resistivity survey technique. The comparison between geophysical methods allows for a determination of a preferred ground geophysical survey method for use in this particular area, where Cenozoic overburden of the Algoa Group can be >50 m thick.
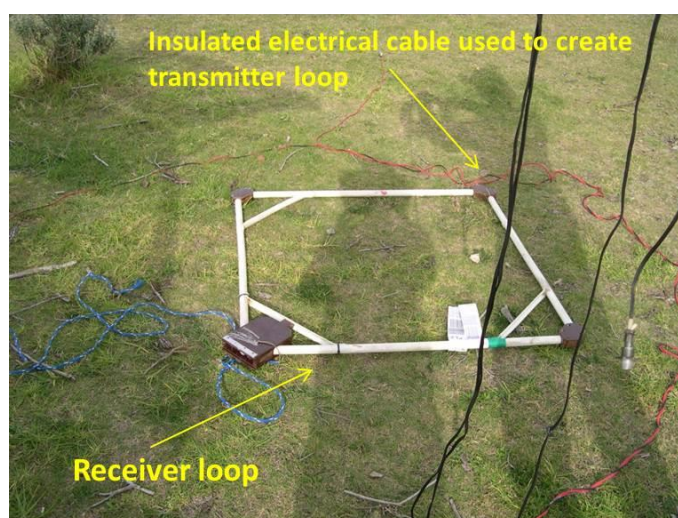
Figure 4.9: Receiver loop used in the TDEM survey of line TDEM-CSF1. A relatively small single 25 m x 25 m transmitter loop size was used to conduct soundings along survey line.

A small single 25 m x 25 m transmitter loop size was used to conduct soundings along TDEM survey line TDEM-CSF1. The small loop size was selected to attain high vertical resolution close to the surface (± 100 m) needed to identify the unconformity between the Cenozoic cover and Palaeozoic bedrock. To increase lateral resolution, a 12.5 m distance was kept between the centres of loop (Figure 4.9). The TEM-FAST 48 system was used to capture receiver readings. The TEM-RESEARCHER (TEM-RES-WIN) software was ultimately used to generate TDEM profiles. The survey line consists of 134 TDEM stations along its length. The location of each TDEM station was captured using a Garmin ETrex GPS with a ± 4m accuracy. The field survey and processing of data was conducted by Dr. V. Zadorozhnaya and D. Eberle from the Geophysics Unit of the Council for Geoscience.
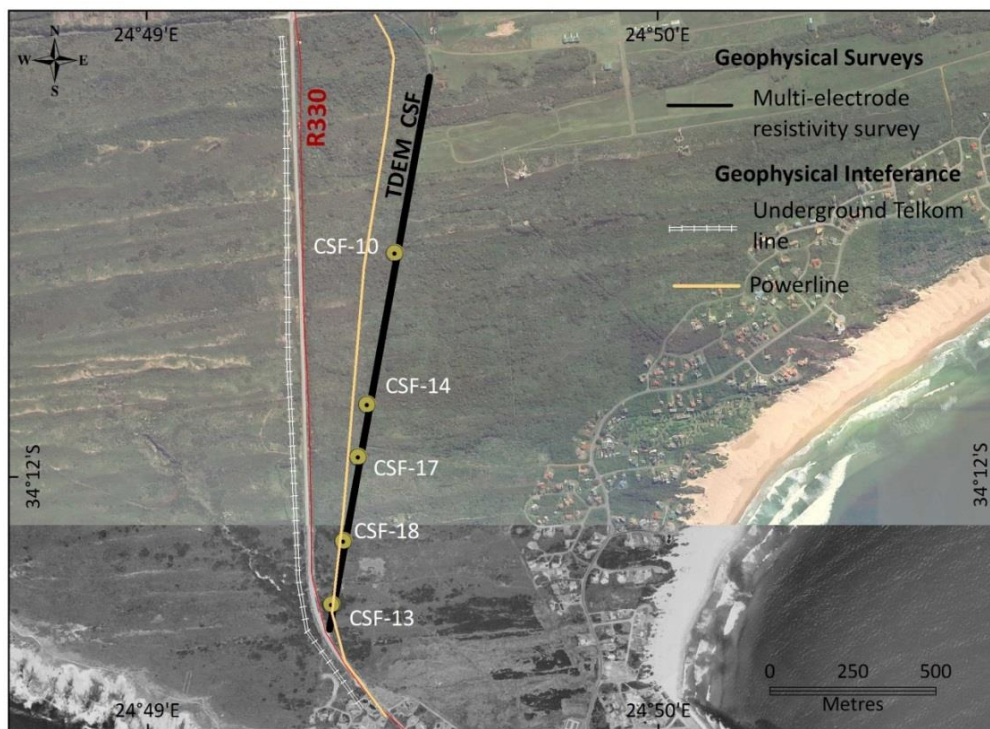
Figure 4.10: Location of the TDEM survey line TDEM-CSF1 located near Cape St. Francis.

Table 4.4: Table summarizing survey attributes of multi-electrode resistivity lines TDEM-CSF1 located near Cape St. Francis.

Line	Line Trend	Length of survey line	To Bedding	Presumed bedrock	Co-ordinates (start of line)		Co-ordinates (end of line)	
					South	East	South	East
TDEM-CSF1	NNW-SSE	1675 m	Oblique	Peninsula, Cedarberg, & Goudini Formations	34°12'14.94"	24°49'21.36"	34°11'21.08"	24°49'33.24"

4.4 Borehole data

This section aims to outline how borehole data were sourced, captured and utilized in conjunction with other data sources to achieve various study aims.

4.4.1 Sourcing and capture of borehole data

A comprehensive literature review was undertaken to find boreholes drilled in the study area. Although hundreds of holes were identified, many did not have geological substrate information and were therefore of no use to the study. This included groundwater boreholes identified during a hydrocensus undertaken by SRK (a geological consultancy) in 2009 (pers. comm. Riona Kruger). Ultimately the data from nine borehole datasets (247 boreholes) were selected for use in this dissertation (Raubenheimer *et al*., 1988 b; Rosewarne & Lomberg, 1989; Maclear, 2002; Maclear, 2005; Maclear, 2006; Eskom, 2010 a; Eskom 2010 b; Hanson *et al*., 2012; Engelsman & Constable, 2012) (Figure 4.11). See Appendix C1 for a spreadsheet of borehole locations, elevations, borehole depths and other associated data and Appendix C2 for borehole metadata. The co-ordinates, elevation, depth of borehole, depth to bedrock, stratigraphy and lithology of each borehole were captured (Appendix C1). Borehole metadata captured included

reasons why boreholes were originally drilled, type and quality of data captured in borehole logs and original co-ordinate systems used (Appendix C2). Maps depicting the location of various boring are available in Appendix C3. Photos of borehole core were obtained for only three datasets, namely Raubenheimer *et al.* (1988 a & b); Eskom (2010 b) and Hanson *et al*., (2012), however the quality of photos obtained from the Raubenheimer *et al*. (1988 a & b) dataset was poor and could not be utilized.

A review of the bedrock stratigraphy was conducted after inconsistencies in certain borehole log descriptions were noticed. Inconsistencies include for example borehole TB46 - logged as intercepting bedrock of the Skurweberg Formation despite surrounding boreholes within a 300 m radius intercepting bedrock of the Goudini Formation. Seven such stratigraphic inconsistencies were noted and subsequently corrected (Appendix C1). Table 4.5 provides a list of incorrectly logged bedrock stratigraphy and outlines reasons why a new formation or group status was assigned. All subsequent results take stratigraphic updates into account.

Figure 4.11: Map showing the location of borings within the study area.

Table 4.5: *A list of boreholes in which bedrock stratigraphy was conceivably incorrectly logged. Original and newly identified stratigraphy is indicated. Reasons for altering bedrock stratigraphy are outlined.*

Borehole	Original bedrock stratigraphy	Newly assigned bedrock stratigraphy	Combination of reasons for change in bedrock stratigraphy
SRK-6	Table Mountain Group	Bokkeveld Group	• North of borehole SRK-6, eight boreholes (SRK-1, SRK-2, SRK-4, SRK-5, SRK-10, SRK-11, SRK-12, SRK-17) intercept bedrock of the Bokkeveld Group. To the south of borehole SRK-6, one borehole (SRK-8) intercepts the Bokkeveld Group. • Borehole SRK-6 is situated too far north for the lithology to be associated with the Table Mountain Group.
TB11	Skurweberg Formation	Goudini Formation	• Boreholes (New Seismic B, NewE18, New17, New18, Thy-RP11, TS20, New21, & TB46) within a 400 m 360° radius of borehole TB11 all intercept bedrock of the Goudini Formation. • Bedrock lithology is consistent with the Goudini Formation. Bedrock consists of siltstone with mudstone lenses.
TB15	Skurweberg Formation	Goudini Formation	• Three boreholes (New H1, BHPP8 & BHDP11) within a 120 m distance to the NNE and SSW log bedrock lithology as Goudini Formation. • Bedrock lithology consists of alternating sandstone and shale. Lithology is more typical of Goudini Formation.
TB22	Goudini Formation	Skurweberg Formation	• 18 boreholes (New29, TB4, TB5, TB14, TB17c, THY-MR9, THY-RP14, BHDB1, BHDB4, BHDB3, BHDB4, BHDB7, BHDB8, BHDB9, BHPB1, BHPB2, BHPB3, BHPB4 & BHPB5) to the south and 3 boreholes (TB30, TB35, TB36) to the N of borehole TB22 all intercept bedrock lithology of the Skurweberg Formation. These boreholes are all within a 300 m radius of borehole TB22.
TB32	Skurweberg Formation	Goudini Formation	• Fourteen boreholes (THY-MR2, THY-RP7, TB39, NEW D1, BHDP7, BHDP9, BHPP1, BHPP2, BHPP3, BHPP4, BHPP5, BHPP6, BHPP7, Thyspunt BH5) in a 200 m radius around borehole TB32 all intercept Goudini Formation. • Borehole log descriptions note alternating layers of siltstone and shale, conceivably more consistent with the lithology of the Goudini Formation.
TB46	Skurweberg Formation	Goudini Formation	• Six boreholes (TS20, TS21, THYRP11, NEW17, NEW18, NEW Seismic B) to the NE, three boreholes (TB39, NEW13, NEW27) to the W and NW and fourteen boreholes (THY-MR2, THY-RP7, TB39, NEW D1, BHDP7, BHDP9, BHPP1, BHPP2, BHPP3, BHPP4, BHPP5, BHPP6, BHPP7, Thyspunt BH5) to the south of TB46 are logged as intercepting the Goudini Formation. These boreholes all occur within a 300 m distance of borehole TB46. • Borehole loggings describe 10 m thick successions of alternating siltstone and shale. In consistent with the arenaceous lithologies of the Skurweberg Formation
TS22	Goudini Formation	Cedarberg Formation	• 150 m SE of borehole TS22 along strike, NEW U1, intercepts Cedarberg shale, in addition 60m NE of borehole TS22, borehole THY-MR12 intercepts quartzitic sandstone of the Peninsula Formation.

4.4.2 Utilization of borehole data

Borehole data were utilized to determine the following geoscientific parameters of the study area:

4.4.2.1 Lithostratigraphic contacts beneath overburden cover

At Thyspunt, Eskom (2009) identified bedrock transition zones between the Skurweberg and Goudini Formations; and the Goudini and Cedarberg Formations beneath sediments of the Algoa Group (Figure 3.1 a). Borehole data is used to re-access these transition zones and identify additional contacts between formations across the entire study area, with previously excluded and subsequently obtained data (Goedhart *et al*., 2008; Stettler *et al*., 2008; Hanson *et al*., 2012; Engelsman & Constable, 2012). The planning, design and construction phases of the NPP will benefit in the identification of bedrock lithostratigraphy as the various formations will have different geotechnical properties that need to be considered during siting and construction of the NPP.

To identify contacts between TMG formations beneath cover sediments, a map of boreholes that intercept bedrock was created. Boreholes were assigned specific symbology based on their assigned bedrock lithostratigraphy. Contacts between stratigraphic units were drawn from these maps, while adhering to geophysical results obtained along coastal embayments by Stettler *et al*., (2008).

4.4.2.2 Thickness distribution of cover sediments (Algoa Group)

A total of 232 (out of 247) boreholes were used in determining thickness of the Algoa Group. Thickness within each borehole is calculated from top of borehole to first occurrence of bedrock. Inclined boreholes (Raubenheimer *et al*., 1988a; 1988b) were corrected to vertical (Appendix C1, C2 & C3). Boreholes not intercepting bedrock were excluded from thickness calculations. Individual borehole surface elevations, bedrock elevations and the resultant thicknesses were graphically plotted against their distance from the coastline. The impact of surface relief and bedrock elevation on the thickness of the Algoa Group were further investigated by means of cross-sections perpendicular to the coastline at Thyspunt and Cape St. Francis.

Investigation into the thickness distribution of Cenozoic overburden, aids in accessing safety during proposed construction at the Thyspunt site. Eskom, (2009) indicated that any construction of a NPP will be done on bedrock and that significant excavation of overburden will be required. Excavations will require cut backs to tolerable angles to ensure safety during the construction phase of NPP. Results aim to re-access the three 'sensitivity' or risk classes that overburden material may pose to site construction since last evaluation by Eskom in 2009 (§ 3.2, Figure 3.2).

4.4.2.3 Palaeotopograhy of bedrock

The first interception of bedrock within boreholes loggings is referred to as the 'top of bedrock' surface and represents the palaeotopographic surface in an ancedant landscape prior to the deposition of Cenozoic cover. Interpolation between points of bedrock elevation enables the creation of a continuous palaeotopographic (bedrock) surface. Data points utilized to determine the bedrock surface include (Figure 4.12):

• Bedrock elevation values derived from borings (Appendix C1)

• Elevation values at localities where bedrock and Cenozoic deposits are in direct contact at the surface

• Estimated bedrock elevation values derived from ground bourne geophysics

Various interpolation methods were considered. Ultimately a visual inspection of the various interpolation output surfaces, density of data points and accuracy in reflecting landscape features were factors considered in choosing the interpolation methods. At Thyspunt dense and fairly evenly distributed data points suit the method of Kriging interpolation best and allows for the creation of a bedrock contour map with a 1 m interval. Bedrock elevation values covering the remainder of the study area are somewhat sparse and did not allow for this method of interpolation. Instead interpolated palaeotopography was derived using the vector-based Delaunay triangular irregular network (TIN) method with a 5 m interval. ArcGIS software was used to produce bedrock contour maps.

4.5 Geomodelling

Geological modelling or geomodeling is defined as the applied science of generating a computerized model that visualizes the physical topology and geometry of the earth's surface from measurable (numerical) or interpretive data (Mallet, 2002; Caumon *et al.*, 2009). Geomodeling incorporates two-dimensional (2D) geological data sources such as structural geology, sedimentology, stratigraphy and geophysics in an integrated manner with a multi-dimensional perspective.

4.5.1 Software utilization

The Thyspunt geomodel was created using a combination of ArcMap 9.3 & 10.1, Google SketchUp 7 and Google Earth software programs. Google SketchUp is a freeware 3D drawing software and was utilised for the creation of TINs and conversion of 2D spatial data into 2½D. Data that could not be presented in 2D (e.g. fold structures) in ArcGIS was drawn in 2½D utilizing this software. The software was chosen in lieu of costly commercial 3D software unavailable to the author. Google SketchUp was also chosen for its ease of use and easy integration functionality with Google Earth that ensures accessibility to end users. Google Earth is utilized to display the Thyspunt geomodel created in SketchUp.
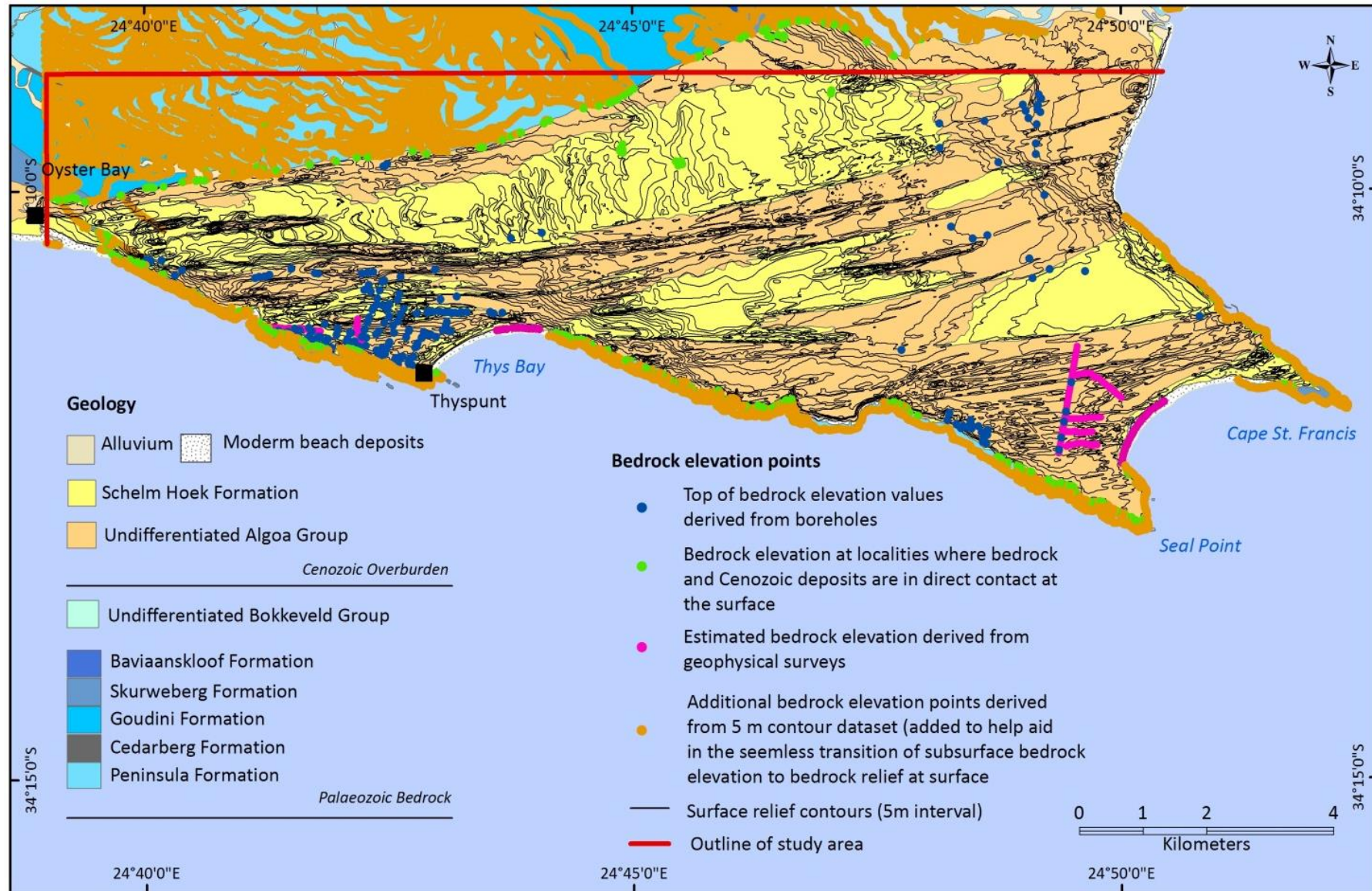
Figure 4.12: Map of study area, indicating the location of bedrock elevation points within the study area.

4.5.2 Data sources considered

Table 4.6 outlines the various data sources (geographical, geophysical and borehole used in the construction of the geomodel.

4.5.3 Methodology for model construction

This section aims to deal with the scale at which the model was constructed, the interpolation methods used in the creation of topographical surfaces, and to instruct the end user in the use and view of the final model. A flow chart outlining the processes used in the construction of the Thyspunt model is also provided (Figure 4.13).

Table 4.6: Table summarizing data sources, their origin, selection for use and ultimate use in the Thyspunt geomodel.

Data sources	Data origin	Interpretation / analysis or altering of original data for use in model	Reason/s for use	How data is used in construction of model
Geographical data				
Surface relief (5m contour dataset)	Chief Surveyor General (2008)	None	Most complete, smallest contour interval set (most detailed) that could be obtained for the entire study area.	Utilized to interpolate a 3D topographic surface for the model
Surface geology for study area	Goedhart *et al.*, 2008	None	Most recent mapping of the study area	Surface geology in model, structural readings aid in determining the structural character of the stratigraphic units in the subsurface
Borehole data				
Borehole datasets	Raubenheimer *et al.*, 1988 b; Rosewarne & Lomberg, 1989; Maclear, 2002; Maclear, 2005; Maclear, 2006; Eskom, 2010 a; Eskom 2010 b; Hanson *et al.*, 2012; Engelsman & Constable, 2012	Original data logged in boreholes were predominantly kept, expect were stated otherwise (refer to Table 4.5)	Data provide subsurface geological information	Partial stratigraphic subdivision of subsurface geology, interpolation of the Palaeozoic topography (top of bedrock beneath Cenozoic cover)
Geophysical data				
Multi-electrode res.	Loots *et al.*, 2009;	Re-interpretation of the geological substrate from resistivity-depth section	Provide detailed geoscientific information of the subsurface	Partial stratigraphic subdivision of subsurface geology, interpolation of the Palaeozoic topography (top of bedrock beneath Cenozoic cover), validity of possible faults beneath Cenozoic cover
TDEM	Stettler *et al.*, 2008; Zadorozhnaya *et al.*, 2012	Re-interpretation of the geological substrate from the geoelectrical model of Zadorozhnaya et al., 2012.		
Aeromagnetics	Cole & Cole, 2007	None – interpretation of subsurface was conducted by Cole & Cole (2007)		
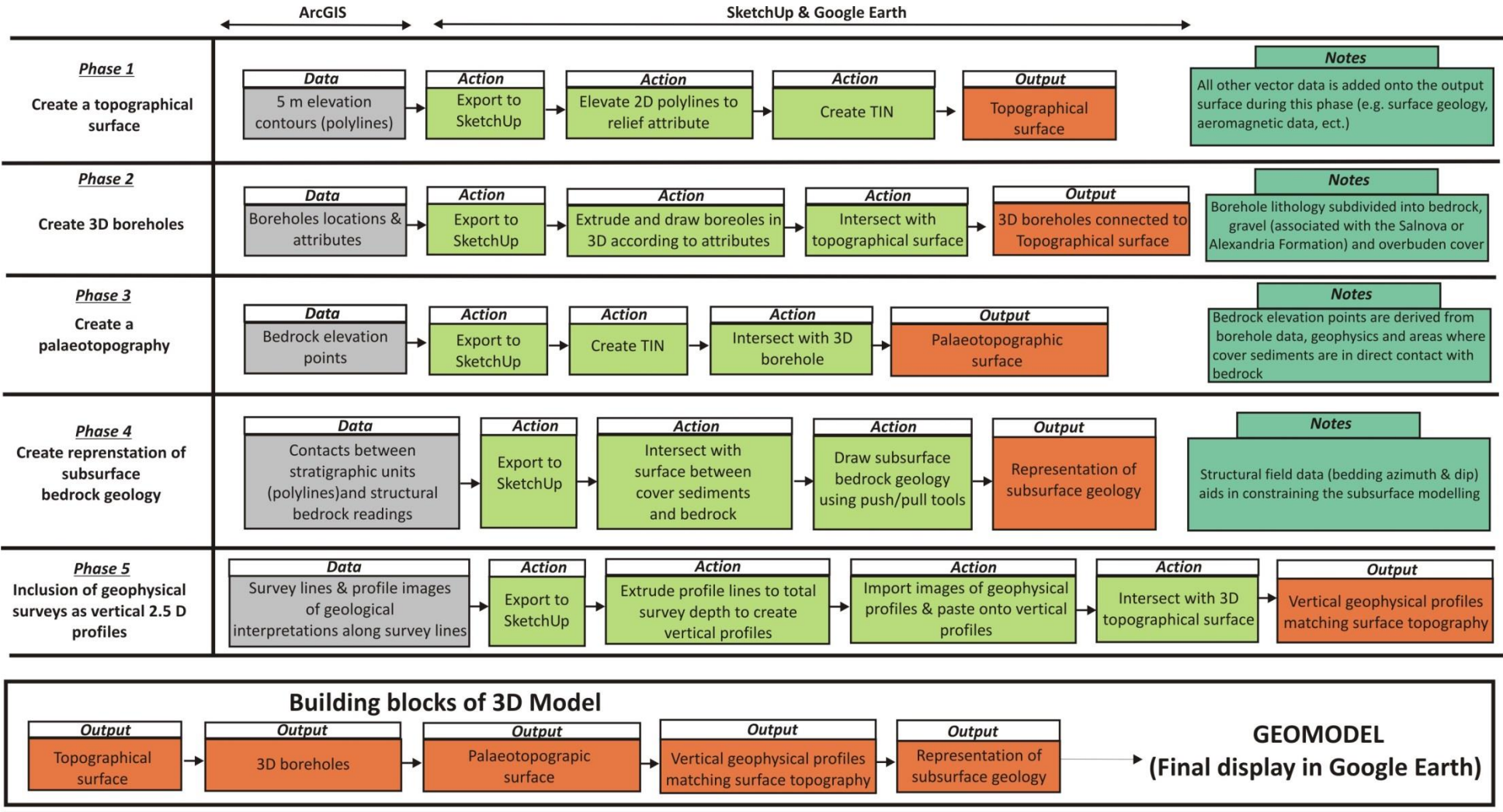
Figure 4.13: Flow chart outlining the geomodel construction process composed of five phases.

4.5.3.1 Scale of 3D model

The model was constructed on a 1:1:1 scale (scaleX(1), scaleY(1), scaleZ(1)) with no vertical exaggeration. This was done to maintain an accurate depiction of fold structures in the substrate.

4.5.3.2 Spatial interpolation methods for geomodel

Interpolation methods are utilized to create 3D surfaces of the topography and palaeotopography beneath cover sediments of the Algoa Group from known and/or calculated 2D vector data (relief points and contour lines) (Table 4.6). The selection of an interpolation method took certain known and assumed characteristics about the current and antecedent landscape relief into consideration. The various terrain complexities within the study area include:

• Highly variable and dynamic E-W striking and undulating dune topography forming part of the Oyster Bay–St. Francis headland bypass dune field

• Coastal and inland bedrock relief exhibit linear NW-SE trending topographic highs and depressions in response to differential weathering of the varying lithologies comprising formations within the study area.

• Along coastal exposures, bedrock is cut by numerous gullies that trend parallel, perpendicular and oblique to NW-SE bedding. It is assumed that the antecedent landscape topography beneath overburden will exhibit similar gullies.

The Delaunay triangulated irregular network (TIN) method of interpolation was used to create the 3D surfaces. The method interpolates a surface composed of a network of contiguous, non-overlapping triangles that satisfies the requirement that a circle drawn through three vertices (in this case elevation points) of a triangle will contain no other vertex and thereby ensures that no vertex lies within the interior of any of the circumcircles of the triangles in the network (Figure 4.14) (Jones, 2014.)

The Delaunay TIN interpolation method satisfies the requirements of the study area's data distribution, its topography and palaeotopography, by interpolating surfaces at different levels of resolution. The method is able to provide higher resolution in areas where relief is highly variable and / or more detail is required or by providing lower resolution in areas that are less variable. The precision of input data is preserved while modeling the relief points between known points. The method is able to interpolate effectively between areas of no or very limited data with favourable visual appearance. In addition SketchUp software allows modification of individual TIN surface if and where required, with the option of various smoothing techniques (Murdock, 2010).

4.5.3.3 Process of model construction

Figure 4.14 outlines the model construction process. The geomodel is composed of five construction phases. Any additional data such as borehole attribute data, field photos, stereonets or graphs are displayed in pop-up windows using keyhole markup language.

(a)

Vertices
(in this case bedrock elevation points)

Delaunay TIN surface

Circle drawn through 3 vertices only

Interpolated surface

(b)

(c)
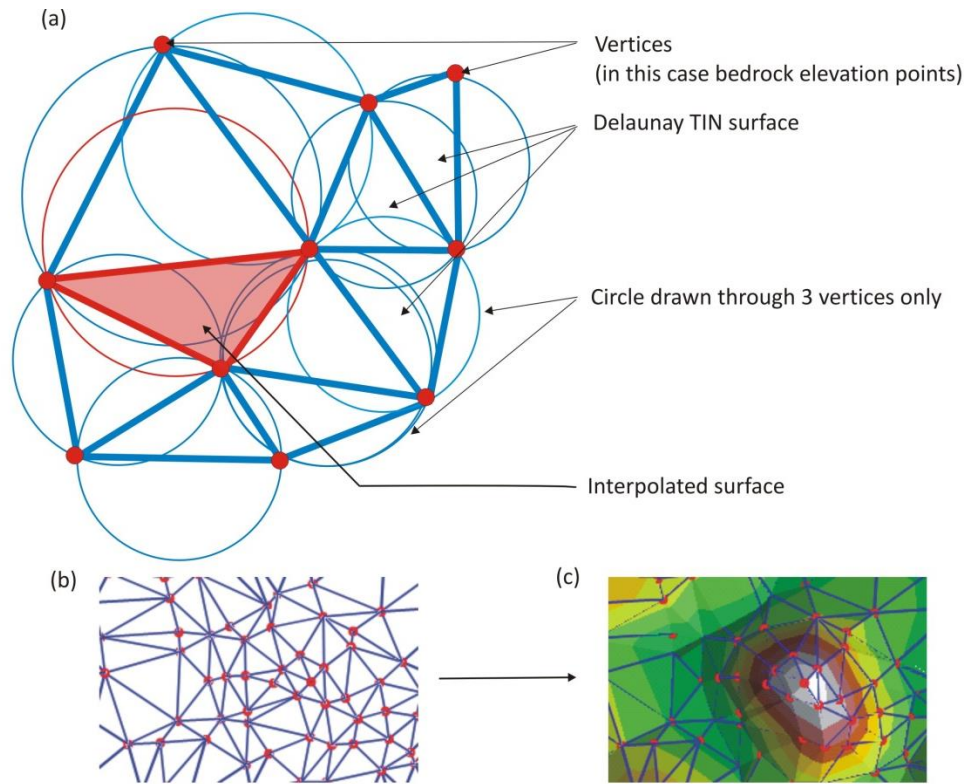
Figure 4.14: (a) Methodology applied to the creation of a Delaunay TIN (Jones, 2014). (b) An example of a Delaunay TIN. (c) An example of a Delaunay TIN showing interpolated surfaces (Jones, 2014).

5. Results

5.1 Field investigation

The study area exhibits minimal exposed outcrop. Outcrop of the Cedarberg and Baviaanskloof Formations (TMG) and Bokkeveld Group are not exposed within the study area. The lithologies and structure of the TMG are described predominantly from exposed outcrop along a narrow (30-250 m wide) NW-SE trending, south-facing, relatively straight and rocky coastline south of vegetated dune deposits associated with the Algoa Group. Consequently, additional, but limited field work was undertaken in areas immediately outside the study area and is presented here in combination with borehole data. For the location of specific boreholes mentioned below, refer to borehole maps in Appendix C3.

The sections below detail the lithologies of the TMG and Bokkeveld Group. See chapter 4.2 for detailed characterisation of the study area's structural geology. Table 5.1 provides a summary of lithostratigraphic units within the study area.

Table 5.1: A lithostratigraphic summary of rock types in the study area (modified after SACS, 1980; Goedhart et al., 2008).

Age	Super-group	Sub-group	Group	Formation	Lithological Description	Outcrop Exposure
Cenozoic (cover sediments) Holocene 0 - 11.7 ka			Algoa	Schelm Hoek	Aeolian sand, soil horizons, and middens	Well exposed
Pleistocene 11.7 ka - 1.8 Ma				Nahoon	Aeolian calcareous sandstone, palaeosols, and subordinate calcrete	Limited exposure
				Salnova	Marine and/or estuarine calcareous sandstone, siltstone, coquinite and basal gravels	Not exposed
Pliocene Miocene - 1.8 Ma - 23 Ma				Nanaga	Calcareous sandstone (aeolianite), palaeosols, subordinate and calcrete,	Not exposed
				Alexandria	Calcareous sandstone, semi-consolidated conglomerate, coquinite and basal gravels	Not exposed Limited exposure outside study area
~~ UNCONFORMITY ~~~~~~						
Palaeozoic (Bedrock) Devonian 359 Ma - 416 Ma	Cape		Bokkeveld		Black to brown shale, subordinate siltstone and is fossilferous	Limited exposure
		Nardouw	Table Mountain	Baviaanskloof	Impure feldspathic sandstone, subordinate shale	Not exposed Limited exposure outside the study area
Silurian 416 Ma - 444 Ma				Skurweberg	Quartzite, medium- to coarse-grained, profusely cross-bedded, subordinate shale	Well exposed
				Goudini	Brown-weathering thinly bedded siltstone, mudstones, quartzite	Limited exposure Limited exposure outside the study area
Ordovician 444 Ma - 488 Ma				Cedarberg	Black shale, laminated	Not exposed Limited exposure outside the study area
				Peninsula	Quartzite, massive and laminar and cross bedded, medium- to coarse-grained	Well xposed
~~ UNCONFORMITY ~~~~~~						
Basement Namibian 542 Ma - 630 Ma			Gamtoos		Quartzite, phyllite, conglomerate, limestone	Not exposed

5.1.1 Table Mountain Group

5.1.1.1 Peninsula Formation

The Peninsula Formation comprises white to light grey (N9 – N7), supermature and medium-grained, quartzite, interbedded with subordinate fine-grained dark grey (N3) to black (N1) carbonaceous shale horizons (Figure 5.1 a & b). The quartzites are well bedded and bedding layers are generally medium (10 - 30 cm) to very thick bedded (>100 cm), but do appear massive in places, containing no discernible bedding planes. Sedimentary structures in quartzites include large-scale (> 6cm) trough cross-bedding and planar cross-bedding (Figure 5.1 a). Tabular cross-bedding display both angular and tangential basal contacts. Herringbone cross-bedding is often observed west of Seal Point (Figure 5.2 a & b). Cross-lamination with set heights of <6 cm is also observed. Other frequent sedimentary structures include horizontal lamination and channel structures. Soft sediment deformation structures occur sporadically within the formation. Cross-beds are often folded over and contortion is observed at the top of beds (Figure 5.3). Quartzites occasionally display normally graded bedding (Figure 4.4). In most cases the grading of particle sizes are subtle and coarse particles located at the base of the graded bed are generally <5 mm in size. Thin to medium bedded layers of matrix supported conglomerate contain sub-angular to well rounded clasts of granular (2 – 4 mm) to pebble size (4 - 64 mm) (Figure 5.4). Quartzites are occasionally stained pink or red by iron oxides.

Subordinate shale horizons, generally <1.5 m in thickness are documented west of the Seal Point lighthouse along coastal exposures (Figure 5.1 a & b). Shale units are thinly bedded (3-10 cm) and contain planar lamination in a parallel sequence. Farther inland (250 m from De Hoek) borehole data (Raubenheimer *et al*., 1988 a; Raubenheimer *et. al*., 1988 b) intercept "*greenish grey to dark grey*" shale layers of up to 3 m thick.

Herringbone cross-bedding is a frequent occurrence and indicate a bimodal flow direction (Figure 5.2 a & b). Subtle normally graded bedding is indicative of waning flow in a turbidity or storm current (Figure 5.4). These sedimentary structures in combination with predominant arenaceous lithology of the Peninsula Formation support work by previous authors (Theron & Thamm, 1990, Thamm & Johnson, 2006) indicating a tidal, shallow marine palaeo-environment for the Peninsula Formation. Soft sediment deformation features (overturned cross-beds) observed at the top of beds (Figure 5.3). These structures are formed when newly laid sediment is deformed by a successive pulse of sedimentation, prior to lithification (e.g. Tucker, 2011) and indicate that some deformation of sedimentary structures may have taken place prior to lithification.
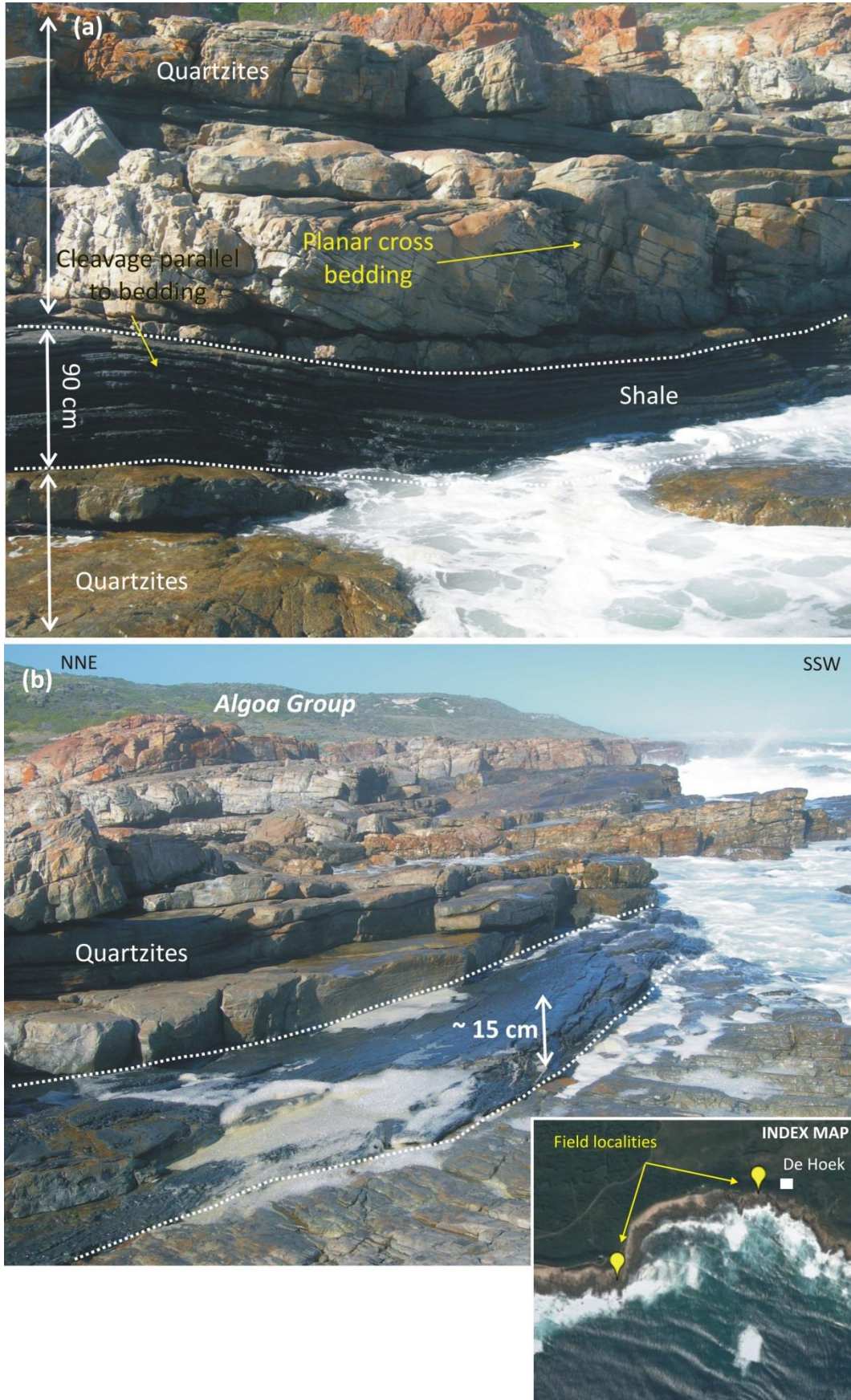
Figure 5.1: (a) A coastal exposure of competent quartzites of the Peninsula Formation, interbedded with very subordinate dark-grey mudrock (90 cm in thickness) at De Hoek (Lat: 34° 11' 48.1" Long: 24° 47' 39.0"). (b) Looking east along coastal exposures immediately east of De Hoek. A ~15 cm thick black shale unit is interbedded with quartzites of the Peninsula Formation. Note the undulating dune cover (Algoa Group) in the background.
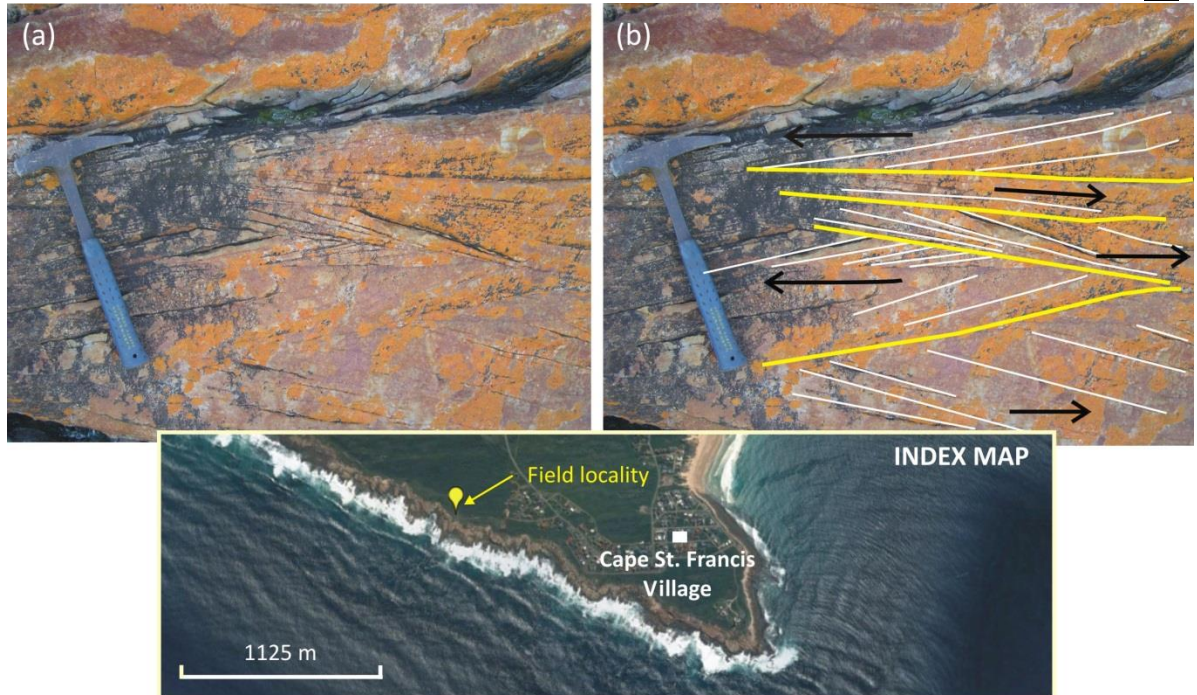
Figure 5.2: (a & b) Photo without and with annotation showing herringbone cross-bedding observed in quartzites of the Peninsula Formation (Lat: 34° 12' 25.3" Long: 24° 49' 08.1"). Cross beds display tangential basal contacts. Cross-bedding is depicted by black lines; the direction of flow is indicated with black arrows and the cut-off (erosion) surface between bi-direction cross-bedding is annotated by yellow lines.
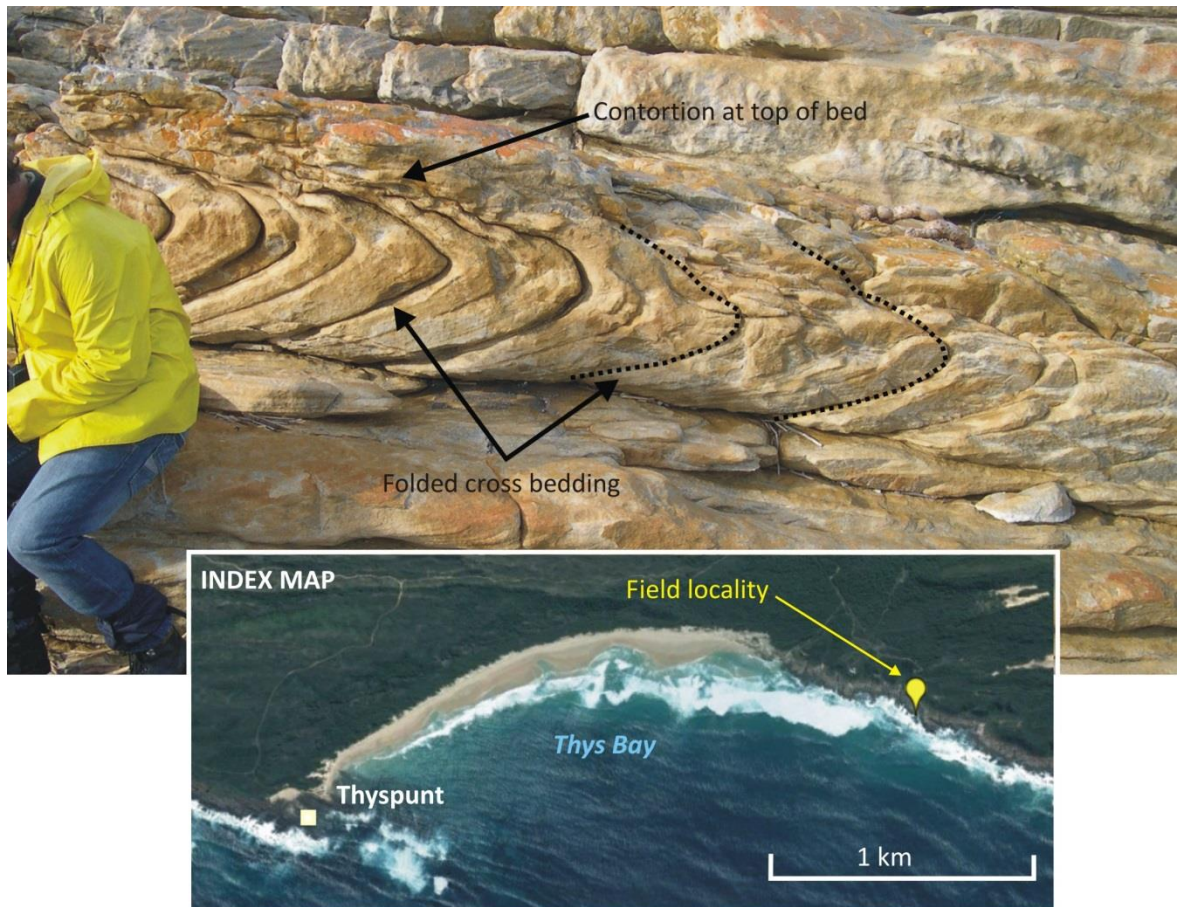
Figure 5.3: Soft sediment deformation in quartzites of the Peninsula Formation along coastal exposures east of Thys Bay (Lat. 34° 11' 20.6" Long. 24° 44' 34.1").
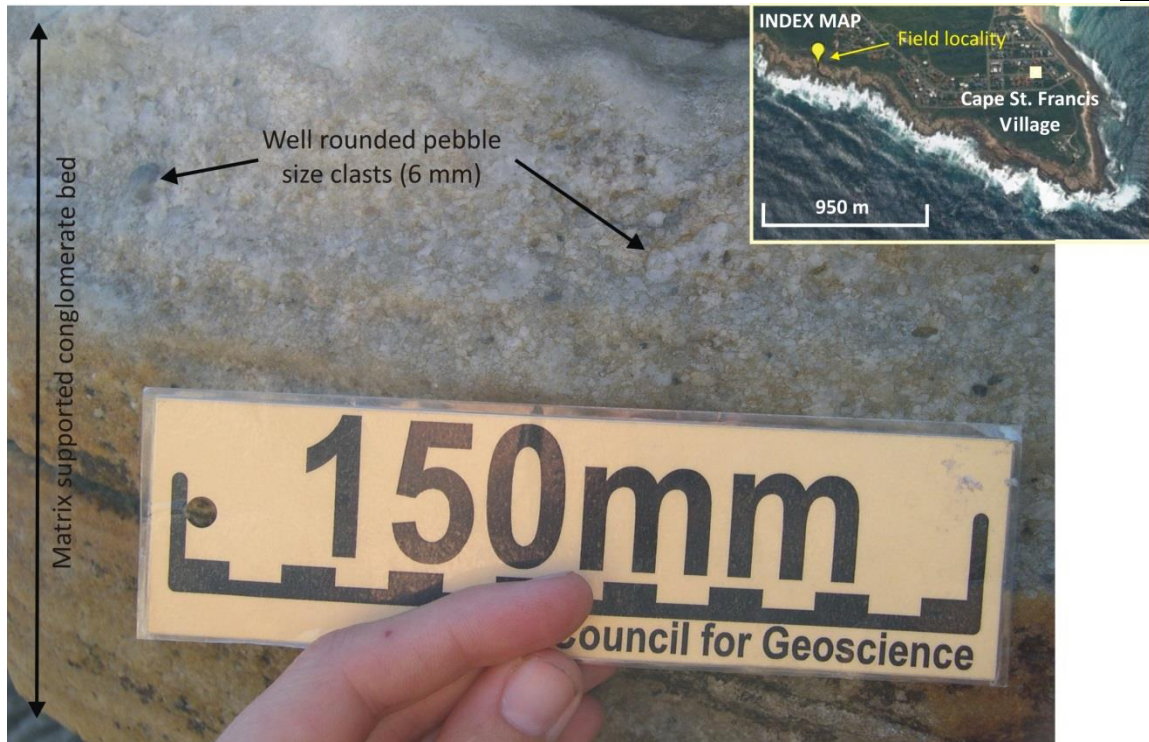
*Figure 5.4: Matrix supported conglomerate bed within the Peninsula Formation (Lat: 34° 12' 27.0"
Long: 24° 49' 15.9").*

The Peninsula Formation is unconformably overlain by Algoa Group sediments (Figure 5.5). Limited
outcrop exposure prevented description of formation's upper contact with the Cedarberg Formation.
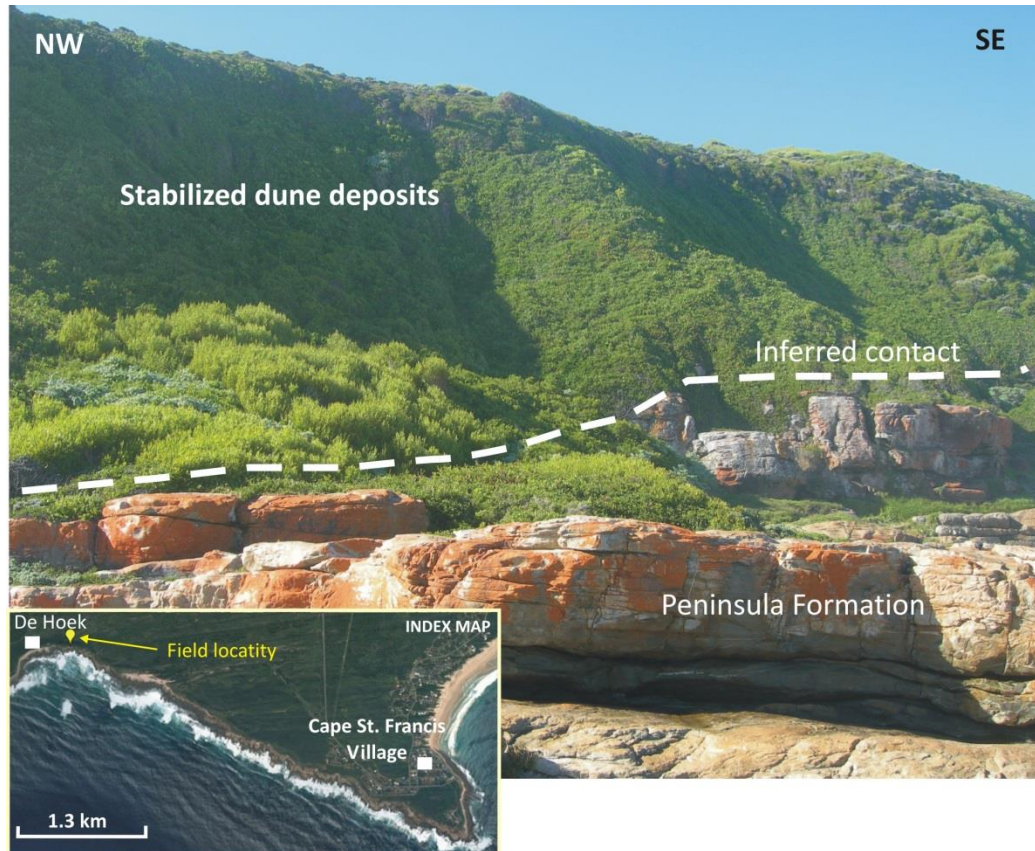
*Figure 5.5: Coastal quartzites exposures of the Peninsula Formation overlain by sediments of the Algoa
Group (Lat: 34° 11' 48.1" Long: 24° 47' 39.0").*

5.1.1.2 Cedarberg Formation

The Cedarberg Formation consists of very dark grey (N3) to black (N1), fine-grained carbonaceous shale (Figure 5.6a & b) containing infrequent thin bedded siltstone (Figure 5.7). Shales are predominantly thin to medium bedded and display few sedimentary structures. Shales exhibit planar lamination of a horizontal, wavy or discontinuous nature. Weathered exposures appear moderate yellow (5Y 6/4), light olive brown (5Y 5/6) and greyish yellow (5Y 8/4) (Figure 5.7). The contact could not be directly observed within the field due to limited outcrop exposure. The formation's lower contact with the Peninsula Formation (Figure 5.7) is described by other others as sharp, while the upper contact with the Goudini Formation is gradational (Toerien & Hill, 1989; Johnson *et al.*, 1999). Limited exposed outcrop also hampered differentiation between the lower Soom and upper Disa Member across the study area. In borehole data the occurrence of dark grey to black shale is association with the basal Soom Member (Figure 5.6 b) while more argillaceous and pale coloured shales are associated with the Disa Member.

Figure 5.6: (a) Rarely exposed dark grey to black, fine-grained Cedarberg Formation visible at the base of a valley NW of Humansdorp, outside the study area (Lat: 33° 51' 44.5"; Long: 24° 35' 42.1"). Photograph taken by M.L Goedhart. (b) Black, thinly laminated carbonaceous shale of the Cedarberg Formation (possibly Soom Member). The formation is intercepted at Thyspunt in borehole core as seen in borehole CSF-14 (Hanson et al., 2012) between 56.68 m and 57.18 m below ground level. Location of the borehole: Lat: 34° 11' 52.9"; Long: 24° 49' 25.9".
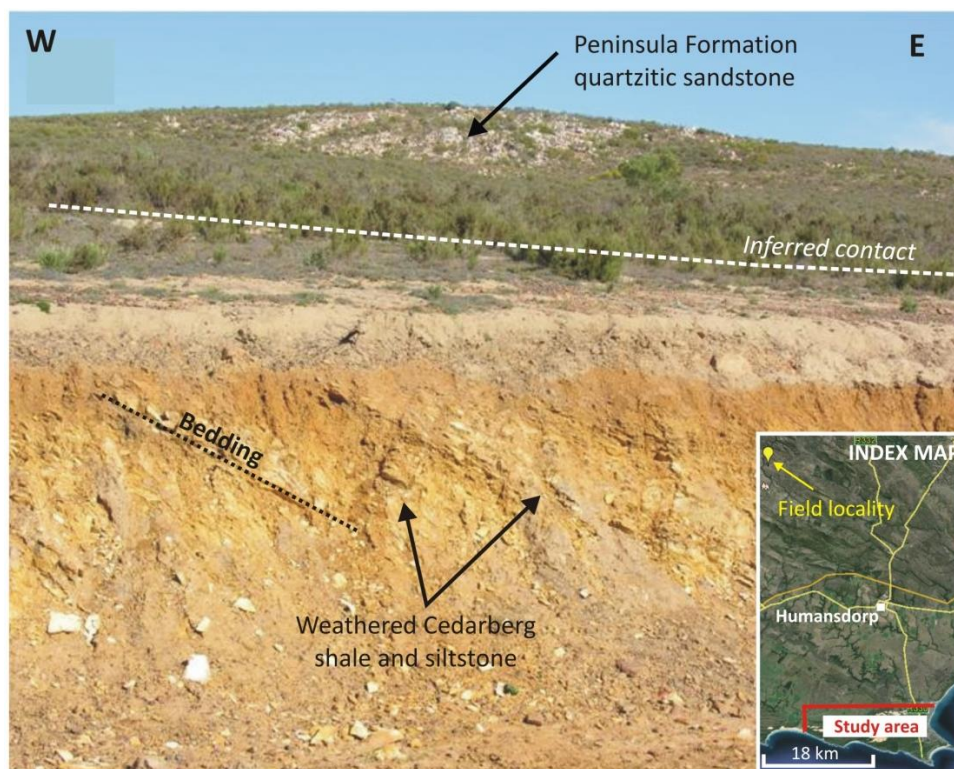
Figure 5.7: Light brown to yellowish brown weathered shale and siltstone units of the Cedarberg Formation (possibly the Disa Member). Note the elevated quartzitic ridge of the Peninsula Formation in the background (Lat: 33° 52' 13.0"; Long: 24° 36' 35.1").

5.1.1.3 Goudini Formation

Outside the study area, east of Humansdorp and NW of Kruisfontein outcrop of the Goudini Formation is well exposed in low relief areas flanked by quartzite ridges associated with the Skurweberg Formation. Within the study area, exposures of the formation are limited, but can be observed along a small, still uneroded strip towards the eastern end of the Cape St. Francis Bay (Figure 5.8 a). A similar uneroded strip of outcrop occurs along the western end of Thys Bay where its basal contact with the Skurweberg Formation is transitional over at least 25 m (Goedhart *et al.*, 2008) (Figure 5.8 b & c).

The Goudini Formation is comprised of fine to medium-grained quartzose sandstone interbedded with subordinate shale and siltstone horizons. In unweathered exposures, sandstones appears very light grey (N4) to medium dark grey (N8) (Figure 4.9), pinkish grey (5YR 8/1) or greyish yellow (5Y 8/4) (Figure 5.10 a). Weathered exposures appear moderate yellow (5Y 7/8) and light yellowish orange (10 YR 8/6). Yellow-brown to reddish weathering hues are imparted on rocks as a consequence of iron and manganese oxidation. Sandstones are generally medium (10-30 cm) to thick bedded (30-100 cm) and are commonly cross-bedded and less commonly laminated. Finer-grained sandstone is generally more massive, showing no discernable sedimentary structures. Tabular sandstone also appears siliceous in places. Subordinate shale and siltstone is more frequently thin bedded (3-10 cm) and is generally structureless or contain planar parallel lamination. Thin <0.5 m very light grey micaceous shale layers were observed north of Humansdorp (Figure 5.10 b). The very dark grey (N3) siltstones and occasional sandstone beds are frequently highly bioturbated obliterating nearly all primary sedimentary structures (Figure 5.11 a & b).
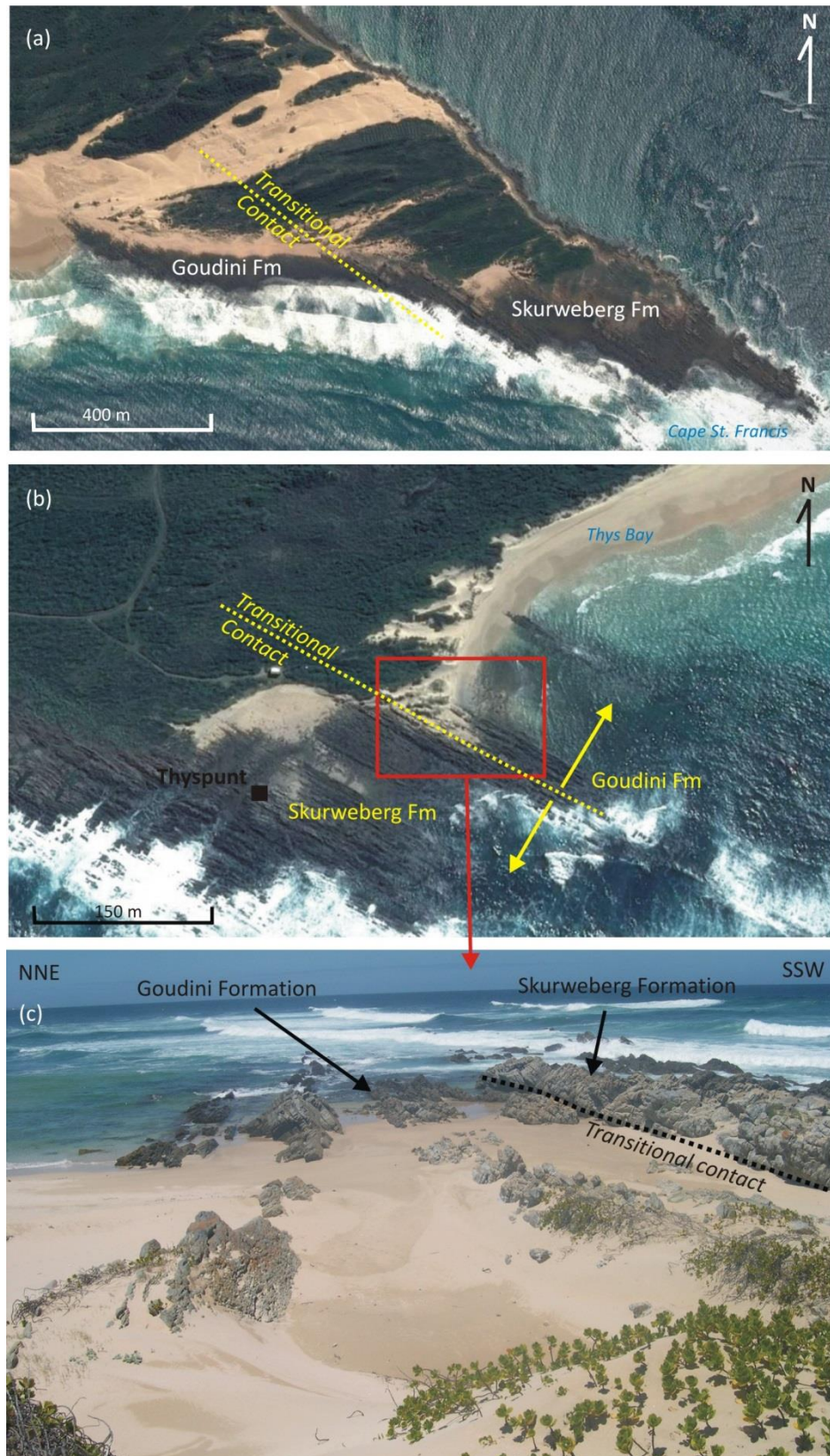
Figure 5.8: (a) The upper transitional contact of the Goudini Formation with the Skurweberg Formation at Cape St. Francis and (b) Thyspunt. (c) Enlarged area of at Thyspunt (Lat: 34° 11' 32.8"; Long: 24° 42' 57.1").

Figure 5.9: Medium dark grey, fine-grained and fractured sandstone of the Goudini Formation observed on borehole NEW24, between 39.56 – 47.16 m below ground level, 1.5 km NNW of Thyspunt. Note the cross-bedding.
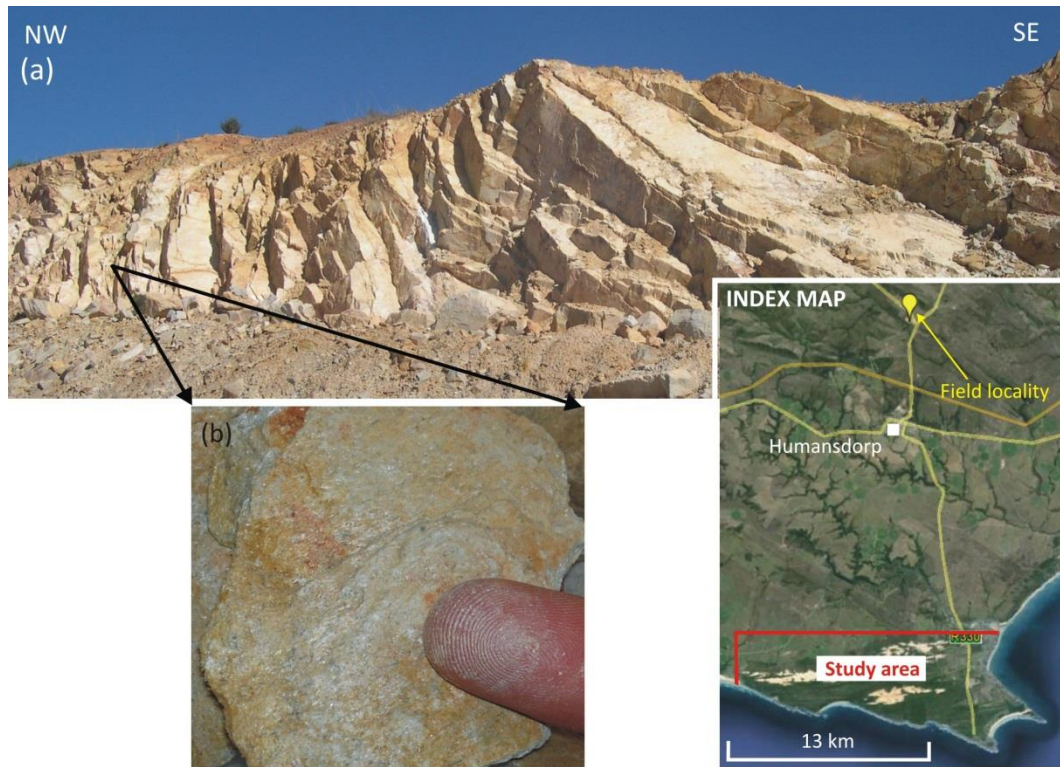
Figure 5.10: (a) Fine to medium-grained sandstone of the Goudini Formation exposed along the northeastern wall the Zwartebosch Quarry (Lat: 33° 58' 09.7"; Long: 24° 46' 30.2"). (b) Very pale grey and thin (<0.5 m) micaceous shale with pale orange-brown iron and manganese oxidation observed taken from at the same quarry (Lat: 33° 58' 09.8"; Long: 24° 46' 30.7").
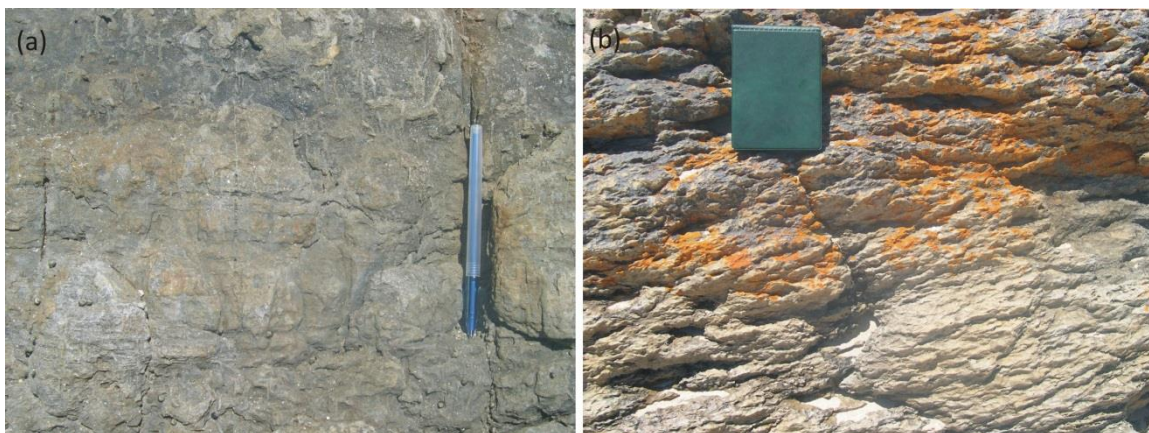
Figure 5.11: (a) Bioturbated siltstone of the Goudini Formation, showing vertical tubes at Thyspunt (Lat: 34° 11' 32.2"; Long: 24° 42' 57.6"). (b) Bioturbated sandstone of the Goudini Formation has completely obliterated primary sedimentary structures (Lat: 34° 11' 31.7"; Long: 24° 42' 57.1").

5.1.1.4 Skurweberg Formation

The Skurweberg Formation is composed of white (N9) to light grey (N7) mature quartzites (Figure 5.12) interbedded with subordinate greyish green (10GY 5/2) to medium grey (N5) shale and grey-wacke units (Figure 5.13 a & b), medium grey (N5) siltstones and conglomerate stringers. Quartzites are moderately sorted and medium to coarse-grained. The formation is generally medium (10 -30 cm) to thickly bedded (30-100 cm) and although beds can appear massive; planar and trough cross-bedding are frequent occurrences. Tabular cross-bedding display both angular and tangential basal contacts. Asymmetrical ripple marks atop bedding surfaces were also noted (Figure 5.14).

Subordinate grey-wacke units are generally <10 m thick and are laterally persistent. Thinning and thickening of siltstone units along strike is however observed (Figure 5.13 a). Grey-wackes are thin bedded (1-3 cm) to medium bedded (10 -30 cm). Grey-wackes are generally structureless or display planar horizontal lamination (Figure 5.15 a). Bioturbation is a common occurrence (Figure 5.15 b). Along coastal exposures the lithologically less competent grey-wacke and shale units form a favourable erosion zone, producing bedding parallel gullies west of Oyster Bay.

Borehole log descriptions (Raubenheimer *et. al.*, 1988 b; Eskom, 2010 a, Eskom, 2010, b) indicate an increase in the number of shale units in close proximity to the contact between the Skurweberg and Goudini Formations. Near Tony's Bay borehole data show quartzites frequently interbedded with red shales layers. These iron rich shales occur as lenses, stringers or medium thick beds and are predominantly observed NW of Tony's Bay in boreholes TB16 (Figure 5.16), NEW30, NEW29 and BHDH2. The occurrence of thinly bedded, highly cleaved medium grey shales interbedded with fine-grained sandstones is responsible for the development of the NW-SE trending linear embayment at Tony's Bay. Descriptions of borehole core by Raubenheimer *et. al.* (1988 b) indicate the presence of conglomerate units <1 m with pebble sized clasts in the Thyspunt and Tony's Bay area.

Figure 5.12: NW-SE trending, steeply dipping (60° SW) bedding of light grey quartzites from the Skurweberg Formation (Lat: 34° 10' 34.4" Long: 24° 39' 46.3").
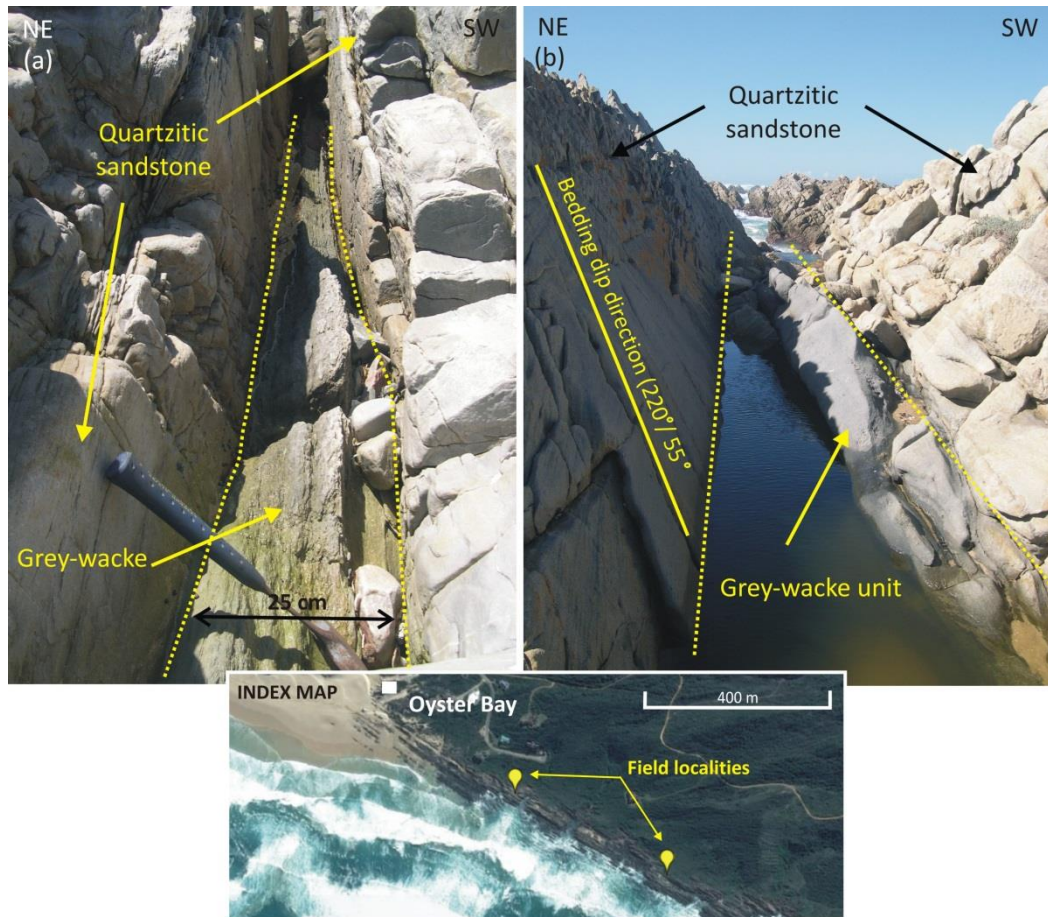
Figure 5.13: *(a) A ~25 cm light olive grey grey-wacke thinning in a southeasterly direction (Lat: 34° 10' 35.5" Long: 24° 39' 48.4"). (b) Quartzites of the Skurweberg Formation interbedded with a 3 m grey grey-wacke unit. Note the development of a gully trending parallel to bedding as the lithologically less competent grey-wacke unit erodes out (Lat: 34° 10' 41.1" Long: 24° 40' 01.1").*
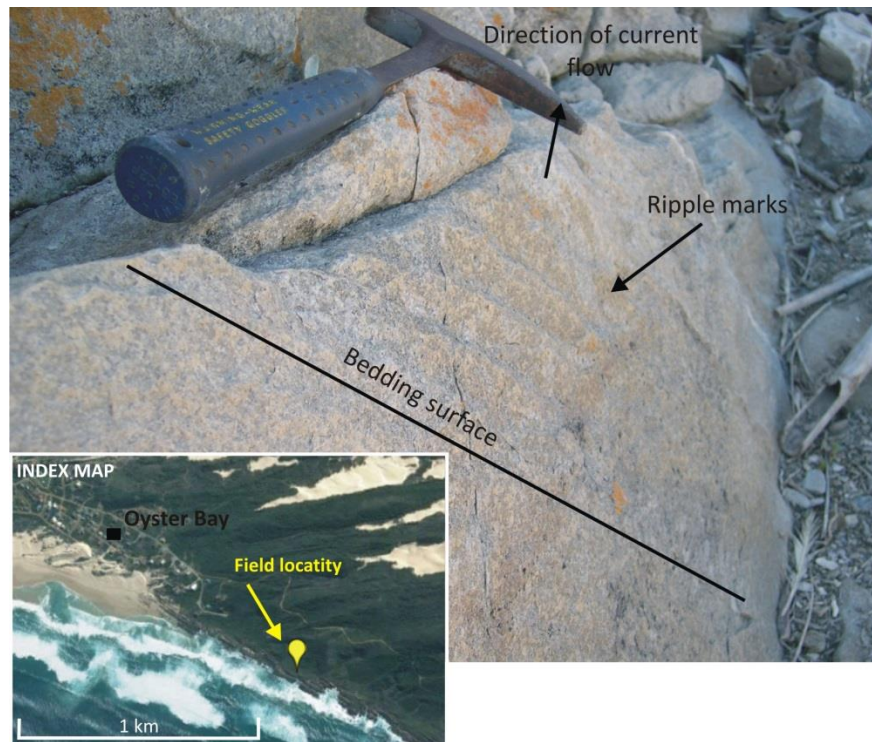
Figure 5.14: *(a) Asymmetrical ripple marks observed on the bedding surface of a quartzite within the Skurweberg Formation (Lat: 34° 10' 41.5" Long: 24° 40' 03.5").*
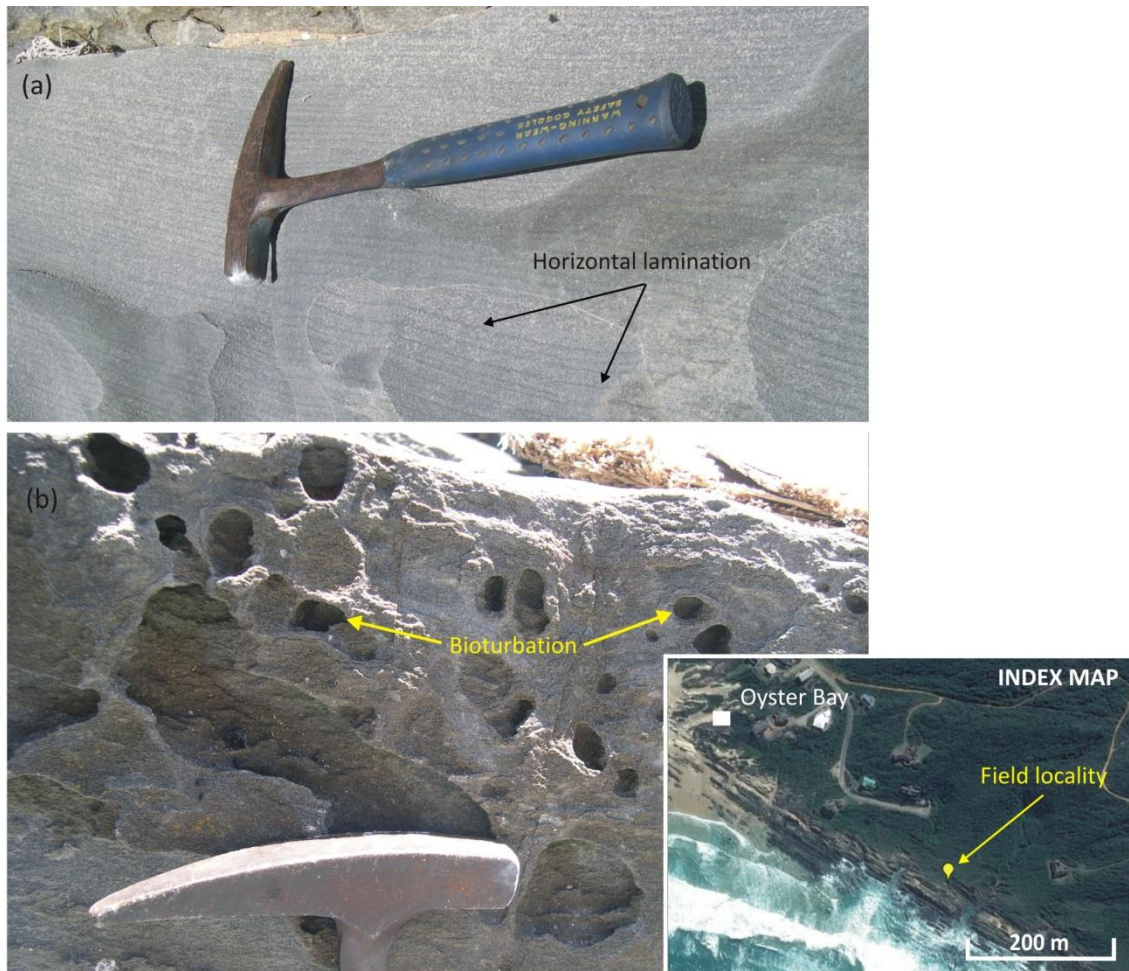
Figure 5.15: (a) Grey-wacke unit within the Skurweberg Formation showing planar horizontal lamination (Lat: 34° 10' 36.4" Long: 24° 39' 52.0"). (b) Bioturbated bedding surface of siltstone unit within the Skurweberg Formation (Lat: 34° 10' 36.4" Long: 24° 39' 52.0").
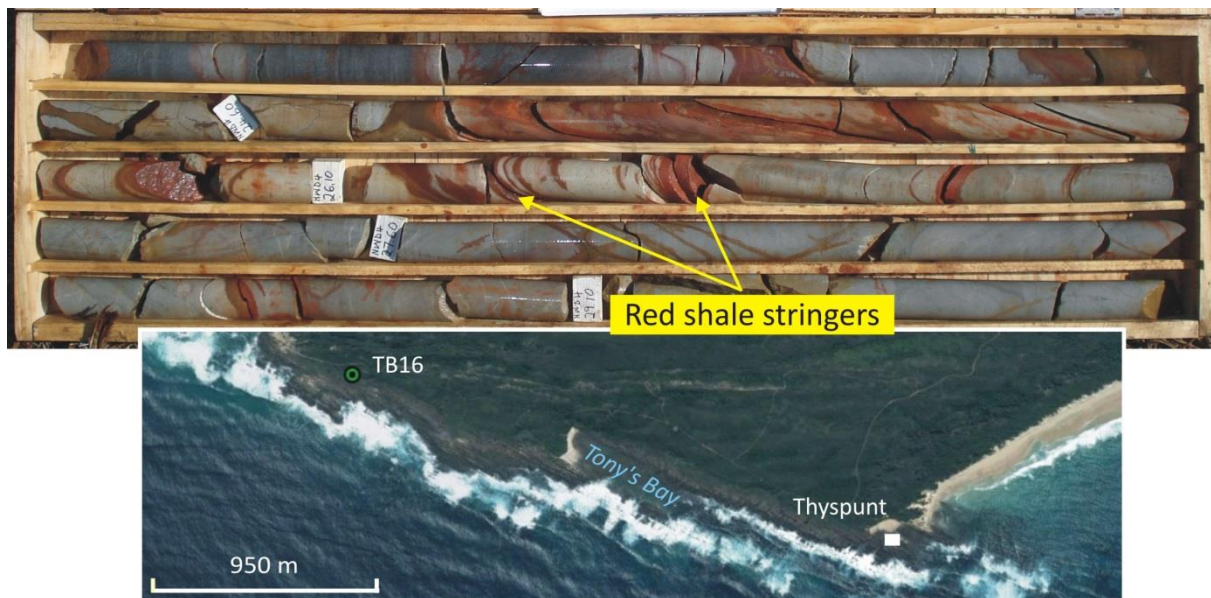
Figure 5.16: Grey quartzitic sandstone of the Skurweberg Formation display layers of red possibly ferruginous shale stringers observed in borehole TB16 at a depth between 23.1-29.8 m below ground surface (Lat: 34° 11' 10.9" Long: 24° 41' 22.0").

5.1.1.5 Baviaanskloof Formation

Northeast of Humansdorp the Baviaanskloof Formation is exposed in road cuttings along the N2, 13 km NNE of the study area and field observations presented here, are mainly based on these exposures. The Baviaanskloof Formation is comprised of immature fine and coarse-grained sandstone (Figure 5.17), mature feldspathic sandstone, mudrock and siltstone. Although minor rhythmite is reported within the Baviaanskloof Formation (Hill, 1991), the lithology was not observed during field investigation. Sandstone of the Baviaanskloof Formation is light grey (N7) to dark grey (N3) in colour and weathers to a light grey (N8) or light yellowish orange (10YR 8/6) colour (Figure 5.18). Grain sizes are generally fine to very fine-grained. Near the middle of the formation, more medium to coarse-grained and mottled sandstone, possibly associated with the Kareedouw Member, is observed approximately 5 km west of Jeffreys Bay, along a road cutting on the R102 (Figure 5.17). Sedimentary structures observed in sandstone include planar parallel and curved parallel lamination (Figure 5.19), micro-cross lamination and wavy bedding. Hill, (1991) observed rare cross-bedding and ripple marks; however these structures were not observed during field investigation. Sandstones appear predominantly massive. The thickness of sandstone units were difficult to determine without substantial and continuous exposure, however Hill (1991) reported sandstone units within the Baviaanskloof Formation varying between 7 to 40 m in thickness.

Subordinate siltstone within the Baviaanskloof Formation is light grey (N7) to dark grey (N3) (Figure 5.20). Siltstones are lenticular-bedded and display planar parallel lamination (Figure 5.20) and planar wavy lamination. Structureless siltstones were also observed. Siltstone units are generally <2 m in thickness. Siltstones and dirty sandstones are frequently bioturbated and contain invertebrate casts, shells, crinoids and horizontal tube-like burrows (De Beer, 2000), although none were identified during field investigation.

Exposures of pale grey (N7) to dark grey (N3) mudrock units within the Baviaanskloof Formation were very limited. Mudrock units were thin, usually <1 m in thickness and appear to be devoid of sedimentary structure.

Figure 5.17: Grey, medium to coarse-grained mottled sandstone of the Baviaanskloof Formation (possibly associated with the Kareedouw Member) exposed along a road cutting 5 km west of Jeffreys Bay. (Lat: 34° 01' 41.0" Long: 24° 51' 24.1").

Figure 5.18: Highly weathered immature and fine-grained feldspathic sandstone of the Baviaanskloof Formation at Sunny Side Dam, 22 km NE of Thyspunt. The sandstone is imparted with brown to yellow iron and manganese oxidising hues (Lat: 34° 00' 55.5" Long: 24° 51' 32.3").
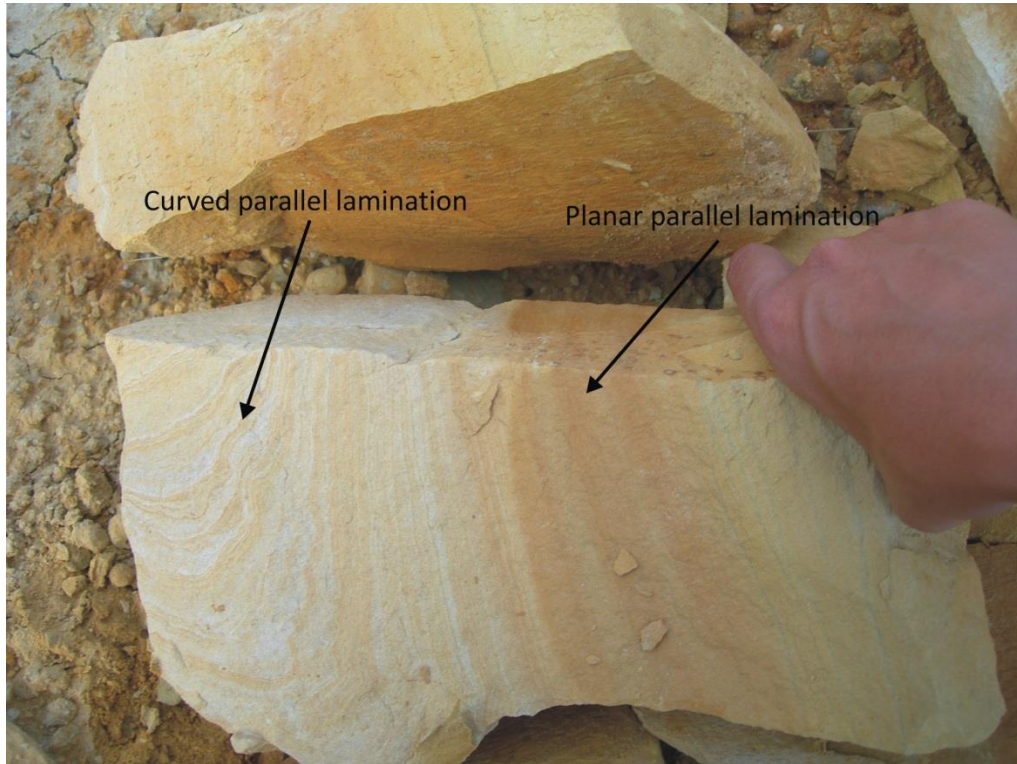
Figure 5.19: Weathered, immature and fine-grained sandstone of the Baviaanskloof Formation showing curved parallel and planar parallel lamination. Photo taken in close proximity to the locality indicated in Figure 5.18 's index map (Lat: 34° 00' 55.5" Long: 24° 51' 32.3").

Figure 5.20: Weathered light grey siltstone of the Baviaanskloof Formation with planar parallel lamination Photo taken at the same locality as indicated in Figure 5.17's index map (Lat: 34° 01' 40.5" Long: 24° 51' 13.8").

5.1.2 Bokkeveld Group

The incompetent argillaceous lithologies comprising the Bokkeveld Group erode easily to produce low topographic relief within the study area and surroundings. Consequently outcrop exposures of the Bokkeveld Group are limited. Descriptions presented here are based on exposures of strata in road cuttings along the R330 (road between Humansdorp and Cape St. Francis) 7 km outside the study area. Boreholes SRK-4, SRK-5, SRK-6, SRK-8, SRK-10, SRK-11, SRK-12 and SRK-17 (Maclear; 2002; Maclear, 2005; Maclear, 2006) within the study area west of St. Francis intercepted strata of the Bokkeveld Group, but borehole cores were poorly described and could not aid in defining detailed characteristics of the group. Limited outcrop exposure also did not allow for differentiation of strata to formation level.

The Bokkeveld Group comprises of medium dark grey (N4) to dark grey (N3) carbonaceous often "pencil" fractured shale and light olive brown (5Y 5/6), yellowish grey (5Y 7/2) and very light grey (N8), fine grained sandstone. Shales contain planar parallel, planar wavy, micro-cross lamination and lenticular bedding (Figure 5.21 a & b). Shale units contain elongated and oval shaped sandstone lenses. Sandstone lenses are 4 -10 cm in width and generally < 1.5 m in length (Figure 5.22 a). Shales are occasionally interbedded with thin light grey quartzose units of less than 30 cm in thickness (Figure 5.22 b). Unweathered shales occasionally contain scattered pyrite in borehole core (SRK-1). At the surface pyrite oxidizes to form limonite, producing reddish and yellow brown 'rust' spots up to 2 cm in size on weathered shale exposures. Exposures are often fossiliferous, containing mainly invertebrate fossils and early plant remains, however no fossils were observed in roadside cuttings.
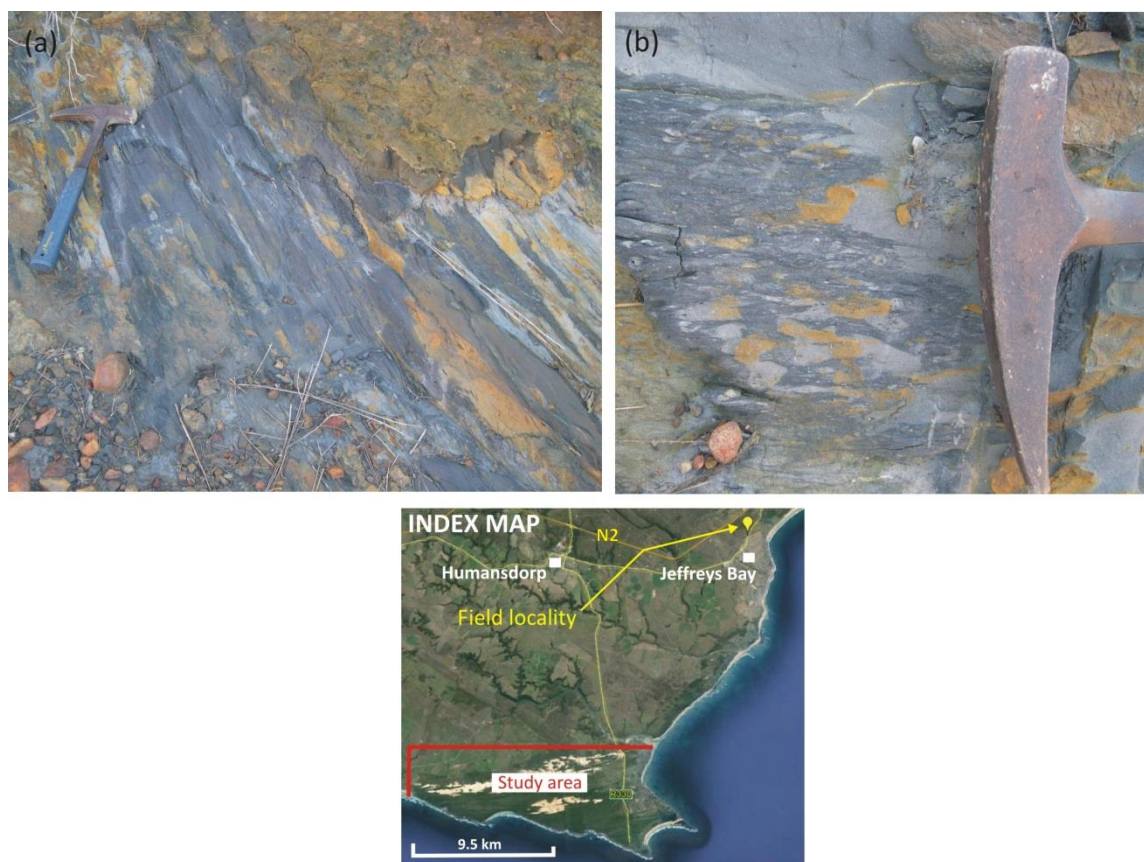
Figure 5.21: (a & b) Lenticular bedding observed in dark grey weathered shale of the Bokkeveld Group (Lat: 34° 00' 45.9" Long: 24° 54' 50.4").
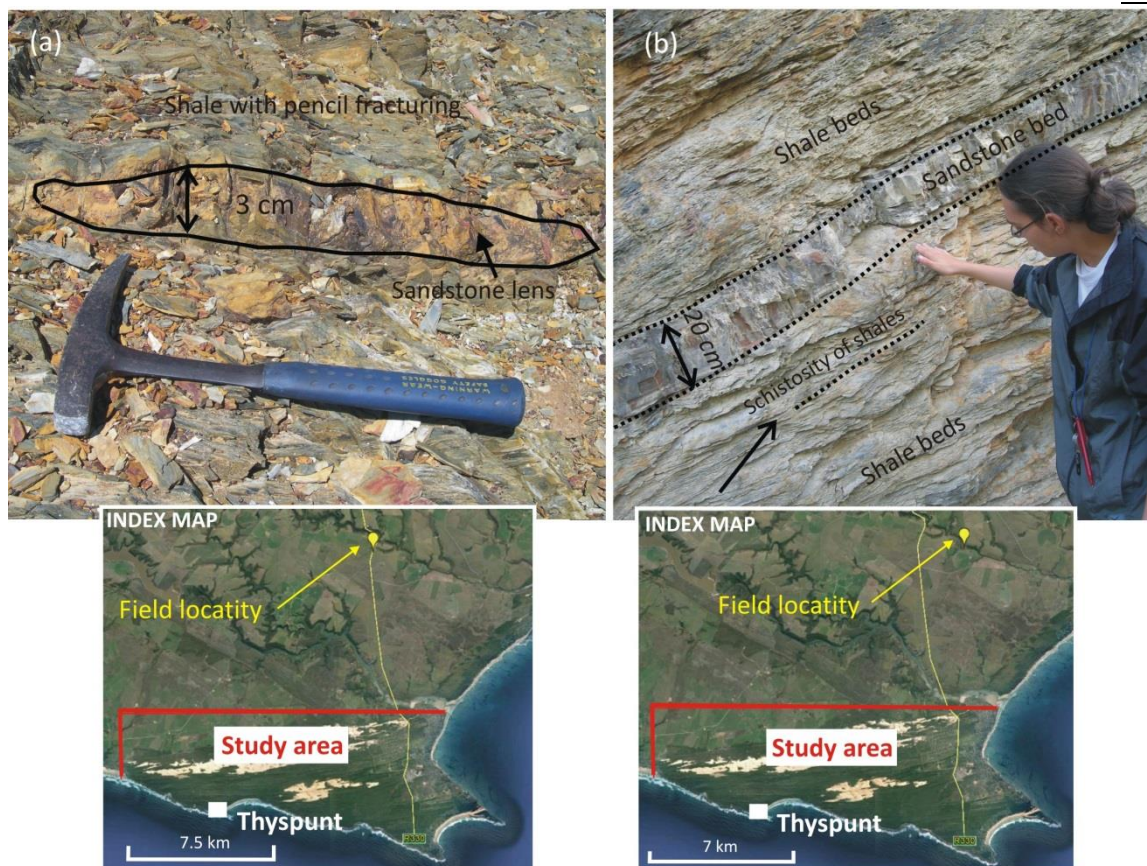
Figure 5.22: (a) A 3 cm thick sandstone lens interbedded with weathered light grey "pencil" fractured shale of the Bokkeveld Group (Lat: 34° 03' 27.4" Long: 24° 47' 41.0"). (b) Weathered schistose shales of the Bokkeveld Group interbedded with a 20 cm thick quartzose sandstone (Lat: 34° 04' 35.1" Long: 24° 49' 19.9").

5.1.3 Algoa Group

Within the study area the Algoa Group sediments make up the Cenozoic overburden above the Palaeozoic bedrock geology. The Algoa Group comprises of the Alexandria, Nanaga, Salnova, Nahoon, and Schelm Hoek Formations (Table 5.1), which consist predominantly of unconsolidated to semiconsolidated clastic nearshore-marine and coastal aeolian-derived sediments (Table 2.1). These mainly aeolian deposits form part of the Oyster Bay–St. Francis bypass dune field which within the study area, extends approximately 4 – 10 km into the hinterland (Figure 1.7). Differentiation between the formations that comprise the Algoa Group is complex due to limited outcrop exposure (obstructed by thick coastal vegetation) and poorly described borehole core. Goedhart *et al.,* (2008) were only able to differentiate between formations in specific locations. They chose to predominantly define the Algoa Group as undifferentiated. Certain detailed borehole log descriptions in combination with photos of the borehole core, did allow for partial differentiation of sediments to formation level (Figure 5.23). The lithostratigraphic description of the Algoa Group provided below is predominantly based on borehole data.

Schelm Hoek Formation

Moderate brown (5YR 4/4) to dusky brown (5YR 2/2), organic, loose to medium dense, silty, fine sand often containing fine shell fragments (topsoil)

Moderate yellowish brown (10YR 5/4), dense to very dense, fine aeolian sand

Yellowish grey (5Y 7/2), very dense often cemented, aeolian sand with very fine shell fragments

Nahoon Formation

Moderate brown (5YR 4/4) to dusky brown (5YR 2/2), highly organic, fine sand, possible palaeo-topsoil

Yellowish grey (5Y 7/2), very dense often cemented, aeolian sand with fine shell fragments

Moderate yellowish brown (10YR 5/4), medium dense, fine aeolian sand

Salnova Formation

Moderate reddish orange (10R 6/6), dense to very dense, silty fine marine sand with fine to occasional coarse shell fragments

Dense, subrounded quarzitic sandstone gravel or pebbles / cobbles / boulders set in a fine to course marine sand matrix with the frequent occurrence of shell fragments

Weathered bedrock contact (associated with topographic bedrock lows)

Bedrock

Figure 5.23: Schematic of the typical lithostratigraphic sequence of the Algoa Group in close proximity to the coastline near Thyspunt.

Borehole loggings describe sporadic thin organic rich relict pedogenic or palaeosoil horizons, generally < 3 m in thickness occurring at various elevations throughout the Algoa Group. Palaeosols appear very dusky red (10R 2/2), moderate brown (5YR 4/4), dusky brown (5YR 2/2), greenish black 5GY 2/1) in colour (Figure 5.24 a & b). Discontinuous pedocretes or calcretes layers of <10 m occur at various depths throughout the Algoa Group. Pedocretes are white (N9) and yellowish grey and are comprised of fine-grained sand generally well cemented in a calcium rich supported matrix. Pedocretes range from brittle in nature, often containing small cavities (1mm – 20 mm) to well cemented, hardpan calcrete layers with no cavities (Figure 5.25 a & b).
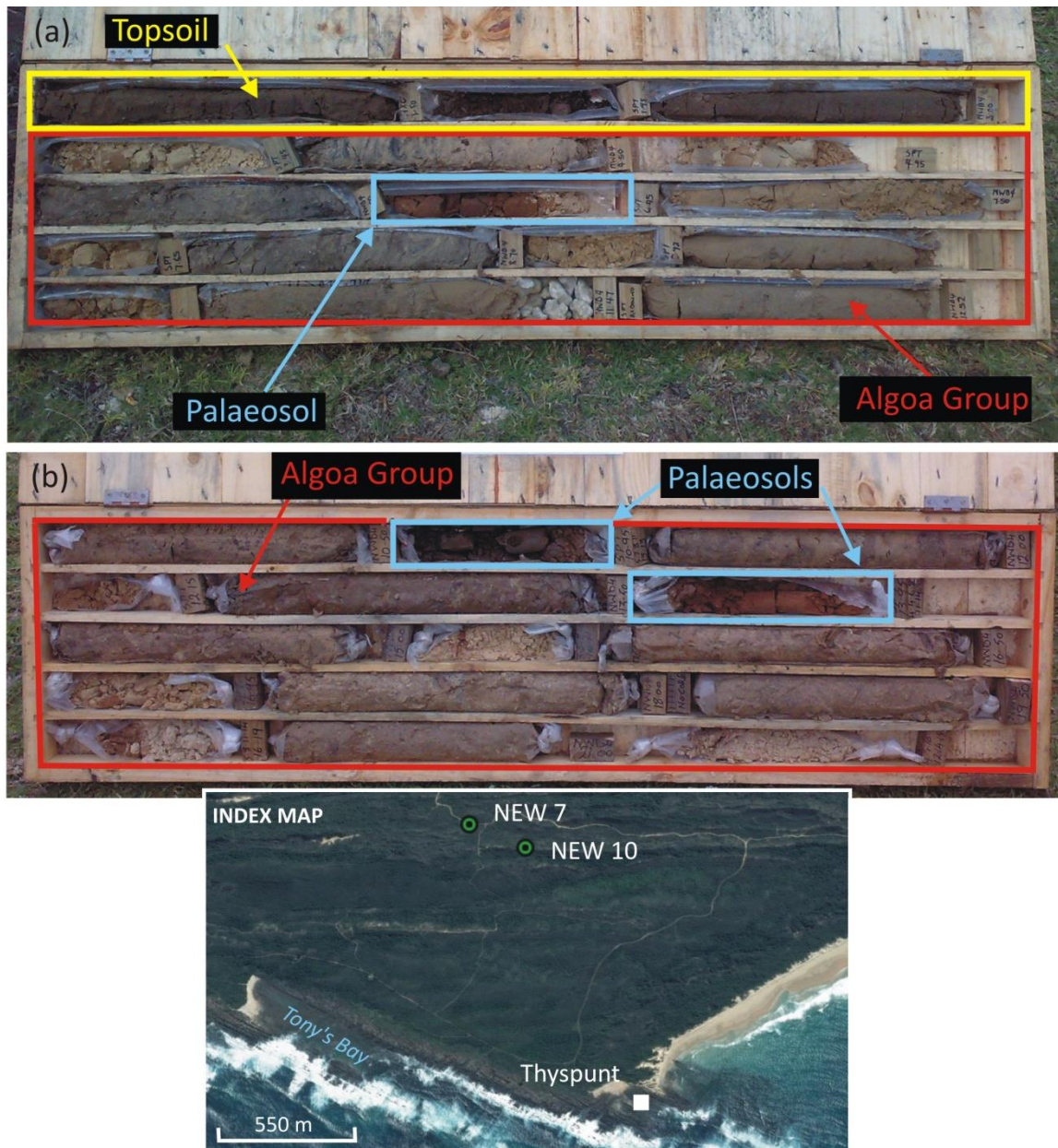
Figure 5.24: (a) A 45 cm thick, moderate brown, fine-grained and silty palaeosol intercepted at a depth of 6 m below ground surface (38 m asl) in borehole NEW7 within the Algoa Group. (b) Palaeosols intercepted within borehole NEW10. A medium brown palaeosol occurs between 10.50 – 10.95 m below ground surface (38.067 – 37.617 m asl). A second light very dusty red palaeosol is intercepted at depths of between 13.50 – 13.95 m below ground surface (35.067 – 34.617 m asl) within the Algoa Group.

Figure 5.25: (a) A 5.15 m thick pedocrete (calcrete) intercepted in borehole NEW6. The fine-grained pedocretes range from brittle, semi-consolidated, containing cavities to well cemented hardpan calcrete at depths between 18 – 23.15 m below ground surface (33.206 – 28.056 m asl) in borehole NEW6. (b) Pedocrete layers intercepted at depths between 10.45 – 10.50 m (29.844 – 29.794 m asl) and 15.45 – 16.50 m (24.844 – 23.794 m asl) in borehole NEW8.

The contact between Algoa Group sediments and underlying Palaeozoic bedrock is unconformable and is often characterized by the presence of a gravel layer of marine or fluvial origin stratigraphically correlated with either the basal conglomerate unit of the Alexandria Formation (Smuts, 1987) or the Salnova Formation (Hanson *et al*; 2012). These basal deposits are not laterally persistent and spatially show great variation in thickness. A maximum gravel thickness of 19 m is encountered in borehole CSF17 in the Cape St. Francis area and 11.5 m in borehole TS06 at Thyspunt (See § 5.5.2 v for detailed thickness distribution of basal units).

Groundwater movement at the contact between the Algoa Group overburden and TMG bedrock is evident from the numerous moderately strong flowing springs occurring along the coast (Figure 4.26). In addition borehole data indicate frequent water strikes at or close to the contact. As rainwater filters through the highly permeable aeolian deposits, leaching of carbonate minerals occurs and is precipitated out at the surface by springs as tufa (limestone) deposits (Figure 5.27). Tufa deposits are porous and range from superficial <5m thick deposits that occur close to, or a few meters above the highwater mark. Borehole loggings indicate in-situ weathering of the underlying bedrock, especially in areas of low bedrock relief, a direct consequence of groundwater movement along this contact (Figure 5.28 a & b). Within the study area the Algoa Group reaches a maximum of 61 m in borehole CSF10 (See § 5.5.2 for detailed descriptions on the thickness distribution of the Algoa Group).
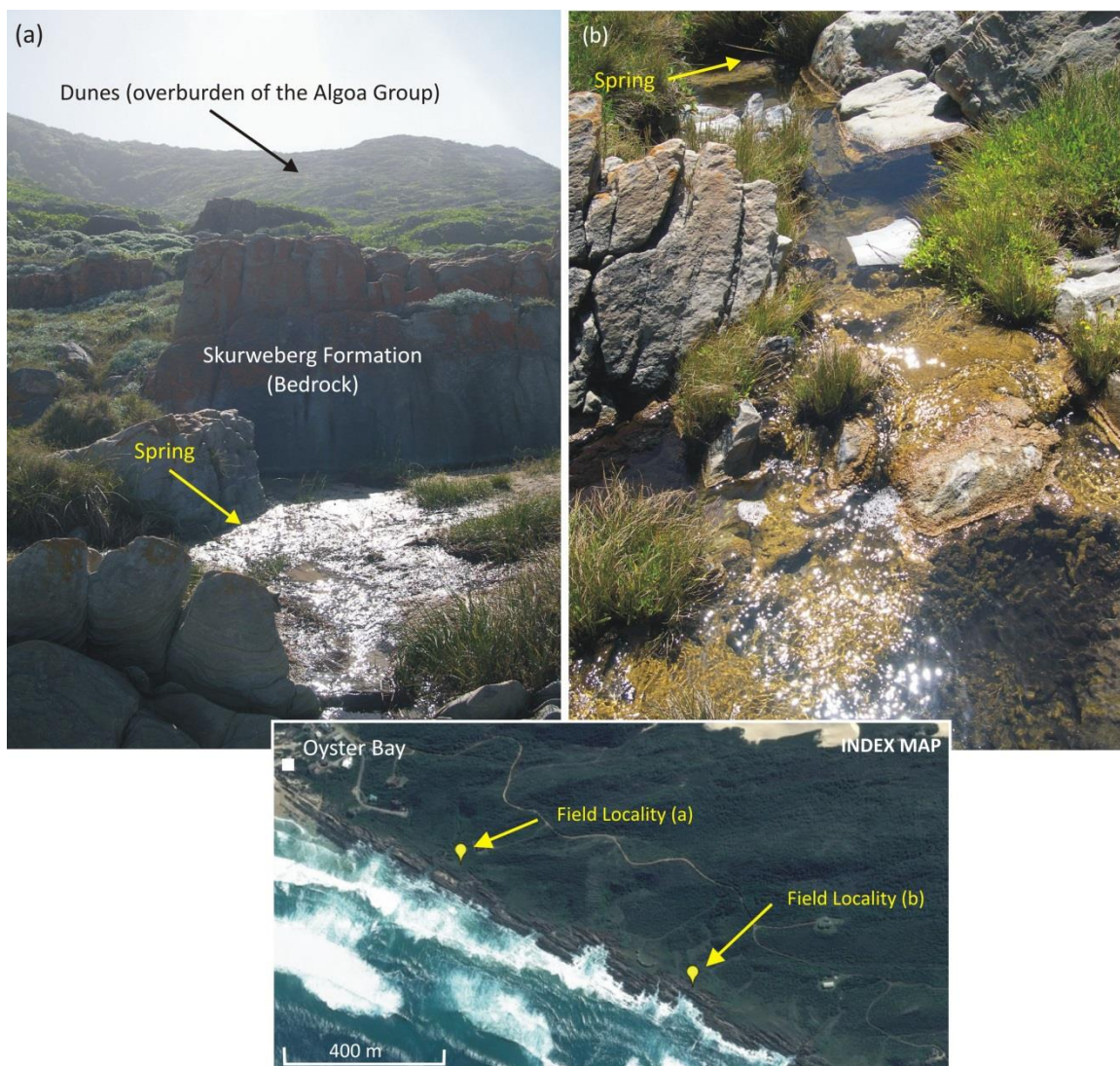
Figure 5.26: (a) A fresh water spring located at the contact between Cenozoic overburden deposits (Algoa Group) and bedrock (Skurweberg Formation). Lat: 34° 10' 37.3" Long: 24° 39' 56.3". (b) Moderately strong flowing spring east of Oyster Bay (Lat: 34° 10' 47.4" Long: 24° 40' 19.5").
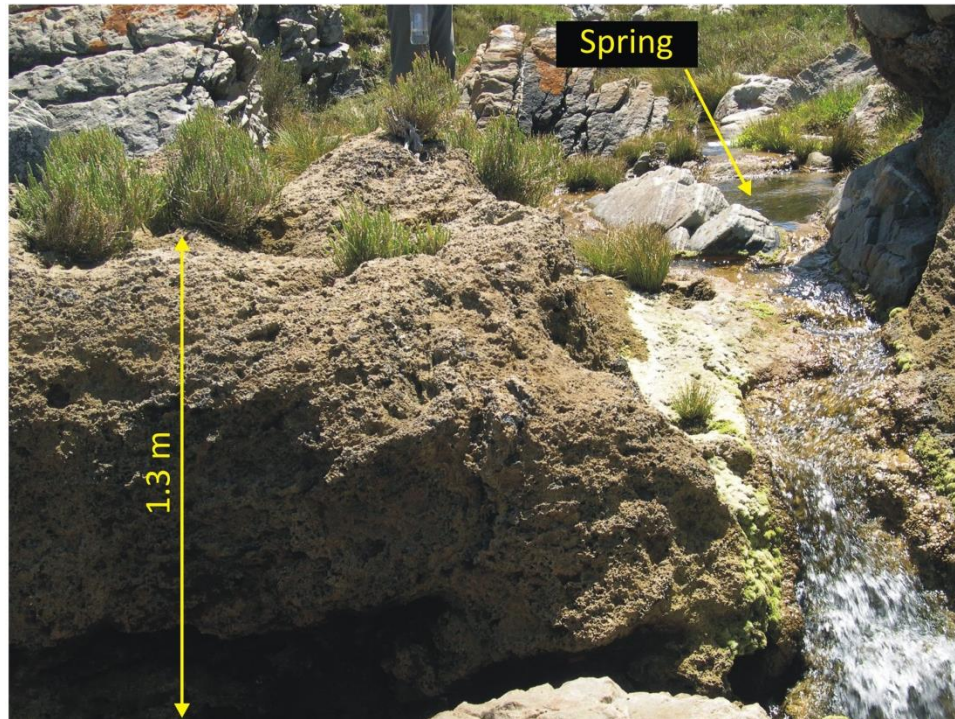
Figure 5.27: A 1.3 m thick tufa deposited along coastal exposures of the Skurweberg Formation, west of Oyster Bay. Note the spring to the right of tufa deposit (Lat: 34° 10' 47.0" Long: 24° 40' 19.2"). Refer to Figure 5.26 (b)'s index map for location.
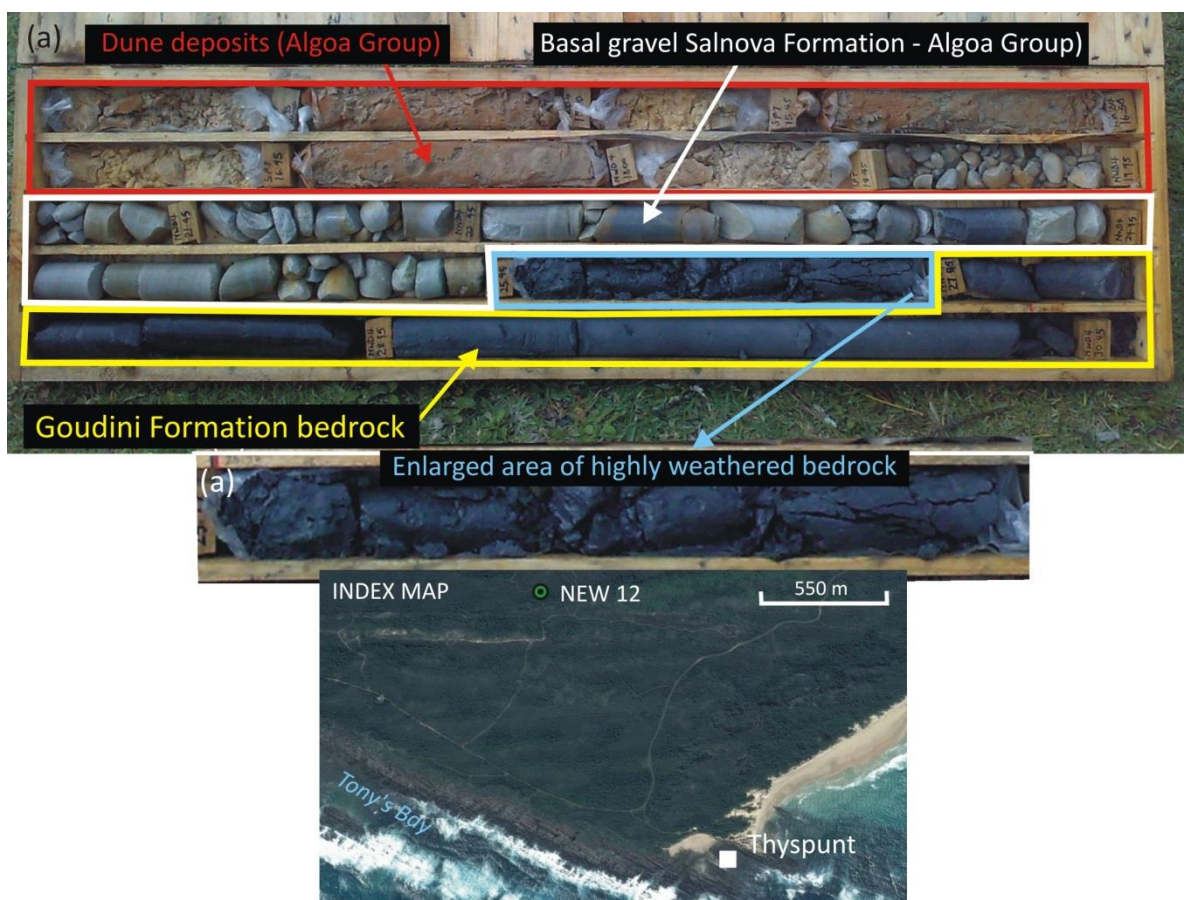
Figure 5.28: (a) Highly weathered shale below the unconformable contact between overlying sediments of the Algoa Group and the underlying bedrock of the Goudini Formation observed in borehole NEW12. (Lat: 34° 11' 08.3" Long: 24° 42' 32.4"). (b) Enlarged view of highly weathered shale highlighted in figure (a) occurring between depths of 25.95 m (0.768 m asl) to27.45 m (-0.732 m asl) in a topographic bedrock low.

5.1.3.1 Alexandria Formation

Within the study area, the Miocene to Early Pleistocene (Smuts, 1987; Roberts *et al.*, 2006) Alexandria Formation is not exposed within the study area, but is possibly present in the subsurface overlying higher bedrock platforms with elevations of approximately ≥18 - 30 m asl (Le Roux, 1987 a). Outside the study area exposures are also limited. Sediments of the Alexandria Formation rest unconformably on a narrow, planar, seaward sloping marine platform that is cut into older Palaeozoic successions (Roberts, 2006; Goedhart *et al.*, 2008; Hanson *et al.*, 2012). Outcrop mapped outside the study area and elsewhere in the Eastern Cape consists of alternating layers of calcareous fine to coarse-grained, moderately to well sorted sandstone, imbricated conglomerate consisting of pebbles and cobbles set in a sandy matrix, and coquinite consisting of shell fragments that generally vary in size from 5 - 15 mm (Le Roux, 1987 a). The composition of the conglomerate depends on the underlying source materials, and within the site vicinity (40 km radius around Thyspunt), clasts consist mostly of Table Mountain Group quartzite (Goedhart *et al.*, 2008). Sedimentary structures include horizontal lamination, low angle bedding and biogenic structures. Fossil assemblages are very common (Le Roux, 1987 b; Le Roux, 1989), but not noted in the limited exposure outside the study area.

Outside the study area, exposures of the conglomerate lithology can be seen along a road cutting north of Oyster Bay, 5 km NNE of the study area. Surface exposure of the Alexandria Formation is often highly weathered with conglomerate containing ferruginised quartzite clasts of pebble and cobble size set in a sandy matrix (Figure 5.29). The Alexandria Formation is generally not laterally persistent and spatially shows great thickness variation (Le Roux, 1989). The formation is generally overlain by coastal dune deposits of the Nanaga- and Schelm Hoek Formations along the coast and in the study area and surroundings overlies bedrock of the Cape Supergroup.

Figure 5.29: Deeply weathered exposure of Alexandria Group conglomerate comprising ferruginised quartzite clasts set in a sandy to silty matrix observed in a road cutting on the Oyster Bay road. (Lat: 34° 06' 17.9" Long: 24° 43' 01.3").

5.1.3.2 Nanaga Formation

The Nanaga Formation is a multiple-generation ENE striking palaeodune deposit that form smooth rounded hills with undulating ridges along the coastal margins (Norman *et al.*, 1987 a, Norman *et al.*, 1987 b; Le Roux, 1989). These dune deposits are generally not part of the Holocene mobile dune corridors (Schelm Hoek Formation) exposed at Oyster Bay and Cape St. Francis, but rather are characterised by older, more stable and vegetated dune deposits. The formation accumulated in coastal dunefields along Late Miocene to Pleistocene's receding shorelines, and as a result, formation deposits become gradually younger from its inland extent towards the coast (Le Roux, 1992; Maud & Botha, 2000; Roberts *et al*, 2006). The formation is composed of unconsolidated to semiconsolidated medium-grained, cross-bedded, calcareous dune sand and calcretes. The formation is very thick bedded and has a greyish yellow (5Y 8/4) to light yellowish orange (10YR 8/6) colour. Occasional thin <10 m, dense, and dark to light brown organic rich silty pedogenic horizons generally <3 m occur throughout the formation.

Le Roux (1992) indicated a maximum thickness for the formation of ≤ 250 m in the Port Elizabeth area. The maximum recorded thickness of the Algoa Group as a whole within the study area is only 61 m as derived from borehole CSF10, therefore the Nanaga Formation thickness is assumed to be at least <61 m. The formation is generally overlain by the younger unconsolidated mobile dunes of the Schelm Hoek Formation or represents the upper Cenozoic deposits in the area. In addition, the Nanaga Formation may sporadically be overlain by the Nahoon Formation.

5.1.3.3 Salnova Formation

Outcrop exposure is limited within the study area. The lithological descriptions of the formation within the study area are predominantly based on borehole data. The Salnova Formation is comprised of light grey (N7), greyish yellow (5Y 8/4) or light yellowish orange (10YR 8/6), fine to coarse-grained calcareous sandstone, shelly limestone and coquinite; or unconsolidated fine to coarse-grained moderately to well-sorted calcareous sand, gravel, coquina and conglomerate deposited on wave cut platforms below 18 m asl. The conglomerate units are composed of imbricated, disc- to roller-shaped clasts of pebble to cobble size set in a fine to medium-grained sandy matrix, frequently containing shell material (Figure 5.30 a & b). The composition of the conglomerate depends on the underlying source materials. Within the study area Goedhart *et al*., (2008) associated clasts with the Table Mountain Group sandstone.

Between interdune hollows near the western edge of the bypass dune field, west of Cape St. Francis, a continuous ~100 m long, ~1 m thick pavement exposure of the Salnova Formation occurs (Figure 5.31). The consolidated beach rock is overlain by unconsolidated dune sand of the Schelm Hoek Formation. Within the study area, the Salnova Formation is overlain by sands of the Schelm Hoek Formation, consolidated aeolianites of the Nahoon Formation, pedosols or calcrete.
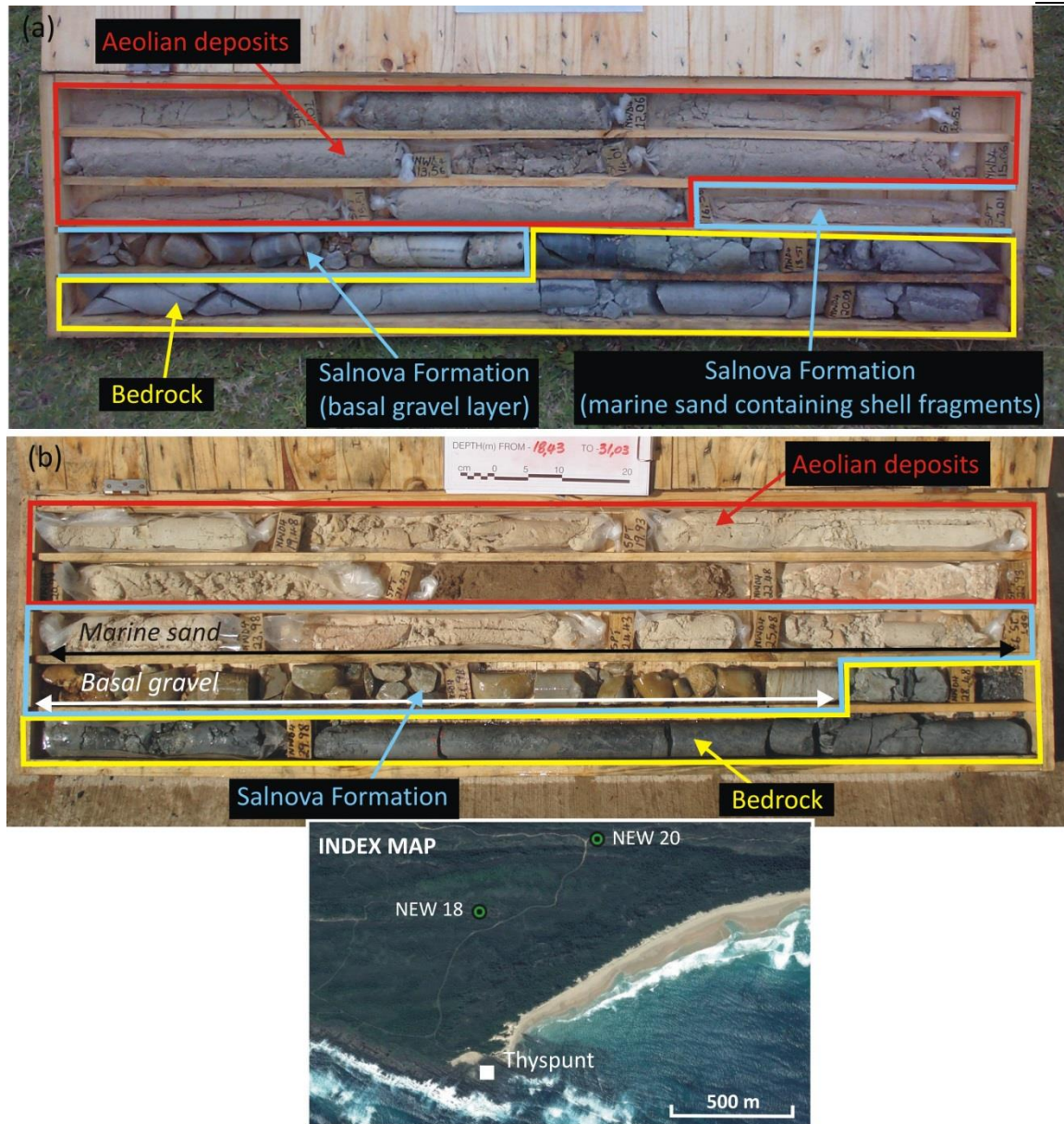
Figure 5.30: (a) The Salnova Formation occurring as fine sand with coarse shell fragments and occasional sub-rounded pebbles between 0.726 & -1.224 m asl and as a conglomerate / gravel layer between -1.224 & -2.484 m asl in borehole NEW20. The extent of the Salnova Formation is encompassed by blue rectangle shape. Location of borehole: Lat: 34°11'02.03"; Long: 24°43'10.49". (b) The Salnova Formation is composed of two lithologies; a 1.95 m thick fine-grained marine sand occurring between (0.77 - -1.18 m asl), underlain by a 2.41 m basal gravel layer occurring between -1.18 - -3.59 m asl in borehole NEW18 (Lat: 34°11'11.78"; Long: 24°42'51.37").

Figure 5.31: A ~1 m thick, interdune exposure of the Salnova Formation along the western edge of the small scale bypass dune field at Cape St. Francis.

5.1.3.4 Nahoon Formation

The Nahoon Formation forms the core of the larger coastal dunes a few kilometres inland of Cape St. Francis. Isolated remnant exposures of the formation are located adjacent to and seaward of, active dunes of the Schelm Hoek Formation. Noticeable exposures occur between Oyster Bay and Thyspunt (Figure 5.32).

The Nahoon Formation is comprised of well consolidated palaeodunes composed of calcareous sandstone (aeolianite), interbedded palaeosols and isolated thin calcrete layers. The calcareous sandstone varies in colour from light grey (N8) to medium grey (N5), grey yellow (5Y 8/4) or moderate yellow (5Y 7/6) and is composed of fine to medium-grained cross bedded dune sand (Figure 4.32). The formation is not laterally persistent. The humic palaeosol component of the formation is semi-consolidated and varies in colour from greyish-yellow (5Y 8/4) or light olive grey (5Y 5/2). The Nahoon Formation is <15 m in thickness, (Le Roux, 1989). The formation is frequently referred to as palaeodune rock or beach rock in borehole logs (Eskom, 2010 a; Eskom, 2010 b; Raubenheimer *et al.,* 1998a). The formation is generally underlain by the Salnova or Nanaga Formation.

Figure 5.32: Aeolianite of the Nahoon formation exposed SE of Oyster Bay. Note the large scale cross-bedding.

5.1.3.5 Schelm Hoek Formation

Outcrop of the Holocene Schelm Hoek formation is well exposed within the study area as mobile dunes within the NNE-SSW trending Cape St Francis – Oyster Bay bypass dune field (Figure 5.33). The formation is composed of moderate yellow (5Y 7/6), greyish yellow (5Y 8/4) or moderate yellowish brown (10YR 5/4), unconsolidated to semi-consolidated calcareous aeolian sands (Figure 4.34 a & b). Aeolian sands are comprised of fine-grained, well sorted quartz grains, with a lesser calcareous shell component. Trace amounts of heavy minerals are often visible in hand sample. The formation is interbedded with shell midden horizons, thin poorly developed soils and palaeosols. Sedimentary structures include wind ripples and high angled planar aeolian cross-bedding. Palaeosols consist mainly of sand and a small amount of organic matter.

Within the study area, a large portion of the formation is defined by active (mobile) dunes. The mobile sand is derived from sandy beaches in the surrounding areas, its main source being the sandy beach at Oyster Bay. Aeolian transport of sand occurs along the headland in an easterly direction by SSW winds (La Cock & Burkinshaw, 1996). An active process of accumulation and deposition is still taking place (Goedhart *et al*., 2008). In general the size and extent of active, mobile dune fields have been shirking over the last 50 years due to human development at the eastern end of the Oyster Bay – Cape St. Francis bypass dune field. Disruption in the sediment transport function of the dunefield and subsequent vegetation encroachment has been the main drivers of its shrikage (Burkinshaw, 1998). More recently, (since 2011) NE dune migration at Oyster Bay is encroaching on developed land and holiday homes (Figure 5.35).
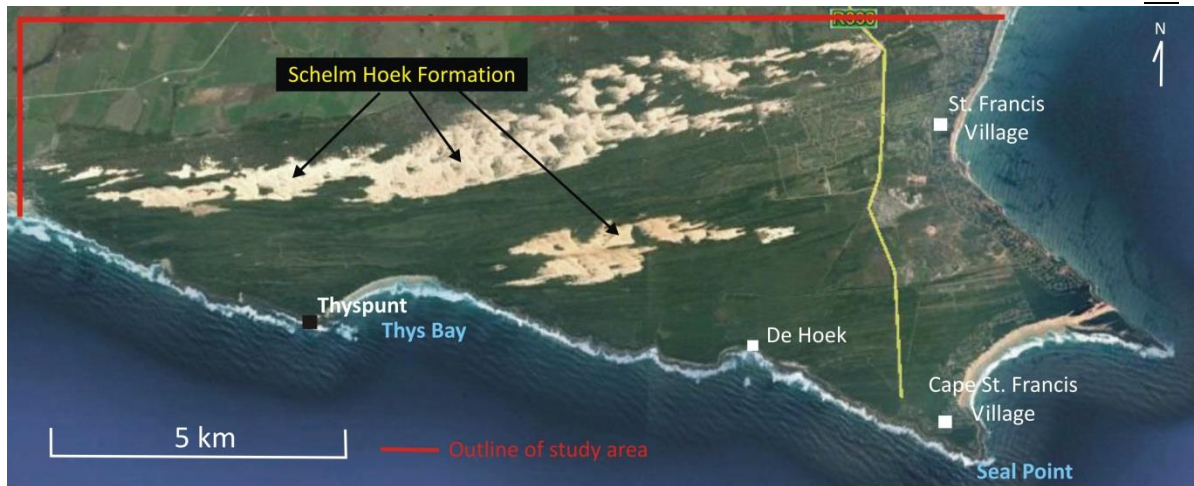
Figure 5.33: Outcrop exposure of the Schelm Hoek Formation within the study area.
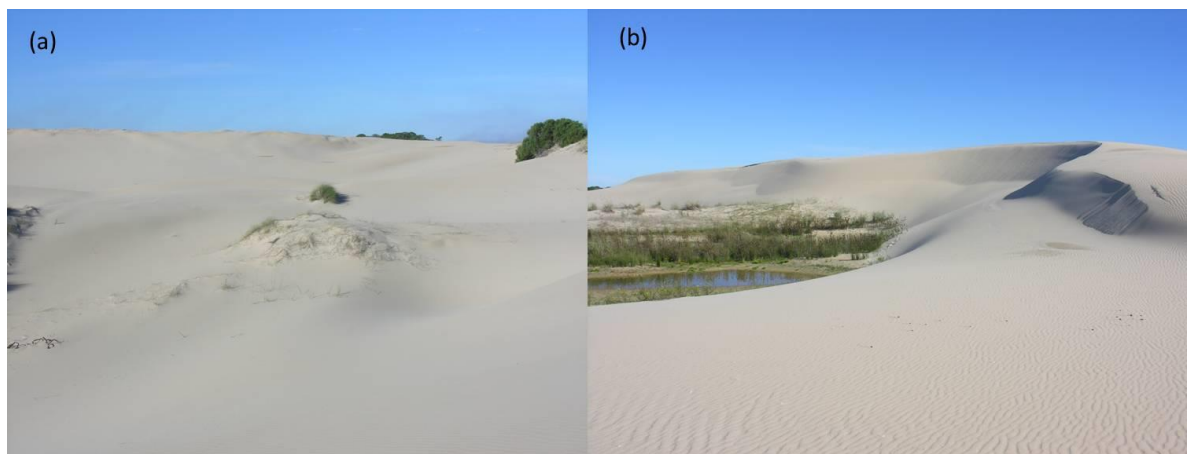
Figure 5.34: (a) Unconsolidated mobile dune sand of the Schelm Hoek Formation forming part of the Oyster Bay dunefield (Lat: 34° 10' 14.1" Long: 24° 44' 11.0"). (b) Ephemeral wetlands are common in the Thys Bay and Oyster Bay dunefields, forming in between dune depressions (Lat: 34° 10' 20.2" Long: 24° 44' 16.0").

Figure 5.35: Dunes encroaching onto developed land, and holiday home properties in Oyster Bay.

5.2 Structural geology

The structural characteristics of strata within the study area are described predominantly from the narrow 30-250 m wide strip of coastal outcrops exposures between Oyster Bay and Cape St. Francis; exposures south of the Oyster Bay–St. Francis headland bypass dune field; and isolated outcrop exposures outside the study area.

5.2.1 Bedding and folds

Trough cross-bedding and channel structures were used to determine the facing direction of bedding. Bedding azimuth and dip measurements are depicted by means of a stereogram (Figure 5.36). Stereograms depicting bedding along coastal outcrop exposures across the Cape St. Francis anticline (Figure 5.37 a & b) are shown within subareas: zones 1, 2 and 3 (Figure 5.37 a & c) and a cross section perpendicular to bedding strike, along the southern portion of the Cape St. Francis anticline is constructed from field data (Figure 5.37 b).

Bedding orientation and inclination of the Table Mountain Group strata are controlled by the regional NW-SE striking, SE plunging, very slight north verging and open Cape St. Francis anticline (Figure 5.37 b) with an interlimb angle of 89°. Although the anticline is described by Goedhart *et al.*, (2008) as a north verging fold, measurements of bedding along the southern portion of the fold are more consistent with observations made by De Beer, (2000) who describes the anticline as upright (Figure 5.37 b). Bedding inclination is mostly controlled by this anticline and the parallel distance away from its sub-horizontal fold axis that exhibits a trend and very shallow plunge of 124°/3° (Figure 5.36). The axial plane shows a sub-vertical SW dipping axial plane (214°/87°), depicting an almost upright fold. Near the Cape St. Francis fold axis, around the broad fold hinge area (Figure 5.36 & Figure 5.37 c, Zone 2), bedding inclination is shallow, with dip values ranging from 5° - 20°. With increasing distance away from the fold axis, dip values show a steady increase to moderately steeper inclinations of 30° to 40° east and west of De Hoek. Towards Oyster Bay, bedding inclination reaches steep inclinations ranging between 50°- 65°. Greater dip values are documented, but rare and localised (Figure 5.37 a). At the Thyspunt site bedding remains relatively consistent at 210° / 50° (azimuth/dip) (Figure 5.37 a).
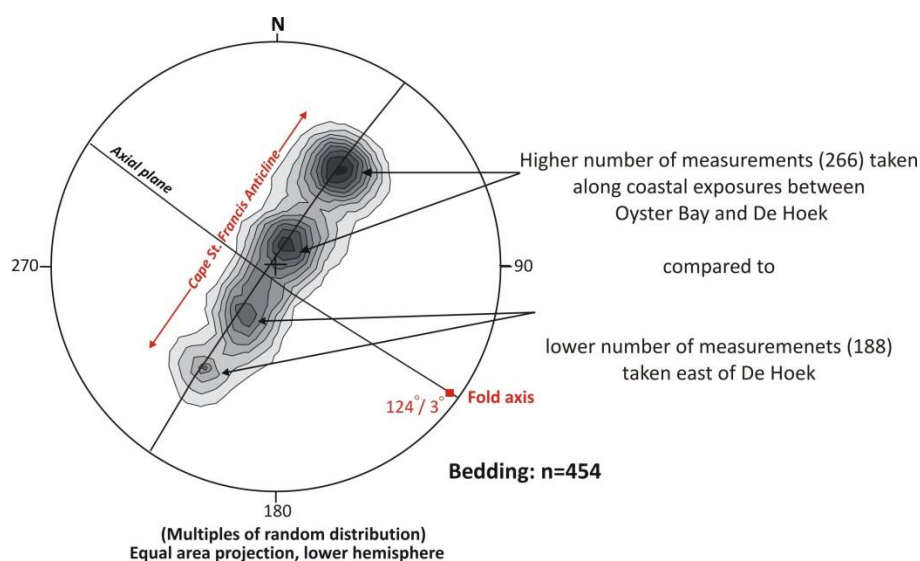
Figure 5.36: Stereogram showing contoured poles to bedding planes. Bedding strikes NW-SE.
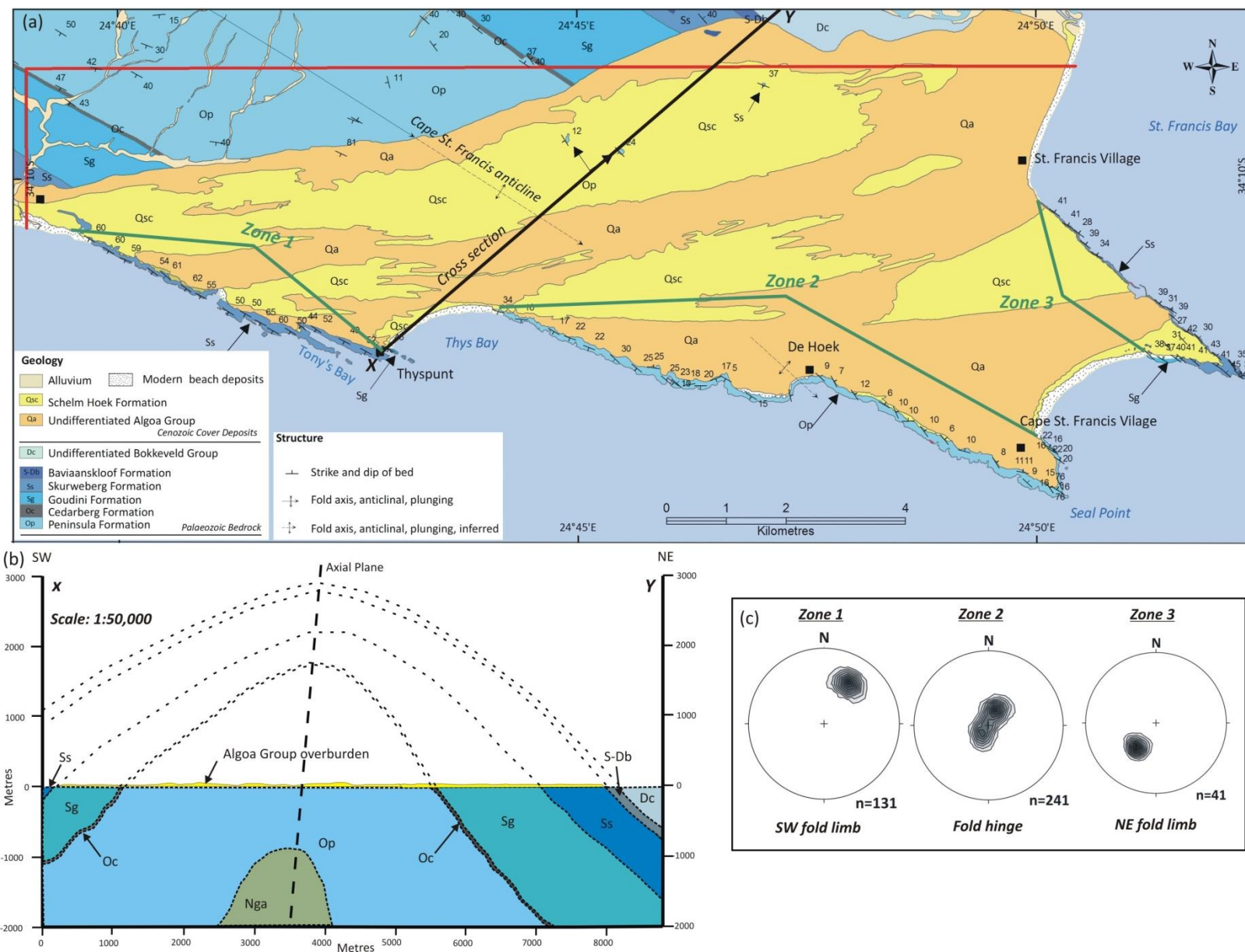
Figure 5.37: (a) Geological map of study area depicting the Cape St. Francis anticline, bedding measurements (azimuth/dip) and the location of cross section X-Y. (b) Geological cross section X-Y. (c) Stereograms of poles to bedding planes as measured along coastal outcrop exposures over the extent of the Cape St. Francis anticline. The area is divided into three subareas: zone 1, 2 and 3.

The regional Cape St. Francis anticlinorium exhibit secondary parasitic meso-scale folds on its limbs. Secondary meso-scale anticlines and synclines show a variety of fold characteristics, with some mimicking or closely resembling; and others deviation from the fold characteristics of the regional Cape St. Francis anticline. Parasitic folds are generally north verging, overturned or recumbent with axial planes predominantly dipping steeply SW or occasionally NE (Figure 5.38 a & b). These folds ranges from open to tight (Figure 5.38 a & Figure 5.39) with fold axes predominantly plunging subhorizontal or gently towards the SE (Figure 5.40). Isolated isoclinal folds were noted ~2km SE of Oyster Bay (Figure 5.39). Meso-scale folds with fold axes orientated oblique to the fold axis of the regional Cape St. Francis anticline may indicate localised compressive forces oblique to the main NE-ward directed compression (Figure 5.40).
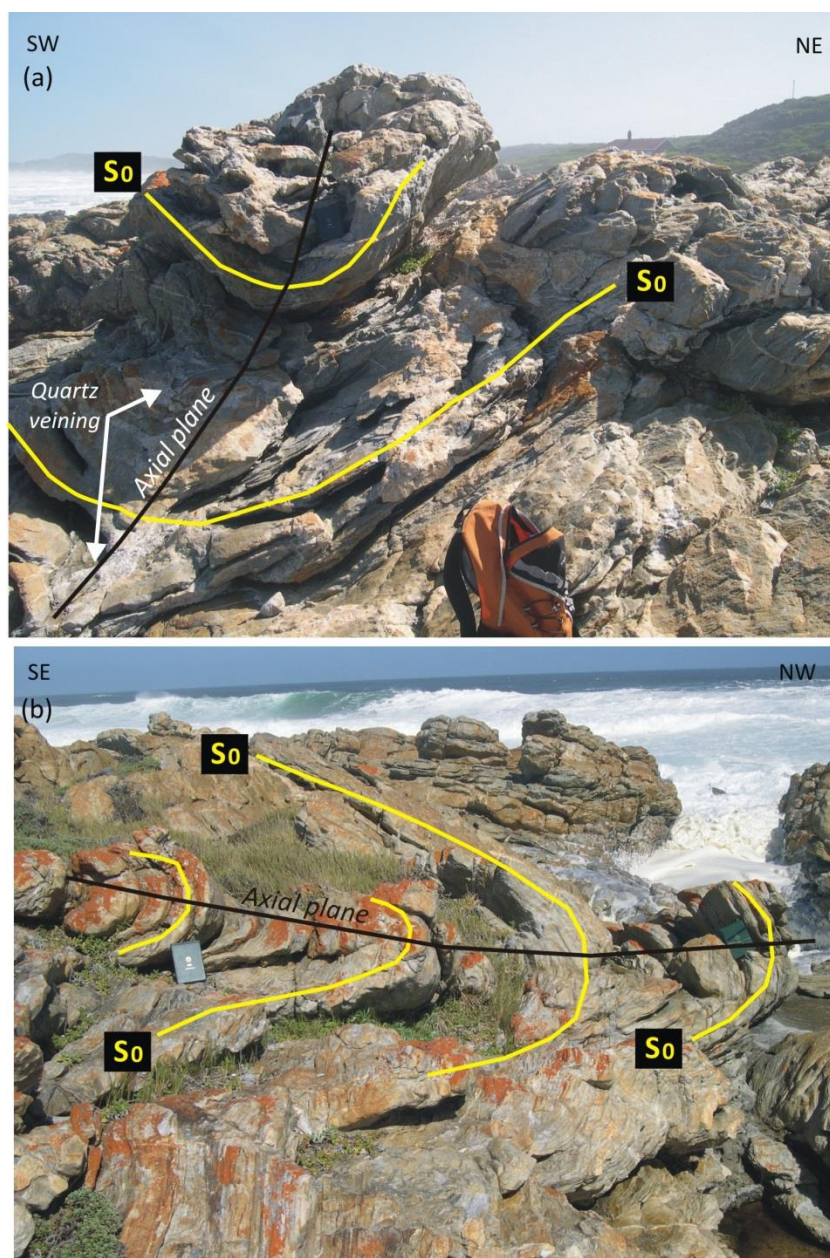
Figure 5.38: (a) An open syncline exposed in coastal outcrop of the Peninsula Formation. The syncline displays a NW-SE striking and SW dipping axial plane (Lat: 34° 11' 17.1" Long: 24° 44' 22.8"). Note the quartz veining in the area where folds occur. (b) An open overfolded, recumbent fold in quartzitic sandstone of the Peninsula Formation. The axial plane strikes roughly NW-SE and steeply dips southwesterly (Lat: 34° 11' 17.9" Long: 24° 44' 22.1"). S0 indicates bedding.
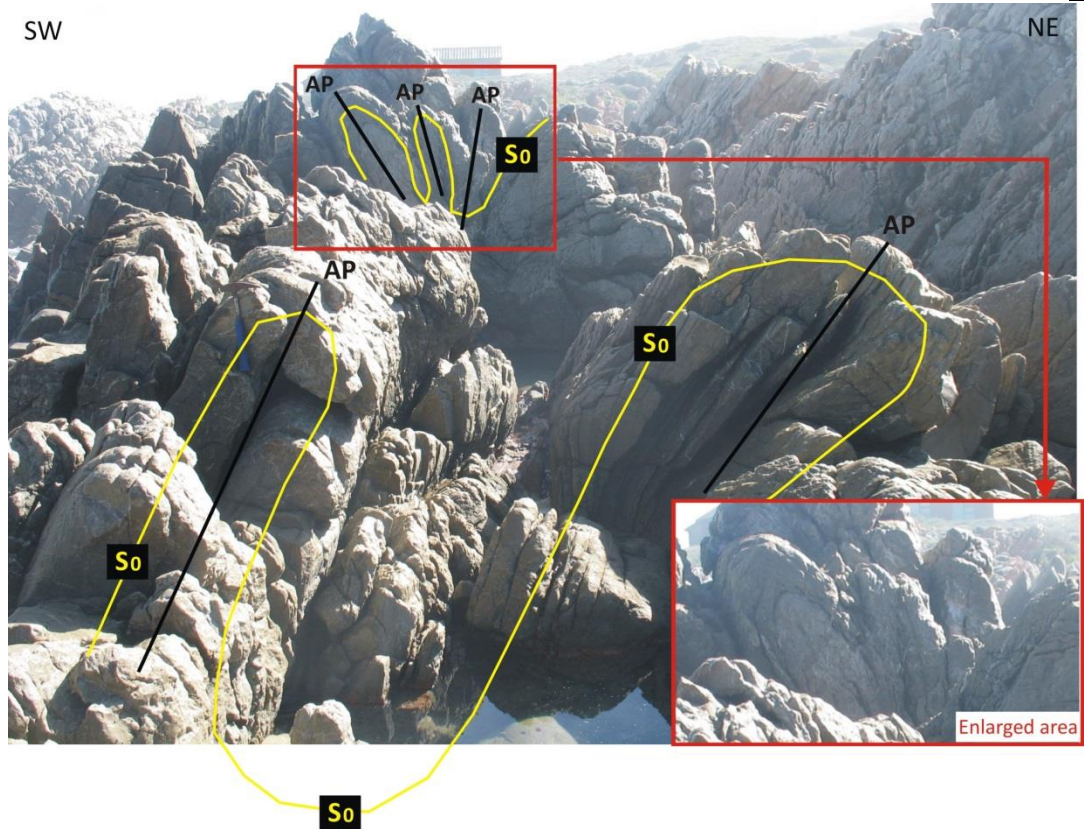
Figure 5.39: Tight inclined isoclinal folds observed in quartzitic sandstone of the Skurweberg Formation, approximately 2 km SE of Oyster Bay (Lat: 34° 10' 47.2" Long: 24° 40' 17.6"). Note both the SW and NE dipping axial planes (AP). S_0 indicates bedding.
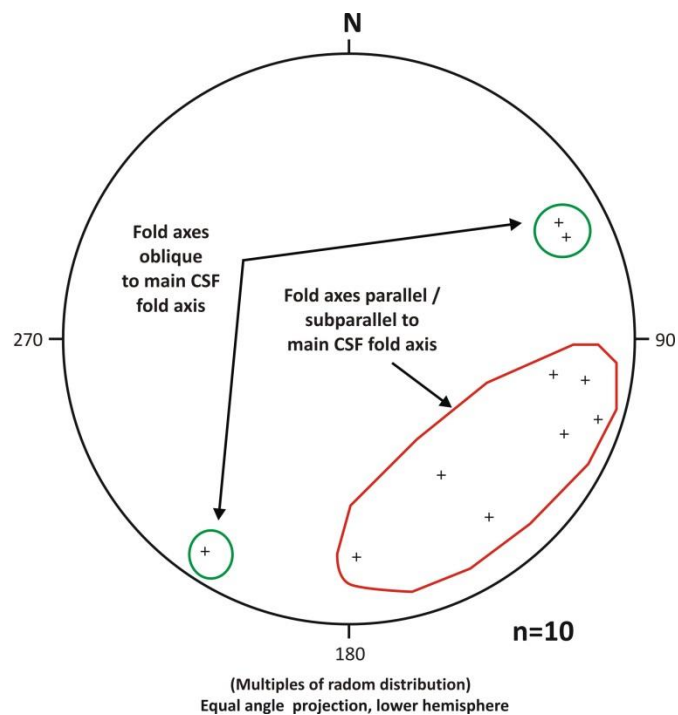
Figure 5.40: Stereogram showing fold axes of parasitic folds measured within the study area and surroundings. Note the dominant trend and plunge of mesoscale fold axes at shallow to moderate angles to the ESE and SE – parallel to subparallel to the main Cape St. Francis anticline. Occasionally fold axes trend and plunge at shallow angles oblique to the regional Cape St. Francis anticline.

The amplitude and wavelength of folds are also linked to the lithological competency and bed thicknesses of the various formations. More incompetent formations, such as the Cedarberg, Baviaanskloof Formations and Bokkeveld Group, tend to produce asymmetrical to tight isoclinal folds that are smaller in size and more closely spaced (Figure 5.41), which in turn leads to substantial shortening, and volume reduction. This is clearly seen in strata of the Baviaanskloof Formation in the areas north of Jeffrey's Bay and NW of Humansdorp, outside the study area. Competent, brittle units such as the Skurweberg and Peninsula Formations are more likely to produce larger scale broad and open folds with open interlimb angles.
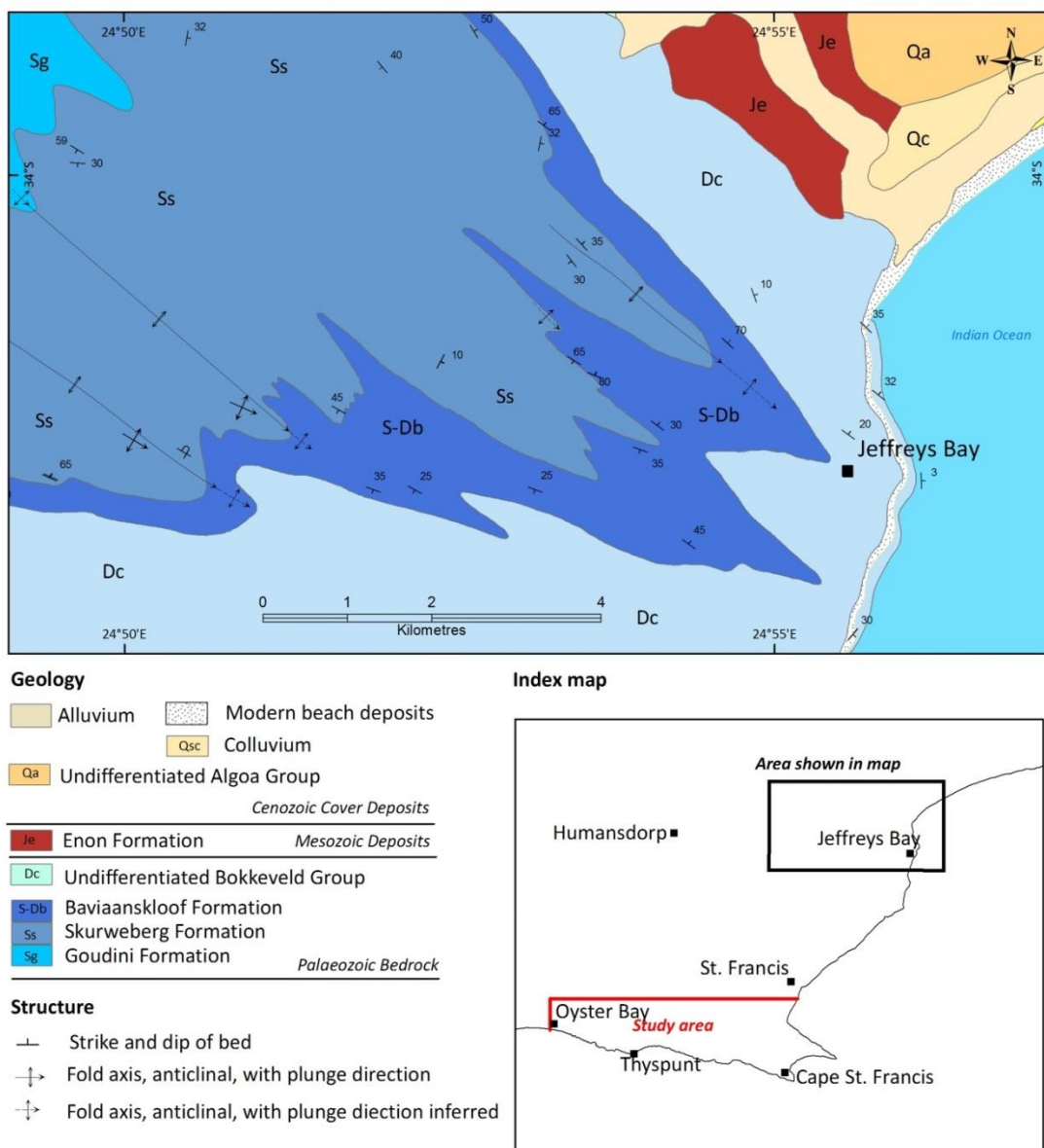
Figure 5.41: Closely spaced folds mapped near Jeffreys Bay, outside the study area (after Goedhart et al., 2008).

Slickensides and slikenfibres are occasionally documented along bedding planes and possibly facilitated differential movement during folding (Figure 5.42). Flexture-slip movement is common on fold limbs and slickensides are often found between bedding planes.

Figure 5.42: Slickenfibres along bedding planes in strata of the undifferentiated Bokkeveld Group 7 km NW of Paradise Beach, outside the study area (Lat: 34° 04' 34.9" Long: 24° 49' 19.4").

5.2.2 Faults

During field investigation, the validity of inferred AEC faults noted as extending through coastal exposures at Thyspunt and De Hoek (§ 3.4 & Figure 3.3) were investigated. Strata in areas where these faults are interpreted to occur were inspected for signs of offset/displacement, the presence of breccia or mylonite and/or variations in bedding orientation and dip. During the review process field observations were combined with borehole data and more recent aeromagnetics (Cole & Naude, 2007) to evaluate the validity of inferred AEC faults.

5.2.2.1 Fault AEC DH1

West of De Hoek, coastal exposures of the Peninsula Formation were investigated to determine the validity of two inferred faults, AEC DH1 and AEC DH3 (Figure 5.43 a, b & c). Fault AEC DH1 is interpreted as a 10.5 km in length with a 250-500m left-lateral displacement (Van Wyk, 1987; Norman *et al.*, 1987b). Coastal exposures in the area where the inferred fault is shown to occur, coincides with a ~400 m long, 60-100 m wide NW-SE trending zone of densely fractured rock of the Peninsula Formation (Figure 5.43 b & Figure 5.44 a-f). Within this zone bedding is highly fractured. Exposures exhibit very closely spaced jointing frequently <5 cm apart (Figure 5.44 a - f). The intersection of mainly joints set J1 (N-S to NNE-SSW) and to a lesser degree J2 (NE-SW), J3 (NW-SE) and J4 (ENE-WSW) (see § 5.2.3 for greater detail on jointing within the study area) greatly facilitated the weathering of rock mass in this area immediately east of the Cape St. Francis anticline axis where bedding dips near horizontal (Figure 5.44 d – f). However close inspection of bedding revealed no evidence indicative of a fault. It should be noted that the investigation of certain portions of the area were partially obstructed by presence of boulders and/or the presence of gullies filled with sea water.
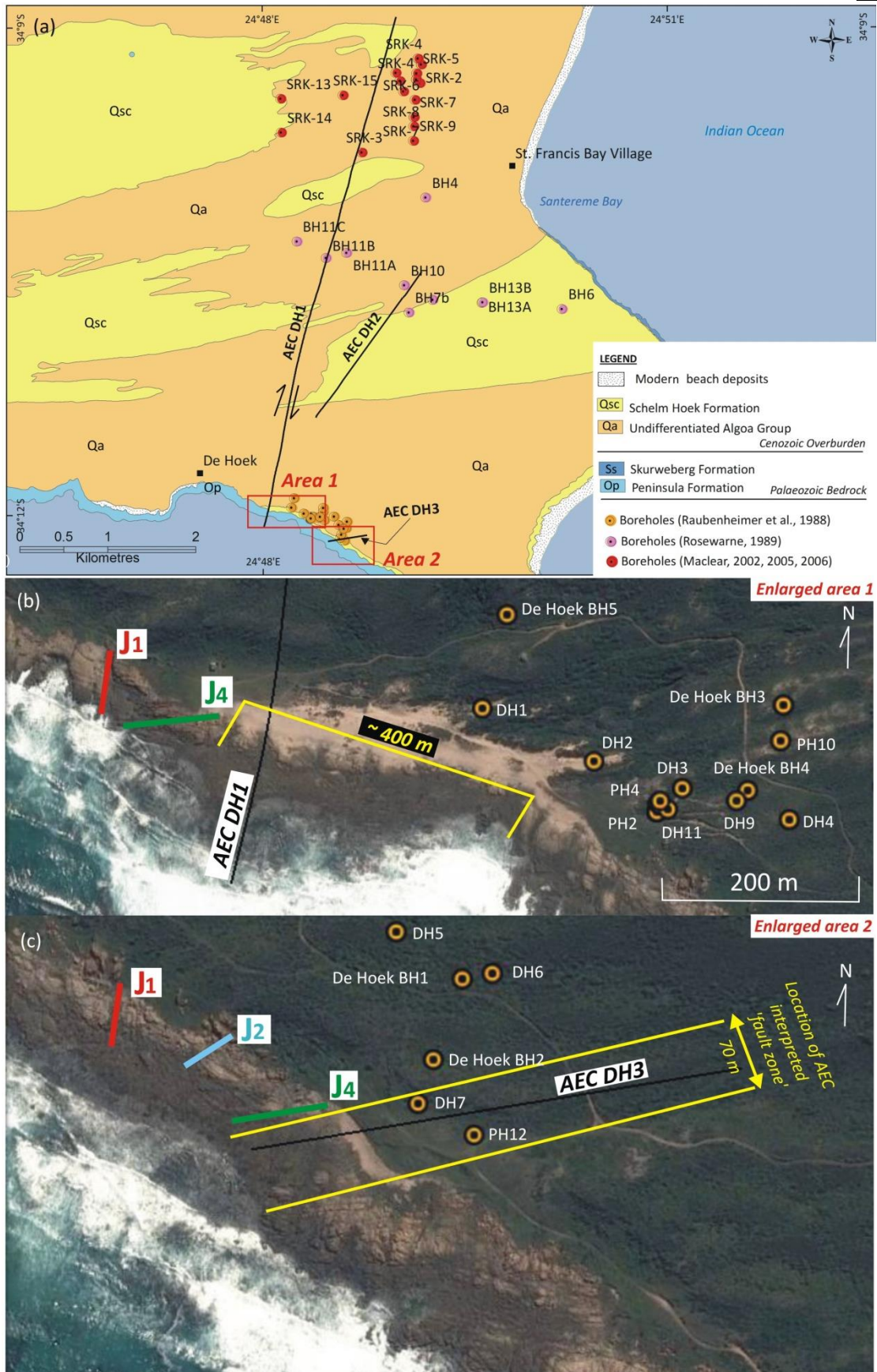
Figure 5.43: (a) Map showing the location of inferred AEC faults in the De Hoek area. Boreholes in the vicinity of faults are also depicted. Areas of interest are outlined in red and an enlarged viewed of these areas are shown in figure b and c. (b) Enlarged view of area 1 outlined in figure a. (c) Enlarged view area of 2 outlined in figure a. J1, J2 and J4 indicate joint sets. Refer to § 5.2.3 for greater detail on joint sets.
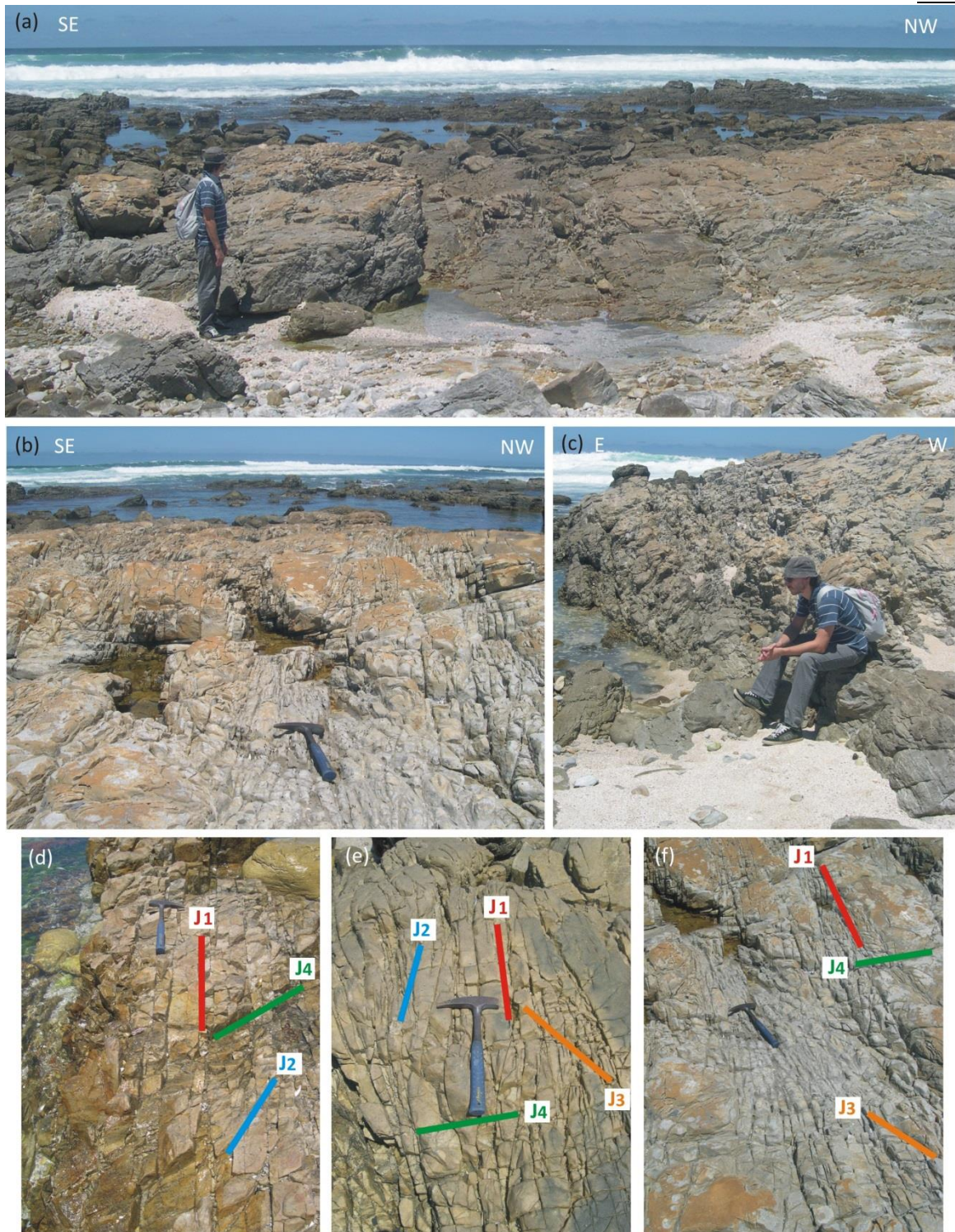
***Figure 5.44:** (a) An overview of the area along coastal exposures, east of De Hoek, where fault AEC DH1 is interpreted to occur. The overview faces SW. Note densely fractured quartzite of the Peninsula Formation at this locality. (b) & (c) Exposures of very closely jointed and fractured exposures of the Peninsula Formation encountered along the ~400 m long, 60 -100 m wide NW-SE trending zone where fault AEC DH1 is interpreted to possibly occur at the coast. (d, e & f) Exposures are very closely spaced jointing. The dominant joint set J1 is NNE-SSW. Joint sets indicated in figures relate to the study area's joint patterns (see § 5.2.3 for greater detail on the area's jointing pattern).*

Borehole loggings in the vicinity of where fault AEC DH1 is interpreted to occur were reviewed. Only borehole DH2 (Raubenheimer *et al.*, 1988 a), located ~100 m NE of the 400 m zone of densely fractured strata (Figure 5.43 b) make reference to a "*small fault zone*" intercepted at a depth of 19.3. The 1.7 m zone of fractured quartzite described as "*fault breccia in a mylonitic matrix*" could not be traced to coastal exposures. Rather the location of the interpreted fault zone coincides along strike with a NNE-SSW shatter zone that trends parallel to joint set J1. Farther inland, beneath Cenozoic cover and along strike of fault AEC DH1, boreholes BH11 A, B and C (Rosewarne & Lomberg, 1989) (Figure 4.43 a), intercept intensely fractured, but not brecciated strata of the Goudini Formation (Figure 5.43 a). More towards the northern sections of the fault line, Maclear, (2002) logged a fault zone intercepted at a depth ~30 m in borehole SRK-3. However the core is only described as highly fractured, not brecciated and the fault zone is therefore an interpretation only. In addition high resolution aeromagnetics (Cole & Naude, 2007) did not recognize a fault in this area (§ 3.4, Figure 3.4).

5.2.2.2 Fault AEC DH2

The validity of fault AEC DH2 located in bedrock beneath Cenozoic overburden (Figure 5.43 a) is difficult to assess, because AEC maps show the fault to have no apparent displacement (Figure 3.4). Van Wyk (1987) described this fault as a possible shatter zone; a zone of high intensity jointing without displacement. It is therefore difficult to ascertain why it is presented on AEC maps as an inferred fault. Borehole BH10 (Rosewarne & Lomberg, 1989) located near the fault line (Figure 5.43 a), confirms the fractured nature of the strata at a depth of 70 m where it intercepts a zone of fractured, but not brecciated rock. High resolution aeromagnetic imagery (Cole & Naude, 2007) depict a possible NE-SW horst-like structure with a 1.5 km displacement near Cape St. Francis that coincides with the position of fault AEC DH2 (Figure 5.45). This structure was not identified as a possible lineament or fault in the original interpretation of aeromagnetic results by Cole & Naude, (2007) (§ 3.4, Figure 3.4).
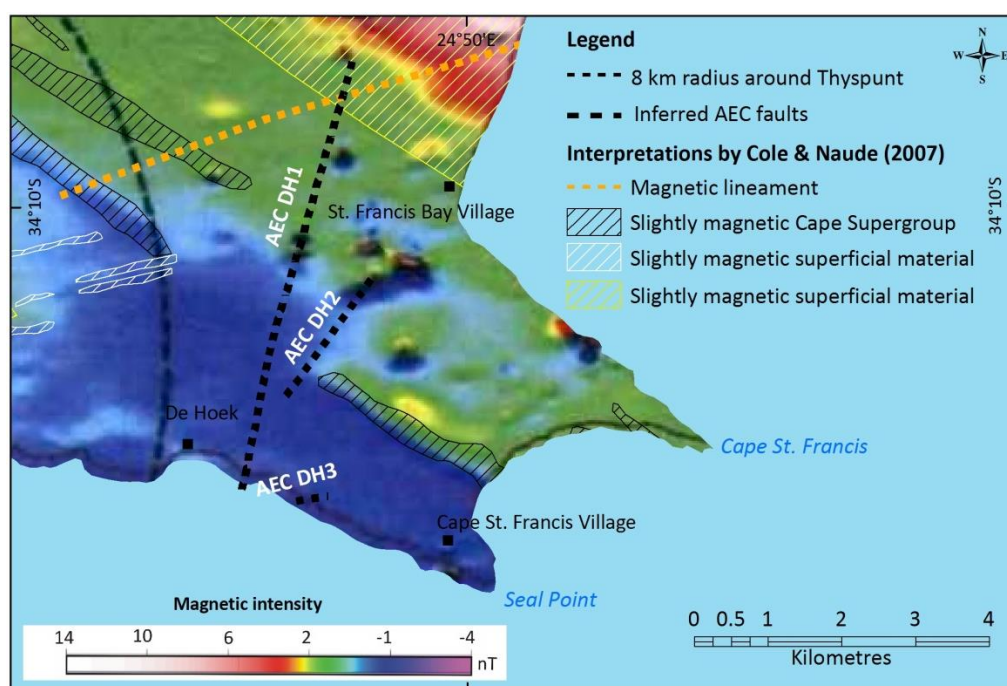
Figure 5.45: Inferred AEC faults (Muller et al., 1986; Anderson et al., 1986 b; Van Wyk, 1987) overlain on high resolution aeromagnetics and associated interpretations by Cole & Naude (2007).

5.2.2.3 Fault AEC DH3

Inferred fault AEC DH3 is interpreted by Van Wyk, (1987) as a 500 m long, NE-SW trending fault with a 70 m wide fault zone (Figure 5.43 a). Coastal exposures of the Peninsula Formation where the fault is interpreted to occur coincide with a 60-70 m wide NW-SE trending area of highly fractured, very closely spaced jointed rock partially overlain by loose bounders (Figure 5.43 c & Figure 5.46 a - d). Strata appear densely fractured with very closely spaced jointing associated with joints set J1 (N-S to NNE-SSW) and to a lesser degree J2 (NE-SW), J3 (NW-SE) and J4 (ENE-WSW) (see § 5.2.3 for greater detail on jointing within the study area). No signs indicative of faulting were identified during this study along these coastal exposures. The validity of fault AEC DH3 in this area cannot be positively confirmed by the investigation of coastal outcrop exposures only. Two boreholes are located further inland along strike of the interpreted fault zone (Figure 5.43 c). Log descriptions of borehole DH7 and PH12 were reviewed; however core is described as fractured with no signs of faulting or brecciated rock. It may also be worth noting that a small ~400 m long NNW-SSE trending cross section perpendicular to bedding and across the AEC DH3 fault drawn by Raubenheimer *et al*., (1988 a), did not include the presence of a fault in the De Hoek area. In addition high resolution aeromagnetics (Cole & Naude, 2007) does not depict a fault zone in this area (Figure 3.6). Closely spaced jointing suggests that the inferred fault can rather be interpreted as a shatter zone (zone of closely spaced jointing).

5.2.2.4 Fault AEC TSP 2

West of De Hoek, two faults, AEC TSP2 and AEC TSP3 are also interpreted to extend through coastal outcrop exposures west of Thyspunt, near Tony's Bay (Figure 5.47 a - d). AEC maps (Van Wyk, 1987; Norman *et al*., 1987b) indicate a roughly 500 m right-lateral displacement of the Cedarberg- and Peninsula Formations along fault AEC TSP 2's northern extent and a roughly 200 m displacement of the Peninsula- and Goudini Formations along its southern extent (§ 3.4, Figure 3.3). Coastal exposures do not show signs indicative of fault in the area. Approximately 300 m west of where the fault line is interpreted to occur, a 170 m long NNE-SSW trending lineament is noted (Figure 5.47 d). Upon investigation of coastal exposures along the southern option of the lineament, no major left-lateral displacement could be established.

5.2.2.5 Fault AEC TSP 3

Bedding in the immediate vicinity, 100 m east and west of where fault AEC TSP3 is interpreted to occur (Figure 5.47 a, b & c) shows no evidence indicative of a fault. Individual beds could easily be traced across the interpreted fault line, showing no obvious displacement. AEC maps (Van Wyk, 1987; Norman *et al*., 1987 b) show the fault as having no displacement, nor does the area correspond to a particular shatter zone. It is therefore uncertain why it was denoted as a fault. Along the northern portion of the interpreted fault line, borehole TS06 situated on the fault line, intercepts fractured to highly fractured mudstone, siltstone and fine-grained sandstone of the Goudini Formation at depths between 56 – 62.44 m. Detailed borehole log descriptions make no mention of a possible fault zone, nor did interpretation of results from the high resolution aeromagnetics by Cole and Naude, (2007) recognize a lineament, possible or probable fault in the area immediately west of Tony's Bay.
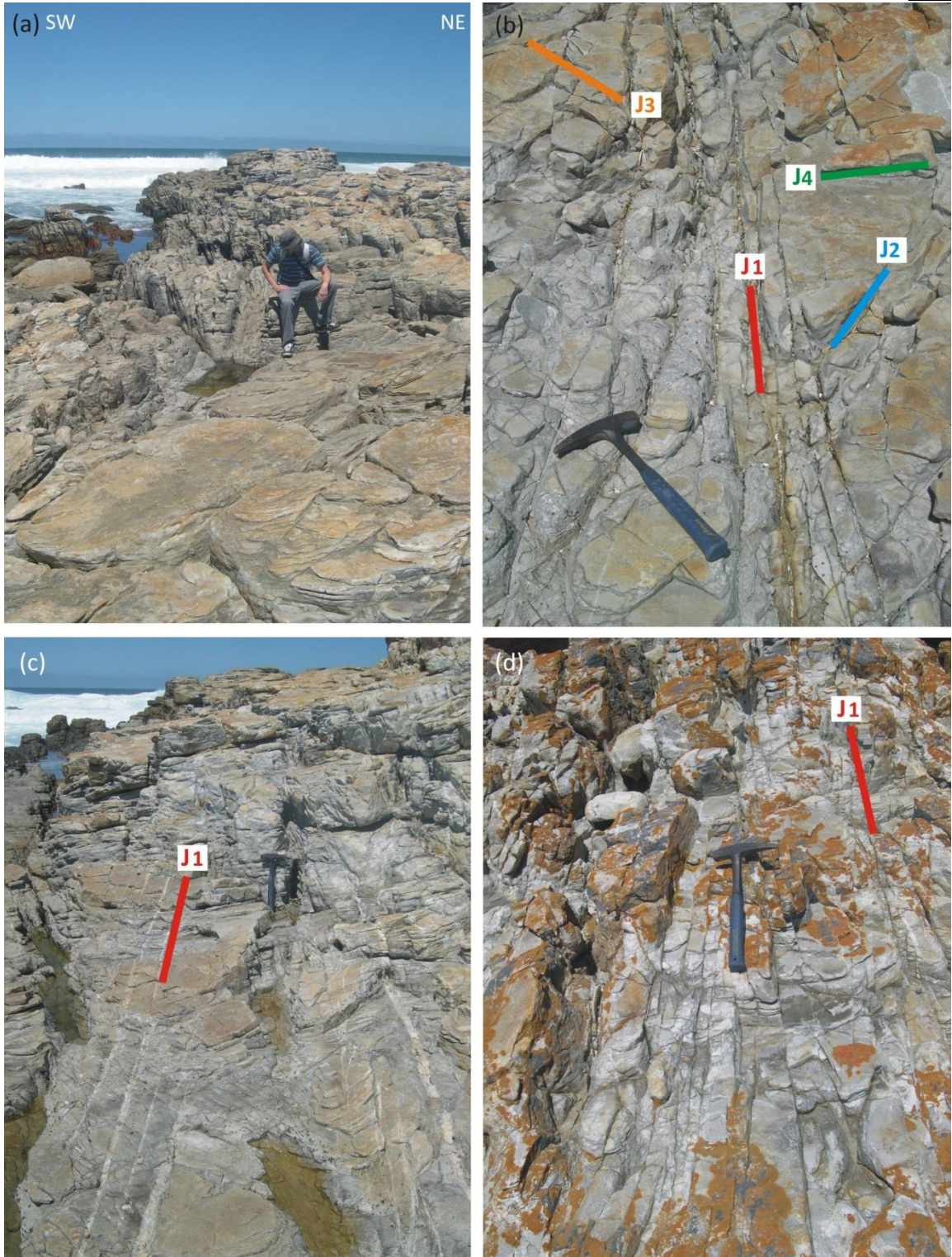
Figure 5.46: (a, b, c & d) Highly fractured quartzite of the Peninsula Formation encountered along the 70 m wide, NE-SW trending zone of coastal exposures where fault AEC DH3 is interpreted to occur. Exposures show closely spaced jointing. Note the veining along joint set J1 in figure c.
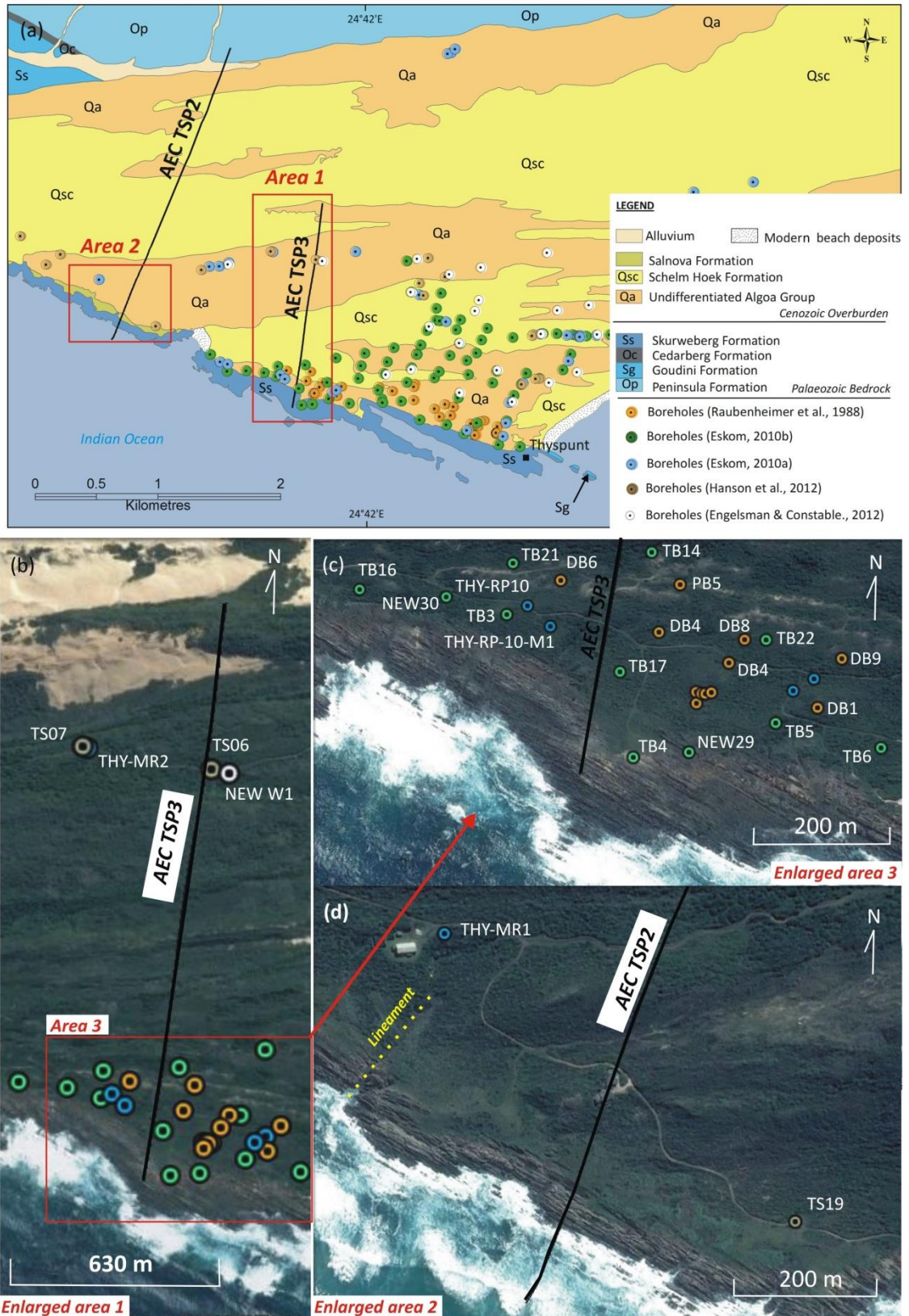
Figure 5.47: (a) Map showing the location of inferred AEC faults in the Thyspunt area. Boreholes in the vicinity of faults are also depicted. Areas of interest are outlined in red and an enlarged view of these areas are shown in figure b, c & d. (b) Enlarged view of area 1 outlined in figure a. An additional area of interest is outlined in red. (c) Enlarged view of area 3 outlined in figure b. (d) Enlarged view of area 2 outlined in figure a. No obvious signs of displacement were observed.

5.2.2.6 Micro-faults

The occurrence of smaller scale normal right-lateral and left-lateral micro or minor faults striking parallel and oblique to bedding is not uncommon along coastal exposures of the Skurweberg and Peninsula Formations between Oyster Bay and Cape St. Francis (Figure 4.48 a & b). These NNE-SSW and ENE-WSW striking, steeply south and north dipping faults (Figure 4.48 c) show displacement ranging between 10 cm to 300 cm (Figure 5.48 d). Micro-faults are associated with areas where joints are closely spaced. Displacements are parallel to joint sets J1 (N-S to NNE-SSW) and J3 (NW-SE) (Figure 5.48 e). Micro-faults do not extend through Cenozoic cover.

5.2.2.7 Thrusts

Localized thrust faulting is observed in the vicinity NE of Thys Bay in quartzite of the Peninsula Formation (Figure 5.49 a & b). Several bedding parallel to subparallel thrusts displaying flat and ramps structures trend NW-SE and have a shallow to very shallow dip towards the SW (Figure 5.49 c & d). Quartz veining is a frequent occurrence in the vicinity of or along these thrust planes (Figure 5.49 a). The amount of displacement along thrust planes could not be established. Thrusts postdate folding, as seen by cut-off relationships. No reverse or back thrusts were noted and no thrusts were found to extend into Cenozoic cover.
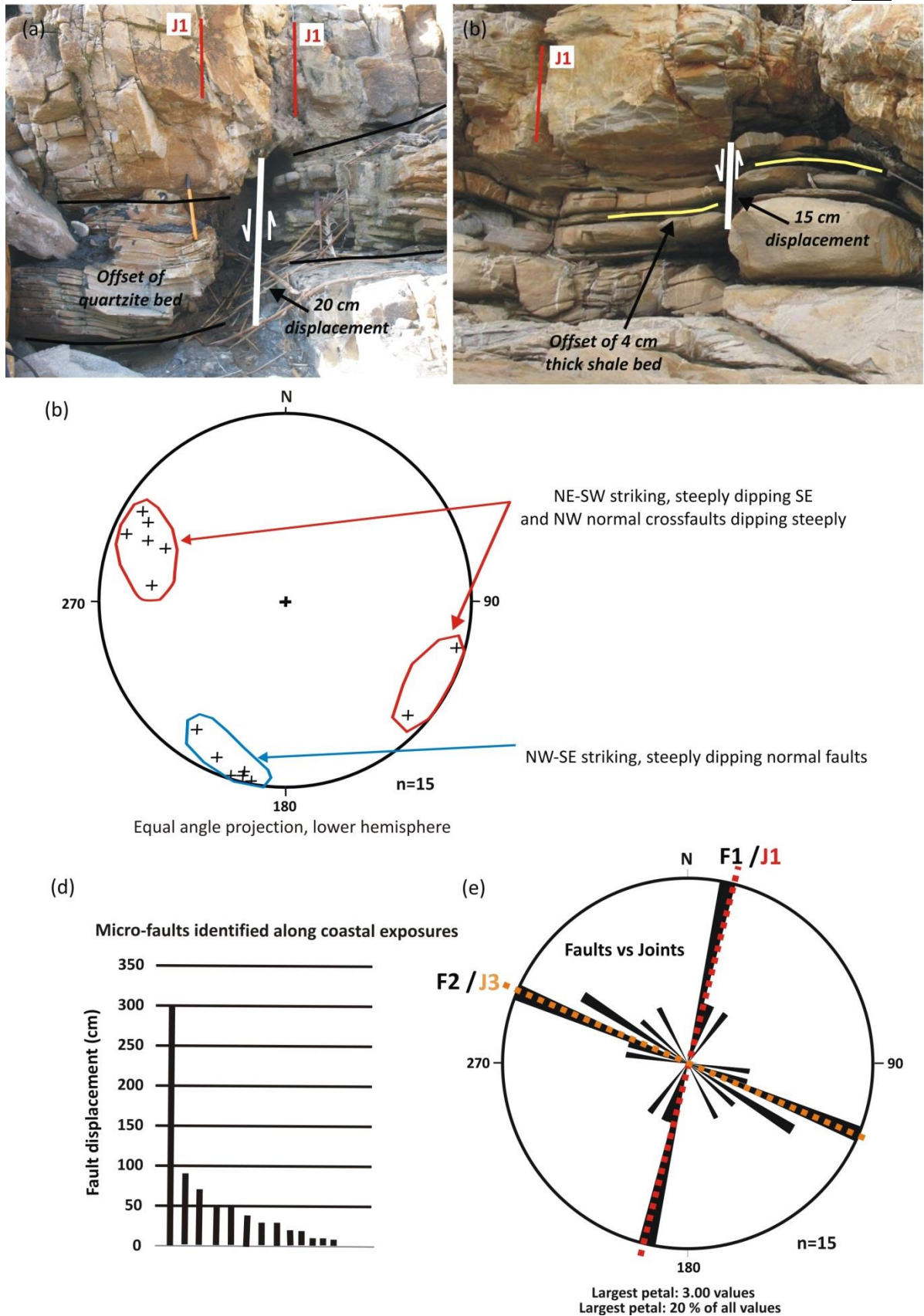
Figure 5.48: (a) A ~15 cm displacement of bedding in the Peninsula along joint set 1, west of Thyspunt. (b) A ~20 cm displacement of a quartzitic sandstone bed within the Peninsula Formation. (c) Stereogram depicting poles to micro-fault planes measured along coastal exposures between Oyster Bay and Cape St. Francis. (d) Displacement along micro-faults (measured in centimetres). (e) Rose diagram showing the strike of micro-faults within the study area. Note how the orientation of micro-faults is parallel to joint sets J1 and J3.
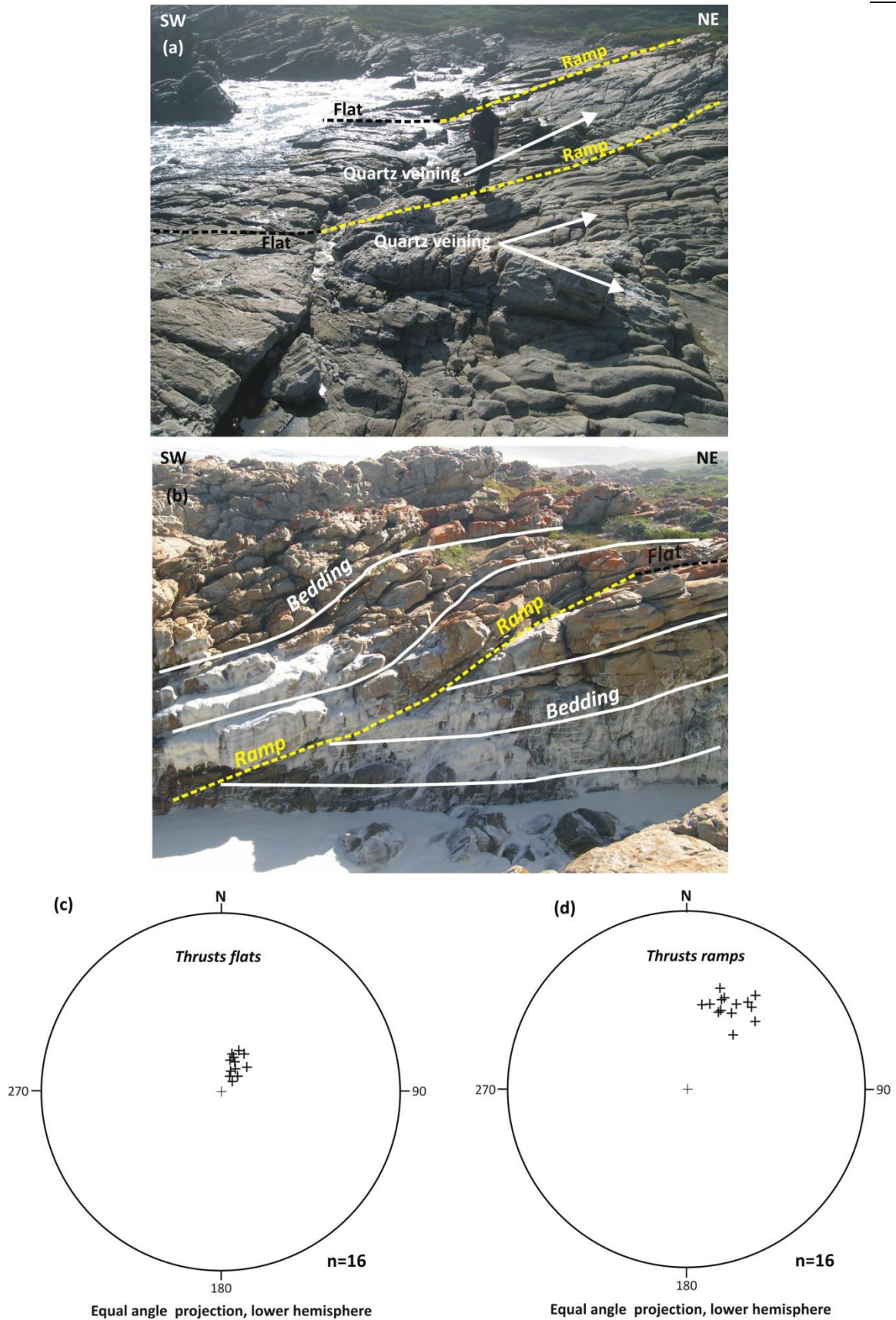
Figure 5.49: (a & b) Thrust fault flats and ramps seen in coastal exposures of the Peninsula Formation quartzitic sandstone immediately east of Thys Bay. All photographs were taken in the same vicinity (Lat: 34° 11' 15.9", Long: 24°44' 21.7"). Note the presence of quartz veining parallel to fault planes (c) Stereogram of poles to thrust fault flat planes and, (d) thrust fault ramp planes.

5.2.3 Joints and fractures

Joint measurements were predominantly obtained from coastal outcrop exposures between Oyster Bay and Cape St. Francis. Due to limited outcrop exposure of the Cedarberg, Goudini, and Baviaanskloof Formation as well as strata of the Bokkeveld Group, joint measurements were taken in surrounding areas outside the study area. Figure 4.50 a & b show a rose diagram and stereonet of all joint measurements taken. The dominant joint direction, joint set J1, trends N-S to NNE - SSW; perpendicular to the NW-SE bedding strike. The joint set has a general strike of 020° (± 20°). Along coastal exposures the joint set is easily identified, trending perpendicular to the coastal margin between Oyster Bay and Seal Point.   Well-developed joint set, J2, strikes NE-SW with a 040° (±15°) strike. Joint sets J1 and J2 dip vertical or subvertical with a northwesterly dip. Joint set J1 frequently also exhibits a steep SE dip. Together joints J1 and J2 form conjugate set X. Joint set J3 trends NW-SE with a 300° (± 30°) strike, parallel or subparallel to bedding and dip either vertically or dip 65-90° E or ESE. Joint set J4 trends ENE-WSW with a 055° (± 30°) strike and dip vertically or subvertical with a northwesterly dip. Joint sets J3 and J4 produce conjugate set Y. A horizontal to subhorizontal joint set, J5 is also identified (Figure 5.50 b).
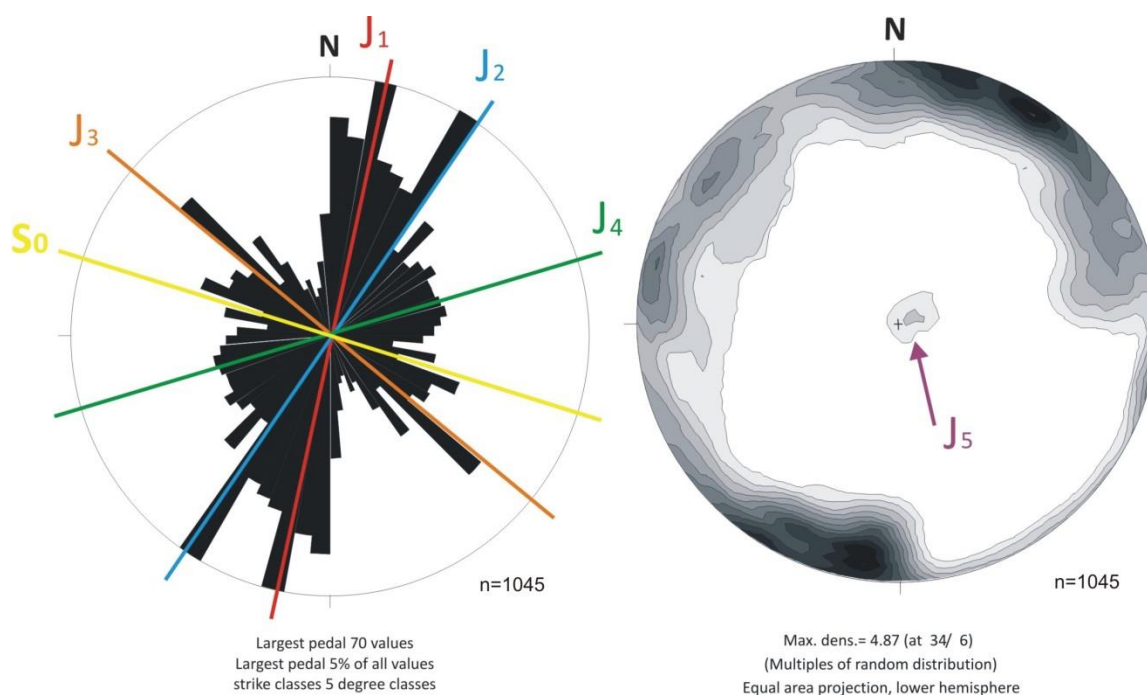
Figure 5.50: (a) Rose diagram showing strike direction of joints. (b) Contoured stereonet of poles to joint planes. S0 indicates bedding. J1-J5 indicates joint sets 1-5.

Locally, joint sets may vary in orientation and some subordinate sets may locally be more dominant depending on the area and the lithological nature of bedrock strata. Rose diagrams for joint direction in the individual formations are depicted in Figure 5.51. Jointing is generally less pervasive in argillaceous lithologies. Due to limited outcrop exposure and pencil shale fracturing of some shale units within the study area, the number of joint readings within the Cedarberg, Goudini, Baviaanskloof Formations and Bokkeveld Group were limited to <15. Strata of the Peninsula and Cedarberg Formations show a dominant N-S to NNE-SSW trending J1 joint set. The Goudini, Skurweberg and Baviaanskloof formations show a more dominant NNE-SSW to NE-SW J1 joint set. The undifferentiated Bokkeveld Group shows a dominant NW-SE trending joint set.   Within the arenaceous Peninsula and Skurweberg Formations

subordinate argillaceous shale, siltstone and grey-wacke horizons show lesser and more widely spaced jointing than the overlying and underlying quartzite units. Joints occurring within the quartzite often do not transect or extend through to interbedded argillaceous and lithologically less competent units (Figure 5.52 a, b & c). The strike of major joint planes can however be traced; extending through different lithologies (Figure 5.52 c).

Figure 5.51: Rose diagrams depicting joint and fracture trends measured in the Peninsula, Cedarberg, Goudini, Skurweberg and Baviaanskloof Formations and undifferentiated Bokkeveld Group.
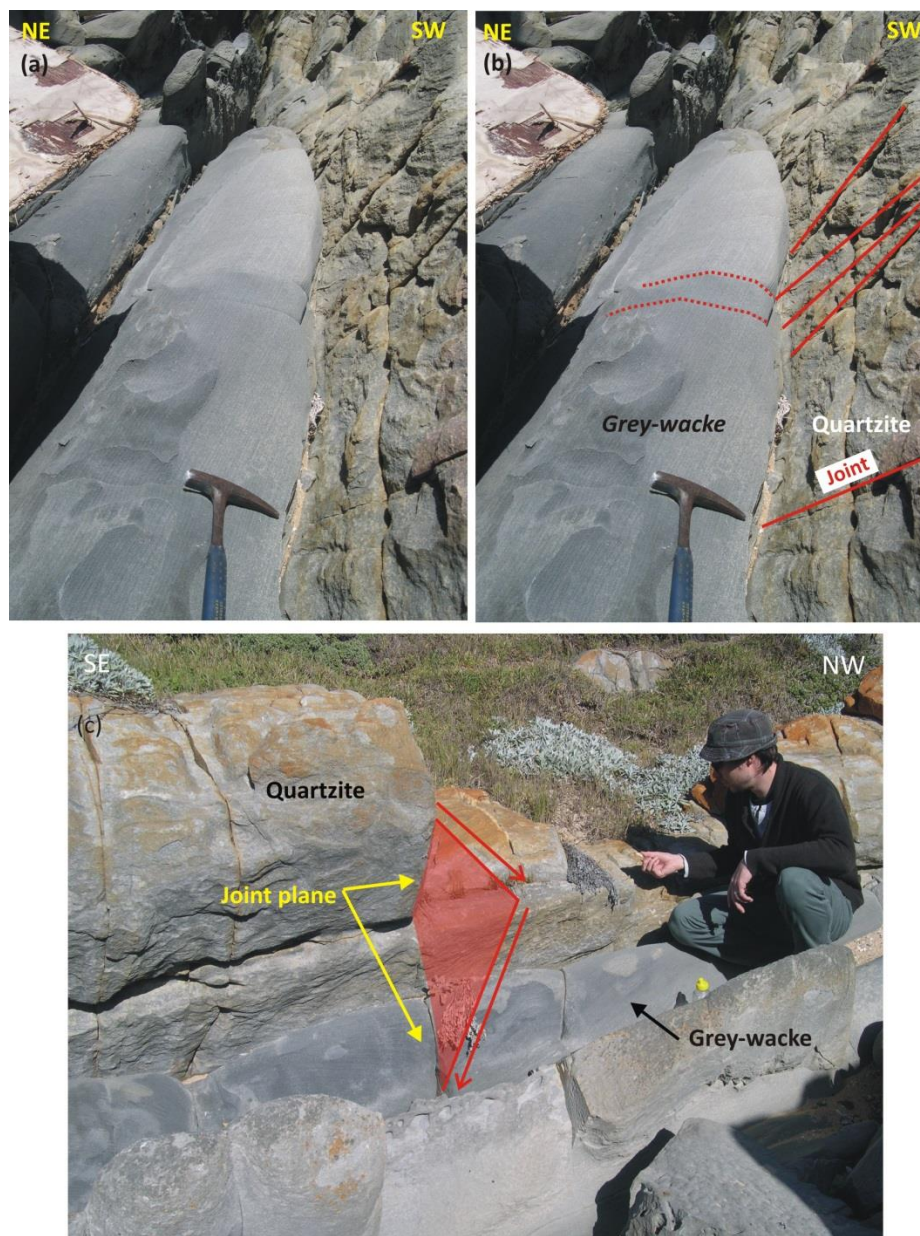
Figure 5.52: (a & b) Photo (a) without and (b) with annotation showing a subordinate greywacke within the predominantly arenaceous Skurweberg Formation. Jointing is less pervasive and more widely spaced within the more argillaceous unit than the arenaceous quartzite. (c) Major joint plane extending through both greywacke and quartzite lithologies.

The spacing of joints varies considerably. Joint spacing range between very widely spaced (1- 3 m) to closely spaced (10 - 30 mm) (Figure 5.53 a & b). A distinctive pattern in the spacing of joints is observed where areas of very widely spaced jointing alternate with areas of closely spaced jointing. Along coastal exposures, areas of closely spaced (30 - 100 mm) to very closed spaced jointing create zones of structural weakness that weather negatively to produce deep gullies and surge channels described as 'shatter zones' (Raubenheimer *et al.*, 1988a; Goedhart *et al.*, 2008) that trend perpendicular or oblique to the coastline and parallel to the strike of joint sets J1, J2. J3 and J4 (Figure 5.53 a & Figure 5.54 a). In areas where joint sets exhibit closely spaced jointing in close proximity, a broad coastal inlet within the rugged coastal is formed. Gullies that form parallel to the coastline and bedding strike can often be attributed to erosion of softer inter-bedded units rather than joint-related shatter zones (Figure 5.54 b & Figure 5.13).
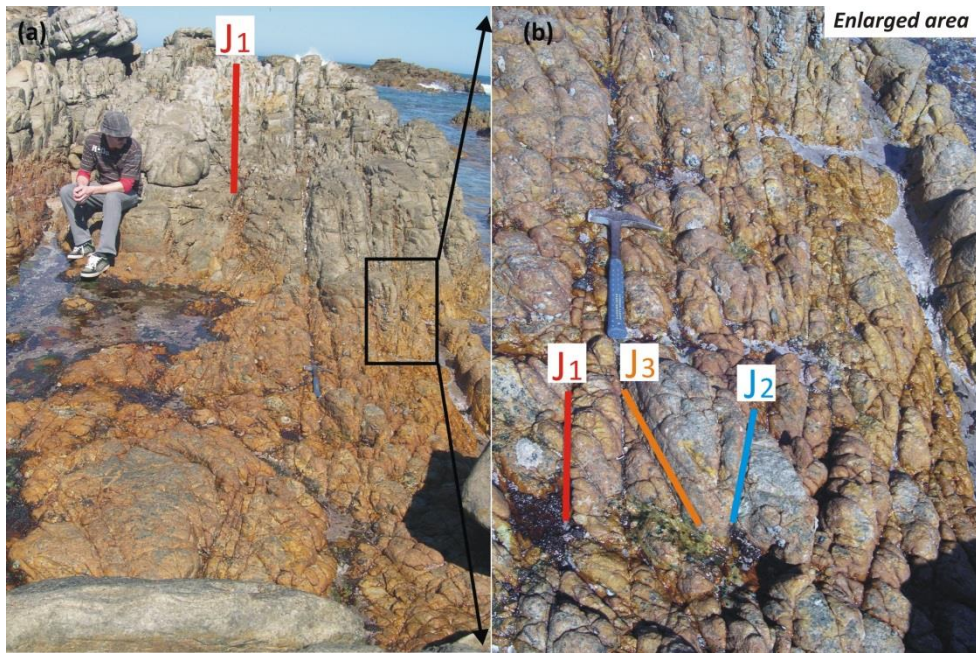
Figure 5.53: (a) Closely spaced jointing in quartzite of the Peninsula Formation. Note the development of a gully towards the northwest. (b) Enlarged area seen in figure a showing joint direction and spacing.
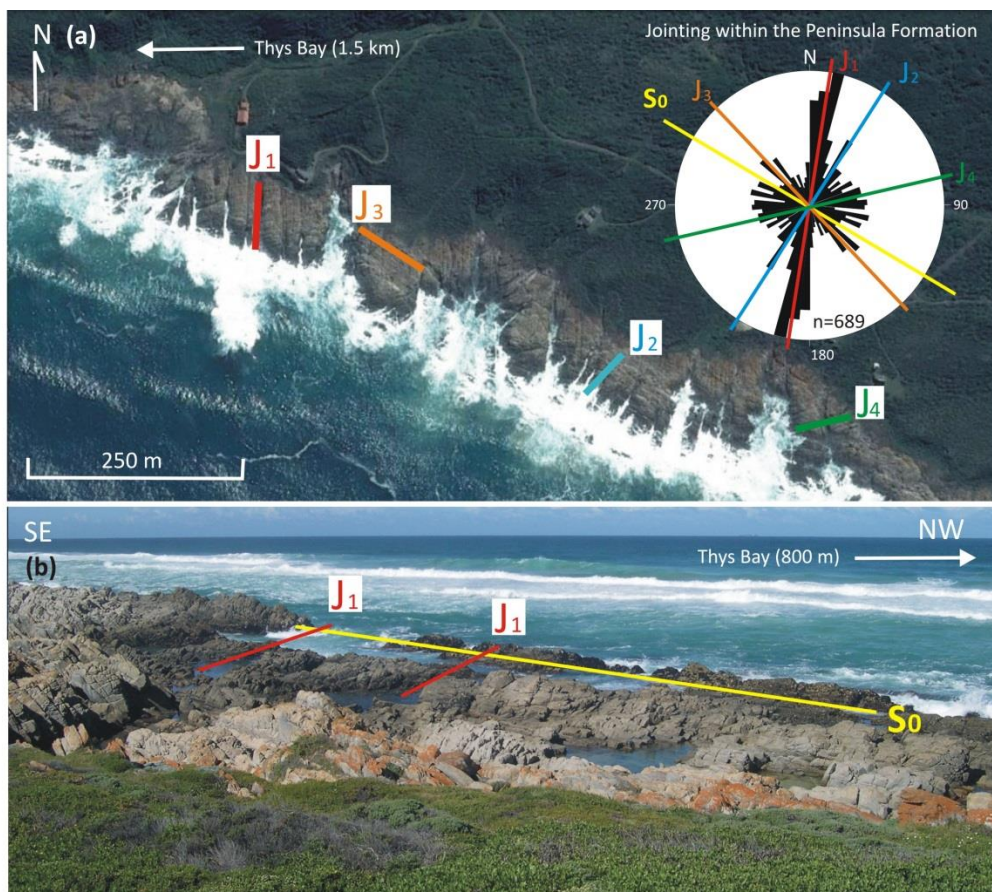
Figure 5.54: (a) An aerial view of gully formation observed in the Peninsula Formation, just east of Thys Bay. Gullies form in areas where jointing is closely spaced. Gully trends match joints trends found in the area. (b) Gullies forming along closely spaced joints are associated with the joint set orientations of joint set J1, perpendicular to bedding strike east of Oyster Bay. Gullies forming parallel to bedding are the result of erosion of softer inter-bedded units (Lat: 34° 10' 37.3", Long: 24° 39' 56.3"). S0 indicates bedding.

Generally, joint apertures range from slightly open (<1 mm) to moderately open (10 – 30 mm) with wide apertures openings (> 30 mm) of 50 mm noted in response to weathering. Joint and fracture openings are empty or filled with rusty brown iron precipitate (Figure 5.55 a, b & c), or milky white quartz (Figure 4.56 d). Joint openings in arenaceous strata of the Skurweberg and Peninsula Formation show quartz fillings (Figure 5.55 d & e). Quartz veins typically range from thin (3 -10 mm) to thick (> 30 mm). Joint openings in argillaceous strata of the Baviaanskloof Formation are filled with very thin (<1 mm) to thin (3-10 mm) iron precipitate (Figure 5.55 a, b & c). De Beer (2000) noted that within the Peninsula and Skurweberg Formations, apertures of northerly trending joint sets (joints set J1) are typically quartz filled, while north-northeastly while northeasterly joints apertures are generally open. Field mapping shows this observation does not consistently hold true.   Quartz filled sigmoidal tension gashes indicative of more ductile shear deformation are occasionally observed in quartzite of the Peninsula and Skurweberg Formations (Figure 5.56 a & b). The tension gashes are S or Z-shaped and are rotated en-echelon along joint sets.

Joint sets transect all other structural features, however no joint set or fracture was found to extend into Cenozoic overburden.
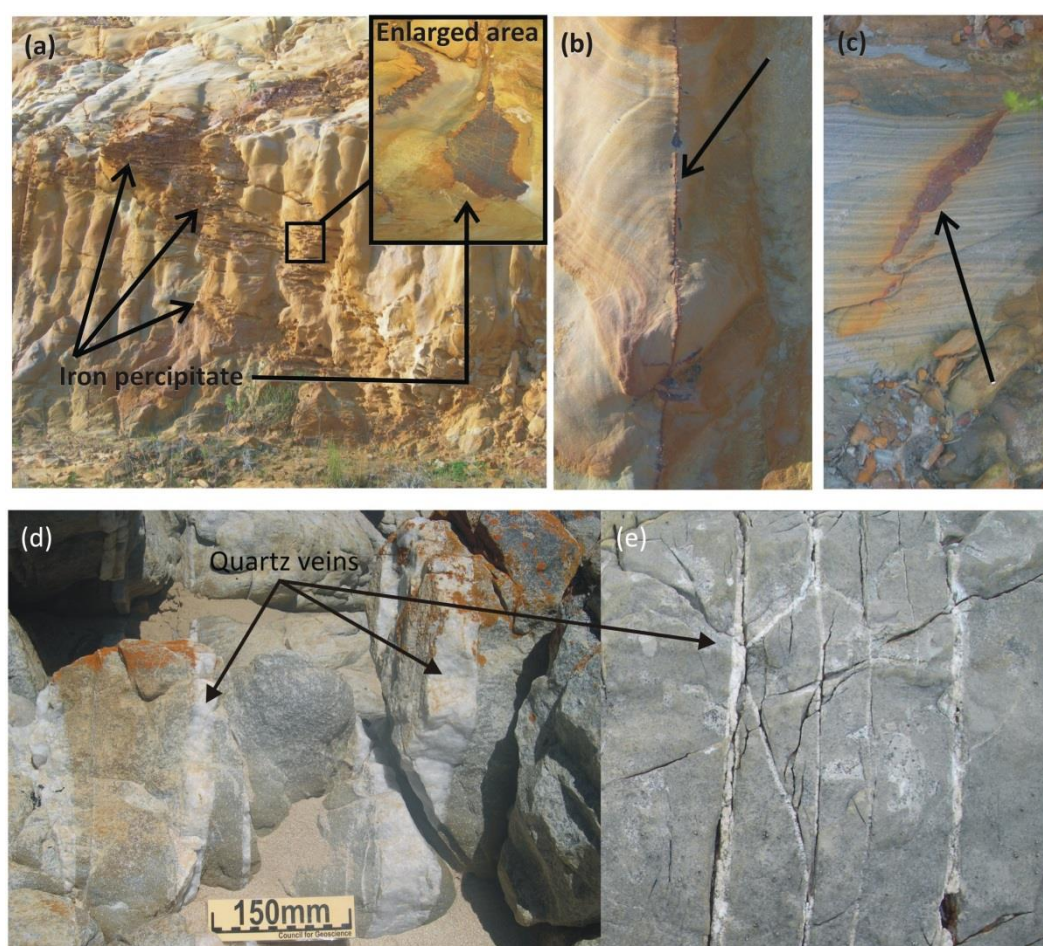
Figure 5.55: (a & b) Joint and fracture planes filled with iron precipitate within highly weathered sandstone of the Baviaanskloof Formation (Lat: 34° 00' 55.5" Long: 24° 51' 32.2"). (c) Fracture filled with iron precipitate in siltstone of the Baviaanskloof Formation (Lat: 34° 01' 41.1" Long: 24° 51' 25.4"). (d & e) Quartz filled joints and fractures in quartzitic sandstone of the Skurweberg Formation (Lat: 34° 11' 31.8" Long: 24° 42' 54.7") and Peninsula Formation (Lat: 34° 11' 52.3" Long: 24° 46' 28.4").
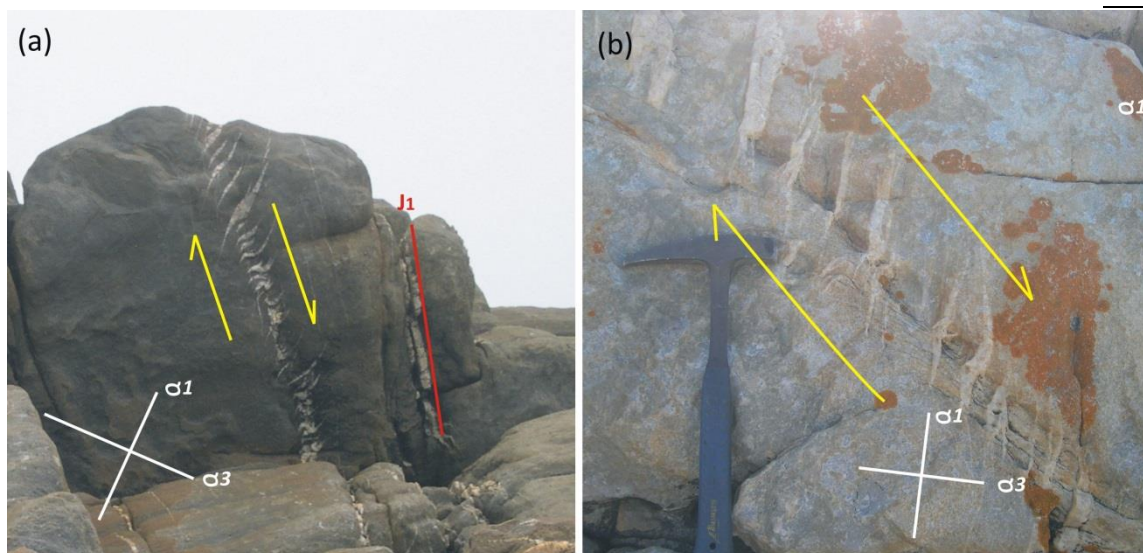
Figure 5.56: (a & b) Quartz filled sigmoidal tension gashes in quartzitic sandstone of the Skurweberg Formation, SE of Oyster Bay along coastal outcrop exposure (Lat: 34° 10' 35.5" Long: 24° 39' 48.4").

5.2.4 Cleavage

Cleavage is most prevalent and well developed in argillaceous (shale) formations, horizons or layers. At Thyspunt, along the southwestern limb of the regional Cape St. Francis anticline, interbedded shale within the Skurweberg Formation show a pervasive, NE-SW trending and moderately dipping NE cleavage with an average azimuth and dip of 052°/ 46° (Figure 5.57 a, b & c). The cleavage is axial planar. Slaty cleavage indicative of the fissility of the strata is also often noted in argillaceous units of the Baviaanskloof Formation and Bokkeveld Group. The lithologically less competent shales of the Bokkeveld Group generally show pencil cleavage (Figure 5.22 a). Cleavage is far less pervasive in arenaceous formations and more difficult to identify. Shallow, 25-45° SW dipping fractures along the northeastern limb of the main Cape St. Francis anticline is interpreted as axial planar fracture cleavage associated with sandstones of the Peninsula and Skurweberg Formation (Figure 5.58). The intersection of cleavage and bedding is manifested in structures seen in Figure 5.59.
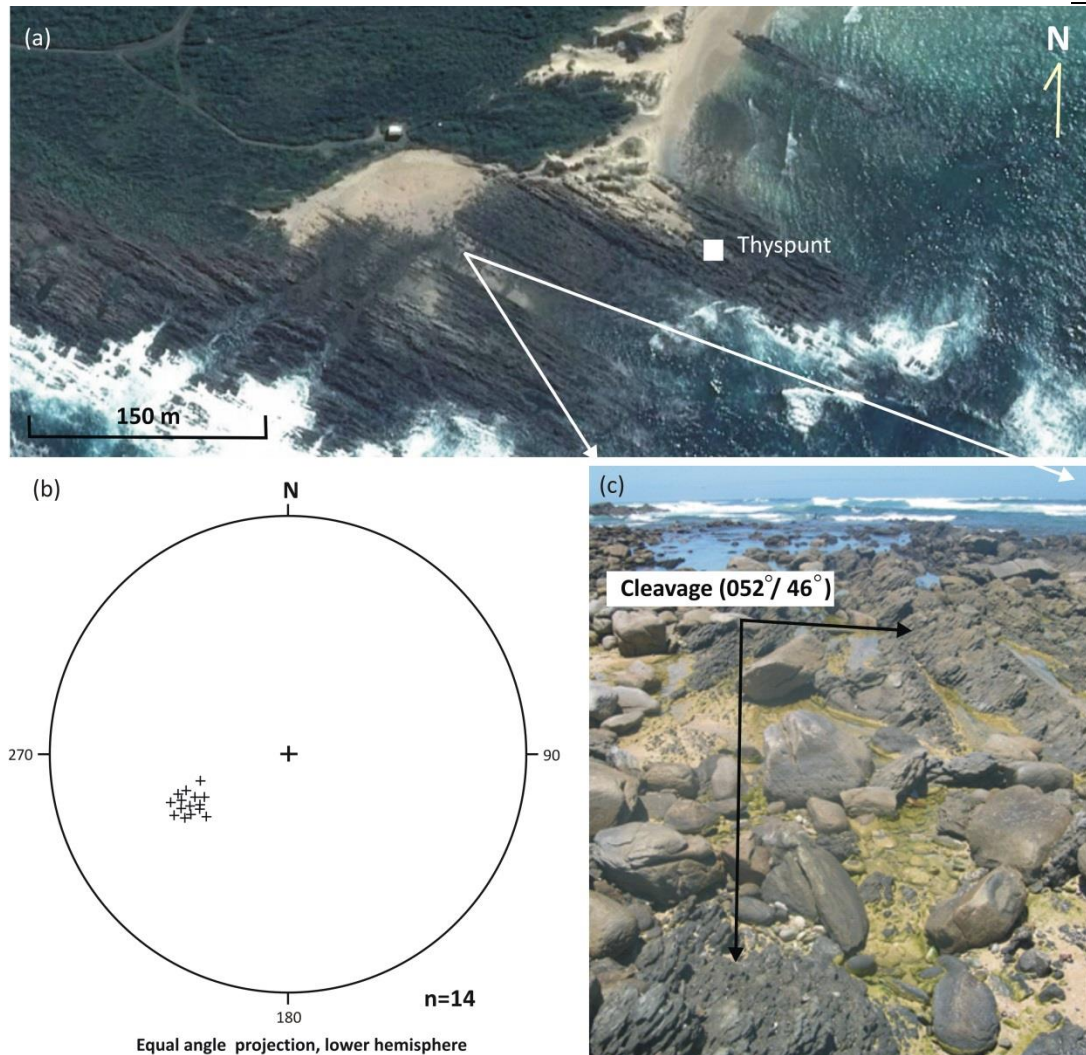
Figure 5.57: (a) Overview map, indicating the location of interbedded shale within the Skurweberg Formation at Thyspunt where pervasive NE dipping cleavage is encountered. (b) Stereogram depicting poles to cleavage planes measured at Thyspunt. (c) Cleavage observed at Thyspunt in shale of the Skurweberg Formation (Lat: 34° 11' 32.0" Long: 24° 42' 51.7").
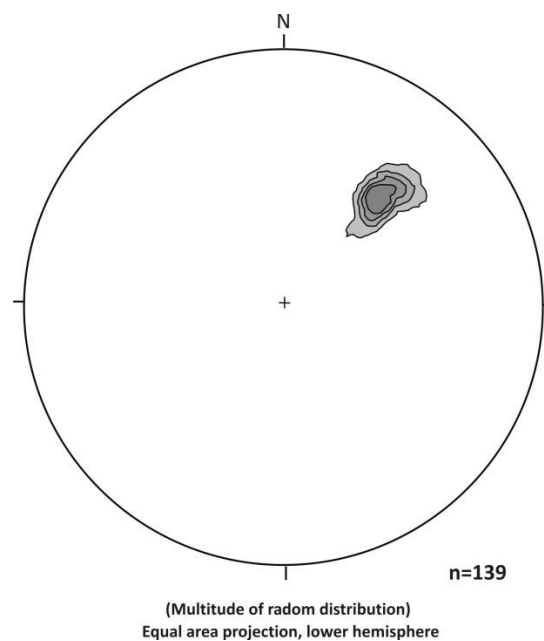
Figure 5.58: Southwest dipping axial planar cleavage in arenaceous sandstones of the Peninsula and Skurweberg Formation along the NE fold limb of the Cape St. Francis anticline.
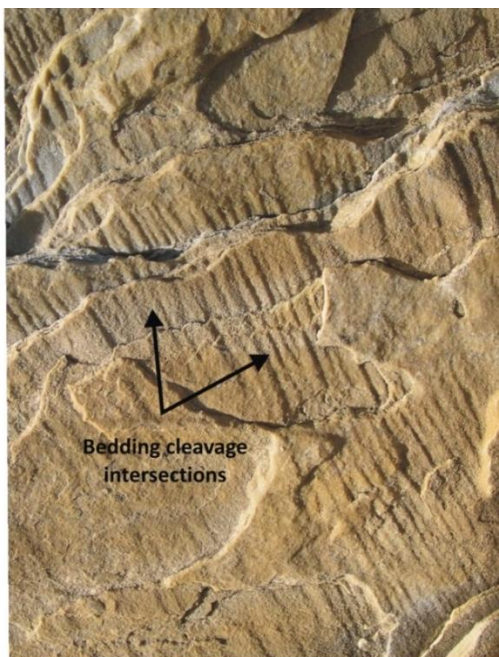
Figure 5.59: Possible intersections between bedding and fracture cleavage in quartzite of the Peninsula Formation west of Thys Bay (Lat: 34° 11' 16.9" Long: 24° 44' 23.0").

5.3 Petrography

5.3.1 Table Mountain Group

5.3.1.1 Peninsula Formation (Sample D22)

Petrographic light microscopy of quartzite from the Peninsula Formation, located east of Thyspunt reveal a lithology that consists almost entirely of recrystallized monocrystalline and occasional polycrystalline quartz grains (98%) and very minor rock fragments (1%) (Figure 5.60 a & b). Accessory minerals are rare and include mica (Figure 5.60 c), zircon (Figure 5.60 d & e) and opaque minerals (1%). Feldspars appear to be totally absent. Whilst the sample should be classified as a compositionally supermature quartz arenite, it is effectively an orthoquartzite (>99% quartz grains). The sample is well sorted and coarse-grained with equigranular grain sizes ranging on average between 800 – 1200 µm. Well sorted subrounded to well rounded quartz grains are cemented by authigenic quartz (chemical compaction) that has formed outgrowths and overgrowths on the original sand grain (Figure 5.60 e), producing an interlocking crystalline granular grain texture. The original outline of the framework grains are preserved as fine dirt lines visible under plane polarised light (Figure 5.60 d). Grain boundaries are sutured (Figure 5.60 c), embayed (Figure 5.60 b) or straight trending towards the presence of triple junctions (120° grain boundary intersections) (Figure 5.60 b) in isolated places similar to a granoblastic polygonal texture. Embayed grain boundaries indicative of grain boundary migration are rare. Irregular grain boundaries are the result of pressure dissolution in response to the increased stress as sediment undergoes diagenesis and grains were compacted (Vernon, 2004). No preferred orientation could however be established. Deformation effects are noted in shadow staining (undulose extinction) and rare fracturing of framework grains. Siliceous rock fragments range from 500 - 1200 µm in diametre and are composed of quartz and microcrystalline quartz (chert) grains (Figure 5.60 b). The small grain size of micas makes it difficult to identify individual minerals according to their optical properties. Mica minerals occur in cracks and spaces between quartz grains (Figure 5.60 c). High relief zircon grains are <200 µm and are generally euhedral to subhedral (Figure5.60 d & e). The sample is textural and compositional mature.
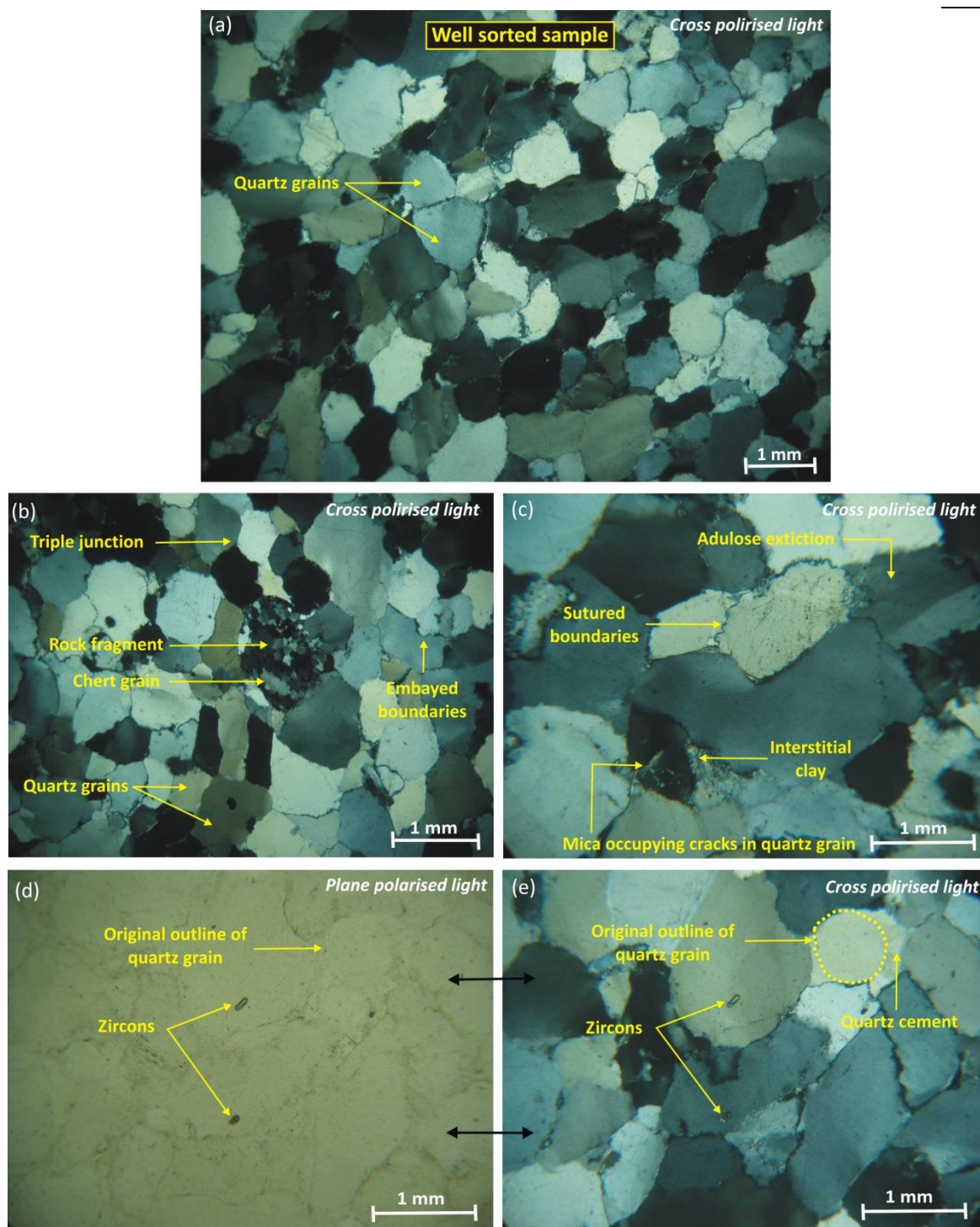
Figure 5.60: (a) Photomicrographs of the Peninsula Formation orthoquartzite depicting: (a) the overall composition of sample D22, (b) sample composed predominantly of quartz grains and minor rock fragments, embayed and straight grain boundaries trending to the formation of triple junctions (120° grain boundary intersections), (c) undulose extinction of quartz grains, sutured grain boundaries and interstitial clay (mica) filling fractures in quartz grains, (d) zircons and fine-grained 'dirt' lines outlining the original rounded to well rounded grain shapes, (e) the same image in figure (d) viewed under cross polarized light, showing quartz cement.

5.3.1.2 Goudini Formation (Samples D14 & D14.1)

Petrographic analysis of Goudini Formation sandstone sampled at Thyspunt and Cape St. Francis reveal a lithology comprised of predominantly recrystallized monocrystalline equigranular quartz grains with minor rock fragments (90%-95%) and mica flakes (<5%) (Figure 4.61 a, b & c). Accessory minerals include zircon (Figure 5.61 d), rutile and other unidentified heavy mineral opaques (Figure 5.61 e). No feldspars were identified. The sandstone sample is well sorted and original framework grains are subrounded to subangular. At Thyspunt (sample D14) some framework grains are cemented by quartz that appear to have formed outgrowths and overgrowths on the original sand grain (Figure 5.61 a). Fine to medium quartz grains (200-500 μm) exhibit an interlocking texture where framework grain boundaries are in contact with each other. The boundaries between framework grains are serrated (Figure 5.61 a), sutured (Figure 5.61 d), embayed (Figure 5.61 b) and straight. Triple junction grain boundary intersections are less frequently observed. The majority of quartz grains show shadow strain (undulose extinction) and fractured sand grains indicative of mechanical compaction or brittle deformation are not uncommon (Figure 5.61 a). Crushed quartz grains produce a mylonitic texture indicative of dynamic recrystalisation in places. The fractures in sand grains appear to have a common orientation. Quartz grains do occasionally exhibit strain induced elongation with a preferred orientation. Clay and larger mica flakes (100-400 μm) show a strong preferred orientation in sandstone from Cape St. Francis (sample D14.1) (Figure 5.61 c). Rock fragments are well rounded and siliceous with microcrystalline quartz (Figure 5.61 b). Heavy minerals are generally subhedral to euhedral in shape and <250 μm in diameter. Sandstones sampled at Thyspunt and Cape St. Francis, at the base of the Goudini Formation is classified as compositionally and texturally mature quartz arenites possibly deposited in a high energy environment.

5.3.1.3 Skurweberg Formation

(i)   Quartzite sample (Sample D4)

Quartzite of the Skurweberg Formation is composed of well sorted, medium to coarse-grained recrystallized monocrystalline and infrequent polycrystalline quartz grains (>95%) with minor rock fragments (1%) and very minor interstitial clay (2%) (Figure 5.62 a, b & c). Feldspars appear to be absent. Accessory minerals include mica (occasionally identified as muscovite and biotite) (Figure 5.62 a), zircon, rutile (Figure 5.62 d) and opaque minerals (2%). The sample is classified as a texturally and compositionally supermature quartz arenite - lithologically and texturally very similar to the Peninsula Formation. The tightly interlocking equigranular quartz grains range on average between 400 - 800 μm in size. Original sand grains are predominantly subrounded to rounded and cemented by quartz that has formed outgrowths and overgrowths on the original sand grains (secondary enlargement) to give them a subrounded to angular appearance. The boundaries between grains are sutured (Figure 5.62 c), embayed (Figure 5.62 a) and straight (Figure 5.62 c) with rare triple junctions (120° grain boundary intersections). The numerous sutured and embayed boundaries provide evidence of grain boundary migration, indicative of strain in a region which has undergone deformation (e.g. Vernon, 2004). Quartz grains exhibit shadow strain (Figure 5.62 c). Minor very fine-grained authigenic interstitial clay occurs between sand grain boundaries and act as fill in fractured quartz grains (Figure 5.62 b). Biotite laths do occasionally occur as larger crystals (<500 μm in length) (Figure 5.62 a). Detrital zircon grains are well rounded and <200 μm in size. Detrital subhedral to anhedral rutile grains are of similar size to framework grains (500 -

800 µm) (Figure 5.62 d). Based on the maturity of the sample, a depositional environmental similar to the Peninsula Formation is envisaged.
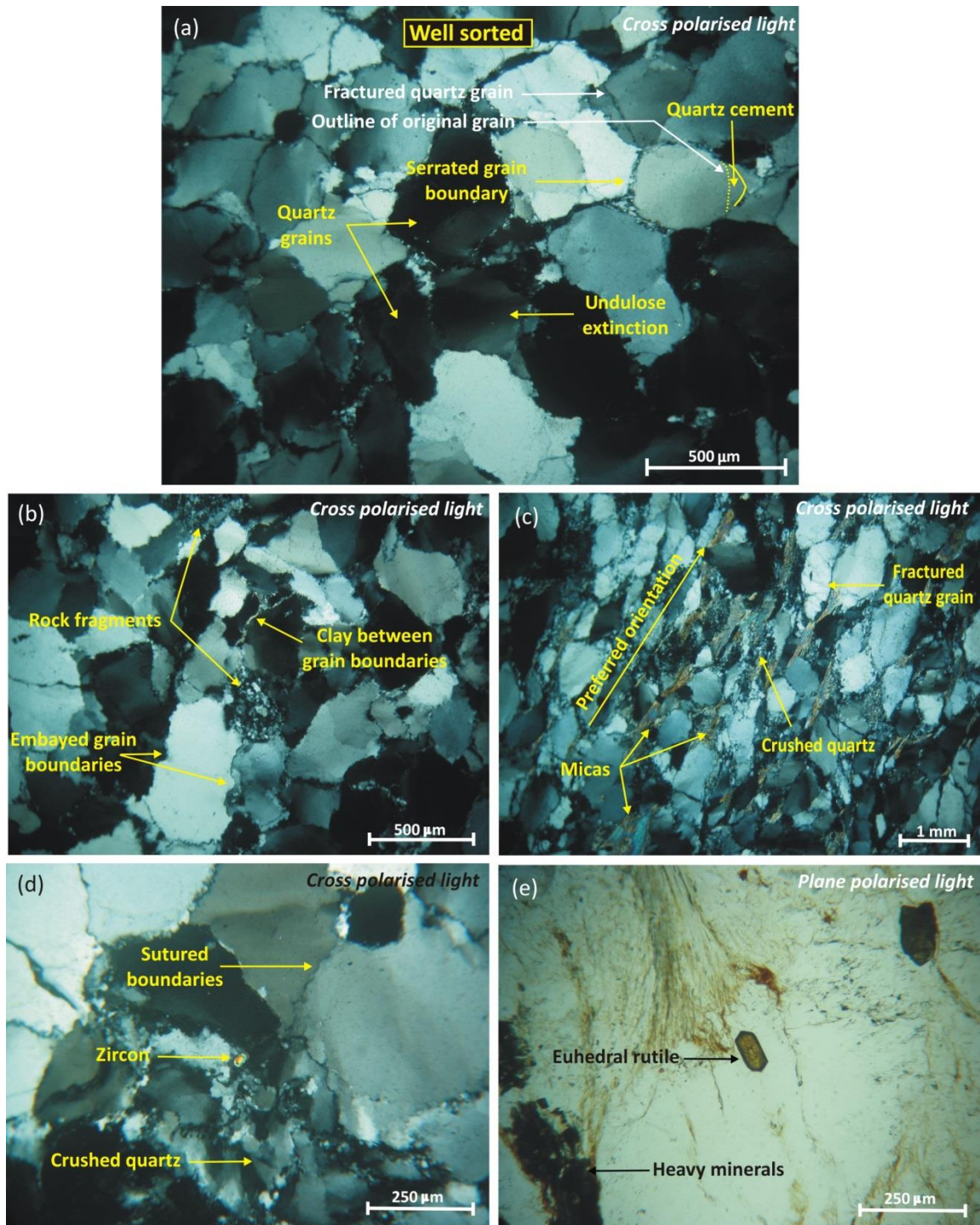
Figure 5.61: Photomicrographs of the Goudini Formation sandstone depicting: (a) the overall composition of sample D14, (b) minor occurrence of rock fragments, interstitial clay between grain boundaries and sutured grain boundary contacts (c) preferred orientation of quartz grains, crushed quartz, interstitial clay and larger mica flakes (d) deformed quartz and zircon, (e) euhedral rutile and opaque heavy minerals.
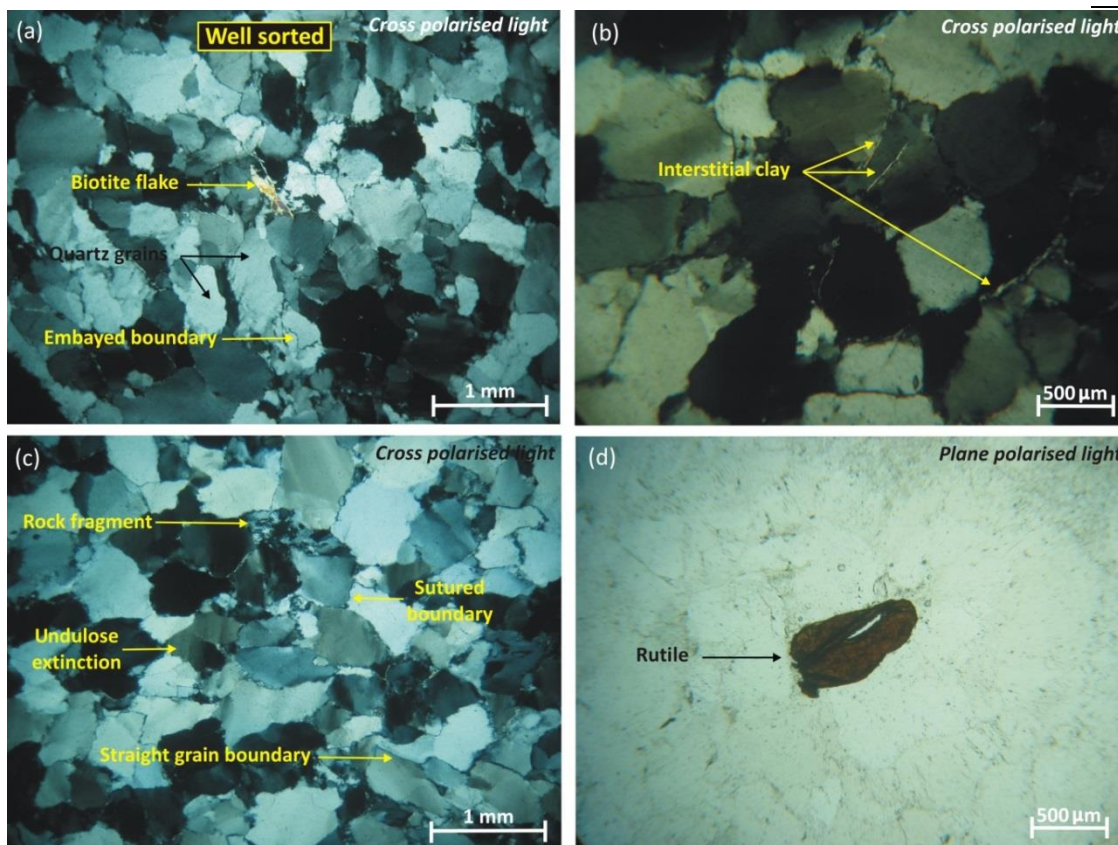
Figure 5.62: *Photomicrographs of the Skurweberg Formation quartz arenite depicting: (a) overall composition comprising predominantly quartz grains, (b) minor interstitial clay between grain boundaries, (c) rock fragment, undulose extinction, straight and sutured grain boundaries, (d) detrital anhedral rutile.*

(ii) Grey-wacke sample (Sample D3)

Petrographic light microscopy of argillaceous sandstone sampled from the Skurweberg Formation reveal a moderately to poorly sorted lithology comprised of recrystallized fine to medium-grained monocrystalline quartz grains (75-80%) set in a fine-grained detrital clay matrix (20-25%) (Figure 5.63 a) that fills spaces between the larger clastic framework grains. The high percentage of allogenic clay matrix is too fine-grained to allow the identification of individual minerals. Certain larger grains (150 - 200 μm) within the matrix are however identified as muscovite and biotite. Sample D3, is classified as an immature quartz wacky based on a >15% matrix and >95% quartz grain framework. Detrital accessory minerals include zircons, rutile and other unidentified heavy opaque minerals (<5%) (Figure 5.63 b & c). No feldspars grains identified. Equigranular framework grains range between 200 - 300 μm in size and are generally subangular to subrounded, however angular grains are not uncommon. The sample exhibits grain-to-matrix boundaries, rather than grain-to-grain boundary contacts (Figure 5.63 d). Where framework grains are in contact with each other, boundaries are straight or sutured. Minerals in the clay matrix are aligned (preferred orientation) (Figure 5.63 d). Subhedral zircon grains are <300 μm in diametre and fractured (Figure 5.63 d). Rutile grains are subhedral and roughly <300 μm in size (Figure 5.63 b & c). Layering of heavy minerals is observed (Figure 5.63 e). Deformation is evident in shadow straining in recrystallized quartz grains and kinked micas. Folded and bent micas flakes (Figure 5.63 d) exhibit wavy extinction and are indicate of more plastic deformation (E.g. Vernon, 2004).
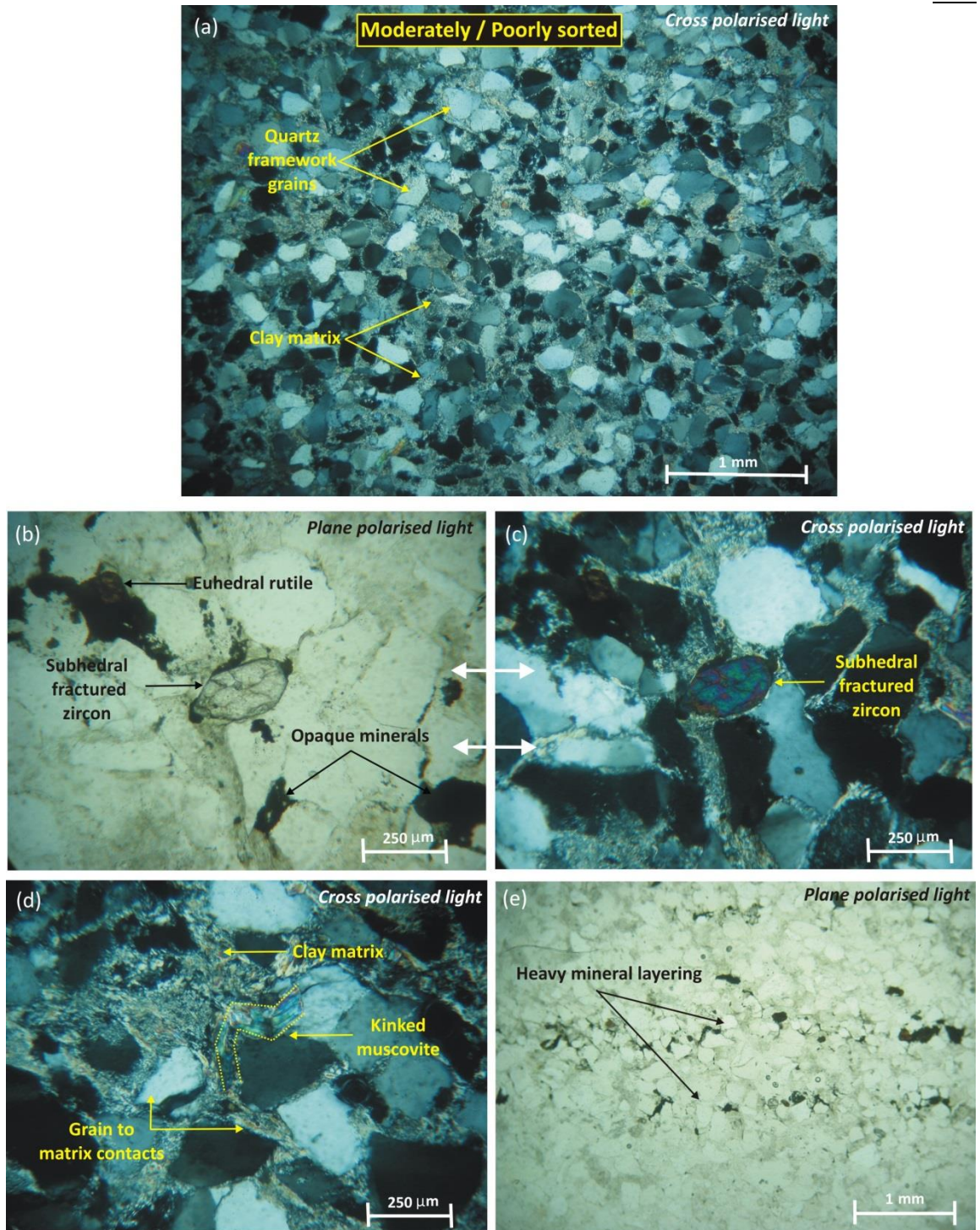
Figure 5.63: *Photomicrographs of Skurweberg Formation quartz wacke depicting: (a) overall composition quartz wacke (sample D3) comprising > 15% matrix and >95% quartz framework grains, (b) euhedral rutile and subhedral zircon viewed under plane polarized light and, (c) under cross polarized light, (d) fine-grained clay matrix, kinked muscovite flake and grain to matrix contacts, (e) heavy mineral layering.*

5.3.1.4 Baviaanskloof Formation (Samples D12 & D13)

The epiclastic sandstone of the Baviaanskloof Formation (possible the Kareedouw Member) sampled along the N2, 7km NE of Humansdorp, is well sorted and comprised predominately of recrystallized monocrystalline and polycrystalline quartz grains, minor rock fragments (92%) and interstitial clay (5%) (Figure 5.64 a). Accessory minerals include larger biotite flakes (not associated with clay matrix), zircon (Figure 4.64 b) and other unidentified opaque heavy minerals (3%) (Figure 5.64 c). No feldspar grains were identified. The sample is therefore classified as a compositionally mature quartz arenite. Framework grains are generally tightly interlocked and grain boundaries are in contact with each other or interstitial clay (Figure 5.64 d). Dissolution of quartz grains (chemical compaction) is observed where quartz framework grains are cemented by quartz. Original medium-grained (400 – 500 μm) sand grains visible under plane polarised light are rounded to subrounded (Figure 5.64 c & d). Grain boundary contacts are sutured (Figure 5.64 b) and straight. Triple junctions (120° grain intersections) grain contacts are rare. Deformation effects are seen as shadow strain in quartz grains (Figure 5.64 b). Subrounded siliceous rock fragments are >500 μm in size and composed of quartz and microcrystalline quartz (chert). Detrital euhedral to subhedral zircons are <150 μm in size (Figure 5.64 b). The textural and compositional maturity of the sample is indicative of a high energy environment.
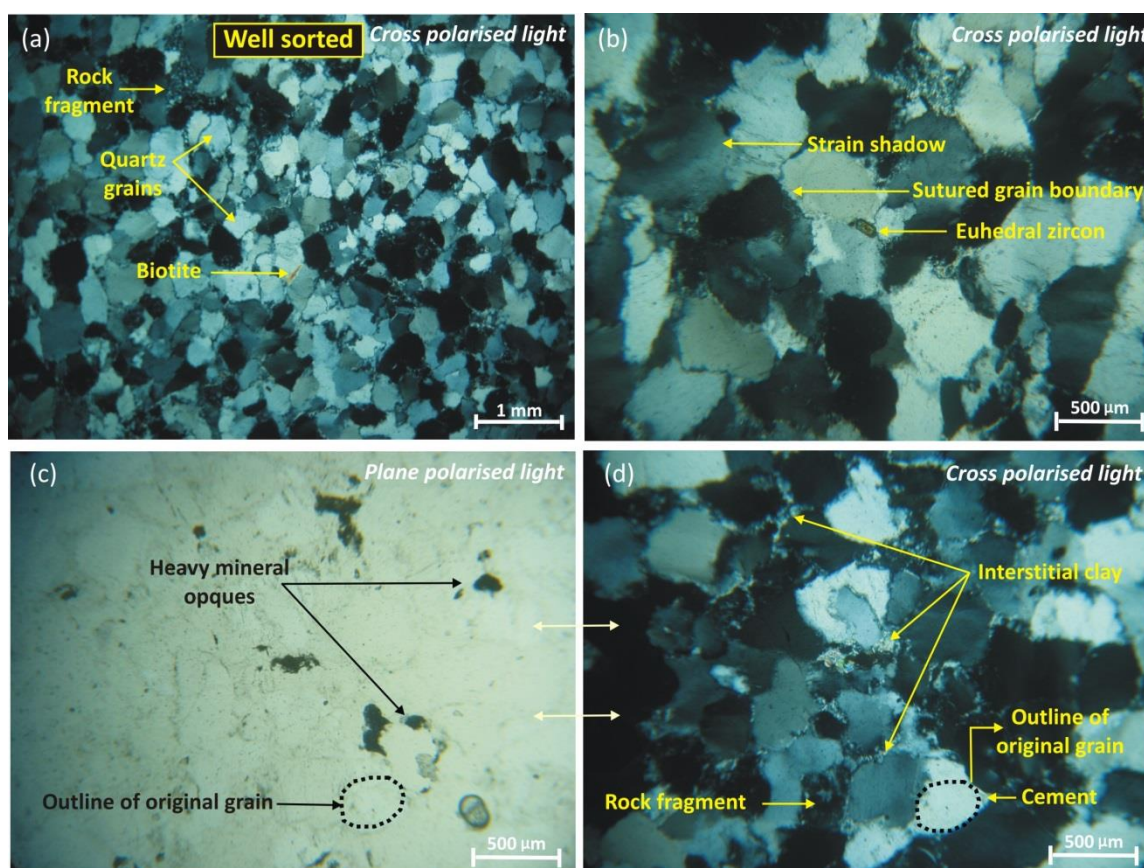
Figure 5.64: *Photomicrographs of Baviaanskloof Formation sandstone depicting: (a) Overall composition, (b) strain shadow observed in quartz grains, sutured grain boundaries and euhedral zircon, (c) heavy mineral opaques, (d) same image viewed under cross polarized light showing interstitial clay, rock fragments and quartz cement.*

5.3.2 Bokkeveld Group (Sample D11)

Grains of the Bokkeveld Group shale are fine-grained and inequigranular. The small grain sizes (10-100 µm) makes it difficult to identify minerals according to their optical properties (Figure 5.65 a), however a few of the larger (<250 µm) grains are confirmed as: quartz, glauconite, rutile and other heavy mineral opaques. Finer grains show a strong foliation (preferred orientation) (Figure 5.65 b). Quartz grain boundaries are recrystallized and show shadow strain. Post deformation glauconite is tabular in shape and is orientated oblique to the main foliation (S1).
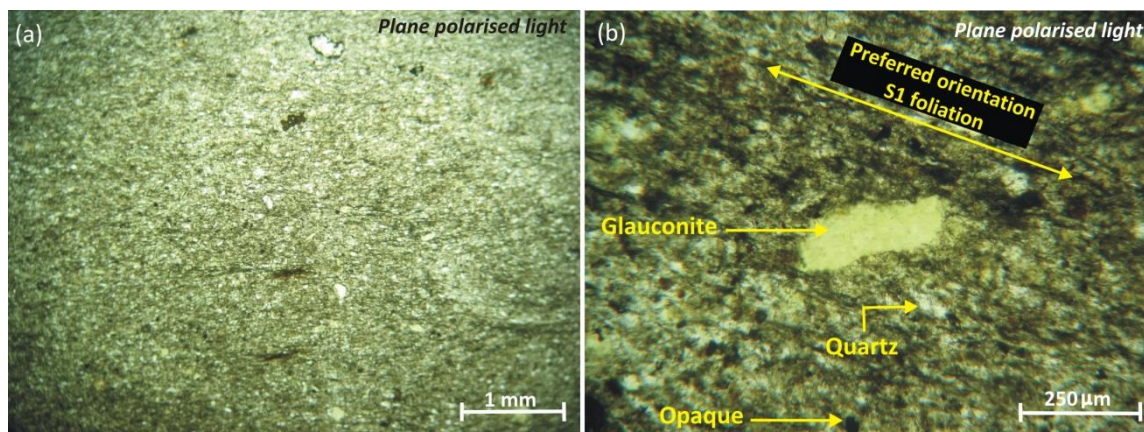
Figure 5.65: *(a) Photomicrograph showing overall fine-grained composition of shale from the Bokkeveld Group. (b) Grains of the Bokkeveld Group shale show a foliation. Quartz grains, glauconite and heavy mineral opaques are identified in sample D11.*

5.4 Geophysics

Results obtained from both multi-electrode (Loots *et al*., 2009) and TDEM resistivity surveys (Zadorozhnaya *et al*., 2012) are presented in the form of geoelectrical profiles. Survey localities, geological site descriptions and anticipated geological findings along all survey lines are discussed in § 4.3.1 and § 4.3.2. New and alternative geological interpretations of geoelectrical profiles initially undertaken by the author as part of the Loots *et al*., (2009) and Zadorozhnaya *et al*., (2012) reports, are presented here with an updated geological model taking subsequently drilled boreholes and a better understanding of the area's geological setting into account. Initial reports by Loots *et al*., (2009) and Zadorozhnaya *et al*., (2012) are provided for in Appendix A2 & A3. Geophysical profiles aid in defining the contacts between Palaeozoic formations and in identifying contacts between Palaeozoic bedrock and Cenozoic overburden at Thyspunt and Cape St. Francis. In addition surveys assist in further verifying the possible occurrence of fault AEC TSP3 at Thyspunt and the possible onland continuation of the Cape St. Francis fault. Comparing results between the array variations (Dipole-dipole and Werner-Schlumberger arrays) used during multi-electrode resistivity surveys, also allows comment on which array choice is better suited for the study area's geological setting, should future surveys be undertaken.

5.4.1 Multi-electrode resistivity

Geological interpretations of the lithostratigraphic substrate are mainly derived from the Werner-Schlumberger electrode array soundings that produce a higher signal to noise ratio. Interpretations of the structural geology were predominantly made from the Dipole-dipole electrode array soundings, as this electrode array is better suited for the inference of vertical and sub-vertical tectonic features. The variation in results obtained between the Dipole-dipole and Werner-Schlumberger arrays may be attributed to the very resistive nature of the ground (contact surface) electrodes are placed into, which in the study area, consists of mostly dry, unconsolidated aeolian sand. The Dipole-dipole electrode array is more likely to have a poor signal to noise ratio in an area where electrode contact with the ground is poor (pers. comm. E.Chirenje, 2014; Loots *et al*., 2009). Interpretation and geological model of survey results are therefore based on the geoelectrical profile of the Werner-Schlumberger electrode array rather than the Dipole-dipole electrode array.

5.4.1.1 Thyspunt

(i) Survey line TS1

Geoelectrical profiles of survey line TS1 (Dipole-dipole and Werner-Schlumberger arrays) (Loots *et al*., 2009) are annotated with updated geological interpretations of the substrate (Figure 5.66 a & b). The E-W trending, 810 m long survey line is orientated oblique to bedding strike and is anticipated to transect bedrock of the Skurweberg Formation on the SW dipping limb of the Cape St. Francis anticline, overlain by overburden sediments of the Algoa Group. Boreholes TB16, NEW30, TB3, TB21, BHDB6, Tony's Bay BH5, TB14 and BHPB5 (Raubenheimer *et al*., 1988 a & b; Eskom, 2010 b) occurring within a 50 m radius are projected onto survey line TS1 (Figure 5.66 a & b).

Boreholes TB16, NEW30, TB3, TB21, BHDB6, Tony's Bay BH5, TB14, and BHPB5 identify the Skurweberg Formation as the bedrock strata along survey line TS1. Bedrock is intercepted at 2.978 m asl, 4.65 m asl, 6.096 m asl, 6.043 m asl, 9.08 m asl, 6.97 m asl, 11.418 m asl, 8.73 m asl, respectively (Figure 5.66 a & b).

From this data a contact surface along the remainder of the survey line between boreholes can be extrapolated along both the Dipole-dipole and Werner-Schlumberger electrode array profiles. Along the Werner-Schlumberger electrode array profile, the contact is consistently marked by the inception of a conductive layer occurring at a depth of 4-18 m (> 2 m above sea level). Consequently the Werner-Schlumberger electrode array profile is able to more accurately define top of bedrock and is deemed a more successful electrode array method upon which geological interpretations can be based.
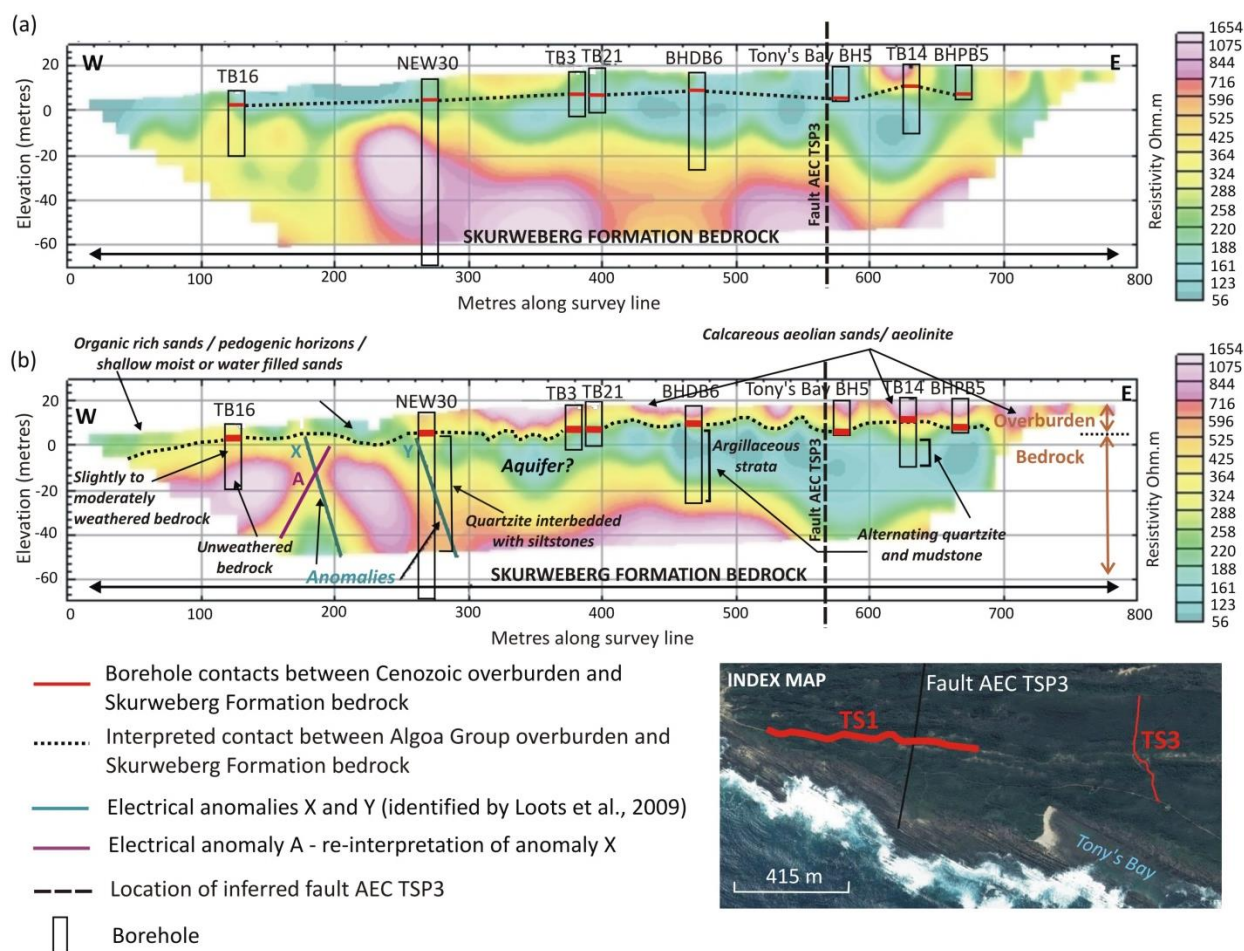
Figure 5.66: Revised geological interpretation of the geoelectrical profile derived from survey line TS1 using the (a) Dipole-dipole and (b) Werner-Schlumberger electrode array (Loots et al., 2009).

Goedhart *et al*., (2008) describe the contact between the Algoa Group overburden and bedrock (Peninsula and Skurweberg Formations) as an interface surface along which groundwater movement takes place. The contact and strata below it is often wet or water logged. An observation substantiated by field investigation (Figure 5.26). Boreholes TB3 and TB21 intercept the conductive layer at 6.096 m and 6.043 m asl to reveal medium to highly jointed, quartzitic sandstone. Highly fractured bedrock strata would facilitate the development of an aquifer. Therefore the conductive (~ 56-250 Ohm.m) 10-45 m thick layer east of borehole NEW30 may reflect the presence of wet or water filled Skurweberg Formation strata at a depth of 60 m, 580 m along the survey line (Figure 5.66 b). Towards the east boreholes BHDB6 and TB14 indicate that similar conductive values in bedrock at 480 m and 640 m along survey line TS1 can also be associated with the occurrence of thin bedded mudstones, shales or siltstones within the predominantly arenaceous Skurweberg Formation.

At 130 m along survey line TS1, data from borehole TB16 confirm resistivity values of 300-500 Ohm.m are associated with slightly, to moderately weathered sandstone of the Skurweberg Formation to a depth of 18.78 m below cover sediments. Borehole data reveal that below this depth, highly resistive substrate (600-1500 Ohm.m) is related to less fractured and unweathered sandstone of the Skurweberg Formation. It is assumed that similar resistivity values at depths of 20 m and 50 m at 240 m and 450 m along the survey line may thus reflect comparable structure and lithology (Figure 5.66 b).

Borehole NEW30 situated 270 m along the geoelectrical profile confirm that resistivity values of 250-600 Ohm.m are reflective of a zone within the Skurweberg Formation comprising "*streaky and mottled dark grey, brown and reddish brown siltstone*" interbedded with quartzitic sandstone layers. This zone and the area west of it, marked by geophysical anomalies X and Y (Loots *et al.*, 2009), if extended along strike to coastal exposures, coincides with the location of the NW-SE trending Tony's Bay (Figure 5.66 a & b, index map). Electrical anomalies, interpreted by Loots *et al.*, 2009 (Figure 4.66 b), therefore coincides with an area of lithological change within the predominantly quartzitic Skurweberg Formation. These anomalies probably dip towards the west, parallel to bedding dip as indicated by newly interpreted anomaly A, and not east as indicated by Loots *et al.*, 2009. No evidence exist that that these anomalies are associated with faults or that they extend through overburden sediments.

Results from line TS1 also allows investigation into the validity of inferred fault AEC TSP3. The fault shows no recognisable displacement of strata on AEC maps (Van Wyk, 1987) (§ 3.4 & Figure 3.3   for greater detail). The projected location of inferred fault AEC TSP 3 occurs at 570 m along the survey line. No electrical anomalies possibly indicative of a fault could however be identified along this section of the survey line. It should be noted that the presence of a conductive layer associated with the possible occurrence of groundwater, may obscure indications of a fault, while possibly substantiating the presence of fractured strata. No disruption of cover sediments is noted in this region.

Borehole data reveal that a <15 m thick, resistive layer (200-1654 Ohm.m) occurring at surface along the entire length of survey line TS1 can be associated with cover sediments of the Algoa Group. Towards the east above 0 m asl, data from boreholes TB3, BHDB6, Tony's Bay BH5, TB14 and BHPB5 indicate that isolated occurrences of slightly more resistive material (700-800 Ohm.m) located close to surface and within the interpreted Algoa Group are predominantly associated with medium to dense calcareous aeolian sands containing abundant shell fragments, aeolianite and/or calcrete <10 m in thickness. Organic rich sands and pedogenic horizons noted in the field and in surrounding boreholes in the greater Thyspunt area (Figure 5.24 a & b) west of borehole NEW30, may account for the presence of <10 m thick slightly more conductive material (150-220 Ohm.m) detected near surface along the initial 250 m of the survey line within the Algoa Group. In addition these sediments may also contain moisture/water, aiding in a slightly more conductive reading.

Based on these interpretations, an updated geological model of results obtained from multi-electrode resistive survey TS1 (Werner-Schlumberger array) is presented in Figure 5.67.
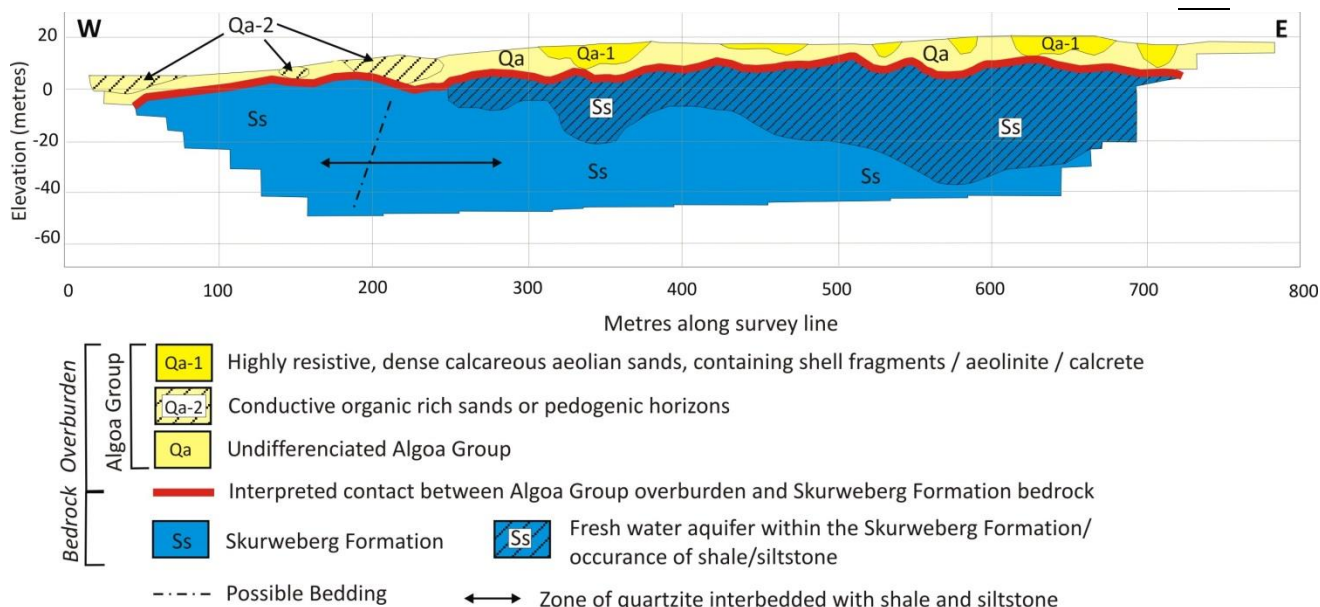
Figure 5.67: Revised geological model of results obtained from multi-electrode resistivity survey line TS1.

(ii) Survey line TS3

The N-S trending, 400 m long survey line TS3, was conducted 100 m north of Tony's Bay, oblique to NW-SE bedding along the southern limb of the Cape St. Francis anticline and is anticipated to transect bedrock of the Skurweberg Formation, overlain by cover sediments of the Algoa Group. The multi-electrode resistivity survey results (Dipole-dipole and Werner-Schlumberger electrode arrays) are presented as geoelectrical profiles in Figures 5.68 a & b (Loots *et al.*, 2009). These figures are annotated with updated geological interpretations of the substrate. Boreholes BHDB5, Thyspunt BH3, Thyspunt BH4, TB31, NEWN1, NEWS1, TB37, TB13 and TB43 (Raubenheimer *et al.*, 1988 a & b; Eskom, 2010 b; Engelsman & Constable., 2012) occurring in close proximity (~100 m) are projected onto the survey line (Figure 4.68. a & b). Boreholes Thyspunt BH4, TB13 and TB43 did not intercept bedrock.

Boreholes BHDB5, Thyspunt BH3, TB31, NEWN1, NEWS1 and TB37 intercept strata of the Skurweberg Formation at 9.04 m, 8.49 m asl, 8.35 m asl, 8.349 m asl, 9.258 m asl and 10.162 m asl along survey line TS3 (Figures 5.68 a & b). From this data a contact surface is interpreted between boreholes along both the Werner-Schlumberger electrode array profile (Figures 5.68 b). As observed along geoelectrical profile TS1, the interpreted contact surface is consistently located at or close to the inception of a conductive zone (<200 Ohm.m) occurring here at elevations of <20 m asl. Geological interpretations are therefore based on the Werner-Schlumberger electrode array and not the Dipole-dipole array results.

Borehole TB31 intercepts the conductive zone located between 40 – 225 m along the survey line at a depth of 8.49 m. Core is described as moderately weathered quartzitic sandstone that exhibits closely spaced jointing. The densely jointed strata would facilitate the development of an aquifer (Figure 5.68 b). The conductive zone could thus conceivably be associated with water filled / moist strata. However to the south boreholes BHDB5 and Thyspunt BH3 reveal that geophysical bodies with similar conductivity may also reflect the occurrence of shale units. If the area to the south is extrapolated along strike to coastal exposures, the area coincides with the basal portion of the Skurweberg Formation mapped as quartzite

with numerous interbedded shales. Boreholes TB16, NEW30, NEW29 and BHDH2 (not located close to survey line TS3, but along the same strike / stratigraphic position) indicate iron rich shales occurring as lenses, stringers or medium thick beds (§ 5.1.1.4, Figure 5.16).

Borehole NEW S1 reveals a highly resistive body (800 - >3000 Ohm.m) detected between 210-270 m at -5 m asl between anomaly X and Y, along the Werner-Schlumberger array profile (Figure 5.68 b). This is related to homogeneous, fracture free quartzitic sandstone within the Skurweberg Formation.
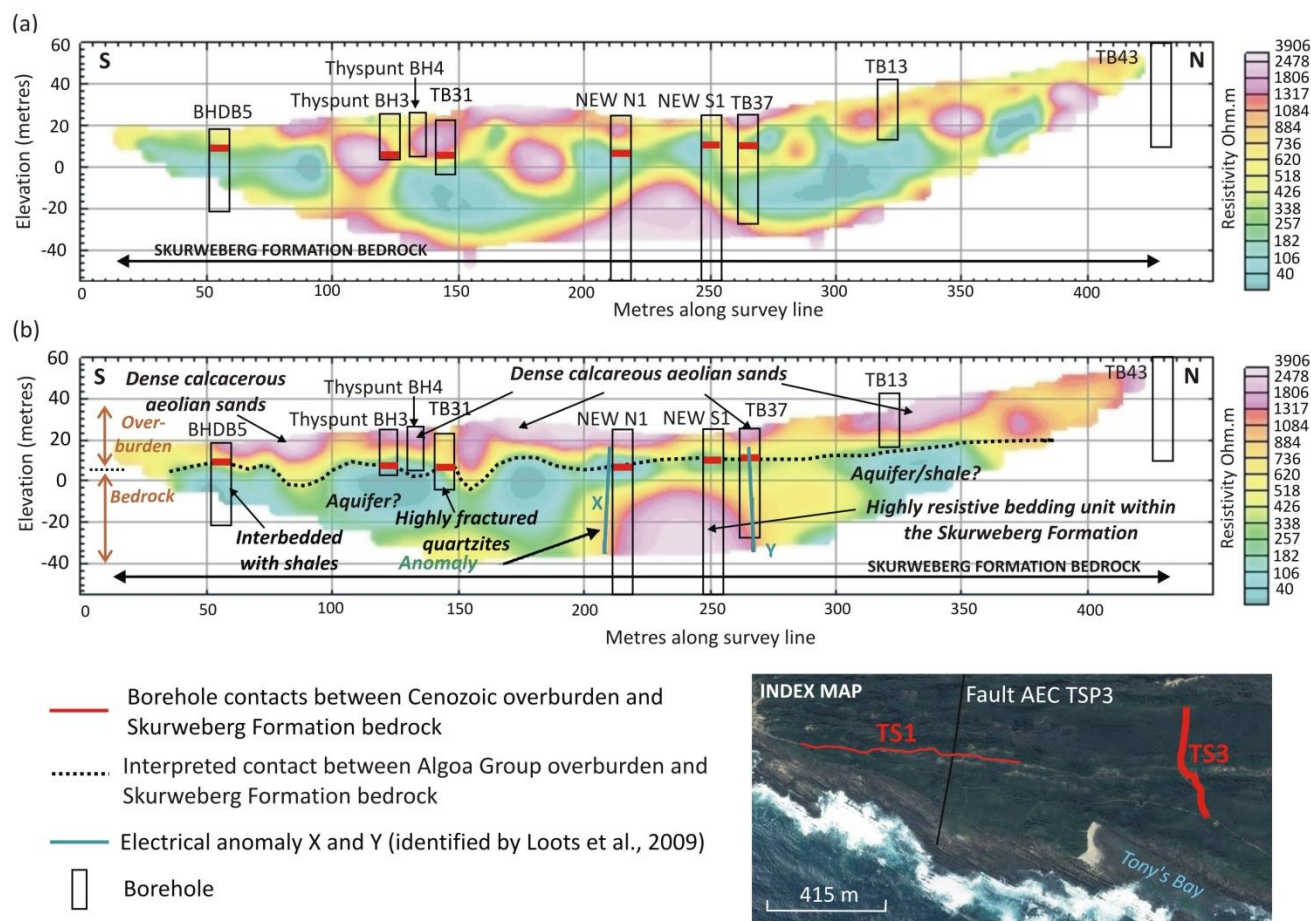
Figure 5.68: Interpretation of the geoelectrical profile derived from survey line TS3 using the (a) Dipole-dipole and (b) Werner-Schlumberger electrode array (Loots et al., 2009) annotated with updated geological interpretations.

A resistive (200-2500 Ohm.m), 10-35 m thick horizontal surface layer occurs along the entire length of survey line TS3. Boreholes BHDB5, Thyspunt BH3, Thyspunt BH4 and TB31, NEWN1, NEWS1, TB37, TB13 and TB43 confirm these resistivity values are associated with sediments of the Algoa Group (Figure 4.68 b). Field observations and borehole data (BHDB5, NEWN1, NEWS1, TB37, TB13 and TB43) indicate that sporadically located, <20 m thick pockets of highly resistive (1300-2500 Ohm.m) material (Figure 5.68 b) occurring at surface within the Algoa Group reflect medium to very densely compacted calcareous aeolian sands often containing numerous shell fragments.

Electrical anomalies X and Y identified by Loots *et al.*, (2009) as possibly joints, fractures or faults are shown as partially extending through into overburden material. Since Loots *et al.*, (2009) only considered borehole TB31 (located towards the south) and were unable to determine where the contact between cover sediments and bedrock would be, it is unlikely that this is the case. In addition there is no evidence

to substantiate that either anomaly X or Y are faults (Figure 5.68 b); and no disruption of overburden sediments is noted.

Based on these interpretations, an updated geological model of results obtained from multi-electrode resistivity line TS3 (Werner-Schlumberger array) is presented in Figure 5.69.
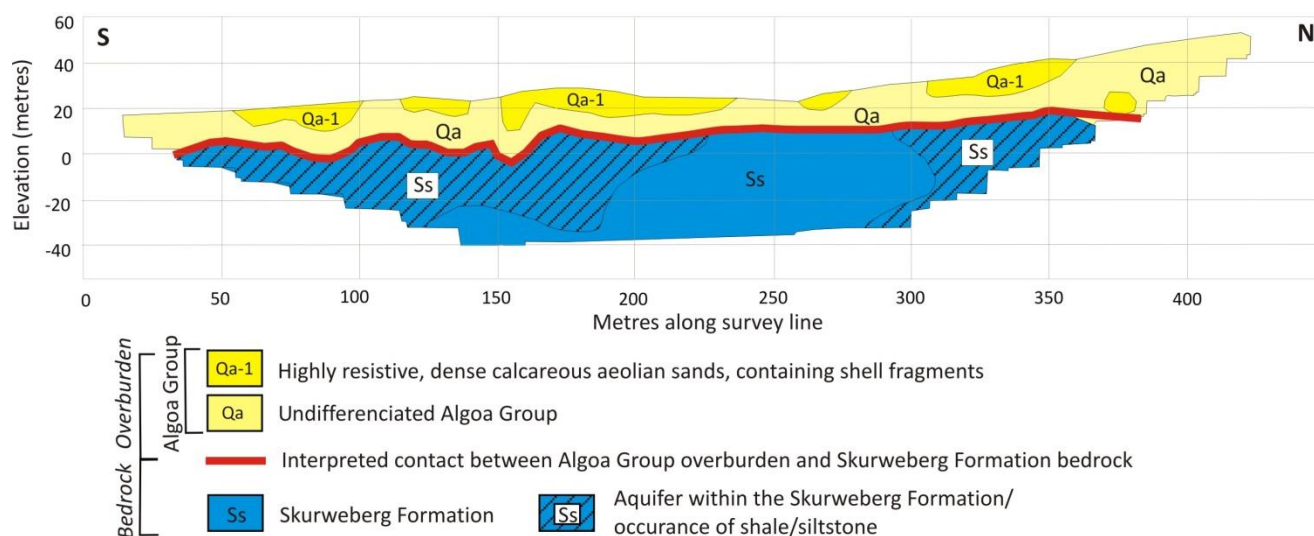
Figure 5.69: Revised geological model of results obtained from multi-electrode resistivity survey line TS3.

5.4.1.2 Cape St. Francis

(i) Survey line CSF1

Results from the S-N trending, 1800 m long, multi-electrode resistivity survey line CSF1 (Dipole-dipole and Werner-Schlumberger electrode arrays), are presented as geoelectrical profiles in Figure 5.70 a & b (Loots *et al*., 2009). Geoelectrical profiles are annotated with updated interpretations of the geological substrate. The survey line is orientated roughly perpendicular to bedding strike and is anticipated to transect NE dipping, NW-SE striking bedrock strata of the Peninsula and Cedarberg Formations towards the south and strata of the Goudini Formation towards the north. In addition to identifying the contacts between bedrock formations, the position of survey line CSF1 also allows the opportunity to explore the onland continuation of the Cape St. Francis Fault (§ 3.4; Figure 3.7).

Boreholes CSF13, CSF18, CSF17, CSF14 and CSF10 (Hanson *et al*., 2012), previously unavailable to Loots *et al*., (2009) and occurring within 25 m of the survey line, are projected onto both the Dipole-dipole and Werner-Schlumberger electrode array profiles. Observations on the ability of the Werner-Schlumberger electrode array to accurately predict the contact between overburden sediments and bedrock at Thyspunt, suggest that geological interpretations of multi-electrode resistivity results obtained in the Cape St. Francis area, which share a similar geological setting, should also be made using the Werner-Schlumberger electrode array technique.
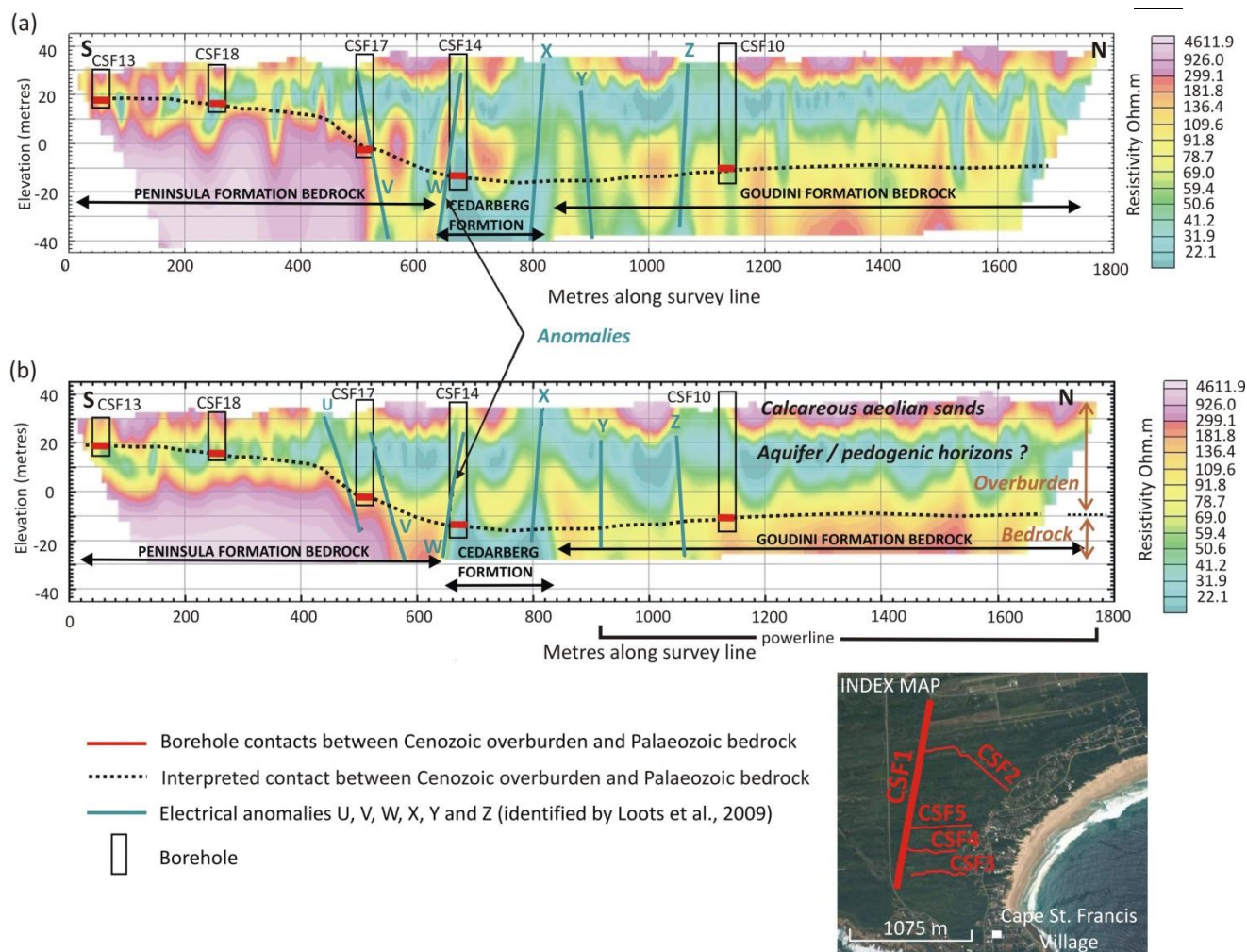
Figure 5.70: Interpretation of the geoelectrical profile derived from survey line CSF1 using the (a) Dipole-dipole and (b) Werner-Schlumberger electrode array (Loots et al., 2009) annotated with updated geological interpretations.

Borehole contacts between the Algoa Group (Cenozoic overburden) and Ordovician-Silurian Palaeozoic bedrock are depicted in Figure 5.70 a & b. From this data a contact surface or palaeotopography along the remainder of the survey line between boreholes can be interpreted. Towards the south, boreholes CSF13, CSF18 and CFS17 situated at 60 m, 260 m and 510 m along survey line CSF1 intercept the Peninsula Formation at 18.41 m asl, 17.64 m asl and -1.23 m asl (Figure 5.70 b). Boreholes confirm that the Peninsula Formation exhibits resistivity values ranging between 50-4200 Ohm.m. Consequently the Peninsula Formation is interpreted to occur between 0 – 640 m along the profile at depths <20 m asl (Figure 5.70 b). Bordering the highly resistive substrate of the Peninsula Formation is a conductive body (20 – 100 Ohm.m) occurring between 640 – 840 m along the profile at a depth of <-10 m asl. Borehole CSF14 intercepts the conductive body at a depth of -11.52 m asl and confirms conductive soundings reflect black shale associated with the Cedarberg Formation (possibly the basal Soom Member).

North of the Cedarberg Formation, an extensive 960 m long, resistive body (100 - 3000 Ohm.m) detected between 840 – 1800 m along profile CSF1 (Werner-Schlumberger electrode array) at a depth of 40 m is expected to stratigraphically correlate with the Goudini Formation. Borehole CSF10 confirms the presence of the Goudini Formation intercepted at -9.44 m asl, 1130 m. A highly resistive body (<3000 Ohm.m) is observed between 1100 – 1660 m. Although highly resistive, its resistivity measures lower

than strata associated with the Peninsula Formation and is therefore not considered as part of the same geological unit towards the south (Figure 5.70 b). Rather, the resistive body is interpreted as a quartzitic unit within the Goudini Formation. A decrease in palaeotopography is noted towards the north in areas underlain by the lithologically less competent argillaceous Cedarberg and Goudini Formations (Figure 5.70 b), indicating the presence of a possible palaeovalley.

Borehole data reveal that cover sediments range in thickness from 12.46 m (borehole CSF13) in the south to 51.04 m (borehole CSF10) northward and can be associated with resistivity values ranging between 20 – 1500 Ohm.m. At surface more resistive material (>300 Ohm.m) <15 m in thickness occurring within the Algoa Group are associated with medium to dense calcareous aeolian sands, calcrete and/or shell-rich horizons (boreholes CSF13, CSF18, CSF17, CSF14 and CSF10). More conductive soundings (20- 55 Ohm.m) at depths ranging between 10 - 40 m (>-10 m asl) along the survey line may possibly be interpreted as moist or water filled sediments within the Algoa Group (intergranular aquifer) (Figure 5.70 b). Alternatively conductive material could also be associated with pedogenic organic rich horizons. These overburden interpretations are substantiated by descriptions of borehole core and similar interpretations of resistivity values made along survey lines TS1 and TS3 at Thyspunt (§5.4.1.1 i, ii).

Electrical anomalies, possibly associated with joints, fractures or faults (U, V, W, X, Y, Z) identified along profile CSF1 by Loots *et al*., (2009), occur in bedrock strata and are interpreted to extend into overburden sediments. No evidence that these anomalies are associated with a particular structural feature or that they extend through into cover sediments could be established (Figure 5.70 b). These features were identified prior to the acquisition of borehole data and Loots *et al.*, (2009) could not constrain a contact between overburden and bedrock. No evidence occurs to substantiate that these anomalies are faults (Figure 5.68 b); and no disruption of overburden sediments is noted. Anomalies U, V, W and possibly X, may be interpreted as indications of lithological change within Palaeozoic bedrock.

Based on results from TDEM survey CSF (Figure 3.9) conducted NE of Seal Point, Stettler *et al*., (2008) initially interpreted the Cape St. Francis fault as possibly continuing its offshore occurrence onland within strata of the Goudini Formation The fault is interpreted to coincide with a ~300 m zone of fault mélange (§ 3.4, Figure 3.9). If the interpreted location of the Cape St. Francis fault and zone of fault mélange is extended inland along strike, these features should intersect survey line CSF1. However, no geophysical anomaly associated with a fault or zone of fault mélange is interpreted to occur within the Goudini Formation along survey line CSF1. The absence of these features could then serve to substantiate the alternative geological model later proposed by Stettler *et al*., (2008) that eliminates the occurrence of a fault and zone of fault mélange through folding (See § 3.4, Figure 3.10 for greater detail on the alternative geological model).

Based on these interpretations, an updated geological model of results obtained from multi-electrode resistivity line CSF1 (Werner-Schlumberger electrode array) is presented in Figure 5.71.
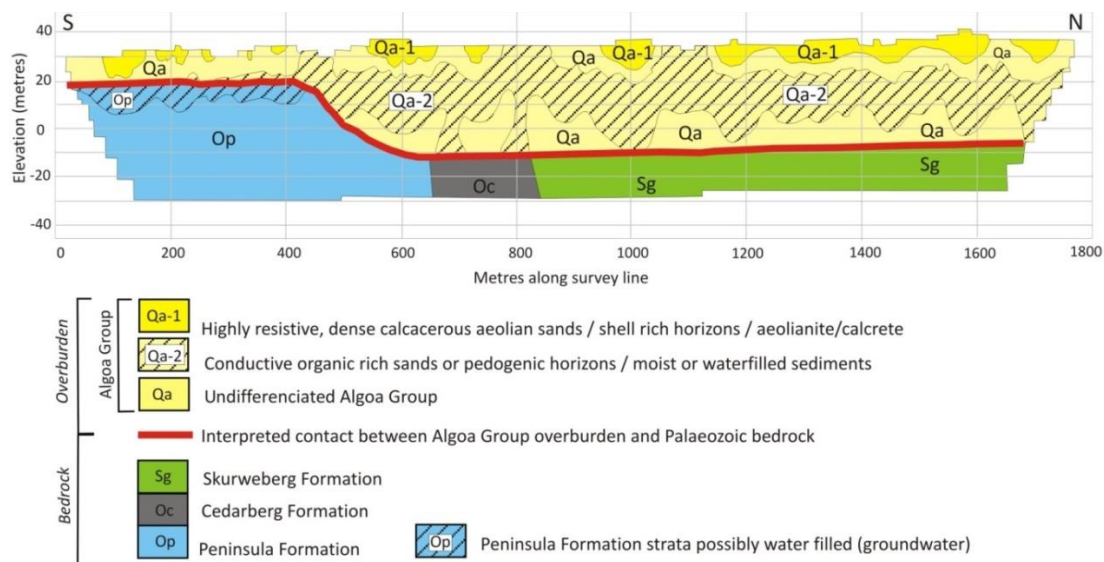
Figure 5.71: Revised geological model of results obtained from multi-electrode resistivity survey line CSF1.

(ii) Survey line CSF2

Results for multi-electrode resistivity survey line CSF2 (Dipole-dipole and Werner-Schlumberger electrode arrays) are presented in the form of geoelectrical profiles (Loots *et al.*, 2009) (Figure 5.72 a & b) and annotated with updated interpretations of the geological substrate. The dual trending survey line is orientated oblique and parallel to bedding strike. Survey line CSF2 is expected to reflect resistivity values representative of the Goudini Formation (bedrock) overlain by sediments of the Algoa Group.

No boreholes occur along survey line CSF2. However, borehole CSF10 located 120 m south of survey line CSF2's western extent, indicates that thickness of cover sediments along the western sections of the survey line, should be in the range of 45 m. Borehole CSF10 also confirms the Goudini Formation as likely bedrock in the area. With this information and interpretations made of resistivity values associated with the Goudini Formation and its accompanying cover sediments along survey line CSF1 (Werner-Schlumberger electrode array), the contact between bedrock and overburden is assumed to be below a conductive layer with resistivity values in the range of 20-55 Ohm.m. Conductive (20-90 Ohm.m) zones <40 m thick, detected between 100-700 m and partially between 700-920 m along survey line CSF2 above argillaceous bedrock are assumed to reflect either moist/water filled sediments possibly associated with the occurrence of differential fresh water penetration or the occurrence of organic rich sands/pedogenic horizons. This layer is used as a guide to delineating the contact surface depicted in Figure 5.72 b.

 A resistive (<15 - >2700 Ohm.m) 12-50 m thick horizontally orientated layer occurring at surface along the entire survey line is interpreted as sediments associated with the Algoa Group (Figure 5.72 b). Similar observations are made along the northern portions of survey line CSF1. Within the Algoa Group <15 m thick highly resistive (>1000 Ohm.m) bodies detected directly at surface are interpreted to possibly reflect densely compacted calcareous sands, possibly containing shell fragments, aeolianite and/or calcrete based on the location of similar resistivity values at Thyspunt (survey lines TS1 & TS3) and survey line CSF1.
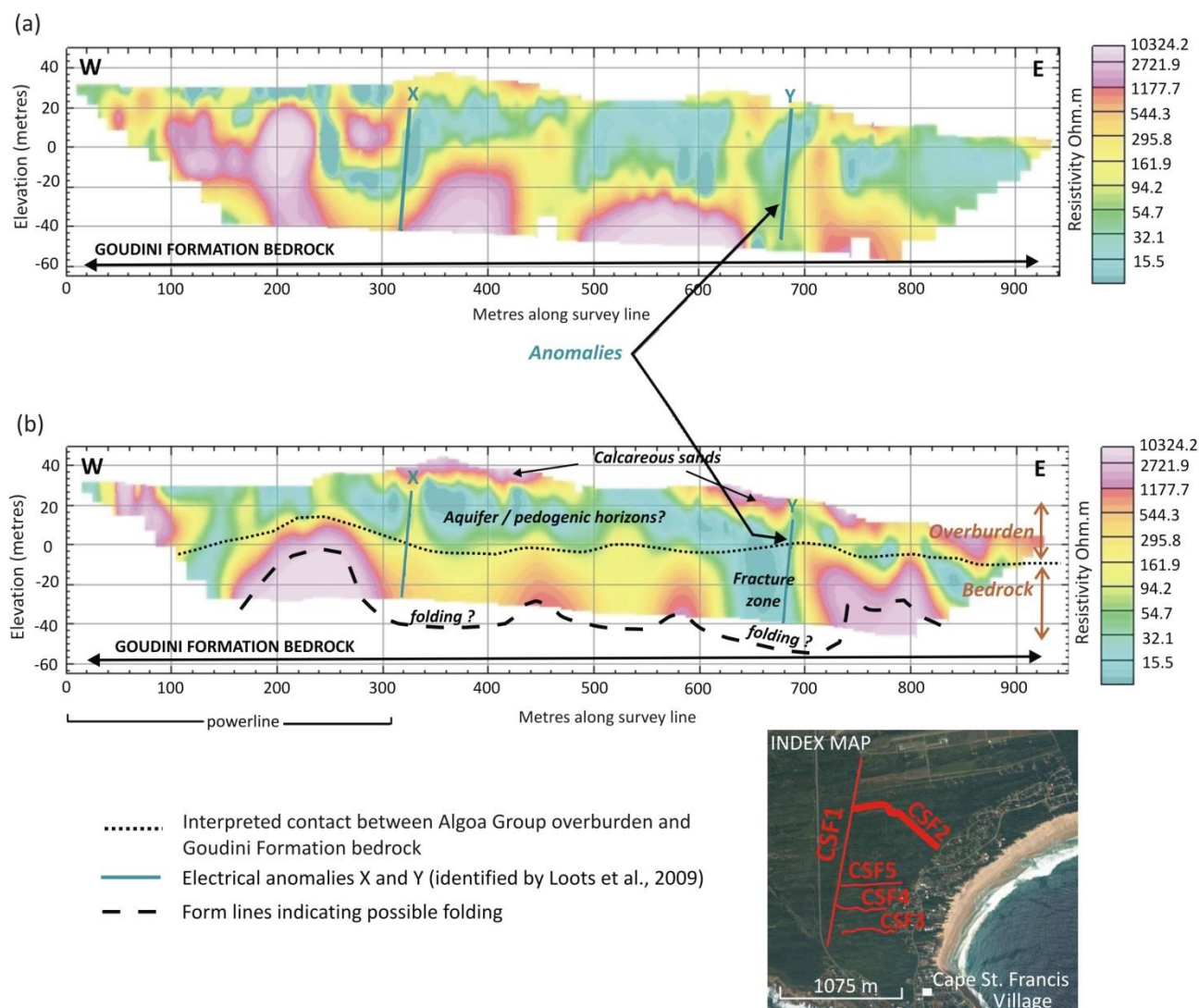
Figure 5.72: *Interpretation of the geoelectrical profile derived from survey line CSF2 using the (a) Dipole-dipole and (b) Werner-Schlumberger electrode array (Loots et al., 2009) annotated with updated geological interpretations.*

Resistive bodies (>1000 Ohm.m) within bedrock strata detected along the Werner Schlumberger array geoelectrical profile, at 160 – 310 m, 420 – 480 m, 570 – 600 m and 720 – 830 m possibly reflect the same geological unit and could be interpreted as localized folding of a highly resistive lithology unit (quartzite?) within the Goudini Formation (Figure 5.72 b). Alternatively these resistivity values could reflect a similar, but unconnected lithology.

Towards the east a 70 m wide zone (20 – 100 Ohm.m), situated at a depth below ~ 25 m (0 m asl) between 630 – 700 m along survey line CSF2 and marked by electrical anomaly Y, could reflect a fracture or shatter zone similar to those identified by Raubenheimer *et al.*, (1988 a) and Goedhart *et al.*, (2008) and during field investigation (Figure 5.44 a-f & Figure 5.46 a-d). The possible occurrence of groundwater along the interpreted shatter zone, could account for the high conductive signal. Anomaly X is not associated with a particular structural feature, rather is interpreted as a lithological change within the Algoa Group.

Electrical anomalies X and Y identified by Loots *et al.*, (2009) as possibly joints, fractures or faults are shown to occur in both overburden sediments and bedrock strata. No evidence that anomaly Y actually

extends through into cover sediments can be established (Figure 5.72 b). The lack of borehole data at the time these anomalies were identified did not allow the establishment of a realistic contact between bedrock and overburden. It is suspected that anomalies were perhaps capriciously indicated. New data and interpretations suggest that anomalies do not extend into younger sediments.

Based on these interpretations, an updated geological model of results obtained from multi-electrode resistivity line CSF2 (Werner Schlumberger array) is presented in Figure 5.73.
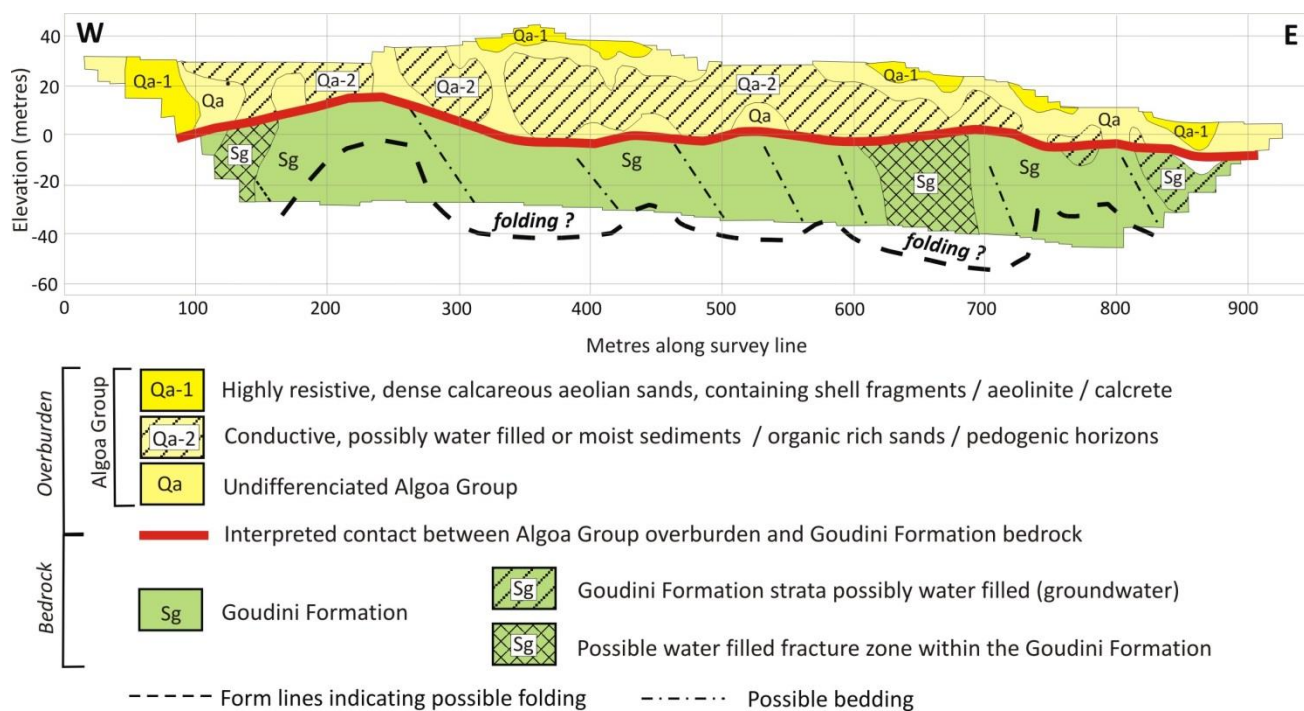
Figure 5.73: Revised geological model of results obtained from multi-electrode resistivity survey line CSF2.

(iii) Survey line CSF3

The geoelectrical profiles (Dipole-dipole and Werner-Schlumberger electrode arrays) derived from results obtained during the conduction of survey line CSF3 are presented in Figures 5.74 a & b (Loots *et al*., 2009) and annotated with updated interpretations of the geological substrate. E-W trending survey line CSF3 is orientated oblique to bedding and is expected to reflect resistivity values (50-4200 Ohm.m) similar to those encountered along the southern portions of survey line CSF1. This assumption is based on data from boreholes CSF13 and CSF18 located north and south of survey line CSF3 that identify Peninsula Formation quartzite as bedrock in the area. Boreholes also indicate that thickness of cover sediments towards the western portions of survey line CSF3 should be <15 m. Based on this information; and geological interpretations of profiles TS1 and TS3 that share a similar type of bedrock lithology (Skurweberg Formation quartzite); proximity to the coast line and line orientation (survey line TS1); it is assumed that the contact between overburden and bedrock along survey line CSF3 should also be marked by the inception of a conductive zone (<200 Ohm.m) associated with the presence of wet or fresh water filled strata (aquifer). The interpreted contact between cover sediments and bedrock strata is depicted in Figure 5.74 b.

Resistivity values ranging between 50-4200 Ohm.m at elevations of <20 m asl along survey line CSF3 are associated with strata of the Peninsula Formation. A ~220 wide zone of highly resistive material (1500-5500 Ohm.m) detected below 0 m asl, between 90-310 m along geoelectrical profile CSF3 (Werner-Schlumberger electrode array), may be indicative of relatively more compacted, less fractured and possibly unweathered bedrock strata within the Peninsula Formation.

Overburden sediments are interpreted to be 5-15 m thick. Overburden containing sporadically distributed thin 5-10 m thick pockets of highly resistive material (1500-2500 Ohm.m) occurring at 30 m, 220 m, 280 m and 450 m along the geoelectrical profile (Werner-Schlumberger electrode array) are possibly associated with medium to dense calcareous sands containing shell fragments /aeolianite / calcrete. Slightly more conductive material (150-250 Ohm.m) occurring close to surface towards the west along the geoelectrical profile, could possibly reflect organic rich sands and/or pedogenic horizons. These overburden interpretations are substantiated by borehole confirmation of similar resistivity values made along survey lines TS1 and TS3 at Thyspunt.

Based on these interpretations, an updated geological model of results obtained from multi-electrode resistivity line CSF3 (Werner-Schlumberger electrode array) is presented in Figure 5.75.
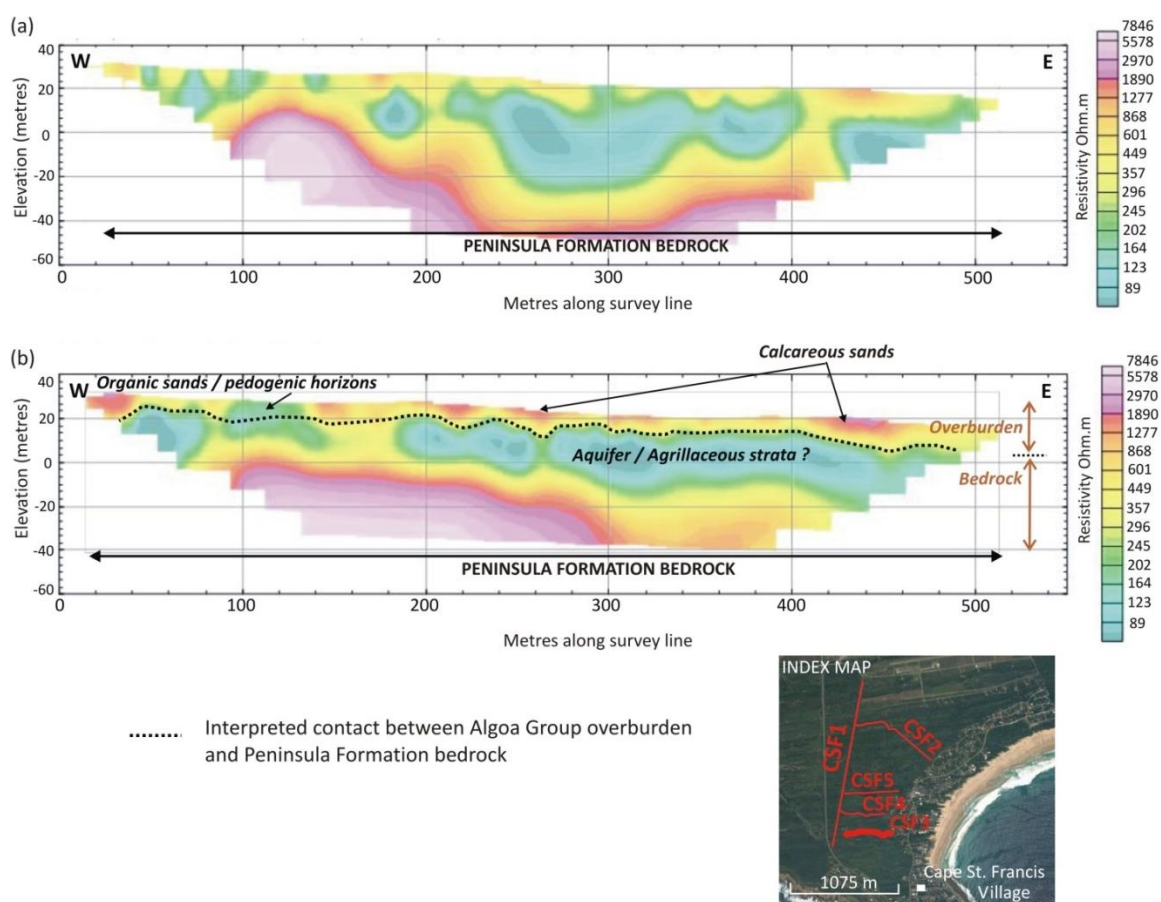
Figure 5.74: Interpretation of the geoelectrical profile derived from survey line CSF3 using the (a) Dipole-dipole and (b) Werner-Schlumberger electrode array (Loots et al., 2009) annotated with updated geological interpretations..
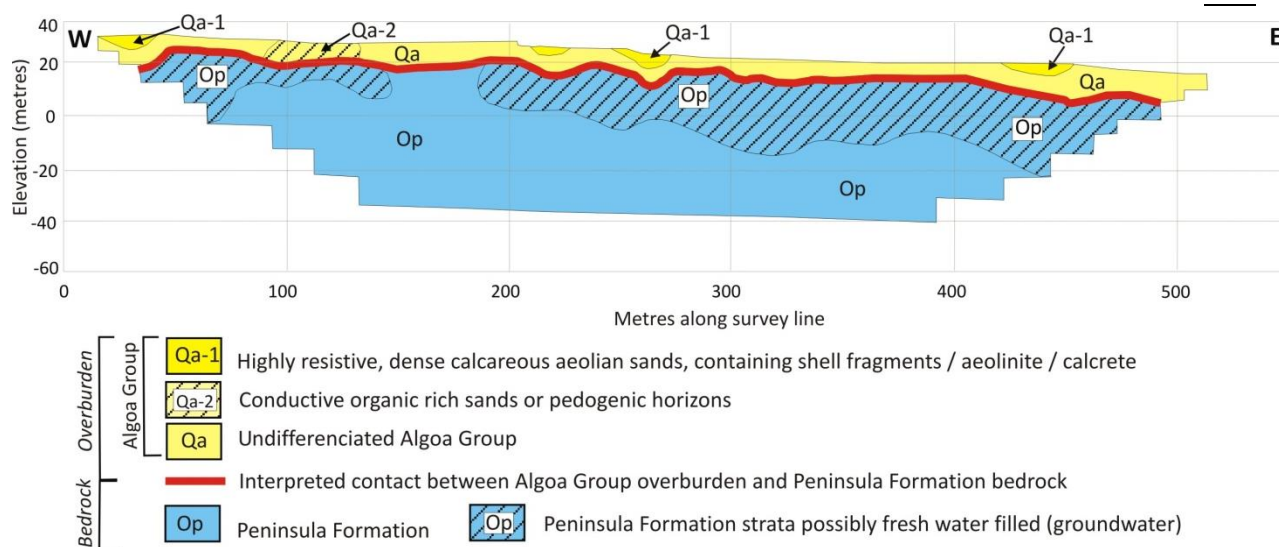
Figure 5.75: Revised geological model of results obtained from multi-electrode resistivity survey line CSF3.

(iv) Survey line CSF4

Survey line CSF4 was conducted oblique to bedding and is anticipated to transect resistive bedrock of the Peninsula Formation overlain by cover sediments of the Algoa Group along its 540 m length and W-E trend. Results of survey line CSF 4 (Dipole-dipole and Werner-Schlumberger electrode array) are presented as a geoelectrical profiles in Figures 5.76 a & b (Loots *et al*., 2009). Profiles are annotated with updated geological interpretations. No boreholes occur along the survey length. Borehole CSF18 occurs 60 m SW of the western extent of survey line CSF4 and encounters Peninsula Formation bedrock overlain by Algoa Group sediments in the range of 15 m.

Based on data from borehole CSF18 and assumptions about the location of the contact between cover sediments and Peninsula Formation bedrock (discussed in the previously section, § 5.4.1.2 iii, Survey line CSF3), the contact is interpreted to occur at a depth of <15 m, but above conductive bodies with resistivity values of <250 Ohm.m. The interpreted contact is depicted in Figure 5.67 b.

Resistivity values ranging between (120-3200 Ohm.m) are associated with overburden sediments <20 m in thickness (Figure 5.76 b). Highly resistive bodies (1400 - >3600 Ohm.m) detected towards the east, at surface between 330-460 m along the Werner-Schlumberger array profile, is interpreted to reflect more densely compacted calcareous sands, aeolianite and/or calcrete layers <18 m in thickness. Conductive bodies detected above the inferred overburden/bedrock contact between 30-260 m along profile CSF4 are interpreted to possibly represent organic sands or pedogenic horizons within the Algoa Group (Figure 5.76 b).

Resistive bodies (>1000 Ohm.m) within bedrock strata present along the Werner Schlumberger array profile, between 110 – 290 m and 310 – 380 m, may reflect the same geological unit and is interpreted as localized folding of a highly resistive, possibly unweathered and unfractured lithology (quartzite) within the Peninsula Formation (Figure 5.76 b). Alternatively these resistivity values could reflect a similar, but unconnected lithology.

Geophysical anomaly X, identified by Loots *et al.*, (2009) as a possibly joint, fracture or fault is only recognised along the Dipole-dipole array profile of survey line CSF4. The anomaly is shown to occur in both overburden and bedrock strata. No evidence that these anomalies are associated with a particular structural feature or that they extend through into cover sediments could be established (Figure 5.76 a). The lack of borehole data at the time these anomalies were identified did not allow the establishment of a realistic contact between bedrock and overburden. It is suspected that anomalies were perhaps capriciously indicated.

Based on these interpretations, an updated geological model of results obtained from multi-electrode resistivity line CSF4 (Werner-Schlumberger electrode array) is presented in Figure 5.77.
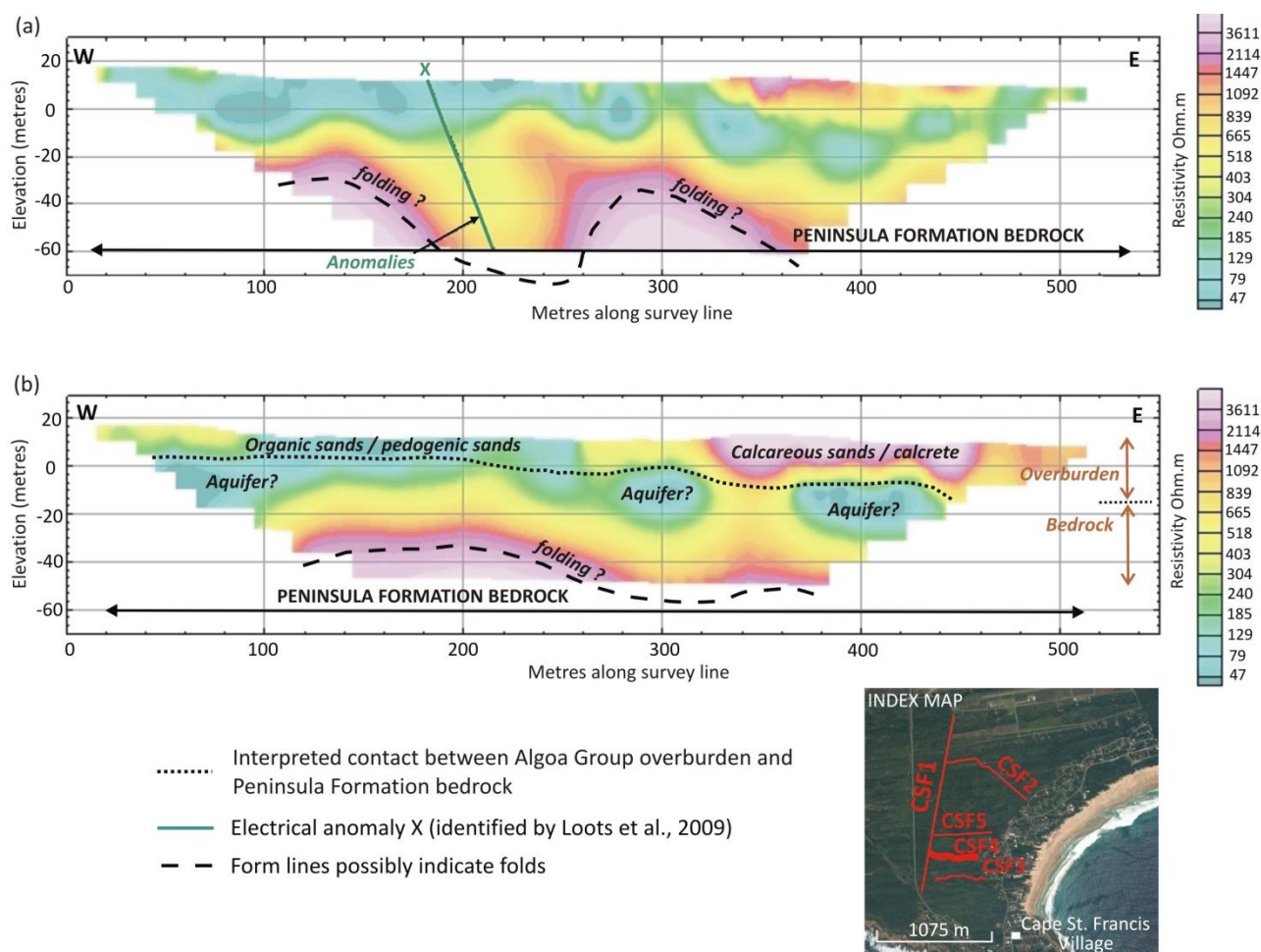
Figure 5.76: Interpretation of the geoelectrical profile derived from survey line CSF4 using the (a) Dipole-dipole and (b) Werner-Schlumberger electrode array (Loots et al., 2009) annotated with updated geological interpretations.
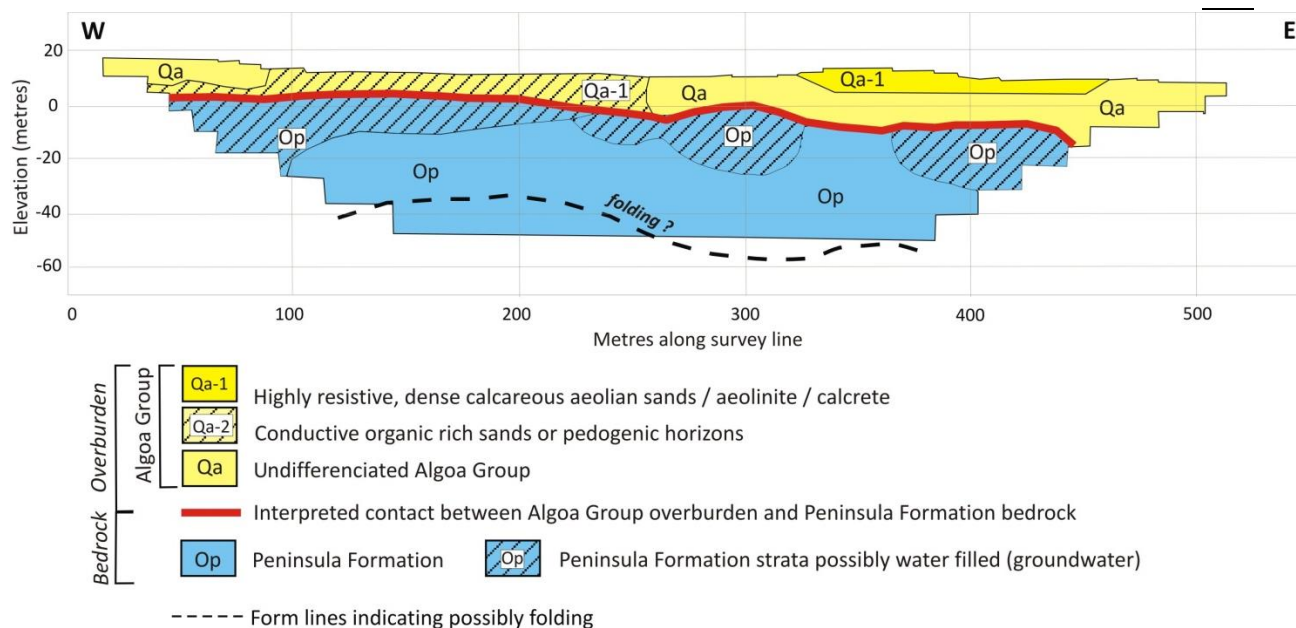
Figure 5.77: Revised geological model of results obtained from multi-electrode resistivity survey line CSF4.

(v) Survey line CSF5

Results from multi-electrode resistivity survey line CSF5 (Dipole-dipole and Werner-Schlumberger electrode arrays) are presented as geoelectrical profiles in Figures 5.78 a & b (Loots *et al.*, 2009). Profiles are annotated with updated geological interpretations. No elevation data was recorded along survey line CSF5. The E-W trending, 540 m long multi-electrode resistivity survey line CSF5, is orientated oblique to the NW-SW bedding trend and is expected to transect NE dipping bedrock of possibly the Peninsula, Cedarberg and Goudini Formation overlain by sediments of the Algoa Group. Borehole CSF17, situated south of survey line CSF5's western extent confirms Peninsula Formation quartzite as the bedrock to the west. Borehole CSF14 confirms the presence of Cedarberg Formation bedrock ~100 m north of the starting point of survey line CSF5 (Figure 4.7). These boreholes indicate that cover sediments towards the west of survey line CSF5 should be in the range of 39-50 m in thickness with bedrock elevations expected to decrease across the lithologically less competent Cedarberg and Goudini Formations, similar to observations made along geoelectrical profiles of survey line CSF1.

The contact between overburden sediments and bedrock strata along geoelectrical profiles of survey line CSF5 is poorly defined. This may, in part be due to the thickness of overburden cover and the capability of multi-electrode resistivity to reach depths of only 60 m - 70m in this type of lithostratigraphic setting. An interpreted contact is however shown in Figure 5.78 b. Two formations may conceivably transect survey line CSF5. Towards the west, at depths below 50 m and between 120-210 m along the geoelectrical profile (Werner-Schlumberger array) a 90 m wide conductive body (<30 Ohm.m) could reflect argillaceous strata of the Cedarberg Formation. Resistive bodies bordering the conductive body east of 210 m are stratigraphically associated with the Goudini Formation.

A resistive (200-2300 Ohm.m), <50 m thick, horizontally trending near surface layer occurring along the entire survey (Werner-Schlumberger array) is interpreted as overburden sediments of the Algoa Group.

As interpreted along previous multi-resistivity profiles at Cape St. Francis and Thyspunt, highly resistive bodies (100 - >2300 Ohm.m) occurring at 210 m, 260 m, 360 m and 440 m along the geoelectrical profile line are possibly associated with the presence of calcareous sands, aeolianite and/or calcrete within the Algoa Group (Figure 5.78 b). At surface thin >10 m horizontal conductive bodies (20-35 Ohm.m) are interpreted to represent organic sands. Larger and more conductive bodies (<30 Ohm.m) below 10 m agl between 120-220m and 220-340 m along the geoelectrical profile (Werner-Schlumberger array) could possibly be associated with groundwater occurrence above argillaceous strata of the Cedarberg and Goudini Formations.

Electrical anomalies possibly associated with joints, fractures or faults (anomalies X and Y) are identified along profile CSF5 by Loots *et al.*, (2009) (Figure 5.78 a & b). These anomalies are depicted as occurring within overburden sediments. The occurrence of these anomalies cannot confidently be linked to the presence of a structural feature; but is rather interpreted to indicate changes in the lithologically diverse Algoa Group and/or possible presence of groundwater above less impermeable argillaceous bedrock strata.

Based on these interpretations, an updated geological model of results obtained from multi-electrode resistivity line CSF5 (Werner-Schlumberger electrode array) is presented in Figure 5.79.
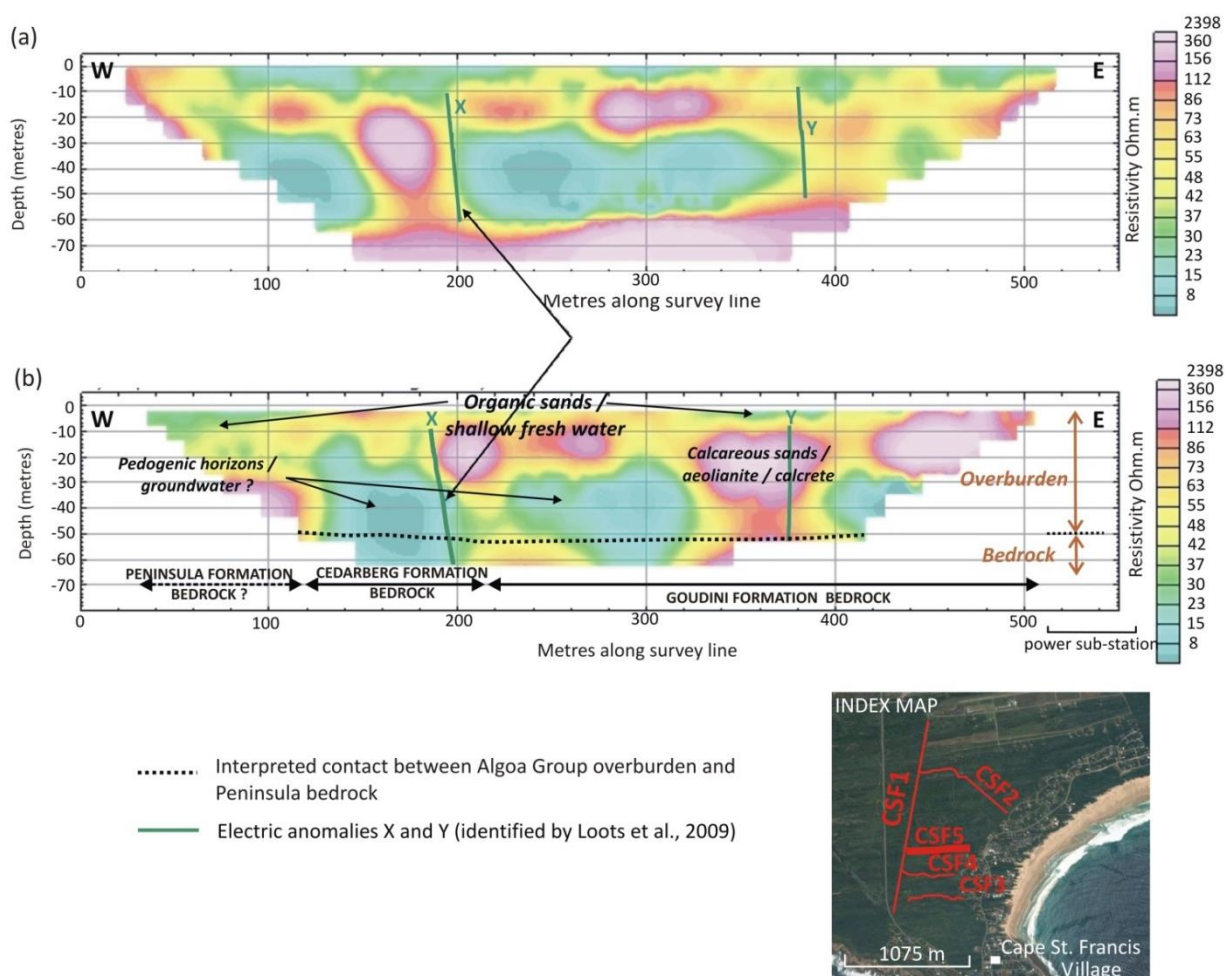
Figure 5.78: Interpretation of the geoelectrical profile derived from survey line CSF5 using the (a) Dipole-dipole and (b) Werner-Schlumberger electrode array (Loots et al., 2009) annotated with updated geological interpretations.
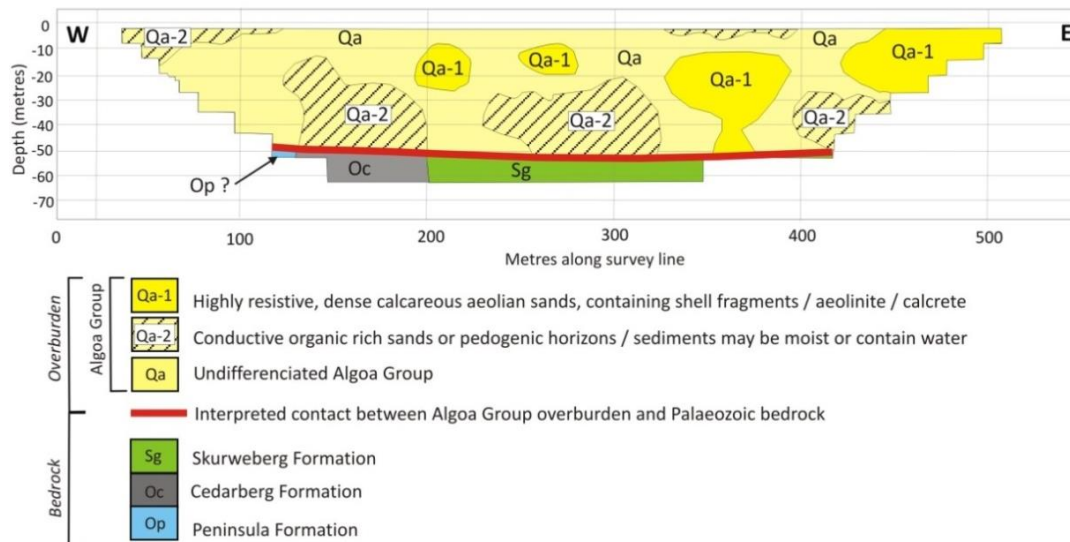
Figure 5.79: Revised geological model of results obtained from multi-electrode resistivity survey line CSF5.

5.4.2 Time domain electromagnetics

5.4.2.1 Survey TDEM-CSF1

Results from the time domain electromagnetic survey TDEM-CSF1 are presented in the form of a geoelectrical profile in Figure 5.80 (Zadorozhnaya *et al.*, 2012). The profile is annotated with updated geological interpretations. The geoelectrical profile reaches depths of between 40m – 90 m over the S-N trending, 1675 m survey length. The surface is located in the same position and along the same trend as multi-electrode resistivity survey line CSF1 and is anticipated to transect NE-SW trending, NE dipping bedrock of the Peninsula, Cedarberg and Goudini Formations overlain by sediments of the Algoa Group. Boreholes CSF13, CSF18, CSF17, CSF14 and CSF10 occurring within 25 m of the survey line are projected onto the geoelectrical profile. Anomalies A, B, C, D, E and F were identified by Zadorozhnaya *et al.*, (2012) as possible faults.

A zone of highly resistive substrate (>800 Ohm.m) is detected between 0 – 560 m along survey line TDEM-CSF1 at < 10 m asl, towards the south and <-10 m asl farther north (Figure 4.80). Boreholes CSF13, CSF18 and CSF 18, situated at 80 m, 275 m and 530 m along the survey line confirms the presence of the Peninsula Formation intercepted at a depths of 12.46 m (18.41 m asl), 15.28 m (17.64 m asl) and 43.6 m (-1.23 m asl) (Figure 5.80). The sharp contrast in resistivity between the compact quartzites of the Peninsula Formation and the overlying less resistive, less compacted, semi-consolidated overburden (40-60 Ohm.m) enables identification of the contact between the Peninsula Formation bedrock and Algoa Group overburden as indicated by Zadorozhnaya *et al.*, (2012) (Figure 5.80).

A less resistive/more conductive zone bordering the highly resistive Peninsula bedrock occurs between anomalies A and B, 550 - 640 m along the survey line at <0 m asl (Figure 5.80). It is unclear whether this zone marks a change in lithology or more weathered strata within the Peninsula Formation. The zone may also be representative of a fractured/highly jointed zone similar to shatter zones described along the coastal exposures (§ 5.2.3) (Raubenheimer *et al.*, 1988 b; Goedhart *et al.*, 2008). Alternatively the zone

could form part of the Cedarberg Formation. This zone was also detected along multi-electrode resistivity line survey CSF1 (§ 5.4.1.2 i).

A highly conductive substrate is detected at a depth of 50 m (>15 m asl) 460-760m along the survey line (Figure 5.80). Borehole CSF14 intercepts the conductive body at -11.52 m asl and confirms it as Cedarberg Formation shale (possibly basal Soom Member). North of 760 m, resistivity values reflect the lithologically varied Goudini Formation comprised of alternating beds of mudstone, shale, siltstone and quartzite. Borehole CSF10 confirms the presence of the Goudini Formation intercepted at a depth of 51.04 m (-9.44 m asl) at 1130 m along the survey line. A resistive substrate body along the northern end of the profile between 1500 – 1675 m at a depth of 50 m (<-10 m asl) within the Goudini Formation shares a similar resistivity with strata of the Peninsula Formation seen along the southern end of the survey line (Figure 5.80). The resistive body may represent a similar type of quartzitic lithology.

Borehole contacts between the Algoa Group and Ordovician - Silurian bedrock are depicted in Figure 4.80. The contact surface along the remainder of the survey line between boreholes is interpreted and depicted in Figure 5.80. As seen along multi-electrode resistivity survey line CSF1, a decrease in the elevation of the interpreted palaeotopographic surface is noted towards the north in areas underlain by the lithologically less competent argillaceous Cedarberg and Goudini Formations (Figure 5.80). The palaeotopographic depression allows for greater accumulation of cover sediments towards the north. Overburden thickness range from 12.46 m (borehole CSF13) in the south to 51.04 m (borehole CSF10) towards the north.

Anomalies A, B, C, D, E and F, identified by Zadorozhnaya et al., (2012) as possible faults, are all shown to extend into cover sediments. These anomalies appear to be drawn on the basis of variations in resistivity values observed predominantly in bedrock. It is unlikely that these anomalies extend into Cenozoic sediments. Zadorozhnaya et al., (2012) did not have access to borehole data in the area, and were thus unable to correlate resistivity values and anomalies to depth of bedrock in the area. Consequently anomalies E and F are interpreted as indicators of lithological change within the Goudini Formation. Similarly anomalies A and C are interpreted to represent stratigraphic change between the Peninsula, Cedarberg and Goudini Formation rather than faults.

Anomaly D, interpreted to occur 1190 m along geoelectrical profile TDEM-CSF1, seemingly extends through both Cenozoic overburden and bedrock and shows a vertical inclination (Figure 5.80). Anomaly D's origin is uncertain, but may be related to a heterogeneous groundwater circulation system. If the anomaly is extended along NW-SE bedding strike it aligns with a similar feature identified by Stettler, et al., (2008) along their initial geological model of a TDEM survey conducted along the beach between Seal Point and Cape St. Francis interpreted to possibly reflect the Cape St. Francis fault (§ 3.4, Figure 3.9). However his initial interpretation of the Cape St. Francis fault and associated zone of fault mélange were later re-interpreted. A re-interpretation of the same TDEM sounding results indicated that steeper anticlinal folding could also fit the measured data collected along the length of the TDEM traverse CSF (Figure 3.10). The alternative geological model suggests a duplication of the Cedarberg Formation along

the bay and eliminates the interpreted onland extension of the Cape St. Francis fault and associated zone of fault mélange.

Based on these interpretations, an updated geological model of results obtained from multi-electrode resistivity line TDEM-CSF1 is presented in Figure 5.81.

Figure 5.80: Interpretation of the geoelectrical profile derived from survey line TDEM-CSF1 (Zadorozhnaya et al., 2012) annotated with updated geological interpretations.
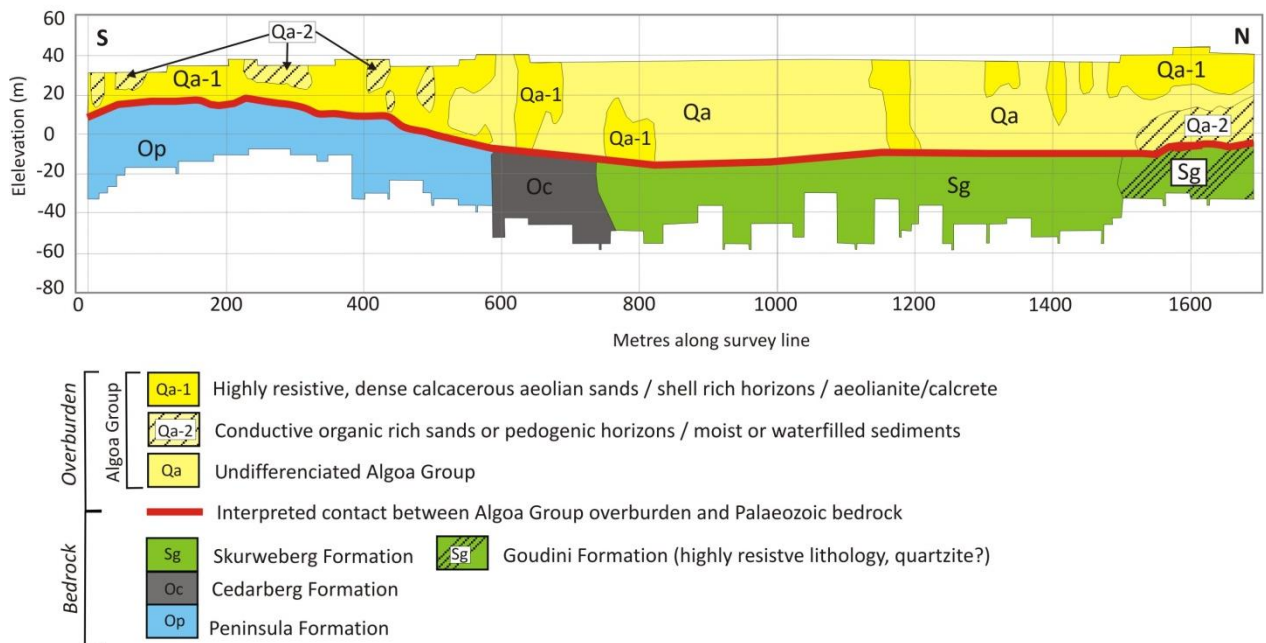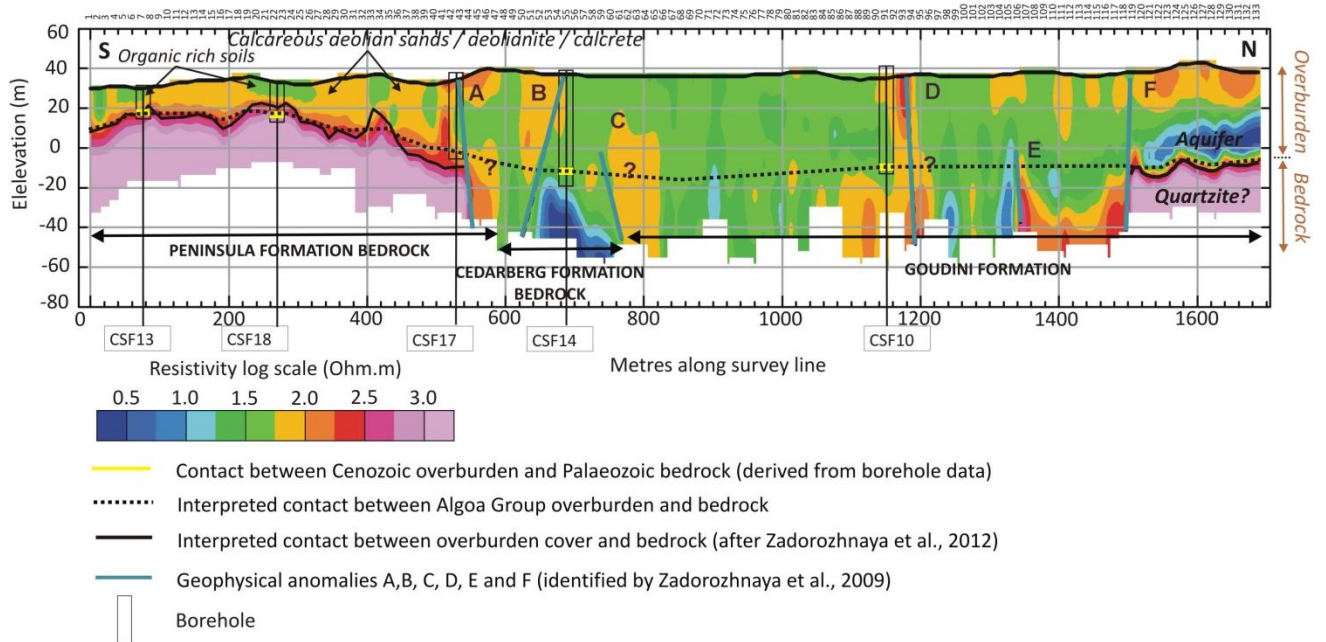
Figure 5.81: Revised geological model of results obtained from time domain electromagnetic survey line TDEM-CSF1.

5.5 Borehole data

Within the study area borehole data (232 from a total of 247 boreholes) are utilised to determine the thickness of the Algoa Group; the stratigraphic contacts between Palaeozoic strata and palaeotopography prior to deposition of overburden sediments. The author has published certain portions of the results presented in § 5.5.1 & § 5.5.2 as part of a bursary condition defined by the CGS (Claassen, 2014) See Appendix A1.

The level of lithostratigraphic detail captured within each borehole dataset varied considerably, consequently tracing out of individual units or possible marker beds was ultimately not possible.

5.5.1 Stratigraphic contacts beneath Cenozoic cover

Borehole data (Raubenheimer *et al.*, 1988a; 1988b; Rosewarne & Lomberg, 1989; Maclear, 2002; Maclear, 2005; Maclear, 2006; Eskom, 2010 a; Eskom, 2010 b; Engelsman & Constable, 2012; Hanson *et al.,* 2012) allowed for partial differentiation between stratigraphic bedrock units at Thyspunt (Figure 5.82), De Hoek, Cape St. Francis (Figure 5.83) and St. Francis (Figure 5.84). Boreholes that reached bedrock were assigned specific symbology based on their bedrock lithostratigraphy. Inferred contacts between stratigraphic units are derived from the borehole data and the extension of coastal outcrop exposures along strike, inland.
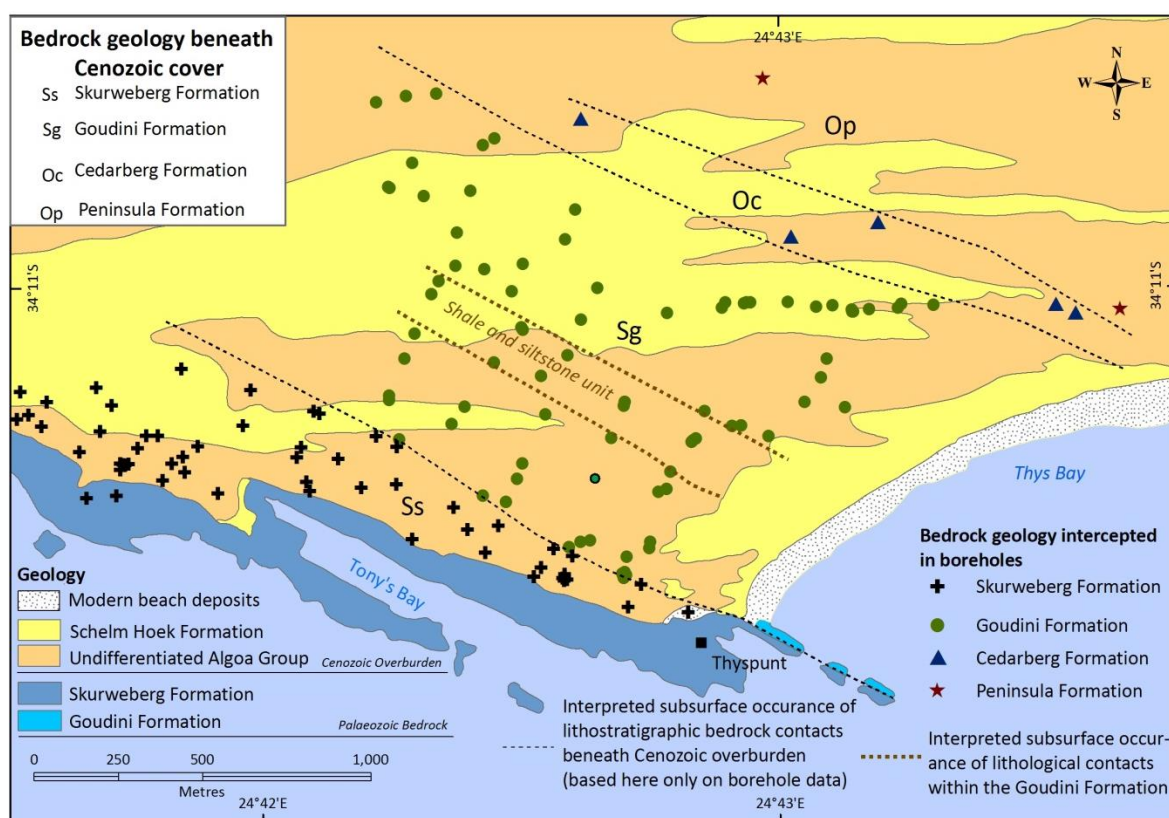
Figure 5.82: Inferred stratigraphic contacts between Palaeozoic bedrock beneath Cenozoic cover deposits at Thyspunt. Contacts are derived from borehole data and geology mapped along coastal outcrop exposures.
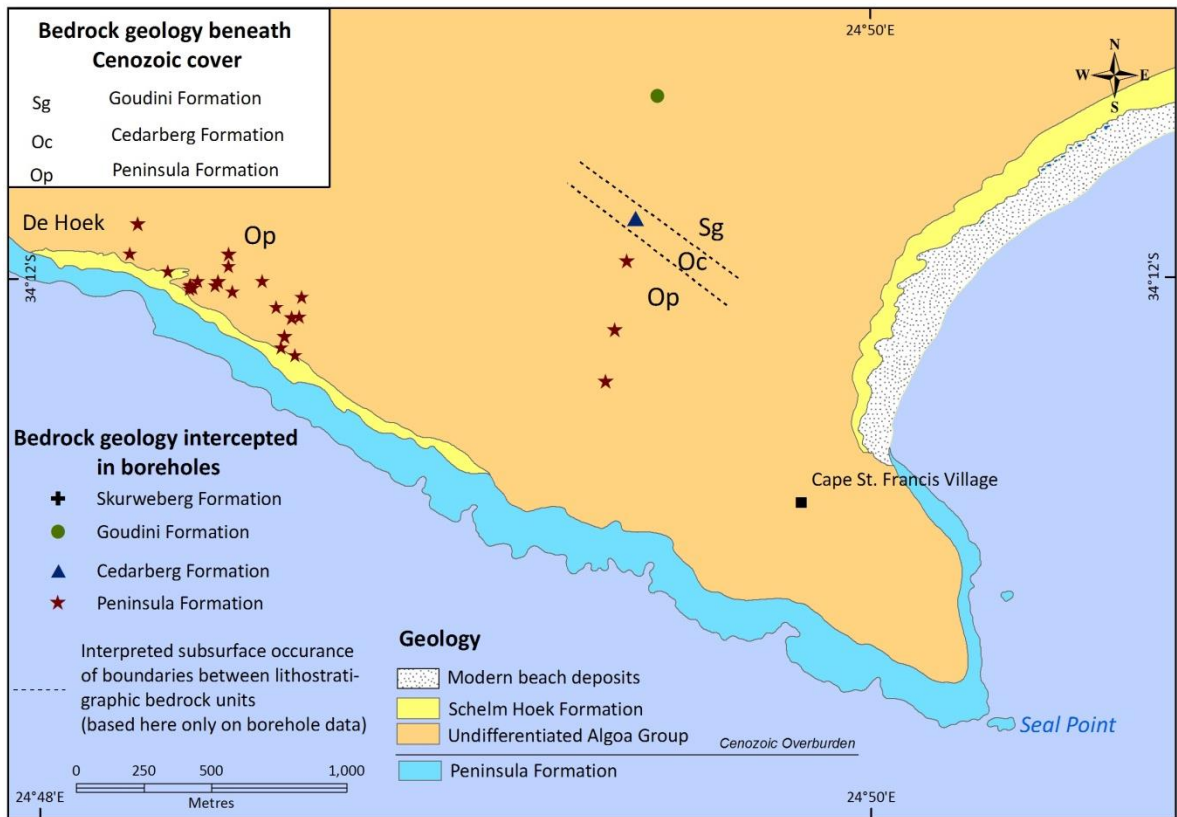
Figure 5.83: Inferred stratigraphic contacts between Palaeozoic bedrock units beneath Cenozoic deposits at De Hoek and Cape St. Francis. Contacts are inferred from borehole data.
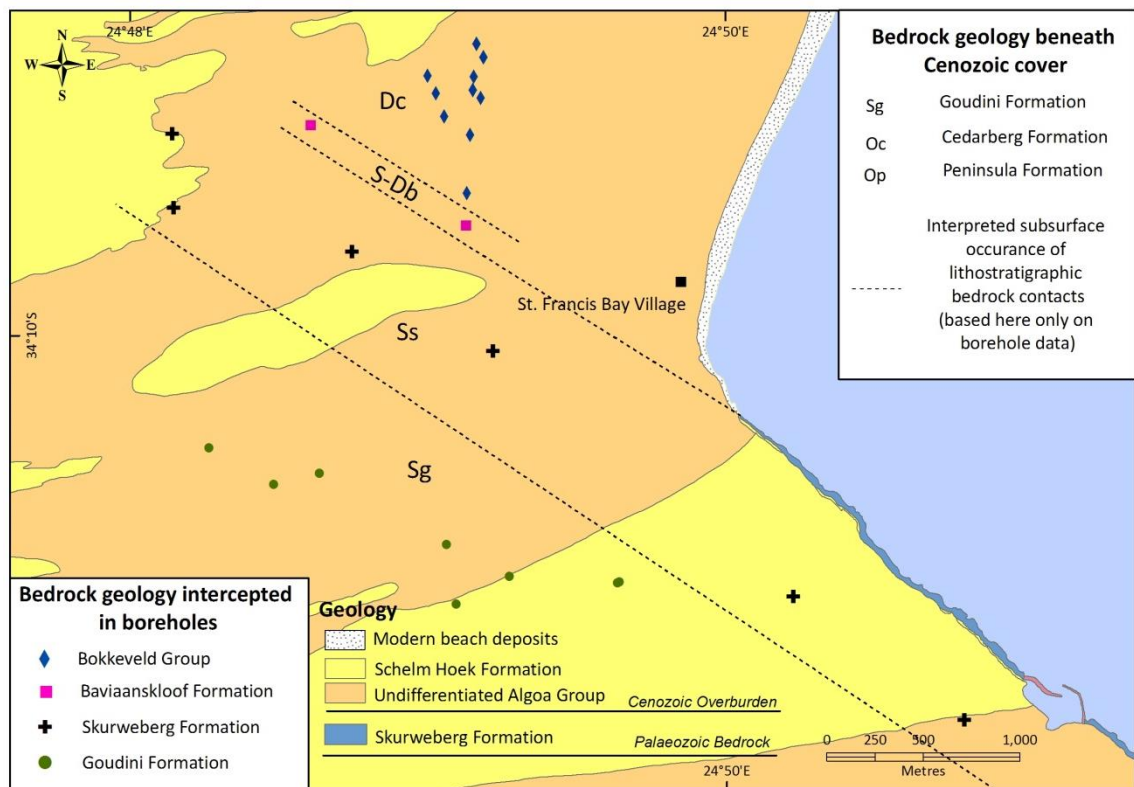
Figure 5.84: Inferred stratigraphic contacts between Palaeozoic bedrock units beneath Cenozoic deposits at St. Francis. Contacts are inferred from borehole data.

5.5.2   Thickness distribution of the Cenozoic Algoa Group

A total of 232 boreholes (Raubenheimer *et al*., 1988 a; 1988 b; Rosewarne & Lomberg, 1989; Maclear, 2002; Maclear, 2005; Maclear, 2006; Engelsman & Constable, 2012; Hanson *et al.,* 2012) were used in determining thickness of the Algoa Group. Delineating thickness of individual formations within the Algoa Group is problematic. Difficulty in differentiating between formations of Cenozoic age within the study area is attributed to limited exposure and borehole log descriptions that are often not formation specific, nor provide adequate lithological descriptions of Cenozoic deposits to facilitate accurate differentiation to formation level. Therefore, the Algoa Group is treated here, predominantly as a composite undifferentiated unit.   Similarly Goedhart *et al*., (2008) also defined the Algoa Group as mainly undifferentiated.

Thickness of the Algoa Group is derived from individual boreholes within the study area (Figure 5.85). Individual borehole surface elevations, bedrock elevations and the resultant thicknesses are graphically plotted against their distance from the coastline in areas where borehole density was sufficient enough to produce a meaningful result or substantiate a trend in the data. These areas include Thyspunt (Figure 5.86 a & b), the combined areas of De Hoek and Cape St. Francis (Figure 5.87 a & b) and St. Francis (Figure 5.88 a & b). The impact of surface relief and bedrock elevation on the thickness of overburden sediments is further investigated by means of cross sections perpendicular to the coastline at Thyspunt (Figure 5.89 and Figure 5.90 a, b & c) and Cape St. Francis (Figure 5.91 & Figure 5.92). Variations in the thickness of the Cenozoic Algoa Group relative to the distance from shoreline, revealed four coast parallel trending zones referred to here as zones A to D (Figure 5.85).
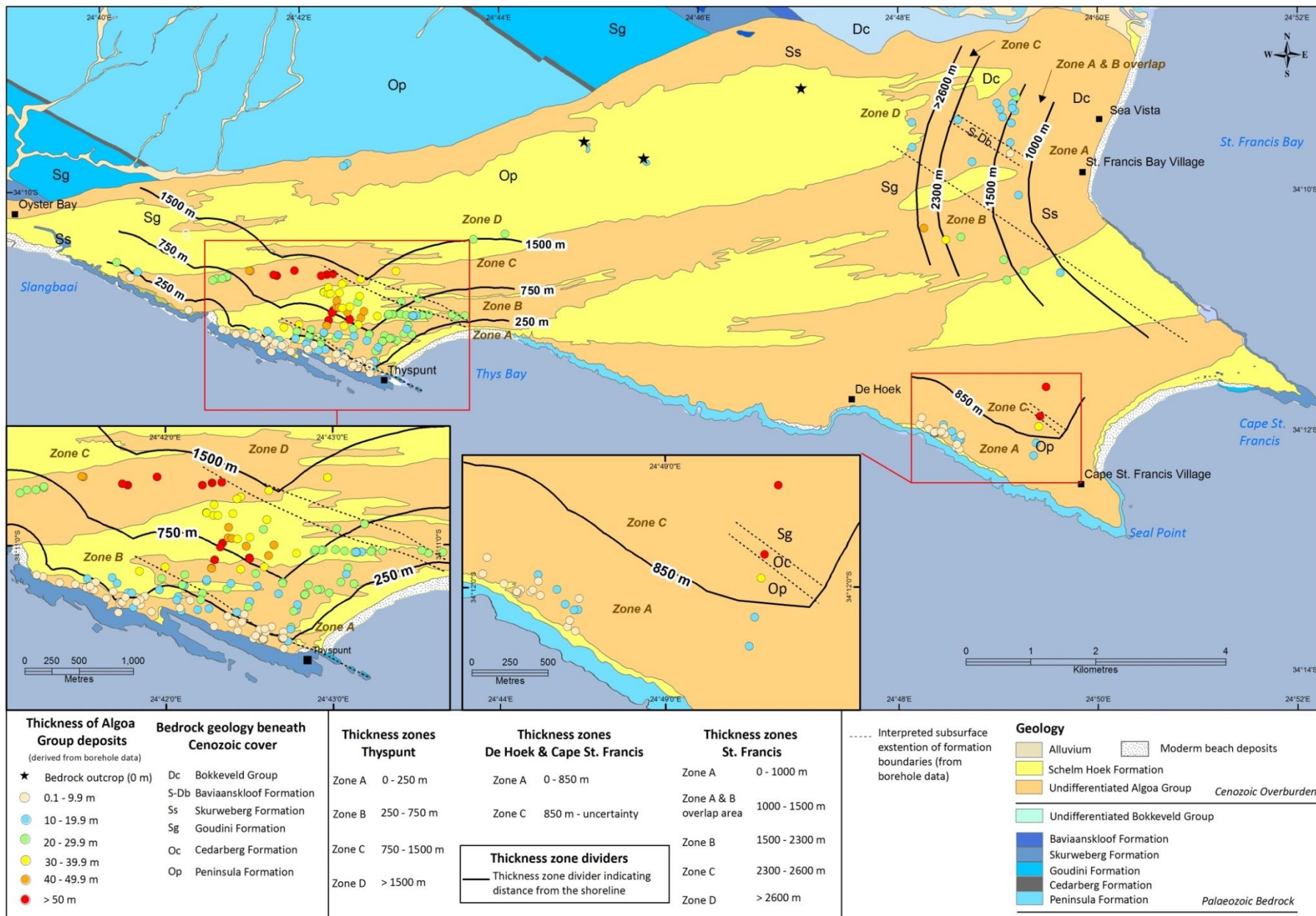
Figure 5.85: Thickness of the overburden sediments (Algoa Group) within the study area, as derived from borehole data. Various thickness zones are identified (A to D). Zones relate to distance from the shoreline (Claassen, 2014).
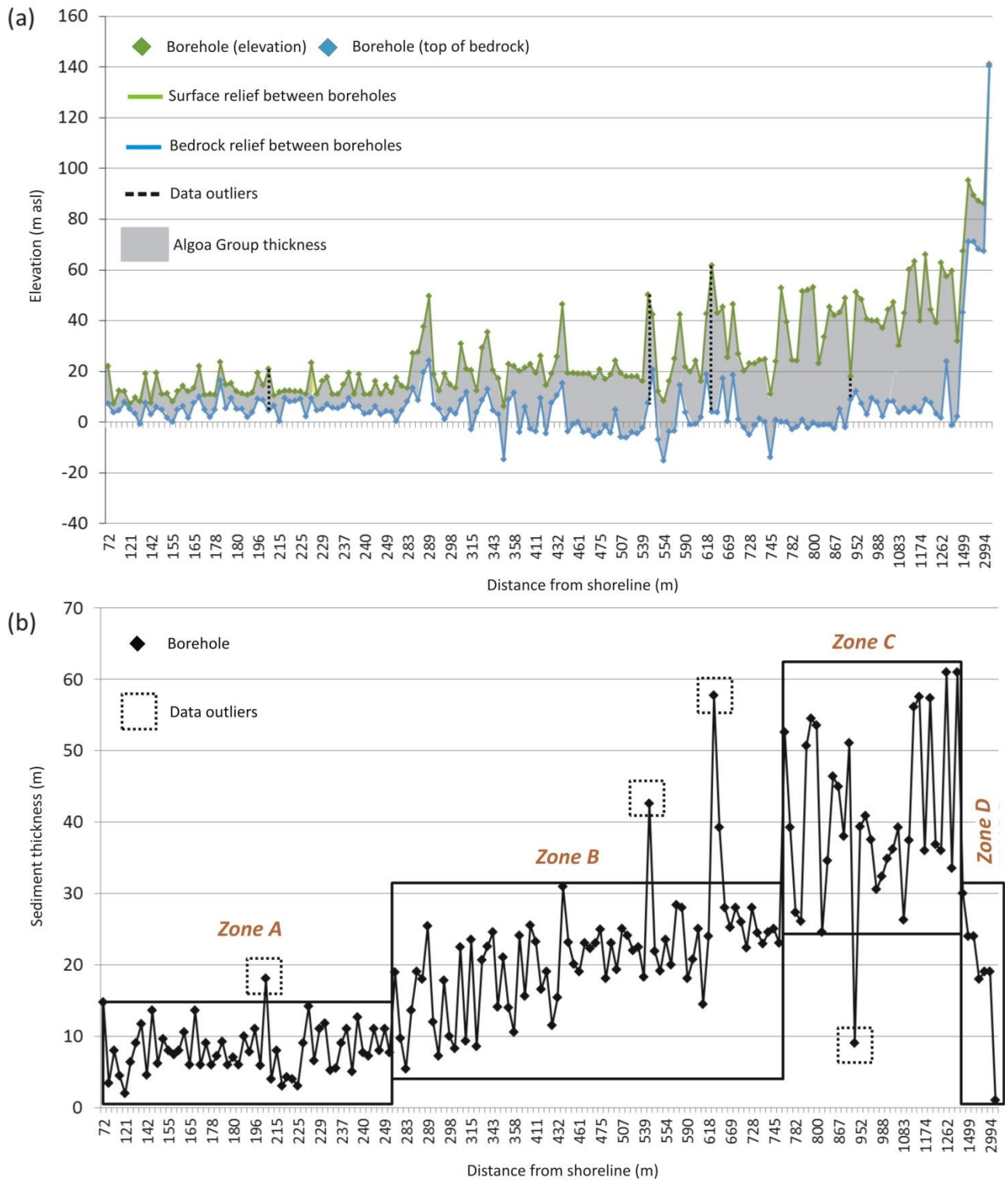
Figure 5.86: (a) Individual borehole surface relief and bedrock elevations in the vicinities of Thyspunt are plotted against their distance from the shoreline. (b) Individual borehole thicknesses of the Algoa Group in the vicinity of Thyspunt plot against their distance away from the coastal margin. Four thickness zones, A to D, can be identified. Data outliers refer to boreholes that either show surface relief or bedrock elevation and resultant cover thickness not in range of the general trend within a defined zone (Claassen, 2014).
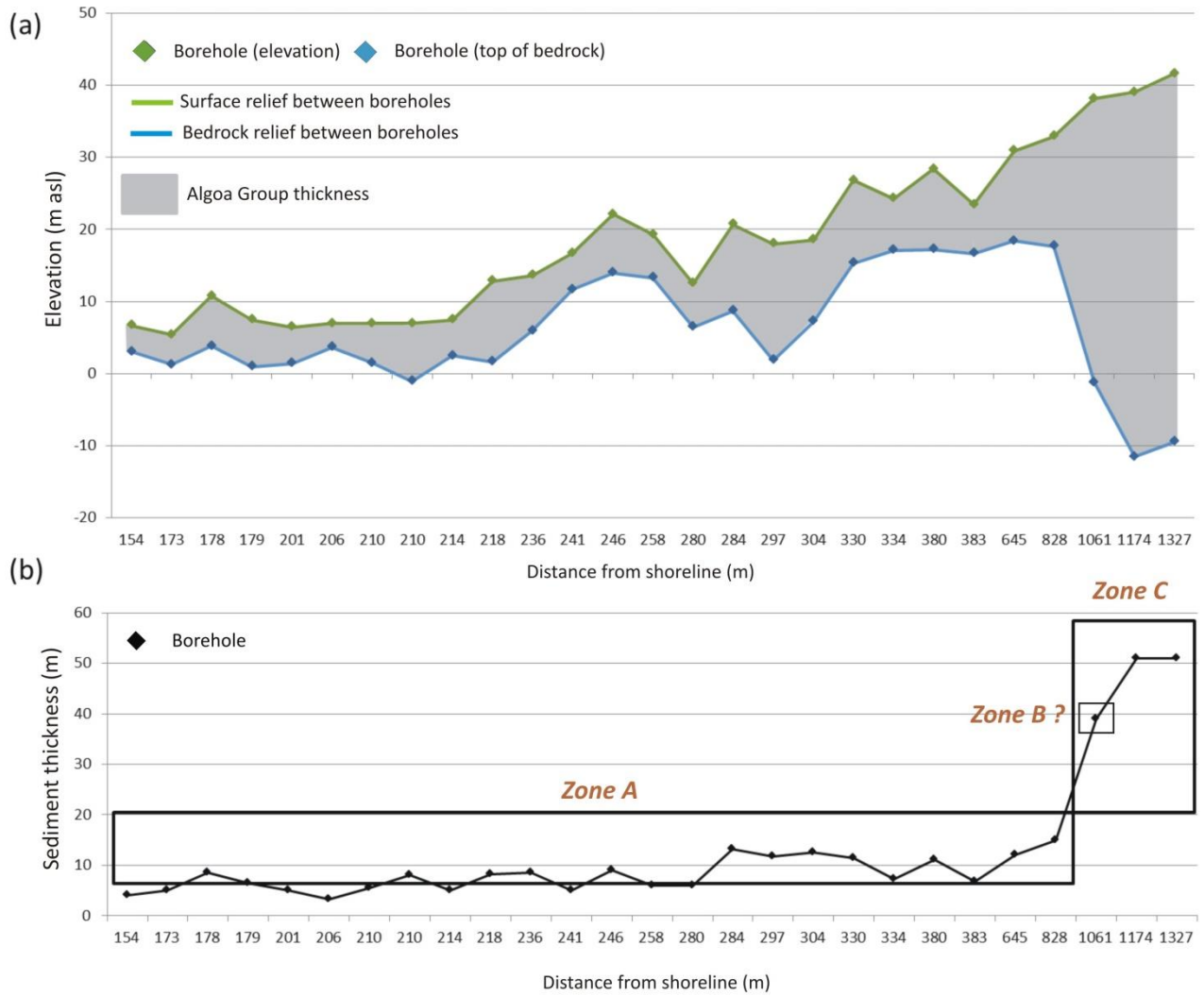
Figure 5.87: (a) Individual borehole surface relief and bedrock elevations in the vicinity of De Hoek and Cape St. Francis are plotted against their distance from the shoreline. (b) Individual borehole thicknesses of the Algoa Group in the vicinity of De Hoek and Cape St. Francis plotted against their distance away from the coastal margin. Thickness zones A and C are identified (Claassen, 2014).
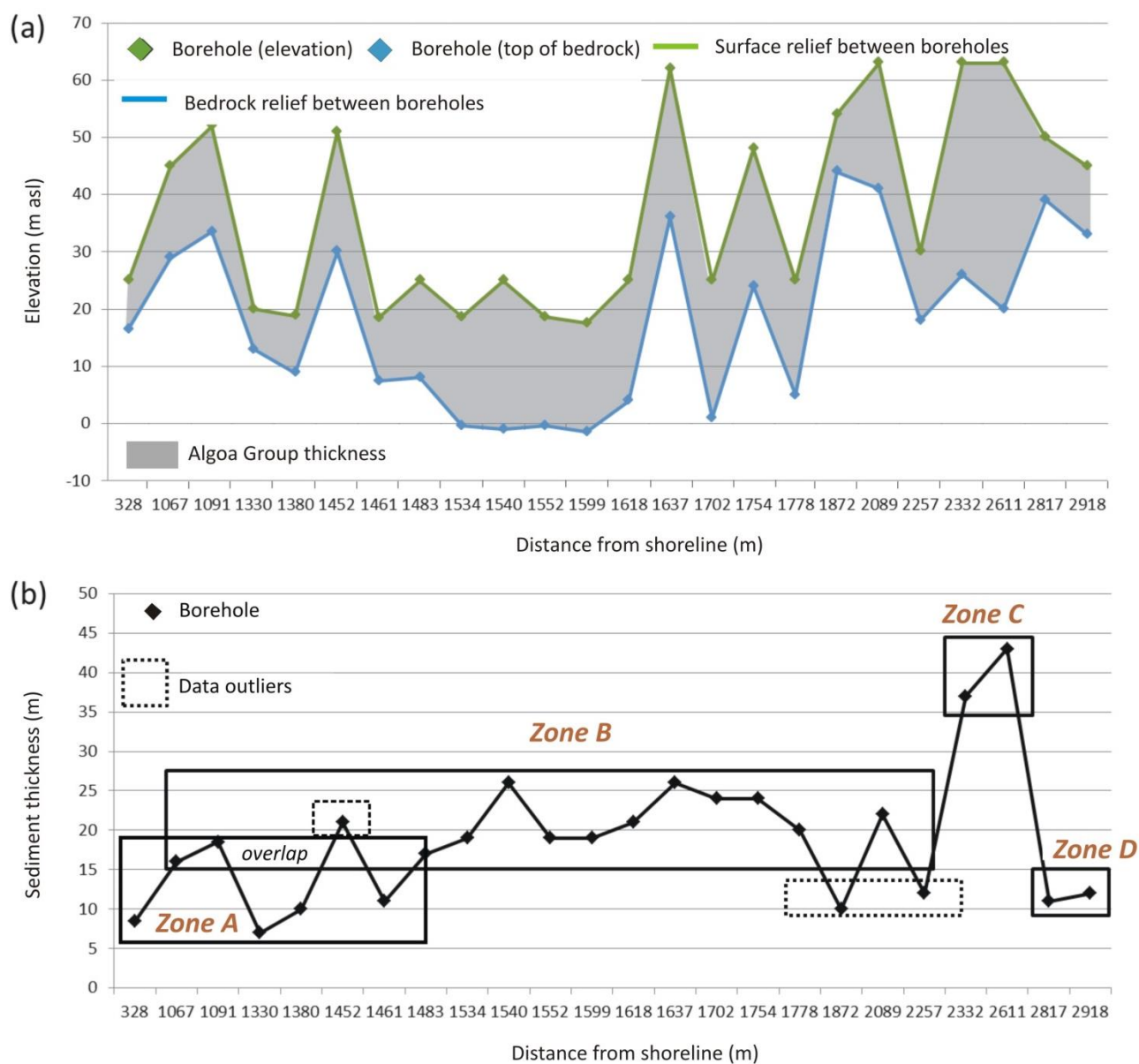
Figure 5.88: (a) Individual borehole surface relief and bedrock elevation in the vicinity of St. Francis plotted against their distance from the shoreline. (b) Individual borehole thicknesses of the Algoa Group in the vicinity of St. Francis plotted against their distance from the shoreline. Thickness zones A - D are primarily identified, with an interpreted overlap between zone A and B. Data outliers refer to boreholes that either show surface relief or bedrock elevation and resultantly cover thicknesses not in range of the general trend within a defined zone (Claassen, 2014).
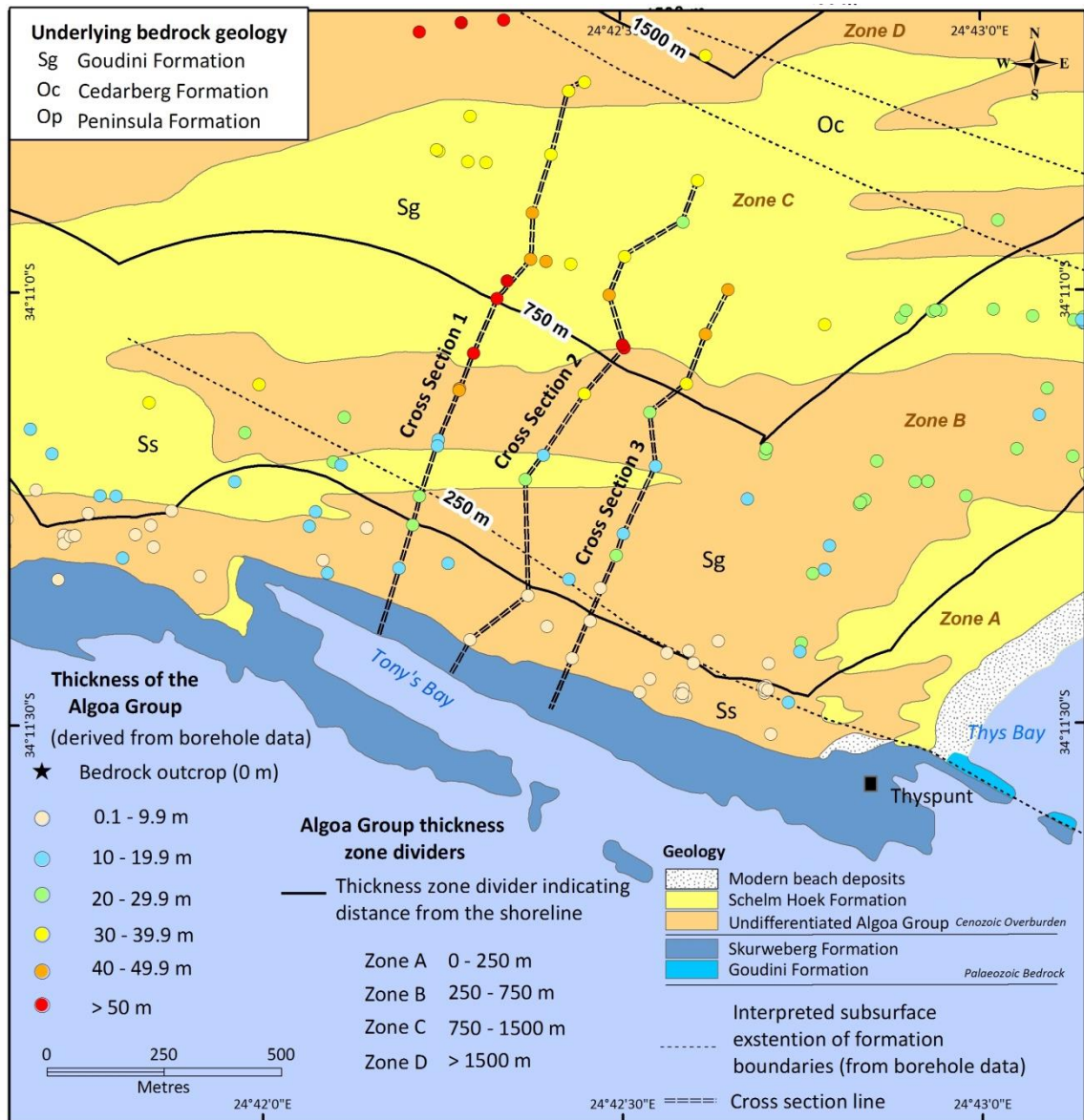
Figure 5.89: Thicknesses of the Algoa Group derived from individual boreholes occurring at Thyspunt and Tony's Bay. Thickness zones A, B, C and D are outlined. The location of cross sections 1, 2 and 3 are also indicated.
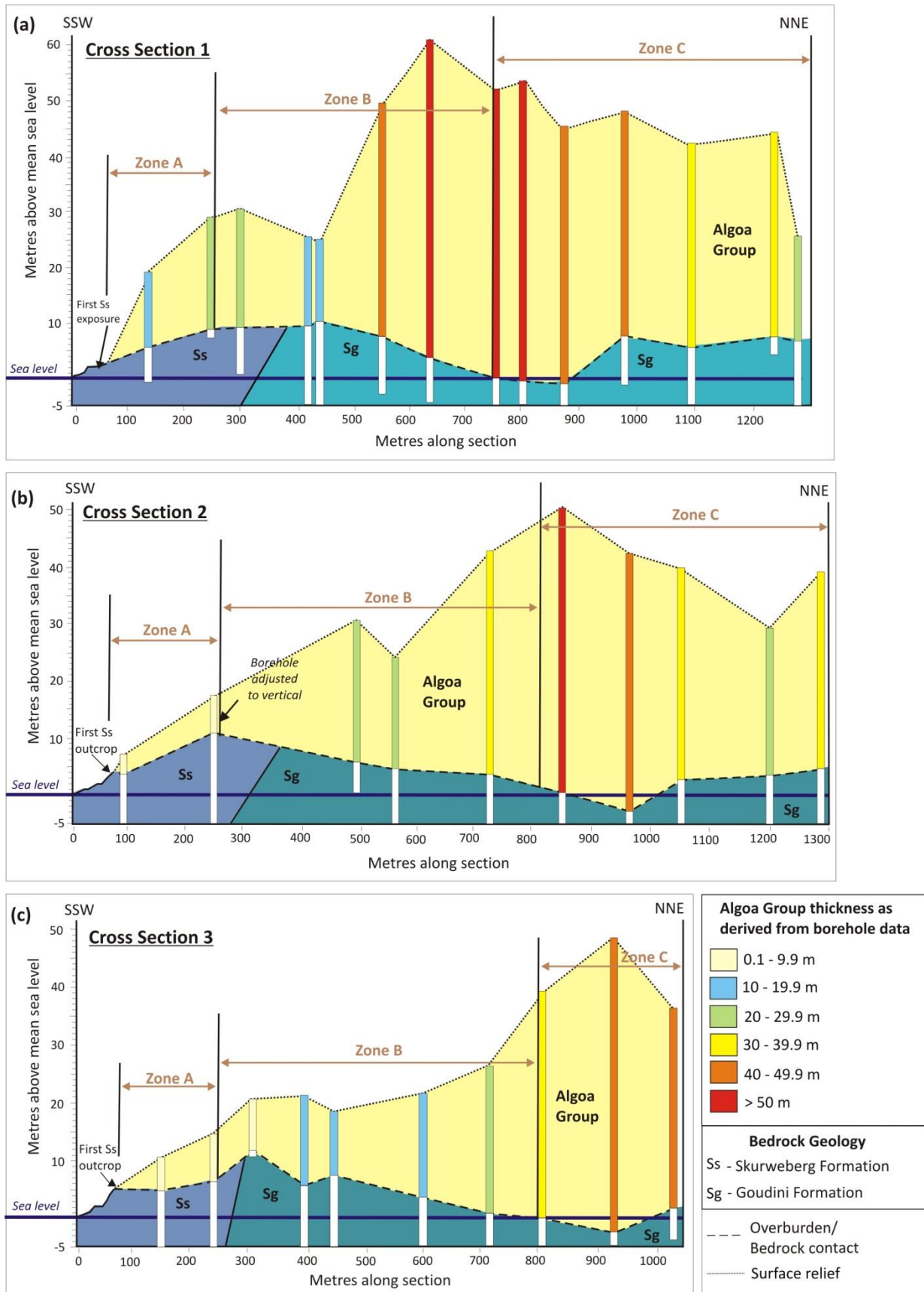
Figure 5.90: Cross sections 1, 2 and 3. See Figure 5.89 for location of these cross sections at Thyspunt. Areas where boreholes indicate the greatest thickness occurrences of the Algoa Group coincide with bedrock lows and surface elevation highs (Claassen, 2014).
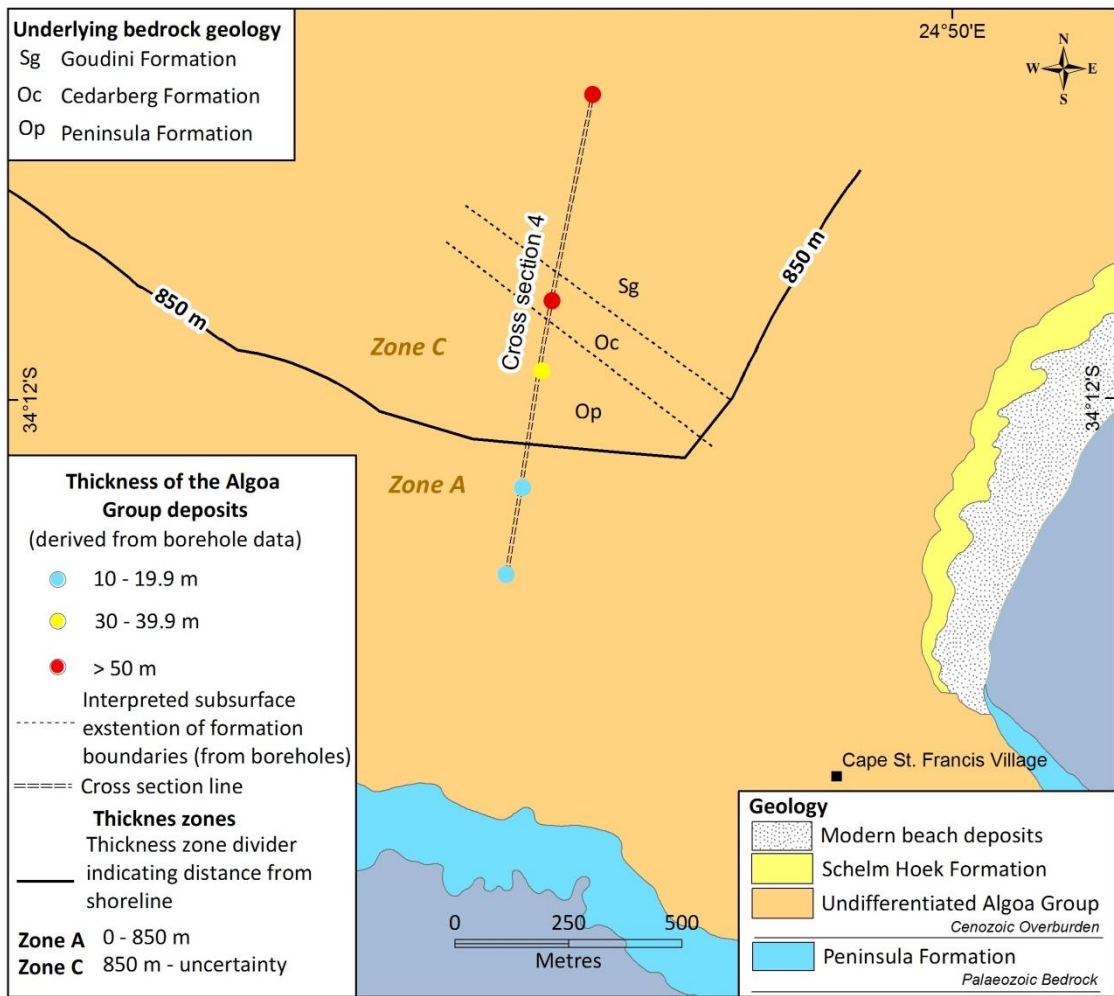
Figure 5.91: The sediment thickness of the Algoa Group from borehole data in the Cape St. Francis area. Thickness zones A to C are identified. The location of cross section 4 is also indicated (Claassen et al., 2014).
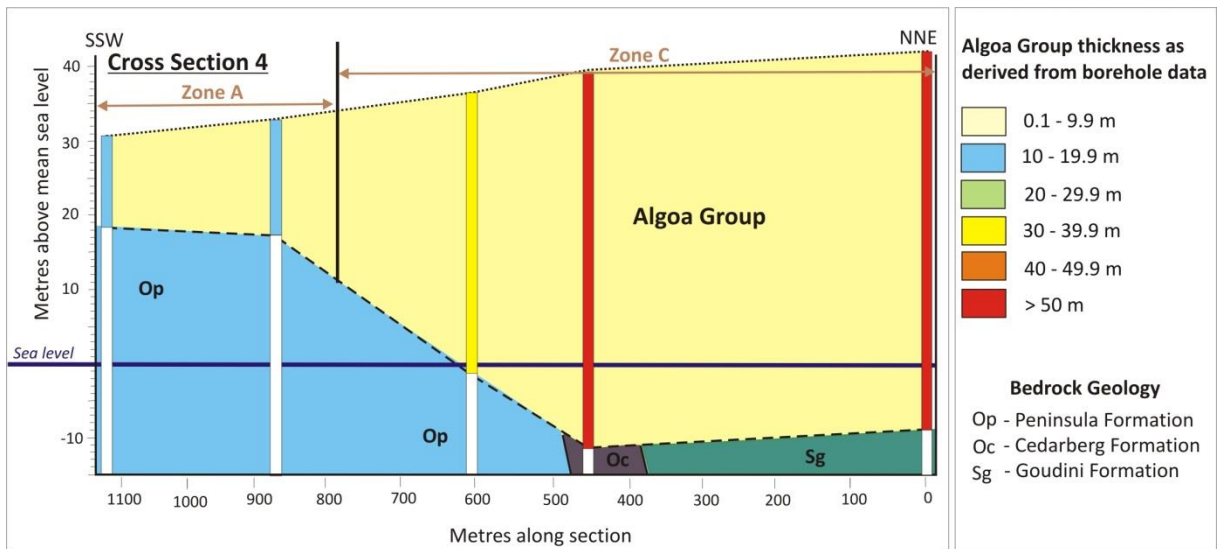
Figure 5.92: Cross section 4. See Figure 5.91 for the location of this cross section at Cape St. Francis. Areas where boreholes indicate the greatest thickness occurrences of the Algoa Group coincide with bedrock lows and surface elevation highs (Claassen, 2014).

(i) Zone A

Zone A (Figure 5.85 & Figure 5.89) represents Algoa Group deposits in the vicinity of Thyspunt that occupy the area extending inland from the coastal margin for ~250 m (Figure 5.86 b); ~830 m in the combined vicinities of De Hoek and Cape St. Francis (Figure 5.87 b) and up to 1500 m in the St. Francis region (Figure 4.88 b). Sediment thicknesses within this coast proximal belt range on average between 3-12 m and rarely exceed a 15 m thickness (Figure 5.86 b).

In the vicinity of Thyspunt, Algoa Group sediments occupying zone A are exclusively underlain by competent NW-SE striking quartzite of the Skurweberg Formation (Figure 5.85 and Figure 5.89). Here, bedrock elevations are below 10 m and very rarely below sea level (Figure 5.86 a & Figure 5.90 a, b & c). Borehole elevations indicate that surface relief does not exceed 25 m (Figure 5.86 a). Sediments range in thickness from a minimum of 2 m near the shoreline, to an isolated 16 m maximum approximately 200 m inland from the coastal margin near Tony's Bay (Figure 5.86 b and Figure 5.89). The sediment thicknesses typically range between 3-11 m (Figure 5.86 b).

In the areas of De Hoek and Cape St. Francis boreholes that occupy zone A are exclusively underlain by competent NW-SE trending quartzite of the Peninsula Formation (Figure 5.85 & Figure 5.91). Bedrock elevation steadily rises with increasing distance from the coastal margin and is coupled with a steady rise in surface relief (Figure 5.87 b). A thickness range similar to Thyspunt is calculated in the De Hoek and Cape St. Francis areas where Cenozoic deposits typically range between 6-9 m (Figure 5.87 a). In the combined areas of De Hoek and Cape St. Francis a maximum sediment thickness of 15 m is recorded, 828 m from the coastline at the inland boundary of zone A (Figure 5.87 b). In the central part of zone A, east of De Hoek, a maximum thickness of 13 m (Figure 5.87 b) is documented for Cenozoic sediments.

At St. Francis, Algoa Group sediments within zone A have extreme thicknesses of up to 22 m, and more frequently sediment accretion values that exceed 10 m (Figure 5.88 b). Zone A is less clearly defined at St. Francis compared to Thyspunt, De Hoek and Cape St. Francis. Here, a greater range in the sediment thickness values is observed than those that would normally define zone A (Figure 5.88 b). In Zone A, accretion values at Thyspunt and the combined areas of De Hoek and Cape St. Francis are below 15 m, with a clear transition to thicker values marking the end of zone A (Figure 5.86 b and Figure 5.87 b). At St. Francis this clear transition to thicker sediment values is more ambiguous. Rather, zones A and B appear to overlap and extend inland from the coastal margin for approximately 1500 m (Figure 5.85). A transition zone where sediment thickness values of zone A and B are shared (Figure 5.85 and Figure 5.88 b), is the preferred interpolation considering the lack of borehole data for the area 1 km parallel to the coastal margin (the area that would more clearly define zone A).

(ii) Zone B

Overburden sediments occurring within zone B show a gradual increase in thickness compared to sediments in zone A. Here Cenozoic deposits frequently exceed 10 m and typically range between 12 – 26 m in thickness (Figure 5.86 b, and Figure 5.88 b).

At Thyspunt, zone B is defined as a 500 m wide zone that occurs inland between ~ 250 – 750 m from the shoreline (Figure 5.85 & Figure 5.88). Algoa Group sediments located towards the southern portions of zone B are underlain by the Skurweberg Formation (Figure 5.85 & Figure 5.89). Sediments that occupy the northern regions of zone B are underlain by the Goudini Formation (Figure 5.89). An increase in both bedrock elevation and surface relief is observed in zone B. (Figure 5.86 a). Unlike zone A, bedrock elevations are also frequently below sea level. This variation in bedrock elevation compared to zone A, is accompanied by an increase in surface relief (Figure 5.86 a). Cenozoic sediment thicknesses occasionally surpassing 30 m and rarely 50 m, are documented at Thyspunt (Figure 4.86 b & Figure 5.89) with extreme thickness value outliers >50 m occurring between ~ 450 – 640 m north of the coastal margin (Figure 5.86 b).

In the vicinity of De Hoek and Cape St. Francis, zone B appears absent (Figure 5.87 b). At Thyspunt, the inception of zone B is marked by a gradual progression from zone A values (3 - 12 m typical thickness range) into thicker accretion values (12 - 26 m typical thickness) (Figure 5.86 b). A similar progression could not be recognized at De Hoek and Cape St. Francis (Figure 5.87 b). Rather a clear transition from zone A accretion values to much thicker sediment values that more closely resemble those associated with zone C is observed (Figure 5.87 b, Figure 5.91 & Figure 5.92). The area may either be devoid of sediment thicknesses associated with zone B or simply contain insufficient borehole data representative of zone B.

Although zone B is identified at St. Francis, its southern extent, is not as well defined compared as at Thyspunt (in part to a perceived overlap between zone A and zone B (Figure 5.85)). Therefore at St. Francis zone B is defined as a broad ~ 800 - 1200 m zone parallel to the coastal margin that extends into the hinterland between ~1050/1480 – 2250 m from the shoreline (Figure 5.85). At St. Francis, Cenozoic sediment thicknesses frequently surpass 15 m and occasionally surpass 25 m (Figure 5.88 b). A few boreholes record sediment thickness outliers below 10 m (Figure 5.88 b). Algoa Group deposits that occupy zone B are underlain by rocks of the Table Mountain Group and Bokkeveld Group at St. Francis (Figure 5.85). A complementary relationship is observed between bedrock elevation and surface relief. A rise in bedrock elevation is coupled by an increase in surface relief. Similarly a decrease in bedrock relief is often coupled by a decrease in surface elevation (Figure 5.88 a).

(iii) Zone C

Boreholes that occupy zone C (Figure 5.85) show a significant increase in the thickness of Cenozoic sediments compared to zones A and B (Figure 5.86 b, Figure 5.87 b & Figure 5.88 b). Zone C is characterized by accretion values that frequently exceed 30 m. (Figure 5.86 b, Figure 5.87 b and Figure 5.88 b).

At Thyspunt, zone C is defined as a 750 m wide inland zone occurring between ~750 – 1500 m from the coastline (Figure 5.85 & Figure 5.89). Cenozoic sediments occupying zone C are underlain by the lithologically incompetent Goudini and Cedarberg Formations. Bedrock elevations for boreholes that occupy zone C are generally below 10 m asl, and frequently below sea level (Figure 5.86 b, Figure 5.90 a, b & c). Borehole elevations indicate that surface relief often exceed 40 m (Figure 5.86 a). Viewed overall, a slight decrease in borehole bedrock elevations is observed compared to zone B. This slight decline in bedrock elevation is accompanied by an increase in surface relief (Figure 5.86 a). The Algoa Group reaches its maximum recorded thickness, 61 m, approximately 1200 m from the coastline at Thyspunt (Figure 5.86 b & Figure 5.90 a).

Near Cape St. Francis Cenozoic deposits occupying zone C are underlain by the Cedarberg and Goudini Formations (Figure 5.91). With zone B absent at this locality (as discussed in the section considering zone B), a sharp increase in surface elevation is observed at the transition from zone A directly to zone C (Figure 5.87 a). Similar to observations made at Thyspunt, this rise in surface relief is also coupled with a decrease in the bedrock elevation (Figure 5.86 a & Figure 5.87 a). At Cape St. Francis borehole bedrock elevation is documented to occur below sea-level by as much as 11 m (Figure 5.87 a & Figure 5.92). Peak accretion values of 51 m are encountered (Figure 5.85) at two localities approximately 1150 m and 1350 m from the shoreline at Cape St. Francis (Figure 5.87 b, Figure 5.91 and Figure 5.92).

The maximum recorded thickness of cover sediments associated with zone C in the vicinity of St. Francis is lower than Thyspunt and Cape St. Francis (Figure 5.86 b, Figure 5.87 b & Figure 5.88 b). Here deposits reach a peak thickness of 43 m at approximately 2600 m from the coastline (Figure 5.88 b). The location of zone C is defined (based on limited borehole data) as a very narrow width approximately 300 m wide, that extends between approximately 2300-2600 m inland from the coastline (Figure 5.85). Boreholes that occupy zone C in the St. Francis area are exclusively underlain by the Goudini Formation (Figure 5.85).

(iv) Zone D

Cover sediments occupying zone D, show a significant decrease in thickness compared to zone C (Figure 5.86 b and Figure 5.88 b). The transition to zone D is marked by the dramatic decline from peak sediment thickness values to thinner accretion values that range between 0 – 25 m (Figure 5.86 b & Figure 5.88 b). Deposits occurring within zone D more closely resemble the thickness values of predominantly zone A and occasionally those of zone B.

At Thyspunt, zone D is situated ~1500 m inland, extending farther into the hinterland towards the northern outcrop extent of the Algoa Group (Figure 5.85 & Figure 5.88 b). Boreholes that occupy zone D are exclusively underlain by the Peninsula Formation. High bedrock elevation values are coupled with prominent surface relief (Figure 5.88 a). Sediment thicknesses frequently range between 0 - 25 m (Figure 5.85 and Figure 5.88 b). Isolated bedrock exposures are documented NE of St. Francis (Goedhart *et al.*, 2008) within zone D (Figure 5.85).

At St. Francis, the start of zone D is situated further inland (Figure 5.85 & Figure 5.88 b). Here zone D is defined only with limited borehole data, but can be described as occurring ~ 2800 m inland towards the northern extent of the Algoa Group (Figure 5.85 & Figure 5.88 b). Boreholes that occupy zone D at St. Francis exclusively intercept Skurweberg Formation bedrock (Figure 5.85). Sediment thicknesses are below 15 m at St. Francis (Figure 5.88 b). Limited data does not allow characterization of zone D at De Hoek and Cape St. Francis.

(v) Algoa Group - basal gravel thickness

One hundred and seventeen boreholes (of 232) record a gravel unit occurring directly above bedrock. These marine and fluvial gravels are stratigraphically correlated with either the basal unit of the Alexandria Formation or the Salnova Formation (Roberts *et al*., 2006; Hanson *et al*., 2012). Within the study area, the gravel unit is composed of highly calcareous light grey to yellowish grey, medium to fine-grained, and moderately to well-sorted sands containing imbricated, disc- to roller-shaped, pebble to cobble-size clasts often containing shell fragments (See § 5.1.3 and Figures 5.23 & 5.28 for greater detail). Certain well described borehole logs allow for partially differentiation of the Algoa Group close to the coastline near Thyspunt (see the generalized scheme in Figure 5.23). Gravels within the study area are not laterally persistent and spatially show great thickness variation. The occurrence and thickness of basal gravels are indicated in Figure 5.93 a and b. No clear thickness distribution pattern for basal gravels could be established in terms of their location relative to the coastal margin. In addition no correlation between the thickness of basal gravels and the elevation of the bedrock surface upon which they were deposited could be established.

Borehole data indicate a greater frequency of occurrence and thickness of basal gravel units in areas underlain by the Goudini Formation, Cedarberg Formations and the undifferentiated Bokkeveld Group than in areas underlain by the Skurweberg- and Peninsula Formation (Figure 5.93 a & b, Figure 5.94). The typical thickness range for basal gravels is calculated between 0.5 m and 5 m, with occasional 5−10 m thicknesses. The thickest gravel layer recorded within the study area is 19 m thick and is documented at Cape St. Francis, where gravels are underlain by Peninsula Formation (Figure 5.94). The maximum thickness of basal gravels recorded at Thyspunt is 11.5 m approximately 1.5 km NW of Tony's Bay, where gravels are underlain by Goudini Formation bedrock.
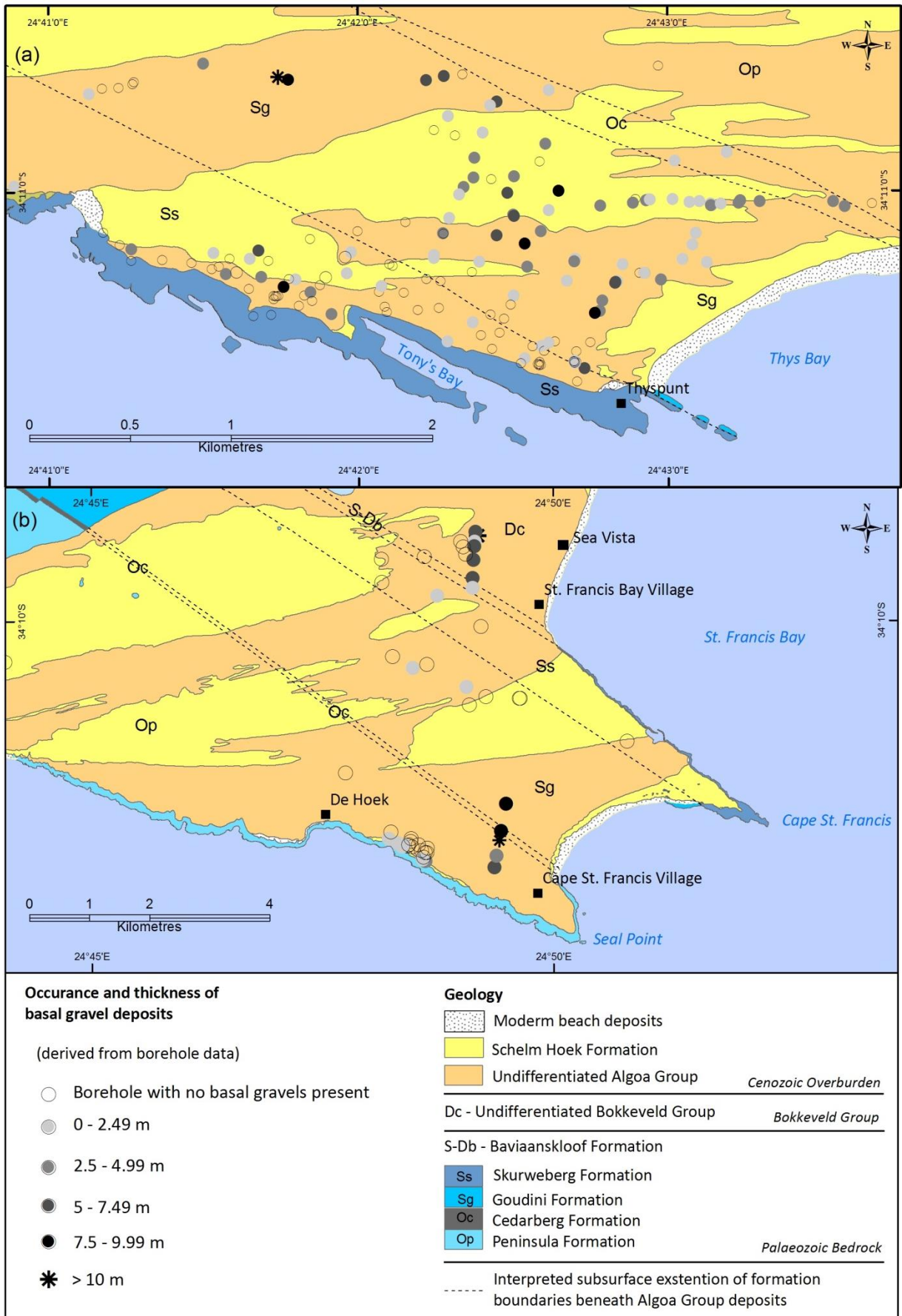
Figure 5.93: (a) Distribution of the Algoa Group basal gravel deposits at Thyspunt and (b) greater Cape St. Francis areas as derived from borehole data (Claassen, 2014).
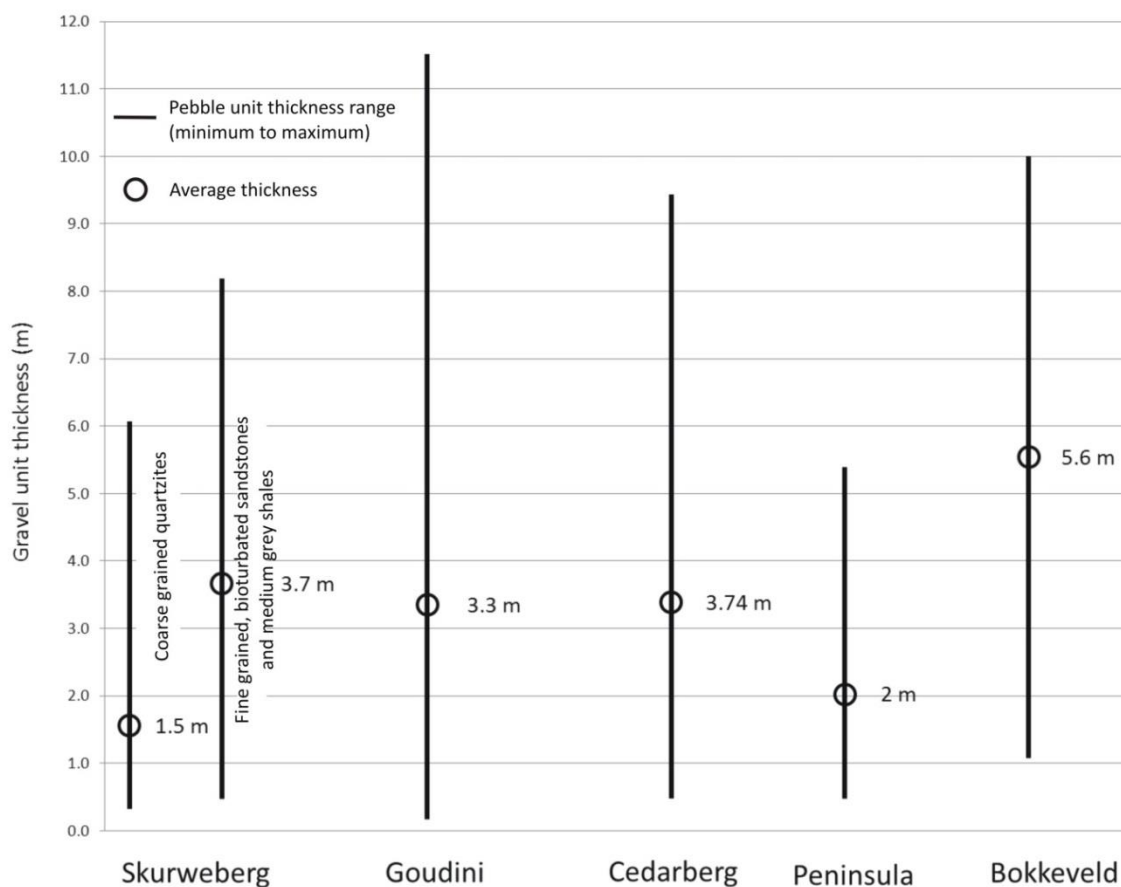
Figure 5.94: The formation specific range and average thickness of basal deposits of the Algoa Group within the study area (Claassen, 2014).

5.5.3 Bedrock elevation beneath Cenozoic cover deposits

The interpolation method of kriging was utilized to create a map of bedrock elevation beneath Cenozoic overburden for the Thyspunt area. The area contains a high density of bedrock elevation values that suite this mode of interpolation best. The data allowed for the creation of a 1 m contour interval interpolation map (Figure 5.96). Bedrock elevation values covering the remainder of the study area are sparse and instead a 5 m bedrock contour interval map utilized the vector-based triangular irregular network (TIN) interpolation method (Figure 5.97).

Within the study area, bedrock elevation ranges between -15.5 m asl (Figure 4.96) to 120 m asl (Figure 5.97) close to the northern outcrop extent of the Algoa Group. Interpolated bedrock surfaces reveal four regions within the study area, beneath overburden where bedrock elevations are at, or below present day sea-level. These areas of negative relief (palaeovalleys) are identified at Tony's Bay, Thyspunt, Cape St Francis and north of St. Francis. Palaeovalleys trend NW-SE, parallel to bedding and occur NW of present day embayments. The widths of palaeovalleys appear slightly wider towards the south along lower reaches, narrowing inland toward upper reaches.
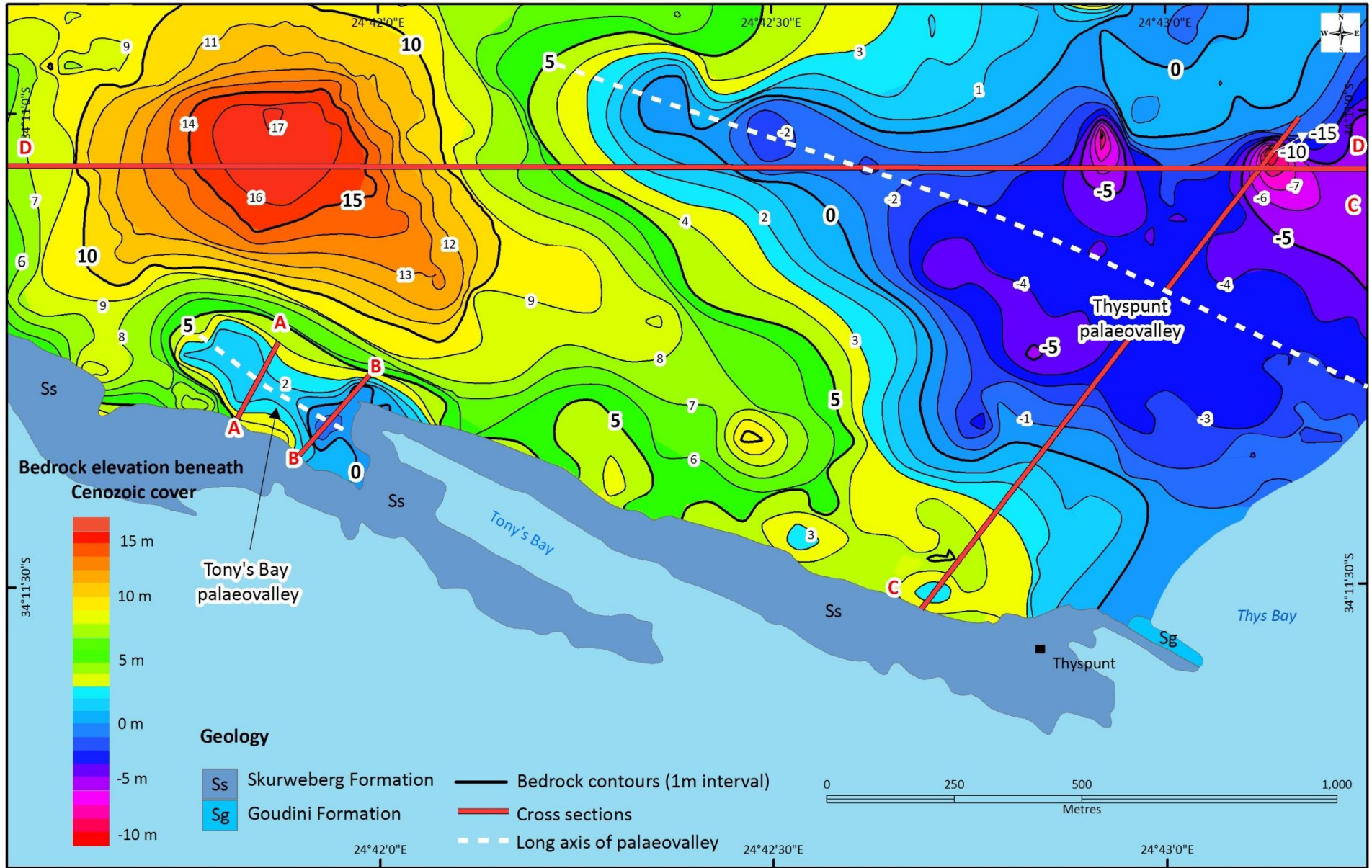
Figure 5.95: Map showing contoured bedrock elevation beneath Cenozoic overburden cover at Thyspunt. Bedrock contour interval spacing is 1m. Contouring reveals the presence of two areas where bedrock elevation is at or below present day sea-level (palaeovalleys), NW of Tony's Bay and Thyspunt, respectively.
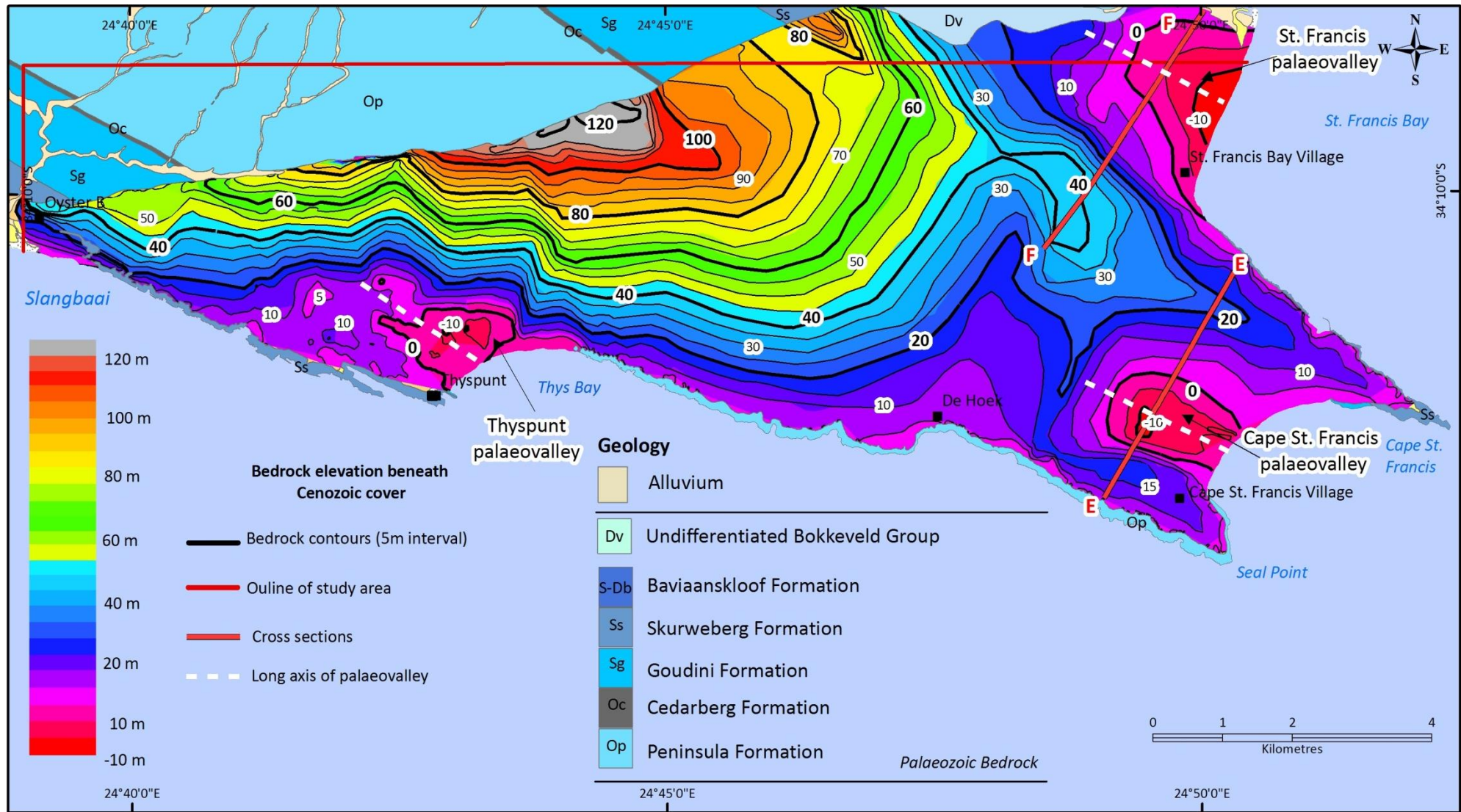
Figure 5.96: Map showing contoured bedrock elevation (palaeotopography) beneath overburden sediments within the study area. Bedrock contour interval spacing is 5 m. Contourings reveal the presence of three areas where bedrock elevation is below present day sea-level (palaeovalleys) at St. Francis, Cape St. Francis and Thyspunt.

A small linear shaped bedrock depression that reaches a maximum depth of -1.129 m asl (Borehole TB6) occurs at Tony's Bay. The valley is U-shaped along its upper reaches, with a 75 m wide flat valley bottom (Figure 5.96). Borehole data (TB22, BHDB1, BHDB3, BHDB9, THY-RP14 & TB6) indicate that the Tony's Bay valley is cut into fine-grained quartzitic sandstones and shale and siltstone units of the Skurweberg Formation. An approximately 50 m wide portion of the valley occurs below sea-level (Figure 5.96 & Figure 5.98 a & b). Portions of the palaeovalley that exhibit negative bedrock relief extend 80 m inland in a NW and NE direction. North of this palaeovalley, a steady rise in bedrock relief occurs to produce a topographic high (17 m asl) associated with quartzites of the Skurweberg Formation (Figure 5.98 d).

Farther eastward a second, larger and deeper palaeovalley is encountered NNE of Thyspunt. Bedrock relief reaches -15.5 m asl (borehole THY-MR11-M3), located 1 km NE of Thyspunt. The valley measures 1.5 km in width near its southern reaches and 150 m wide across its upper reaches. A 1050 m^2 portion of the palaeovalley occurs below sea level (Figure 5.96 & Figure 5.98 c & d). The valley is cut into strata of the Goudini Formation. Portions of the palaeovalley that exhibit negative bedrock relief extend 1,6 km inland in a NW-SE direction.

Between Seal Point and Cape St. Francis, a 7.5 km^2 (onland extent), 2.7 km wide palaeovalley, with a maximum depth of -11.52 m asl (borehole CSF14) is cut into bedrock strata of the Peninsula, Cedarberg and Goudini Formation. The valley extends 2.6 km into the interior (Figure 5.97). Borehole data (Hanson *et al.*, 2012) reveal the valley is cut into strata of the Cedarberg and Goudini Formation. A cross section perpendicular to the palaeovalley's long axis indicates that the southwestern slope of the valley bordered to the south by quartzitic sandstone of the Peninsula Formation, is steeper than the more gradual northeastern slope (Figure 5.98 e). Portions of the palaeovalley that exhibit negative bedrock relief extend 1,7 km inland in a NW-SE direction. A 1087 m^2 1.8 (onland) portion of the palaeovalley occurs below sea level.

Closer to the northeastern boundary of the study area, north of the St. Francis village, a >2.8 km wide palaeovalley is cut into bedrock of the Bokkeveld Group and possibly the Baviaanskloof Formation (Figure 5.97). Interpolation results reveal that the valley may be as deep as -10 m asl, close to its southeastern boundary with the NNE trending coastline. A NE-SW trending cross section perpendicular to bedding strike indicate that a 1.4 km wide portion of the valley occurs below sea level (Figure 5.98 f). Portions of the palaeovalley that exhibit negative bedrock relief extend 1.5 km inland in a NW-SE direction and covers a 2.5 km^2 onland area where elevation is below sea level.
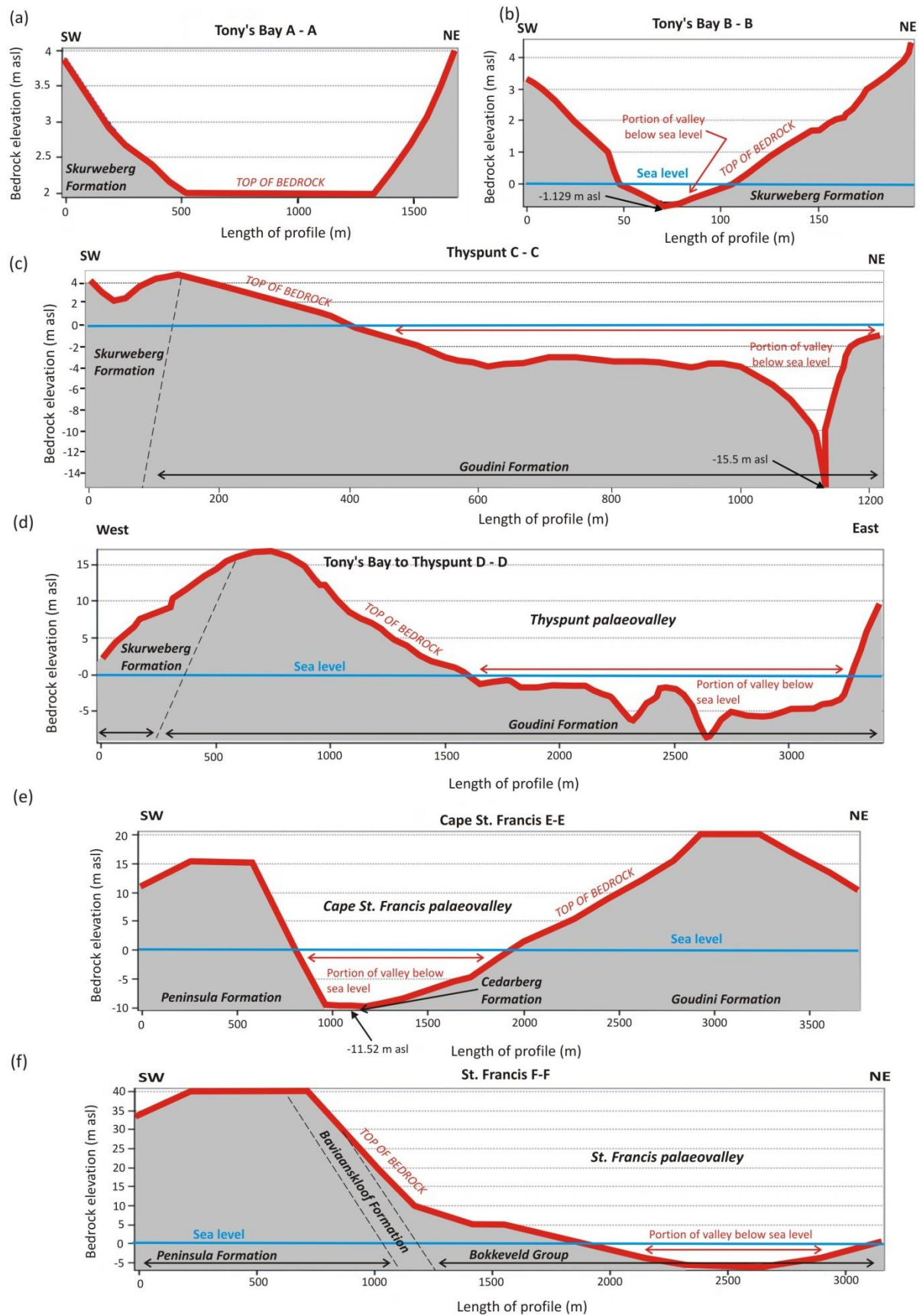
Figure 5.97: (a, b, c, d, e & f) Cross sections perpendicular and oblique to the long axis of palaeovalleys cut into bedrock beneath overburden cover at Tony's Bay, Thyspunt, north of Cape St. Francis and north of the village St. Francis.

5.6 Geomodel

The Thyspunt geomodel assists in visualising and integrating relevant geographical (e.g. topography), geological (e.g. maps), borehole and geophysical data within the study area. Figure 5.98 depicts the various data sources used, actions taken and outputs garnered to produce the geomodel. The geomodel was developed using primarily ArcMap 9.3 software and SketchUp 7.1 freeware in lieu of commercial and often costly 3D geomodelling software packages unavailable to the author. Final visualisation of data is presented in Google Earth enabling end users with even minimum GIS literacy to easily explore, interact and visualise 2D and 2½D data in a spatially referenced setting while partially restricting full access to confidential datasets. Appendix D contains a CD with the Thyspunt geomodel files in .kml or .kmz format. Data comprising the geomodel is grouped as follows:

1. STUDY AREA DATA
2. GEOLOGY
3. PALAEOTOPOGRAPHY
4. BOREHOLE DATA
5. CENOZOIC OVERBURDEN
6. STRUCTURE
7. GEOPHYSICS
8. SITE SAFETY RISKS

Each of the 8 categories contains a large amount of data. It's strongly recommended that the user open each dataset on its own, explore its content before creating an optimised view of the study area from a combination of categories as shown in § 5.6.3 (Model visualisations).

5.6.1 Model assumptions and considerations

During construction of the geomodel, the following assumptions were made (the user should keep these considerations and assumptions in mind when viewing the geomodel):

• Software usage - A basic knowledge of Google Earth operation and its functionality is required.

• Heterogeneity of data used - The large array of data sources gathered and ultimately used in the construction of the geomodel are vast. Datasets varied in extent, scale, detail, metadata information and level of accuracy. The level of accuracy varies between datasets due to the way in which data was captured by original authors. The accuracy of the model is largely depended on the accuracy of the data utilised in its construction. For example, certain borehole locations and elevations were surveyed (Raubenheimer et al., 1988a; 1988b; Eskom, 2010 b; Engelsman & Constable, 2012; Hanson *et al*., 2012), while others were captured with a handheld GPS (Rosewarne & Lomberg, 1989; Maclear, 2002; Maclear, 2005; Maclear, 2006; Eskom, 2010 a). Unless specifically stated otherwise (§ 4.4.1, Table 4.5) it is assumed that the data gathered from external sources and utilised in the construction of the geomodel are correct.
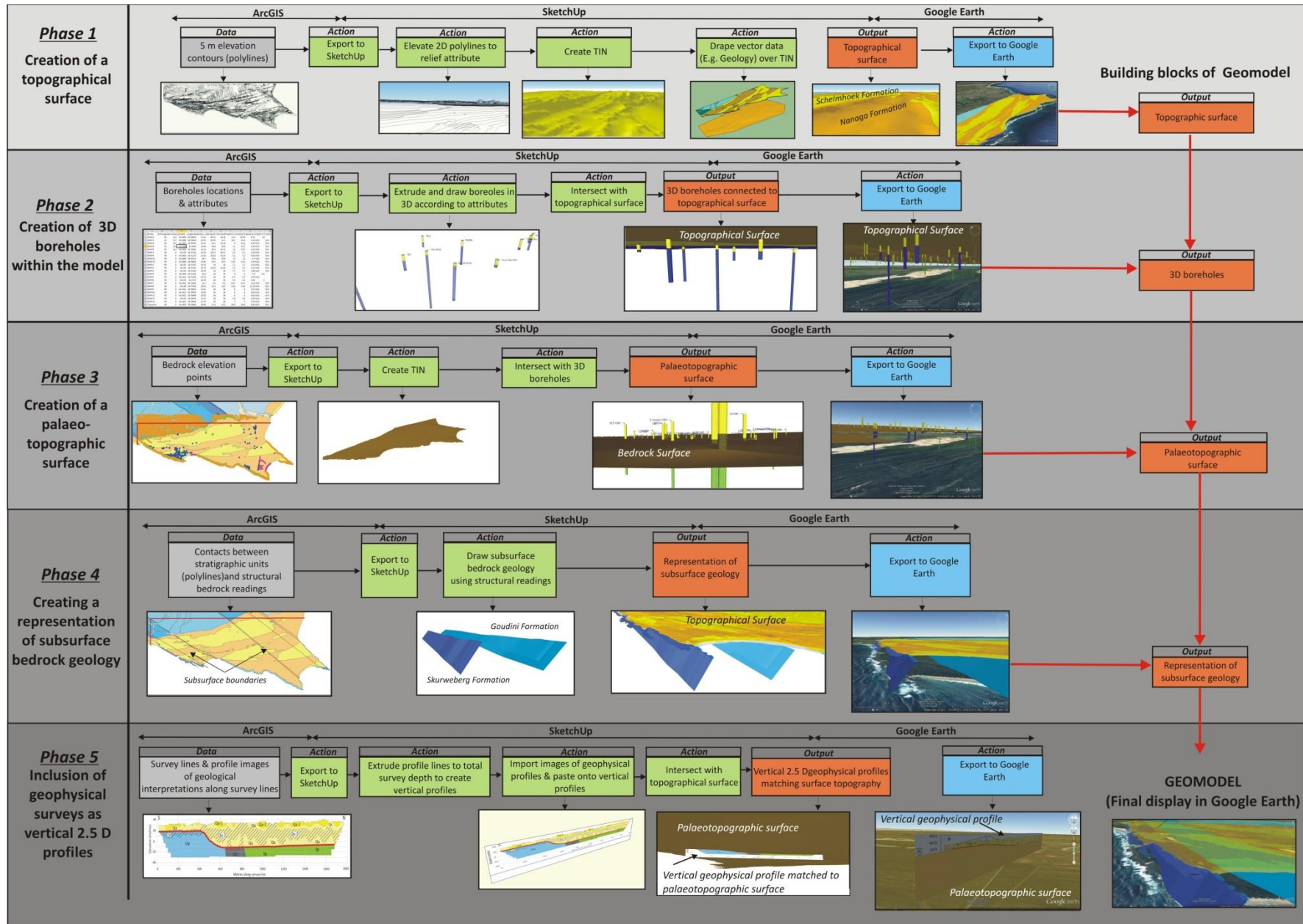
Figure 5.98: A flow chart indicating the data sources utilised and associated actions taken to produce resultant outputs at various stages in the construction of the Thyspunt geomodel.

• Dynamic landscape - The study area is situated in a dynamic landscape setting. The active Oyster Bay–St. Francis headland bypass dune field is continuously reshaping the topographical surface for the southern portions of the study area. It is therefore assumed that the 5 m contour dataset and the topographical surface created from it, are only correct for the year 2010 (the latest available and complete contour dataset that covers the study area in its entirety). Borehole elevations from especially older datasets (e.g. Ruabenheimer *et al*., 1988 a & b, Rosewarne & Lomberg, 1989) were slightly altered on a centimetre to meter scale to match the 2010 topographical surface. Slight variations in the surface relief also occur between the topographical surface and the relief expressed in geophysical profiles.

• Scales – The user should consider the scale at which cross sections and geophysical profiles were drawn at. To display geophysical surveys and geological sections as vertical 2D½ sections matching the actual size and scale appropriate to the model required slight stretching along the X, Y and Z axis of geophysical images. The model was constructed on a 1:1:1 scale (scaleX(1), scaleY(1), scaleZ(1)) with no vertical exaggeration. This was done to maintain an accurate depiction of fold structures in the substrate.

• The geomodel is elevated 315 m above the Google Earth surface, as Google Earth does not allow subsurface view.

• The model contains data sourced from previous authors and data garnered during this thesis. The study area's data can be viewed at 2D, 2½D (surface topography, palaeotopography and subsurface Palaeozoic bedrock contacts) and in the case of some datasets as 3D (borehole data) at full or reduced opacity (Figure 5.99 a-c). Data such as field photos, graphs and tables generated in § 5 (Results) can be viewed with the aid of pop-up windows (Figure 5.100 a - c). Cross sections and geophysical surveys can also be viewed using pop-up windows or as vertical 2D sections that are either clamped to the Google Earth surface or matched to the model's topographical or palaeotopographical surface. Legends are placed in the left and right hand corner and can be switched on or off as required.

5.6.2 Guidelines to model use

The following guidelines for viewing the Thyspunt Geomodel in Google Earth are recommended:

• Set Terrain, Elevation Exaggeration to 0.01 - Go to: Tools tab, select Options. From within the dialog window, select the 3D View and set the Elevation Exaggeration. Untick both 'Use high quality terrain' and 'Use 3D Imagery'.

• Ensure the Sidebar is active - Go to: View tab and ensure that the sidebar option is active.

• Switch all Google Earth vector data off under the 'Layers Panel'.

• If too much data is already stored in the 'My Places' folder under the 'Places' panel on the left hand side of the window view, the addition of large files .kml or .kmz files exceed Google Earth's display capacity and files will not completely load and thus not display. It's recommended to start with an empty 'My Places' folder.

• Allow enough time for files that contain a large amount of data (e.g. Geophysics) to completely load before attempting to view.

• Zoom out to the full extent of the study area when first loading data. Data will only load once full extent is in view, thereafter the user is able to zoom in and out to any desired scale.
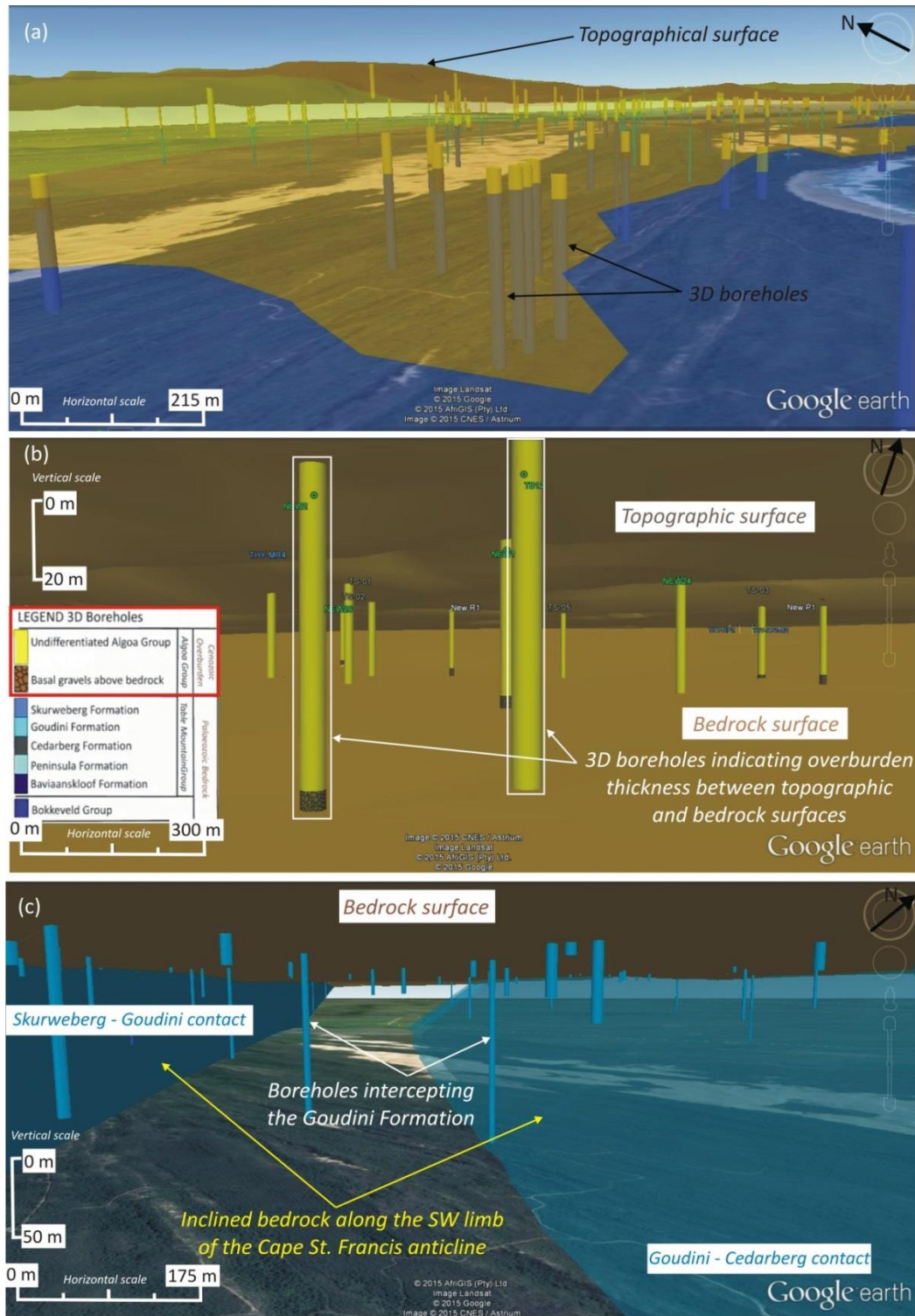
Figure 5.99: *Annotated Google Earth screenshots views depicting (a) the study area's topographic surface and boreholes drilled (3D), (b) observed overburden thickness in 3D boreholes between the topographic and palaeotopographic surface (c) inclined bedrock between stratigraphic units at Thyspunt along the SW limb of the Cape St. Francis anticline.*
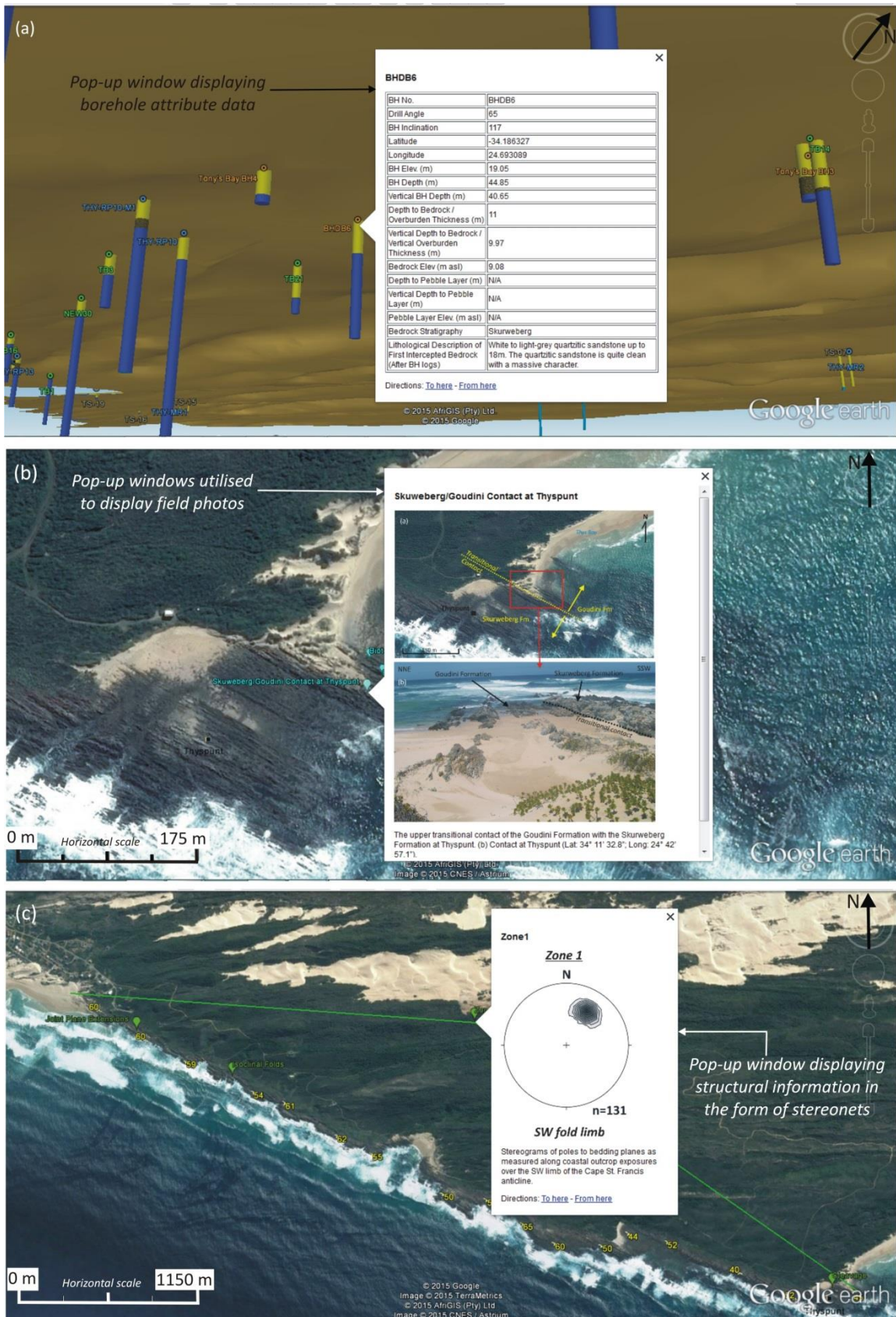
Figure 5.100: Annotated Google Earth screenshot views depicting (a) access to borehole attribute data (e.g. location, elevation, depth and bedrock geology) (b) field photos, (c) and structural data such as stereonets through pop-up windows.

5.6.3 Model visualisations

The geomodel assists in visualising the various datasets occurring in the study area (§ 4.5.2, Table 4.6). This section aims to show how the geomodel is able to visualise how overburden thickness is influenced by the study area's topographical surface relief (Figure 5.101 a), palaetopography (Figure 5.101 b) and Palaeozoic bedrock lithologies (Figure 5.101 c).
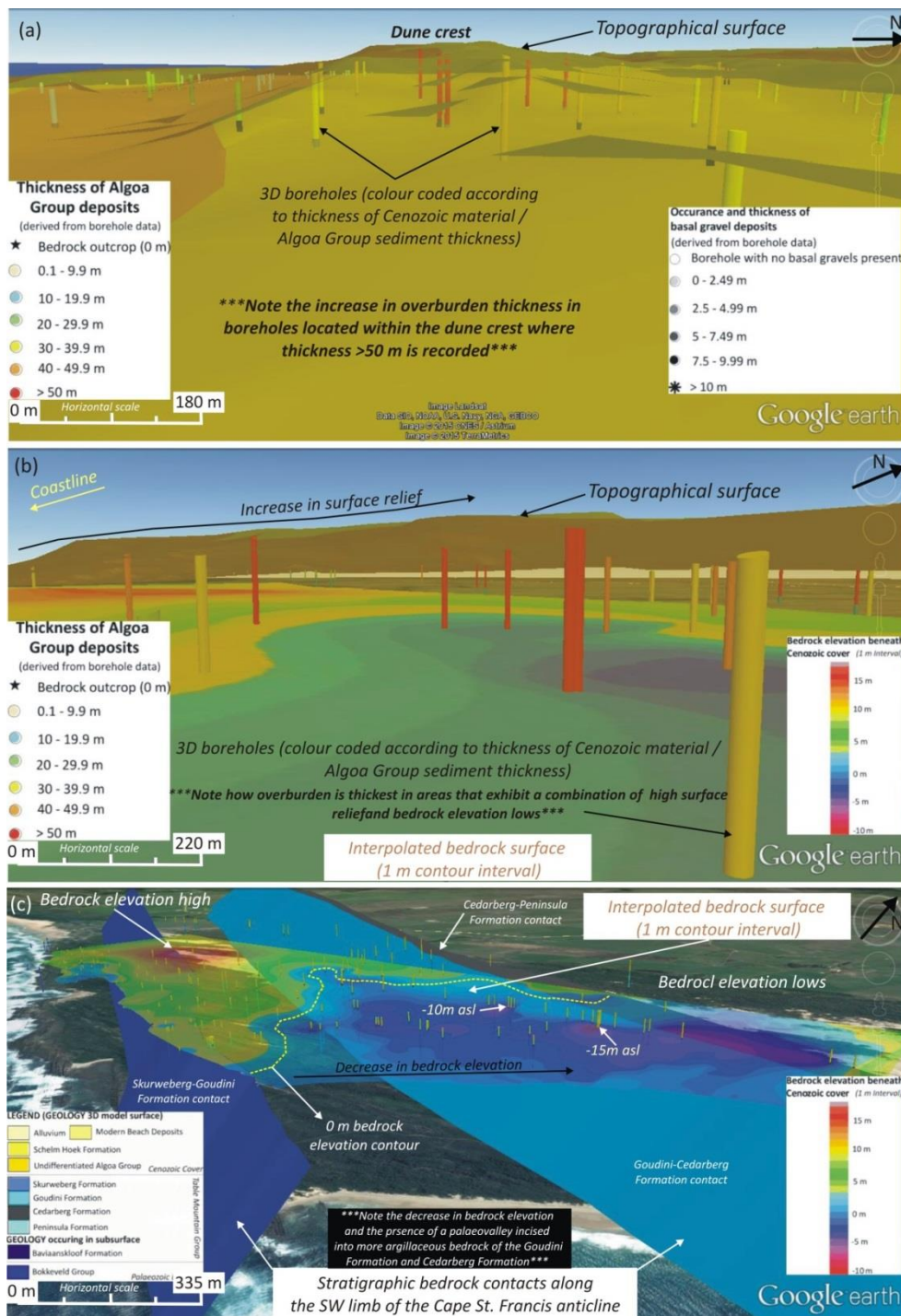
Figure 5.101: (a) Annotated Google Earth screenshot views depicting (a) that thicker overburden deposits (Algoa Group) are associated with higher surface relief (dune crests), (b) that peak overburden thickness of >50 m occurs in areas that exhibit both elevated surface relief (dune crests) and bedrock elevation lows (c) that lower bedrock elevations occur in bedrock of the Goudini and Cedarberg Formation.

Variations in the thickness of the Cenozoic Algoa Group relative to the distance from shoreline (towards the north) revealed by results in § 5.5.2 are depicted by the geomodel in Figure 5.102 a and b.
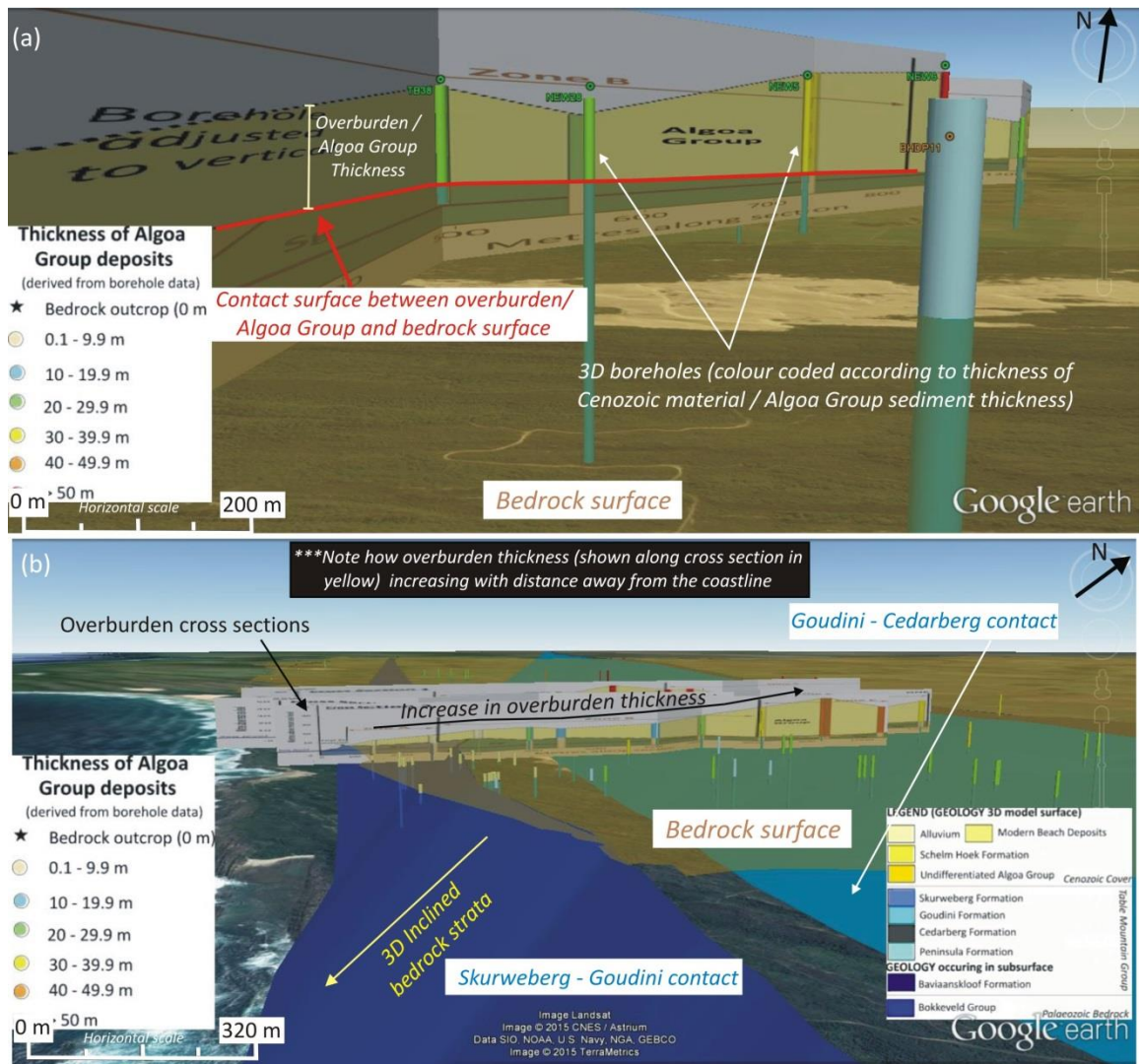
Figure 5.102: Annotated Google Earth screenshot views depicting (a & b) an increase in Cenozoic overburden / Algoa Group sediments with increasing distance away for the coastline.

Figures 5.103 a and b visualises the occurrence of palaeovalleys (marked by the decrease in bedrock elevation to below sea level) and how, for example at Cape St. Francis, they are incised into more incompetent lithologies of the Goudini and Cedarberg Formation.
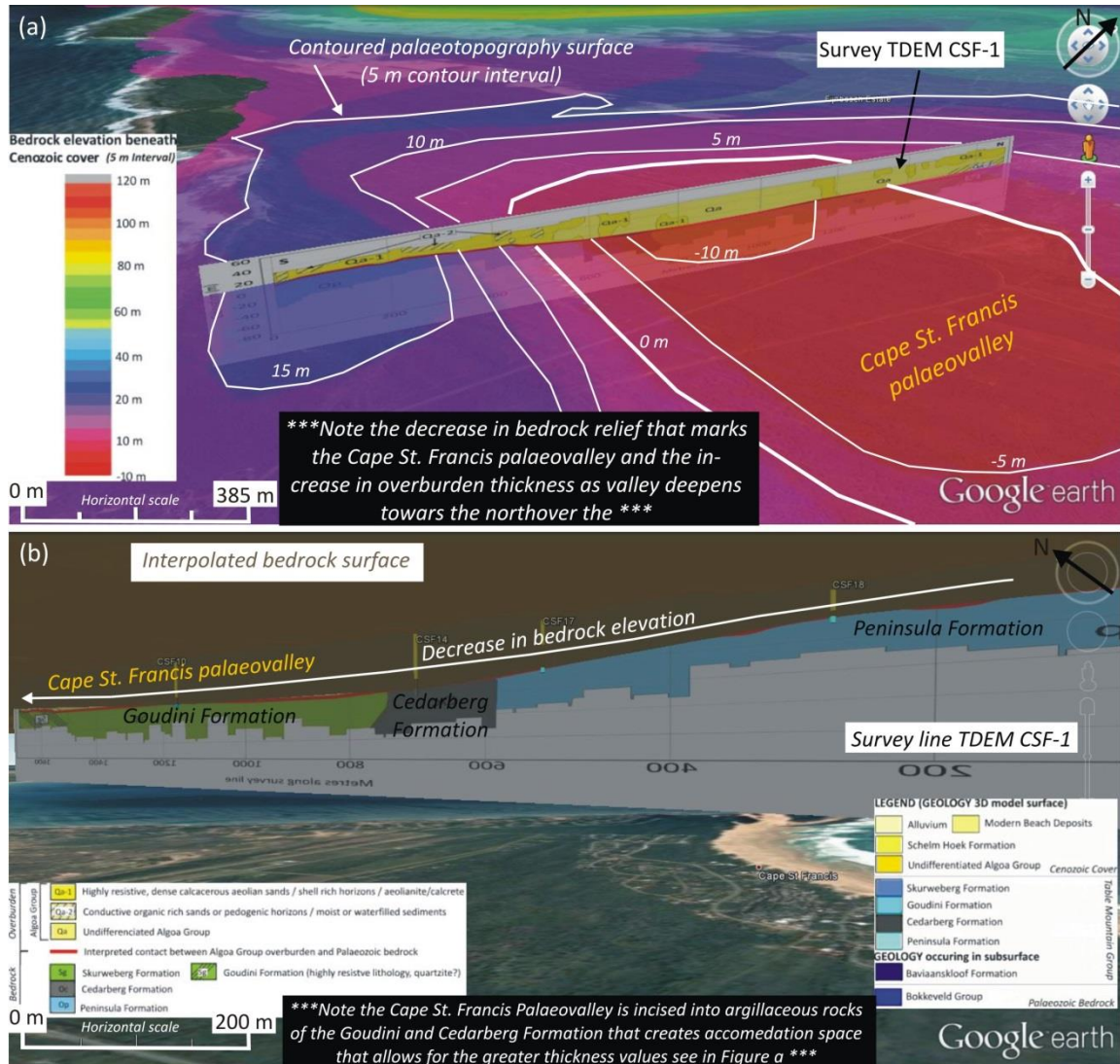
Figure 5.103: Annotated Google Earth screenshot views depicting (a) the survey line TDEM CSF-1 intersected with the interpolated bedrock surface (5 m interval) depicting the decrease in bedrock elevation that marks the Cape St. Francis palaeovalley, (b) the Cape St. Francis palaeovalley incised into argillaceous rocks of the Cedarberg and Goudini Formation.

6. Summary and discussion

This summary and discussion on the geoscientific characteristics of the Palaeozoic bedrock (§ 6.1), Cenozoic overburden (Algoa Group) (§ 6.2) and geological structure (§ 6.3) of the study area are derived from field investigations (§ 5.1 & § 5.2), thin section analyses (§ 5.3), geological re-interpretation of multi-electrode and TDEM resistivity results (§ 5.4) and a holistic review of borehole data (§ 5.5); in combination with work undertaken by previous authors (§ 2 & 3). The potential influence these geological characteristics may bear on siting of the NPP location, its design and construction are then outlined in § 6.4 in the form of an initial geological risk analysis for the Thyspunt site.

6.1 Geoscientific characteristics of the Palaeozoic bedrock

This section provides a lithostratigraphic overview of the TMG and Bokkeveld Group and places specific focus on the delineation of stratigraphic contacts between; and topography of; the Palaeozoic bedrock beneath Cenozoic cover as these aspects will influence where the NPP foundings will be situated. Refer to Figure 6.1 a for revised bedrock contacts. Figure 6.1 b & Figure 6.1 c provide comparison between previously defined (Anderson *et al*., 1986; Van Wyk, 1986; Eskom, 2009) and now revised bedrock contacts.

6.1.1 Lithostratigraphy

Results confirm lithostratigraphic observations made by previous authors who studied the Palaeozoic Table Mountain (Peninsula, Cedarberg, Goudini, Skurweberg and Baviaanskloof Formations) and Bokkeveld Group within the Eastern and Western Cape (§ 2).

• Peninsula Formation

Outcrop of the >562 m thick (Goedhart *et al*., 2008) Peninsula Formation is contained within the crest of the main NW-SE trending, SE plunging Cape St. Francis anticline and is well exposed along the coastal margin between Thys Bay and Cape St. Francis. Thin section images and field investigation reveal the formation consists of compositionally supermature, medium to course grained (800-1200 μm), light grey (Figure 5.1 a & b) quartz arenite that can effectively be described as orthoquartzite (>99% quartz grains) (Figure 5.60). Quartz grains composing the orthoquartzite underwent lower grade greenschist metamorphism during the Cape Orogeny (Hälbich & Cornell, 1983). The recrystallisation of framework grains is typical of all samples collected in the study area. Sample D22 shows the outline of the original detrital framework grains remain preserved as fine dirt lines visible under plane polarised light (Figure 5.60 d). Well sorted subrounded to well rounded quartz grains are cemented by authigenic quartz (chemical compaction) that has formed outgrowths and overgrowths on the original sand grain (Figure 5.60 e), producing an interlocking crystalline granular grain texture that further lends to the strong (75.9 MPa) to extremely strong (279 MPa) rock strength results obtained by Engelsman & Constable, 2012.

The lithological competency of the Peninsula Formation produces elevated relief structures like ridges or linear hills within the surrounding landscape. Cross sections transecting interpolated palaeotopography

beneath overburden cover reveal similar elevated relief associated with the Peninsula Formation within the study (Figure 5.96; Figure 5.97 e & f).

The lithologically homogeneous formation is interbedded with very subordinate fine-grained dark grey to black carbonaceous shale (Figure 5.1 a & b). Thinly bedded shale horizons are generally less than <1.5 m in thickness (Figure 5.1 a & b), but reach a maximum documented thickness of 3 m in borehole data (Raubenheimer *et al.*, 1988) near Seal Point and De Hoek located roughly 7 km from the Thyspunt site. Orthoquarzites are well bedded and bedding layers are generally medium to very thickly bedded.

Limited outcrop exposure in a region predominantly blanketed by Cenozoic overburden prevented delineation of the formation's upper contact with the Cedarberg Formation over much of the study area. However, TDEM and multi-electrode resistivity methods proved especially useful in identifying the contact between the Cedarberg and Peninsula Formation in suboutcrop. The highly conductive signal of the argillaceous Cedarberg Formation shale (20-100 Ohm.m) against the arenaceous highly resistive (50-4200 Ohm.m) Peninsula Formation makes for a relatively easily detectable resistivity contrast and contact identification.

At Cape St. Francis the contact between the Peninsula Formation sandstone and the Cedarberg shale is identified along multi-electrode resistivity lines CSF1, CSF5 and TDEM survey CSF TDEM in conjunction with previous TDEM results derived from Traverse CSF (Figure 3.10) situated further south (Stettler *et al.*, (2008). Towards the south, immediately north of the Cape St. Francis Village, extrapolation between these survey lines reveals the contact to continue without deviation along the area's NW-SE bedding strike (Figure 6.1 a). Farther north, along strike, the contact is interpreted by Anderson *et al.*, (1986 b) and Van Wyk, (1987) as being offset by inferred fault AEC DH1. Lack of evidence for this fault (see § 6.3.3) now means the contact continues without displacement to match with its mapped hinterland location. The contact is defined 250-800 m SW from where it was originally interpreted at Cape St. Francis.

The greater availability of data has facilitated a more precise delineation of the contact along the NE fold limb compared to initial attempts basing definition of lithostratigraphic contacts solely on a medium-sensitivity aeromagnetic survey (Figure 3.4 & Figure 6.1 c). It should be noted that Eskom (2009) made no attempt to define a Peninsula / Cedarberg contact at Thyspunt or Cape St. Francis (Figure 3.1 & Figure 6.1 b).
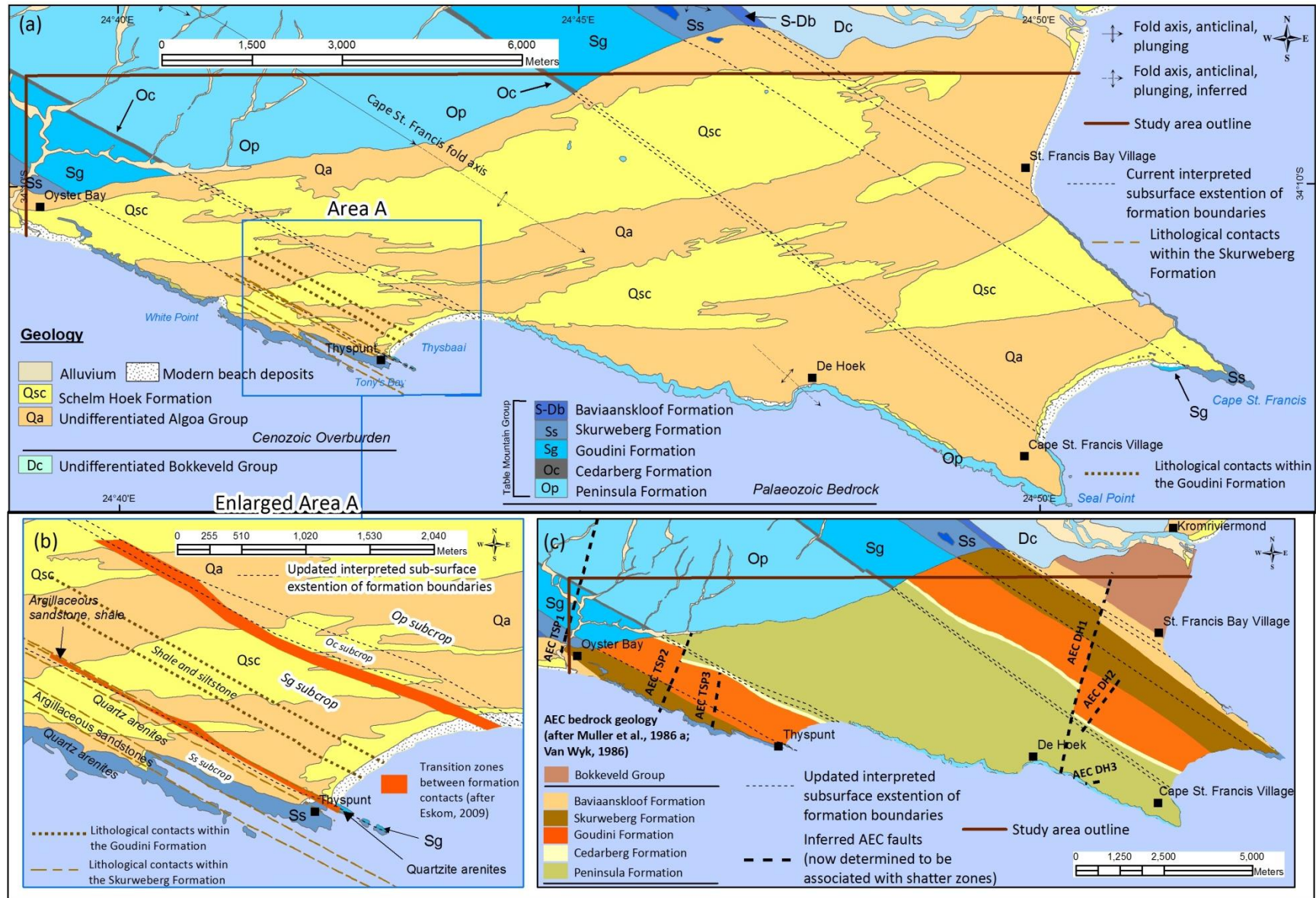
Figure 6.1: (a) Revised contacts between Palaeozoic lithostratigraphic units underlying Cenozoic cover within the study area. (b) An enlarged view of updated Palaeozoic lithostratigraphic contacts beneath Cenozoic cover at Thyspunt in comparison with initial contacts demarcated by Eskom (2009) (c) Revised Palaeozoic lithostratigraphic contacts at Thyspunt in comparison with initial contacts across the entire study area demarcated by Anderson et al., (1986) and Van Wyk, (1986).

At Thyspunt, extrapolation of the inferred hinterland contact (north of Cenozoic cover sediments) along strike to align with the interpreted contact determined from the holistic review of borehole data (Figure 5.82 & Figure 5.83), and results obtained by Stettler *et al*., (2008) along TDEM Traverse T (Figure 3.9 a & b) enables more precise delineation of the contact between the Peninsula and Cedarberg Formation beneath overburden cover (Figure 6.1 a & c). The contact is here defined 250 m NE from where it was originally interpreted to occur at Thyspunt by Eskom (2009). Close to the northern outcrop extent of the Algoa Group, a small right-lateral off-set of the Cedarberg Formation is indicated by inferred fault AEC TSP2 (Figure 3.1 & Figure 6.1 c). A similar fault was not identified by recent aeromagnetics (Cole & Naude, 2007). If interpretations by Cole & Naude (2007) holds true the contact continues uninterrupted along its NW-SE strike in line with the mapped hinterland contact.

• Cedarberg Formation

The rarely exposed ~62 m thin (Goedhart *et al*., 2008) laterally persistent Ordovician Cedarberg Formation comprises very dark grey, fine-grained carbonaceous shale containing infrequent thin bedded siltstone (Figure 5.6 & Figure 5.7). Differentiation between the basal Soom comprising dark grey shale and upper Disa Member (pale coloured shale and siltstone) are hindered by limited outcrop exposure. The argillaceous formation's mineralogy and very weak (1.49 MPa) to weak (7.61 MPa) rock strengths (Engelsman & Constable, 2012) facilitate weathering processes, producing long linear NW-SE landscape depressions adjacent to elevated quarzitic ridges of the Peninsula Formation (Figure 5.7) as evidenced by field mapping and cross section transecting palaeotopography bedrock beneath overburden sediments that show the development of palaeovalleys (Figure 5.97 e).

At Thyspunt a holistic review of various borehole datasets (Figure 5.82) and subsequent reassignment of one borehole's bedrock stratigraphy (borehole TS22) (Table 4.5) confirm the formation's presence below Cenozoic cover in 5 boreholes (TS22, New G1, New M1, New Q1 and New U1) at Thyspunt. These findings in combination with TDEM results (Stettler *et al*., 2008) along Traverse T (Figure 3.9 a & b) (that were omitted or not available to Eskom (2009) in determining the lithostratigraphic contacts) allow the suboutcrop extent of the Cedarberg Formation to now be more accurately demarcated (Figure 6.1 a & b). Along the SW limb of the regional anticline, the Cedarberg Formation's interpreted suboutcrop shows a slightly wider extent from ~150 m along the eastern portion of Thys Bay to ~220 m between 700 – 2000 m inland along its NW bedding strike (Figure 6.1 a & b). The wider suboutcrop extent may be attributed to a slightly shallower bedding dip or a localized thickening of the formation. Alternatively a small right-lateral fault similar to the one identified by Raath & Cole, (2007) north of Oyster Bay (§ 3.4; Figure 3.7) also displacing the Cedarberg Formation could be present. However this is just speculation. Additional investigation is required to confirm this. The Cedarberg Formation's suboutcrop extent is interpreted to occur slightly more towards the NE compared to initial determinations by Anderson *et al*., (1986b), Van Wyk (1987) and Eskom, (2009) (Figure 6.1 a, b & c).

At Cape St. Francis the formation's suboutcrop (Figure 5.1) is determined by borehole CSF14 and geological reinterpretation of multi-electrode resistivity surveys CSF1 (Figure 5.71), CSF5 (Figure 5.79),

TDEM survey line TDEM-CSF1 (Figure 5.81) and inclusion of results previously obtained along TDEM traverse CSF by Stettler *et al*., (2008) (Figure 3.10 a & b). Although the suboutcrop extent or width is consistent with interpretations by Anderson *et al*., (1986 b), the formation is now determined as occurring up to 500 m farther towards the SE (Figure 6.1 a & c).

• Goudini Formation

Strata of the Goudini Formation represent the main suboutcrop directly north of Thyspunt (Figure 5.82). Field investigation and borehole data show the formation is composed of fine to medium-grained and medium to thick bedded arenites (Figure 5.9) interbedded with subordinate very light grey to dark grey, often micaceous shale (Figure 5.10 b) and very dark grey bioturbated siltstones (Figure 5.11 a). Borehole data reveal the presence of a shale and siltstone unit within the Goudini Formation with an areal extent of ~220 m occurs roughly half way through the Formation (Figure 5.82).

Thin section images show sandstones of the Goudini Formation can be classified as fine to medium-grained (200-500 µm), well sorted (Figure 5.61 a), compositionally and texturally mature quartz arenites (90-95% quartz grains) with a higher clay (>5% mica flakes) content than sandstones of the Peninsula Formation. Framework grains exhibit an interlocking texture where framework grain boundaries are in contact with each other. Crushed quartz grains produce a mylonitic texture indicative of dynamic recrystalisation during the Cape Orogeny. Medium to thick bedded arenites are commonly cross bedded (Figure 5.9) while fine-grained arenites generally appear massive with no discernible sedimentary structure.

The subordinate shale and fine-grained argillaceous sandstones (grey-wacke) make the formation more susceptible to weathering generally producing lower landscape relief. East of Humansdorp more competent medium-grained arenites within the Goudini Formation can however produce elevated landscape relief. Cross sections at Thyspunt and Cape St. Francis (Figure 4.97 c & d) transecting interpolated palaeotopograhy (Figure 5.95 & Figure 5.96) reveal the formation is associated with the development of palaeovalleys that exhibit bedrock elevations below present day sea-level (Figure 5.95 & Figure 5.96). The formation's heterogeneous lithology also accounts for the range of rock strengths varying from very weak (1.35 MPa) to very strong (350 MPa) (Constable & Engelsman, 2012).

Lack of outcrop exposure and extensive Cenozoic cover hinders direct field identification of the formation's upper contact with the Cedarberg Formation in the southern portion of the study area. However, geological re-interpretation of geophysics and a review of borehole stratigraphy at Thyspunt and Cape St. Francis enable demarcation of the formation's upper contact in suboutcrop. At Cape St. Francis geological reinterpretation of results obtained from multi-electrode surveys CSF1 (Figure 5.71), CSF5 (Figure 5.79); and survey TDEM-CSF1 (Figure 5.81) identify the contact occurring between a broad zone of slightly more resistive lithologies (100-3000 Ohm.m) (Goudini Formation) and a zone of more conductive (20-100 Ohm.m) and thin (<200 m) lithology, interpreted to represent the Cedarberg shale. Boreholes CSF14 and CSF10 confirm geological interpretations of these resistivity values. Results from TDEM survey CSF conducted along the bay north of Seal point (Stettler *et al*., (2008), were unable to

clearly delineate the contact between the Goudini and Cedarberg Formation, depicting only a postulated upper contact for the Cedarberg. The formation is bordered by a zone Stettler *et al.,* (2008) interpreted as a 240 m wide zone of fault mélange. An anomaly identified at 450 m along the survey line possibly within the Goudini Formation, is interpreted to be the CSF fault inclined at approximately 60–70° SW (Figure 3.9). Stettler *et al* (2008) considered an alternative geological interpretation to the TDEM results. The alternative geological model suggests a duplication of the Cedarberg Formation along the bay due to steep anticlinal folding (Figure 3.10). This interpretation eliminates the postulated onland extension of the Cape St. Francis fault and associated zone of fault mélange. However, if the alternative model is accepted it means steep folding does not extend north or south of multi-resistivity survey line CSF1, CSF5 and TDEM-CSF1 because duplication of a similar conductive zone matching the Cedarberg Formation is not found to occur along these surveys. Consequently the Goudini Formation's upper contact is defined 300 m SW of its original location (Anderson *et al.*, 1986; Van Wyk, 1987) near Cape St. Francis Village (Figure 6.1 c). Re-interpretation of results obtained from surveys CSF1 and TDEM-CSF1, also shows the NW-SE trending updated contact to be situated 200 m farther SW in the area where surveys were conducted (Figure 6.1 a & c).

The contact between the Cedarberg and Goudini Formation at Cape St. Francis is interpreted by Anderson *et al.*, (1986) as offset by inferred fault AEC DH1. Lack of evidence for this fault (see § 6.3.3) now means the contact continues without displacement 500 m farther SW to match with its mapped hinterland location.

At Thyspunt along the SW limb of the Cape St. Francis anticline, the formation's upper contact with the Cedarberg Formation (Figure 6.1) is defined by a review of bedrock stratigraphy denoted in boreholes (Table 4.5; Figure 5.82), results obtained along TDEM traverse T (Stettler *et al.*, 2008) (Figure 3.8 a & b) and extrapolation of coastal contacts along strike to match inferred hinterland contacts. Results obtained and interpretations made in this dissertation are combined with data sources omitted by Eskom (2009) to determine a revised contact, and not just a zone of transition between the Cedarberg and Goudini Formations as shown by Eskom (2009) (Figure 6.1 a, b & c). Although the contact occurs close to the transition zone identified by Eskom (2009), the updated contact is interpreted as occurring a farther ~100 m NE (Figure 6.1 a & b).

• Skurweberg Formation

Thyspunt is predominately underlain by arenaceous bedrock of the Skurweberg Formation. Mapping of coastal exposures between Oyster Bay and Thyspunt, thin section analysis and a universal review of borehole data show the formation is composed of white to light grey, well sorted, medium to coarse-grained (400-800 μm), textually and supermature quartz arenite (>95% quartz grains) with very minor interstitial clay (2%) (Figure 5.12 & Figure 5.61 a) similar to quartz arenites of the Peninsula Formation (Figure 5.61 a). Thin section images show recrystallized quartz grains in a tightly interlocking texture adding in the formation's overall very strong (117 MPa) to extremely strong (160 MPa) rock strength averages (Eskom, 2009; Engelsman & Constable, 2012).

Medium to thickly bedded quartz arenites are interbedded with subordinate greyish green to medium grey shale, <10 m thick grey-wacke units (Figure 5.13 a & b) and medium grey siltstones. Borehole data Raubenheimer et al., 1988 a & b) also indicate the presence of sporadic <1 m thick conglomerate stringers with pebble size clasts close to the coastal margin at Thyspunt and Tony's Bay. Petrographic light microscopy of argillaceous sandstone sampled east of Oyster Bay reveals a moderately to poorly sorted lithology comprised of recrystallized fine to medium-grained monocrystalline quartz grains (75-80%) set in a fine-grained detrital clay matrix (20-25%) (Figure 5.63 a). Argillaceous sandstones can be classified as immature quartz wackys based on a >15% matrix and >95% quartz grain framework. The occurrence of lithologically less competent grey-wacke and shale units form favourable erosion zones, producing bedding parallel gullies west of Oyster Bay (Figure 5.13 a & b). The occurrence of thinly bedded, highly cleaved medium grey shales interbedded with grey-wacke or argillaceous sandstones and siltstones is also responsible for the development of the NW-SE trending linear embayment at Tony's Bay (§ 5.4.1.1 (i)).

Close to the formation's upper contact with the Skurweberg Formation, the number of argillaceous sandstones/grey-wacke and shale units increases with shale beds appearing darker and more carbonaceous (Raubenheimer et al., 1988 a; Raubenheimer et. al., 1988 b). Borehole data (Raubenheimer et. al., 1988 b; Eskom, 2010 a, Eskom, 2010, b) also indicates an increase in the occurrence of red iron rich shale units. These iron rich shales occur as lenses, stringers or medium thick beds and are predominantly observed NW of Tony's Bay in boreholes TB16 (Figure 5.16), NEW30, NEW29 and BHDH2.

The formation's lower contact with the Goudini Formation is defined as the base of the first quartzitic sandstone unit that indicates a recognisable change in the depositional setting (SACS, 1980; Theron et al., 1989). Goedhart et al (2008) interpreted this change as being represented by a 13.5 m thick, massive quartzitic sandstone unit that marks the 'first major influx of sand' in the depositional environment (Figure 3.1 a & b). Field investigation at Thyspunt where a 50 wide and 200 m long exposure of Goudini formation outcrop remains uneroded confirms these interpretations (Figure 5.8 a & b). The contact is however transitional over 25 m. If the observed contact is extrapolated along its NW-SE strike in line with the inferred contact derived from borehole data (Figure 5.82), no displacement of the contact near Thyspunt is observed. Comparison of the contact's current location is consistent with the transitional contact location determined by Eskom, (2009) (Figure 6.1 b)

The Skurweberg Formation's lower contact with the Goudini Formation along the regional anticline's NE limb near Cape St. Francis Village is determined by extrapolating the mapped contact along coastal outcrop exposure (Figure 5.8 a) to align with the inferred contact derived from borehole data (Figure 5.84) and the inferred hinterland contact mapped by Goedhart et al., (2008). Towards the south the current contact is situated ~500 m SW from where it was originally interpreted to occur (Muller et al., 1986; Anderson et al., 1986 b; Van Wyk, 1987). As noted previously, lack of evidence for this fault (see § 6.3.3) now means the contact continues without displacement 500 m farther SW to match with its mapped hinterland location.

• Baviaanskloof Formation

The Baviaanskloof Formation is not exposed within the study area. Suboutcrop of the formation beneath overburden sediments of the Algoa Group along the northeastern limb of the Cape St. Francis anticline, is confirmed west and NW of the Cape St. Francis Bay Village by boreholes SRK-9 and SRK-15 (Maclear, 2005 & 2006) (Figure 5.84). Limited outcrop exposure in the immediate surroundings north and NE of Humansdorp reveals the formation is comprised of light grey to dark grey immature fine and coarse-grained sandstone (Figure 5.17), mature feldspathic sandstone , mudrock units usually <1 m thick and lenticular-bedded siltstone (Figure 5.20). Thin section analysis of a sandstone sample near the middle of the formation, possibly associated with the Kareedouw Member, ~5 km west of Jeffreys Bay, is classified as a well sorted, and medium-grained, compositionally mature quartz arenite (Figure 5.64 a-d).

Although the formation's upper and lower contacts were not directly observed within the study area (blanketed by Cenozoic cover) and immediate surroundings (lack of outcrop exposure), Hill, (1991) described the formation's lower contact with the Skurweberg Formation as gradational, while the upper contact with the Bokkeveld Group is conformable. Borehole data and the extrapolation along strike of inferred hinterland contacts to match last outcrop exposures of the Skurweberg Formation mapped during field investigation, show the formation's lower contact in suboutcrop as interpreted to occur 200 - 450 m NE from where it was originally interpreted to be by Anderson *et al*., (1986 b) (Figure 6.1 a & c).

• Bokkeveld Group *(Undifferentiated)*

Strata of the Devonian Bokkeveld Group are not exposed within the study area. Boreholes (Maclear; 2002; Maclear, 2005; Maclear, 2006) confirm the Group suboutcrops beneath overburden cover ~9.5 km NE of Thyspunt. The predominantly incompetent argillaceous lithologies comprising the Bokkeveld Group erode easily and produce low topographic relief with very limited outcrop exposure that does not allow for differentiation to formation level. Field investigation of limited exposures in road cuttings along the R330 (road between Humansdorp and Cape St. Francis), 7 km outside the study area together with thin section analysis, show the strata composed of medium dark grey to dark grey, fine-grained (<250 μm) carbonaceous shale and fine-grained light olive brown, yellowish grey and very light grey sandstone. The sporadic occurrence of elongated and oval sandstone lenses 4-10 cm in width and <1.5 m in length occur occasionally. Petrographic light microscopy reveals the presence of authogenic glauconite in shales of the Bokkeveld Group. The contact between the strata of the Baviaanskloof Formation and Bokkeveld Group's beneath Cenozoic overburden (Figure 6.1 a & c) is determined from the extrapolation of mapped hinterland exposures along strike to align with borehole data.

6.1.2 Palaeotopography

The interpolated Palaeozoic topographic surfaces at Thyspunt (1 m contour interval) (Figure 5.96) and across the entire study area (5 m contour interval), reveal an antecedent landscape that has undergone weathering sufficient enough to erode bedrock to elevations well below present day sea-level at Thyspunt (-15.5 m asl), Tony's Bay (-1.129 m asl), Cape St. Francis (-11.52 m asl) and north of St. Francis (interpolated -10 m asl). Although previous authors (Eskom, 2009; Hanson *et al.*, 2012), eluded to the occurrence of topographical depressions cut into Palaeozoic bedrock, interpolation results (Figure 5.96) and cross sections traversing palaeotopography perpendicular and oblique to the NW-SE trending long axes of palaeovalleys (Figure 5.98 a - f) enable for the first time characterisation of the size, shape and overall depth profile of these NW-SE trending palaeovalleys (§ 5.5.3). Cross sections (Figure 5.98 a - f) reveal palaeovalley development is linked to the lithological competency of the underlying bedrock and the process of differential weathering. Comparably less competent lithologies predominantly comprising the Goudini and Cedarberg Formations as well as the Bokkeveld Group are more susceptible to erosion resulting in the development of bedrock depressions. More competent arenaceous formations of the Peninsula and Skurweberg Formations tend to produce elevated topography within the palaeolandscape. The process of differential weathering must have already started in the ancedent landscape prior to deposition of the Cenozoic deposition, however near shore deepening, shaping and subsequent infill of palaeovalleys are likely associated with factors such as climate changes, involving change in sea level and variation in sediment discharge, and/or tectonic and isostatic processes that may have modified coastal gradients (Roberts et al., 2006) Palaeovalleys likely underwent some incision during the last glacial when sea level was much lower than present and subsequently filled with sediment reworked by the following Pleistocene to Holocene sea-level highstands.

6.2 Geoscientific characteristics of the Cenozoic cover

This section provides a summary of Cenozoic lithostratigraphy based on results obtained during field investigations (§ 5.1.3), re-interpretation of geophysical surveys, (§ 5.4) and the holistic review of borehole data (§ 5.5.2 & 5.5.3). Discussions predominantly focus on defining the geological and geographical controls that possibly bear influence on the thickness distribution of the Cenozoic cover defined in § 5.5.2. Understanding thickness distribution is important as construction of the NPP will be done on bedrock requiring major excavation of cover deposits (Eskom, 2009).

6.2.1 Lithostratigraphy of the Algoa Group (undifferentiated)

Field descriptions of the Cenozoic overburden confirm observations made by previous authors who mapped the Algoa Group within the Eastern Cape (§ 2.5.1). Differentiation to formation level and correlation between stratigraphic units of the Algoa Group within the study area is hindered by limited outcrop exposure and inadequate borehole log descriptions. Therefore within the study area, the Algoa Group is mainly described as undifferentiated.

Overburden material lithostratigraphically associated with the Algoa Group comprises predominantly unconsolidated, clastic, nearshore-marine and coastal aeolian-derived sediments (Roberts *et al.*, 2006).

These mainly aeolian deposits form part of the Oyster Bay–St. Francis bypass dune field and reflect a passive coastal margin that underwent a series of glacio-eustatic marine transgressions and regressions superimposed on uplift and seaward tilting of the subcontinent during the Cenozoic Era (Roberts *et al.*, 2006). Cover deposits are interbedded with sporadically occurring thin, dark brown, dark grey and black organic rich relict pedogenic or palaeosoil horizons. Palaeosoils are generally <3 m in thickness occurring at various elevations throughout the Algoa Group (Figure 5.24 a & b). Palaeozoic horizons are frequently semiconsolidated. White to pale grey pedocretes or calcretes layers of <10 m occur occasionally at various depths throughout the Algoa Group. Pedocretes are comprised of fine-grained sand generally well cemented in a calcium rich supported matrix and range from brittle in nature, often containing sporadic small (1 mm – 20 mm) cavities to well cemented hardpan calcrete layers with no cavities (Figure 5.25 a & b).

Borehole data show the contact between Algoa Group sediments and underlying Palaeozoic bedrock as unconformable and as often characterized by a sporadic, laterally non-persistent gravel layer of marine or fluvial origin stratigraphically correlative with either the basal unit of the Alexandria Formation or the Salnova Formation. The basal gravel unit comprises imbricated, disc- to roller-shaped clasts of pebble to cobble size set in a fine- to medium-grained sandy matrix, frequently containing shell material (Figure 5.23 & Figure 5.28). Gravel units deposited on wave cut platforms below ~18m amsl are generally stratigraphically associated with the Salnova Formation (Figure 5.23), while gravels units above ~18m amsl are more closely related to younger deposits of the Alexandria Formation (Le Roux, 1989; Smuts, 1987).

A holistic review of borehole data shows the typical thickness for basal gravels range between 0.5 - 5 m, with occasional 5–10 m thicknesses. The thickest gravel layer recorded within the study area is 19 m thick at Cape St. Francis, where gravels are underlain by Peninsula Formation (Figure 5.94). The maximum thickness of basal gravels recorded at Thyspunt is 11.5 m, approximately 1.5 km NW of Tony's Bay, where gravels are underlain by Goudini Formation bedrock.

Groundwater movement occurs at the contact between overlying highly permeable Cenozoic sediments and relatively less permeable Palaeozoic bedrock. Consequently numerous springs occur along coastal exposures (Figure 5.26 a & b).

6.2.2 Overburden thickness distribution

Results indicate a clear trend in thickness distribution for the Algoa Group sediments between Oyster Bay and St. Francis (Figure 5.85, Figure 5.86 b, Figure, 5.87 b and Figure 5.88 b). Thickness trends are observed in what appears to be a coast-parallel trending zonation. Two initial zones; zone A and B, characterized by a general trend of increasing thickness with increasing distance from coastal margins occur in the first few hundred metres. Zone A, the zone closest to the coastal margin records the lowest sediment thickness. Further inland zone C, a zone of peak thickness values occurs in areas where sediment is underlain by incompetent, argillaceous lithologies of the Goudini and Cedarberg Formation, only to peter out to a zone of lower thickness values near northern outcrop boundaries (Figure 5.85).

Between Oyster Bay and St. Francis results indicate that the distribution of thickness values for the Algoa Group is influenced or controlled by a combination of the following geological and geographical factors:

•Bedrock lithology and bedrock elevation

The prominent headlands and embayments that make up the coastline morphology of the study area are in part the consequence of variation in the competency of lithological units that comprise the bedrock geology and the process of differential weathering. The prominent headlands at Seal Point, Cape St. Francis, Thyspunt and the surrounding NW-SE trending straight and rocky coastlines are constructed of the lithologically competent quartzitic bedrock units of the Skurweberg and Peninsula Formations. In contrast the Thys Bay embayment is underlain by lithological incompetent of thinly bedded sandstones, shales, and mudstones that comprise the Goudini and Cedarberg Formations. North of St. Francis, the coastline exhibits a SW-NE trending, SE facing undulating coastal embayment underlain by the lithologically incompetent argillaceous units of the Bokkeveld Group and Baviaanskloof Formation. Erosion of incompetent fine-grained, bioturbated sandstone unit within the Skurweberg Formation west of Thyspunt led to the development of an elongated NW-SE trending embayment known as Tony's Bay. This variation in the competency of bedrock lithologies and the processes of differential weathering that appears to have led to the formation of alternating headlands and embayments along the present day coastline, would likely also have been active in an ancedent landscape prior to the deposition of the Algoa Group. Differential weathering would have produced an uneven palaeolandscape relief with topographic highs and depressions allowing for variation in the way the accretion of sediments took place. Topographic highs would facilitate a lower accretion of sediments than surrounding topographic lows.

At Thyspunt thicker Algoa Group deposits (including thicker basal gravels) are more frequently underlain by incompetent lithologies of the Goudini and Cedarberg Formation (Figure 5.89, Figure 5.92 and Figure 4.94). Cenozoic deposits underlain by these formations (associated with northern regions of zones B and zone C) are generally 20 m to 60 m in thickness (Figure 5.85 b). Thinner Cenozoic deposits (<20 m) identified within zones A and D, reflect regions within the study area where Cenozoic deposits are underlain by relatively elevated bedrock relief, associated with the more erosion resistant Peninsula and Skurweberg Formations (Figure 5.85 & Figure 5.94).

Within the area occupied by zone C, where peak thickness values are observed, bedrock elevations are often below sea level (Figure 5.86 a and Figure 5.90 a, b and c). NW of Thys Bay, borehole bedrock elevations of -6 m to -15 m asl is documented and associated with the Thyspunt palaeovalley (Figure 5.96).

The presence of a comparable inland palaeovalley, striking NW-SE, near Cape St. Francis, is based on an abrupt fall in bedrock elevations to -11.52 m and -9.44 m asl (Figure 5.92 & Figure 5.98 e). Here too the presence of similar lithologically incompetent bedrock facilitated a greater degree of erosion than surrounding arenaceous bedrock within the palaeolandscape. At Cape St. Francis the peak accretion value (51 m) documented to occur in zone C (Figure 5.87 b), corresponds to the presence of the Cape St.

Francis palaeovalley cut into argillaceous bedrock. Although a steady rise in surface relief occurs transitioning from zone B to C, this represents only a small component of the overall thickness increase. Instead, it is the extreme decrease in bedrock elevation that appears to primarily facilitate these peak values (Figure 5.87 a and b). In areas like zone C where prominent bedrock lows occur with elevated surfaces (dune crests), greater accretion of Algoa Group sediments is present (Figure 5.90 a, b, c and Figure 5.92).

A greater accretion of basal gravels is also recognized within both of these palaeovalley areas (Figure 5.93 a & b). No direct correlation between the thickness of basal gravels and the bedrock elevation height upon which they were deposited were recognized.

Near St. Francis boreholes occupying incompetent bedrock of the argillaceous Bokkeveld Group, show lesser Algoa Group thicknesses than comparable less erosion resistant bedrock units of the Goudini and Cedarberg Formations at Thyspunt and Cape St. Francis (Figure 5.86 b, Figure 5.87 b and Figure 5.88 b). At St. Francis lower accretion values can be attributed to a complementary relationship between bedrock elevation and surface relief. A rise in borehole bedrock elevation is coupled by an increase in surface relief and vice versa (Figure 5.88 a).

Localised erosion pockets or bedrock peaks within the ancedent landscape, may be responsible locally for slightly thicker or thinner deposits within a particular thickness zone. This is the assumed case with Cenozoic thickness outliers documented in the study area (Figure 5.86 a & b and Figure 5.90 a, b & c). The development of these localized erosion pockets may be influenced by the presence of a slightly less erosion resistant unit within a particular formation. Such a less erosion resistant, fine-grained, bioturbated sandstone unit interbedded with shale and siltstone west of Thyspunt, facilitated the development of the elongated NW-SE trending embayment known as Tony's Bay. If this unit continues along its trend inland beneath Cenozoic cover, it explains the concentration of boreholes with thicker basal gravels in that area (Figure 5.93 a & Figure 5.94).

Another factor that may influence the development of bedrock lows, are zones of structural weakness. Shatter zones like those identified along coastal exposures (Figure 5.44 a – f & Figure 5.46 a - d) are locally more susceptible to erosion, possibly producing lower bedrock relief and ultimately facilitating greater sediment accretion. The location and extent of these shatter zones is however difficult to predict beneath Cenozoic cover.

• Surface relief and sediment supply

A steady progression of increasing surface elevation is observed from coastal margins into the interior (Figure 5.86 a, Figure 5.87 a and Figure 5.88 a). The portion of the study area blanketed by Cenozoic dune cover is characterized by undulating topography; a consequence of alternating E-W trending dune crests and troughs. Locally areas with higher elevation associated with dune crests facilitate greater accretion of sediments compared to surrounding areas where lower surface relief occur (such as dune depressions or troughs). The more dominant role surface relief plays in affecting accretion values is clearly observed at

Thyspunt. Here the transition from thicker accretion values (zone A to B) is facilitated mainly by a rise in surface relief and only a marginally lower bedrock elevation (Figure 5.86 a & b & Figure 5.90 a & b).

It appears unlikely that elevation can be the sole factor influencing accretion values.   At Thyspunt extreme thickness outliers occurring within zone B at approximately 550 and 640 m north of the coastline, mark the edge of the interpolated palaeovalley at Thyspunt incised into lithologically less erosion resistant Goudini Formation. The topographic depression within the palaeolandscape coupled with a more elevated surface relief may have stimulated greater accretion of sediments (Figure 5.86 a and b & Figure 5.90 a, b, c). Surface relief and distribution of dune heights are influenced by sand supply, wind regime and bedrock topography (Burkinshaw, 1998). Surface relief and dune heights show greater elevation towards the northwestern sections of the study area. This area is located close to the area's upwind sand supply source, e.g Slang Bay (Figure 1.8). An overall decrease in surface relief and dune heights is observed downwind, likely due to a lower rate of sand supply further east towards St. Francis (Burkinshaw, 1998). Locally sand supply is also influenced by the NW-SE trending Cape St. Francis anticline, the core of which produces a quartzitic (Peninsula Formation) bedrock ridge over much of the central portions of the study area (Figure 1.8). The ridge impedes sediment transfer to the east, and results in a concentration of dune mass in the northwestern areas along the western limb of the anticline where bedrock topography is lower. In addition the northeastern regions of the St. Francis area are located downwind of the west-east migrating dunefield, towards the distal end of the sediment source. At St. Francis the accretion of sediment is less compared to Thyspunt, which is located closer to its sediment source. Along the northern edge of the Algoa Group outcrop and along the eastern limb of the Cape St. Francis anticline; prevailing W-WSW winds have already exposed the Peninsula Formation in two localities (Figure 5.85).

Variation in sediment accretion is also influenced by factors such as sea level changes driven by climate changes, and/or tectonic and isostatic processes that may have modified coastal gradients and influenced the sediment discharge (Burkinshaw, 1998). Evidence for the marine isotope stage 11 highstand is observed at Mossel Bay (Roberts, 2006; Roberts *et al*. 2009; Jacobs & Roberts, 2009; Roberts *et al*; 2012) where Roberts *et al.* (2012) estimated eustatic sea level during marine isotope stage 11 to be at +13 ± 2 m above modern sea-level. The last intergacial sea-level associated with marine isotope stage 5e was most likely between 6 and 8.5 m above current sea-level (Carr *et al*., 2010). Substantial reworking of aeolianite and dune deposits occurred during the Holocene highstand, the last interglacial, and continues at present. This alludes to the combined role that sea-level change and bedrock topography can play in creating accommodation space for accretion. At Thyspunt, bedrock elevation typically ranges from 3-9 m above sea-level within zone A. The reduced thickness of sediments (3-12 m) within Zone A could partly be a function of the limited time available for sediment accretion since the last major highstand and/or the reduced likelihood of preservation throughout the majority of the Middle to late Pleistocene as a result of limited sediment supply. More detailed investigation, not part of the scope for this thesis, is required to define the role of sea-level change or tectonic uplift (despite its low rates), in accretion of sediments within these zones.

6.3 Structural characteristics of the Palaeozoic bedrock

The structural deformation of Palaeozoic rocks is predominantly attributed to the northward directed compressional forces from the south associated with the Permian-Triassic Cape orogeny (~245 and ~278 Ma) and the Mid to Late Mesozoic extensional forces associated with the break-up of southern Gondwana (180-170 Ma). Thick bedded competent arenaceous rocks associated with the Skurweberg and Peninsula Formations in the study area, have undergone predominantly brittle deformation. Lithologically less competent, more argillaceous sandstone, siltstone and shale units with a higher clay content generally exhibiting thinner bedding, underwent more ductile deformation as evidenced by field observations that show asymmetrical to tight isoclinal folds that are smaller in size and more closely spaced (Figure 5.41) and thin section analysis that show folded and bent mica flakes (Figure 5.63 d) exhibiting wavy extinction indicative of more plastic deformation (e.g. Vernon, 2004). Structural features (faults and joints) do not extend into younger cover deposits of the Algoa Group and are therefore older than 23 Ma years.

6.3.1 Bedding and folds

Structural analysis of the TMG confirms that NE-SW striking strata within the study area form part of the regional shallow SE plunging open Cape St. Francis anticlinorium that shares a sub-parallel orientation to other folds of the Cape Orogeny (Figure 2.9). The aniclinorium exhibits an interlimb angle of 89° (Figure 5.36) and steep SW dipping axial plane (214°/87°). The fold is therefore interpreted as verging slightly to the north. Although bedding measurements reflects a SE plunging fold axis (within the study area), Goedhart et al., (2008) also noted that the same Cape St. Francis anticline that extends past the Kareedouw area (farther NW outside the study area) also exhibits a NW plunge. Therefore the Cape St. Francis anticline may be described across its entirety as a doubly plunging fold. Bedding inclination is controlled by the distance away from the anticline's sub-horizontal fold axis (124°/3°) (Figure 5.36). Near De Hoek, the broad fold hinge area (Figure 5.36 & Figure 5.37 c, Zone 2) shows shallow bedding inclination, with dip values ranging from 5° - 20°. With increasing distance away from the fold axis, dip values show a steady increase to moderately steeper inclinations of 30° to 40° east and west of De Hoek. Towards Oyster Bay, bedding inclination reaches steep inclinations ranging between 50°- 65°. At Thyspunt, bedding remains relatively consistent at 210° / 50° (azimuth/dip) (Figure 5.37 a). Asymmetrical, parasitic, meso-scale folds on the NE and SW limbs of the Cape St. Francis anticlinorium gently plunge southeastward at shallow to moderate angles with axial planes dipping steeply SW. This type of north verging are characteristic of folds in the eastern portion of the CFB where the upper hinge area of folds is commonly dragged over in a northerly direction exhibiting SW dipping axial planes (Hälbich, 1983; Hälbich, 1992; De Beer, 1995). Coaxial folding is prevalent in the study area however fold axes of parasitic folds orientated oblique or perpendicular to the fold axis of the Cape St. Francis anticline (Figure 5.40) may indicate a secondary stress orientation oblique to the main palaeostress direction. Fold styles vary throughout the study area and include open to tight folds (Figure 5.39). Tight Isoclinal, overfolded and recumbent (Figure 5.38 b) folds indicate the increased intensity of deformation. The variety of fold styles, amplitude and wavelength of folds documented in the study area and in the CFB as a whole, are closely

associated with the competency contrasts and bedding thickness (Hälbich, 1983; De Beer, 1989; De Beer, 1990; De Beer, 1995; Tankard *et al*., 2012). More incompetent formations, such as the Cedarberg, Baviaanskloof Formations and Bokkeveld Group, are developed as asymmetrical to tight isoclinal folds that are smaller in size and more closely spaced (Figure 5.41), which in turn leads to substantial shortening. Competent, brittle units such as the Skurweberg and Peninsula Formations are more likely to produce larger scale broad and open folds with open interlimb angles. Bedding-parallel lineations in the form of slickenfibres, on bedding planes indicate a possible flexural-slip mechanism for initial folding in the study area (Figure 5.52).

6.3.2 Cleavage

Slaty penetrative cleavage is well developed in argillaceous strata consisting of platy minerals (micas) that allow even distribution in a preferred orientation (Figure 5.6 a & Figure 5.22 b). Pencil fracture cleavage is most notably seen in shales of the Bokkeveld Group (Figure 5.22 a). Cleavage is far less pervasive in arenaceous sandstones and more difficult to identify. Sandstones of the Peninsula and Skurweberg Formation exhibit shallow, 25-45° SW dipping fractures along the northeastern limb of the main Cape St. Francis anticline that are interpreted as axial planar fracture cleavage. In the CFB axial planar cleavage is well documented as dipping south at moderate to steep angles due to the asymmetric northward verging open to tight mega-anticlines and synclines. However the more upright and near symmetrical nature of the Cape St. Francis anticline dictates that axial planar cleavage will be sub-parallel to the fold axis. The axial planar cleavage is formed syn-Cape folding. At Thyspunt, along the southwestern limb of the regional Cape St. Francis anticline and within the Skurweberg Formation, interbedded shales show a pervasive, NE-SW trending and moderately dipping NE axial planar cleavage with an average azimuth and dip of 052°/ 46° (Figure 5.57 a, b & c).

6.3.3 Evaluation of inferred AEC normal faults

The AEC interpreted several inferred NNE-SSW trending faults along the Eastern Cape coastline from results of a medium sensitivity broad scale aeromagnetic survey (Muller *et al*., 1986; Anderson *et al*., 1986 b) (§ 3.1). Six of these faults occur within the study area. These inferred faults are almost invariably blanketed by Cenozoic overburden, making direct field investigation into the validity of the faults cumbersome. Following a brief review by Goedhart *et al*., (2008) into the validity of inferred AEC faults (that mainly considered results from a near regional aeromagnetic and a site vicinity aeromagnetic survey (Cole & Naude, 2007)), uncertainty as to the legitimacy of these features still remained. However, results from the multi-electrode resistivity survey TS1 (§ 4.4.1.1 (i); Figure 4.66) a review of borehole data previously unavailable to Goedhart *et al*., (2008) and targeted mapping of coastal exposures now enable the validity of these inferred faults to be re-avaluated (§ 4.2.2.1 - § 4.2.2.5).

A summary of conclusions derived from the after afore mentioned data sources are detailed below:

• Field investigation shows no evidence of faulting along coastal exposures where inferred faults were indicated to occur (§ 4.2.2.1 - § 4.2.2.5). Outcrop exposures appear highly fractured but show no signs of offset/displacement, breccia/mylonite or variations in bedding orientation or dip, indicative of a fault.

Although centimetre displacement is occasionally observed (micro-faults) no evidence of large scale faulting were observed, keeping in mind that during field investigation certain portions of the coastal outcrop were partially obstructed by boulders and/or the presence of gullies filled with sea water. In addition the absence of marker beds within the lithologically homogeneous Peninsula and Skurweberg Formations (§ 5.2.2) did make fault investigation cumbersome.

• Boreholes in close proximity (<100 m) of inferred fault lines show no evidence of breccia. Strata is only described as highly fractured, but not brecciated at De Hoek or Thyspunt (§ 5.2.2).

• High resolution aeromagnetics (Cole & Naude, 2007), do not support the presence of inferred AEC faults (Goedhart *et al.*, 2008) (§ 3.1; Figure 3.4 and Figure 3.5). No inferred faults or probably faults were identified in areas where AEC faults are indicated.

• AT Thyspunt, the location of inferred fault AEC TSP 3 is projected to occur at 570 m along survey line TS1. However, no electrical anomalies possibly indicative of a fault were identified (§ 5.4.1.1 i) - keeping in mind that the presence of a conductive layer associated with the possible occurrence of groundwater in the area may obscure the presence of a fault, while possibly substantiating the presence of fractured strata (§ 5.2.2.5, Figure 5.46) that act as a reservoir for groundwater occurrence.

• Inferred AEC faults AEC TSP3 and AEC DH3 show no recognizable displacement on original AEC maps (Muller *et al.*, 1989; Anderson *et al.*, 1986 b; Van Wyk, 1987). Denoting these features as faults is thus technically unjustified.

• Numerous zones of high frequency, closely spaced jointing (shatter zones) occur within the study area. These zones share a similar NNE-SSW orientation as inferred AEC faults and correlates well with the main joint set, J1's orientation.

Therefore, based on a lack of strong evidence supporting the presence of inferred AEC faults at De Hoek and Thyspunt, these features are interpreted to be shatter zones (areas of closely spaced jointing or high frequency jointing) with no recognizable displacement that exceed 3 m (micro-fault scale - § 5.2.2.6). It should be noted, uncertainty still remains as to the extent of these shatter zones beneath Cenozoic cover. Whether their length or extent is accurately portrayed by AEC interpretations is uncertain.

6.3.4 Micro-faults

Micro-faults with displacement <3 m are occasionally observed (Figure 4.58 a & b). The occurrence of smaller scale normal right and left-lateral micro or minor faults striking parallel and oblique to bedding is mainly observed along coastal exposures of the Skurweberg and Peninsula Formations between Oyster Bay and Cape St. Francis (Figure 4.48 a & b). These NNE-SSW and ENE-WSW striking, steeply south and north dipping faults (Figure 4.48 c) show displacement ranging between 10 cm to 300 cm (Figure 5.48 d). Micro-faults occur in areas where joints are closely spaced with displacements parallel to the area's J1 (N-S to NNE-SSW) and J3 (NW-SE) joint set strike (Figure 5.48 e). The development of micro-faults are associated with compressive events of the Cape Orogeny. Faults form either perpendicular or parallel to

the CSF fold axis and are interpreted to have formed as space accommodation features during CFB folding. Micro-faults do not extend through Cenozoic cover.

6.3.5 Thrust faults

NE of Thys Bay, in quartzite of the Peninsula Formation localised bedding-parallel to subparallel thrusts (Figure 5.49 a & b) with an unknown amount of displacement display flat and ramps structures that strike NW-SE and have a shallow to very shallow dip towards the SW (Figure 5.49 c & d), with a northward movement on forethrusts. Thrusts are tectonically related and formed during the same northward directed stress (Cape Orogeny) that developed folding features. No reverse or back thrusts were noted and no thrusts were found to extend into Cenozoic cover.

The large body of competent Peninsula Formation quartzitic sandstone that forms the core of the anticline acts as a structural buttress to compression. Folds in thinner-bedded formations are piled up tightly against the anticline's southern limb, rupturing in places to form small ESE thrusts (§ 5.2.4) oblique to the main regional fold axis (Goedhart *et al.*, 2008).

6.3.6 Possible onland continuation of the Cape St. Francis Fault

The 40 km long NW-SE trending Cape St. Francis fault occurs offshore and comes within ~17.5 km of Thyspunt. The fault and associated faults along the Cape St. Francis Arch are extensional faults and are of tectonic origin and Mesozoic age (Goedhart *et al.*, 2007). Although the presence of the Cape St. Francis fault is based on offshore seismic data, (McMillian *et al.*, 1997; Bate & Malan, 1992, Roux, 2011) its onshore continuation is speculative. The uncertainty as to its onshore occurrence arises due to a lack of an intermediate nearshore dataset that would enable correlation between onshore (Davidson & Smith, 2007; Goedhart, 2008; Stettler *et al.*, 2008; Zadorozhnaya *et al.* 2012; Hanson *et al.*, 2012) and offshore datasets (Horwood, 2009; Roux, 2011). Goedhart (2007) and Goedhart *et al.*, (2008) postulated a possible onshore extension of the fault in two localities within the study area. At Thys Bay the fault is proposed to possibly occur south or north of the Cedarberg Formation (Figure 4.27). Results obtained along TDEM Traverse T (Figure 3.8 a & b) (Stettler *et al.*, 2008) and a review of borehole data, do not however support its presence at Thyspunt.

Towards the east, the fault is postulated as continuing onland north of Seal Point, bordering the Cedarberg Formation or possibly occurring within the Goudini Formation (Goedhart, 2007) (Figure 4.27 – Option 1). A brief summary of data that aids in determining the viability of the Cape St. Francis fault north of Seal Point is summarized below:

- A near regional aeromanetics survey conducted in the area, did not detect or recognize a discontinuity that could be possibly be interpreted as the Cape St. Francis fault (Figure 3.4) (Cole & Naude, 2007). The fault is however anticipated to retain its NW-SE strike, parallel to bedding, if extended inland, and could therefore remain undetected by airbourne geophysics.

- Extensive Cenozoic overburden hinders any possible fault verification in the southern portions of the study area. Mapping of limited hinterland exposures north of Cenozoic cover did not reveal any evidence indicative of a fault, suggesting the fault is either not present or remains undetected in the limited exposures available north of Cenozoic outcrop. Alternatively, if present, the fault may terminate in bedrock blanketed by Cenozoic sediments.

- TDEM Traverse CSF conducted along the embayment north of Seal point, (Figure 3.9 a & b) perpendicular to the projected likely onshore extension of the fault (Figure 3.7) reveals an anomaly occurring 450 m along the survey line within bedrock of the Goudini Formation. The ~60–70° SW dipping anomaly is interpreted as the Cape St. Francis fault bordered to the south by a zone interpreted as fault mélange (Stettler *et al.,* 2008) (Figure 3.9 b). The interpreted zone of fault mélange shares a similar conductivity to the shale and siltstone lithologies of the Cedarberg Formation, making it difficult to understand how resistivity signals were ultimately used to discriminate between the Cedarberg Formation and zone of fault mélange. The alternative geological interpretation by Stettler *et al.,* (2008) from the same TDEM sounding results show that steeper anticlinal folding can also fit the measured data collected along the length of TDEM traverse CSF. The alternative geological model suggests a duplication of the Cedarberg Formation eliminates the interpreted onland extension of the CSF fault and associated zone of fault mélange (§ 3.4). Stettler *et al.,* (2008) did not however consider the close proximity (25 – 100 m) of the survey line's locality to the ocean's edge and possible influence sea water penetration could exhibit on survey results. The conductive (5 Ohm.m) zone of fault mélange located between 100-525 m and 850-1350 m along the traverse could also likely represent complex zones of conductive shales and siltstones within the Cedarberg and Goudini formation and fine-grained sandstones in the Goudini Formation reflecting a greater conductivity as a consequence of sea water infiltration. Great difficulty arises in defining a fault, zone of fault mélange or even stratigraphic contacts in an area this close to the ocean where resistivity values will undoubtable be affected and generally be far more conductive compared to drier inland areas situated away from the effects of salt water infiltration.

- Multi-electrode resistivity survey CSF1 (Figure 5.70 a & b; Figure 71 a & b) and TDEM survey TDEM-CSF1 (Figure 5.80 & Figure 5.81) were conducted in the same location and along the same NE-SW trend. These surveys are situated 1.5 km NW of TDEM traverse CSF (Stettler *et al.,* 2008) and were conducted sub-perpendicular to the postulated onshore location of the CSF fault north of the Cape St. Francis village. Re-interpretation of survey results suggests conductive readings ranging between 20 – 100 Ohm.m below Cenozoic over are associated with the Cedarberg Formation. A wide zone of similar conductivity suggested by Stettler *et al.*, (2008) to possibly reflect a zone of fault mélange bordering the Cedarberg shale, is not detected along multi-resistivity line CSF1 and TDEM survey TDEM-CSF1. Instead higher resistivity values (100 - 3000 Ohm.m) bordering the Cedarberg Formation are associated with shale, siltstone and sandstone lithologies of the Goudini Formation. No duplication of resistivity values associated with the Cedarberg Formation is encountered elsewhere along survey lines. Consequently results from CSF1 and TDEM survey line TDEM-CSF1 also do not support the alternative model proposed

by Stettler et al., (2008) of steeper anticlinal folding in the area. A geophysical anomaly similar to the one identified and interpreted by Stettler et al (2008) as the Cape St. Francis fault is identified further NW and along strike at 1190 m along survey line TDEM-CSF1. The anomaly occurs immediately north of borehole CSF10 and was referred to 'anomaly D' by Zadorozhnaya *et al.*, (2012). Alignment of these anomalies along the postulated CSF fault strike can not be construed as proof for the onshore extension of the CSF fault. The anomalies may simply represent a particular lithological unit within the Goudini Formation. In addition, neither the resistivity values nor dip of anomalies appear similar between surveys. The closest borehole located 50 m south of anomaly D is borehole CSF-10 (Hanson *et al.*, 2012). No breccia was denoted in the borehole log descriptions of CSF10.

These findings and lack of any strong evidence supporting therefore do not support the inland continuation of the Cape St. Francis fault.

6.3.7 Joints

Systematic tectonic jointing is pervasive throughout Palaeozoic strata in the study area. Jointing is associated with compressional stresses present during the Permo-Triassic formation of the Cape Orogeny (Raubenheimer *et al.*, 1988 a; Goedhart *et al.*, 2008). Competent strata of the Peninsula and Skurweberg Formations and more arenaceous lithologies of the Goudini Formation show the best developed joint planes. More poorly developed jointing occurs in argillaceous formations and argillaceous litholgies of the Goudini and Cedarberg Formations. No joint planes extend through into Cenozoic overburden.

Four joint sets are identified within the study area. The dominant joint direction, joint set J1, trends N-S to NNE - SSW; perpendicular to the NW-SE bedding strike and fold axis trend. The joint set strikes 020° (± 20°). Along coastal exposures the joint set is easily identified, trending perpendicular to the coastal margin between Oyster Bay and Seal Point. Well-developed joint set, J2, strikes NE-SW with a 040° (±15°) strike. Joint sets J1 and J2 dip vertical or subvertical with a northwesterly dip. Joint set J1 frequently exhibits a steep SE dip. Together joints J1 and J2 form conjugate set X. Joint set J3 trends NW-SE with a 300° (± 30°) strike, parallel or subparallel to bedding and dip either vertically or dip 65-90° E or ESE. Joint set J4 trends ENE-WSW with a 055° (± 30°) strike and dip vertically or subvertical with a northwesterly dip. Joint sets J3 and J4 produce conjugate set Y. A fifth subhorizontal joint set, J5 is interpreted as unloading joints that form due to a release of compressive stress during uplift and erosion of overlaying strata. Although these four joint sets appear most prominent, joint planes can exhibit a range of strike directions (Figure 5.50 a & b) related to variance in the orientation and magnitude of the palaeostresses that generally change with position in the fold and the development of the fold trough time (e.g. Price & Cosgrove, 1990). Variation in joint set orientations is also related to the lithological nature of bedrock strata. The orientation of some subordinate sets may locally be more dominant depending on the area and strata's lithology. The Goudini, Skurweberg and Baviaanskloof formations show a more dominant NNE-SSW to NE-SW J1 joint set. The undifferentiated Bokkeveld Group shows a dominant NW-SE trending joint set. Within the arenaceous Peninsula and Skurweberg Formations subordinate argillaceous shale, siltstone and grey-wacke horizons show lesser and more widely spaced jointing than the overlying

and underlying quartzite units. Joints occurring within the quartzite often do not transect or extend through to interbedded argillaceous and lithologically less competent units (Figure 5.52 a, b & c). The strike of major joint planes can however be traced; extending through different lithologies (Figure 5.52 c).

Joint spacing aids greatly in modifying the coastal physiography. Areas of closely spaced jointing produce zones of weakness within the structural fabric of the rock exposure. These areas weather negatively and are associated with deep gullies and surge channels that trend perpendicular or oblique to the coastline and parallel to the strike of joint sets J1, J2. J3 and J4 (Figure 5.53 a & Figure 5.54 a). In areas where joint sets exhibit closely spaced jointing in close proximity, a broad coastal inlet within the rugged coastline is formed.

Quartz filled sigmoidal tension gashes indicative of more ductile shear deformation are occasionally observed in quartzite of the Peninsula and Skurweberg Formations (Figure 5.56 a & b). The tension gashes are S or Z-shaped, rotated en-echelon along joint sets and are associated with the late stage of deformation during the Cape Orogeny.

6.4 Geological factors influencing the NPP's footprint location

Within this dissertation; factors considered to influence siting of the proposed NPP's footprint location, its layout design and construction include: bedrock lithology (§ 5.4.1), stratigraphic bedrock contacts (§ 5.4.2; Figure 6.1 a, b & c), bedrock palaeotopography (§ 5.4.3; Figure 5.95 & Figure 5.96), thickness of overburden sediments (§ 5.4.4; Figure 5.85) and structural geology (§ 5.45). Discussions do not aim to comment on the seismicity of the area or seismic hazard geological features may pose to site safety. This task is assigned to the probabilistic seismic hazard analysis (PSHA) team and involves the seismic characterisation of the site in terms of vibratory ground motions due to natural earthquakes. These studies are governed by a different set of criteria: the Regulatory Guide 1.208, '*A Performance-Based Approach to Define the Site-Specific Earthquake Ground Motion*' (USNRC, 2007) and ASCE/SEI 43-05 '*Seismic Design Criteria for Structures, Systems, and Components in Nuclear Facilities'* (ASCE, 2005).

Influencing factors are discussed separately and presented holistically with a map that shows overall geological risk to site safety (§ 6.4.6). Although no geohydrological investigations were undertaken, the influence of groundwater on site safety cannot be omitted and is thus briefly alluded to, were applicable.

6.4.1 Bedrock lithology

Siting of the proposed NPP on strata of the lithologically more homogeneous, very strong to extremely strong (MPa average range, Engelsman & Constable, 2012) arenaceous Skurweberg Formation is scientifically more justifiable than siting on the lithologically heterogeneous, argillaceous, weak to medium strong (MPa average range, Engelsman & Constable, 2012) strata of the Goudini Formation. Site placement and design should avoid lithologically high risk areas underlain by the very weak to weak incompetent shale and siltstone lithologies such as those comprising the Cedarberg Formation (Engelsman & Constable, 2012). The competent, arenaceous and very strong to extremely strong orthoquartzites of the Peninsula Formation (Engelsman & Constable, 2012), pose little risk. Lithologies composing the Baviaanskloof Formation and Bokkeveld Group are situated too far (9.5 km) to bear any direct influence on the site placement and design of the NPP at Thyspunt.

Although the lithology of the predominantly arenaceous Skurweberg Formation is less risk adverse, the formation too has more argillaceous units directly NW of Tony's Bay (1.2 km from Thyspunt) deemed less favourable as founding substrate for the NPP. Approximately 13 m and 212 m SW of the contact between the Skurweberg and Goudini Formation, the 51 m and 84 m thick NW-SE striking units of argillaceous sandstone and shale (Figure 3.1 a & b; Figure 6.1 a & b) should be avoided if possible. Similarly, so should the zone of shale and siltstone with an areal width of ~220 m within the Goudini Formation (Figure 5.82).

6.4.2 Stratigraphic bedrock contacts

Fieldwork confirms observations by Goedhart *et al*., (2008) that the contact between the Goudini to Skurweberg Formation is transition over 25 m at Thyspunt. Consequently a 50 m buffer around this stratigraphic bedrock contact zone should be enforced. The buffer serves to include the first argillaceous sandstone and shale unit at the base of the Skurweberg Formation. A similar 50 m buffer is enforced around the upper and lower extent of the Cedarberg Formation at Thyspunt. The 50 m buffer serves as a possible range of inaccuracy in the identification of the Cedarberg Formation beneath overburden and aids in safely avoiding potentially siting NPP infrastructure on incompetent strata. Site design and layout should preferably not occur within these buffer zones.

6.4.3 Palaeotopography

Since the proposed NPP will be constructed on bedrock, awareness of bedrock palaeotopography and especially topographic depressions (palaeovalleys) are important as these areas may require greater removal of overburden and are prone to flooding as sea-level rises in future. These regions also indicate areas of lithologically less competent strata, more susceptible to erosional processes deemed more risk adverse to siting of the proposed NPP footprint foundings.

Interpolated bedrock elevations reveal four regions beneath overburden within the study area where bedrock elevations are below present day sea-level (Figure 5.96). In terms of proximity, size and lowest bedrock relief, the Thyspunt palaeovalley poses the greatest palaeotopographic risk to site safety. The palaeovalley is incised into bedrock of the Goudini Formation reaching depths of -15.5 m asl only 300 m NE from Thyspunt. A 1050 m^2 km wide portion of the palaeovalley occurs below sea level (Figure 4.96 &

Figure 4.98 c & d). The smaller sized, 150 m wide Tony's Bay palaeovalley cuts into a zone of argillaceous sandstones, shales and siltstone within the Skurweberg Formation reaches a maximum depth of -1.129 m asl. Based on size and depth, the Tony's Bay palaeovalley poses much less of a risk to site safety, compared to the larger and much deeper Thyspunt palaeovalley. These palaeotopographical depressions also act as an area of groundwater confluence and storage and should preferable be avoided or given special consideration. Palaeovalleys developed in the vicinity of the Cape St. Francis and St. Francis villages are situated too far to pose any direct risk to the Thyspunt site.

6.4.4 Overburden thickness

Founding of the NPP on bedrock requires significant excavation of overburden material. Excavations will need to cut back overburden to tolerable angles (<20°) to ensure safety during construction (Eskom, 2009). Overburden thicknesses are assigned to one of three classes that define the potential risk to site safety during excavation (§2.4, Figure 2.14) (Eskom, 2009). Classes are defined as areas. Areas that pose the greatest safety risk during construction activities are those areas exhibiting overburden thicknesses >20 m. These areas should preferably be avoided. With the inclusion of omitted and subsequently drilled borehole data, an updated map of overburden thickness categorised according to these 3 risk classes is presented in Figure 6.2. Although Eskom (2009) only defined 3 risk categories, an additional subdivision of high risk sediment thicknesses greater than 30 m, 40 m and 50 m are also indicated (Figure 6.2). Within the study area, high risk areas are partially associated with thickness distribution defined by zone B, predominantly zone C, and potentially zone D located further north (Figure 4.85).

Unconsolidated to semi-consolidated overburden material form an interganular aquifer. Excavation of overburden material should take into account the depth of the groundwater table. Dry, loose and unconsolidated sediments may become wet or waterlogged material that may require dewatering before excavation and may be prone to liquefaction.

6.4.5 Structural geology

Fractures are discontinuities in a rock mass that ultimately detract from the rocks overall strength. Jointing is the most pervasive rock discontinuity within the study area. Four well developed vertical to subvertical and one subhorizontal joint set are identified (Figure 5.50 a & b). The strike of joints sets vary slightly among stratigraphic units. Overall rock strength is diminished in areas where joint sets are closely spaced (shatter zones) (Figure 4.54 a & b).

Strata of the Peninsula and Cedarberg Formations show a dominant N-S to NNE-SSW trending J1 joint set. The Goudini, Skurweberg and Baviaanskloof formations show a more dominant NNE-SSW to NE-SW J1 joint set. Jointing is generally more pervasive in arenaceous lithologies (sandstones) composing the Skurweberg and Peninsula formations. Argillaceous lithologies tend to show either pencil shale fracturing or a well-developed cleavage. The spacing of joints varies considerably ranging from very closely spaced to very widely spaced. Arenaceous strata within the study area show slightly open to moderately open joint and fracture openings that are empty or filled with milky white quartz (Figure 4.56 d). Quartz veins generally act to 'seal' fractures and return some or all of the cohesive nature and strength to rock units.

No normal faults with displacement >3 m (micro-faults) are currently identified within the onland extent of the site locality (1 km radius around Thyspunt) or site vicinity (8 km radius around Thyspunt) (Figure 4.48 d). Thrust faults with an unknown amount of displacement were identified ~3km east of Thyspunt. These fault types thus bear no direct influence on the siting of the NPP's footprint. Inferred fault AEC TSP3 occurs within 2 km of Thyspunt and is reassessed as a shatter zone. It is however difficult to determine the extent of the shatter zone or other areas with extensive fractures or closely spaced joints sets, in bedrock below overburden cover. Thick overburden sediments blanket most of the Thyspunt site preventing any *in situ* structural analysis that may serve to guide the NPP's footprint placement. These structural characteristics should be considered closer to the time of construction of the NPP when detailed geotechnical investigations will be undertaken and removal of overburden will occur. No structural feature/s currently directly influence or pose a direct risk to footprint location, layout design and construction within the site locality.
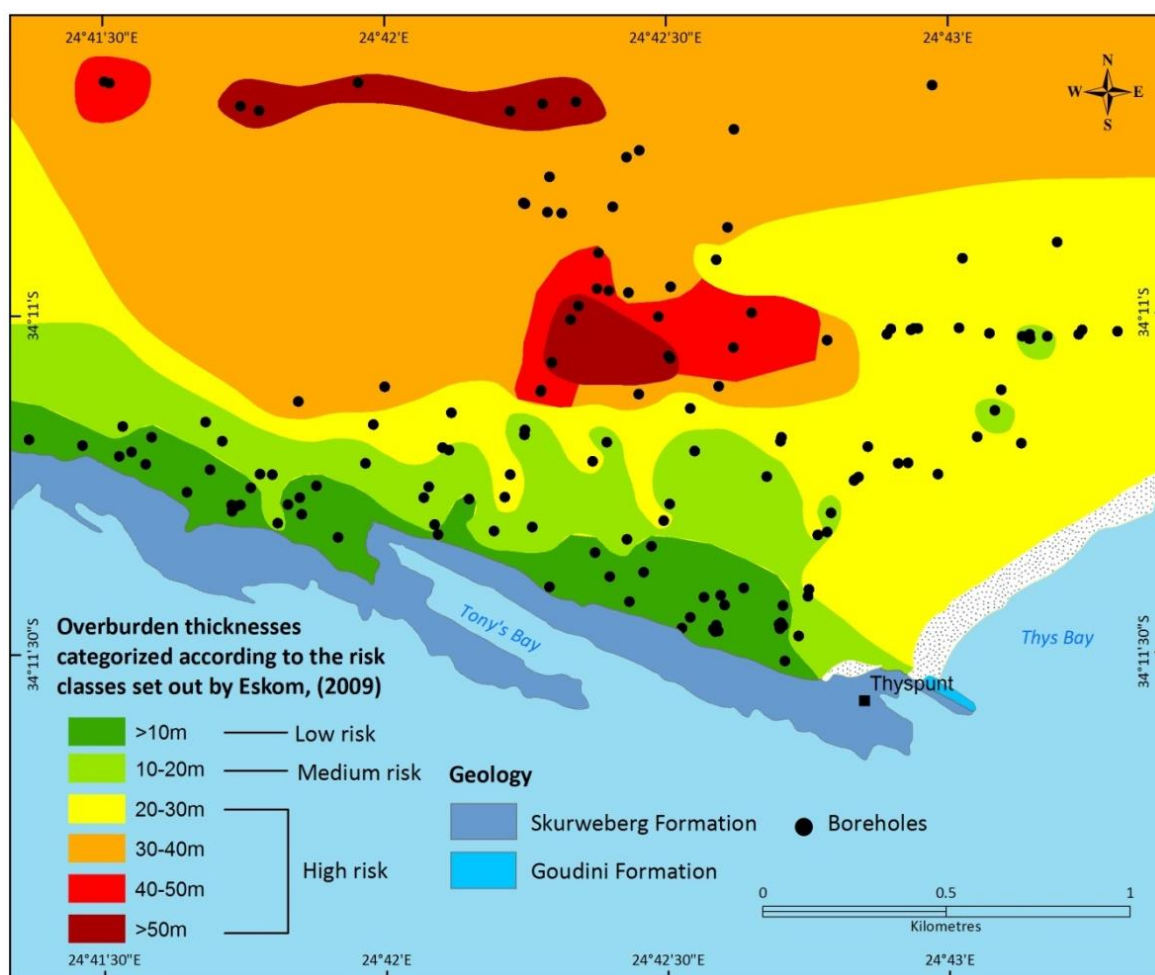
Figure 6.2: Map showing the thickness of Cenozoic cover at Thyspunt as categorized according to the safety risk classes set out by Eskom (2009) for excavation of overburden material. Areas that pose the greatest safety risk are those areas where overburden thicknesses exceed 20 m.

6.4.6 Geological risk assessment

Geological factors considered to influence siting of the NPP's foundings (§ 6.4.1 -6.4.5), are presented as a factor of combined risk to site safety (Figure 6.3). Areas are assigned a geological risk factor ranging from 0-11. Areas assigned a 0 risk factor; pose no risk, while areas assigned a risk factor of 11 pose the greatest risk to siting and construction of the proposed NPP. Areas that exhibit bedrock elevations below sea-level (palaeovallys) are assigned a higher risk ranking than areas underlain only by incompetent bedrock lithologies; this is because areas exhibiting bedrock elevation below sea-level already represent bedrock of comparatively less competent lithologies more susceptible to erosion. Shatter zone AEC TSP3, occurring ~2km from Thyspunt is indicated in Figure 6.3, however is not directly assigned a risk factor because of uncertainty with regard to the fault's extent beneath overburden cover (§ 6.4.5). The map presented in Figure 6.3 provides an initial site specific geological risk assessment for the proposed NNP at Thyspunt.

The future rise in sea level, will pose a significant risk to site safety. Future sea level projections are based on complex scenarios that take palaeoclimatic evidence from past interglacial periods, the thermal expansion of oceans and melting of onland ice into account while considering variations in the amount of future greenhouse gas releases. The International Panel on Climate Change and others (Kopp *et al*., 2009; Church *et al*., 2013) project a maximum <1 m rise in sea level by 2100. The US National Research Council and others (Pfeffer *et al*., 2008; Vermeer & Rahmstorf, 2009) however, project a maximum ~2 m rise in sea level. The complete meltdown of the world's second largest ice sheet (Greenland ice sheet), already showing rapid volumes of melt, will contribute a maximum global rise in sea-level of 7.2 m by the end of the millennium (Church *et al*., 2013). At Thyspunt, the impact of a 2 m sea level rise will cause coastal inundation of the rocky coastline for 30-40m inland. A rise of 7 m will drown the entire rugged coastline as we see it today up to 180 m inland (Figure 6.3).
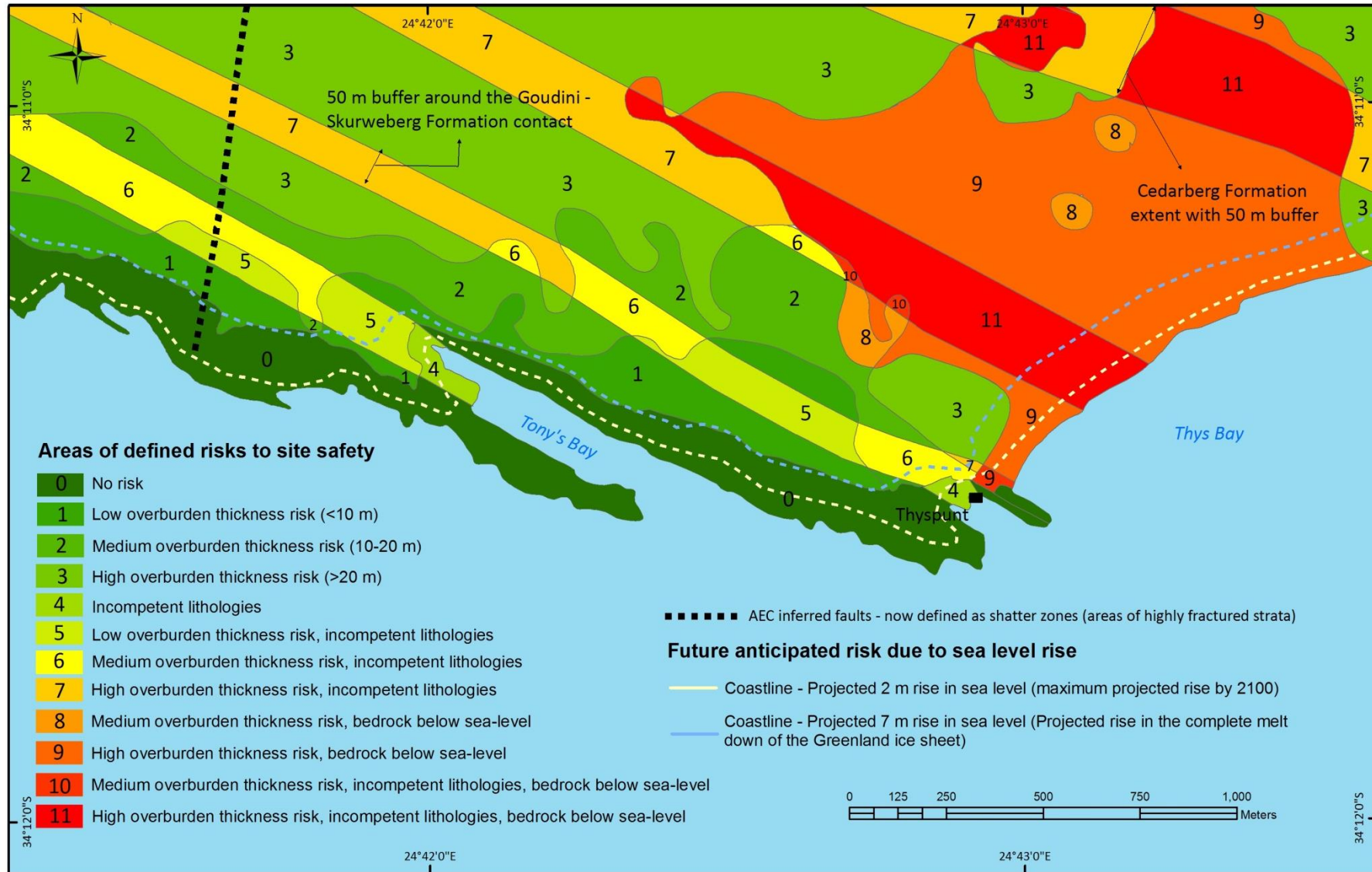
Figure 6.3: Map showing areas of defined risk to site safety based on bedrock lithology, stratigraphic contacts, bedrock palaeotopography, and overburden thickness. Although structural geology is also a factor considered to influence site safety. No faults occur within the site locality. Areas marked as 0 pose the lowest site safety risk. An area marked as 10 pose the greatest risk to site safety. Future sea level induntation is also indicated.

7. Conclusions

This study aimed to supplement information to the geoscientific topic 'Geological Setting' as outlined in section 2.5.1.1 of the USNRC Standard Review Plan NUREG-800, which details the geological information required for review in the proposed construction of a NPP. Information required and provided for include physiography (§ 1.2.3), geomorphology (§ 1.2.4), tectonic setting (§ 2.1, §2.2 & § 2.4), geological history (§ 2), (§ 2.1, §2.2 & § 2.4) stratigraphy (§ 2.3, § 3.1, § 5.1, §5.5, § 6.1.1, § 6.2.1), lithology (§ 2.3, § 2.5, § 5.1.1, § 5.3, § 6.1.1) and faulting and folding characteristics of the region encompassing the site (§ 2.4, § 3.4, § 5.2, § 6.3) with associated geological history (§ 2).

Studies undertaken focussed on geological aspects bearing influence on the siting location, and construction of the NPP. This was achieved by defining characteristics of the Ordovician to early Devonian (485-419 Ma) TMG Palaeozoic bedrock, the characteristics of the Miocene to Holocene (<23 Ma) Cenozoic overburden sediments and the structural geology of the study area. These factors are then utilised to determining an initial site specific geological risk assessment for the proposed NPP.

Geological factors considered influencing siting of the NPP's footprint, layout design and construction at the proposed Thyspunt NPP include: bedrock lithology, stratigraphic bedrock contacts, bedrock palaeotopography, thickness of overburden sediments and structural geology. Geological factors are presented as a factor of combined risk to site safety (Figure 6.3).

In conclusion:

• At Thyspunt, siting the proposed NPP on strata of Skurweberg Formation is geologically less risk adverse than siting on strata of the Goudini Formation. Site foundings on rocks of the Cedarberg Formation will pose a higher risk to site safety and these areas should be avoided. Stata of the Peninsula Formation, pose little risk.

• Areas exhibiting palaeovalley development will require greater removal of overburden sediments and may be prone to flooding especially with increasing climate change and the anticipated future rise in sea level. These areas also indicate regions of lithologically less competent strata, more prone to erosional process that pose a greater risk to site safety. Based on proximity, size and lowest bedrock relief, Thyspunt palaeovalley poses the greatest risk to site safety. The palaeovalley is incised into bedrock of the Goudini Formation reaching depths of -15.5 m asl only 300 m NE from Thyspunt. A 1050 m^2 portion of the palaeovalley occurs below sea level.

• Areas reflecting overburden thickness exceeding 20 m pose the greatest risk to site safety during excavation activities.

• No structural feature/s currently directly influence or pose a direct risk to footprint location, layout design and construction within the site locality.

8. References

Anderson, N.J.B., Faurie, J.N., Levin, N., Muller, J.A., Norman, N.G., and Hambleton-Jones, B.B., 1986 a. Investigations for the siting of nuclear power stations, Executive summary: Preliminary geotechnical investigations conducted between Cape St. Francis and the Tsitsikamma River during March 1985 and April 1986, Atomic Energy Corporation of South Africa, NSIP-EC-005663#P1-20, Pretoria, 20 pp. *(Confidential)*

Anderson, N.J.B., Muller, J.A., Faurie, N., and Hambleton-Jones, B.B., 1986 b. A geological interpretation of the detailed aeromagnetic survey carried out south of Humansdorp, Progress report No. 9 during March 1985 and April 1986, Atomic Energy Corporation of South Africa, NSIP-EC-006289#P1-26, Pretoria, 21 pp. *(Confidential)*

AEC, 1987. Escom Eastern Cape Nuclear Siting Project, Geological map of the coastal strip between Tsistsikamma River mouth and Cape St. Francis, Department of geotechnology, Atomic Energy Corporation of South Africa Ltd., 1:50,000-scale. *(Confidential)*

ASCE, 2005. Seismic Design Criteria for Structures, Systems, and Components in Nuclear Facilities. ASCE/SEI 43-05, American Society of Civil Engineers, Reston, VA.

Bate, K.J. and Malan, J.A., 1992. Tectonostratigraphic evolution of the Algoa, Gamtoos and Pletmos Basins, offshore South Africa. In: de wit, M.J. and Ransome, I.G. D. (Eds.), Inversion tectonics of the Cape Fold Belt, Karoo and Cretaceous Basins of Southern Africa, Balkema, Rotterdam, pp. 61-73.

Bierman, P.R., 2012. Report #1 Cosmogenic Geochronology, Southern Africa Fault Corridor Investigation, Appendix B.3 in Hanson, K., Slack, C. and Coppersmith, R., Thyspunt Geological Investigations—Kango Fault Study, Council of Geoscience Report Number 2012-0035 Rev. 0, 126 pp. *(Confidential)*

Booth, P.W.K., 1996. The relationship between folding and thrusting in the Floriskraal Formation (ipper Witteberg Group), Steytlerville, Eastern Cape, South Afr. J. Geol. 99, 235-243.

Booth, P.W.K., 1998. The effect of thrusting on fold style and orientation, Weltevrede Formation (Cape Supergroup), Steytlerville, Eastern Cape, S. Afr. J. Geol., 101, 27-37.

Booth, P.W.K., 2002. Thrust faults and fold vergence in the Paleozoic middle and upper Witteberg Group, Cape Supergroup (Cape Fold Belt), Steytlerville: an interpretation of their relationship. South African Journal of Geology 105: 25-38.

Booth, P.W.K., and Shone, R.W., 1992. The pre-Cape—Table Mountain Group contact west of Port Elizabeth, South African Journal of Geology 95(1/2), 34-39.

Booth, P.W.K., and Shone R.W., 1999. Complex thrusting at Uniondale, Eastern sector of the Cape fold belt, Republic of South Africa: structural evidence for the need to revise the lithostratigrapphy, J. Afr. Earth Sci. 29, 125-133.

Booth, P.W.K., Brunsdon, G., and Shone, R.W., 2004. A duplex model for the eastern Cape fold belt? Evidence from the Palaeozoic Witteberg and Bokkeveld Groups (Cape Supergroup), near Steytlerville, South Africa, Gondwana Res. 7, 211-222.

Broad, D.S., Jungslager, E.H.A., McLachlan, I.R., and Roux, J., 2006. Offshore Mesozoic basins, In: Johnson, M.R., Anhaeusser, C.R., and Thomas, R.J. (Eds.). The Geology of South Africa. Geological Society of South Africa, Johannesburg/Council for Geoscience, Pretoria, pp. 553-571.

Broad, D.S., Jungslager, E.H.A., McLachlan, I.R., Roux, J., and Van der Spuy, D., 2012. South Africa's offshore Mesozoic basins. In: Phanerozoic Passive Margins, Cratonic Basins and Global Tectonic Maps, D.G. Roberts & A.W. Bally (eds.), pp. 535-564, Elsevier, Rotterdam.

Brown, R.W.K., Gallagher, K., Gleadow, A.J.W., and Summerfield, M.A., 2000. Morphotectonic evolution of the South Atlantic margins of Africa and South America, in Geomorphology and Global Tectonics, edited by M. A. Summerfield, John Wiley, New York, pp. 257-283.

Brown, R.W., Summerfield, M., and Gleadow, A., 2002. Denudational history along a transect across the Drakensberg Escarpment of southern Africa derived from apatite fission track thermochronology. Journal of Geophysical Research, 107, NO. B12, 2350.

Brown, R., Summerfield, M., Gleadow, A., Gallagher, K., Carter, A., Beucher, R., and Wildman, M., 2014. Intracontinental deformation in southern Africa during the Late Cretaceous. J. Afr. Earth Sci. 100, 20–41.

Burke, K., 1996. The African Plate, South African Journal of Geology 99(4), 341-409.

Burkinshaw, J., 1998. Morphodynamics of headland bypass dunefields with special reference to the Cape St. Francis headland, Eastern Cape, South Africa, P.hD. Thesis, University of Port Elizabeth, pp. 373 (unpublished).

Carr, A.S., Bateman, M.D., Roberts, D.L., Murray-Wallace, C.V., Jacobs, Z., and Holmes, P.J. 2010. The last interglacial sea-level high stand on the southern Cape coastline of South Africa. Quaternary Research, 73, 351-362.

Caumon, G., Collon-Drouaillet, P., Le Carlier deVeslud, C., Viseur, S., and Sausse, J., 2009. Surface-based 3D modelling of geological structures, Math. Geosci., 41, 927-945.

Chief Surveyor General, 2008. 1:10,000-scale digital spatial cadastrial data, 5m interval for maps 3424BA and 3424BB.

Church, J.A., Clark, P.U., Cazenave, A., Gregory, J.M., Jevrejeva, S., Levermann, A., Merrifield, M.A., Milne, G.A., Nerem, R.S., Nunn, P.D., Payne, A.J., Pfeffer, W.T., Stammer D., and Unnikrishnan, A.S., 2013. Sea Level Change. In: Climate Change 2013: The Physical Science Basis. Contribution of Working Group I to the Fifth Assessment Report of the Intergovernmental Panel on Climate Change [Stocker, T.F., D. Qin, G.-K. Plattner, M. Tignor, S.K. Allen, J. Boschung, A. Nauels, Y. Xia, V. Bex and P.M. Midgley (eds.). Cambridge University Press, Cambridge, United Kingdom and New York, NY, USA, pp. 1137-1216.

Claassen, D., 2014. Geographical controls on sediment accretion of the Cenozoic Algoa Group along the southern Eastern Cape coastline between Oyster Bay to St. Francis, Eastern Cape, South Africa, South African Journal of Geology, Vol.117.1, 109-128.

Cloetingh, S., Lankreijer, A., De Wit, S.M., and Martinez, I., 1992. Subsidence history and forward modelling of the Cape and Karoo Supergroups, In: Inversion Tectonics of the Cape Fold Belt, Karoo and Cretaceous Basins of Southern Africa. Eds. De Wit, M. J. and Ransome, I. G. D. Balkema, Rotterdam, pp. 239-248.

Cole, J., 2006 a. Preliminary interpretation of high resolution airborne geophysical data collected at Thyspunt, Report NSIP-NSI-018902#P1-9, 9 pp. *(Confidential)*

Cole, J., and Cole, P., 2007. Geophysical interpretation of the marine magnetic data collected in the offshore site area (8 km radius) of Thyspunt. CGS Report No 2007-0189, NSIP-NSI-020268#P1-12, 12 pp. *(Confidential)*

Cole, J., and Naudé, C., 2007. Final report: Airborne survey of Thyspunt. Council for Geoscience, Report No. 2007-0006, ESKOM, NSIP-NSI-019039#P1-67, Pretoria, 67 pp. *(Confidential)*

Conrad, C.P., and Gurnis, M., 2003. Seismic tomography, surface uplift, and the breakup of Gondwanaland: Integrating mantle convection backwards in time, Geochemistry, Geophysics, Geosystems 4 (3), doi:10.1029/2001GC000299.

Cooper, M.R., 1986. Facies shifts, sea-level changes nd event stratigraphy in the Devonian of South Africa, S. J. Sci., 82, 255-258.

Cotter, E., 2000. Depositional setting and cyclic development of the lower part of the Witteberg Group (Mid-to Upper-Devonian), Cape Supergroup, Western Cape, South Adrica, S. J. Geol., 103, 1-14.

Council for Geoscience, 1991. Geological Survey of South Africa, 1:250,000-scale 3324, Port Elizabeth, geological series map.

Davidson, A., and Smith, S., 2007. Geophysical survey report for Thyspunt Eskom Site Surveys South Africa, Fugro Survey Africa (PTY) Ltd. Report Number MZ581za-01-RPT-03-01 (Client Reference: NSIP-NSI-019130#P1-215), prepared for Eskom Holdings Limited, South Africa, 85 pp., plus appendices. *(Confidential)*

De Beer, C. H., Van Zijl, J. S. V. and Bahnemann, F. K., 1974. Plate Tectonic origin for the Cape Fold Belt? Nature (252): 675-676.

De Beer, C.H., 1989. Structure of the Cape Fold Belt in the Ceres syntaxis, M.Sc. thesis (unpubl.) Univ. Stellenbosch, 136 pp.

De Beer, C.H., 1990. Simultaneous folding in the western and southern branches of the Cape Fold Belt. S. Afr.J. Geol. 93, pp. 583-591.

De Beer, C.H., 1995. Fold interface from simultaneous shortening in different directions: the Cape fold belt syntaxis, J.Afr.Earth Sci. 21, pp. 157-169.

De Beer, C.H., 2000. Geology and tectonics of the Thyspunt site, Humansdorp. Internal CGS report to the seismology unit, 21 pp. *(Confidential)*

De Beer, C.H., 2001. Summary of the subsurface geology at the Brazil, Schulpfontein, Koeberg, Bantamsklip and Thyspunt sites. Internal CGS report to the seismology unit, 10 pp. *(Confidential)*

De Beer, C.H., 2005. Investigation into evidence for neotectonic deformation within inland Neogene to Quaternary deposits between Alexander Bay and Port Elizabeth – South Coast Report. Council for Geoscience, Report No. 2005-0180, NSIP-SHA-016311#P1-197, 197 pp. *(Confidential)*

De Swardt, A.M.J., and Rowsell, D.M., 1974. Note on the Relationship between Diagenesis and Deformation in the Cape Fold Belt. Transactions of the Geological Society of South Afirca 77: 239-245.

De Villiers, J., 1944. A Review of the Cape Orogeny. Ann. Univ. Stell., 22-A: 183-208.

De Wit, M.J., 2007. The Kalahari Epeirogeny and climate change: differentiating cause and effect from core to space. South Afr J. Geol 110(2–3):367–392.

De Wit, M. J., and Ransome, I.G.D., 1992 a. Preliminary investigations into a microplate model of the South Western Cape. In: Inversion Tectonics of the Cape Fold Belt, Karoo and Cretaceous Basins of Southern Africa. Eds. De Wit, M. J. and Ransome, I. G. D. Balkema, Rotterdam, 269 pp.

De Wit, M.J., and Ransome, I.G.D., 1992 b. Regional inversion tectonics along the southern margin of Gondwana. In: Inversion tectonics of the Cape Fold Belt, Karoo and Cretaceous Basins of Southern Africa. Eds. de Wit, M. J. and Ransome, I. G. D. A.A Balkema, Cape Town, 269 pp.

Dingle, R.V., Siesser, W.G., and Newton, A.R., 1983. Mesozoic and Tertiary geology of southern Africa. Balkema, Rotterdam, 375 pp.

Doucouré, C.M. and de Wit, M.J., 2003. Old inherited origin for the present nearbimodal topography of Africa. Journal of African Earth Sciences, v. 36,. 371-388.

Duncan, R.A., Hooper, P.R., Rehacek, J, Marsh J.S., and Duncan, AR., 1997. The timing and duration of the Karoo igneous event, southern Gondwana. J Geophys Res 102:18127–18138

Engelsman, B. and Constable, B., 2012. Thyspunt Shear Wave Velocity Measurements, Report Number 449376, SRK Consulting Ltd, 16 pp. *(Confidential)*

Erlanger, E.D., Granger, D.E., and Gibbon, R.J., 2012. Rock uplift rates in South Africa from isochron burial dating of fluvial and marine terraces, Geology 40, 1019-1022.

Eskom, 2009. Evironmental impact assessment for a proposed nuclear power station ('nuclear-1') and associated infrastructure, Geotechnical Characterisation Assessment Study, Eskom holdings limited, SRK Consulting, 46 pp. *(Confidential)*

Eskom, 2010 a. Thyspunt Site Safety Report, Section 5.11, Geohydrology, Exploration Borehole Data and Logs, Draft Report, June 2010. *(Confidential)*

Eskom, 2010 b. Thyspunt Site Safety Report, Section 5.15, Geotechnical Characterization, Borehole Logs, Draft Report, June 2010. *(Confidential)*

Eskom, 2014. Eskom Holdings SOC Limited, Standard presentation, July, 2014. Available at <http://www.eskom.co.za/OurCompany/Investors/Presentations/Documents/StandardPresentationJuly2014.pdf>

Fawkes, H., 2005. Energy efficiency in South African industry, Journal of Energy in Southern Africa, Vol 16 No. 4, pp. 18-25.

Fitch, F.J., and Miller, J.A., 1984. Dating Karoo igneous rocks by the conventional K-Ar and 40Ar/39Ar age spectrum methods. In: Erlank, A.J. (Ed.), Petrogenesis of the Volcanic Rocks of the Karoo Province. Geological Society of South Africa, Special Publication 13, pp. 247–266.

Fleming, A., Summerfield, M.A., Stone, J.O., Fifield, L.K., and Cresswell, R.G., 1999. Denudation rates for the southern Drakensberg escarpment, SE Africa, derived from in-situ-produced cosmogenic 36Cl: initial results. Journal of the Geological Society, London, v. 156, pp. 209-212.

Forman, S.L., 2012. Optical ages for aeolian and littoral sediments from drill-core, Eastern Cape, South Africa, (Appendix E.2 in Hanson, K.L., Glaser, L., Coppersmith, R., Roberts, D.L, Claassen, D., & Black, D.E. (2012). Thyspunt Geological Investigations—Marine Terrace Studies, Report Number 2012-0034, Rev. 0, Council for Geoscience, Pretoria. *(Confidential)*

Fouché, J., Bate, K. J., and van der Merwe, R., 1992. Plate tectonic setting of the Mesozoic Basins, southern offshore, South Africa: A review. In: Inversion Tectonics of the Cape Fold Belt, Karoo and Cretaceous Basins of Southern Africa. Eds. De Wit, M. J. and Ransome, I. G. D. Balkema, Rotterdam, 269 pp.

Gilchrist, A.R., and Summerfield, M.A., 1990. Differential denudation and flexural isostasy in formation of rifted-margin upwards, Nature 346, 739-742.

Goedhart, M.L., 2007. Onshore and Offshore Geohazards for the Thyspunt Nuclear Power Plant: A Summary of New Airborne and Marine Geophysical Data, and Existing Offshore Seismic Reflection Data (Rev. 0), Report No. 2007–0257, Council for Geoscience, Pretoria, 16 pp. *(Confidential)*

Goedhart, M.L., and Cole, J., 2007. Nuclear Siting Investigation Program: Remote sensing assessment of the length of aeromagnetic lineament SV1, Thyspunt., CGS Report No. 2007-0211, NSIP-NSI-020327#P1-29, 29 pp. *(Confidential)*

Goedhart, M.L., and Hattingh, J., 1997. The geology of the Coega River mouth and proposed Industrial Development Zone, Eastern Cape. Council for Geoscience, Report No. 1997 0008 (unpublished), 106 pp & 5 map pockets.

Goedhart, M.L., Reddering, J.S.V., Kilian, D, Mitha, V., Bosch, P.J.A., and Black, D., 2008. Surface geology and update of on-land geological hazards for the 40km Site Vicinity and 8km Site Area around the proposed Thyspunt nuclear power plant, Eastern Cape, South Africa, Council for Geoscience, Report No. 2008–0222, 219 pp. *(Confidential)*

Gresse, P.G., Theron, J.N. T., Fitch, F.J., and Miller, J.A., 1992. Tectonic inversion and radiometric resetting of the basement in the Cape Fold Belt. In: Inversion Tectonics of the Cape Fold Belt, Karoo and Cretaceous Basins of Southern Africa. Eds. De Wit, M. J. and Ransome, I. G. D. Balkema, Rotterdam, 269 pp.

Grunow, A., Hanson, R., and Wilson, T., 1996. Were aspects of Pan-African deformation linked to Iapetus opening? Geology 24, 1063–1066.

Hälbich, I.W., 1983. A tectogenesis of the Cape Fold Belt. In: Sohnge, A.P.G. & Hälbich, I.W. (eds.), Geodynamics of the Cape Fold Belt, Spec. Publ. Geol. Soc. S. Afr., 12,165 175.

Hälbich, I.W., 1992. The Cape Fold Belt Orogeny: State of the art 1970s – 1980's. In: De Wit, M.J., and Ransome, I.G.D. (Eds.). Inversion tectonics of the Cape Fold Belt, Karoo and Cretaceous Basins of Southern Africa. Balkema, Rotterdam, 141-158.

Hälbich, I.W. and Cornell, D.W., 1983. Metamorphic history of the Cape FoldBelt. In: A.P.G. Söhnge and I.W. Hälbich (Editors), Geodynamics of theCape Fold Belt. Special Publication of the Geological Society of South Africa, 12, 131-148.

Hälbich, I.W., Fitch, F.J., and J.A., Miller., 1983. Dating the Cape Orogeny. In: Söhnge, A.P.G & Hälbich, I.W. (Eds.), Geodynamics of the Cpe Fold Belt. Spec. Publ. Geol. Soc. Afr., 12, 149-164.

Hansma, J., Tohver, E., Schrank, C., Jourdan, F., and Adams, D., 2015. The timing of the Cape Orogeny: New 40Ar/39Ar age constraints on deformation and cooling of the Cape Fold Belt, South Africa, Gondwana Research, doi:10.1016/j.gr.2015.02.005, p.16 *(in press)*.

Hanson, K.L., Coppersmith, R., Glaser, L., Roberts, D.L., Claassen, D., and Black, D.E., 2012. Thyspunt Geological Investigations—Marine Terrace Studies, Report No. 2012-0034, Council for Geoscience, Pretoria. *(Confidential)*

Henop, F., 1987. Investigation for the siting of nuclear power stations, Progress report no.18 - Land survey co-ordinates of boreholes of the candidate sites: De Hoek; Thyspunt; Tony's Bay; Klippepunt; Morgan's Bay and Brakkeduine, Atomic Energy Corperation of South Africa, NSIP:N002566, Pretoria. *(Confidential)*

Hill, R.S., 1991. Lithostratigraphy of the Baviaanskloof Formation (Table Mountain Group), including the Kareedouw sandstone member. South African Committee for Stratigraphy (SACS) - Lithostratigraphic Series 11, 7 pp.

Hobday, D.K., and Tankard, A.J., 1978. Transgressive-barrier and shallow-shelf interpretation of the lower Paleozoic Peninsula Formation, South Africa. Bulletin of the Geological Society of America, 89, 1733-1744.

Horwood, S., 2009. Thyspunt 8 km Radius Marine Survey: Structural Geology Report, CGS Report 2009-0027, 11 pp. *(Confidential)*

Huskins, L.R., 1981. Eastern Cape Nuclear sites – siting study, Memorandum from General manager to Serior General Manager, NSIP-EC-006703#P1-14, 14 pp *(Confidential)*

Illenberger, W.K., 1992. Lithostratigraphy of the Schelm Hoek Formation (Algoa Group). South African Committee for Stratigraphy (SACS), Lithostratigraphic Series, 21, 7 pp.

Illenberger, W., and Burkinshaw, J., 2007 (update of December 2001 report). The Cape St. Francis headland bypass dune system and beach erosion at St. Francis Bay, and sediment accumulation in the Kromme Estuary, description for Heritage Center, December 2001, Illenberger and Associates, 6 pp.

Illenberger, W.K. and Rust, I.C., 1988. A sand budget for the Alexandria coastal dunefield, South Africa. Sedimentology, 35, 513-521.

Illenberger, W., Rust, I., Burkinshaw, J., Vogel, J. and Woodborne, S., 2005. Luminescence dating of coastal dunes of the southern-eastern Cape: paper presented at the South African Coast Paleoclimate, Paleoenvironment, Paleoecology, Paleoanthropology Project SACP4 Workshop, 5-6 November, Munro House, Dias Museum, Mossel Bay.

Jacobs, Z., and Roberts, D.L., 2009. Last Interglacial Age for aeolian and marine deposits and the Nahoon fossil human footprints, Southeast Coast of South Africa. Quaternary Geochronology, 4, 160-169.

Johnson, M.R., 1976. Stratigraphy of the Cape and Karoo Systems in the Eastern Cape Province. M.Sc. Thesis, Rhodes University (unpublished).

Johnson, M.R., 1991. Sandstone petrography, provenance and plate tectonic setting in Gondwana context of the southeastern Cape-Karoo basin, S. Afr. J. Geol. 94, 137-154.

Johnson, S.T., 2000. The Cape Fold Belt and syntaxis and the rotated Falkland Islands: dextral transpressionaltectonics along the southwest margin of Gondwana, Journal of African Sciences, Vol.31, No 1, pp. 51-63.

Johnson, M.R., Theron, J.N., and Rust, I.C., 1999. Table Mountain Group, In: Johnson, M.R. (Ed.). Catalogue of South African Lithostratigraphic Units, 6, 6-43 – 6-45.

Jones, C.B., 2014. Geographical information systems and computer cartography, Pearson Education Limited, New York, 344 pp.

Jones D.L, Duncan R.A, Briden J.C, and Randall D.E, Macniocaill C., 2001. Age of the Batoka basalts, northern Zimbabwe, and the duration of Karoo large igneous province magmatism. Geochem Geophys Geosyst 2:14 pp.

Jourdan F., Fe´raud G., Bertrand H., Watkeys M., and Renne PR., 2007. Distinct brief major events in the Karoo large igneous province clarified by new 40Ar/39Ar ages on the Lesotho basalts. Lithos 98 (1–4):195–209

Kopp, R.E., Simons, F.J., Mitrovica, J. X., Maloof, A.C., and Oppenheimer, M., 2009. Probabilistic assessment of sea level during the last interglacial stage. Nature, 462, 863–868.

La Cock, G.D., and Burkinshaw, J.R., 1996. Management implications of development resulting in disruption of a headland bypass dunefield and its associated river, Cape St. Francis, South Africa, Landscape and urban planning, 34, 373-381.

Le Roux, F.G., 1987 a. Lithostratigraphy of the Alexandria Formation. South African Committee for Stratigraphy (SACS), Lithostratigraphic Series, 1, 18 pp.

Le Roux, F.G., 1987 b. Tertiary macrofossils of the Alexandria Formation a supplementary list: Ann. geol. Surv. S. Afr., 21, 65-74.

Le Roux, F.G., 1989. The lithostratigraphy of Cenozoic deposits along the south Cape coast as related to sea level changes. M.Sc. Thesis, University of Stellenbosch, 247pp (unpublished).

Le Roux, F.G., 1991. Lithostratigraphy of the Salnova Formation. Lithostratigraphic Series, Geological Survey of South Africa 9: 1-14.

Le Roux, F.G., 1992. Lithostratigraphy of the Nanaga Formation (Algoa Group). South African Committee for Stratigraphy (SACS), Lithostratigraphic Series, 15, 9 pp.

Le Roux, F.G., 2000. Explanation of sheets 3325DC&DD, 3425BA Port Elizabeth, 3325CD&3425AB Uitenhage, 3325CB Uitenhage Noord, and 3325DA Addo. Council for Geoscience, 55 pp.

Lindeque, A., De Wit, M.J., Ryberg, T., Weber, M., and Chevallier, L., 2011. Deep crustal profile across the southern Karoo Basin and Beattie magnetic anomaly, South Africa: An integrated interpretation with tectonic implications. South African Journal of Geology,114, 265 pp.

Linol, B., De Wit, M.J., Milani, E.J., Guillocheau F., and Scherer, C. Chapter b: New Regional Correlations between the Congo, Paraná and Cape-Karoo Basins of southwest Gondwana. In: De Wit, M.J., Guillocheau, F., (Eds.) The Geology and Resource Potential of the Congo Basin (in press due to be published).

Lock, B.E., 1980. Flat plate subduction and the Cape Fold Belt of South Africa. Geology, 8, 35 39.

Loke, M.H., 1999. Electrical imaging surveys for environmental and engineering studies, A practical guide to 2-D and 3-D surveys, Copyright (1997, 1999) M.H.Loke, Penang, Malaysia, pp57. Avalible at : <http://www.abem.se/files/res/2dnotes.pdf> (viewed 05.19.2014)

Loke, M.H., 2001. Tutorial : 2-D and 3-D electrical imaging surveys, (Revision date : 1 Sept. 2001) Copyright (1996-2001) M.H.Loke, Penang, Malaysia, pp.120. Avalible at : <https://pangea.stanford.edu/research/groups/sfmf/docs/DCResistivity_Notes.pdf> (viewed at 05.19.2014)

Loke, M.H., Chambers, J.E., and Kuras, O., 2011. Instrumentation, electrical resistivity. In Solid Earth Geophysics Encyclopedia (2nd Edition), Electrical & Electromagnetic, Gupta, Harsh (ed), 2nd ed. Berlin: Springer, pp. 599–604.

Loots, L., Chirenje, E., Claassen, D., and Black, D., 2009. A multi-eletrode survey near Cape St. Francis and Thyspunt, Eastern Cape with the position of marine terraces and possible faults buried under Cenozoic cover, Council for Geoscience, Report nr. 2009-0211, Rev0. *(Confidential)*

Marshall, C.G.A., and Von Brunn, V., 1999. The stratigraphy and origin of the Natal Group, S.Afr. J. of Geol., 102, 15-25.

Maclear, M., 2002. St Francis Bay Golf Estate: Groundwater development, exploration phase, SRK Consulting, Report nr. 291491/1, 20 pp.

Maclear, M., 2005. St. Francis Golf Links: Phase 2, Groundwater Development, SRK Consulting, Report nr. 344065.

Maclear, M., 2006. St Francis Golf Links Groundwater Supply, Routine Groundwater Quality Monitoring, SRK Consulting, Port Elizabeth, May.

Magubane, N., 2013. Speech by the Director General at the NIASA Convention on Nuclear Power: An Essential Component of our Energy Mix. Avalible at: http://www.energy.gov.za/files/media/speeches/2013/DG-Speech-%20NIASA-2013-Conference-14August2013.pdf> (viewed 04.05.2014)

Malan, J.A., Theron, J.N., and Hill, R.S., 1989. Lithostratigraphy of the Goudini Formation (Table Mountain Group). South African Committee for Stratigraphy (SACS) - Lithostratigraphic Series 2, 5 pp.

Mallet, J.L., 2002. Geomodelling. Oxford University Press, New York, 624pp.

Maud, R.R., 2008. The macro-geomorphology of the Eastern Cape. In: Lewis, C.A. (Ed.). Geomorphology of the Eastern Cape, South Africa (Second Edition). NISC, Grahamstown, 1–20.

Maud, R.R., and Botha, G.A., 2000. Deposits of the South Eastern and Southern Coasts. In: Partridge, T.C., and Maud, R.R. (Eds.). The Cenozoic of Southern Africa. Oxford Monographs on Geology and Geophysics, 40, 19-32.

McLachlan, A., Illenberger, W.K., Burkinshaw, J.R., and Burns, M.E.R., 1994. Management implications of tampering with littoral sand sources, Journal of Coastal Research 12 (Special Issue on Coastal Hazards), 51-59.

McMillan, I.K., Brink, G.I., Broad, D.S., and Maier, J.J., 1997. Late Mesozoic sedimentary basins off the south coast of South Africa. In: African Basins, R.C. Selley (ed.), vol. 3 in Sedimentary Basins of the World series, pp. 319-376, Elsevier, Amsterdam.

McNeill, J.D., 1994. Principles and application of time domain electromagnetic techniques for resistivity sounding, Technical note TN27, Geonics Limited, Ontario, Canada, pp.15. Avalible at: <http://www.geonics.com/pdfs/technicalnotes/tn27.pdf>

Mfundisi, Z., 2013. In pursuit of Vision 2030: Reforming South Africa's electricity sector, Entry number 1289. Avalible at: <http://www.budgetspeechcompetition.co.za/download_files/winners-and-finalists/2013/zwelihle-mfundisi.pdf> (viewed 04.05.2014)

Milani, E.J., and De Wit, M.J., 2008. Correlations between the classic Paraná and Cape Karoo sequences of South America and southern Africa and their basin infills flanking the Gondwanides: du Toit revisited. In: Pankhurst, R.J., Trouw, R.A.J., Brito Neves, B.B., De Wit, M.J. (Eds.), West Gondwana: Pre-Cenozoic Correlations Across the South Atlantic Region. Geological Society, Special Publications, Vol. 294, pp. 319-342. London.

Mielke, C.H., and De Wit, M.J., 2009. Large-scale structural map of the Cape Fold Belt derived by remote sensing analysis, 11th SAGA, Biennial Technical Meeting and Exhibition Swasiland, 16-18 September 2009, pp. 521-523.

Milsom, J., 2003. Field Geophysics, 3rd Edition, John Wiley and Sons, Chichester, UK, pp. 232.

Moorman, R., 2008. A safety re-elvaluation of the AVR pebble bed reactor operation and its consequences for future HTR concepts, Berichte des Forschungszentrums Jülich, ISSN 0944-2952, 37 pp.

Muller, J.A., Anderson, N.J.B., and Hambleton-Jones, B.B, 1986. Results and geophysical interpretation of the detailed aeromagnetic survey conducted in the coastal area of the Humansdorp district, Report No.14, PIN-982 (B/R), GEA 721, Atomic Energy Corperation, Pretoria, 13 pp. *(Confidential)*

Murdock, K.L., 2010. Google Sketchup and Google Sketchup Pro 7 Bible, Wiley Publishing Inc., Indiana, US, 524 pp.

Newton, A.R., 1973. A gravity folding model for the Cape Fold Belt, Transactions of the Geological Society of South Africa, 76, 145 152.

Newton, A.R., Shone., R.W., and Booth, P.W.K., 2006. The Cape fold belt, In: Johnson, M.R., Anhaeusser, C.R., Thomas, R.J. (Eds.), The geology of South Africa, Geological Society of South Africa, Johannesburg and Council for Geoscience, Pretoria, pp. 521-530.

Norman, N.G., 1985. Geological investigations for the siting of nuclear power stations; Progress report No.1; Seismicity and structure as site criteria, preliminary notes, Atomic Energy Corporation of South Africa, NSIP-EC-006291#P1-27, Pretoria, 17 pp. *(Confidential)*

Norman, N.G., Anderson, N.J.B., Faurie, J.N and Hambleton-Jones, B.B., 1986. Investigations for the siting of nuclear stations, Progress report No. 5, A preliminary assessment of regional and coastal geology from Cape St. Francis to the Tsitsikamma River with the view to the selection of candidate sites for a nuclear power station, Atomic Energy Corporation of South Africa, NSIP-EC-005760#P1-59, Pretoria, 59 pp. *(Confidential)*

Norman, N.G., Raubenheimer, E., Muller, A., Anderson, N.J.B., Faurie, J.N and Hambleton-Jones, B.B., 1987 a. Investigations for the siting of nuclear stations, Progress report No.15, Final report on the geology of the area between Cape St. Francis and the Tsitsikamma River mouth, Vol.1, Atomic Energy Corporation of South Africa, PIN-988 (B/R) GEA-730, Pretoria, 27 pp. *(Confidential)*

Norman, N.G., Raubenheimer, E., Muller, A., Anderson, N.J.B., Faurie, J.N and Hambleton-Jones, B.B., 1987 b. Investigations for the siting of nuclear stations, Progress report No.15, Final report on the geology of the area between Cape St. Francis and the Tsitsikamma River mouth, Vol.2, Atomic Energy Corporation of South Africa, PIN-988 (B/R) GEA-730, Pretoria, 27 pp. *(Confidential)*

Partridge, T.C., and Maud, R.R., 1987. Geomorphic evolution of southern Africa since the Mesozoic. South African Journal of Geology, 90, 179–208.

Partridge, T.C., and Maud, R.R., 2000. Macroscale geomorphic evolution of southern Africa, in The Cenozoic of Southern Africa, Eds., T. C. Partridge and R. R. Maud, Oxford Univ. Press, New York, pp. 3-18.

Partridge, T.C., Botha, G.A. and Haddon, I.G., 2006, Cenozoic deposits of the interior. In Johnson, M.R., Anhaeusser, C.R. and Thomas, R.J. (eds.):Geology of South Africa, Geological Society of South Africa, Johannesburg/Council for Geoscience, Pretoria, pp. 585-604.

Paton, D.A., Macdonald, D.I.M., and Underhill, J.R., 2006. Applicability of thick or thin skinned structural models in a region of multiple inversion episodes; southern Africa. J. Struct. Geol. 28, 1933-1947.

Pfeffer, W.T., Harper, J.T., and O'Neel, S., 2008. Kinematic constraints on glacier contributions to 21st-century sea-level rise. Science, 321, 1340–1343.

Price, N.J., and Cosgrove, J.W., 1990. Analysis of geological structures, Cambridge Press, New York, 502 pp.

Raath, C.J. de W, and Cole, J., 2007. Ground geophysical survey investigating a feature identified during the airborne geophysical study of the area around Thyspunt (Revision 1). CGS Report No. 2007-0198, NSIP-NSI-020068#P1-11, 11 pp. *(Confidential)*

Rosewarne, P.N., and Lomberg, C.R., 1989. Groundwater resource evaluation at St. Francis, SRK Consulting, Report nr: 171719/3, 36 pp.

Raubenheimer, E., and Hambletone-Jones, B.B., 1988 a. Detailed geology of the De Hoek, Thyspunt and Tony's Bay, Eskom Eastern Cape Project - Investigations for the siting of nuclear power stations,

Atomic Energy Corporation of South Africa, Ltd., Dept of Geotechnology, Progress report No. 20. Vol 1 geological description of borehole core, PIN-1072 (B/R) GEA 801. NSIP-N002557 & NSIP-EC-005421#P1-143, 143 pp. *(Confidential)*

Raubenheimer, E., and Hambletone-Jones, B.B., 1988 b. Detailed geology of the De Hoek, Thyspunt and Tony's Bay, Eskom Eastern Cape Project - Investigations for the siting of nuclear power stations, Atomic Energy Corporation of South Africa, Ltd., Dept of Geotechnology, Progress report No. 20., Vol 2 geotechnical maps, PIN-1072 (B/R) GEA 801. NSIP-N002557 & NSIP-EC-005421#P1-202, 202 pp. *(Confidential)*

Reeves, C., 1999. Aeromagnetic and gravity features of Gondwana and their relation to continental break-up: more pieces, less puzzle. J Afr. Earth Sci 28:263–277.

Reddering, J.S.V., Rohwer, M.H., Majokweni, M.P. and Roberts, M.P., 2006. Explanation of the geology of the Wild Coast area (1:50 000-scale map sheets) 3129BC Lusikiski, 3129CB Tombo, 3129CC AND CD, Coffee Bay, 3129DA Port St. Johns – publication in progress, Council for Geoscience, Pretoria, 84 pp.

Roberts, D.L., 2006. Dating and preliminary correlation of raised marine and estuarine terraces on the western and southern coast of South Africa, Final Report. NSIP-SHA-018230#P1-206, Council for Geoscience, Report No. 2006-0186, 206 pp. *(Confidential)*

Roberts, D.L., Botha, G.A., Maud, R.R., and Pether, J., 2006. Coastal Cenozoic deposits, In: Johnson, M.R., Anhaeusser, C.R., and Thomas, R.J. (Eds.). The Geology of South Africa. Geological Society of South Africa, Johannesburg/Council for Geoscience, Pretoria, pp. 541–552. *(Confidential)*

Roberts, D.L., Bateman, M.D., Murray-Wallace, C., Carr, A.S. and Holmes, P.J., 2009. West coast dune plumes: Climate driven contrasts in dunefield morphogenesis along the western and southern South African coasts, Palaeogeography, Palaeoclimatology, Palaeoecology 271, 24–38.

Roberts, D.L., Karkanas, P., Jacobs, Z., Marean, C.W., and Roberts, R.G., 2012. Melting ice sheets 400,000 yr ago raised sea level by 13 m: Past analogue for future trends. Earth and Planetary Science Letters, 357/358, 226-237.

Roux, J., 2011. Offshore geophysical data, PowerPoint presentation (given by A. Davids on behalf of the author) at SSHAC Workshop 1, April 16, Cape Town.

Rust, I.C., 1967. On the sedimentation of the Table Mountain Group in the western Cape Province, Unpublished D.S.c Thesis, University of Stellenbosch, 110 pp.

Rust, I.C., 1973. The evolution of the Paleozoic Cape basin, southern margin of Africa, In: Nairn, A.E.M., Stehli, F.G. (Eds.), The ocean Basins and Margins, vol.1. Plenum, New York, pp. 247-276.

SACS, 1980. (See South African Committee for Stratigraphy).

Shone, R.W., 2006. Onshore post-Karoo Mesozoic deposits, In: Johnson, M.R., Anhaeusser, C.R., and Thomas, R.J. (Eds.). The Geology of South Africa. Geological Society of South Africa, Johannesburg/Council for Geoscience, Pretoria, pp. 541–552.

Shone, R.W., 1976. The sedimentology of the Mesozoic Algoa Basin. M.Sc. dissertation, University of Port Elizabeth, 48 pp. (unpubl.).

Shone, R.W., Nolte, C.C., and Booth., P.W.K., 1990. Pre-Cape rocks of the Gamtoos area – a complex tectonostratigraphic package preserved as a horst block, Trans. Of the Geol. Soc. of SA., 93, 616-621.

Shone R.W., and Booth P.W.K., 1993. Trusting in the Bokkeveld Group of the southern Cape, S. Afr. J. Geol. 96, 220-225.

Shone, R.W., and Booth, P.W.K., 2005. The Cape Basin, South Africa – A Review. Journal of African Earth Sciences, 43, 196-210.

Simmons, N.A., Forte, A.M., and Grand, S.P., 2007. Thermochemical structure and dynamics of the Africa superplume: Geophysical Research Letters 34, doi:10.1029/2006GL028009.

Smuts, W.J., 1987. The sedimentology of the Alexandria Formation: M.Sc. thesis, Univ. Port Elizabeth. (unpubl.).

Söhnge, A.P.G., 1983. The Cape Fold Belt-Perspective. In: Geodynamics of the Cape Fold Belt. Eds. Söhnge, A. P. G. and Hälbich, I. W. The Geological Society of South Africa, Johannesburg. pp.

South African Committee for Stratigraphy (SACS), 1980. Stratigraphy of South Africa, Part 1 (L.E. Kent, Comp.): Lithostratigraphy of the Republics of Bophuthatswana, Transkei and Venda: Handb. geol. Surv. S. Afr., 8.

Stettler, E.H., Zadorozhnaya, V.Y. and Goedhart, M.L., 2008. Results of a Time Domain Electromagnetic Survey Over Four Possible Fault Positions Signifying the Landward Continuation of the Cape St. Francis Fault, Cape St. Francis and Oyster Bay, Eastern Province. Council for Geoscience, Pretoria, Report No. 2008-0171 - Addendum, 30 pp. *(Confidential)*

Steyn, G., 2003. Administered Prices: Electricity. Pretoria: Report for National Treasury, pp.32. Available at <http://www.treasury.gov.za/publications/other/epir/Electricity.pdf> (viewed 06.05.2014)

Summerfield, M.A., 1996, Tectonics, geology, and long-term landscape development. In Adams, W.M., Goudie, A.S. and Orne, A.R. (eds.): The Physical Geography of Africa, Oxford University Press, New York, 17 pp.

Tankard, A.J., Jackson, M.P.A., Eriksson, K.A., Hobday, D.K., Hunter, D.R., and Minter, W.E.L., 1982. Crustal evolution of southern Africa: New York, Springer-Verlag, 523 pp.

Tankard, A., Welsink, H., Aukes, P., Newton, R., and Stettler, E., 2009. Tectonic evolution of the Cape and Karoo basins of South Africa, Marine Petrol. Geol. 26, 1379-1412.

Tankard, A., Welsink, H., Aukes, P., Newton, R., and Stettler, E., 2012. Geodynamic interpretation of the Cape and the Karoo basins, South Africa. Phanerozoic Passive Marigins, Cratonic Basins and Global Tectonics Maps. USA & UK: Elsevier, 869 pp.

Thamm, A.G., 1989. Sedimentology of the Ordovician Piekenierskloof and Graafwater Formations, South Africa: a fluvial-earshore transition, Abstracts 4th International Conference Fluvial Sedimentology, Barcelona, 230.

Thamm, A.G., and Johnson M.R., 2006. The Cape Supergroup. In: Johnson, M.R., Anhaeusser, C.R., and Thomas, R.J. (Eds.). The Geology of South Africa. Geological Society of South Africa, Johannesburg/Council for Geoscience, Pretoria, pp. 443–460.

Theron, J.N., and Johnson, M.R., 1991. Bokkeveld Group (including the Ceres, Bidouw and Traka Subgroups). Catalogue of South African Lithostratigraphic Units 3: 3-5. Council for Geoscience. Pretoria.

Theron, J.N., and Thamm, A.G., 1990. Stratigraphy and sedimentology of the Cape Supergroup in the Western Cape, Guidebook Geocongress '90.Geol.Soc.S. Afr.PR2, 1-64.

Theron, J.N., Malan, J.A., and Hill, R.S., 1989. Lithostratigraphy of the Skurweberg Formation (Table Mountain Group). South African Committee for Stratigraphy, Lithostratigraphic Series 3, 6 pp.

Thomas, R.J., Marshall, C.G.A., Watkeys, M.K., Fitch, F.J. and Miller, J.A., 1992. K-Ar and $^{40}Ar/^{39}Ar$ dating of the Natal Group, southeast Africa – a post-Pan-African molasses?, J.Afr. Earth Sci., 15, 453-471.

Thomas, S., 2010. The economics of nuclear power: An update, Heinrich-Böll Stiftung publication series on ecology, European Union, Brussels, 68 pp. Avalible at: <https://www.google.co.za/#q=The+Economics+of+Nuclear+Power%3A+An+Update+thomas+2010> (viewed 05.05.2014)

Tinker, J., De Wit, M., and Brown, R., 2008. Mesozoic exhumation of the southern Cape, South Africa, quantified using apatite fission-track thermochronology, Tectonophysics 455(1 4), 77-93.

Toerien, D.K., 1973. Geological Survey of South Africa, 1:50,000-scale geological maps of areas 3424BA and 3424BB, unpublished.

Toerien, D.K., and Hill, R.S., 1989. The geology of the Port Elizabeth area. Explanation of sheet 3324 (1:250 000). Geological Survey of South Africa, 35 pp.

Trouw, R.A.J., and De Wit, M.J., 1999. Relation between the Gondwanide Orogen and contemporaneous intracratonic deformation, J. Afr. Earth Sci., 28 (1), 203-213.

Tucker, M.E., 2011. Sedimentary Rocks in the Field: A Practical Guide, Wiley Publishers, 276 pp.

Turner, B.R., 1991. Continental sediments in South Africa, J, Afr. Earth Sci., 10, 139-149.

USNRC, 2007. A performance-based approach to define the site-specific earthquake ground motion. Regulatory Guide 1.208, US Nuclear Regulatory Commission, Washington D.C.

Van Wyk, J.H., 1987. Eskom Eastern Cape Nuclear Siting Project: Geological map of the coastal strip between Tsitsikamma River mouth and Cape St. Francis. Compiled by the Department of Geotechnology, Atomic Energy Corporation of South Africa Ltd. *(Confidential)*

Van Wyk, J., 2013. South Africa's nuclear future, South African Institute of International Affairs, Governance of Africa's resource programme, Occasional paper No.150, June 2013. Avalible at: <http://www.saiia.org.za/doc_download/337-south-africa-s-nuclear-future> (viewed 04.04.2014)

Vermeer, M., and Rahmstorf, S., 2009. Global sea level linked to global temperature. Proc. Natl. Acad. Sci. U.S.A., 106, 21527–21532.

Vernon, R.H., 2004. A practical guide to rock microstructure, Cambridge University Press, Cambrige, United Kingdom, 579 pp.

Watkeys, M. K., 2006. Gondwana Break-Up: A South African Perspective. In: The Geology of South Africa. Eds. Johnson, M. R., Anhaeusser, C. R. and Thomas, R. J. The Geological Society of South Africa and Council for Geoscience, Pretoria. pp. 531-539.

Young, C.G., Bradley, N.A., and Heidstra, N.N., 1981. Eastern Cape Nuclear Siting Study, Sections I & II, Appendix I, Copy No.3, Electricity Supply Commission, Civil Engineering – NW6, NSIP-EC-019569#P1-169, 14 pp.

Zadorozhnaya, V., Eberle, D. and Claassen, D., 2012. Results of a Time Domain Electromagnetic Survey Conducted at Cape St. Francis with the Intent of Locating the Bedrock Surface Buried Beneath Cenozoic Cover, Eastern Cape, South Africa, CGS Report No. 2012-0152, Rev. 0, 11 pp. *(Confidential)*

Websites

http://data.wordbank.org[1] – Available at:

> http://data.worldbank.org/indicator/EG.USE.PCAP.KG.OE (viewed 21.10.2014)

http://data.wordbank.org[2] – Available at:

> <http://data.worldbank.org/indicator/EN.ATM.CO2E.PC/countries/ZA?display=graph> (viewed 21.10.2014)

http://environmentalresearchweb.org – Avalible at:

> <http://environmentalresearchweb.org/cws/article/news/30499> (viewed 17.10.2014)

http://unfccc.int – Avalible at:

> <http://unfccc.int/kyoto_protocol/items/2830.php> (viewed 21.10.2014)

www.brics.co.za - Available at:

> <http://www.brics5.co.za/> (viewed 04.05.2014)

www.energy.gov.za[1] - Available at:

> <http://www.energy.gov.za/IRP/irp%20files/IRP2010_2030_Final_Report_20110325.pdf> (viewed 04.05.2014)

www.energy.gov.za[2] - Available at:

> <http://www.energy.gov.za/files/policies/electrification/Suite%20of%20Supply%20policy%20guidelines%202012.13.pdf> (viewed 04.05.2014)

www.enigeeringnews.co.za - Available at:

> <http://www.engineeringnews.co.za/print-version/eskom-may-need-to-raise-r50bn-more-debt-than-initially-forecast-2013-07-11> (viewed 04.05.2014)

www.eskom.co.za[1] – - Available at:

> <http://www.eskom.co.za/AboutElectricity/FactsFigures/Documents/Nuclear.pdf> (viewed 04.05.2014)

www.eskom.co.za[2] - Available at:
> <http://www.eskom.co.za/OurCompany/SustainableDevelopment/EnvironmentalImpactAssessments/Documents/DEIR_APP_E17_Economic_Assessment.pdf> (viewed 04.05.2014)

www.eskom.co.za[3] - Available at:
> <http://www.eskom.co.za/Whatweredoing/NewBuild/Pages/Renewable_Energy.aspx> (viewed 04.05.2014)

www.eskom.co.za[4] - Available at:
> <http://www.eskom.co.za/OurCompany/MediaRoom/Documents/AFD_LoanAgreement15Oct2013.pdf> (viewed 04.05.2014)

www.iaea.org - Avalible at:

> <http://www.iaea.org/PRIS/WorldStatistics/OperationalReactorsByCountry.aspx>(viewed 17.11.2014)

www.ncwater.org - Avalible at:

> <http://www.ncwater.org/?page=562> (viewed 05.12.14)

www.world-nuclear.org – Avalible at:

   <http://www.world-nuclear.org/info/Country-Profiles/Countries-O-S/South-Africa/> (viewed 17.10.2014)

www.world-nuclear-news.org – Avalible at:

   <http://www.world-nuclear-news.org/NN-South_Africa_and_France_sign_nuclear_accord-1410147.html> (viewed 19.10.2014)

Appendix A1 - Claassen, D., 2014. Geographical controls on sediment accretion of the Cenozoic Algoa Group along the southern Eastern Cape coastline between Oyster Bay to St. Francis, Eastern Cape, South Africa., Vol.117.1, 109-128.

GEOGRAPHICAL CONTROLS ON SEDIMENT ACCRETION OF THE CENOZOIC ALGOA GROUP BETWEEN OYSTER BAY AND ST. FRANCIS, EASTERN CAPE COASTLINE, SOUTH AFRICA

D. CLAASSEN

Regional Eastern Cape Unit, Council for Geoscience, PO Box 5347, Walmer, Port Elizabeth, 6001, South Africa.
e-mail: dkilian@geoscience.org.za or debclaassen@gmail.com

ABSTRACT

Borehole data provide an opportunity to explore the thickness distribution of Late Cenozoic Algoa Group sediments along the southern Eastern Cape coastline, between Oyster Bay and Cape St. Francis, South Africa. Bedrock lithology, bedrock elevation, surface relief and sediment supply are factors considered to influence thickness variations locally. Variations in accretion values allow recognition of four coast-parallel trending zones, referred to here as zones A to D. Zones A and B are characterised by a general trend of increasing thickness, with increasing distance from the coastal margin and occur in the first few hundred metres from shore. Zone A occurs closest to the shoreline and records the lowest sediment thicknesses. At Thyspunt zone A extends inland from the coastal margin for ~250 m and sediment thicknesses here range between 3 to 12 m. Zone B defines the inland area between ~250 to 750 m from the shoreline. A clear progression from zone A accretion values into thicker zone B sediment thicknesses is recognized at Thyspunt, where sediment thickness typically range between 12 to 26 m. Further inland, zone C, a zone of peak thickness values (61 m) occurs where the Algoa Group is underlain by the argillaceous Goudini and Cederberg Formations. Bedrock elevations below sea-level and the occurrence of fluvial deposits above these argillaceous bedrock lithologies indicate the presence of a possible palaeo-valley near Thyspunt and Cape St. Francis. Such a palaeo-valley allowed for greater accretion of sediments. Greatest accretion values occur in these areas especially where coupled with elevated surface relief as is the case towards the northwestern regions of the study area where elevated dune heights occur close to the area's upwind sand supply. Furthermore here the occurrence of the Cape St. Francis anticline cored by quartzite of the Peninsula Formation form a bedrock ridge impeding sediment transfer to the east, concentration dune mass along the western limb of the anticline. The transition to zone D is marked by the dramatic decline from peak sediment thickness values to thinner accretion values (<25 m) near the inland extent of the Algoa Group.

Introduction

Onshore Cenozoic deposits of littoral marine, beach, nearshore estuarine, fluvial and aeolian origin, are irregularly deposited along the coastal plains of southern Africa. These deposits reflect a coastal margin that underwent a series of glacio-eustatic marine transgressions and regressions superimposed on uplift and seaward tilting of the subcontinent during the Cenozoic Era (Roberts et al., 2006).

The South African Committee for Stratigraphy (SACS) accepted a lithostratigraphic framework that geographically partitions these deposits into distinct groups. Five geographical partitions are recognized; the east coast region (Maputaland Group), the southeastern coast (Algoa Group), the southern coast (Bredasdorp Group), the southwestern coast (Sandveld Group) and the west coast (West Coast Group) (Roberts et al., 2006). The Algoa Group deposits are restricted to the Eastern Cape; occurring east of Oubosstand (35 km west of Cape St. Francis) to East London. Deposits equivalent to those of the Algoa Group have recently been identified on a limited scale (Reddering et al., 2006) along the wild coast, between East London and Port St. Johns, with a new lithostratigraphic terminology (Mount Thesiger Formation) proposed by Reddering et al., (2006), but not yet accepted by SACS for marine conglomerates in the vicinity of Port St. Johns. If these equivalents are truly part of the Algoa Group it will lead to an extension of the Cenozoic Algoa Group to the majority of the Eastern Cape coastline.

Observations regarding the variation in accretion or thickness of the Algoa Group as a composite unit within the Eastern Cape are limited. Le Roux (1990a) describes the thickness of the Algoa Group in the Algoa Bay region as variable. Towards the northern hinterland of the Algoa Bay and along coastal areas west of Port Elizabeth, portions of the Algoa Group are documented as attaining a thickness of >250 m (Le Roux, 1990). Sediment accretions in the region of the Alexandria dune field often attain 160 m (Le Roux 1990a). Le Roux (1987a, 1987b; 1990a, 1990b; 1989; 1992) was one of few authors (Illenberger, 1992; Burkinshaw, 1998) who made an attempt to document the thickness of either portions or the Algoa Group as a whole, in combination with factors that may possibly influence the distribution of accretion values.

A large collection of boreholes occurring in the area between Oyster Bay and St. Francis (the study area) provide an opportunity to explore the thickness distribution of Late Cenozoic Algoa Group sediments
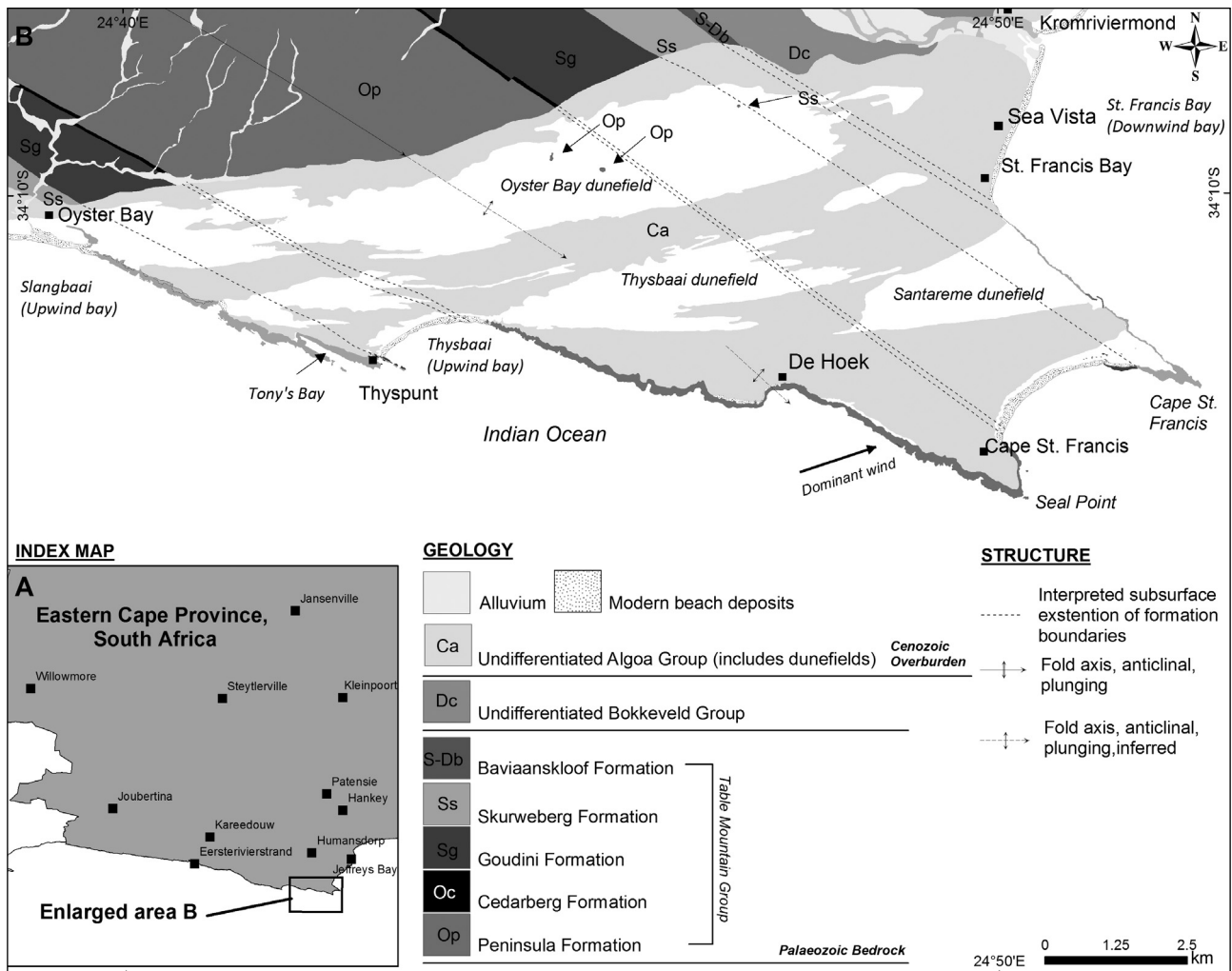
Figure 1. Location of study area, showing the outcrop extent of the Algoa Group. Headlands-bypass dunefields in the Cape St. Francis area (modified after Illenberger and Burkinshaw, 2008; Goedhart et al., 2008).

and the geographical factors that may locally influence thickness along this section of the southern Eastern Cape coastline (Figure 1). The results may aid in a greater stratigraphic understanding of the Algoa Group and may serve as a valuable dataset for future groundwater or infrastructure development studies in the area.

Geology of the study area

The study area is underlain by folded northwest-southeast-striking Palaeozoic bedrock strata of the Ordovician to Silurian age Table Mountain Group and the undifferentiated Devonian age Bokkeveld Group (Figure 1) that underwent deformation as a result of northerly-directed intercontinental compression associated with the Permo-Triassic Cape Orogeny 280-230 Ma (De Beer, 2000; Bate and Malan, 1992; Halbich, 1983). Within the study area, the Table Mountain Group bedrock comprises five sedimentary formations: the Peninsula, Cedarberg, Goudini, Skurweberg and Baviaanskloof Formations (Figure 1 and Table 1). Inadequate exposure prevented differentiation of the predominantly argillaceous Bokkeveld Group (Figure 1

and Table 1) to formation level. Subsurface mapping of individual Cape Supergroup formations beneath Cenozoic sediments was initially attempted by geophysical means (Anderson et al., 1986 a; Anderson et al., 1986 b; Cole and Naudé, 2007). Later, Goedhart et al., (2008), extended on this scheme by correlating inland exposures along strike with mapped coastal exposures. However a more holistic interpretation of borehole data (Raubenheimer et al., 1988a; 1988b; Rosewarne and Lomberg, 1989; Maclear, 2002; Maclear 2005; Maclear 2006; Engelsman and Constable, 2012; Hanson et al., 2012), geophysical results (Cole and Naudé 2007; Stettler et al., 2008; Loots et al., 2009; Zadorozhnaya et al., 2012) and mapped exposures (Figure 1); have succeeded in better defining the formation contacts beneath overburden (Figure 1).

Between Oyster Bay and Cape St. Francis bedrock strata are controlled by a regional-scale northwest-southeast-striking, southeast-plunging anticline, known as the Cape St. Francis anticline (Goedhart et al., 2008). The anticline is cored by quartzite of the Peninsula Formation. The fold axis of the anticline trends parallel

to the northwest-southeast bedding strike and verges to the north (Figure 1). Bedding inclination is mostly controlled by this anticline and the parallel distance away from its fold axis. Near the fold axis, bedding inclination is shallow (5 to 20°) with dip increasing away from the fold axis to reach inclination values of 50 to 65° along the Thyspunt-Oyster Bay coastline and 30 to 40° west of De Hoek. Raubenheimer et al., (1988a; 1988b) and Goedhart et al., (2008) identified numerous shatter zones (areas described as closely spaced jointing) along coastal exposures that weather negatively cutting deep gullies and surge channels into bedrock.

Marine transgressions and regressions from the Late Cretaceous to Holocene induced by both uplift and seaward tilting of the subcontinent and sea-level changes resulted in the development of well-planed, seaward-sloping erosional platforms incised into the structurally deformed Palaeozoic bedrock. These deposits formed a base for the deposition of predominantly unconsolidated to semiconsolidated clastic nearshore-marine and coastal aeolian-derived Algoa Group cover deposits (Table 1) that generally young in a seaward direction as a result of progradation on successive sea-level highstands (Illenberger 1996; Roberts et al. 2006, Roberts et al, 2009; Bateman et al. 2011).

The Algoa Group is stratigraphically subdivided into six formations; from oldest to youngest, the Bathurst, Alexandria, Nanaga, Salnova, Nahoon, and Schelm Hoek, Formations (Table 1). The Bathurst Formation is not documented within the study area or its immediate surroundings (Table 1). Exposure of the Algoa Group is largely obscured by coastal vegetation making differentiation of formations that compose the Algoa Group, difficult. In addition borehole logs are often poorly described. Goedhart et al. (2008) mapped not only the study area, but also the area west of Oyster Bay, and were only able to differentiate between formations in small isolated localities, and thus locally chose to predominately define the Algoa Group as undifferentiated.

Between Oyster Bay and Cape St. Francis, the Algoa Group occurs along a coastal corridor (Goedhart et al., 2008) north of either coastal rock exposures or modern beach sands (Figure 1). In the study area, these predominantly aeolian deposits form part of the Oyster Bay-St. Francis headland bypass dune field (Figure 1). The dunefields are characterised by undulating topography formed by a series of linear east-west trending dune ridges and troughs (Figures 2 a and b) extending ~10 km inland from the coastline near Cape St Francis (Figure 1). Two active large-scale headland-bypass dune corridors are recognised within the study area, the Oyster Bay dunefield and the Thysbaai dunefield (Figure 1). A third dunefield, the Santareme dunefield (Figure 1), which occurs near the village of St. Francis was completely stabilised during the 1970s and 1980s to enable development of a holiday resort in the area (McLachlan et al. 1994; La Cock and Burkinshaw 1996; Illenberger and Burkinshaw, 2007). These dunefields receive their sand supply from sandy beaches in the area. Sand from Oyster Bay beach (Slangbaai) supplies the larger Oyster Bay dunefield, while the beach at Thysbaai serves as the sand source for the smaller Thysbaai dunefield. A dominant west and west-southwest wind distributes sand in an easterly direction. The Oyster Bay, Thysbaai and Santareme dunefields are currently predominantly cut off from their sand sources and are slowly becoming vegetated (Illenberger and Burkinshaw, 2008). The Oyster Bay dunefield, which varies in width from about 500 to 1,200 m, is active over a length of about <13 km. Transverse dune height varies from 22 m in the upwind (western) end of the dunefield to 5 m at the downwind (eastern) end. The smaller Thysbaai dunefield has a maximum length of about 6 km, a maximum width of about 1,000 m, and average transverse dune height within the field of about 11 m (Burkinshaw, 1998).

Luminescence ages for dune deposits of the Algoa Group in the Oyster Bay and Thysbaai dunefields (Figure 1) range from Holocene to middle Pleistocene (>490 ka) (Illenberger et al., 1997). Fossil dune ridges at

Table 1. A lithostratigraphic summary of the study area.

Age	Age	Supergroup	Group	Formation	Lithological Description
Cenozoic	Holocene		Algoa	Schelm Hoek	Aeolian sand, soil horizons and shell middens
	Pleistocene			Nahoon	Aeolianite, palaeosols and minor calcrete
				Salnova	Marine and/or estuarine calcareous sandstone, siltstone, coquinite, and basal gravels (conglomerate)
				Nanaga	Calcareous sand/sandstone, palaeosols and calcrete
	Mio-Pliocene			Alexandria	Calcareous sandstone, coquinite and basal gravels (conglomerate)
Palaeozoic	Devonian	Cape	Bokkeveld		Fine grained sandstone, mudrock and siltsone
	Silurian		Table	Baviaanskloof	Impure feldspathic sandstone, subordinate shale
			Mountain	Skurweberg	Medium to course grained quartzitic sandstone
				Goudini	Medium grained sandstone, and subordinate shales
	Ordovician			Cedarberg	Black shale, subordinate siltstone
				Peninsula	Medium to course grained quartzitic sandstone
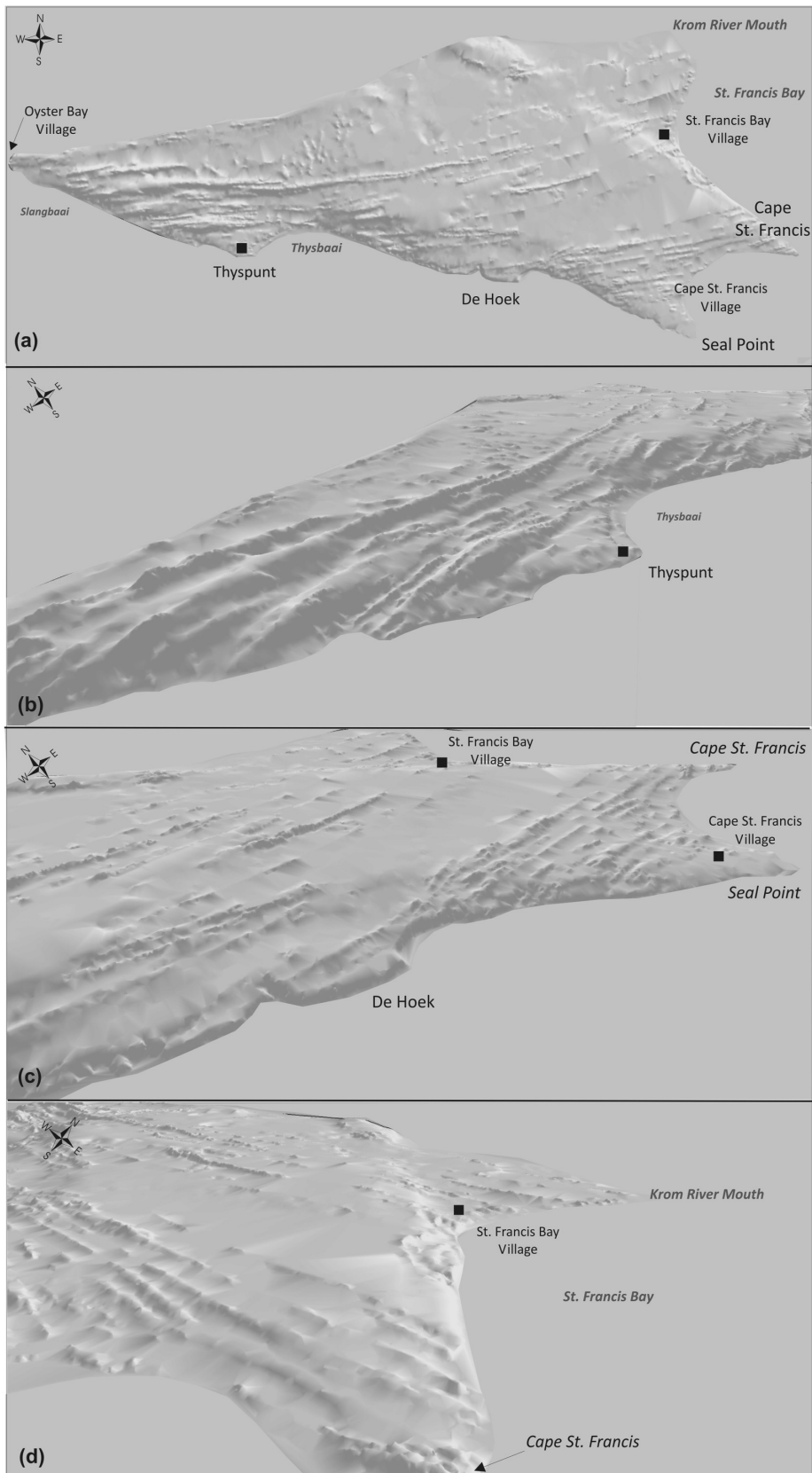
Figure 2. (**a**) *Digital elevation model (DEM) of the Cenozoic Algoa Group outcrop within the study area,* (**b**), *the Thyspunt area,* (**c**) *the De Hoek and Cape St. Francis areas and* (**d**) *the St. Francis area. Model is derived from a 5m contour interval.*
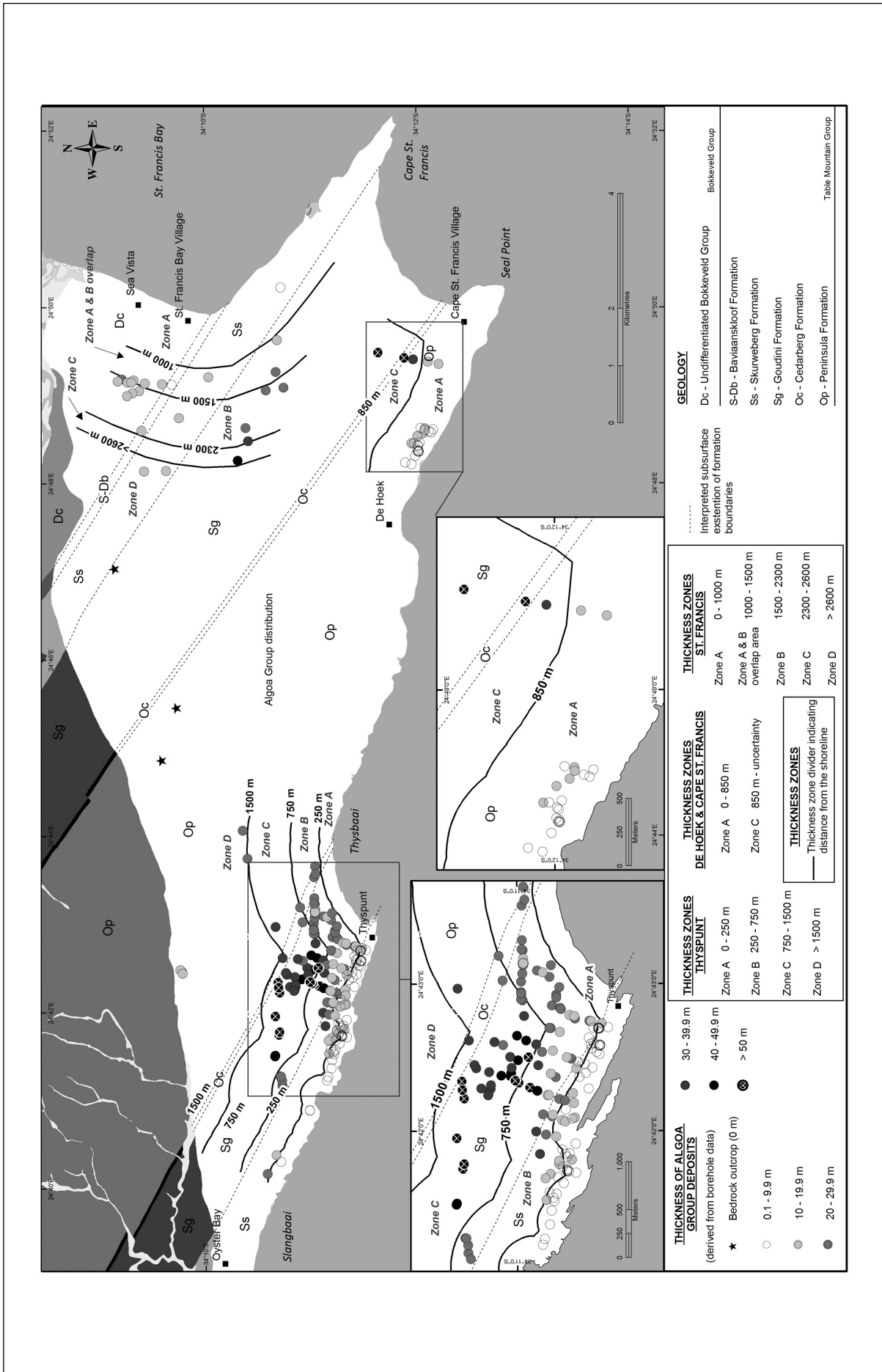
Figure 3. *Thickness of the Algoa Group as derived from borehole data. Thickness zones A to D relate to distance from the shoreline.*

the windward (western) end of the Oyster Bay dunefield confirmed dune activity associated with Late Pleistocene interglacials. Weathered dune rock from a ridge flank was dated at ~105 ka, and case-hardened aeolianite from the downwind nose of another ridge was dated at ~225 ka. Iron-enriched sands found on the flanks of the fossil ridges were dated at ~225 ka (Oyster Bay dunefield) and at ~490 ka (Thysbaai dunefield) (Illenberger et al. 1997; Illenberger and Burkinshaw 2007). Optically stimulated luminescence ages derived from core samples (Hanson et al., 2012) collected at Thyspunt ranged in age from ~22.5 ka to >130 ka (Forman, 2012).

The interface between Palaeozoic bedrock and Cenozoic cover deposits is often associated with sporadically deposited marine and fluvial gravels, stratigraphically correlative with either the basal unit of the Miocene to Early Pliocene Alexandria Formation or the Quaternary Salnova Formation (Hanson et al., 2012; Roberts et al., 2006). Le Roux (1991) describes the Salnova Formation generally occurring below 18 m amsl. The basal gravel deposits consist of sand and/or gravels on a number of well-planed, seaward-sloping platforms in shoreface and foreshore to lagoonal and/or estuarine depositional settings (Roberts et al., 2006). The composition of the gravel depends on the underlying source materials and along the southern Cape coastal area such clasts consist mostly of Table Mountain Group quartzite (Goedhart et al., 2008). The occurrence and thickness of these Algoa Group basal gravels are discussed later.

A regional marine terrace study (Hanson et al., 2012) and cosmogenic analysis of gravel clasts and underlying bedrock from boreholes (Bierman, 2012) indicate that the lower marine platforms (elevations <18 m) in the Thyspunt area are probably Quaternary in age. Cosmogenic dating (Bierman, 2012) of a gravel unit in borehole core located ~800 m north-northeast of Thyspunt, indicated that the Salnova Formation ranged in age from 747 to 802 ka.

Calculating Algoa Group sediment accretion values
Data considerations
A total of 247 boreholes (Raubenheimer et al., 1988a; 1988b; Rosewarne and Lomberg, 1989; Maclear, 2002; Maclear, 2005; Maclear, 2006; Engelsman and Constable, 2012; Hanson et al., 2012) were used in determining thickness of the Algoa Group. Thickness within each borehole is calculated from top of borehole to first occurrence of bedrock. Inclined boreholes (Raubenheimer et al., 1988a; 1988b) were corrected to vertical for the purpose of thickness calculation. Boreholes that did not reach bedrock were excluded from accretion calculations.

Delineating thickness of individual formations within the Algoa Group is problematic. Difficulty in differentiating between formations within the study area is attributed to limited exposure and borehole log descriptions that are often not formation specific, nor provide adequate lithological descriptions of Cenozoic

deposits to facilitate accurate differentiation to formation level. Therefore the Algoa Group is treated here predominantly as a composite undifferentiated unit.

Results
Algoa Group thickness
The thickness of the Algoa Group as derived from individual boreholes is indicated in Figure 3. Individual borehole surface elevations, bedrock elevations and the resultant thicknesses were graphically plot against their distance from the coastline in areas where borehole density was sufficient to produce a viable result. These areas include Thyspunt (Figures 4 a and b), the combined areas of De Hoek and Cape St. Francis (Figure 5 a and b) and St. Francis (Figures 6 a and b). The impact of surface relief and bedrock elevation on the thickness of the Algoa Group are further investigated by means of more detailed cross sections perpendicular to the coastline in areas such as Thyspunt (Figures 7, 8 a, b and c) and Cape St. Francis (Figures 9 and 10). Variations in the thickness of the Cenozoic Algoa Group allowed for the recognition of four coast parallel trending zones referred to here as zones A to D (Figure 3).

Zone A
Zone A (Figures 3 and 7) represents Algoa Group deposits that occupy the area extending inland from the coastal margin for ~250 m in the vicinity of Thyspunt (Figure 4 b), ~830 m in the combined vicinities of De Hoek and Cape St. Francis (Figure 5 b) and conceivably up to 1500 m in the St. Francis region (Figure 6 b). Sediment thicknesses within this coast proximal belt, range on average between 3 and 12 m and rarely exceeds a 15 m thickness (Figure 4 b).

In the vicinity of Thyspunt, Algoa Group sediments occupying zone A are exclusively underlain by competent northwest to southeast trending quartzitic sandstone of the Skurweberg Formation (Figures 3 and 7). Here bedrock elevations are below 10 m and very rarely below sea level (4 a and Figure 8 a, b and c). Borehole elevations indicate that surface relief does not exceed 25 m (Figure 4 a). Sediments range in thickness from a minimum of 2 m near the shoreline; to an isolated 16 m maximum ~200 m from the coastal margin (Figures 4 b and 7) near Tony's Bay. The sediment thicknesses typically range between 3 to 11 m (Figure 4b).

In the areas of De Hoek and Cape St. Francis boreholes that occupy zone A are exclusively underlain by competent northwest to southeast trending quartzitic sandstone of the Peninsula Formation (Figures 3 and 9). The bedrock elevation steadily rises with increasing distance from the coastal margin and is coupled with a steady rise in surface relief (Figure 5 b). A thickness range similar to Thyspunt is calculated in the De Hoek and Cape St. Francis areas where Cenozoic deposits typical range between 6 to 9 m (Figure 5 a). The maximum recorded sediment thickness for the Algoa Group in the combined areas of De Hoek and
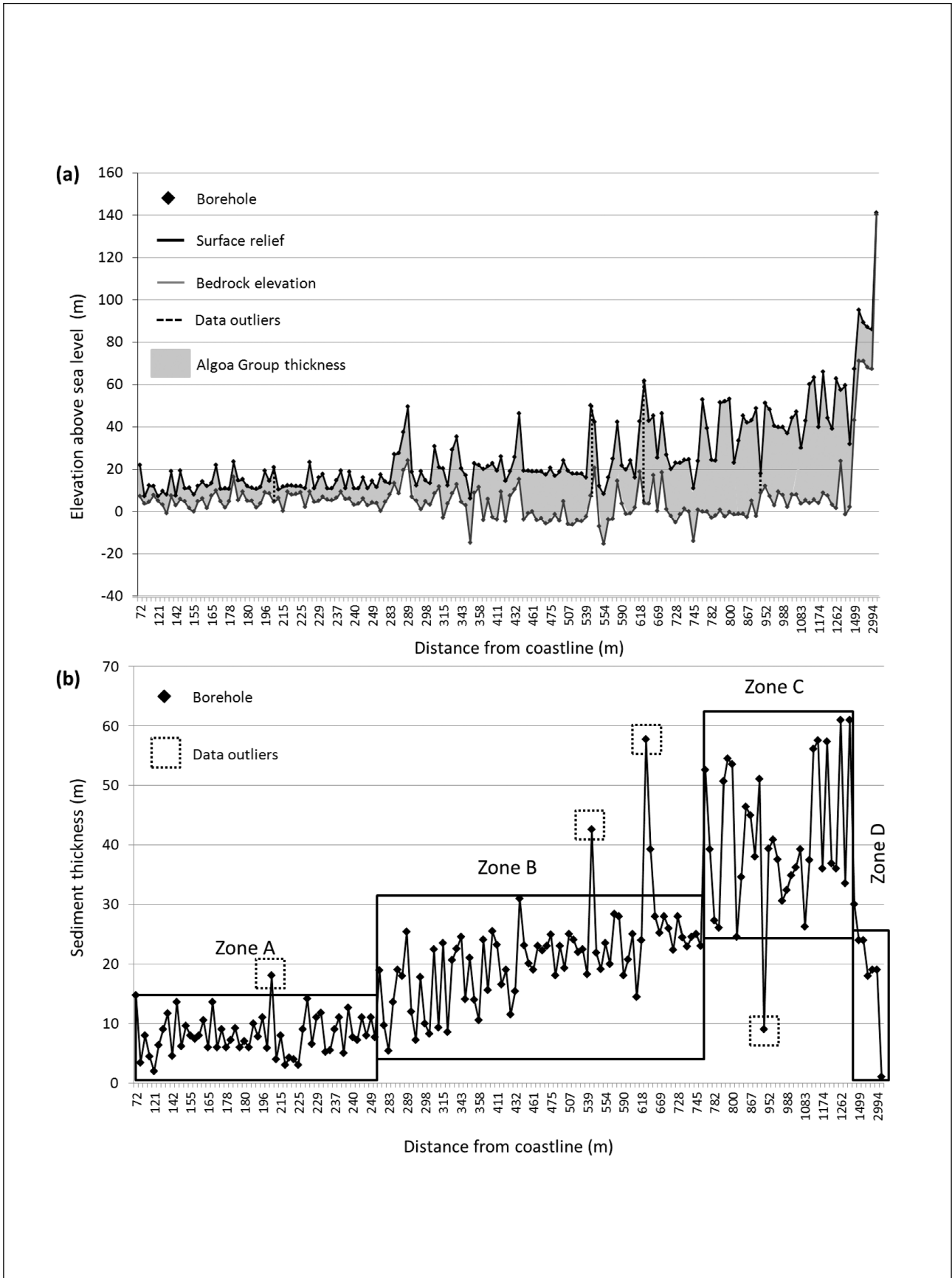
Figure 4. (**a**) *Individual borehole surface relief and bedrock elevation in the vicinities of Thyspunt plot against their distance from the shoreline.* (**b**) *Individual borehole thicknesses of the Algoa Group in the vicinity of Thyspunt plot against their distance away from the coastal margin. Four thickness zones, A to D, can be identified.*
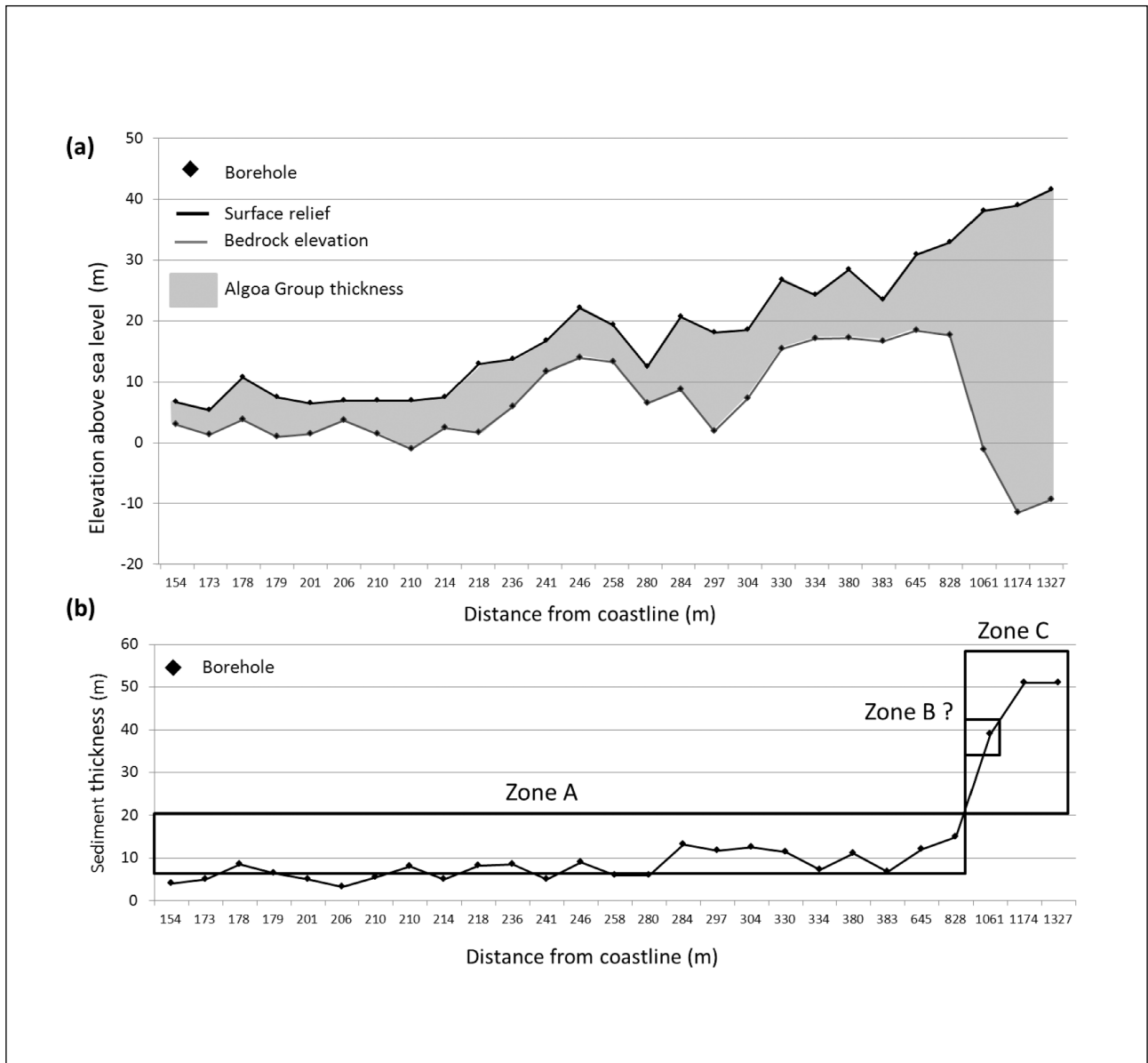
Figure 5. (***a***) *Individual borehole surface relief and bedrock elevation in the vicinity of De Hoek and Cape St. Francis plot against their distance from the shoreline.* (***b***) *Individual borehole thicknesses of the Algoa Group in the vicinity of De Hoek and Cape St. Francis plot against their distance away from the coastal margin. Thickness zone A and C can be identified.*

Cape St. Francis is 15 m and occurs 828 m from the coastline at the inland boundary of zone A (Figure 5 b). In the central part of zone A east of De Hoek, a maximum thickness of 13 m for the Algoa Group sediments (Figure 5 b) is recorded.

At St. Francis zone A has extreme thicknesses of up to 22 m and more frequently sediment accretion values that exceed 10 m (Figure 6 b). Zone A is less clearly defined at St. Francis compared to the Thyspunt, De Hoek and Cape St. Francis areas. Here a greater range in the sediment thickness values are observed than those that would normally define zone A (Figure 6 b). Zone A accretion values at Thyspunt and the combined areas of De Hoek and Cape St. Francis are below 15 m, with a clear transition to thicker accretion values marking the end of zone A (Figures 4 b and 5 b).

At St. Francis this clear transition to thicker sediment values is more ambiguous. Rather, zones A and B appear to overlap, which implies that boreholes that occupy zone A will extend inland from the coastal margin for approximately 1500 m (Figure 3). A transition zone where accretion values of zone A and B are shared (Figures 3 and 6 b), is supported by the lack of borehole data for the area 1 km parallel to the coastal margin (the area that would more clearly define zone A).

Zone B
Algoa Group sediments that occupy the area defined by zone B show an increase in thickness compared to zone A. Cenozoic deposits more frequently exceed 10 m within zone B and typically range between 12 to 26 m in thickness (Figures 4 b and 6 b).

At Thyspunt zone B is defined as a 500 m wide zone that occurs inland between ~250 and ~750 m from the shoreline (Figures 3 and 7). Algoa Group sediments located towards the southern portions of zone B are underlain by the Skurweberg Formation (Figure 3 and Figure 7). Sediments that occupy the northern regions of zone B are underlain by the Goudini Formation (Figure 7). An increase in both bedrock elevation and surface relief is observed in zone B. (Figure 4 a), however bedrock elevations, unlike zone A, are also frequently below sea level. This variation in bedrock elevation compared to zone A, is accompanied by an increase in surface relief (Figure 4 a). Cenozoic sediment thicknesses occasionally surpassing 30 m and rarely 50 m, are documented at Thyspunt (Figures 4 b and 7). Extreme 50 m thickness value outliers occur

between ~450 and ~640 m north of coastal margins (Figure 4 b).

In the vicinity of De Hoek and Cape St. Francis zone B appears absent (Figure 5 b). At Thyspunt, the inception of zone B is marked by a clear progression from zone A values (3 to 12 m typical thickness range) into thicker accretion values (12 to 26 m typical thickness) (Figure 4 b). A similar progression could not be recognized at De Hoek and Cape St. Francis (Figure 5 b). Rather a clear transition from zone A accretion values into much thicker sediment values that more closely resemble those associated with zone C is observed (Figures 5 b, 9 and 10). The area may either be devoid of sediment thicknesses associated with zone B or simply contain insufficient borehole data representative of zone B.
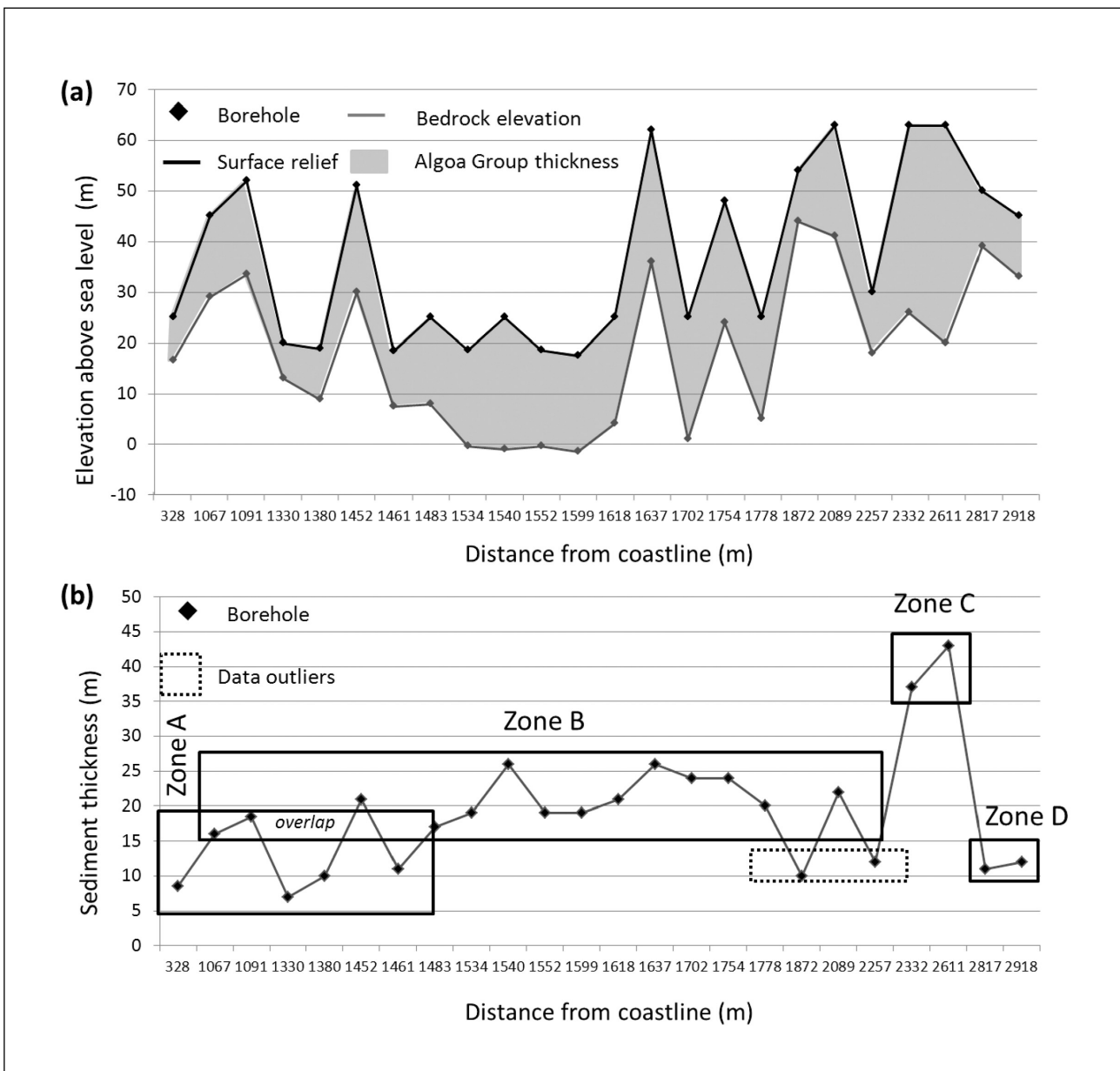
Figure 6. (*a*) *Individual borehole thicknesses of the Algoa Group in the vicinity of St. Francis plot against their distance from the shoreline.* (*b*) *Thickness zones A - D are primarily identified, with a interpreted overlap between zone A and B.*
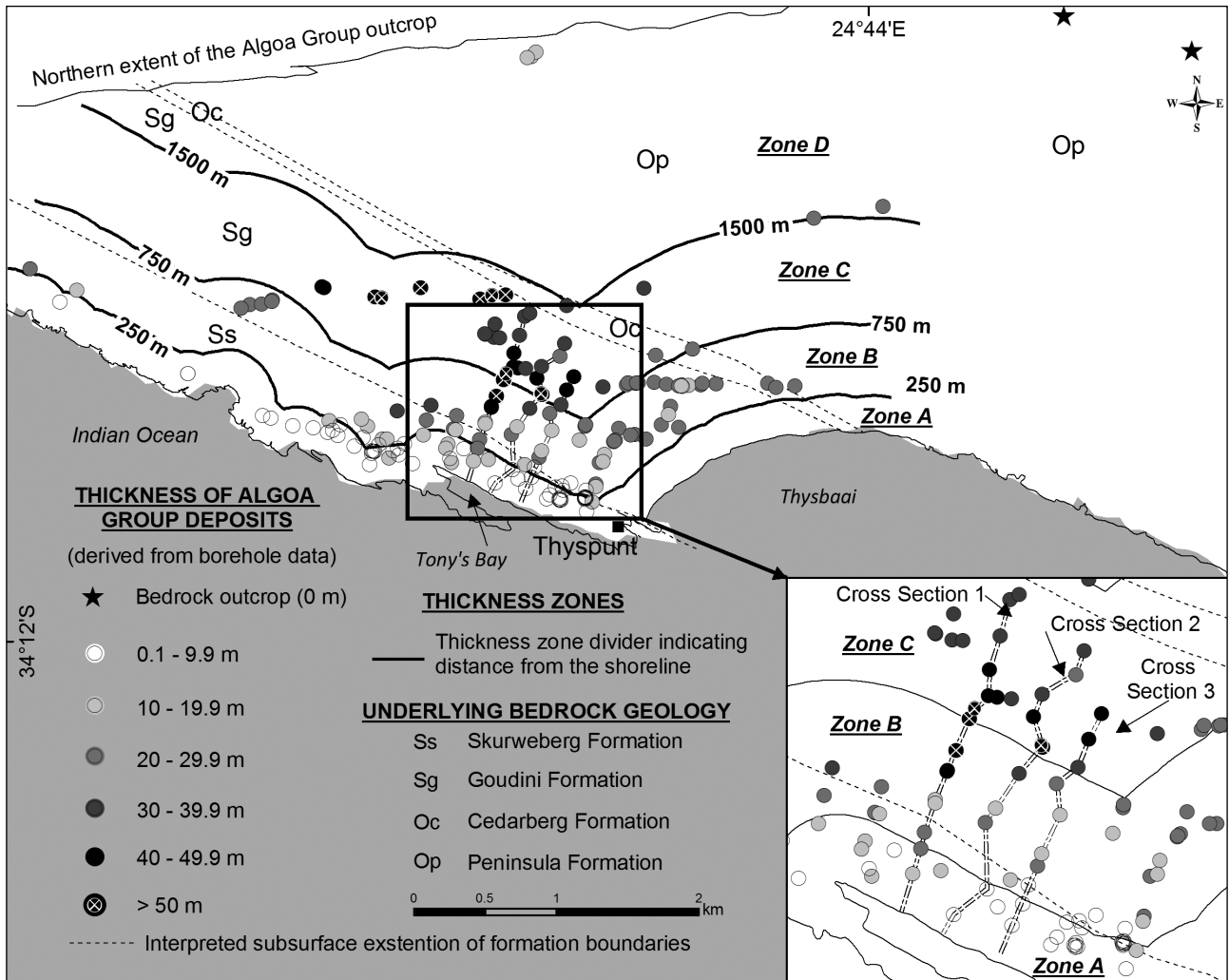
Figure 7. *The distribution of Algoa Group sediment thickness from borehole data in the southern Thyspunt vicinity. The location of cross sections 1, 2 and 3 are also indicated.*

Although zone B is identified at St. Francis, its southern extent is not as well defined compared to Thyspunt. This is due to a perceived overlap between zone A and zone B (Figure 3). Therefore at St. Francis zone B is defined as a broad ~800 to ~1200 m zone parallel to the coastal margin that extends into the hinterland between ~1050/1480 to ~2250 m from the shoreline (Figure 3). At St. Francis Cenozoic sediment thicknesses frequently surpass 15 m and occasionally surpass 25 m (Figure 6). A few boreholes record sediment thickness outliers of below 10 m (Figure 6 b). Algoa Group deposits that occupy zone B are underlain by rocks of the Table Mountain Group and Bokkeveld Group at St. Francis (Figure 3). A complementary relationship is observed between bedrock elevation and surface relief. A rise in borehole bedrock elevation is coupled by an increase in surface relief and vice versa (Figure 6 a).

Zone C
Boreholes that occupy the area defined by zone C (Figure 3) show a significant increase in the thickness of

Cenozoic sediments compared to zones A and B (Figures 4 b, 5 b and 6 b). Zone C is characterized by accretion values that frequently exceed 30 m. (Figures 4 b, 5 b and 6 b).

At Thyspunt zone C is defined as a 750 m wide inland zone that occurs between ~750 to ~1500 m from the coastline (Figure 3 and Figure 7). Cenozoic sediments that occupy zone C are underlain by the lithologically incompetent Goudini and Cedarberg Formations. Here bedrock elevations for boreholes that occupy zone C are generally below 10 m amsl and frequently below sea level (Figures 4 b, 8 a, b and c). Borehole elevations indicate that surface relief often exceed 40 m (Figure 4 a). Viewed overall, a slight decrease in borehole bedrock elevations are observed compared to zone B. This slight decline in bedrock elevation is accompanied by an increase in surface relief (Figure 4 a). The Algoa Group reaches its maximum recorded thickness of 61 m ~1200 m from the coastline at Thyspunt (Figures 4 b and 8 a).

Near Cape St. Francis Cenozoic deposits that occupy zone C are underlain by the Cedarberg and Goudini
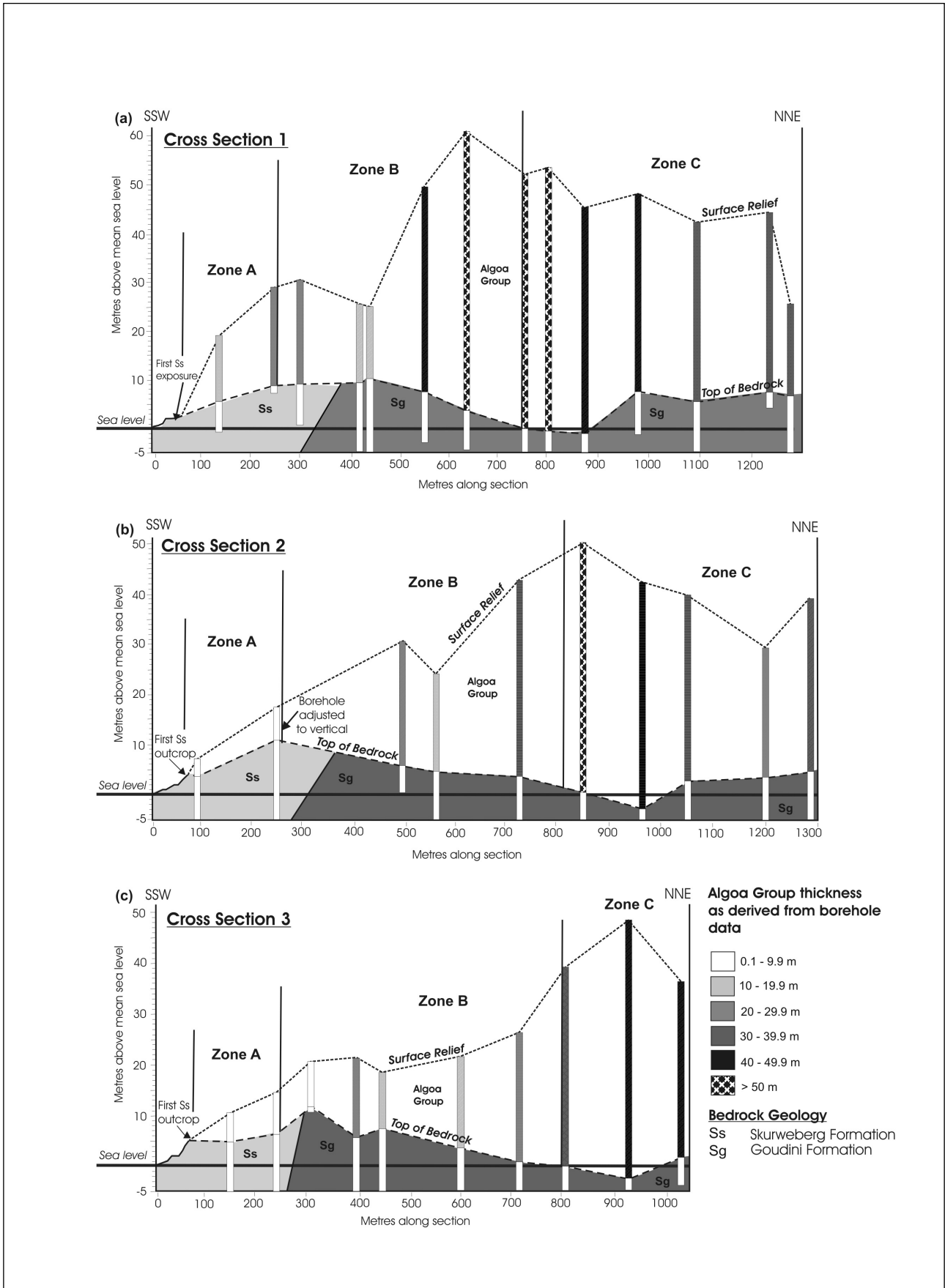
Figure 8. *Cross sections 1, 2 and 3. See figure 10 for location of these cross sections at Thyspunt. Areas where boreholes indicate the greatest thickness occurrences of the Algoa Group coincide with bedrock lows and surface elevation highs.*
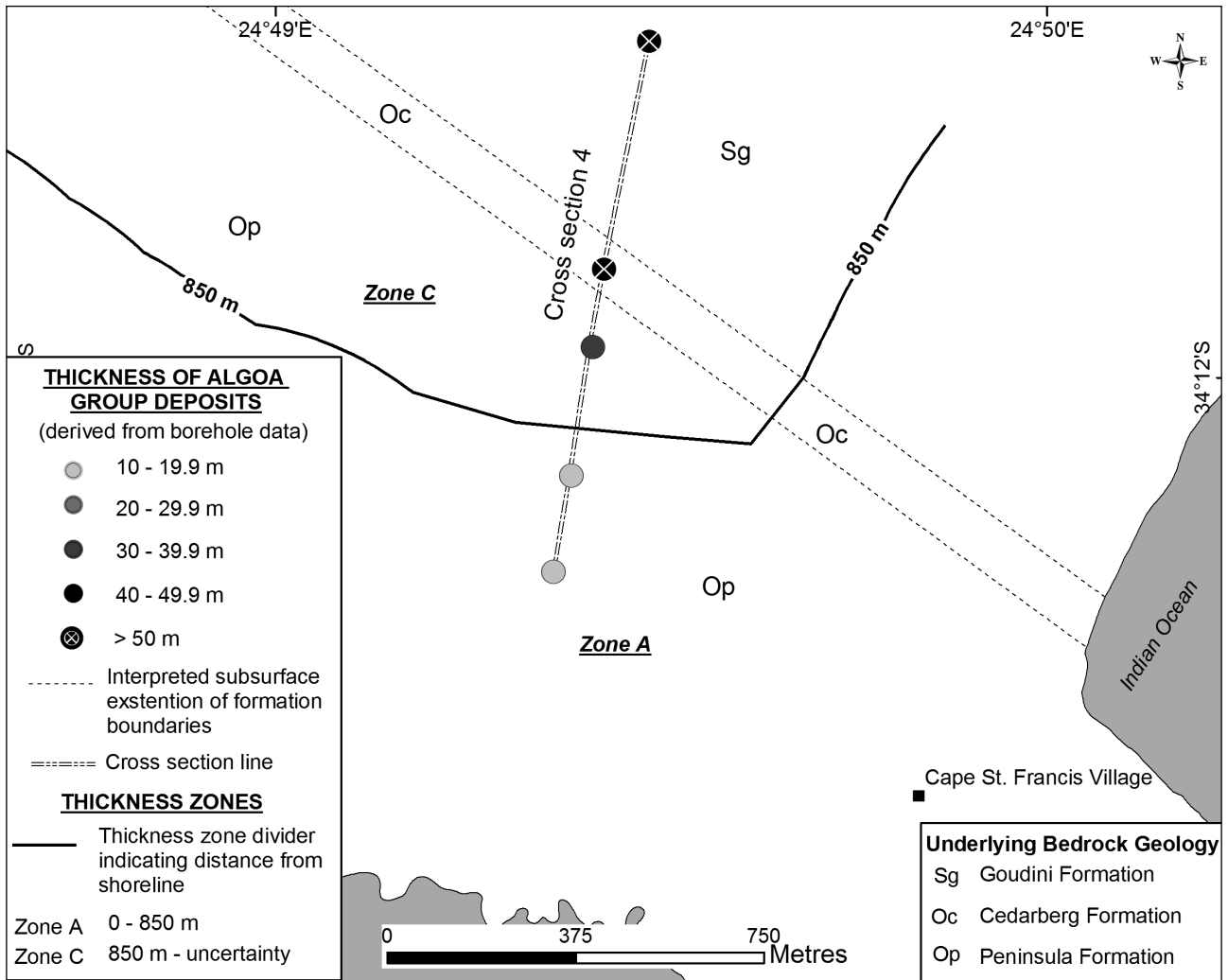
Figure 9. *The distribution of Algoa Group sediment thickness from borehole data in the Cape St. Francis area. Thickness zones A to C are identified. The location of cross section 4 is also indicated.*

Formations (Figure 9). With zone B absent here (as discussed in the section considering zone B), a sharp increase in the surface relief is observed at the transition from zone A to C (Figure 5 a). Similar to Thyspunt, this rise in surface relief is also coupled with a decrease in the bedrock elevation (Figures 4 a and 5 a). At Cape St. Francis borehole bedrock recordings are documented to occur below sea-level by as much as 11 m (Figures 5 a and 10). Peak accretion values of 51 m are encountered (Figure 3) at two localities ~1150 m and ~1350 m from the shoreline at Cape St. Francis (Figures 5 b, 9 and 10).

The maximum recorded thickness of cover sediments associated with zone C in the vicinity of St. Francis is relatively lower than Thyspunt and Cape St. Francis (Figures 4 b, 5 b and 6 b). Here deposits reach a peak thickness of 43 m at ~2600 m from the coastline (Figure 6 b). The location of zone C is defined (based on limited borehole data) as a very narrow ~300 m wide area that extends between ~ 2300 and ~2600 m inland from the coastline (Figure 3). Boreholes that occupy zone C in the St. Francis area are exclusively underlain by the Goudini Formation (Figure 3).

Zone D

Cover sediments occupying zone D, show a significant decrease in thickness compared to zone C (Figure 4 b and Figure 6 b). The transition to zone D is marked by the dramatic decline from peak sediment thickness values to thinner accretion values that range between 0 to 25 m (Figures 4 b and 6 b). Deposits occurring within zone D more closely resemble the thickness values of predominantly zone A and occasionally those of zone B.

At Thyspunt, zone D is situated ~1500 m inland, extending further into the hinterland towards the northern extent of the Algoa Group (Figures 3 and 6 b). Boreholes that occupy zone D are exclusively underlain by the Peninsula Formation. High bedrock elevation values are coupled with prominent surface relief (Figure 6 a). Here sediment thicknesses frequently range between 0 to 25 m (Figures 3 and 6 b). Isolated bedrock exposures are documented northeast of St. Francis (Goedhart et al., 2008) within zone D (Figure 3).

At St. Francis, the inception of zone D is situated further inland (Figure 3 and Figure 6 b). Here zone D is

defined only with limited borehole data, but can be described as occurring ~2800 m inland towards the northern extent of the Algoa Group (Figure 3 and Figure 6 b). Here the boreholes that occupy zone D exclusively intercept Skurweberg Formation bedrock (Figure 3). Sediment thicknesses are below 15 m at St. Francis (Figure 6 b). Limited data does not allow characterization of zone D at De Hoek and Cape St. Francis.

Basal gravel thickness of the Algoa Group

A total of 117 boreholes contained basal gravels directly above bedrock. These gravel deposits are stratigraphically correlative with either the basal unit of the Alexandria Formation or the Salnova Formation (Roberts et al., 2006; Hanson et al., 2012a). Within the study area, the gravel unit is composed of highly calcareous light grey to yellowish grey, medium- to fine-grained, and moderately to well-sorted sands containing imbricated, disc- to roller-shaped, pebble to cobble-size clasts and often shell fragments (Figures 11 and 12). Certain well described borehole log descriptions did allow for partially differentiation of the Algoa Group close to the coastline near Thyspunt (see the generalized scheme in Figure 11). Gravels within the study area are not laterally persistent and spatially show great thickness variation. The occurrence and thickness of basal gravels are indicated in Figures 13 a and b. No clear thickness distribution pattern for basal gravels could be established in terms of their location relative to the coastal margin. In addition no correlation between the thickness of basal gravels and the elevation of the

bedrock surface upon which they were deposited could be established. Borehole data does however indicate that basal gravels were more frequently encountered and are thicker in areas underlain by the Goudini Formation, Cedarberg Formations and the undifferentiated Bokkeveld Group and less frequently in areas underlain by the Skurweberg- and Peninsula Formation (Figures 13 a and b, Figure 14). The typical thickness range for basal gravels is calculated between 0.5 m and 5 m, with occasional 5 to 10 m thicknesses. The thickest gravel layer recorded within the study area is 19 m and occurs at Cape St. Francis, where gravels are underlain by Peninsula Formation (Figure 14). The maximum thickness of basal gravels recorded at Thyspunt, is 11.5 m ~1.5 km northwest of Tony's Bay where gravels are underlain by Goudini Formation bedrock.

Discussion

Results indicate a clear trend in thickness distribution for the Algoa Group sediments between Oyster Bay and St. Francis (Figure 3, Figure 4 b, Figure, 5 b and Figure 6 b). Thickness trends are observed in what appears to be a coast-parallel trending zonation. Two initial zones; zone A and B, characterized by a general trend of increasing thickness with increasing distance from coastal margins occur in the first few hundred metres. Zone A, the zone closest to the coastal margin records the lowest sediment thickness. This progressive trend escalates further inland to reach zone C, a zone of peak thickness values in areas where sediment is underlain by incompetent, argillaceous
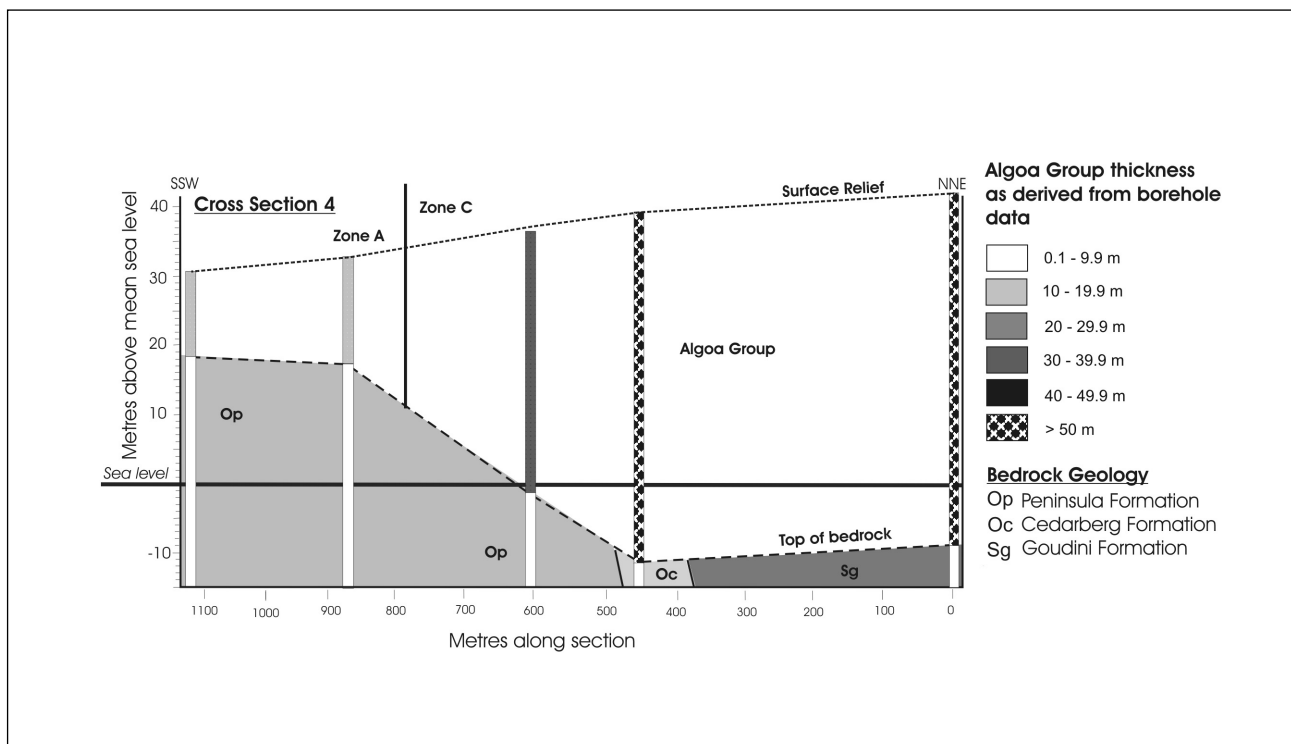
Figure 10. *Cross section 4. See figure 12 for the location of this cross section at Cape St. Francis. Areas where boreholes indicate the greatest thickness occurrences of the Algoa Group coincide with bedrock lows and surface elevation highs.*
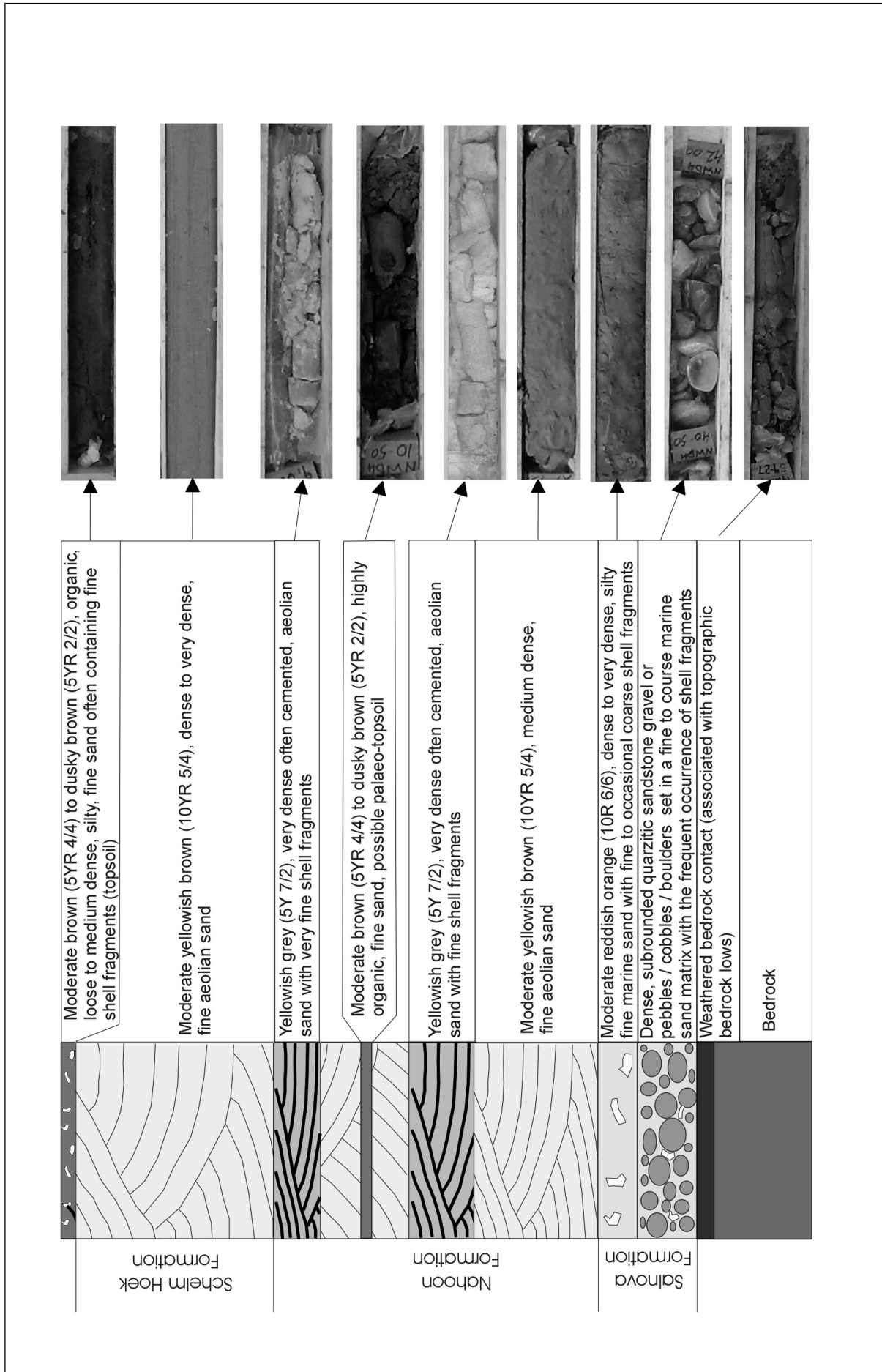
Figure 11. *Schematic of the typical lithostratigraphic sequence of the Algoa Group in close proximity to the coastline near Tbyspunt.*
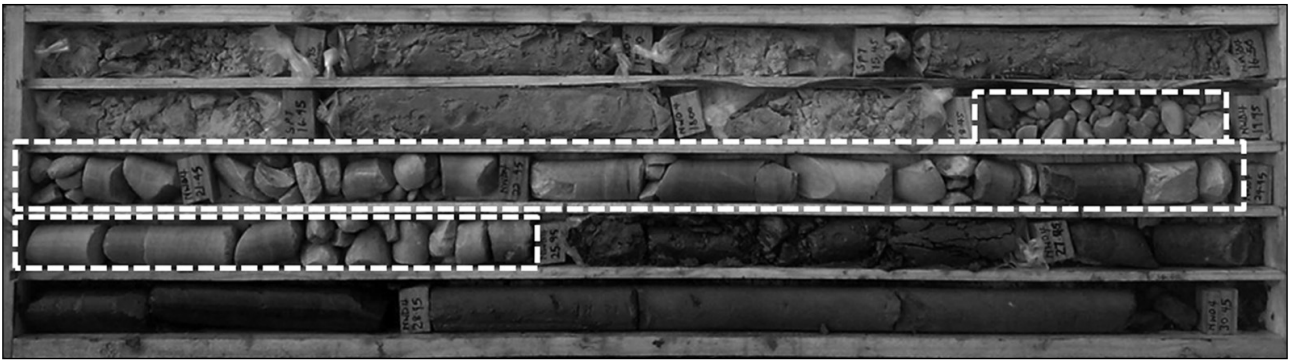
Figure 12. *The Miocene to early Pliocene Alexandria Formation or early Quaternary Salnova Formation basal gravels (highlighted in white) composed of imbricated, disc- to roller-shaped clasts of pebble to cobble size set in a fine- to medium-grained sandy matrix observed in borehole core (Hanson et al., 2012) (34°11 08.3 S, 24°42 32.4 E) between 13.50 m and 30.49 m below ground level.*

lithologies of the Goudini and Cederberg Formation, only to peter out to a zone of lower thickness values near northern outcrop boundaries (Figure 3).

Between Oyster Bay and St. Francis results indicate that the distribution of thickness values for the Algoa Group is influenced by a combination of the following factors:

Bedrock nature and bedrock elevation

The prominent headlands and embayments that make up the coastline morphology of the study area; is in part the consequence of the variation in the competency of lithological units that comprise the bedrock geology and the process of differential weathering. The prominent Seal Point, Cape St. Francis, Thyspunt headland and surrounding northwest-southeast trending straight and rocky coastlines are the result of the lithologically competent quartzitic bedrock units of the Skurweberg and Peninsula Formations. In contrast the development of the Thysbaai embayment is the consequence of the lithological incompetence of thinly bedded sandstones, shales, and mudstones that comprise the Goudini and Cedarberg Formations. North of St. Francis, the coastline exhibits a southwest-northeast trending, southeast facing undulating coastal embayment underlain by the lithologically incompetent argillaceous units of the Bokkeveld Group and Baviaanskloof Formation. An incompetent fine grained, bioturbated sandstone unit within the Skurweberg Formation west of Thyspunt allowed for the development of an elongated northwest-southeast trending embayment known as Tony's Bay. This variation in the competency of bedrock lithologies and the processes of differential weathering that led to the formation of alternating headlands and embayments along the present day coastline would also have been active in an ancedent landscape prior to the deposition of the Algoa Group. Differential weathering would have produced an uneven palaeo-landscape relief with topographic highs and depressions allowing for variation in the way the accretion of sediments took place. Topographic highs would facilitate a lower accretion of sediments than surrounding topographic lows.

At Thyspunt thicker Algoa Group deposits (including thicker basal gravels) are more frequently underlain by incompetent lithologies of the Goudini and Cedarberg Formation (Figure 7, Figure 10 and Figure 14). Cenozoic deposits underlain by these formations (associated with northern regions of zones B and zone C) are generally 20m to 60 m in thickness (Figure 4 b). Thinner Cenozoic deposits (>20 m) identified within zones A and D, reflect regions within the study area where Cenozoic deposits are underlain by relatively elevated bedrock relief, associated with the more erosion resistant Peninsula and Skurweberg Formations (Figures 3 and 14).

Within the area occupied by zone C, where peak accretions values occur, bedrock elevations are often below sea level (Figures 4 a and 8 a, b and c). Towards the western side of Thysbaai, borehole bedrock elevations of -6 m to as low as -15 m below sea level, towards the eastern extent of Thysbaai are documented. Hanson et al. (2012a) associated the low bedrock elevations with the presence of a possible palaeo-channel or palaeo-valley that shares a similar trend to the Thysbaai embayment and other surrounding modern day drainage systems such as the Klipdrift and Krom rivers. Further evidence supporting the presence of a palaeo-channel is provided by associated borehole logs overlapping the depression (Hanson et al., 2012; Engelsman and Constable, 2012) that indicate the presence of fluvial deposits above bedrock.

Hanson et al., (2012) also proposed the presence of a comparable inland palaeovalley, possibly striking northwest to southeast near Cape St. Francis based on an abrupt fall in bedrock elevations to -11.52 m and -9.44 m below sea-level (Figure 10). Here too the presence of similar lithologically incompetent bedrock would facilitate a greater degree of erosion than surrounding arenaceous bedrock within the palaeoland-scape. At Cape St. Francis the peak accretion value (51 m) documented to occur in zone C (Figure 5 b), is mainly due to the presence of this palaeo-valley cut into argillaceous bedrock (Hanson et al., 2012). Although a steady rise in surface relief occurs transitioning from zone B to C, this represents only a small component of
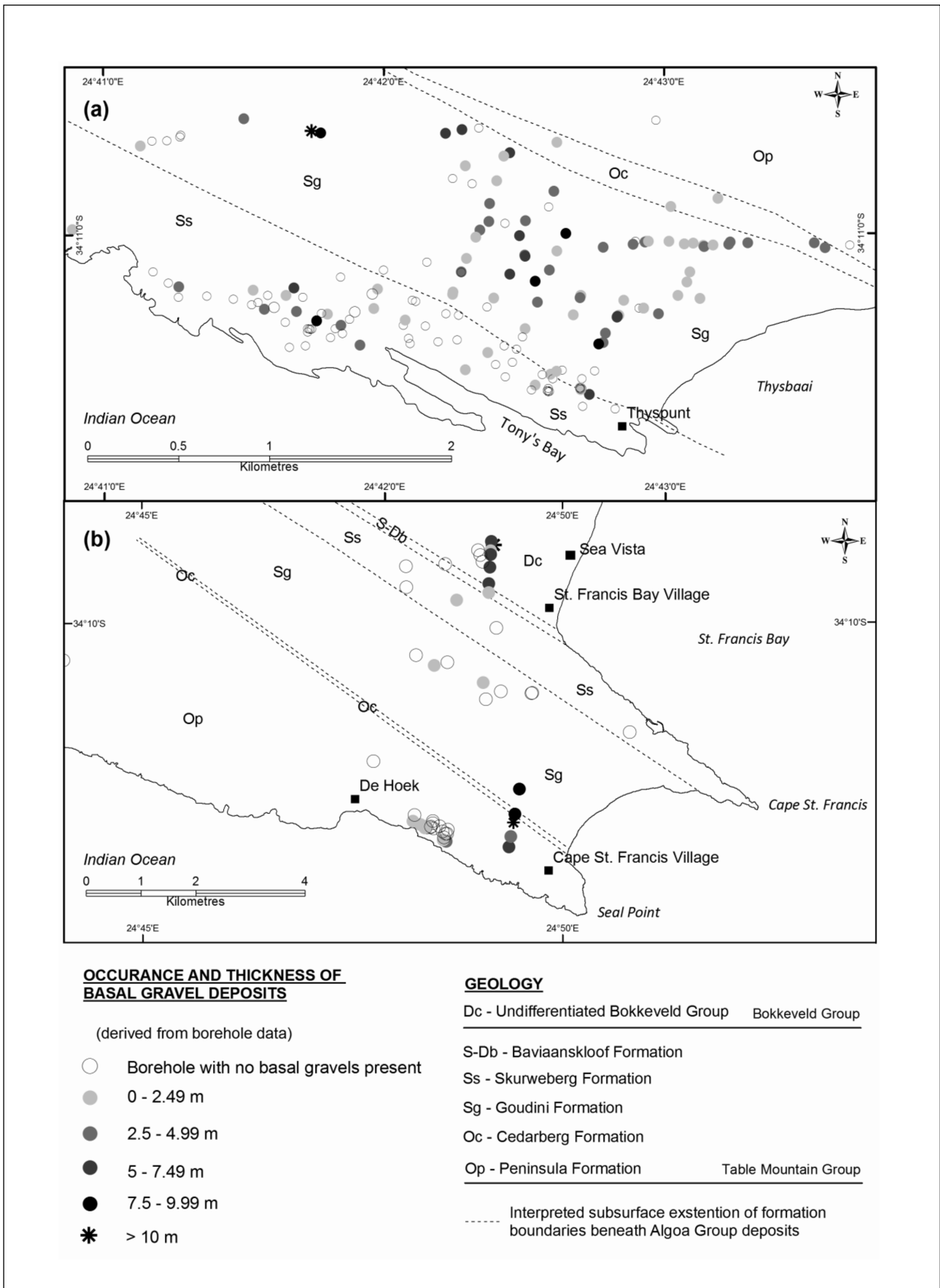
Figure 13. (**a**) Distribution of the Algoa Group basal gravel deposits at Thyspunt and (**b**) greater Cape St. Francis areas as derived from borehole data (Raubenheimer et al., 1988a, 1988b; Hanson et al., 2012a; Engelsman and Constable, 2012).

the overall thickness increase. Instead, it is the extreme decrease in bedrock elevation that primarily facilitates these peak values (Figures 5 a and b). In areas like zone C where prominent bedrock lows occur with elevated surface (dune crests), greater accretion of Algoa Group sediments are present (Figures 8 a, d and c and 10).

A greater accretion of basal gravels are also recognized within both of these palaeovalley areas (Figures 13 a and b). However no direct correlation between the thickness of basal gravels and the bedrock elevation height upon which they were deposited could be recognized.

Near St. Francs boreholes occupying incompetent bedrock of the argillaceous undifferentiated Bokkeveld Group, show lower Algoa Group thicknesses than comparable less erosion resistant bedrock units of the Goudini and Cedarberg Formations at Thyspunt and Cape St. Francis (Figures 4 b, 5 b and 6 b). At St. Francis lower accretion values can be attributed to a complementary relationship between bedrock elevation and surface relief. A rise in borehole bedrock elevation is coupled by an increase in surface relief and vice versa (Figure 6 a). Bedrock also appears to be slightly higher in boreholes within the St Francis vicinity, with no bedrock elevation below -1 m amsl or palaeovalley interpretation (Figure 6 a).

Localized erosion pockets or bedrock peaks within the setting of the ancedent landscape, may be responsible locally for slightly thicker or thinner deposits within a particular thickness zone. This is the case with data outliers documented in the study area (Figures 4 a
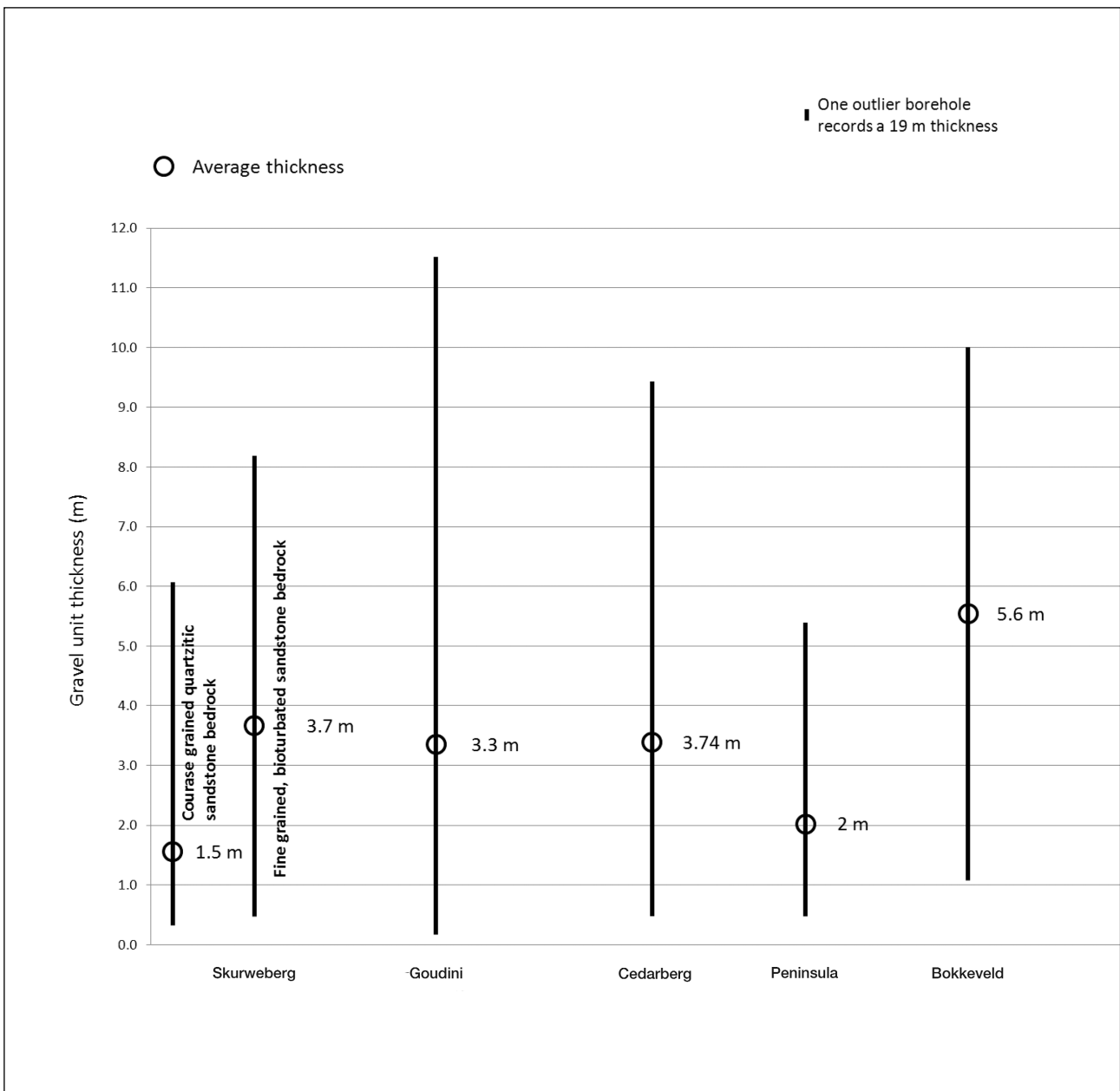
Figure 14. *The formation specific thickness range and average of basal deposits of the Algoa Group within the study area.*

and b and 8 a, b and c). The development of these localized erosion pockets may be influenced by the presence of a slightly less erosion resistant unit within a particular formation. Such a less erosion resistant, fine grained, bioturbated sandstone unit west of Thyspunt allowed for the development of the elongated northwest-southeast trending embayment known as Tony's Bay. If this unit continues along its trend inland beneath Cenozoic cover, it explains the concentration of boreholes with thicker basal gravels in that area (Figures 13 a and 14).

Another factor that may influence the development of bedrock lows, are zones of structural weakness. Shatter zones like those identified along coastal exposures by Raubenheimer et al., (1988a; 1988b) and Goedhart et al., (2008) would be more susceptible to erosion in the antecedent landscape and locally possibly produced lower bedrock relief and ultimately facilitating greater sediment accretion. The location and extent of these shatter zones is however difficult to predict beneath Cenozoic cover.

Surface relief and sediment supply

A steady progression of increasing surface elevation is observed from coastal margins into the interior (Figures 4 a, 5 a and 6 a). The portion of the study area blanketed by Cenozoic dune cover is characterized by undulating topography; a consequence of alternating east-west trending dune crests and troughs (Figures 2 a to d). Locally areas with higher elevation associated with dune crests would have greater accretion of sediments compared to surrounding areas where lower surface relief occur such as dune depressions or troughs. The more dominant role surface relief plays in affecting accretion values are clearly observed at Thyspunt. Here the transition from thicker accretion values (zone A to B) is facilitated mainly by a rise in surface relief and only a marginally lower bedrock elevation (Figures 4 a and b and 8 a and b).

It appears unlikely that elevation can be the sole factor influencing accretion values. At Thyspunt extreme thickness outliers occurring within zone B between ~550 and ~640 m north of the coastline, mark the edge of the interpreted palaeo-valley at Thyspunt (Hanson et al., 2012a) incised into the underlying lithologically less erosion resistant Goudini Formation. The topographic depression within the palaeolandscape coupled with a more elevated surface relief, allows for greater accretion of sediments (Figures 4 a, b, 8 a, b and c). Surface relief and distribution of dune heights are influenced by sand supply, wind regime and bedrock topography (Burkinshaw, 1998). Surface relief and dune heights show greater elevation towards the northwestern sections of the study area (Figures 2 a to d). This area is located close to the area's upwind sand supply source, Slangbaai (Figure 1). An overall decrease in surface relief and dune heights is observed downwind due to a lower rate of sand supply further east towards St. Francis (Burkinshaw, 1998). Locally sand supply is also influenced by the northwest-southeast trending Cape St. Francis anticline, the core of which produces a quartzitic (Peninsula Formation) bedrock ridge over much of the central portions of the study area (Figure 1). The ridge would impede sediment transfer to the east and result in a concentration of dune mass in the northwestern areas along the western limb of the anticline where bedrock topography is lower. In addition the northeastern regions of the St. Francis area, are located downwind of the west-east migrating dune field, towards the distal end of the sediment source. At St. Francis the accretion of sediment is less compared to Thyspunt, which is located closer to its sediment source. Along the northern edge of the Algoa Group outcrop along the eastern limb of the Cape St. Francis anticline, prevailing west westsouthwest winds have already exposed the Peninsula Formation in two localities (Figure 3).

The variation in sediment accretion would have been influenced by factors such as climate change, involving change in sea level and variation in sediment discharge, or tectonic and isostatic processes that may have modified coastal gradients (Burkinshaw, 1998). Although this study does not directly focus on these aspects, they cannot be ignored. Evidence for the marine isotope stage 11 high stand is observed at Mossel Bay (Roberts, 2006; Roberts et al. 2009; Jacobs et al; 2011; Roberts et al; 2012) where Roberts et al. (2012) estimated eustatic sea level during marine isotope stage 11 at +13 ± 2 m above modern sea-level. The last intergacial sea-level associated with marine isotope stage 5e was most likely between 6 and 8.5 m above current sea-level (Carr et al., 2010). Substantial reworking of aeolianite and dune deposits which occurred during the Holocene highstand, the last interglacial and continues at present, eludes to the combined role that sea-level change and bedrock topography can play in creating accommodation space for accretion. At Thyspunt, bedrock elevation typically ranges from 3 to 9 m above sea-level within zone A. The reduced thickness of sediments (3 to 12 m) within Zone A could partly be a function of the limited time available for sediment accretion since the last major highstand (marine isotope stage 5e) and/or the reduced likelihood of preservation throughout the majority of the Middle to late Pleistocene as a result of limited sediment supply. More detailed investigation, not part of the scope for this study, is required to define the role of sea-level change in accretion of sediments within these zones.

matter of this paper. Reviews by Professor Jay Barton and an anonymous helped to improve this paper and are greatly appreciated.

References

Anderson, N.J.B., Muller, J.A. and Faurie, J.N., 1986. A geological interpretation of the detailed aeromagnetic survey carried out south of Humansdorp, Eskom Eastern Cape project investigations for the siting of nuclear power stations, progress report no.9, Department of Geotechnology AEC, PIN-937 (b/R) GEA 671. Pretoria, 13pp (Confidential)

Bate, K.J. and Malan, J.A., 1992. Tectonostratigraphic evolution of the Algoa, Gamtoos and Pletmos Basins, offshore South Africa. In: M.J. De Wit and I.G.D. Ransome (Editors). Inversion tectonics of the Cape Fold Belt, Karoo and Cretaceous Basins of Southern Africa. Balkema, Rotterdam, 61-73.

Bateman, M.D., Carr, A.S., Dunajko, A.C., Holmes, P.J., Roberts, D.L., McLaren, S.J., Bryant, R.G., Marker, M.E. and Murray-Wallace, C.V., 2011. The evolution of coastal barrier systems: A case study of the Middle-Late Pleistocene Wilderness barriers, South Africa, Quaternary Science Reviews, 30, 63-81.

Bierman, P.R., 2012. Report #1 Cosmogenic Geochronology, Southern Africa Fault Corridor Investigation, Appendix B.3 in Hanson, K., Slack, C. and Coppersmith, R., Thyspunt Geological Investigations-Kango Fault Study, Council of Geoscience Report Number 2012-0035 Rev. 0, 126pp (Confidential).

Burkinshaw, J., 1998. Morphodynamics of headland bypass dunefields with special reference to the Cape St. Francis headland, Eastern Cape, South Africa, unpublished PhD. Thesis, University of Port Elizabeth, South Africa, 373pp.

Carr, A.S., Bateman, M.D., Roberts, D.L., Murray-Wallace, C.V., Jacobs, Z. and Holmes, P.J., 2010. The last interglacial sea-level high stand on the southern Cape coastline of South Africa. Quaternary Research, 73, 351-362.

Cole, J. and Cole, P., 2007. Geophysical interpretation of the marine magnetic data collected in the offshore site area (8 km radius) of Thyspunt. CGS Report No 2007-0189, NSIP-NSI-020268#P1-12, 12pp.

Cole, J. and Naudé, C., 2007. Final report: Airborne survey of Thyspunt. CGS Report No. 2007-0006, NSIP-NSI-019039#P1-67, 68pp (Confidential).

De Beer, C.H., 2000. Geology and tectonics of the Thyspunt site, Humansdorp. Internal Council For Geoscience Report to the seismology unit, 21pp.

Engelsman, B. and Constable, B., 2012. Thyspunt Shear Wave Velocity Measurements, Report Number 449376, SRK Consulting Ltd, 16pp (Confidential).

Goedhart, M.L., Reddering, J.S.V., Kilian, D., Mitha, V., Bosch, P.J.A. and Black, D., 2008. Surface Geology and Update of Onland Geological Hazards for the 40 km Site Vicinity and 8 km Site Area Around the Proposed Thyspunt Nuclear Power Plant, Eastern Cape, South Africa. Council for Geoscience, Pretoria, Report No. 2008-0222, 218pp.

Hälbich, I.W., 1983. A tectonogenesis of the Cape Fold Belt. In: Geodynamics of the Cape Fold Belt, A.P.G. Sönghe and I.W. Hälbich (Editors), Geological Society of South Africa, Special Publication, 12, 165-175

Hanson, K.L., Coppersmith, R., Glaser, L., Roberts, D.L., Claassen, D., and Black, D.E., 2012. Thyspunt Geological Investigations – Marine Terrace Studies, Report No. 2012-0034, Council for Geoscience, Pretoria, 111pp (Confidential).

Illenberger, W.K., 1992. Lithostratigraphy of the Schelm Hoek Formation (Algoa Group). South African Committee for Stratigraphy (SACS), Lithostratigraphic Series, 21, 7pp.

Illenberger, W.K., 1996. The geomorphologic evolution of the Wilderness dune cordons, South Africa, Quaternary International 33, 11-20.

Illenberger, W.K. and Rust, I.C., 1988. A sand budget for the Alexandria coastal dunefield, South Africa. Sedimentology, 35, 513-521.

Illenberger, W., Rust, I. and Vogel, J.C., 1997. Luminescence Dating of Coastal Dunes of the Southern Cape. Abstract, XIII SASQUA, Biennial Conference. Rhodes University, Grahamstown, 6-7.

Illenberger, W. and Burkinshaw, J., 2007 (update of December 2001 report). The Cape St. Francis headland bypass dune system and beach erosion at St. Francis Bay, and sediment accumulation in the Kromme Estuary,

description for Heritage Center, December 2001, Illenberger and Associates, 6pp.

Illenberger, W.K.I. and Burkinshaw, J.R., 2008. Coastal dunes and dunefields, In: C.A., Lewis (Editor), Geomorphology of the Eastern Cape, NISC Publishing, Grahamstown. South Africa, 85-106.

Jacobs, Z., Roberts and D.L., 2009. Last Interglacial Age for aeolian and marine deposits and the Nahoon fossil human footprints, Southeast Coast of South Africa. Quaternary Geochronology, 4, 160-169.

La Cock, G.D. and Burkinshaw, J.R., 1996. Management implications of development resulting in disruption of a headland-bypass dunefield and its associated river, Cape St Francis, South Africa, Landscape and Urban Planning 34, 373-381.

Le Roux, F.G., 1991. Lithostratigraphy of the Salnova Formation. Lithostratigraphic Series, Geological Survey of South Africa 9: 1-14.

Le Roux, F.G., 1990a. Algoa Group. In: M.R. Johnson (Editor), Catalogue of South African Lithostratigraphic Units, 2, 2-1 – 2-2.

Le Roux, F.G., 1987a. Lithostratigraphy of the Alexandria Formation. South African Committee for Stratigraphy (SACS), Lithostratigraphic Series, 1, 1-18.

Le Roux, F.G., 1987b. Palaeontological aspects of Tertiary marine deposits near Port Elizabeth, South African Journal of Science, 83, 508pp.

Le Roux, F.G., 1989. The lithostratigraphy of Cenozoic deposits along the south Cape coast as related to sea level changes, unpublished M.Sc. Thesis, University of Stellenbosch, South Africa, 247pp.

Le Roux, F.G., 1992. Lithostratigraphy of the Nanaga Formation (Algoa Group). South African Committee for Stratigraphy (SACS), Lithostratigraphic Series, 15, 9pp.

Loots, L., Chirenje, E., Claassen, D. and Black D., 2009. A multi-eletrode survey near Cape St. Francis and Thyspunt, Eastern Cape with the position of marine terraces and possible faults buried under Cenozoic cover, Council for Geoscience, Report nr. 2009-0211, Rev0, unpublished, 38pp (Confidential).

Maclear, M., 2002. St Francis Bay Golf Estate: Groundwater development, exploration phase, SRK Consulting, Report nr. 291491/1, 20pp.

Maclear, M., 2005. St. Francis Golf Links: Phase 2, Groundwater Development, SRK Consulting, Report nr. 344065, 17pp.

Maclear, M., 2006. St Francis Golf Links Groundwater Supply, Routine Groundwater Quality Monitoring, SRK Consulting, Port Elizabeth, Project nr. 344065, 5pp.

Maud, R.R., 2008. The macro-geomorphology of the Eastern Cape. In: C.A. Lewis (Editor), Geomorphology of the Eastern Cape, South Africa (Second Edition). NISC Publishing, Grahamstown, South Africa, 1-20.

McLachlan, A., Illenberger, W.K., Burkinshaw, J.R. and Burns, M.E.R., 1994. Management implications of tampering with littoral sand sources, Journal of Coastal Research 12 (Special Issue on Coastal Hazards), 51-59.

Reddering, J.S.V., Rohwer, M.H., Majokweni, M.P. and Roberts, M.P., 2006. Explanation of the geology of the Wild Coast area (1:50 000-scale map sheets) 3129BC Lusikiski, 3129CB Tombo, 3129CC AND CD, Coffee Bay, 3129DA Port St. Johns – publication in progress, Council for Geoscience, Pretoria, 84pp.

Roberts, D.L., 2006. Dating and preliminary correlation of raised marine and estuarine terraces on the western and southern coast of South Africa, Final Report. NSIP-SHA-018230#P1-206, Council for Geoscience, Report No. 2006-0186, 206pp.

Roberts, D.L., Botha, G.A., Maud, R.R. and Pether, J., 2006. Coastal Cenozoic deposits, In: M.R. Johnson, C.R., Anhaeusser and R.J. Thomas, (Editors.). The Geology of South Africa. Geological Society of South Africa/Council for Geoscience, 541-552.

Roberts, D.L., Bateman, M.D., Murray-Wallace, C., Carr, A.S. and Holmes, P.J., 2009. West coast dune plumes: Climate driven contrasts in dunefield morphogenesis along the western and southern South African coasts, Palaeogeography, Palaeoclimatology, Palaeoecology 271, 24-38.

Roberts, D.L., Bateman, M.D., Murray-Wallace, C.V., Carr, A.S. and Holmes, P.J., 2008. Last Interglacial fossil elephant trackways dated by OSL/AAR in coastal aeolianites, Still Bay, South Africa. Palaeogeography Palaeoclimatology Palaeoecology, 257, 261-279.

Roberts, D.L., Karkanas, P., Jacobs, Z., Marean, C.W. and Roberts, R.G., 2012. Melting ice sheets 400,000 yr ago raised sea level by 13 m: Past analogue for future trends. Earth and Planetary Science Letters, 357/358, 226-237

Raubenheimer, E., Hambleton-Jones, B.B. and Toens, P.D., 1988a. Detailed

geology of De Hoek, Thyspunt and Tony's Bay: in two volumes – Investigations for the siting of nuclear power stations, Atomic Energy Corporation of South Africa, Ltd., Department of Geotechnology, Progress Report Number 20, Volume 1 – Geological description. PIN-1072(B/R), GEA 801, NSIP-N002420-≠P1– 190.

Raubenheimer, E., Hambleton-Jones, B.B. and Toens, P.D., 1988b. Detailed geology of De Hoek, Thyspunt and Tony's Bay: in two volumes – Investigations for the siting of nuclear power stations, Atomic Energy Corporation of South Africa, Ltd., Deparetment of Geotechnology, Progress Report Number 20, Volume 2 – Geotechnical maps of De Hoek, Thyspunt and Tony's Bay. PIN-1072(B/R), GEA 801, NSIP-N002420-≠P1– 190.

Rosewarne, P.N., and Lomberg, C.R., 1989. Groundwater resource evaluation at St. Francis, SRK Consulting, Report nr: 171719/3, 36pp.

Stettler, E.H., Zadorozhnaya, V.Y. and Goedhart, M.L., 2008. Results of a Time Domain Electromagnetic Survey Over Four Possible Fault Positions Signifying the Landward Continuation of the Cape St. Francis Fault, Cape St. Francis and Oyster Bay, Eastern Province. Council for Geoscience, Pretoria, Report No. 2008-0171 - Addendum, 30pp (Confidential).

Van Wyk, J.H., 1987. Eskom Eastern Cape Nuclear Siting Project: Geological map of the coastal strip between Tsitsikamma River mouth and Cape St. Francis. Compiled by the Department of Geotechnology, Atomic Energy Corporation of South Africa Ltd.

Zadorozhnaya, V., Eberle, D. and Claassen, D., 2012. Results of a Time Domain Electromagnetic Survey Conducted at Cape St. Francis with the Intent of Locating the Bedrock Surface Buried Beneath Cenozoic Cover, Eastern Cape, South Africa, Council For Geoscience, South Africa, Report No. 2012-0152, Review 0, 15pp.

Editorial handling: E. Bordy.

Access to reports/studies listed as confidential can only be obtained with permission of Eskom.

Appendix A2 - Loots, L., Chirenje, E., Claassen, D., and Black D., 2009. A multi-electrode survey near Cape St. Francis and Thyspunt, Eastern Cape with the position of marine terraces and possible faults buried under Cenozoic cover, Council for Geoscience, Report nr. 2009-0211, Rev0.

A multi-electrode resistivity survey near Cape St. Francis and Thyspunt, Eastern Cape with the intent to locate the position of marine terraces and possible faults buried under Cenozoic cover

Compiled by Letticia Loots, Emmanuel Chirenje, Debbie Claassen and Dawn Black

Council of Geoscience
Report Number 2009- 0211
Rev. 0

CONFIDENTIAL

DOCUMENT APPROVAL SHEET

	COUNCIL FOR GEOSCIENCE (Geophysics Unit)		REFERENCE: CGS REPORT 2009 - 0211
			REVISION 0
COPY No.	**A multi-electrode resistivity survey near Cape St. Francis and Thyspunt, Eastern Cape with the intent to locate the position of marine terraces and possible fault positions under Cenozoic cover.**		DATE OF RELEASE: 22 July 2009
			CONFIDENTIAL

AUTHORS			
			ACCEPTED BY:
L. Loots	E. Chirenje		E. Hattingh
EDITED BY:	ACCEPTED BY:	ACCEPTED BY:	AUTHORISED BY:
L. P. Maré	D. Eberle 22/07/2009	P.Cole	G. Graham

REVISION	DESCRIPTION OF REVISION	DATE	MINOR REVISIONS APPROVAL

Executive Summary

A DC multi-electrode direct current resistivity survey was conducted at two sites namely Cape St. Francis which is located in the 40km site vicinity around the proposed nuclear site and Thyspunt which is located in the 8km site area, near the town of Humansdorp, about 100km from Port Elizabeth.

The main objective of the survey was to acquire new data that would be integrated with the ever expanding database of geological information so as to highlight any new geological features that may influence the existing seismic hazard assessment of the proposed nuclear site at Thyspunt.

The objective of these surveys was to:
● Map bedrock depth below the Aeolian sands with the intent to locate the positions of   marine terraces.
● Map discontinuities, such as fractures and faults.
● Try and locate the possible landwards extension of the Cape St. Francis fault.

The datasets used in the integration process include:
● Fugro offshore survey (Fugro, 2007) and TDEM study of the potential on-land extension of the Cape St. Fault
● Airborne and ground geophysical survey (Cole and Naudé, 2007) for the identification of lineaments that may show potential for offset strata
● SRK geotechnical and groundwater borehole data provide accurate location of depth to bedrock for the location of marine terraces.

Results show the stratigraphic sequences, discontinuities/fractures, bedrock elevation and topography.

Table of Contents

Tables

Figures

1. Introduction

Resistivity is a geophysical technique that employs measurements of electrical potential associated with subsurface electrical current flow generated by a DC, or slowly varying AC, source. Factors that affect the measured potential, and thus can be mapped using this method, include the presence and quality of pore fluids and clays and this in turn can be used to map depth of weathering, stratigraphy, and structures such as faults, dykes and fracture zones.

As part of mandatory site investigations for a planned nuclear power station, the Council for Geoscience was tasked by Eskom to conduct multi-electrode resistivity surveys at two sites, namely Cape St. Francis and Thyspunt with the intent to identify bedrock elevation, to locate marine terrace positions, discontinuities such as faults and fractures and the possible on-land extension of the Cape St. Francis fault.

1.1 Site locations and description

Two separate areas were chosen for the resistivity survey. The first area is located near the town of Cape St. Francis (CSF). In this area 5 traverses were chosen for surveying. Start and end co-ordinates of each line are given in Table 1. The location of these traverses is also shown on Figure 1. Lines CSF 2, 3, 4 and 5 is approximately perpendicular to CSF 1 and the coastline, and it is anticipated that they will reveal the positioning of marine terraces buried beneath Aeolian sand cover. Line CSF 1 was chosen with the intent of locating the possible on-land extension of the offshore identified Cape St. Francis fault. This line is perpendicular to the geologic strike direction and runs approximately north-south and would thus possibly intercept the fault line.

Table 1: Locality of resistivity lines

Line	Direction	Latitude (beginning)	Longitude (beginning)	Latitude (end)	Longitude (end)
CSF 1	S-N	34.2041 S	24.8226 E	34.1883 S	24.8256 E
CSF 2	W-E	34.1963 S	24.8335 E	34.1930 S	24.8252 E
CSF 4	W-E	34.2005 S	24.8232 E	34.2010 S	24.8285 E
CSF 5	W-E	34.2029 S	24.8292 E	34.2032 S	24.8239 E
CSF3	W-E	34.1992 S	24.8237 E	34.1998 S	24.8294 E
TS 1	W-E	34.1859 S	24.6882 E	34.1865 S	24.6966 E
TS 3	S-N	34.1847 S	24.7030 E	34.1883 S	24.7039 E
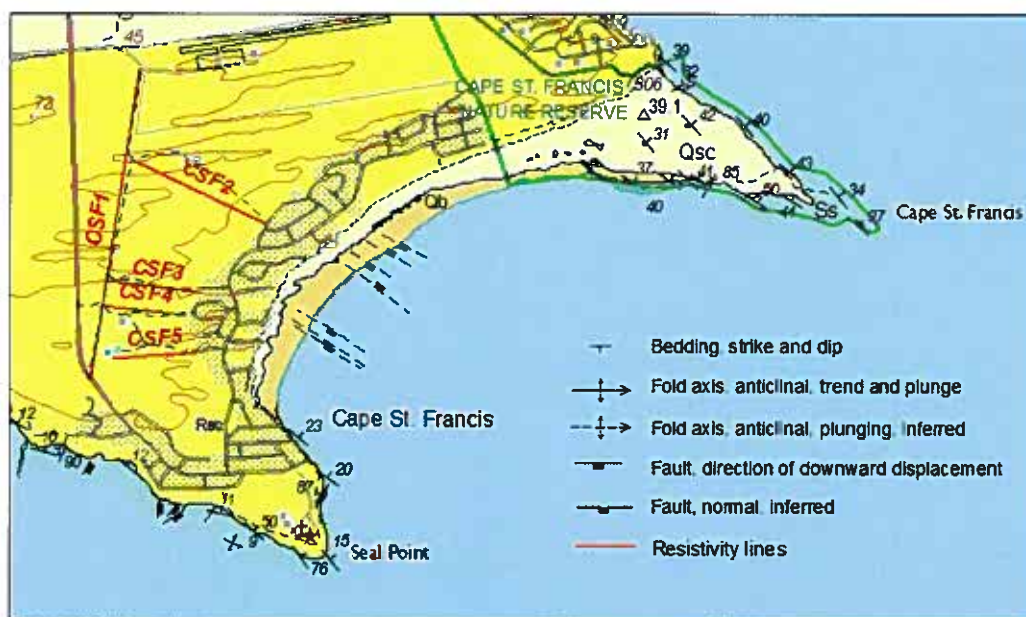
Figure 1: Map of Cape St. Francis showing the traverses

Thyspunt (TS) is located between Oyster Bay and Cape St. Francis approximately 100km west of Port Elizabeth. In this area 3 traverses were chosen, of which only two traverses are interpreted due to localized field conditions that made the traverse too short for it to be of any real value. As a result only data from line TS1 and TS3 are presented. The location of these two traverses is presented in Table 1 and is shown on Figure 2. TS 1 trend roughly west-east, parallel to the ocean and TS 3 lies perpendicular to TS 1 and the coastline.
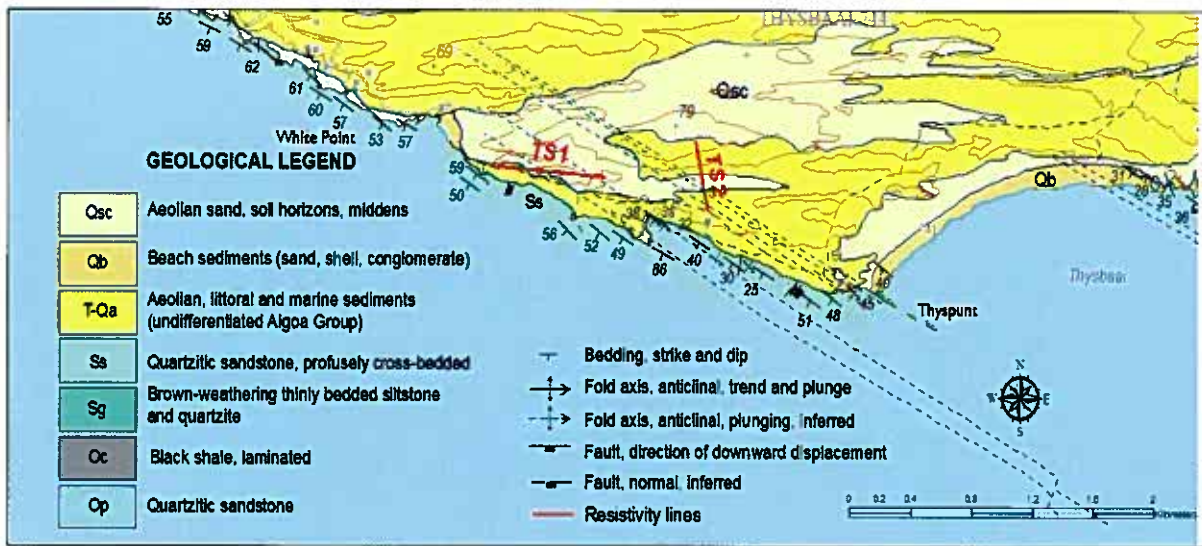
Figure 2: Map of Thyspunt showing the traverses and the borehole locations

2. Geology

2.1 Introduction

The Thyspunt area is distinguished by a south-facing fairly straight rocky coastline which is caused by the sharp southward-dipping hard rocks of the Skurweberg Formation. The bays of Thysbaai and Cape St. Francis are underlain by the siltstones and sandstones of the Goudini Formation (Cole and Naudé, 2007; Cole and Cole, 2007 and Fugro, 2007). The northern part of Thysbaai is crossed by the shales of the Cedarberg Formation which is only detected by projection along strike from thinned inland outcrops to the NW and by airborne and ground geophysical methods (Cole and Naudé. 2007 and Stettler *et al.*, 2008). The northern edge of Thysbaai is formed by the resistant quartzite of the southward-dipping Peninsula Formation. All formations mentioned in this paragraph occur within the Table Mountain Group.

To the south of Cape St. Francis Bay the Peninsula Formation dips shallowly to the northeast. North of Cape St. Francis Bay, the Skurweberg sediments stretch all along the coastline at medium gradients. West of Thysbaai, steep, southwesterly dipping Skurweberg Formation sediments strike NW-SE. To the east of Thysbaai, sediments of the Peninsula Formation dip more moderately.

3

Formation thickness varies from place to place. The Peninsula Formation is reported up to 1600m thick in some areas, the Cedarberg Formation from 80-120m, the Goudini Formation around 300m and the Skurweberg Formation up to 400m. Datasets on Tertiary and Quaternary stratigraphic composition and thickness overlaying bedrock in the St. Francis Bay and Cape St. Francis area are derived from:

• Boreholes at the De Hoek site (Raubenheimer *et al.*, 1988a&b), roughly 1-2km from newly surveyed geophysical CSF 1

• Borehole data (Rosewarne and Lomberg, 1989) collected for a groundwater resource evaluation study. Boreholes are collected mostly along the northern coast, near Sea Vista and Santareme Bay.

2.2 Stratigraphy

2.2.1 Paleozoic sediments

The Table Mountain Group forms part of the Cape Supergroup. The group consists of a 3500m thick clastic succession which is composed of arenaceous super mature quartzose sandstone. Five formations are defined in the group; Peninsula and Cedarberg Formation which are Ordovician in age; and the Goudini, Skurweberg and Baviaanskloof Formation which are Silurian in age. The Baviaanskloof Formation is not present in the location where the traverses are situated and as a result not discussed below.

Figure 3 provides an overview of the Table Mountain Group stratigraphy in the Thyspunt vicinity.
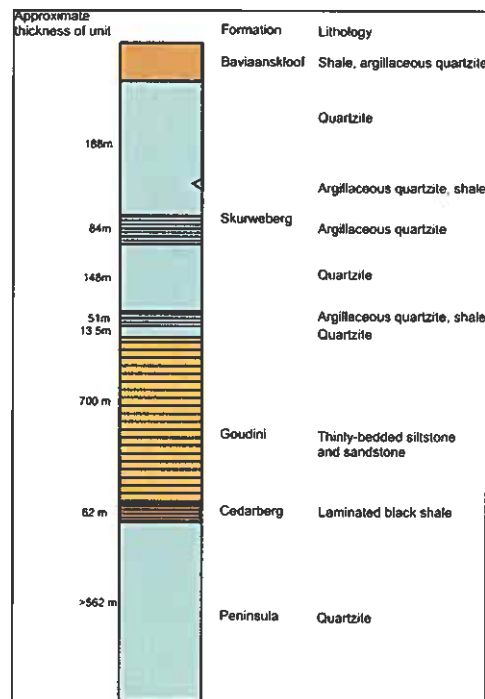
Figure 3: Stratigraphy of the Table Mountain Group in the vicinity of Thyspunt, showing the transition from Goudini to Skurweberg Formation. (Stratigraphic thicknesses are approximate) (Goedhart *et al.*, 2008).

The Peninsula Formation is made up of light-grey, super mature quartzitic sandstone interbedded with small subordinate argillaceous horizons that are generally very thin. Outcrops are massive, well-bedded and usually medium grained. Along the coast outcrops are flat, due to planing by extensive marine erosion. The resulting marine-planed surface dips moderately towards the sea and exposes scattered but inclined remnant bedrock.

The Cedarberg Formation consists of a fine grained, approximately 150m thick, thinly laminated argillaceous unit that is horizontally very persistent. The unit may have been deposited due to a world wide change in sea level. In its un-weathered state, the argillaceous unit consists of black shale. When weathered the sediments take on a variety of colors ranging from grey, greenish-grey to yellow. Topographically the easily erodible formation weathers into long linear landscape depressions (Toerien and Hill, 1989) adjacent to the high erosion resistant hills of

5

the Peninsula Formation. Although this formation is horizontally persistent, it is poorly exposed in the vicinity of the proposed site.

The Goudini Formation consists of alternating supermature quartzitic sandstones and mudstones, with thin interbedded shale and siltstone lenses. Topographically, the Goudini Formation forms prominent low relief areas and embayment along coastal margins.

The Skurweberg Formation consists of white, mature siliceous quartzitic sandstone. The moderately sorted, medium- to coarse-grained sandstone of this formation is distinguished by medium to very thick bedding (between 13 and 85 m). Sandstones are interbedded with argillaceous shale units and conglomerate stringers which respectively comprise no more than 1 to 8 % of the Skurweberg Formation. The thinly bedded pebble beds contain quartzite, vein quartz and blue quartz pebbles clasts < 3.5cm in length (Rust, 1967, 1973; Tankard *et al.*, 1982).

2.3 Structure

The stratigraphic framework for the Thyspunt and Cape St. Francis regions are described in detail by Hälbich (1983a, and 1992), and are summarized Goedhart (2007 and 2008).

2.3.1 Faults

Normal faults follow the general strike of the geology and most were recorded with a down-to-the-south sense of displacement. A second set of near-vertical striking to steeply-dipping high-angle cross faults were recorded as normal faults. Around the Thyspunt area, these appear to have resulted mostly to accommodate undulations and competency contrasts along the fold lengths at the time of their formation or by later extension related to Mesozoic extension. They also reflect a regional trend, indicated by similar but much larger scale structures rupturing the regional folding in the Kouga dam region north of the Thyspunt Site area.

Thrust faults developed mostly parallel to the bedding, and are strongly associated with the bedding-parallel normal faults. In terms of order of development, the thrust faults developed first during Permo-Traissic compression, followed by the normal faults, developed during Mesozoic extension, by inversion of the pre-existing thrusts (Hälbich, 1992).

None of these structures, where followed out along their lengths and were observed to have disrupted the overlying Aeolian sands of the Algoa Group, or younger, alluvial or colluvial sediments.

One of the more important faults in the Cape St. Francis and Thyspunt area is the offshore identified normal Cape St. Francis fault that is 42km in length and trends NNW-SSE.

2.3.2 Folds

Within the Peninsula Formation fold amplitude and wavelength reaches a maximum. In strata with thin bedding and a variation in the competency of the lithologies, folding tends to be smaller in size and more closely spaced, with more intense cleavage, in places representing considerable shortening and volume reduction (e.g. folding in the Goudini Formation). Folding in the Eastern Cape Fold Belt region is characterised mainly by north-east verging anticlines and synclines, the upper hinge areas of which are commonly dragged over northward to produce upward north-curving axial planes (Hälbich, 1983a and 1992). This is readily apparent throughout the Thyspunt Site vicinity, both at the regional large kilometre scale folding, and in numerous small secondary folds on the flanks and hinge areas of the larger structures.

On a larger scale, broad cross-folding in the eastern CFB is indicated by double plunging anticlines and synclines, over distances of several tens of kilometers to even a hundred kilometers some of which are described in Cole and Cole (2007).

2.3.3 Joints

During the investigation of surface geology and update of on-land geological hazards for the 40km site vicinity and 8km site area around the proposed Thyspunt nuclear power plant over 1300 joints were measured by Goedhart *et al.* (2008). All joints dip vertical to near vertical with inclinations of 75-90°.

3. Data Acquisition and Survey Methodology

3.1 Resistivity method - Theory

Electrical surveys deduce the subsurface resistivity distribution by making measurements on the ground surface. From these measurements, the true resistivity of the subsurface can be estimated. The ground resistivity is related to various geological parameters such as the mineral and fluid content, porosity and degree of water saturation in the rock. The resistivity measurements are normally made by injecting current into the ground through two current electrodes (C1 and C2), and measuring the resulting voltage difference at two potential electrodes (P1 and P2).
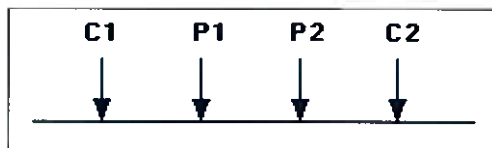
From the current (I) and voltage (V) values, an apparent resistivity (*pa*) value is calculated:

$$pa = k\,V\,/\,I$$

where k is the geometric factor which depends on the arrangement of the four electrodes.

The calculated resistivity value is not the true resistivity of the subsurface, but an apparent value which is the resistivity of a homogeneous half-space which will give the same resistance value for the same electrode arrangement. The relationship between the apparent resistivity and the true resistivity is not a simple relationship.

An inversion of the measured apparent resistivity values, using a computer program, is carried out to determine the true subsurface resistivity.

The choice of the array for a field survey depends on the type of structure to be mapped, the sensitivity of the resistivity meter and the background noise level. Among the characteristics of an array that should be considered are: The sensitivity of the array to vertical and horizontal changes in the subsurface resistivity; the depth of investigation; the horizontal data coverage and the signal strength.

3.1.1 Dipole-dipole array
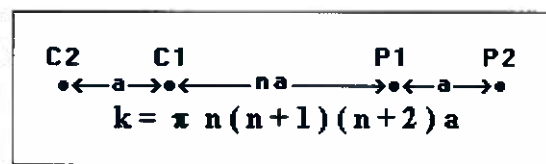
Figure 4: Illustration of dipole-dipole array configuration

This array (Figure 4) is widely used in most surveys because of the low E.M. coupling between the current and potential circuits. The arrangement of the electrodes is shown in Figure 4 and the apparent resistivity is given by:

$$pa = \Pi\ n\ (n+1)(n+2)\ a\ V/I$$

The spacing between the current electrode pair, **C2-C1**, is given as **a** which is the same as the distance between the potential electrodes pair **P1-P2**.The factor **n** is the ratio of the distance between the **C1** and **P1** electrodes to the **C2-C1** (or **P1-P2**) dipole separation **a**. For survey using this array, the **a** spacing is initially kept fixed and the **n** factor is increased up to **8** in order to increase the depth of investigation. The Dipole-Dipole array is more sensitive to vertical structures (Keary *et al.*, 2002).

3.1.2 Wenner-Schlumberger array


```
C1              P1    P2              C2
●←——— n a ———→●←—a—→●←——— n a ———→●
        k =  π n ( n + 1 ) a
```
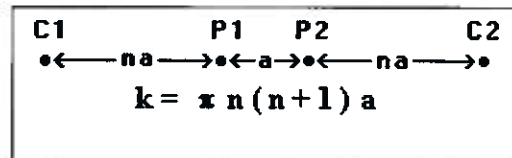
Figure 5: Illustration of the Wenner – Schlumberger array configuration.

The apparent resistivity value for the Wenner-Schlumberger array is given by:

$$pa = \Pi\ n\ (n+1)\ a\ V/I$$

where **a** is the spacing between the **P1** and **P2** electrodes and **n** is the ratio of the distances between the **C1-P1** and the **P1-P2** electrodes. For **n** greater than 2, the array effectively becomes the Schlumberger array and is more sensitive to both horizontal and vertical structures (Keary *et al.*, 2002).

3.2 SYSCAL Pro 72 (Resistivity & IP equipment)

The SYSCAL Pro Switch is a fully automated electrical resistivity meter that combines a transmitter, receiver and switching unit in one single casing.

• The measurements are carried out automatically (output voltage, stacking number, quality factor) after selection of limit values by the operator, and are stored in the internal memory.

• The output specifications are 800V (switch mode), 1 000V (manual mode) for the voltage, 2.5A for the current and 250W for the power using the internal DC/DC converter and the battery.

• The SYSCAL Pro Switch uses multi-core cables for controlling a set of 72 electrodes connected in a line at predefined 5m interval making a single spread of total length 360m.

• The ten channels of the system permit to carry out up to 10 readings at the same time for a high efficiency.

Table 2: Summary of geophysical instrumentation and field procedure

Instrumentation	Field Procedure
SYSCAL Pro 72 unit Stainless steel electrodes	• 10 m dipole-dipole array for greater progress • 10 m Schlumberger array for greater depth of investigation and improved signal to noise ratio
Garmin GPS (Handheld)	• Geo-referencing survey lines • Acquisition of topographical information

3.3 Data acquisition

The DC resistivity survey was done using the Dipole-Dipole array (Figure 4) and the Schlumberger array (Figure 5) with 10m electrode spacing, with a maximum spread separation of 360m. The 10m dipole separation was chosen in both cases as we wanted to achieve the greatest depth of investigation and at the same time map the structures with optimum resolution and also to progress at a satisfactory rate. Due to the high contact resistance from sands on the surface, a maximum voltage of 800V was always applied to ensure maximum transmission power, in particular for the Dipole-Dipole array. For the Schlumberger array the applied voltage depended on the current electrode separation and is determined by the fully automated instrument programmed sequence settings. Sources of noise in electrical surveys such as power lines were noted where they were not avoidable.

Topography was measured with a handheld Garmin GPS. This was done to correct for perturbations in measured voltages due to variations in topography which result from the effect of currents being focused in valleys and dispersed under hills.

Near surface variations were controlled to some extent by ensuring maximum possible ground-electrode contact whilst some unavoidable noise due to poor

ground-electrode contact in the Aeolian sands was minimized by statistical treatment of the data during inversion. During the statistical treatment of data a cut off percentage error between the measured and calculated apparent resistivity data is chosen and the data lying above the cut off percentage error are considered bad data and the data set is trimmed to remove the outliers.

In Table 3 the day-to-day workings in the field is summarized.

Table 3: Summary of time spent in the field

Date	Line	Arrays used	Survey Direction	Instrument Operator	Assistants	Distance covered	Line Length
05/04/ 2009	CSF 1	Dipole-dipole & Schlumb erger	SSW-NNE	E. Chirenje	M. Sethobya L. Loots D. Eberle D. Claassen	810m	1800m
06/04/ 2009	CSF 1	Dipole-dipole & Schlumb erger	SSW-NNE	E. Chirenje	M. Sethobya L. Loots D. Eberle D. Claassen D. Black	900m	1800m
07/04/ 2009	CSF 1	Dipole-dipole & Schlumb erger	SSW-NNE	E. Chirenje	M. Sethobya L. Loots D. Eberle D. Claassen D. Black	720m	1800m
08/04/ 2009	CSF 3	Dipole-dipole & Schlumb erger	SSW-NNE	E. Chirenje	M. Sethobya L. Loots	540m	540m
09/04/	CSF	Dipole-	SE-NW	M.	M.	900m	950m

2009	2	dipole & Schlumberger		Sethobya L. Loots E. Chirenje	Sethobya L. Loots E. Chirenje		
10/04/ 2009	TS1	Dipole-dipole & Schlumberger	W–E	E. Chirenje	M. Sethobya L. Loots D. Claassen D. Black	450m	810m
10/04/ 2009	TS2	Dipole-dipole & Schlumberger	WNW-ESE	E. Chirenje	M. Sethobya L. Loots D. Claassen D. Black	270m	270m
13/04/ 2009	CSF 5	Dipole-dipole & Schlumberger	WSW-ENE	E. Chirenje M. Sethobya L. Loots	E. Chirenje M. Sethobya L. Loots	540m	540m
13/04/ 2009	CSF 2	Dipole-dipole & Schlumberger	SE-NW	L. Loots	M. Sethobya E. Chirenje D. Claassen D. Black	360m	950m
14/04/ 2009	CSF 4	Dipole-dipole &	WSW-ENE	M. Sethobya	E. Chirenje	540m	540m

14

		Schlumb erger		L. Loots	M. Sethobya L. Loots		
15/04/ 2009	TS3	Dipole- dipole & Schlumb erger	WNW-ESE	E. Chirenje	M. Sethobya L. Loots	450m	450m
16/04/ 2009	TS3	Seismic test	WNW-ESE	E. Chirenje	M. Sethobya	120m	120m
16/04/ 2009	TS1	Dipole- dipole & Schlumb erger	W-E	E. Chirenje	M. Sethobya L. Loots D. Eberle	450m	810m
17/04/ 2009	TS1	Dipole- dipole & Schlumb erger	W-E	L. Loots E. Chirenje	M. Sethobya L. Loots D. Eberle E. Chirenje	450m	810m

4. Data Processing

Table 6: Computer processing packages used to process data

Software	Comments
Prosys II	Instrument data dumping to PC, filtering and sorting and conversion to Res2Dinv format.
Res2Dinv	Inverse modeling program that produces apparent resistivity sections as a function of depth.
Geosoft Oasis Montaj	Data processing, gridding and map production software package. Also does geo-referencing of maps.

After the field survey, the resistance measurements were reduced to apparent resistivity values using the Prosys II software. A 2-D model for the subsurface consisting of a large number of rectangular blocks was used for interpretation. A computer program Res2Dinv was used to generate the model blocks and to determine the resistivity of the blocks so that the calculated apparent resistivity values agree with the measured values from the field survey. The computer program Res2Dinv automatically subdivides the subsurface into a number of blocks, and it then uses a least-squares inversion scheme to determine the appropriate resistivity value for each block. The program has a set of default parameters which guide the inversion process. In most cases the default parameters give reasonable results. If the results did not give a reasonable subsurface model, parameters like block size, numbers of iterations, layer depth, etc. were changed. The problem of non-uniqueness is well known in the inversion of resistivity sounding and other geophysical data. For the same measured data set, there is wide range of models giving rise to the same calculated apparent resistivity values. To narrow down the range of possible models, some assumptions were made concerning the nature of

the subsurface that could be incorporated into inversion subroutine, based on known geological information and borehole logs.

The resulting resistivity models were then exported to Geosoft for gridding and adding interpretation annotations.

5. Survey results

For all the traverses, the Dipole-Dipole and Schlumberger resistivity-depth sections are presented together with a detailed interpretation model, based on trying to associate the modeled resistivity-depth distribution with known geology and borehole information. Only boreholes lying within ±50m of the traverses in the Thyspunt area were used for correlation. Modeled depth values were compared with the depth data from the boreholes. Resistivity-depth models were also compared with the stratigraphy of the boreholes.

For the Cape St. Francis survey area, borehole projection was not undertaken as the existing boreholes were considered too far away from the survey lines. However, available information was used to carefully infer geological information for the interpreted resistivity-depth models. Interpretation focused on Schlumberger sounding results due to their higher signal to noise ratio and greater depth of investigation. The Schlumberger sections were also used to infer the underlying geology. The Dipole-Dipole array results reflect smaller depth of investigation, but as opposed to the Schlumberger configuration, they produced greater lateral resolution. Thus, the dipole-dipole data were mostly used to infer vertical to sub-vertical tectonic features such as faults and fracture zones and in some instances, adapt for depth discrepancies with the Schlumberger sections.

The interpreted geological sections are based on the allocation of various resistivities to particular geologic units identified from boreholes and their expected response to the effect of a steady electric current as a function of their composition.

Resistivity values obtained from laboratory measurements on dry rock samples of the Goudini and Skurweberg formations and the Port Elizabeth area in general are shown in Table 4 below. These data were referred to as a control in stratigraphy assignment during the interpretation process, though on-site moisture might diminish the values given in Table 4.

Table 4: Resistivity values of surrounding area (Maré (2002), (2007)).

Formation	Rock Type	Resistivity (Ohm.m)
Skurweberg	Quartzitic Sandstone	2221
Skurweberg	Quartzitic Sandstone	1745
Skurweberg	Quartzitic Sandstone	4367
Skurweberg	Quartzitic Sandstone	5164
Skurweberg	Quartzitic Sandstone	5053
Goudini	Sandstone	7188
Port Elizabeth area	Sandstone	58 – 16061
Port Elizabeth area	Calcrete	180 – 694

5.1 Cape St. Francis L1 (CSF 1)

The survey line trends NNE –SSW, oblique to the bedding strike and measures around 1800m in length, see Figure 1. A communal power line runs parallel to the line for the last 900m from the north and this might influence the quality of the data for that section, although no disruption in data quality was noted in the field. There are four resistivity layers: The resistive surface layer (200Ω.m - 3000Ω.m), the conductive middle layer (20Ω.m - 100Ω.m) and two electric substrates consisting of a resistive substrate (150Ω.m - 3000Ω.m) to the north and a highly resistive substrate (>3000Ω.m) to the south of the section.

Figure 6 shows a resistivity low (20Ω.m - 100Ω.m) approximately 400m wide that extends vertically downwards in the middle of section, around between 600m and 1200m from the south. This conductive feature appears on both the Dipole-dipole and the Schlumberger sections and might be a thrust fault or an iso-clinal fold. This feature might be related to the Cape St. Francis fault, but a few more parallel running traverses are required to correlate this feature with the Cape St. Francis

fault with a high degree of certainty. A TDEM study (Stettler *et al.*, 2008) done along Cape St. Francis Bay has also confirmed this deformed zone. The width of the surveyed fractured zone along CSF 1 is similar to the width of a shear zone detected along Cape St. Francis Bay during the TDEM survey. That may confirm that it is the same zone.

In the conductive layer ($40\Omega.m$ - $200\Omega.m$) there seems to be a lot of very small joints, but this is most likely an effect of poor electrode contact to the ground. There are only a few interpreted joints that run from the conductive layer to the electric substrate and these are indicated on Figure 6 and Figure 7. The top of the resistive electric substrate in the south of the profile is much shallower than the top of the electric substrate in the north of the profile. The resistive electric substrate in the north of the profile is also not as resistive ($100\Omega.m$ - $3000\Omega.m$) as the substrate in the south ($>3000\Omega.m$). This brings us to the conclusion that these are not part of the same lithological unit and are most likely two different geological formations.

The interpreted geology is shown in Figure 7. There are four different lithological units. The resistive surface layer consists of aeolian sands. The conductive layer is interpreted to be fresh water-filled porous sandstone (as indicated by boreholes surrounding the area). The resistive substrate to the north is interpreted to be quartzitic sandstones from the Goudini Formation and the highly resistive substrate to the south is interpreted to be quartzitic sandstones from the Peninsula formation.
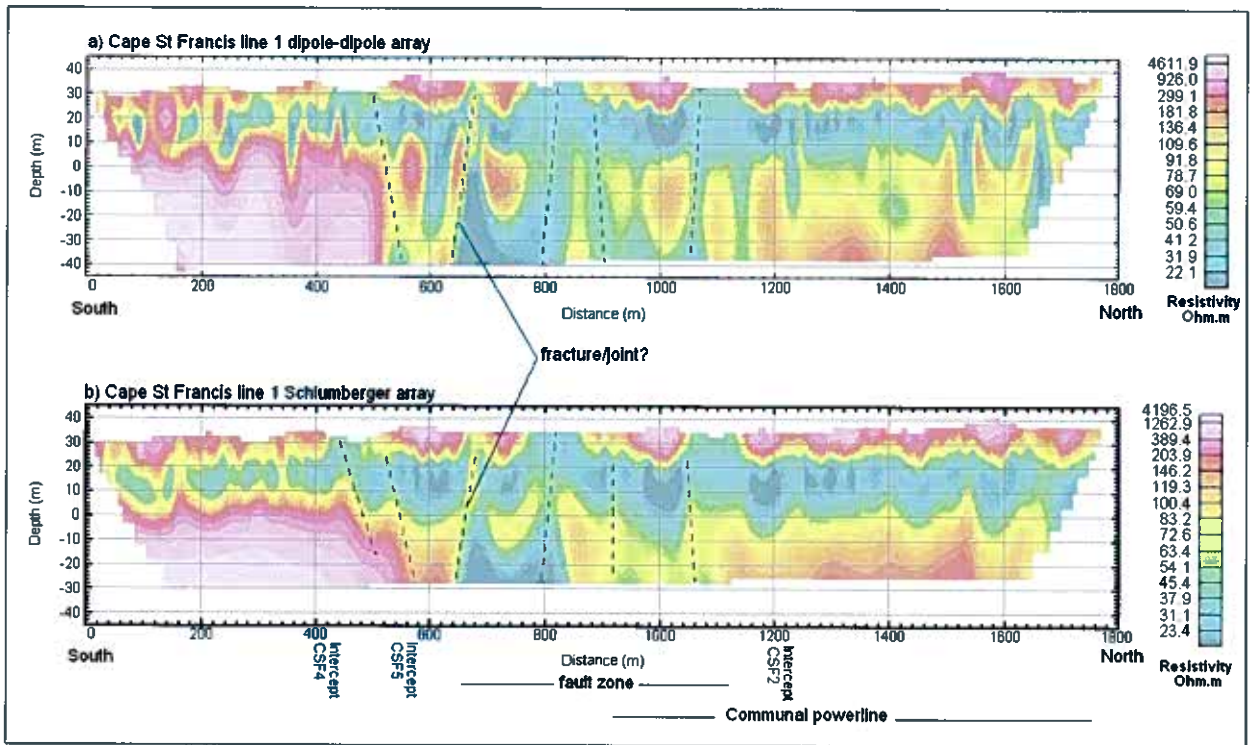
Figure 6: CSF 1 resistivity-depth section.

Legend

Resistive surface layer (200-3000 Ohm.m) probably associated with aeolian sands

Conductive layer (20-100 Ohm.m) probably to be associated with porous/fractured sandstone presumably water filled

Resistive substrate (150-3000 Ohm.m) probably to be associated with less compact quarzitic sandstone from the Goudini Formation

Highly resistive substrate (>3000 Ohm.m) probably to be associated with compact quarzitic sandstone from Peninsula formation

- - - -   Fracture, discontinuity or joint

Figure 7: Interpretation of the CSF 1 resistivity-depth section.

5.2 Cape St. Francis L2 (CSF 2)

CSF 2 (Figure 8) measures 900 meters in length, trends WNW-ESE and runs roughly perpendicular to traverse CSF 1. A power line runs parallel to the traverse for the first 300m from the west of the line and this might influence the quality of the data for that section. Four resistivity layers can be seen on the section: The resistive surface layer (240Ω.m - 1500Ω.m), the conductive layer (20Ω.m - 100Ω.m) and the electric substrate consisting of a resistive substrate in the middle of the profile (150Ω.m - 1000Ω.m) and a highly resistive substrate to the east and west of the profile (>1000Ω.m).

As with CSF 1, the conductive layer changes thickness quite rapidly and this might be explained by poor electrode contact to the ground. Only two joints can be interpreted with certainty and these can be seen in Figure 8. The difference between the Dipole-Dipole section and the Schlumberger section can be explained by the fact that the Dipole-Dipole array is likelier to have a poor signal to noise ratio if the surface is very resistive, which was the case when the measurements were done.

The top of the conductive layer (20Ω.m - 100Ω.m) seems to deepen to the east, where the coast is, as can be seen on Figure 8(b) and this might indicate terracing, but it is only a suspicion as it is not duplicated in the resistive electric substrate. As with CSF 1, the resistive electric substrate seems to consist of two different lithologies. To the very west and very east of the profile the electric substrate is much more resistive (>1000Ω.m) than in the middle of the section (150Ω.m - 1000Ω.m).

The geological interpretation is shown on Figure 9. The resistive surface layer is associated with aeolian sands. The conductive layer is interpreted to be fresh water-filled porous sandstone. The resistive substrate, in the middle of the section, is interpreted to be quartzitic sandstone, which is not as compact as the highly resistive substrate, which is also quartzitic sandstone.
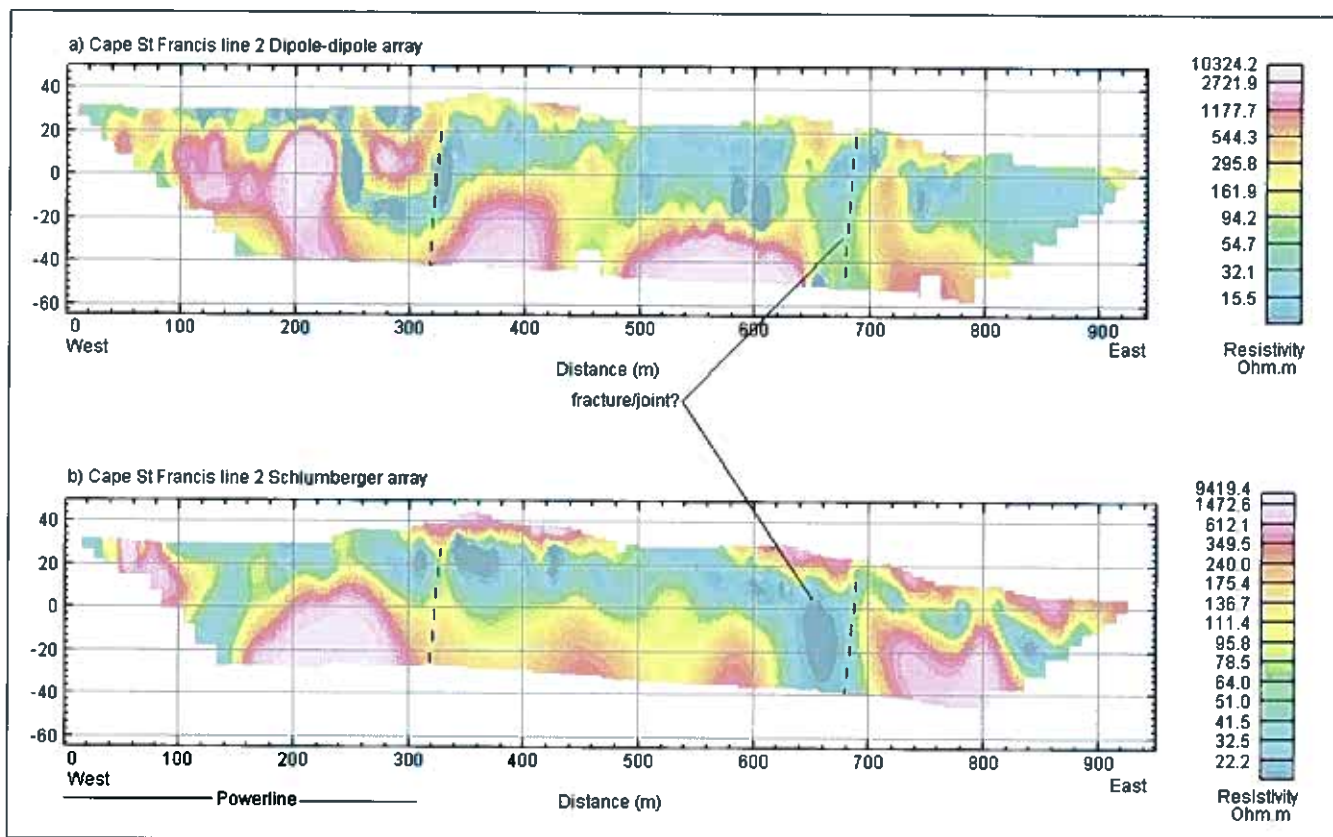
Figure 8: CSF 2 resistivity-depth section.
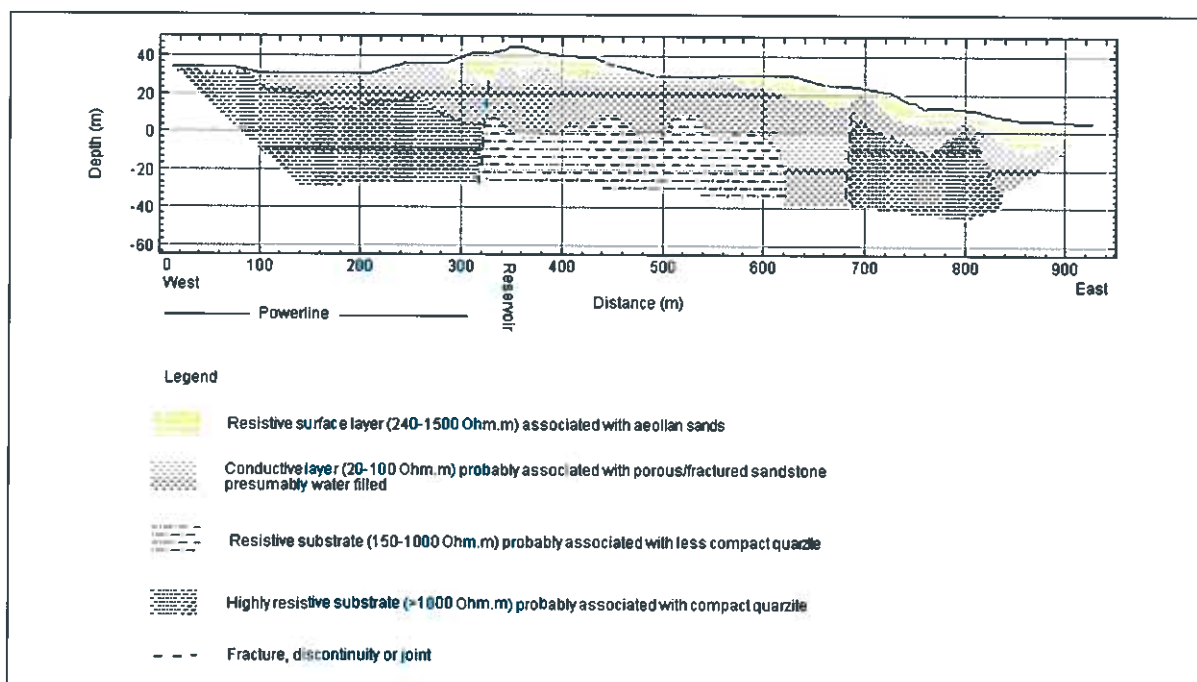
Figure 9: Interpretation of the CSF 2 resistivity-depth section.

5.3 Cape St. Francis L3 (CSF 3)

This line is located roughly 150 meters south of CSF 4 (Figure 1) and strikes oblique to bedding.

The resulting resistivity-depth section (Figure 10) shows the existence of three resistivity layers. The resistive surface layer (200Ω.m - 1550Ω.m) is very shallow (mostly less than 10m). On Figure 10(b) the surface layer is not visible everywhere on the section and this is likely because the layer is too thin in some places to be seen on the section. The top of the conductive layer does not deepen much to the east therefore it does not indicate any terracing. The electric substrate consists of two different lithologies as is the case with CSF1 and CSF2. The electric substrate to the west of the section is highly resistive (>500Ω.m), where the electric substrate to the east of the profile is less resistive (300Ω.m - 500Ω.m). This is clearly indicated on Figure 11.

The geological interpretation of the resistivity data is shown in Figure 11. The surface resistive layer, which is overall approximately 10m deep consist of aeolian sands. The conductive layer is interpreted to be fresh water-filled porous sandstone. The highly resistive electric substrate to the west is interpreted to be compact quartzitic sandstone/quartzite and the less resistive electric substrate to the east is interpreted to be quartzitic sandstone/quartzite that is not as compact as the highly resistive material to the west.

Borehole data used to aid in this interpretation indicate that the resistive surface layer (associated with aeolian sands) is immediately followed by the bedrock. We interpret the top of bedrock where the conductive layer starts at depth.

The deepening of the resistive electric substrate to the east might be an indication of terracing, but this is only speculation.
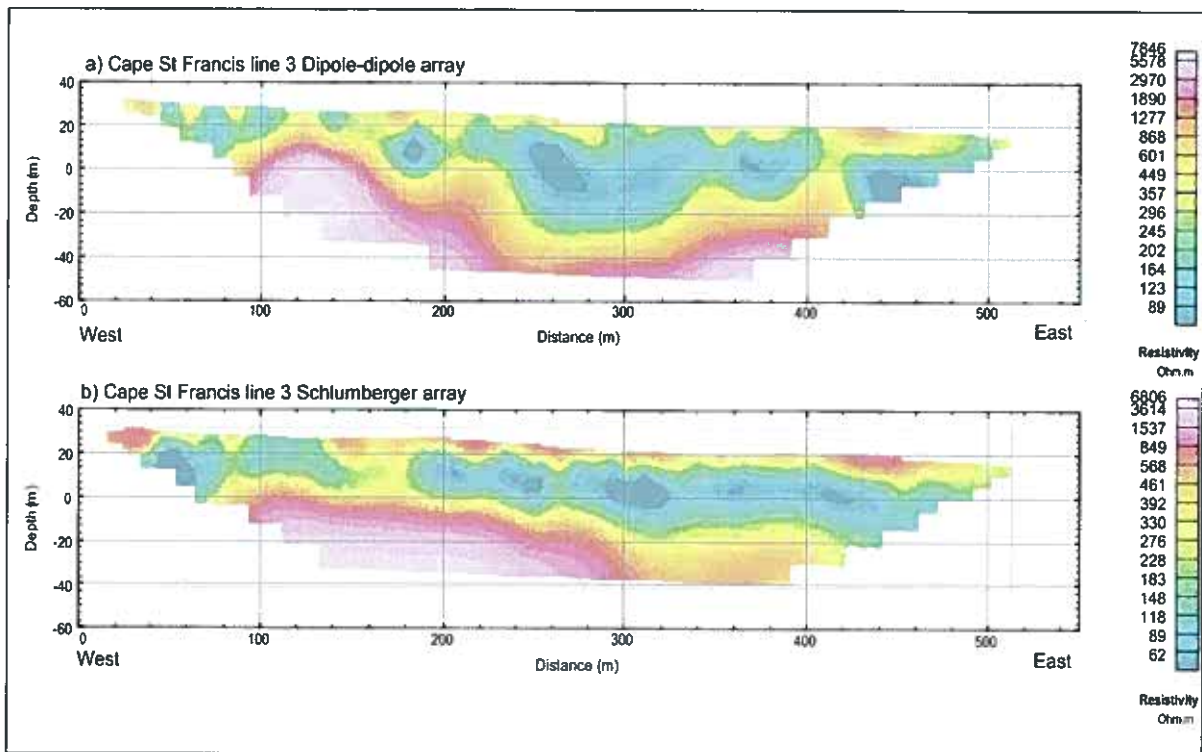
Figure 10: CSF 3 resistivity-depth section.

Legend

Resistive surface layer (200-1550 Ohm.m) associated with aeolian sands

Conductive layer (20-100 Ohm.m) probably associated with porous/fractured sandstone presumably water filled

Resistive substrate (300-500 Ohm.m) probably associated with less compact quarzite

Highly resistive substrate (>500 Ohm.m) probably associated with compact quarzite
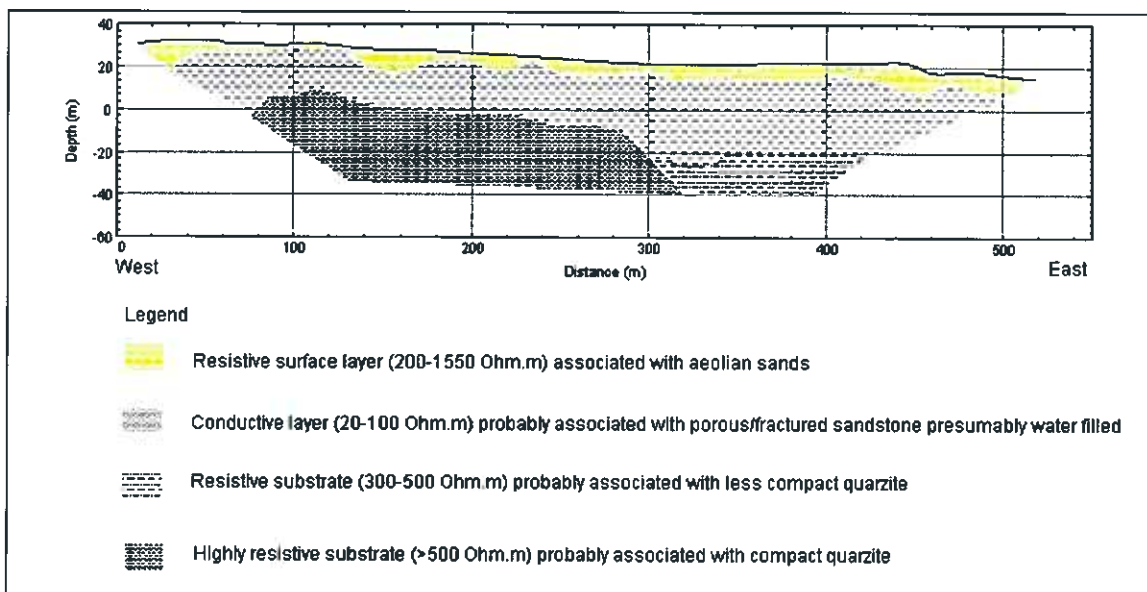
Figure 11: Interpretation of the CSF 3 resistivity-depth section.

5.4 Cape St. Francis L4 (CSF 4)

CSF 4 (Figure 12) is 540 m in length, trends approximately WNW – ESE and runs parallel to CSF 3 and CSF 5 (Figure 1). On the Schlumberger section, Figure 12(b), there are three visible resistivity layers. The resistive surface layer (200Ω.m - 3000Ω.m) is not visible throughout the section and this may be due to the fact that it is extremely thin at some places. The conductive middle layer (20Ω.m - 100Ω.m) can be seen throughout the section and the layer gradually deepens to the east of the section. The top of the resistive electric substrate (300Ω.m - 3000Ω.m) also gradually deepens to the east. Both the conductive layer and the electric substrate show a deepening trend to the east and this can be an indication of terracing. There is only one interpreted joint and it is indicated on both Figure 12 and Figure 13.

In Figure 13 the three resistivity layers are interpreted to be aeolian sands (surface resistive layer), porous fresh water-filled sandstone (conductive layer) and quartzitic sandstone (resistive electric substrate). There is no indication of a fourth lithology as was the case with CSF 1, 2 and 3.
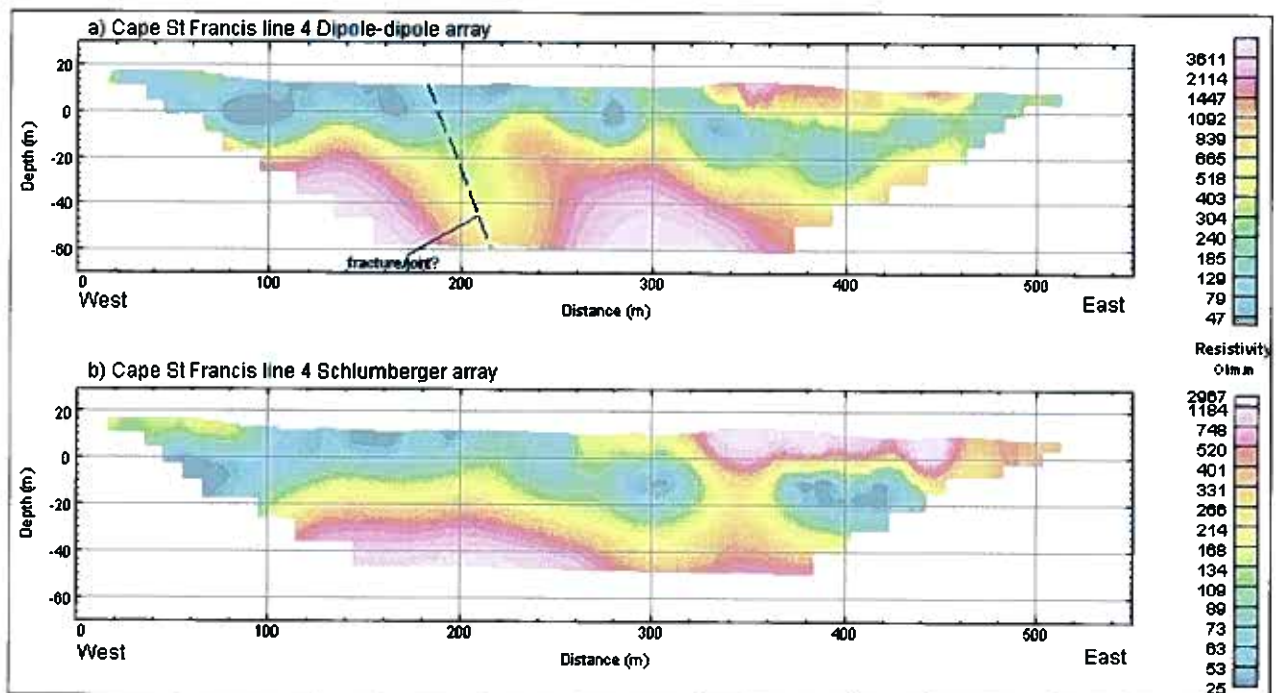
Figure 12: CSF 4 resistivity-depth section.
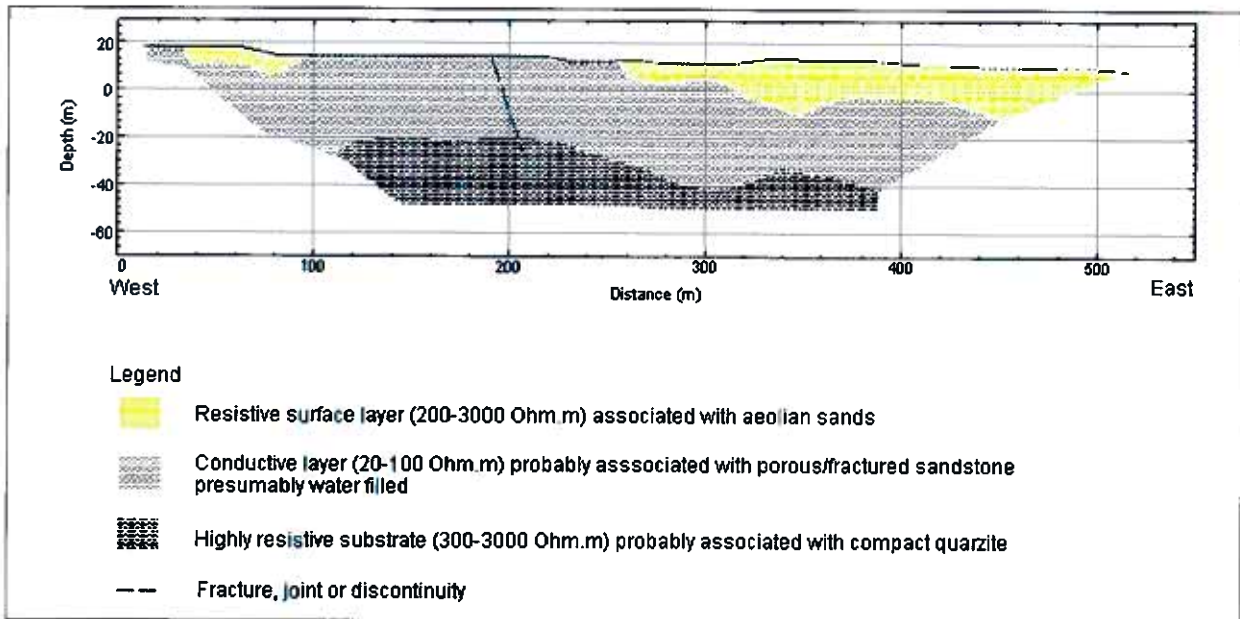
Figure 13: Interpretation of the CSF 4 resistivity-depth section.

5.5 Cape St. Francis L5 (CSF 5)

Before commencing with the interpretation of this traverse (Figure 14), it must be noted that there is no elevation on the section and the data could not be corrected for elevation changes. Thus, the depth of this section will not correlate with the other sections. This traverse is 540m in distance, trend WNW – ESE and lies parallel to CSF 3 and CSF 4. In the far east of the traverse a sub-PowerStation was located roughly 30m from the traverse. This might influence the data quality near the PowerStation.

Three resistivity layers can be seen on the section: A conductive surface layer (10Ω.m - 40Ω.m), a resistive layer (50Ω.m - 400Ω.m) and a conductive layer ($<40\Omega$.m). There are two interpreted joints and these can be seen on both Figure 14 and Figure 15.

The geological interpretation is shown on Figure 15. The three resistivity layers are interpreted as follows: The conductive surface layer is interpreted to be organic sands; the resistive layer is interpreted to be compact sandstone/quartzitic

sandstone and the conductive electric substrate is interpreted to be porous sandstone which is probably filled with water. There is no indication of terracing on this traverse.
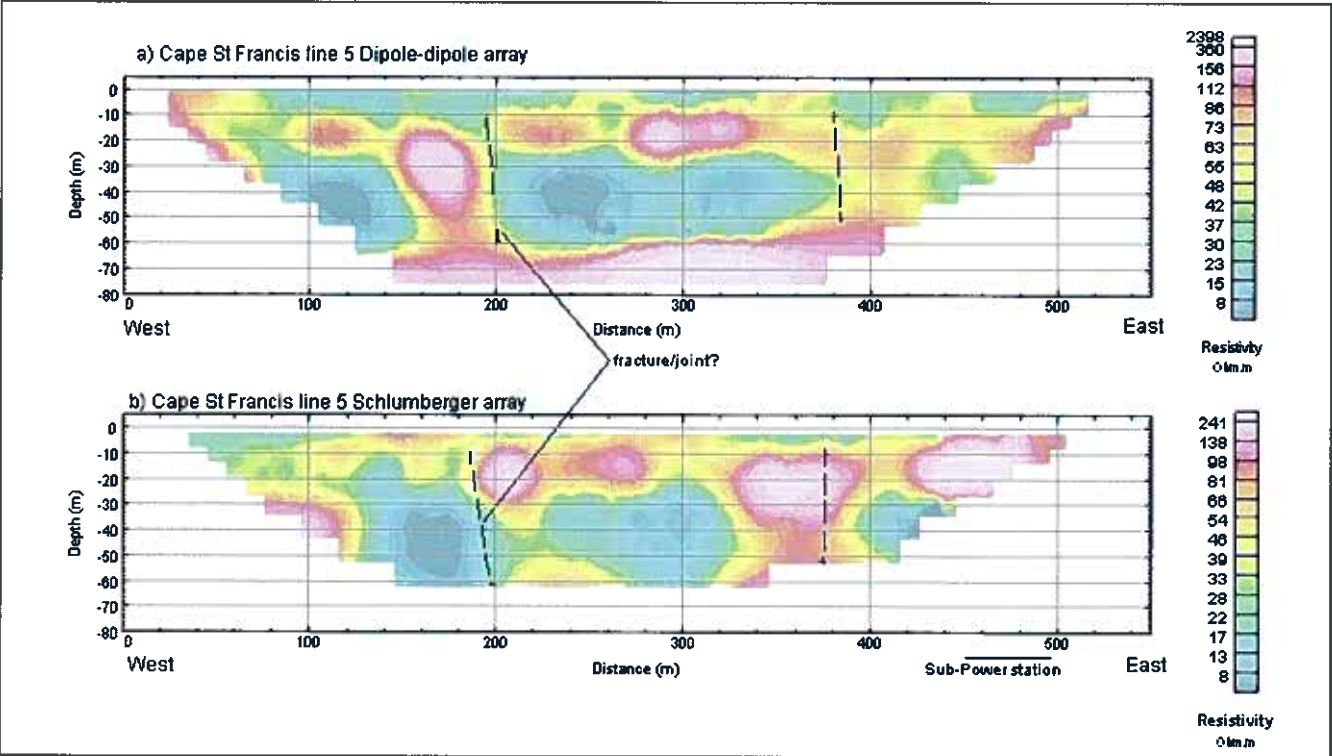
Figure 14: CSF 5 resistivity-depth section.

Legend

Conductive surface (10-40 Ohm.m) probably associated with organic sands

Resistive layer (50-400 Ohm.m) probably associated with fractured to compact sandstone

Conductive layer (<40 Ohm.m) probably associated with porous sandstone presumably water filled

— — Fracture, joint or discontinuity
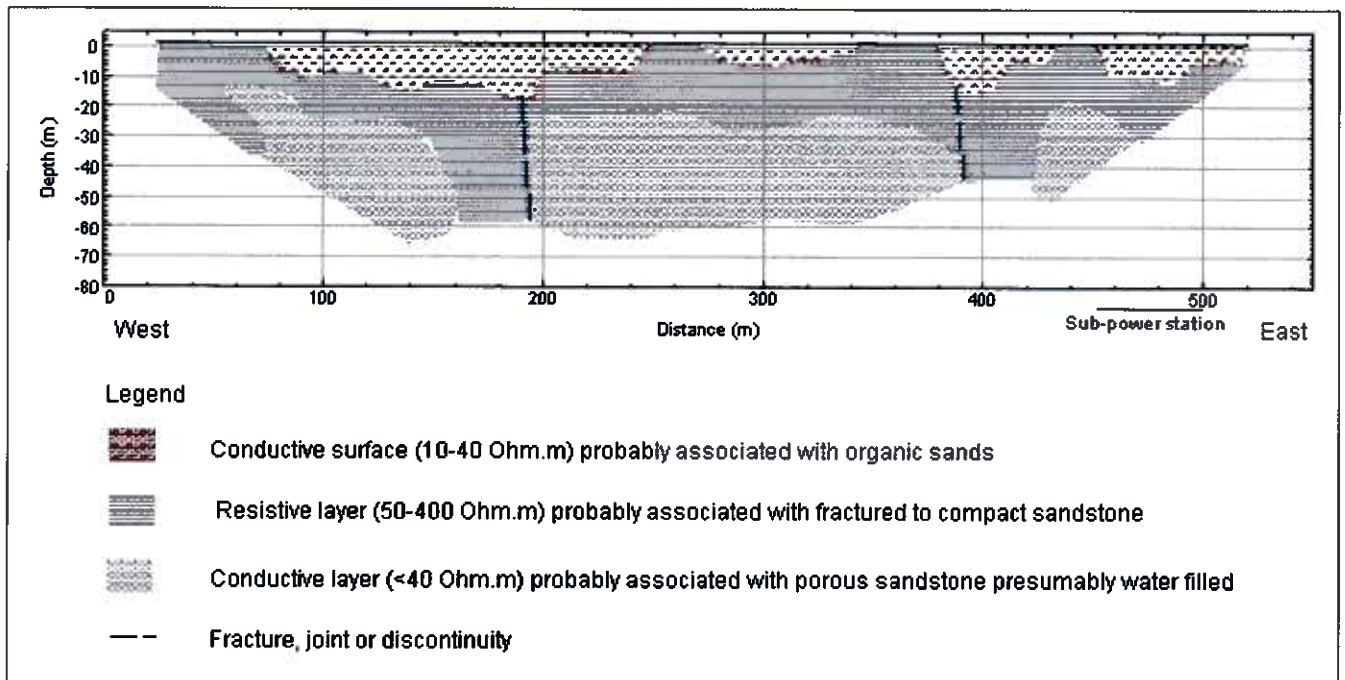
Figure 15: Interpretation of the CSF 5 resistivity-depth section

5.6 Thyspunt L1 (TS 1)

On TS 1 (Figure 16), the boreholes that were projected to the line are TB16, TB3, TB21 and TB14. Three resistivity layers are identified on the resistivity-depth section in Figure 16(b). There is the resistive surface layer ($200\Omega.m$ - $800\Omega.m$), the conductive layer ($< 200\Omega.m$) and the highly resistive electric substrate ($200\Omega.m$ - $1500\Omega.m$) which gradually deepens to the east. There are two interpreted joints which can be seen on both Figure 16(a) and (b).

To aid in the interpretation of the possible geology of this line the borehole data was used to determine the possible depth to bedrock and different lithological units. The borehole data used refers to two main geology layers: aeolian sands (resistive surface layer) and quartzitic sandstones (highly resistive electric substrate). The conductive layer is interpreted to be porous quartzitic sandstone which is presumably filled with water. We come to this conclusion as the traverse runs over beach sands and is very close to the ocean, so presumably there is a lot of water close to the surface. As the conductivity values are quite high, intrusion of sea water

28

can be excluded. If we use the borehole data in aid of determining the depth to bedrock, it seems as though it correlates with the top of the conductive layer. The borehole data and the resistivity data then closely agree on depth to bedrock as can be seen in Figure 18.

Table 5: Lithological summary of the boreholes surrounding TS1

Thyspunt Line 1 (TS 1)				
BHID	**From**	**To**	**Stratigraphy**	**Comments**
TB 3	0.00	7.97	Schelm Hoek Formation	Aeolian succession.
	7.97	20.78	Skurweberg Formation	Quartzitic sandstone varies in hardness, from hard to very hard.
TB 14	0.00	10.50	Schelm Hoek Formation	Aeolian succession, with minor occurrence of marine sediments and a pebble layer.
	10.50	30.92	Skurweberg Formation	Quartzitic sandstone varies in hardness, from hard to very hard.
TB 16	0.00	6.36	Schelm Hoek Formation	Aeolian succession.
	6.36	30.60	Skurweberg Formation	Quartzitic sandstone varies in hardness, from soft, medium hard to very hard.
TB 21	0.00	12.67	Schelm Hoek Formation	Succession of aeolian sand and topsoil, in cases a mixture.
	12.67	19.56	Skurweberg Formation	Quartzitic sandstone varies in hardness, from medium hard to hard.
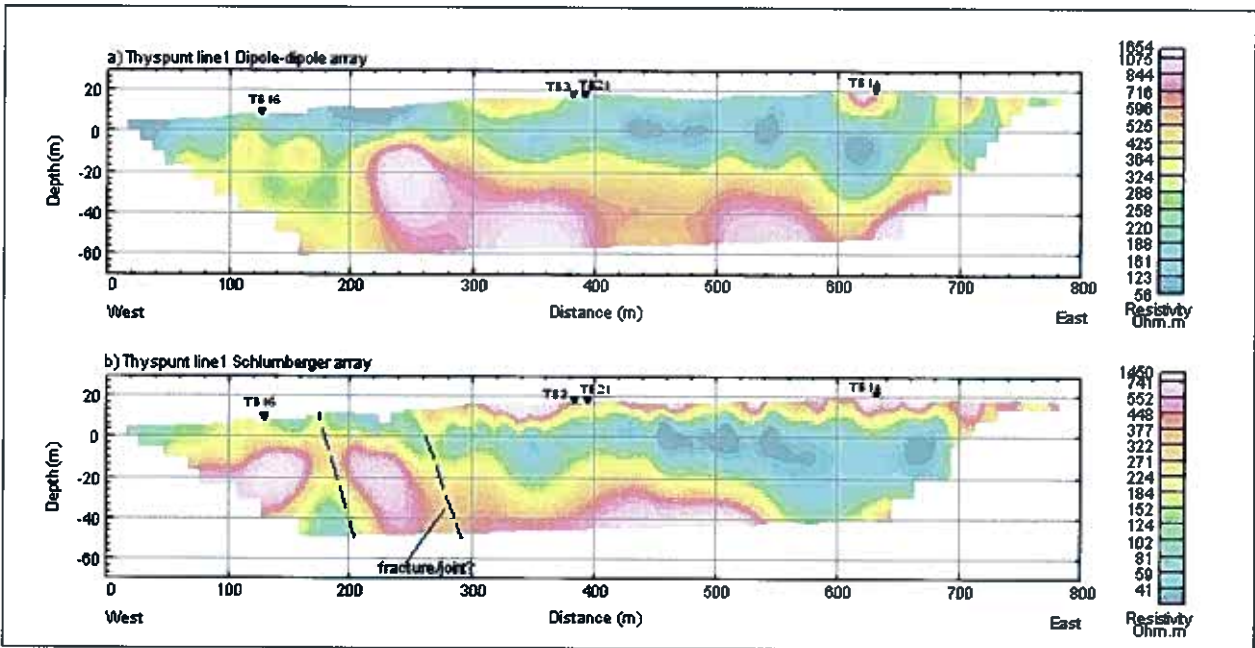
Figure 16: TS 1 resistivity-depth section

Legend

Resistive surface layer (200-800 Ohm.m) associated with aeolian sands

Conductive layer (<200 Ohm.m) probably associated with porous/fractured sandstone, presumably water filled

Resistive to highly resistive substrate (200-1500 Ohm.m) probably associated with compact quarzite

▼ Projected borehole

— · Fracture, joint or discontinuity
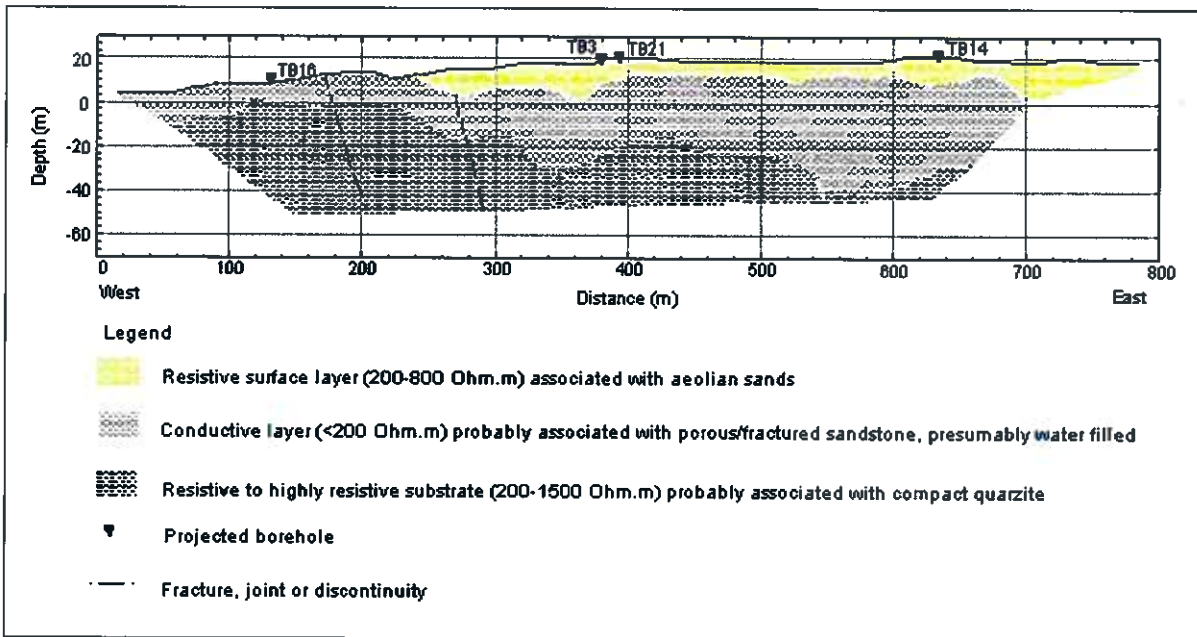
Figure 17: Interpretation of the TS 1 resistivity-depth section.
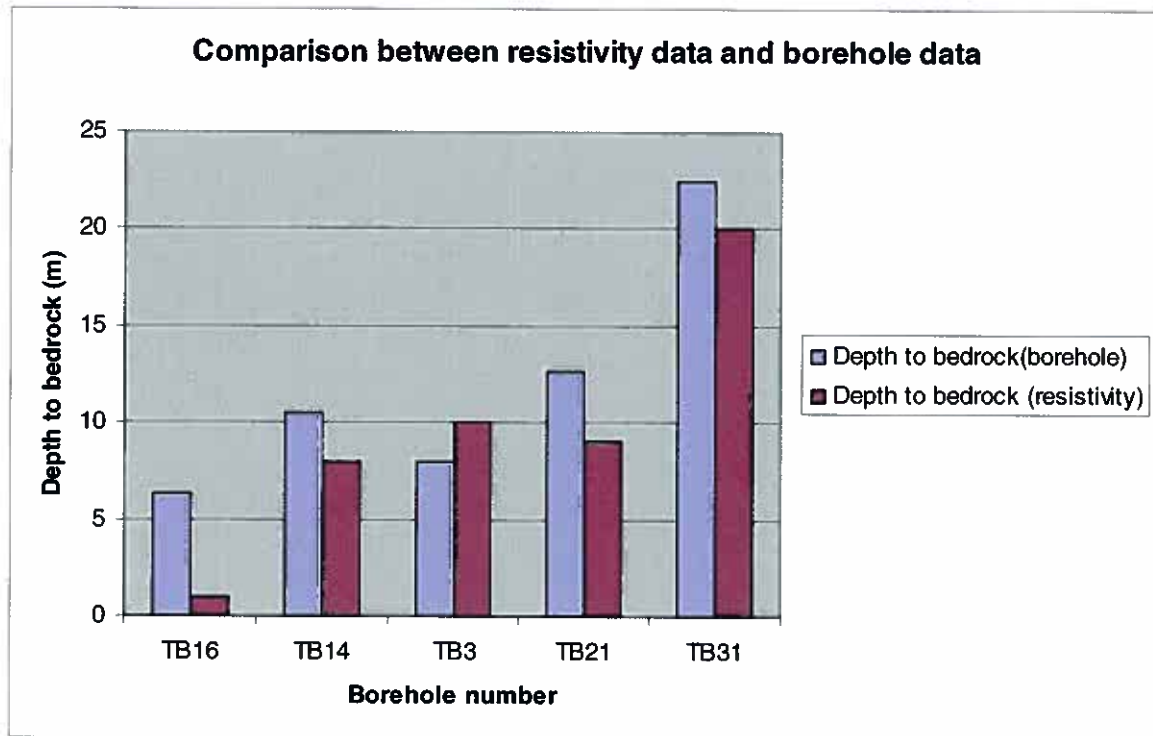
Figure 18: Comparison between resistivity data and borehole data

5.7 Thyspunt L3 (TS 3)

The borehole data used to aid this interpretation is TB31. In this section (Figure 19) there are 3 main resistivity layers. The resistive surface layer (200Ω.m - 800Ω.m) is throughout about 10m thick and from 320m in the profile it thickens to about 20m at the end of the profile. The conductive layer ($<200\Omega$.m) extends throughout the profile to the depth we are able to detect. The highly resistive electric substrate (500Ω.m - 3000Ω.m) is only detected in the middle of the section. There are two interpreted joints which are indicated on both Figure 19 and Figure 20.

With the aid of the borehole data top of bedrock is correlated with the top of the conductive layer (Figure 20). As with TS 1, the conductive layer is thought to be porous, presumably water filled sandstone stressed by cleavages and joints, with the electric substrate consisting of very hard and competent quartzitic sandstone.

Table 6: Lithological summary of the borehole near TS 3

BHID	From	To	Stratigraphy	Comments
Thyspunt Line 3 (TS 3)				
TB 31	0.00	22.43	Schelm Hoek Formation	Succession of aeolian sand and topsoil, in cases a mixture.
	22.43	30.00	Skurweberg Formation	Quartzitic sandstone varies in hardness, from hard to very hard.
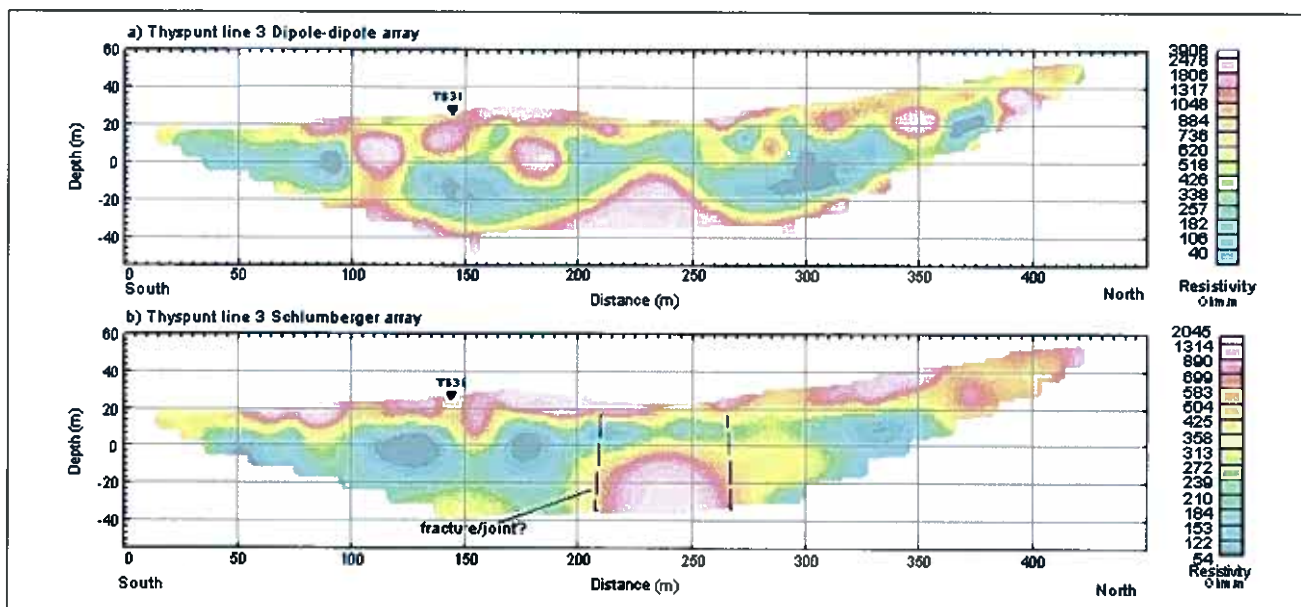
Figure 19: TS 3 resistivity-depth section.

Legend

Resistive surface layer (200-800 Ohm.m) associated with aeolian sands

Conductive layer (<200 Ohm.m) porous/fractured sandstone, presumably water filled

Resistive to highly resistive substrate (500-3000 Ohm.m) probably associated with compact quarzite

▼ Projected borehole

- — Fracture, joint or discontinuity
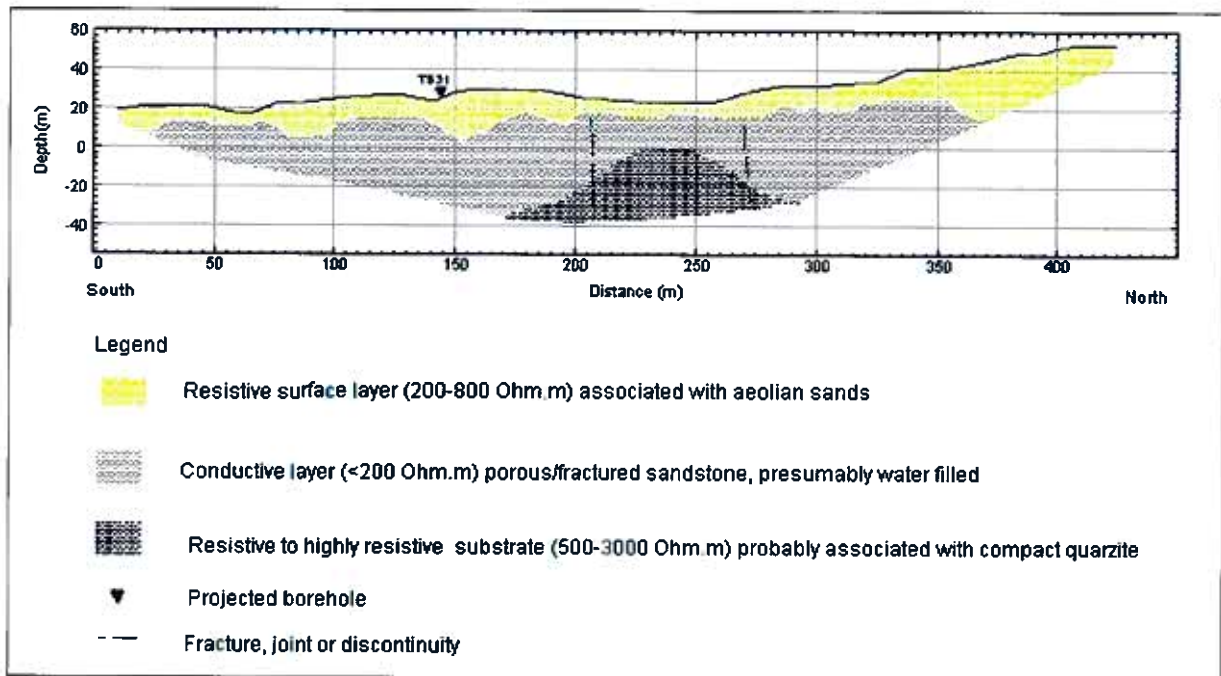
Figure 20: Interpretation of the TS 3 resistivity-depth section.

6. Conclusions

In CSF 1 to CSF 3 four different lithologies were identified from the resistivity data. A surface resistive layer which is associated with aeolian sands, a conductive layer that is interpreted to be porous, fresh water-filled sandstone or quartzite that underwent tectonic stress, a resistive electric substrate interpreted to be sandstone/quartzite and a highly resistive electric substrate interpreted to be very compact quartzitic sandstone/quartzite.

In CSF 4 only three different lithologies were identified from the resistivity data. A resistive surface layer which is associated with aeolian sands, a conductive layer interpreted to be porous fresh water filled sandstone or quartzite that underwent tectonic stress and a resistive to highly resistive electric substrate which is interpreted to be compact quartzitic sandstone/quartzite. In CSF 5, the surface layer encountered was conductive and is interpreted to be organic sands, the resistive middle layer is interpreted to be the same as the resistive electric substrate from

CSF 4 and then the conductive electric substrate is interpreted to be porous sandstone which is possibly filled with water.

In CSF 1 a possible thrust fault/ iso-clinal fold have been identified from the resistivity data, but as in section 5.1, it can only be proved if measurements are run on a parallel traverse.

CSF 2, 3 and 4 shows a deepening trend in the resistivity layers to the east, and this might indicate terracing.

The top of bedrock for CSF 1 – 4 is interpreted to start where the conductive layer starts and the top of bedrock for CSF 5 is interpreted to start where the resistive layer starts.

On TS 1 and TS 3, three main lithological units were identified: The resistive surface layer consisting of aeolian sands, a conductive layer interpreted to be porous sandstone filled with water and a resistive electric substrate interpreted to be compact quartzitic sandstone. Top of bedrock is interpreted to be where the conductive layer starts.

We conclude that the resistivity method was successful for the purpose of this study. It maps the subsurface successfully and display possible faults, joints and displacements very clearly.

7. Recommendations
More resistivity and/or seismic traverses parallel to CSF1 need to be done to confirm the wide conductive zone interpreted as a fault zone possibly related to the Cape St. Francis fault. The Thyspunt site should be investigated in much more detail to receive a more representative DC-dataset from the 8 km site area. Clearing of these proposed additional lines is a absolute necessity. To overcome high surface

resistance, it is recommended to conduct further resistivity work during or immediately after the rainy winter season.

Refraction seismic surveys would verify the resistivity results and provide information that reduces ambiguity in the site investigation. Extra information on bedrock properties, such as rippability, can also be deduced from seismic data.

8. Acknowledgements

9. References

Cole, J. and Naudé, C. (2007). Final report: Airborne survey of Thyspunt. CGS Report No. 2007-0006, NSIP-NSI-019039 #P1-67.

Cole, J. and Cole, P. (2007). Geophysical interpretation of the marine magnetic data collected in the offshore site area (8 km radius) of Thyspunt. CGS Report No. 2007-0189, NSIP-NSI-020268 #P1-12.

Fugro Survey Africa, (2007). Thyspunt Nearshore Final Report. NSIP-NSI-020579#P1-113.

Goedhart. M.L., Reddering, J.S.V., Kilian, D., Mitha, M., Bosch, P.J.A. and Black, D. (2008) Surface geology and update of on-land geological hazards for the proposed Thyspunt nuclear power plant, Eastern Cape, South Africa, Report No.2008-0222.

Goedhart, M.L. (2007). Onshore and offshore geo-hazards for the Thyspunt nuclear power plant: a summary of new airborne and marine geophysical data, and existing offshore seismic reflection data (Rev 0). Council for Geoscience, Report No. 2007–0257, 16 pp.

Hälbich, I.W. (1983a). Disharmonic folding, detachment and thrusting in the Cape Fold Belt. In: Söhnge, A.P.G., and Hälbich, I.W. (Eds.). *Geodynamics of the Cape Fold Belt, Special Publication of the Geological Society of South Africa*, **12**, 115-123.

Hälbich, I.W. (1992). The Cape Fold Belt Orogeny: State of the art 1970s – 1980's. In: De Wit, M.J., and Ransome, I.G.D. (Eds.). *Inversion tectonics of the Cape Fold Belt, Karoo and Cretaceous Basins of Southern Africa*. Balkema, Rotterdam, 141-158.

Keary, P., Brooks, M. and Hill, I. (2002). An Introduction to Geophysical Exploration, Third Edition. Blackwell Publishing, UK, 262pp.

Maré, L.P. (2002). Physical Property Analysis on samples from the Port Elizabeth 1:250 000 Sheet. Council for Geoscience, Report number 2002-0005.

Maré, L.P. (2007). South African Geophysical Atlas, Volume IV, Physical Properties of South African Rocks: Electrical Properties. Council for Geoscience, 687 pp.

Raubenheimer, E., Hambleton-Jones, B.B. and Toens, P.D. (1988a). Detailed geology of De Hoek, Thyspunt and Tony's Bay: in two volumes - Investigations for the siting of nuclear power stations, Atomic Energy Corporation of South Africa, Ltd., Dept of Geotechnology, Progress report No. 20, Vol 1 – Geological description. PIN-1072(B/R), GEA 801, NSIP-N002420-#P1– 190.

Raubenheimer, E., Hambleton-Jones, B.B. and Toens, P.D. (1988b). Detailed geology of De Hoek, Thyspunt and Tony's Bay: in two volumes - Investigations for the siting of nuclear power stations, Atomic Energy Corporation of South Africa, Ltd., Dept of Geotechnology, Progress report No. 20, Vol 2 – Geotechnical maps of De Hoek, Thyspunt and Tony's Bay. PIN-1072(B/R), GEA 801, NSIP-N002420-#P1– 190

Rosewarne, P.N and C.R Lomberg (1989) Groundwater resource evaluation at St. Francis Bay, SRK Consulting – Port Elizabeth, Report no. 171719/3.

Rust, I.C. (1967). On the sedimentation of the Table Mountain Group in the Western Cape Province. D.Sc. Thesis, Stellenbosch University (unpublished).

Rust, I.C. (1973). The evolution of the Paleozoic Cape Basin, southern margin of Africa. In: Nairn, A.E.M., and Stehli, F.G. (Eds.). *The Ocean Basins and Margins*, 1, Plenum, New York, 247-276.

Stettler, E.H., Zadorozhnaya, V.Y. and Goedhart, M.L. (2008). Results of a time domain electromagnetic survey over four possible fault positions signifying the landward continuation of the Cape St Francis fault, Cape St Francis and Oyster Bay, Eastern Province. Council for Geoscience, Report No. 2008-0171, 30 pp.

Tankard, A.J., Jackson, M.P.A., Erikkson, K.A., Hobday, D.K., Hunter, D.R. and Minter, W.E.L. (1982). *Crustal evolution of Southern Africa*. Springer-Verlag, New York, 523 pp.

Toerien, D.K. and Hill, R.S. (1989). The geology of the Port Elizabeth area. Explanation of sheet 3324 (1:250 000). Geological Survey of South Africa, 35 pp.

Appendix A3 - Zadorozhnaya, V., Eberle, D. and Claassen, D., 2012. Results of a Time Domain Electromagnetic survey conducted at Cape St. Francis with the intent of locating the bedrock surface buried beneath cenozoic cover, Eastern Cape, South Africa, CGS Report No. 2012-0152, Rev. 0, 15pp.

Results of a time domain electromagnetic survey conducted at Cape St. Francis with the intent of locating the bedrock surface buried beneath Cenozoic cover, Eastern Cape, South Africa.

by

Dr. V. Zadorozhnaya, Dr. D.Eberle, D. Claassen

CGS Report No. 2012-0152

CONFIDENTIAL

Corresponding authors:

Dr. V. Zadorozhnaya
Specialist Scientist
Council for Geoscience
Geophysics Unit
280 Pretoria Street
Pretoria 0001
Ph: 012 841 1189
E-mail: valeriya@geoscience.org.za

Dr. D. Eberle
Specialist Scientist
Council for Geoscience
Geophysics Unit
280 Pretoria Street
Pretoria 0001
Ph: 012 841 1196
E-mail:deberle@geoscience.org.za

Debbie Claassen (BSc. Hons.)
Geologist/GIS Operator
Council for Geoscience
Eastern Cape Unit
P.O. Box 5347
Port Elizabeth 6065
Tel: +27 (0)41 5811164
Email: dkilian@geoscience.org.za

i

Table of Contents

List of Figures

List of Table

1. Introduction

The Council for Geoscience (CGS) was asked to evaluate and then recommend the most suitable geophysical survey method for discerning subsurface geological structure, in particular a method that would determine bedrock surface beneath Cenozoic overburden in the area of Cape St. Francis. The CGS recommended carrying out a time domain electromagnetic (TDEM) survey because of it would provide a fine resolution of subsurface structures and rapid mobilization.

The survey at Cape St. Francis was conducted in an attempt to gather data for a marine terrace study undertaken in support of SSHAC level 3 investigations that will ultimately be integrated into the Probabilistic Seismic Hazard Assessment (PSHA) for the proposed nuclear power plant at Thyspunt. The survey aims to identify the bedrock surface beneath Cenozoic overburden. Interpretation of bedrock elevations to identify specific terraces and platforms will not be discussed in this report, but will be addressed in Kathryn et al, 2012. This report will aim to explain the methodology behind the TDEM technique and the primary observations obtained from the survey as it pertains to the subsurface geology and structure.

2. Survey locality and site description

The survey line was conducted within the 40 km radius of investigation known as the 'site locality' around the proposed nuclear power station at Thyspunt. The start and end co-ordinates of the survey line are given in table xx. The roughly 1675 m TDEM survey line was conducted sub-parallel to the coastline with a SSW-NNE trend that would enable it to cross three major Palaeozoic lithological units in the subsurface; namely the Peninsula Formation (quartzitic sandstone), Cedarberg Formation (pyritic black shale) and Goudini Formation (sandstone interbedded with shale and siltstone) (Figure xx and table xx). These geological units dip east and are situated along the eastern limb of a NW-SE trending anticline with a southern plunge. Palaeozoic formations are overlain by semi-consolidated Cenozoic sediments comprised of palaeodunes which are interbedded with occasional organic rich pedogenic and shell rich horizons. A sporadic and thin marine terrace gravel, known as the Alexandria Formation lies between the bedrock and dune overburden interface (Goedhart, et al, 2008), this unit often acts as a conduit for groundwater movement. However it must be mentioned; at the time the survey was conducted the area was experiencing a severe drought.

1

Table 1: Start and end co-ordinates of the Cape St. Francis TDEM survey line.

Survey Line	Line start co-ords		Line end co-ords	
TDEM CSF	S34.20415	E24.82260	S34.18919	E24.82590

The elevation of bedrock surface is presumed higher along the southern end of the profile in erosion resistant quartzitic, as opposed to the adjacent and less competent lithological units of the Cedarberg- and Goudini Formations which may form a paleochannel similar to the present day Cape St. Francis Bay at the coast. It may also be more cumbersome to determine the top of bedrock across the Cedarberg- and Goudini Formation because the overburden and bedrock may show a similar resistivity.

Any anomalies within the profile should be viewed in context within the areas structural features, such as the jointing pattern and lithological diversity of units such as the Goudini Formation.
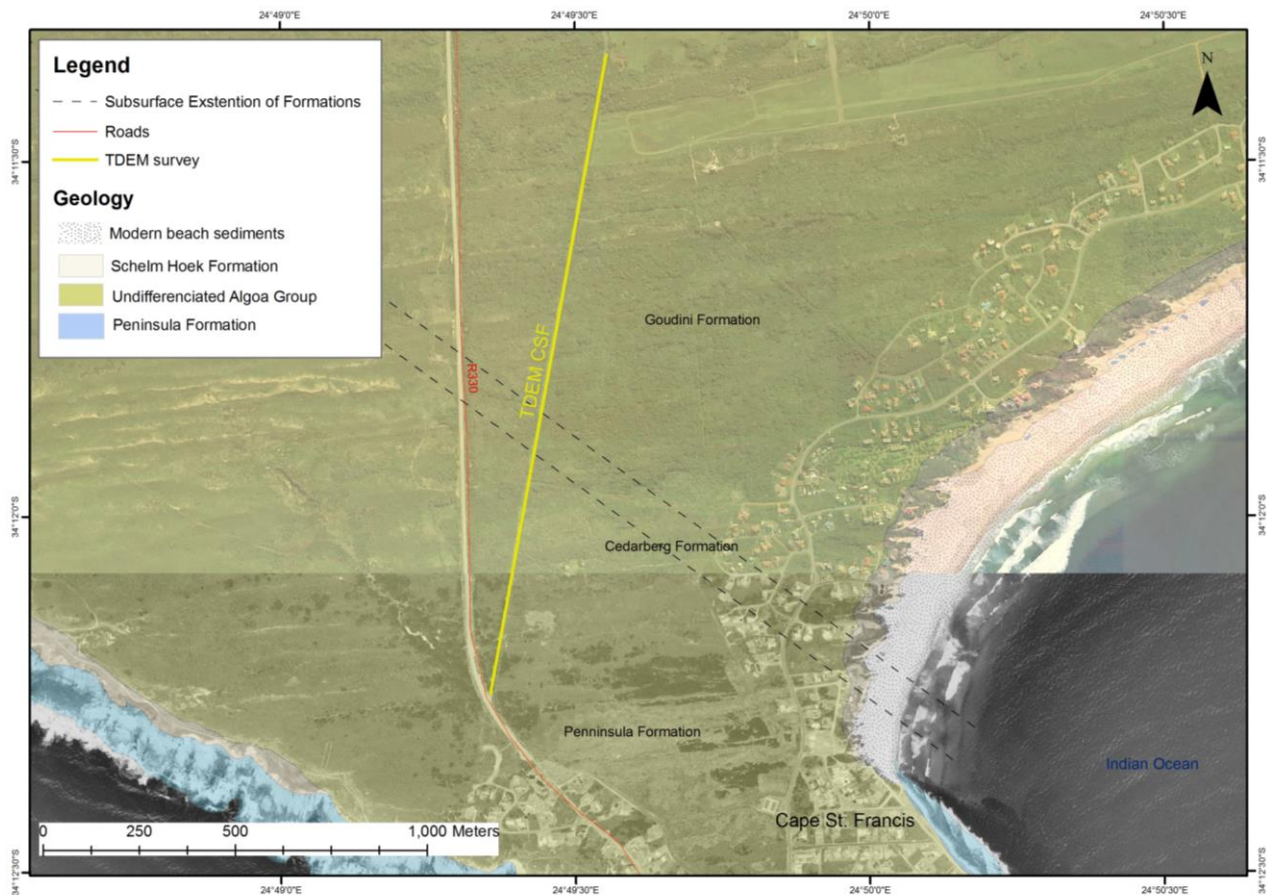
Figure 1: Map showing the location of the Cape St. Francis TDEM survey line. The interpreted position of formation boundaries within the subsurface are also indicated. The boundary interpretations are extrapolated along strike from inland exposures and a TDEM survey conducted along Cape St. Francis Bay in 2008.

Table 2: Resistivity and lithology of geological formations across the TDEM survey

Stratigraphy	Lithology	Resistive nature
Peninsula Formation	Quartzitic sandstone with minor thin shale beds	Very resistive
Cedarberg Formation	Black pyritic shale, minor sandstone	Very conductive
Goudini Formation	Sandstone, siltstone, lesser mudstone and quartzitic sandstone	Variable

3. Methodology

Electromagnetic (EM) survey method utilizes the response of the ground to the penetration of electromagnetic fields, which are composed of an alternating electrical intensity and magnetic force. Primary electromagnetic field is generated by passing an alternating current through a large loop of wire. The response of the ground is the generation of secondary electromagnetic field, the eddy current propagate in the ground and induce a flow in a receiver coil by the process of electromagnetic induction. Time domain electromagnetic sounding uses the primary field which is not continuous but consists of a series of pulses separating by periods when it is inactive. The secondary field induced by the primary is only measured during the interval when the primary is absent. The eddy currents induced in a subsurface conductor tend to diffuse inwards its centre when the inducing field is removed and gradually dissipate by resistive heat loss.

In ground surveys, the primary pulses EM field is generated by a transmitter that sends the electrical pulses in a large transmitter loop. In some TDEM array configurations the transmitter loop can also be utilized as a receiver loop. The decaying secondary field is quantified by measuring the temporal variation of the secondary at a number of fixed times (channels) after primary time-off.

TDEM method was developed in Russia in the middle of sixties. Sidorov and Tikshaev (1967) were the first who carried out field measurements in a case when the distance between transmitter and receiver loops was shorter then depth of investigation, when the response of ground was registered at the earlier time than process generated by plane electrical wave propagating from the surface. Simultaneously A. Kaufman in Novosibirsk (1967) and G. Obukhov in Moscow developed the theoretical foundation of TDEM. After A. Kaufman TDEM found numerous researcher as in Russia as in the West.

Some of the TDEM experiments relating to the search for oil and gas fields at greater depths required a time range of 0.1-10 seconds. However most of the geological problems that required solving can be investigated at shallow Several types of instruments have been designed and manufactured, which able to registration of secondary signals within the period of several microseconds to a few seconds (Geonics, Fenix, etc). The instrument used for fieldwork is TEMFAST -48 developed

in Russia and manufactures in Holland (AEMR). The application of TDEM is very large: hydrogeology, engineering geology, environmental geology, particularly delineation of ground water contamination, prospection of ore deposits, and search for oil contamination, supplementary for the other techniques. Interpretation of TDEM data has been done using the advanced software package TEM- Researcher (TEM-RES-WIN) softwere.

TEMFAST 48 is a new instrument in the family of portable geophysical tools developed by the AEMR company. In spite of the fact that there are in the geophysical market at a minimum a dozen EM and TDEM tools with similar area of application, the family TEMFAST products occupies a stable position in the field for small depth.

TEM-FAST originally was developed within the framework of the international program "MARS-94" and intended installation on the landed Matian module with the purpose of performing TDEM sounding in the surface of the "red planet" It is only natural that during its development the increased requirements for reliability of the instrument in extreme conditions, we set. All these qualities have been inherited by all "terrestrial" variants of TEMFAST. The TEMFAST instrument includes:a generator of uni-polar rectangular pulses (transmitter or Tx), a measuring block that provides the registration of the signals (receiver or Rx), a control block (controller), a power supply (battery). All devices are assembled in a single case. Portative PC type IPaq serves for selection of parameters and registration of the signals and its visualization. A complete set include instrument, antennas (cables), battery and PC, fits in such small case and weights 5 kg (Figure 2). The block of diagram of TEM-FAST 48 is given in the figure 3.

Figure 2. Instrument TEM-FAST 48
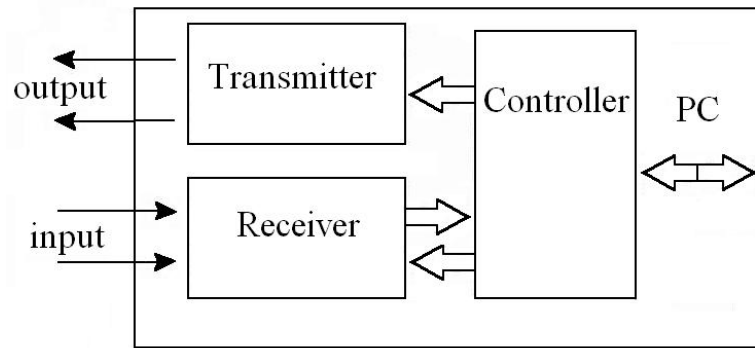
Figure 3. Block-diagram of TEMFAST 48

The TDEM device capable of working as robustly in urban street and industrial areas with level noise in the receiver of one volt and more. This device provides a dynamic range of measurements within the limits of 140 dB. TDEMFAST provides the possibility to start the process of measuring of decay of the current beginning from 4 μs. This parameter, determine the minimal time of registration of the signal and minimal depth of the research in TEMFAST is the shortest of all available TDEM instruments in the world market.

The antennas used by TEM-FAST are coaxial single loop. At time on it serves as a transmitter loop and at time off – as receiver. It is advantage and weakness of this configuration. The advantage is the easiest to lay thin, light and quite short cable on the ground. It accelerates the field work process and allows to record 50-60 sounding per day manipulating by persons only. In TEMFAST the automatic mode of operations is stipulated, at which the device through the given intervals of time (windows) makes measurements and records the data in PC memory. This mode can be used for the continuous monitoring of the conditions of various targets during several weeks or months. The pre-processing include formatting the reading into txt.files for following interpretation. The software provide as automatical interpretations of data as well as manual. It allow to interpret data affect by IP effect. TEMFAST 48HPC system have also advanced software package TEM-RESEARCHER (TEM-RES-WIN) for fast inverse problem solution in the class of gradient and layered sections directly in the field conditions. EM-RES-WIN gives user possibility to do inversion even if induced polarization (IP) and superparamagnetic (SPM) effect complicate experimental data.

5

4. Field work technique and interpretation

To determine the internal structure of the area a single loop of 25m x 25m was used to do soundings. The loop size was kept small on purpose to obtain high resolution of the near surface bedded rocks. For better lateral resolution the distance between centres of loop was kept 12.5 m. The length of the profile is 1675 m. Total number of TDEM stations on the profile is 134. The location of the TDEM stations was marked by GPS.

The pre-processing includes formatting the reading into txt.files for following interpretation. The software provide as automatically interpretations of data as well as manual. TEM-FAST 48HPC system have also advanced software package TEM-RESEARCHER (TEM-RES-WIN) for fast inverse problem solution in the class of gradient and layered sections directly in the field conditions. EM-RES-WIN gives user possibility to do inversion.

The investigated areas consist of different type of rocks and accordingly different types of emf (electromagnetic force) have been recorded. The example forward modeling (apparent resistivity) is given in the figures 4-6 which demonstrate different shape of TDEM signals.
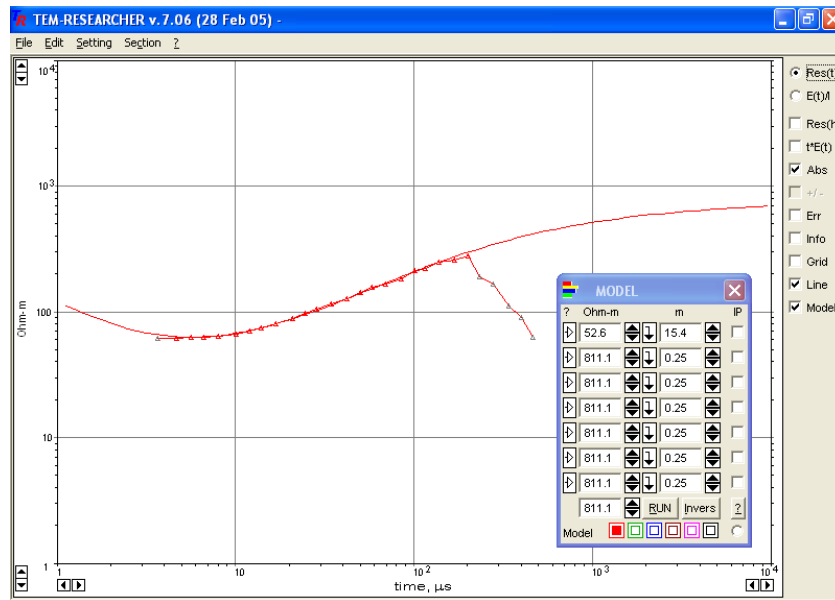
Figure 4. Interpretation of TDEM 6 located on the high resistive block in the Southern partof profile 1. Field and modeled emf curves has been shown. The table on the left demonstrated parameters of the section at this point.

6
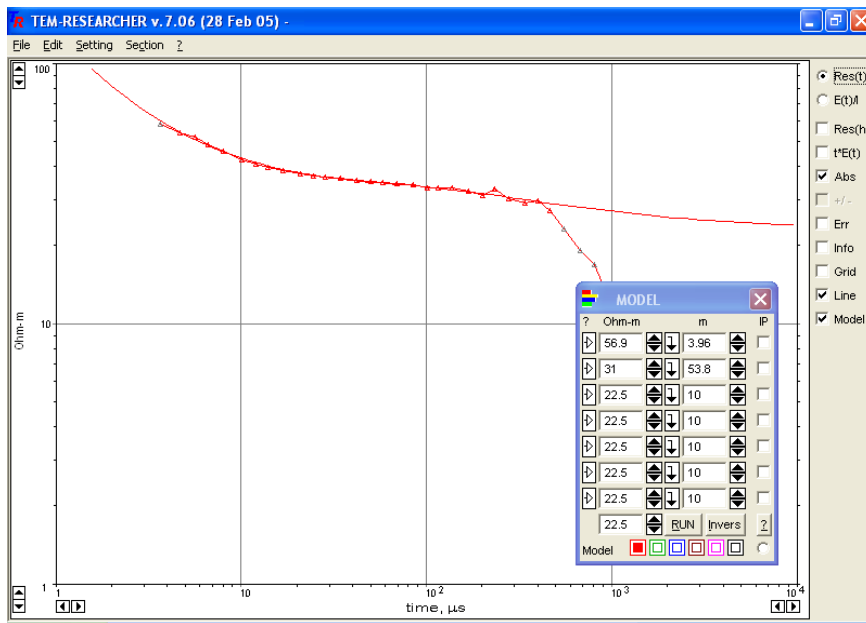
Figure 5. Interpretation of TDEM 77 located on the middle of profile where low resistive sediments are deposited. Field and modeled emf curves has been shown. The table on the left demonstrated parameters of the section at this point.
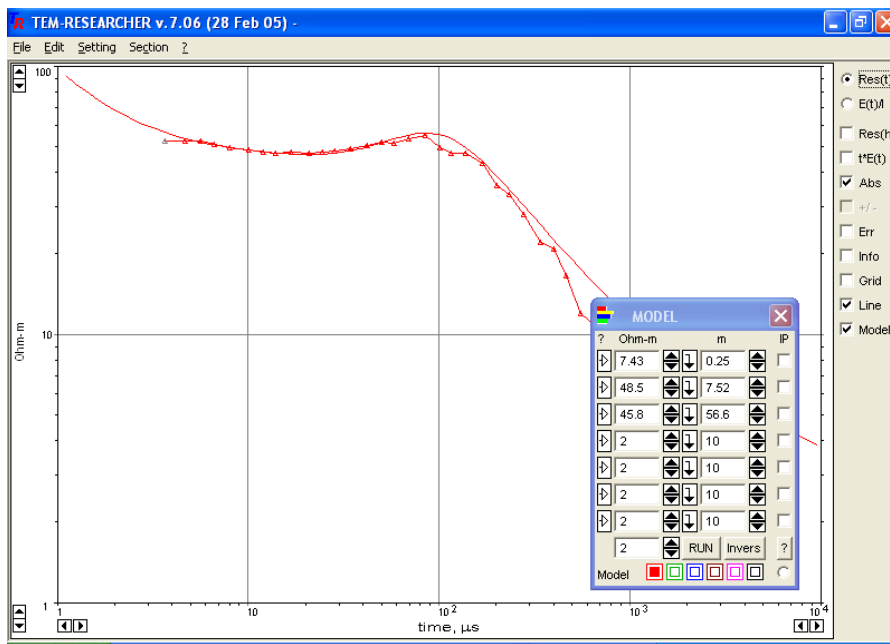
Figure 6. Interpretation of TDEM 55 located close to the anomaly "B" separating relatively conductive Peninsula Formation and very conductive Cederberg Formation (Figure 6). Field and modeled emf curves has been shown. The table on the left demonstrated parameters of the section at this point.

7

The figure 4 demonstrates the curve recorded on the north of profile where high resistive block has been observed. The resistivity of Peninsula Formation quartzite is very high, more than 800 Ohmm. The thickness of overlaid Cenozoic sediments (with resistivity of 56 Ohmm is approximately 15 m. The figure 5 shows the relatively low resistive sediments (56, 32 and 22 Ohmm), possible Goudini Formation . The depth on basement is deeper than electromagnetic field occurring due to using TEMFAST 48 transmitter (1 Amper current) could penetrate.

The figure 6 demonstrates the influence of the high conductive body to the TDEN transformed signal. Let us note that most of the curves at the later time of registration were distorted. The comparison $\rho_\tau(t)$ with emf allow editing the readings.

5. Results and conclusion

The interpretation of results are presented in the geoelectrical profiles (Figure 7). Three blocks characterizing of different geoelectrical feathers can be delineated along this profile. A zone of highly resistive rocks is observed towards the south between stations TDEM 1-43 starting at a depth of roughly 15 m. This resistive zone is interpreted to quartzitic sandstone of the Peninsula Formation. Sediments overlaying the Peninsula Formation show relatively low resistivity (40-60 Ohmm) and are associated with the semi-consolidated sediments of the Algoa Group.

A clear boundary between the resistive quartzitic sandstone and a more conductive zone further north is marked between anomaly A and B and TDEM stations 45-50. It is unclear whether this zone marks a change of lithology within the Peninsula Formation over a length of roughly 30 m or if the area is representative of a fractured / highly jointed zone similar to those seen along the coast that are indicative of gully formation.

A conductive body is observed between TDEM stations 50-60 starting at a depth of 30 m. This conductive zone can stratigraphically be correlated to the black pyritic Cedarberg Formation shale. The projected subsurface location of the formation, taken along strike from inland outcrop and postulated location according to a TDEM survey along the Cape St. Francis bay (Stettler, et al, 2008); is consistent with its position along the survey line.

From TDEM station 60 to the end of the profile a diverse pattern of resistivity is observed. This zone is believed to present the lithological varied Goudini Formation which consists of alternating beds of mudstone, shale, siltstone, sandstone/greywackey. It is extremely difficult to determine the bedrock surface in such a diverse setting, where overburden may share a similar resistive nature than

8

the bedrock. A zone along the southern end of the profile between TDEM stations 118-134 starting at a depth of roughly 50 m within the Goudini Formation share a similar resistivity to the quartzitic sandstone of the Peninsula Formation seen along the southern end of the survey line. The assumption here is the transition from lithological unit into a quartzitic sandstone unit within the Goudini Formation. Therefore anomalies E and F can be seen as indicators of lithological change within the formation.

It must be noted that an assumption is made regarding the bedrock surface. It is assumed is deeper in the Cedarberg and Goudini Formations. A palaeochannel similar to the Cape St. Francis Bay is presumed to be present inland beneath Cenozoic overburden in part due to the formation's less competent units that erode easily.

At TDEM station 94, anomaly D seemingly extends through both Cenozoic overburden and bedrock and show a vertical inclination. Its possible origin is uncertain, but could be associated with the on-land extent of the offshore Cape St. Francis fault. A similar feature was identified by Stettler, et al (2008) further south along the TDEM survey conducted at Cape St. Francis bay and was interpreted as possibly being the Cape St. Francis fault, however the deduction was inconclusive.

A multi-electrode resistivity survey conducted by Loots et al, 2009 in the same area was however unable to detect a similar anomaly, but does verify the positional accuracy of the boundaries between formations as indicated by the survey in this report.
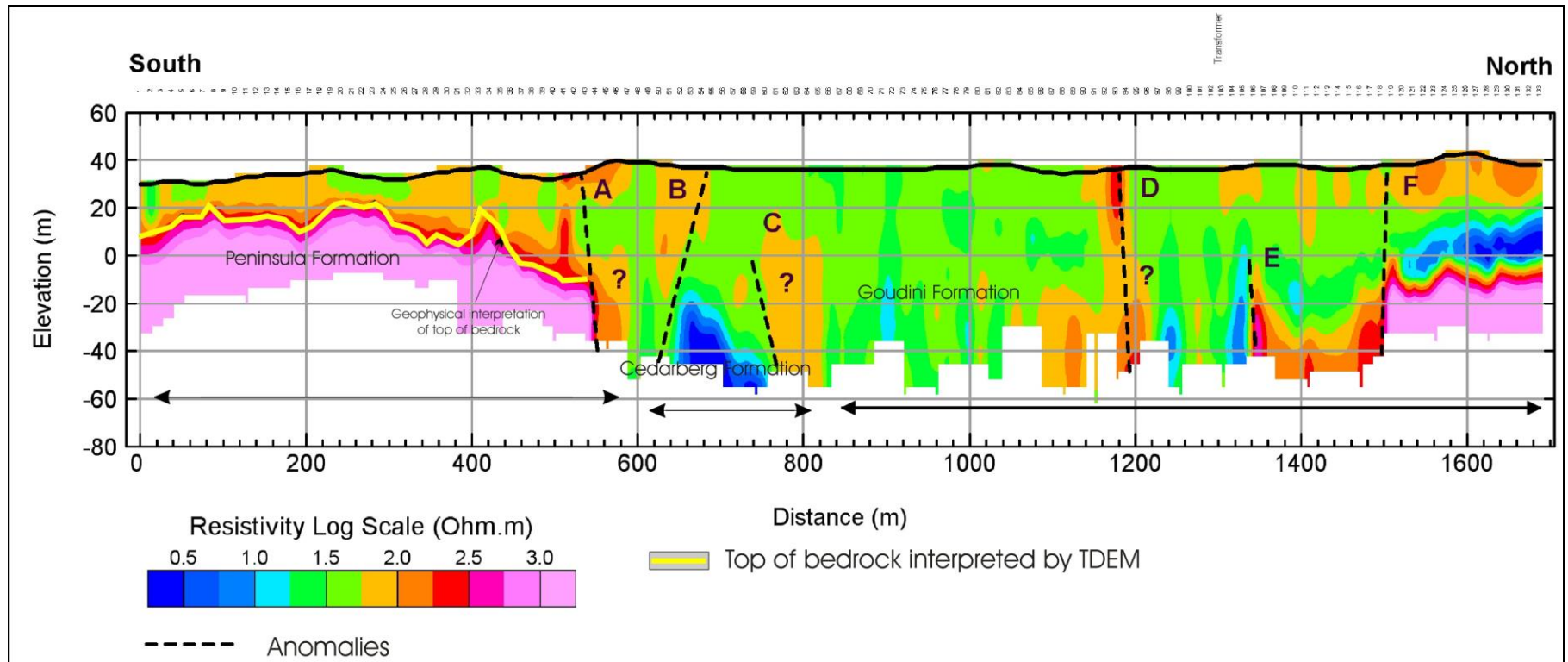
Figure 7: Cape St. Francis geoelectrical profile, showing interpreted bedrock surface along the Peninsula Formation in the south. The area that constrains each formation is also indicated.

10

6. References

Goedhart. M.L., Reddering, J.S.V., Kilian, D, Mitha, M, Bosch, P.J.A, and Black, D (2008) Surface geology and update of onland geological hazards for the proposed Thyspunt nuclear power plant, Eastern Cape, South Africa, Report No.2008-0222.

Loots, L., Chirenje, E., Claassen, D., Black, D. 2009. A multi-electrode resistivity survey near Cape St. Francis and Thyspunt, Eastern Cape with the intent to locate the position of marine terraces and possible faults buried under Cenozoic cover. Council for Geoscience, Report Nr. 2009-0211.

Stettler,E.H., Zadorozhnaya, V.Y., and Goedhart, M.L. 2008. Results of a time domain electromagnetic survey over four possible fault positions signifying the landward continuation of the Cape St. Francis fault, Cape St. Francis and Oyster Bay, Eastern Province. Council for Geoscience, Report Nr. 2008-0171.

Appendix B – Field measurements

APPENDIX B

Bedding Readings			
Latitude	Longitude	Azim.	Dip
24.83502	-34.2071	70	15
24.83541	-34.207419	29	22
24.835999	-34.20796	30	16
24.83717	-34.20937	34	20
24.83727	-34.212709	64	15
24.83733	-34.213649	52	15
24.83665	-34.21385	32	16
24.835539	-34.21344	56	76
24.83415	-34.21257	14	20
24.833239	-34.212409	194	6
24.832599	-34.212079	42	50
24.83214	-34.212089	120	8
24.83147	-34.21275	43	9
24.831429	-34.212089	47	10
24.830519	-34.211259	12	11
24.8304	-34.21077	67	5
24.81436	-34.20558	80	18
24.813749	-34.205449	28	10
24.81277	-34.20489	218	8
24.811349	-34.20446	172	10
24.810109	-34.20306	34	15
24.807549	-34.202029	66	10
24.80535	-34.20093	140	5
24.801989	-34.19969	256	12
24.80016	-34.199399	56	12
24.797319	-34.198309	202	2
24.79627	-34.197359	54	7
24.79525	-34.197199	70	10
24.792969	-34.19672	130	10
24.79089	-34.197099	348	8
24.788469	-34.199259	104	4
24.78772	-34.199979	106	5

Bedding Readings			
Latitude	Longitude	Azim.	Dip
24.787129	-34.19983	40	0
24.78474	-34.19997	186	10
24.783929	-34.19993	175	9
24.78282	-34.19947	152	5
24.78183	-34.199769	212	15
24.78022	-34.199169	12	10
24.778439	-34.19904	174	15
24.77722	-34.197159	162	2
24.77643	-34.196469	220	5
24.77538	-34.1969	220	15
24.77426	-34.1972	22	18
24.772639	-34.19758	14	25
24.77323	-34.19768	192	40
24.77157	-34.1976	188	22
24.769949	-34.197959	212	20
24.76911	-34.19758	22	20
24.768739	-34.19751	12	22
24.76776	-34.19766	42	10
24.76769	-34.196779	20	20
24.76691	-34.19617	34	20
24.76643	-34.19613	28	25
24.76577	-34.197089	40	25
24.76521	-34.196749	28	22
24.76458	-34.19634	14	25
24.76456	-34.195159	22	25
24.763429	-34.195399	10	25
24.65379	-34.161859	215	65
24.65343	-34.162039	226	50
24.65313	-34.162319	234	59
24.65272	-34.162669	242	28
24.747229	-34.154059	35	34
24.70971	-34.157899	200	75

Bedding Readings			
Latitude	Longitude	Azim.	Dip
24.71068	-34.159199	200	75
24.70738	-34.16301	205	81
24.833239	-34.212409	43	15
24.83214	-34.212089	24	12
24.81277	-34.20489	222	10
24.78282	-34.19947	46	22
24.77722	-34.197159	185	29
24.77323	-34.19768	183	21
24.77157	-34.1976	184	20
24.769949	-34.197959	202	22
24.65379	-34.161859	212	86
24.70971	-34.157899	30	86
24.757859	-34.163	226	24
24.74896	-34.190829	200	22
24.747879	-34.19067	251	19
24.747419	-34.19041	211	25
24.746379	-34.19033	216	15
24.74585	-34.189929	221	18
24.745069	-34.189419	212	150
24.74402	-34.189159	201	22
24.7433	-34.189009	236	12
24.74289	-34.18874	221	25
24.74206	-34.187899	201	33
24.74172	-34.18823	224	28
24.741429	-34.18782	231	30
24.683229	-34.18359	216	35
24.74102	-34.188059	188	12
24.74036	-34.187959	197	27
24.739989	-34.18792	181	20
24.739359	-34.187739	214	16
24.738859	-34.18776	212	36
24.73826	-34.18732	195	16

Bedding Readings			
Latitude	Longitude	Azim.	Dip
24.73794	-34.18738	236	30
24.73735	-34.187329	220	32
24.736889	-34.1869	245	35
24.736449	-34.186769	213	32
24.73594	-34.18676	206	40
24.735369	-34.18642	213	28
24.734049	-34.18604	180	27
24.71602	-34.192179	206	60
24.71589	-34.19238	205	45
24.71511	-34.192129	215	42
24.71477	-34.192139	210	40
24.714299	-34.192339	215	30
24.71411	-34.192529	206	41
24.714089	-34.192879	211	42
24.714579	-34.19309	215	48
24.713559	-34.19246	208	62
24.713139	-34.19244	211	54
24.71272	-34.192679	215	48
24.712119	-34.19297	203	53
24.711669	-34.19281	209	52
24.71129	-34.192739	212	51
24.711089	-34.19257	211	49
24.71065	-34.192589	240	51
24.71015	-34.19236	206	54
24.709879	-34.192149	206	42
24.70834	-34.191489	201	47
24.70784	-34.191339	208	40
24.70707	-34.191239	212	45
24.706769	-34.191099	208	55
24.706599	-34.191169	202	45
24.70641	-34.191119	213	52
24.70621	-34.19103	215	50

APPENDIX B

Bedding Readings

Latitude	Longitude	Azimuth	Dip
24.706039	-34.19097	215	55
24.70581	-34.19093	212	60
24.7057	-34.190839	212	53
24.705329	-34.190739	212	46
24.705099	-34.19061	222	45
24.70457	-34.19067	212	56
24.70393	-34.190219	215	42
24.70373	-34.19003	220	26
24.7034	-34.189859	220	40
24.703229	-34.1898	210	40
24.702959	-34.18971	129	39
24.702799	-34.18959	215	52
24.70183	-34.18928	211	49
24.701169	-34.18911	218	45
24.70082	-34.18892	211	45
24.7001	-34.188599	214	54
24.699639	-34.188409	203	46
24.70001	-34.18886	209	56
24.700019	-34.1891	218	44
24.70056	-34.19034	206	86
24.69994	-34.19001	207	53
24.699229	-34.18995	212	57
24.69817	-34.189799	212	50
24.69779	-34.18956	210	49
24.697509	-34.18931	220	56
24.69695	-34.189409	201	57
24.696939	-34.189559	211	45
24.696099	-34.189359	216	52
24.69572	-34.189069	210	45
24.69513	-34.189339	212	50
24.69482	-34.189689	209	60
24.69424	-34.189379	202	62

Bedding Readings

Latitude	Longitude	Azimuth	Dip	Strat
24.69372	-34.18922	221	56	
24.69291	-34.188809	215	52	
24.692549	-34.18854	208	65	
24.69183	-34.18748	215	52	
24.69135	-34.18775	217	45	
24.69106	-34.18746	212	52	
24.690549	-34.187429	202	45	
24.68998	-34.187129	210	50	
24.68961	-34.18702	209	52	
24.68938	-34.1871	216	54	
24.688749	-34.186939	213	53	
24.676699	-34.18227	214	57	
24.83502	-34.2071	70	15	
24.83541	-34.207419	29	22	
24.835999	-34.20796	30	16	
24.83717	-34.20937	34	20	
24.83727	-34.212709	64	15	
24.83733	-34.213649	52	15	
24.83665	-34.21385	32	16	
24.835539	-34.21344	56	76	
24.83415	-34.21257	14	20	
24.833239	-34.212409	194	6	
24.832599	-34.212079	42	50	
24.83214	-34.212089	120	8	
24.83147	-34.21275	43	9	
24.831429	-34.212089	47	10	
24.830519	-34.211259	12	11	
24.8304	-34.21077	67	5	
24.82987	-34.21114	53	16	
24.82951	-34.21115	54	16	
24.8285	-34.211	18	12	
24.827489	-34.21131	48	13	

Bedding Readings

Latitude	Longitude	Azimuth	Dip
24.827489	-34.21131	48	13
24.8273	-34.210959	24	14
24.82572	-34.20966	59	8
24.82475	-34.208769	39	12
24.82342	-34.20876	42	6
24.82239	-34.20841	57	12
24.82175	-34.20841	46	15
24.819939	-34.20805	15	10
24.818509	-34.207379	82	20
24.677739	-34.18243	205	59
24.69406	-34.18944	34	53
24.69306	-34.188079	30	50
24.715999	-34.15244	256	11
24.74642	-34.153999	241	15
24.78414	-34.15283	201	37
24.74792	-34.161189	249	7
24.74792	-34.161189	238	12
24.81798	-34.206619	42	14
24.816489	-34.206329	79	9
24.81639	-34.206169	52	6
24.814289	-34.205659	84	14
24.81375	-34.20543	50	8
24.812719	-34.20486	54	10
24.811369	-34.204449	352	9
24.809729	-34.203569	358	10
24.80759	-34.20217	118	8
24.80539	-34.20095	30	6
24.80191	-34.199709	320	10
24.799609	-34.199299	122	10
24.800119	-34.19932	56	12
24.79732	-34.198259	20	2
24.79632	-34.197339	62	7

Bedding Readings

Latitude	Longitude	Azimuth	Dip
24.7953	-34.19714	41	10
24.793829	-34.196789	42	9
24.792959	-34.19674	127	7
24.790889	-34.19716	3	6
24.78851	-34.19936	78	4
24.787709	-34.20001	230	10
24.78471	-34.19995	212	11
24.782809	-34.19944	162	12
24.781849	-34.1997	229	21
24.780279	-34.19915	169	11
24.77838	-34.19902	210	11
24.777219	-34.19717	215	12
24.777129	-34.19689	231	8
24.77642	-34.19646	183	10
24.77536	-34.196899	158	17
24.774259	-34.197239	69	19
24.77267	-34.19757	192	25
24.77378	-34.19781	203	25
24.77323	-34.19771	183	21
24.77258	-34.198069	179	20
24.77155	-34.19764	202	20
24.769999	-34.197969	198	22
24.76875	-34.197519	7	25
24.76771	-34.197669	216	23
24.767679	-34.19677	190	17
24.76689	-34.196239	201	16
24.76639	-34.19618	195	15
24.764549	-34.196369	201	22
24.76459	-34.19523	219	16
24.76348	-34.19544	184	17
24.762839	-34.195519	212	23
24.762019	-34.19547	210	22

APPENDIX B

Bedding Readings					Bedding Readings					Bedding Readings					Bedding Readings			
Latitude	Longitude	Azimuth	Dip		Latitude	Longitude	Azimuth	Dip		Latitude	Longitude	Azimuth	Dip		Latitude	Longitude	Azimuth	Dip
24.760999	-34.19553	219	25		24.78769	-34.199919	175	6		24.68387	-34.183479	211	45		24.66517	-34.177529	212	60
24.76025	-34.19527	214	27		24.846529	-34.17994	35	35		24.68353	-34.183779	215	46		24.66488	-34.17719	210	54
24.759809	-34.19472	92	22		24.845939	-34.17961	37	33		24.68226	-34.18378	206	57		24.66506	-34.176849	211	56
24.759309	-34.194169	199	22		24.84508	-34.179029	35	30		24.68177	-34.184439	208	55		24.66426	-34.176959	213	60
24.75885	-34.19407	205	26		24.844	-34.17846	30	34		24.681389	-34.183699	210	57		24.663939	-34.176489	221	60
24.75837	-34.194019	206	22		24.843439	-34.178259	35	34		24.6805	-34.183799	215	53		24.66344	-34.176509	217	70
24.75755	-34.19397	193	19		24.842839	-34.17792	39	34		24.67993	-34.183719	213	58		24.66322	-34.176339	210	59
24.756959	-34.194109	223	30		24.842	-34.17685	37	39		24.679639	-34.183399	211	63		24.662769	-34.17613	210	57
24.75653	-34.193839	220	16		24.84169	-34.17664	45	35		24.67924	-34.18333	206	60		24.662279	-34.176029	212	60
24.756129	-34.193469	222	30		24.841449	-34.17653	35	20		24.67859	-34.18305	218	53		24.661689	-34.17574	213	60
24.75572	-34.19315	217	20		24.84106	-34.17606	40	20		24.678209	-34.182979	215	69		24.833239	-34.212409	43	15
24.755049	-34.19274	205	17		24.840749	-34.17519	36	28		24.677729	-34.18251	210	55		24.83214	-34.212089	24	12
24.75436	-34.192659	194	21		24.84007	-34.174749	24	29		24.677079	-34.18231	211	55		24.82951	-34.21115	336	14
24.75334	-34.193009	188	30		24.83874	-34.173979	31	41		24.67653	-34.18213	220	55		24.827489	-34.21131	16	18
24.75316	-34.192159	185	22		24.83783	-34.173189	30	40		24.676069	-34.18222	208	60		24.818509	-34.207379	104	10
24.752779	-34.19172	200	20		24.836339	-34.172009	34	41		24.67545	-34.18141	220	61		24.782809	-34.19944	234	16
24.752439	-34.19234	201	22		24.784709	-34.199919	132	5		24.675209	-34.18107	214	60		24.781849	-34.1997	233	12
24.751799	-34.19174	212	29		24.78395	-34.19995	175	9		24.67489	-34.18123	211	60		24.77838	-34.19902	200	23
24.75126	-34.19163	201	22		24.782809	-34.19947	195	10		24.674039	-34.18104	212	67		24.77323	-34.19771	7	30
24.75056	-34.19106	210	22		24.782809	-34.19947	210	19		24.67315	-34.180759	216	54		24.77155	-34.19764	2	17
24.7498	-34.19096	234	18		24.78185	-34.19975	220	9		24.67247	-34.180219	212	70		24.769999	-34.197969	350	18
24.749359	-34.19107	220	18		24.780229	-34.19921	192	15		24.67233	-34.18014	220	64		24.65889	-34.15566	192	40
24.66469	-34.151309	178	46		24.6882	-34.186909	206	53		24.671789	-34.17984	214	62		24.675079	-34.18114	209	55
24.66351	-34.150319	222	52		24.68809	-34.18684	213	55		24.67124	-34.179579	219	60		24.670259	-34.179489	207	83
24.662359	-34.149709	197	61		24.686899	-34.18679	212	50		24.670399	-34.17974	208	62		24.666009	-34.17732	229	44
24.662919	-34.15	196	50		24.687379	-34.18624	213	59		24.669729	-34.17859	221	54		24.68705	-34.157179	180	22
24.662919	-34.15003	192	42		24.68662	-34.185749	205	62		24.6682	-34.178899	202	59		24.6848	-34.16126	202	45
24.658829	-34.15183	201	62		24.686149	-34.185269	207	55		24.668099	-34.17859	212	57		24.68737	-34.15999	188	37
24.814359	-34.205599	15	9		24.685879	-34.18507	218	60		24.66785	-34.17839	216	61		24.68696	-34.160179	203	32
24.813669	-34.20548	30	7		24.686	-34.18451	212	46		24.667079	-34.178389	210	49		24.6522	-34.154869	208	53
24.811409	-34.2044	8	12		24.685139	-34.183469	205	52		24.66656	-34.17783	214	47		24.65486	-34.152229	234	35
24.78769	-34.199919	175	6		24.68467	-34.18353	215	48		24.66605	-34.177579	208	50		24.656509	-34.15301	207	47

APPENDIX B

Bedding Readings			
Latitude	Longitude	Azimuth	Dip
24.657929	-34.1538	187	44
24.65886	-34.153889	209	40
24.65822	-34.15519	216	43
24.65871	-34.155419	213	45
24.670229	-34.15102	209	40
24.8538	-34.18475	37	36
24.85544	-34.18574	38	39
24.857529	-34.186779	32	31
24.8581	-34.18792	41	39
24.860489	-34.19011	29	27
24.86251	-34.19094	49	30
24.86301	-34.19128	50	40
24.864119	-34.19236	31	43
24.865769	-34.19362	40	43
24.86661	-34.19396	29	46
24.867219	-34.19416	30	36
24.868709	-34.19497	52	34
24.86996	-34.19642	43	37
24.853719	-34.19357	45	38
24.855949	-34.19416	30	37
24.858349	-34.19409	36	40
24.859469	-34.194059	44	41
24.8602	-34.194079	39	39
24.86081	-34.19429	298	85
24.861719	-34.194539	40	41
24.86378	-34.195139	34	50
24.86587	-34.19516	33	41
24.867639	-34.196259	41	45
24.86861	-34.19583	48	35
24.85966	-34.19119	47	42
24.85684	-34.192099	51	31
24.6848	-34.16126	188	40

Bedding Readings			
Latitude	Longitude	Azimuth	Dip
24.68737	-34.15999	204	30
24.868709	-34.19497	58	35
24.678209	-34.18296	208	54
24.679219	-34.18337	215	62
24.665919	-34.150789	200	35
24.77846	-34.198999	215	21
24.777219	-34.19713	210	5
24.77534	-34.19691	175	14
24.774199	-34.197009	180	16
24.77266	-34.197539	185	21
24.70377	-34.18825	185	27
24.749789	-34.19096	215	10
24.749369	-34.191039	213	16
24.749069	-34.19085	200	22
24.7479	-34.190719	225	14
24.7474	-34.190439	211	25
24.746319	-34.190349	220	12
24.745879	-34.18997	211	17
24.74508	-34.18943	200	20
24.744069	-34.189169	212	19
24.74329	-34.18904	174	7
24.74278	-34.188569	210	10
24.7421	-34.187939	205	25
24.74171	-34.188229	225	28
24.74146	-34.18782	225	32
24.74116	-34.188009	190	20
24.74038	-34.18799	195	25
24.739969	-34.18797	185	16
24.73932	-34.187719	214	16
24.73894	-34.187699	215	20
24.738259	-34.18731	195	16
24.73796	-34.18735	219	21

Bedding Readings			
Latitude	Longitude	Azimuth	Dip
24.73737	-34.187289	212	29
24.736899	-34.18688	222	25
24.73648	-34.18672	226	24
24.7358	-34.1868	197	34
24.735319	-34.186449	227	33
24.73405	-34.185979	203	27

APPENDIX B

Joint (Fracture) Readings

Latitude	Longitude	Azimuth	Dip	Strat
-34.01321	24.44614	276	90	Oc
-34.01322	24.44615	145	84	Oc
-33.8702778	24.60975	132	70	Oc
-34.1329038	24.43375301	315	57	Oc
-34.01315	24.44616	276	90	Oc
-34.01315	24.44616	145	84	Oc
-33.97631	24.88323	160	68	S-Db
-34.1497285	24.61516824	116	73	S-Db
-34.14256	24.60592	297	84	S-Db
-34.09613	24.6928	206	28	S-Db
-34.14263	24.60589	317	75	S-Db
-34.14256	24.60592	342	65	S-Db
-34.12461	24.56539	111	89	S-Db
-34.12666	24.5685	112	77	S-Db
-34.09613	24.6928	294	84	S-Db
-34.02079	24.58783	97	88	S-Db
-34.07642	24.8222	44	50	Dc
-34.07642	24.8222	244	75	Dc
-34.07642	24.8222	80	45	Dc
-34.07642	24.8222	40	85	Dc
-34.01628	24.66814	88	52	Dc
-34.01628	24.66814	116	81	Dc
-34.01628	24.66814	160	10	Dc
-34.09052	24.74373	300	78	Dc
-34.10225	24.71949	291	68	Dc
-34.02917	24.76163	332	70	Dc
-34.01997	24.63805	310	80	Dc
-34.07637	24.82206	44	50	Dc
-34.07637	24.82206	244	75	Dc
-34.07637	24.82206	80	45	Dc
-34.07637	24.82206	40	85	Dc
-34.1619	24.65379	340	80	Sg

Joint (Fracture) Readings

Latitude	Longitude	Azimuth	Dip	Strat
-34.16204	24.65343	138	60	Sg
-34.16232	24.65313	149	58	Sg
-34.16267	24.65272	154	70	Sg
-34.16248	24.73943	126	75	Sg
-34.16204	24.65343	131	80	Sg
-34.16232	24.65313	223	83	Sg
-34.16267	24.65272	121	46	Sg
-34.16204	24.65343	144	75	Sg
-34.06982	24.61721	121	90	Sg
-34.10381	24.5387	301	79	Sg
-34.05982	24.3973	120	84	Sg
-34.21414	24.83752	18	90	Op
-34.21415	24.83753	134	90	Op
-34.21416	24.83754	134	90	Op
-34.21417	24.83755	18	90	Op
-34.21404	24.83725	21	85	Op
-34.21405	24.83726	21	85	Op
-34.21385	24.83665	12	90	Op
-34.21386	24.83666	338	90	Op
-34.21387	24.83667	338	90	Op
-34.21388	24.83668	12	90	Op
-34.21382	24.83605	26	74	Op
-34.21383	24.83606	335	81	Op
-34.21384	24.83607	335	81	Op
-34.21385	24.83608	26	74	Op
-34.21365	24.83733	32	90	Op
-34.21366	24.83734	32	90	Op
-34.21344	24.83554	12	76	Op
-34.21345	24.83555	126	82	Op
-34.21346	24.83556	126	82	Op
-34.21347	24.83557	12	76	Op
-34.21324	24.83509	29	80	Op

Joint (Fracture) Readings

Latitude	Longitude	Azimuth	Dip	Strat
-34.21324	24.83509	29	80	Op
-34.21295	24.8345	29	75	Op
-34.21295	24.8345	29	75	Op
-34.21275	24.83147	69	90	Op
-34.21275	24.83147	12	90	Op
-34.21275	24.83147	12	90	Op
-34.21275	24.83147	69	90	Op
-34.21271	24.83727	96	86	Op
-34.21271	24.83727	346	77	Op
-34.21271	24.83727	346	77	Op
-34.21271	24.83727	96	86	Op
-34.21258	24.83414	18	90	Op
-34.21258	24.83414	18	90	Op
-34.21257	24.83415	19	89	Op
-34.21257	24.83415	19	89	Op
-34.21256	24.83387	40	75	Op
-34.21256	24.83387	304	85	Op
-34.21256	24.83387	304	85	Op
-34.21256	24.83387	40	75	Op
-34.21252	24.83167	76	84	Op
-34.21252	24.83167	140	80	Op
-34.21252	24.83167	140	80	Op
-34.21252	24.83167	50	90	Op
-34.21252	24.83167	76	84	Op
-34.21241	24.83324	16	90	Op
-34.21241	24.83324	16	90	Op
-34.21209	24.83143	35	85	Op
-34.21209	24.83143	35	85	Op
-34.21209	24.83214	39	82	Op
-34.21209	24.83214	310	79	Op
-34.21209	24.83214	310	79	Op
-34.21209	24.83214	39	82	Op

Joint (Fracture) Readings

Latitude	Longitude	Azimuth	Dip	Strat
-34.21208	24.8326	19	76	Op
-34.21208	24.8326	19	76	Op
-34.21130944	24.82749123	228	80	Op
-34.21130944	24.82749123	108	90	Op
-34.21126	24.83052	200	86	Op
-34.21126	24.83052	82	82	Op
-34.21126	24.83052	82	82	Op
-34.21126	24.83052	200	86	Op
-34.21114465	24.82986951	0	90	Op
-34.21114465	24.82986951	126	90	Op
-34.21114465	24.82986951	288	80	Op
-34.21100325	24.82849823	304	90	Op
-34.21100325	24.82849823	240	86	Op
-34.21100325	24.82849823	296	82	Op
-34.21096209	24.82729753	222	85	Op
-34.21096209	24.82729753	284	85	Op
-34.21076562	24.82676829	125	72	Op
-34.21076562	24.82676829	144	85	Op
-34.21077	24.8304	26	80	Op
-34.21077	24.8304	66	88	Op
-34.21077	24.8304	66	88	Op
-34.21077	24.8304	67	5	Op
-34.21077	24.8304	26	80	Op
-34.2103	24.83698	300	87	Op
-34.2103	24.83698	300	87	Op
-34.20965955	24.82571955	303	60	Op
-34.20965955	24.82571955	239	90	Op
-34.20965955	24.82571955	286	84	Op
-34.20937	24.83717	4	90	Op
-34.20937	24.83717	338	85	Strat
-34.20937	24.83717	338	85	Op
-34.20937	24.83717	4	90	Op

APPENDIX B

Joint (Fracture) Readings					Joint (Fracture) Readings					Joint (Fracture) Readings					Joint (Fracture) Readings				
Latitude	Longitude	Azimuth	Dip	Strat	Latitude	Longitude	Azimuth	Dip	Strat	Latitude	Longitude	Azimuth	Dip	Strat	Latitude	Longitude	Azimuth	Dip	Strat
-34.2087683	24.8247501	230	88	Op	-34.2071	24.83502	160	86	Op	-34.20445179	24.8113687	174	80	Op	-34.1997	24.78185	50	80	Op
-34.2087683	24.8247501	314	90	Op	-34.2071	24.83502	260	90	Op	-34.20357496	24.809733	215	85	Op	-34.1997	24.78185	272	90	Op
-34.2087683	24.8247501	295	69	Op	-34.2071	24.83502	260	90	Op	-34.20357496	24.809733	301	75	Op	-34.1997	24.78185	338	80	Op
-34.2087559	24.82342358	256	86	Op	-34.2071	24.83502	160	86	Op	-34.20357496	24.809733	175	78	Op	-34.19993	24.78393	270	80	Op
-34.2087559	24.82342358	136	90	Op	-34.206819	24.817175	232	77	Op	-34.20306	24.81011	290	75	Op	-34.19993	24.78393	238	87	Op
-34.2087559	24.82342358	288	85	Op	-34.206819	24.817175	300	78	Op	-34.20306	24.81011	182	82	Op	-34.19992	24.78471	52	80	Op
-34.20869	24.83686	14	85	Op	-34.206819	24.817175	306	71	Op	-34.20217149	24.8075851	210	78	Op	-34.19992	24.78471	350	65	Op
-34.20869	24.83686	14	85	Op	-34.2066231	24.817978	289	84	Op	-34.20217149	24.8075851	280	82	Op	-34.19992	24.78769	283	77	Op
-34.2084099	24.82174686	258	90	Op	-34.2063345	24.816489	250	81	Op	-34.20217149	24.8075851	184	77	Op	-34.19992	24.78769	54	80	Op
-34.2084099	24.82174686	294	80	Op	-34.2063345	24.816489	285	90	Op	-34.20203	24.80755	282	82	Op	-34.19992	24.78769	305	85	Op
-34.2084145	24.82239084	235	90	Op	-34.2061654	24.816387	301	80	Op	-34.20203	24.80755	194	88	Op	-34.19983	24.78702	300	85	Op
-34.2084145	24.82239084	284	83	Op	-34.2061654	24.816387	292	80	Op	-34.20110615	24.8062059	243	90	Op	-34.19983	24.78702	40	70	Op
-34.20814	24.83618	16	75	Op	-34.1992952	24.799608	282	85	Op	-34.20094857	24.8053909	242	90	Op	-34.19983	24.78713	270	80	Op
-34.20814	24.83618	16	75	Op	-34.2056595	24.814286	218	60	Op	-34.20094857	24.8053909	280	70	Op	-34.19983	24.78713	196	80	Op
-34.2080545	24.81993922	250	87	Op	-34.2056595	24.814286	282	75	Op	-34.20094857	24.8053909	366	85	Op	-34.19983	24.78713	128	90	Op
-34.2080545	24.81993922	173	90	Op	-34.2056595	24.814286	162	84	Op	-34.20093	24.80535	105	75	Op	-34.19977	24.78183	230	80	Op
-34.2080545	24.81993922	284	84	Op	-34.2056	24.81436	102	84	Op	-34.20093	24.80535	34	75	Op	-34.19977	24.78183	348	83	Op
-34.20796	24.836	40	90	Op	-34.2056	24.81436	235	47	Op	-34.20093	24.80535	292	75	Op	-34.19977	24.78183	220	90	Op
-34.20796	24.836	334	73	Op	-34.20558	24.81436	82	60	Op	-34.20001	24.78395	233	69	Op	-34.19975	24.78185	355	74	Op
-34.20796	24.836	334	73	Op	-34.20558	24.81436	226	75	Op	-34.20001	24.78395	270	60	Op	-34.19975	24.78185	102	80	Op
-34.20796	24.836	248	80	Op	-34.20545	24.81375	290	85	Op	-34.20001	24.78395	144	86	Op	-34.1997	24.78185	276	90	Op
-34.20796	24.836	40	90	Op	-34.20545	24.81375	60	80	Op	-34.20001	24.78395	116	90	Op	-34.1997145	24.80190706	312	76	Op
-34.2078933	24.81970428	236	90	Op	-34.2054257	24.813751	249	90	Op	-34.20001	24.78771	28	83	Op	-34.1997145	24.80190706	284	90	Op
-34.2078933	24.81970428	295	85	Op	-34.2054257	24.813751	104	85	Op	-34.20001	24.78771	278	80	Op	-34.1997145	24.80190706	164	81	Op
-34.2077715	24.82105292	285	90	Op	-34.2054257	24.813751	151	81	Op	-34.20001	24.78771	306	81	Op	-34.19969	24.80199	118	80	Op
-34.20742	24.83541	20	79	Op	-34.20489	24.81277	122	89	Op	-34.19998	24.78772	276	75	Op	-34.19969	24.80199	200	75	Op
-34.20742	24.83541	332	70	Op	-34.20489	24.81277	232	80	Op	-34.19998	24.78772	190	80	Op	-34.19947	24.78281	52	75	Op
-34.20742	24.83541	332	70	Op	-34.2048629	24.81272	239	90	Op	-34.19997	24.78474	60	80	Op	-34.19947	24.78281	53	76	Op
-34.20742	24.83541	20	79	Op	-34.2048629	24.81272	300	87	Op	-34.19997	24.78474	350	85	Op	-34.19947	24.78281	355	75	Op
-34.2073787	24.81851061	242	80	Op	-34.2048629	24.81272	168	85	Op	-34.19995	24.78395	126	87	Op	-34.19947	24.78282	102	70	Op
-34.2073787	24.81851061	167	90	Op	-34.2044518	24.811369	52	85	Op	-34.19995	24.78395	110	70	Op	-34.19947	24.78282	180	80	Op
-34.2073787	24.81851061	278	90	Op	-34.2044518	24.811369	288	90	Op	-34.19995	24.78395	238	88	Op	-34.19944	24.78281	285	60	Op

APPENDIX B

Joint (Fracture) Readings					Joint (Fracture) Readings					Joint (Fracture) Readings					Joint (Fracture) Readings				
Latitude	Longitude	Azimuth	Dip	Strat	Latitude	Longitude	Azimuth	Dip	Strat	Latitude	Longitude	Azimuth	Dip	Strat	Latitude	Longitude	Azimuth	Dip	Strat
-34.19944	24.78281	0	71	Op	-34.199	24.77846	356	63	Op	-34.19771	24.77323	90	75	Op	-34.19754	24.7692	346	75	Op
-34.1994	24.80016	40	82	Op	-34.199	24.77846	50	75	Op	-34.19771	24.77323	92	80	Op	-34.19754	24.7692	97	85	Op
-34.1994	24.80016	104	90	Op	-34.199	24.77846	325	86	Op	-34.19767	24.76771	145	89	Op	-34.19754	24.7692	312	84	Op
-34.1993559	24.78850566	179	86	Op	-34.199	24.77846	0	60	Op	-34.19767	24.76771	100	72	Op	-34.19754	24.77266	91	82	Op
-34.1993559	24.78850566	284	84	Op	-34.1989942	24.79836	290	85	Op	-34.19767	24.76771	305	71	Op	-34.19754	24.77266	307	75	Op
-34.1993559	24.78850566	150	90	Op	-34.19879	24.77797	272	75	Op	-34.19768	24.77323	278	75	Op	-34.19754	24.77266	55	83	Op
-34.1993559	24.78850566	24	76	Op	-34.19876	24.77802	90	80	Op	-34.19768	24.77323	348	82	Op	-34.19752	24.76875	352	89	Op
-34.1993243	24.80011669	194	90	Op	-34.19874	24.77796	284	75	Op	-34.19768	24.77323	138	85	Op	-34.19752	24.76875	104	74	Op
-34.1993243	24.80011669	310	82	Op	-34.19845	24.79701	126	90	Op	-34.19766	24.76776	278	73	Op	-34.19751	24.76874	376	72	Op
-34.1993243	24.80011669	144	83	Op	-34.19831	24.79732	108	90	Op	-34.19766	24.76776	204	60	Op	-34.19751	24.76874	176	90	Op
-34.1992952	24.79960808	189	87	Op	-34.19831	24.79732	180	85	Op	-34.19766	24.76776	178	90	Op	-34.19736	24.79627	286	75	Op
-34.1992952	24.79960808	284	83	Op	-34.1982586	24.79732	283	81	Op	-34.19765	24.77074	270	90	Op	-34.19736	24.79627	46	85	Op
-34.19926	24.78847	276	90	Op	-34.1982586	24.79732	322	86	Op	-34.19765	24.77074	140	90	Op	-34.19733748	24.7963165	210	90	Op
-34.19926	24.78847	164	80	Op	-34.19809	24.7726	278	80	Op	-34.19765	24.77074	92	88	Op	-34.19733748	24.7963165	284	84	Op
-34.19926	24.78847	220	75	Op	-34.19809	24.7726	6	75	Op	-34.19765	24.77074	94	90	Op	-34.19733748	24.7963165	356	84	Op
-34.19927	24.7997	286	80	Op	-34.19809	24.7726	328	80	Op	-34.19765	24.77074	125	90	Op	-34.19713573	24.79529802	280	88	Op
-34.19927	24.7997	272	85	Op	-34.19807	24.77258	7	76	Op	-34.19764	24.77155	39	74	Op	-34.19713573	24.79529802	314	87	Op
-34.19927	24.7997	190	85	Op	-34.19807	24.77258	95	90	Op	-34.19764	24.77155	70	85	Op	-34.19713573	24.79529802	75	88	Op
-34.19921	24.78023	235	81	Op	-34.19807	24.77258	313	67	Op	-34.19764	24.77155	150	84	Op	-34.1972	24.77426	282	88	Op
-34.19921	24.78023	303	78	Op	-34.19797	24.77	10	80	Op	-34.19764	24.77155	28	89	Op	-34.1972	24.77426	356	50	Op
-34.19921	24.78023	95	76	Op	-34.19797	24.77	82	90	Op	-34.1976	24.77157	96	80	Op	-34.1972	24.77426	302	90	Op
-34.19917	24.78022	274	90	Op	-34.19797	24.77	314	98	Op	-34.1976	24.77157	190	90	Op	-34.19717	24.77722	288	73	Op
-34.19917	24.78022	190	80	Op	-34.19796	24.76995	284	85	Op	-34.1976	24.77157	52	88	Op	-34.19717	24.77722	278	74	Op
-34.19915	24.78028	56	86	Op	-34.19796	24.76995	178	50	Op	-34.1976	24.77157	248	90	Op	-34.19717	24.77722	153	82	Op
-34.19915	24.78028	274	84	Op	-34.19796	24.76995	94	85	Op	-34.19758	24.76911	282	65	Op	-34.1972	24.79525	280	88	Op
-34.19915	24.78028	348	78	Op	-34.19796	24.76995	50	55	Op	-34.19758	24.76911	200	80	Op	-34.1972	24.79525	190	82	Op
-34.19904	24.77844	282	80	Op	-34.19781	24.77378	358	77	Op	-34.19758	24.76911	152	80	Op	-34.19716	24.77722	254	85	Op
-34.19904	24.77844	356	65	Op	-34.19781	24.77378	96	77	Op	-34.19758	24.77264	276	90	Op	-34.19716	24.77722	30	75	Op
-34.19904	24.77844	44	90	Op	-34.19781	24.77378	308	77	Op	-34.19758	24.77264	180	90	Op	-34.19716305	24.79089425	213	75	Op
-34.19902	24.77838	209	90	Op	-34.1978	24.77373	274	90	Op	-34.19757	24.77267	4	80	Op	-34.19716305	24.79089425	286	83	Op
-34.19902	24.77838	66	70	Op	-34.1978	24.77373	346	80	Op	-34.19757	24.77267	102	90	Op	-34.19713	24.77722	330	71	Op
-34.19902	24.77838	90	60	Op	-34.1978	24.77373	138	82	Op	-34.19757	24.77267	72	90	Op	-34.19713	24.77722	248	82	Op

APPENDIX B

Joint (Fracture) Readings					Joint (Fracture) Readings					Joint (Fracture) Readings					Joint (Fracture) Readings				
Latitude	Longitude	Azimuth	Dip	Strat	Latitude	Longitude	Azimuth	Dip	Strat	Latitude	Longitude	Azimuth	Dip	Strat	Latitude	Longitude	Azimuth	Dip	Strat
-34.19713	24.77722	260	82	Op	-34.19676	24.7652	102	72	Op	-34.19619	24.77704	248	84	Op	-34.19472	24.75981	317	83	Op
-34.19709	24.76577	272	85	Op	-34.19676	24.7652	7	80	Op	-34.19617	24.76691	284	75	Op	-34.19472	24.75981	22	80	Op
-34.19709	24.76577	218	73	Op	-34.19675	24.76521	304	75	Op	-34.19617	24.76691	288	85	Op	-34.19472	24.75981	94	79	Op
-34.19709	24.76577	132	85	Op	-34.19675	24.76521	102	80	Op	-34.19617	24.76691	136	80	Op	-34.19417	24.75931	60	74	Op
-34.1971357	24.79529802	284	78	Op	-34.19675	24.76521	88	60	Op	-34.19613	24.76643	284	85	Op	-34.19417	24.75931	49	74	Op
-34.1971357	24.79529802	190	90	Op	-34.1967883	24.793827	220	82	Op	-34.19553	24.761	38	72	Op	-34.19417	24.75931	324	85	Op
-34.1971	24.79089	104	85	Op	-34.1967883	24.793827	270	90	Op	-34.19553	24.761	119	89	Op	-34.19417	24.75931	92	78	Op
-34.1971	24.79089	42	75	Op	-34.1967883	24.793827	332	86	Op	-34.19553	24.761	341	69	Op	-34.19411	24.75696	41	45	Op
-34.1971	24.79089	162	80	Op	-34.19678	24.79397	122	80	Op	-34.19552	24.76284	53	61	Op	-34.19411	24.75696	130	88	Op
-34.19701	24.7742	280	76	Op	-34.19678	24.79397	190	85	Op	-34.19552	24.76284	322	87	Op	-34.19411	24.75696	191	89	Op
-34.19701	24.7742	355	62	Op	-34.19678	24.79397	180	85	Op	-34.19552	24.76284	161	80	Op	-34.19411	24.75696	98	74	Op
-34.19701	24.7742	94	85	Op	-34.1967398	24.792963	199	90	Op	-34.19547	24.76202	82	16	Op	-34.19407	24.75885	60	66	Op
-34.19701	24.7742	325	62	Op	-34.1967398	24.792963	279	70	Op	-34.19547	24.76202	94	83	Op	-34.19407	24.75885	315	86	Op
-34.19691	24.77534	95	81	Op	-34.19672	24.79297	286	75	Op	-34.19547	24.76202	276	70	Op	-34.19407	24.75885	21	87	Op
-34.19691	24.77534	135	80	Op	-34.19672	24.79297	210	85	Op	-34.19544	24.76348	204	69	Op	-34.19407	24.75885	94	77	Op
-34.1969	24.77536	331	61	Op	-34.19647	24.77643	280	90	Op	-34.19544	24.76348	268	90	Op	-34.19402	24.75837	24	68	Op
-34.1969	24.77536	174	99	Op	-34.19647	24.77643	358	75	Op	-34.19544	24.76348	136	80	Op	-34.19402	24.75837	310	81	Op
-34.1969	24.77536	190	87	Op	-34.19646	24.77642	163	88	Op	-34.1954	24.76343	270	86	Op	-34.19402	24.75837	226	87	Op
-34.1969	24.77538	276	85	Op	-34.19646	24.77642	280	90	Op	-34.1954	24.76343	202	75	Op	-34.19397	24.75755	32	60	Op
-34.1969	24.77538	180	65	Op	-34.19646	24.77642	133	88	Op	-34.1954	24.76343	140	80	Op	-34.19397	24.75755	298	85	Op
-34.1969	24.77538	320	65	Op	-34.19637	24.76455	2	87	Op	-34.19527	24.76025	37	75	Op	-34.19397	24.75755	336	85	Op
-34.19689	24.77713	290	46	Op	-34.19637	24.76455	100	77	Op	-34.19527	24.76025	298	78	Op	-34.19397	24.75755	89	87	Op
-34.19689	24.77713	40	81	Op	-34.19637	24.76455	329	80	Op	-34.19527	24.76025	348	77	Op	-34.19384	24.75653	20	60	Op
-34.19683	24.77711	278	50	Op	-34.19634	24.76458	272	85	Op	-34.19527	24.76025	300	89	Op	-34.19384	24.75653	292	84	Op
-34.19683	24.77711	20	55	Op	-34.19634	24.76458	98	80	Op	-34.19523	24.76459	82	77	Op	-34.19384	24.75653	87	70	Op
-34.19678	24.76769	320	80	Op	-34.19624	24.76689	5	84	Op	-34.19523	24.76459	304	88	Op	-34.19347	24.75613	94	74	Op
-34.19678	24.76769	154	80	Op	-34.19624	24.76689	96	81	Op	-34.19523	24.76459	314	97	Op	-34.19347	24.75613	132	80	Op
-34.19678	24.76769	66	75	Op	-34.19624	24.76689	330	70	Op	-34.19516	24.76456	272	85	Op	-34.19347	24.75613	9	73	Op
-34.19677	24.76768	99	70	Op	-34.19618	24.76639	115	76	Op	-34.19516	24.76456	214	65	Op	-34.19315	24.75572	2	85	Op
-34.19677	24.76768	305	80	Op	-34.19619	24.77704	278	50	Op	-34.19516	24.76456	160	45	Op	-34.19315	24.75572	270	76	Op
-34.19677	24.76768	320	66	Op	-34.19619	24.77704	20	55	Op	-34.19516	24.76456	214	65	Op	-34.19301	24.75334	46	64	Op
-34.19676	24.7652	182	79	Op	-34.19619	24.77704	320	75	Op	-34.19472	24.75981	42	71	Op	-34.19301	24.75334	99	71	Op

APPENDIX B

Joint (Fracture) Readings					Joint (Fracture) Readings					Joint (Fracture) Readings					Joint (Fracture) Readings				
Latitude	Longitude	Azimuth	Dip	Strat	Latitude	Longitude	Azimuth	Dip	Strat	Latitude	Longitude	Azimuth	Dip	Strat	Latitude	Longitude	Azimuth	Dip	Strat
-34.19301	24.75334	359	77	Op	-34.19096	24.74979	96	80	Op	-34.18993	24.74585	89	71	Op	-34.18823	24.74172	40	65	Op
-34.19293	24.75539	28	60	Op	-34.19096	24.74979	207	80	Op	-34.18993	24.74585	183	78	Op	-34.18823	24.74172	103	71	Op
-34.19293	24.75539	331	85	Op	-34.19096	24.74979	355	74	Op	-34.18943	24.74508	75	85	Op	-34.18823	24.74172	341	89	Op
-34.19293	24.75539	349	90	Op	-34.19096	24.7498	206	80	Op	-34.18943	24.74508	1	74	Op	-34.18807	-34.18807	210	79	Op
-34.19293	24.75539	91	82	Op	-34.19096	24.7498	96	80	Op	-34.18943	24.74508	300	83	Op	-34.18807	-34.18807	95	75	Op
-34.19274	24.75505	94	85	Op	-34.19096	24.7498	166	88	Op	-34.18942	24.74507	36	66	Op	-34.18807	-34.18807	52	50	Op
-34.19274	24.75505	352	90	Op	-34.19085	24.74907	79	81	Op	-34.18942	24.74507	75	80	Op	-34.18806	24.74102	337	89	Op
-34.19274	24.75505	101	74	Op	-34.19085	24.74907	171	60	Op	-34.18942	24.74507	1	74	Op	-34.18806	24.74102	90	84	Op
-34.19266	24.75436	220	80	Op	-34.19083	24.74896	171	65	Op	-34.18942	24.74507	302	88	Op	-34.18806	24.74102	122	78	Op
-34.19266	24.75436	92	80	Op	-34.19083	24.74896	100	85	Op	-34.18917	24.74407	96	66	Op	-34.18801	-34.18801	115	80	Op
-34.19266	24.75436	341	79	Op	-34.19083	24.74896	312	82	Op	-34.18917	24.74407	342	68	Op	-34.18801	-34.18801	300	84	Op
-34.19234	24.75244	111	90	Op	-34.19072	24.7479	93	63	Op	-34.18916	24.74402	94	62	Op	-34.18801	-34.18801	122	78	Op
-34.19234	24.75244	345	74	Op	-34.19072	24.7479	161	64	Op	-34.18916	24.74402	341	86	Op	-34.18801	-34.18801	40	55	Op
-34.19216	24.75316	53	80	Op	-34.19072	24.7479	0	76	Op	-34.18904	24.74329	94	71	Op	-34.18799	-34.18799	90	83	Op
-34.19216	24.75316	89	80	Op	-34.19072	24.7479	285	78	Op	-34.18904	24.74329	169	64	Op	-34.18799	-34.18799	34	72	Op
-34.19216	24.75316	355	86	Op	-34.19067	24.74788	161	68	Op	-34.18904	24.74329	4	71	Op	-34.18799	-34.18799	160	75	Op
-34.19216	24.75316	269	88	Op	-34.19067	24.74788	98	63	Op	-34.18901	24.7433	184	84	Op	-34.18796	24.74036	13	69	Op
-34.19174	24.7518	347	87	Op	-34.19067	24.74788	342	84	Op	-34.18901	24.7433	86	80	Op	-34.18796	24.74036	100	67	Op
-34.19174	24.7518	265	90	Op	-34.19067	24.74788	285	83	Op	-34.18901	24.7433	14	84	Op	-34.18796	24.74036	286	70	Op
-34.19172	24.75278	97	77	Op	-34.19044	24.7474	100	74	Op	-34.18874	24.74289	194	85	Op	-34.18794	-34.18794	100	89	Op
-34.19172	24.75278	347	84	Op	-34.19044	24.7474	169	86	Op	-34.18874	24.74289	96	82	Op	-34.18794	-34.18794	305	79	Op
-34.19163	24.75126	168	87	Op	-34.19041	24.74742	179	84	Op	-34.18874	24.74289	304	87	Op	-34.18794	-34.18794	354	76	Op
-34.19163	24.75126	96	77	Op	-34.19041	24.74742	100	74	Op	-34.18857	-34.18857	89	85	Op	-34.18792	24.73999	99	74	Op
-34.1915556	24.75202778	1	85	Op	-34.19035	24.74632	89	75	Op	-34.18857	-34.18857	340	86	Op	-34.1879	24.74206	359	77	Op
-34.1915556	24.75202778	282	82	Op	-34.19035	24.74632	172	60	Op	-34.18857	-34.18857	320	82	Op	-34.1879	24.74206	96	89	Op
-34.19107	24.74936	181	57	Op	-34.19033	24.74638	179	70	Op	-34.18848	24.74238	174	72	Op	-34.1879	24.74206	304	87	Op
-34.19107	24.74936	92	70	Op	-34.19033	24.74638	101	70	Op	-34.18848	24.74238	88	85	Op	-34.18782	24.74143	351	72	Op
-34.19107	24.74936	325	74	Op	-34.19033	24.74638	125	84	Op	-34.18848	24.74238	288	80	Op	-34.18782	24.74143	99	65	Op
-34.19106	24.75056	187	74	Op	-34.18997	24.74588	90	83	Op	-34.18846	-34.18846	95	66	Op	-34.18782	24.74143	122	76	Op
-34.19106	24.75056	91	86	Op	-34.18997	24.74588	202	89	Op	-34.18846	-34.18846	30	65	Op	-34.18782	-34.18782	95	65	Op
-34.19104	24.74937	85	77	Op	-34.18997	24.74588	275	78	Op	-34.18823	-34.18823	120	80	Op	-34.18782	-34.18782	320	90	Op
-34.19104	24.74937	190	55	Op	-34.18993	24.74585	53	90	Op	-34.18823	-34.18823	342	79	Op	-34.18782	-34.18782	355	71	Op

APPENDIX B

Joint (Fracture) Readings					Joint (Fracture) Readings					Joint (Fracture) Readings					Joint (Fracture) Readings				
Latitude	Longitude	Azimuth	Dip	Strat	Latitude	Longitude	Azimuth	Dip	Strat	Latitude	Longitude	Azimuth	Dip	Strat	Latitude	Longitude	Azimuth	Dip	Strat
-34.18776	24.73886	42	86	Op	-34.18729	-34.18729	350	75	Op	-34.16126	24.6848	115	65	Op	-34.19626	24.86764	304	85	Ss
-34.18776	24.73886	82	76	Op	-34.18729	-34.18729	329	85	Op	-34.16126	24.6848	105	79	Op	-34.19626	24.86764	207	57	Ss
-34.18776	24.73886	20	78	Op	-34.1869	24.73689	96	65	Op	-34.16119444	24.7479167	58	76	Op	-34.19626	24.86764	276	80	Ss
-34.18776	24.73886	78	79	Op	-34.1869	24.73689	328	81	Op	-34.16119444	24.7479167	155	74	Op	-34.19583	24.86861	290	70	Ss
-34.18774	24.73936	38	75	Op	-34.1869	24.73689	71	76	Op	-34.1579	24.70971	112	65	Op	-34.19516	24.86587	146	85	Ss
-34.18774	24.73936	86	88	Op	-34.18688	-34.18688	58	69	Op	-34.1592	24.71068	290	88	Op	-34.19516	24.86587	229	63	Ss
-34.18774	24.73936	352	63	Op	-34.18688	-34.18688	348	74	Op	-34.1592	24.71068	20	5	Op	-34.19514	24.86378	214	26	Ss
-34.18774	24.73936	292	87	Op	-34.1868	-34.1868	330	65	Op	-34.1587	24.64944	318	78	Op	-34.19514	24.86378	155	87	Ss
-34.18772	-34.18772	89	67	Op	-34.1868	-34.1868	185	85	Op	-34.154	24.7464167	106	69	Op	-34.19497	24.86871	205	43	Ss
-34.18772	-34.18772	352	63	Op	-34.1868	-34.1868	51	89	Op	-34.15244444	24.716	87	78	Op	-34.19497	24.86871	290	74	Ss
-34.18772	-34.18772	350	56	Op	-34.18677	24.73645	220	86	Op	-34.15244444	24.716	111	82	Op	-34.19497	24.86871	290	74	Ss
-34.1877	-34.1877	80	72	Op	-34.18677	24.73645	300	76	Op	-34.15223	24.65486	226	58	Op	-34.19454	24.86172	266	75	Ss
-34.1877	-34.1877	221	77	Op	-34.18677	24.73645	150	82	Op	-34.15223	24.65486	127	85	Op	-34.19454	24.86172	302	82	Ss
-34.1877	-34.1877	344	69	Op	-34.18676	24.73594	38	72	Op	-34.15102	24.67023	355	67	Op	-34.19416	24.86722	301	76	Ss
-34.1877	-34.1877	221	77	Op	-34.18676	24.73594	99	83	Op	-34.15102	24.67023	112	82	Op	-34.19396	24.86661	310	89	Ss
-34.18738	24.73794	102	78	Op	-34.18676	24.73594	322	68	Op	-34.15079	24.66592	230	87	Op	-34.19396	24.86661	297	81	Ss
-34.18738	24.73794	149	82	Op	-34.18672	-34.18672	155	86	Op	-34.15079	24.66592	100	84	Op	-34.19396	24.86661	228	48	Ss
-34.18738	24.73794	49	69	Op	-34.18672	-34.18672	300	67	Op	-34.15079	24.66592	302	77	Op	-34.19396	24.86661	128	87	Ss
-34.18735	-34.18735	110	61	Op	-34.18672	-34.18672	220	86	Op	-34.15	24.66292	118	81	Op	-34.19362	24.86577	272	72	Ss
-34.18735	-34.18735	155	84	Op	-34.18645	-34.18645	155	53	Op	-34.15	24.66292	159	86	Op	-34.19362	24.86577	211	50	Ss
-34.18735	-34.18735	48	70	Op	-34.18645	-34.18645	353	70	Op	-34.15	24.66292	108	80	Op	-34.19362	24.86577	108	81	Ss
-34.18733	24.73735	106	74	Op	-34.18642	24.73537	47	43	Op	-34.14916	24.66813	88	89	Op	-34.19309	24.71458	41	35	Ss
-34.18733	24.73735	326	85	Op	-34.18642	24.73537	290	70	Op	-34.14665	24.72382	109	85	Op	-34.19309	24.71458	112	74	Ss
-34.18733	24.73735	51	64	Op	-34.18642	24.73537	166	59	Op	-34.14472	24.65667	104	82	Op	-34.19309	24.71458	329	80	Ss
-34.18732	24.73826	68	70	Op	-34.18604	24.73405	22	69	Op	-34.14472	24.65667	331	80	Op	-34.19297	24.71212	31	34	Ss
-34.18732	24.73826	96	76	Op	-34.18604	24.73405	278	75	Op	-34.1441	24.73005	286	0	Op	-34.19297	24.71212	318	88	Ss
-34.18732	24.73826	166	87	Op	-34.18604	24.73405	5	82	Op	-34.14365	24.73146	292	85	Op	-34.19297	24.71212	344	71	Ss
-34.18732	24.73826	53	73	Op	-34.18598	-34.18598	70	70	Op	-34.14279	24.72218	282	80	Op	-34.19288	24.71409	19	65	Ss
-34.18731	-34.18731	94	76	Op	-34.18598	-34.18598	354	64	Op	-34.14130556	24.7271111	103	81	Op	-34.19288	24.71409	306	87	Ss
-34.18731	-34.18731	356	71	Op	-34.163	24.757861	103	65	Op	-34.14130556	24.7271111	152	85	Op	-34.19288	24.71409	310	81	Ss
-34.18731	-34.18731	43	73	Op	-34.163	24.757861	137	81	Op	-34.19642	24.86996	217	59	Ss	-34.19281	24.71167	69	60	Ss
-34.18729	-34.18729	55	70	Op	-34.163	24.757861	48	66	Op	-34.19642	24.86996	319	85	Ss	-34.19281	24.71167	119	84	Ss

APPENDIX B

Joint (Fracture) Readings					Joint (Fracture) Readings					Joint (Fracture) Readings					Joint (Fracture) Readings				
Latitude	Longitude	Azimuth	Dip	Strat	Latitude	Longitude	Azimuth	Dip	Strat	Latitude	Longitude	Azimuth	Dip	Strat	Latitude	Longitude	Azimuth	Dip	Strat
-34.19281	24.71167	5	72	Ss	-34.19236	24.71015	326	80	Ss	-34.19112	24.70641	316	82	Ss	-34.19003	24.70373	3	80	Ss
-34.19281	24.71167	285	70	Ss	-34.19236	24.71015	87	72	Ss	-34.19112	24.70641	74	69	Ss	-34.19001	24.69994	39	30	Ss
-34.19274	24.71129	209	47	Ss	-34.19234	24.7143	109	83	Ss	-34.19112	24.70757	333	76	Ss	-34.19001	24.69994	108	80	Ss
-34.19274	24.71129	295	90	Ss	-34.19218	24.71602	54	25	Ss	-34.1911	24.70677	8	50	Ss	-34.19001	24.69994	75	70	Ss
-34.19274	24.71129	310	85	Ss	-34.19218	24.71602	123	89	Ss	-34.1911	24.70677	310	77	Ss	-34.18996	24.69967	347	55	Ss
-34.19274	24.71129	106	66	Ss	-34.19215	24.70988	24	60	Ss	-34.19103	24.70621	34	46	Ss	-34.18996	24.69967	116	72	Ss
-34.19268	24.71272	38	35	Ss	-34.19215	24.70988	276	70	Ss	-34.19103	24.70621	129	72	Ss	-34.18995	24.69923	20	54	Ss
-34.19268	24.71272	131	84	Ss	-34.19215	24.70988	326	75	Ss	-34.19103	24.70621	298	80	Ss	-34.18995	24.69923	122	73	Ss
-34.19268	24.71272	330	67	Ss	-34.19214	24.71477	32	55	Ss	-34.19097	24.70604	44	30	Ss	-34.18986	24.7034	42	47	Ss
-34.19268	24.71272	80	77	Ss	-34.19214	24.71477	108	77	Ss	-34.19097	24.70604	300	80	Ss	-34.18986	24.7034	130	80	Ss
-34.19259	24.71065	41	41	Ss	-34.19214	24.71477	166	68	Ss	-34.19097	24.70604	92	72	Ss	-34.18986	24.7034	338	82	Ss
-34.19259	24.71065	108	75	Ss	-34.19214	24.71477	253	87	Ss	-34.19093	24.70581	52	32	Ss	-34.19011	24.86049	224	66	Ss
-34.19259	24.71065	6	69	Ss	-34.19213	24.71511	120	80	Ss	-34.19093	24.70581	298	73	Ss	-34.19011	24.86049	242	19	Ss
-34.19259	24.71065	64	62	Ss	-34.19213	24.71511	99	82	Ss	-34.19084	24.7057	30	40	Ss	-34.19011	24.86049	297	73	Ss
-34.19257	24.71109	27	42	Ss	-34.19187	24.70972	320	82	Ss	-34.19084	24.7057	110	75	Ss	-34.19011	24.86049	297	73	Ss
-34.19257	24.71109	292	88	Ss	-34.19187	24.70972	172	80	Ss	-34.19084	24.7057	120	90	Ss	-34.1898	24.69817	38	30	Ss
-34.19257	24.71109	118	75	Ss	-34.19149	24.70834	43	50	Ss	-34.19074	24.70533	12	42	Ss	-34.1898	24.69817	104	84	Ss
-34.19253	24.71411	12	24	Ss	-34.19149	24.70834	113	84	Ss	-34.19074	24.70533	139	88	Ss	-34.1898	24.69817	94	75	Ss
-34.19253	24.71411	284	82	Ss	-34.19149	24.70834	10	85	Ss	-34.19074	24.70533	92	69	Ss	-34.1898	24.70323	29	36	Ss
-34.19253	24.71411	110	82	Ss	-34.19149	24.70834	82	74	Ss	-34.19067	24.70457	29	30	Ss	-34.1898	24.70323	110	77	Ss
-34.19246	24.71356	330	65	Ss	-34.19134	24.70784	69	55	Ss	-34.19067	24.70457	300	80	Ss	-34.1898	24.70323	346	80	Ss
-34.19246	24.71356	121	72	Ss	-34.19134	24.70784	316	82	Ss	-34.19067	24.70457	342	65	Ss	-34.18971	24.70296	30	42	Ss
-34.19246	24.71356	8	65	Ss	-34.19134	24.70784	325	80	Ss	-34.19061	24.7051	40	50	Ss	-34.18971	24.70296	312	81	Ss
-34.19244	24.71314	29	63	Ss	-34.19134	24.70784	79	86	Ss	-34.19061	24.7051	310	80	Ss	-34.18969	24.69482	20	40	Ss
-34.19244	24.71314	284	89	Ss	-34.19124	24.70707	47	47	Ss	-34.19043	24.7044	323	85	Ss	-34.18969	24.69482	116	74	Ss
-34.19244	24.71314	326	57	Ss	-34.19124	24.70707	126	88	Ss	-34.19001	24.69994	46	13	Ss	-34.18959	24.7028	24	37	Ss
-34.19244	24.71314	78	80	Ss	-34.19124	24.70707	80	80	Ss	-34.19001	24.69994	112	80	Ss	-34.18959	24.7028	315	81	Ss
-34.19238	24.71589	41	32	Ss	-34.19117	24.7066	33	32	Ss	-34.19001	24.69994	140	20	Ss	-34.18956	24.69694	42	30	Ss
-34.19238	24.71589	302	76	Ss	-34.19117	24.7066	298	84	Ss	-34.19022	24.70393	56	45	Ss	-34.18956	24.69694	130	84	Ss
-34.19238	24.71589	316	80	Ss	-34.19117	24.7066	312	67	Ss	-34.19022	24.70393	314	90	Ss	-34.18956	24.69694	84	82	Ss
-34.19236	24.71015	36	51	Ss	-34.19117	24.7066	78	70	Ss	-34.19003	24.70373	213	65	Ss	-34.18956	24.69779	24	55	Ss
-34.19236	24.71015	122	72	Ss	-34.19112	24.70641	34	33	Ss	-34.19003	24.70373	123	80	Ss	-34.18956	24.69779	112	75	Ss

APPENDIX B

Joint (Fracture) Readings					Joint (Fracture) Readings					Joint (Fracture) Readings					Joint (Fracture) Readings				
Latitude	Longitude	Azimuth	Dip	Strat	Latitude	Longitude	Azimuth	Dip	Strat	Latitude	Longitude	Azimuth	Dip	Strat	Latitude	Longitude	Azimuth	Dip	Strat
-34.18956	24.69779	339	79	Ss	-34.18907	24.69572	91	65	Ss	-34.19094	24.86251	170	75	Ss	-34.18663889	24.68811111	270	70	Ss
-34.18956	24.69779	92	76	Ss	-34.18907	24.69572	71	80	Ss	-34.18748	24.69183	43	32	Ss	-34.18682	24.85756	163	86	Ss
-34.18941	24.69695	29	31	Ss	-34.18923	24.85914	228	74	Ss	-34.18748	24.69183	117	75	Ss	-34.18682	24.85756	280	76	Ss
-34.18941	24.69695	118	82	Ss	-34.18923	24.85914	346	82	Ss	-34.18746	24.69106	36	45	Ss	-34.18682	24.85756	236	54	Ss
-34.18941	24.69695	83	67	Ss	-34.18923	24.85914	302	85	Ss	-34.18746	24.69106	93	66	Ss	-34.18682	24.85756	151	88	Ss
-34.18938	24.69424	301	89	Ss	-34.18923	24.85914	322	80	Ss	-34.18746	24.69106	323	73	Ss	-34.18678	24.85753	237	55	Ss
-34.18938	24.69424	179	79	Ss	-34.18892	24.70082	42	32	Ss	-34.18746	24.69106	85	64	Ss	-34.18678	24.85753	124	80	Ss
-34.18936	24.6961	29	25	Ss	-34.18892	24.70082	330	90	Ss	-34.18743	24.69055	47	39	Ss	-34.18624	24.68738	111	78	Ss
-34.18936	24.6961	300	86	Ss	-34.18892	24.70082	336	70	Ss	-34.18743	24.69055	119	75	Ss	-34.18624	24.68738	346	54	Ss
-34.18936	24.6961	93	68	Ss	-34.18886	24.70001	20	26	Ss	-34.18743	24.69055	341	70	Ss	-34.18624	24.68738	85	68	Ss
-34.18934	24.69513	352	40	Ss	-34.18886	24.70001	293	85	Ss	-34.18738889	24.6915833	291	84	Ss	-34.18575	24.68662	358	55	Ss
-34.18934	24.69513	139	77	Ss	-34.18886	24.70001	328	82	Ss	-34.18713	24.68998	33	35	Ss	-34.18575	24.68662	103	82	Ss
-34.18934	24.69513	86	60	Ss	-34.18881	24.69291	37	30	Ss	-34.18713	24.68998	120	90	Ss	-34.18575	24.68662	323	65	Ss
-34.18931	24.69751	6	30	Ss	-34.18881	24.69291	115	69	Ss	-34.1871	24.68938	31	2	Ss	-34.18587	24.85557	174	68	Ss
-34.18931	24.69751	106	78	Ss	-34.18881	24.69291	325	82	Ss	-34.1871	24.68938	113	82	Ss	-34.18587	24.85557	306	85	Ss
-34.18931	24.69751	94	70	Ss	-34.1886	24.7001	38	38	Ss	-34.1871	24.68938	346	74	Ss	-34.18587	24.85557	232	66	Ss
-34.1893056	24.69761111	105	83	Ss	-34.1886	24.7001	326	84	Ss	-34.18702778	24.6906944	265	74	Ss	-34.18682	24.85756	288	80	Ss
-34.18928	24.70183	54	47	Ss	-34.18854	24.69255	42	26	Ss	-34.18702	24.68961	41	31	Ss	-34.18527	24.68615	119	70	Ss
-34.18928	24.70183	313	76	Ss	-34.18854	24.69255	338	76	Ss	-34.18702	24.68961	11	89	Ss	-34.18527	24.68615	318	74	Ss
-34.18928	24.70183	325	60	Ss	-34.18841	24.69964	37	40	Ss	-34.18694	24.68875	19	35	Ss	-34.18522222	24.68619444	140	69	Ss
-34.18922	24.69372	29	35	Ss	-34.18841	24.69964	312	77	Ss	-34.18694	24.68875	119	75	Ss	-34.18507	24.68588	56	40	Ss
-34.18922	24.69372	119	76	Ss	-34.18841	24.69964	324	27	Ss	-34.18694	24.68875	322	89	Ss	-34.18507	24.68588	120	74	Ss
-34.18922	24.69372	146	80	Ss	-34.18825	24.70377	288	88	Ss	-34.18691	24.6882	20	22	Ss	-34.18507	24.68588	329	62	Ss
-34.18922	24.69372	88	82	Ss	-34.18825	24.70377	5	57	Ss	-34.18691	24.6882	120	74	Ss	-34.18507	24.68588	100	79	Ss
-34.18911	24.70117	5	30	Ss	-34.1880833	24.693056	324	87	Ss	-34.18691	24.6882	348	60	Ss	-34.18451	24.686	68	45	Ss
-34.18911	24.70117	116	70	Ss	-34.18743	24.69055	31	27	Ss	-34.18684	24.68809	24	25	Ss	-34.18451	24.686	108	82	Ss
-34.18911	24.70117	152	76	Ss	-34.18743	24.69055	111	82	Ss	-34.18684	24.68809	120	74	Ss	-34.18451	24.686	322	75	Ss
-34.1891	24.70002	24	42	Ss	-34.18743	24.69055	338	72	Ss	-34.18684	24.68809	332	78	Ss	-34.18444	24.68177	58	15	Ss
-34.1891	24.70002	116	85	Ss	-34.18743	24.69055	85	77	Ss	-34.18684	24.68809	88	66	Ss	-34.18444	24.68177	294	67	Ss
-34.1891	24.70002	310	81	Ss	-34.19094	24.86251	178	61	Ss	-34.18679	24.6869	32	41	Ss	-34.1838	24.6805	35	36	Ss
-34.1891	24.70002	72	69	Ss	-34.19094	24.86251	64	49	Ss	-34.18679	24.6869	122	76	Ss	-34.1838	24.6805	328	72	Ss
-34.18907	24.69572	28	43	Ss	-34.19094	24.86251	282	79	Ss	-34.18679	24.6869	354	56	Ss	-34.1838	24.6805	105	87	Ss

APPENDIX B

Joint (Fracture) Readings					Joint (Fracture) Readings					Joint (Fracture) Readings					Joint (Fracture) Readings				
Latitude	Longitude	Azimuth	Dip	Strat	Latitude	Longitude	Azimuth	Dip	Strat	Latitude	Longitude	Azimuth	Dip	Strat	Latitude	Longitude	Azimuth	Dip	Strat
-34.18378	24.68226	16	36	Ss	-34.18298	24.67821	62	25	Ss	-34.18104	24.67404	42	27	Ss	-34.1789	24.6682	56	32	Ss
-34.18378	24.68226	296	74	Ss	-34.18298	24.67821	113	80	Ss	-34.18104	24.67404	130	88	Ss	-34.1789	24.6682	346	60	Ss
-34.18378	24.68353	318	84	Ss	-34.18296	24.67821	136	90	Ss	-34.18102	24.67526	136	87	Ss	-34.1789	24.6682	102	81	Ss
-34.18378	24.68353	0	64	Ss	-34.18296	24.67821	104	71	Ss	-34.18076	24.67315	24	54	Ss	-34.17903	24.84508	290	72	Ss
-34.18378	24.68353	88	72	Ss	-34.18251	24.67773	41	15	Ss	-34.18076	24.67315	101	81	Ss	-34.17903	24.84508	227	42	Ss
-34.18372	24.67993	29	34	Ss	-34.18251	24.67773	302	83	Ss	-34.18076	24.67315	308	84	Ss	-34.17862	24.66976	280	76	Ss
-34.18372	24.67993	329	76	Ss	-34.18251	24.67773	331	70	Ss	-34.18076	24.67315	94	81	Ss	-34.17859	24.6681	350	60	Ss
-34.1837	24.68139	40	21	Ss	-34.18251	24.67773	85	66	Ss	-34.18022	24.67247	44	2	Ss	-34.17859	24.6681	86	75	Ss
-34.1837	24.68139	120	90	Ss	-34.18243	24.67774	317	59	Ss	-34.18022	24.67247	116	84	Ss	-34.17859	24.66973	126	90	Ss
-34.1837	24.68139	101	80	Ss	-34.18243	24.67774	123	81	Ss	-34.18022	24.67247	320	76	Ss	-34.17859	24.66973	350	65	Ss
-34.18359	24.68322	50	44	Ss	-34.18243	24.67774	90	70	Ss	-34.18022	24.67247	98	75	Ss	-34.17859	24.66973	106	76	Ss
-34.18359	24.68322	112	75	Ss	-34.18231	24.67708	44	22	Ss	-34.18014	24.67233	342	18	Ss	-34.17839	24.66708	38	45	Ss
-34.18359	24.68322	345	83	Ss	-34.18231	24.67708	115	89	Ss	-34.18014	24.67233	119	87	Ss	-34.17839	24.66708	324	75	Ss
-34.18359	24.68322	88	90	Ss	-34.18231	24.67708	308	84	Ss	-34.18014	24.67233	146	85	Ss	-34.17839	24.66708	94	63	Ss
-34.18359	24.68323	336	80	Ss	-34.18227	24.6767	146	70	Ss	-34.18014	24.67233	108	85	Ss	-34.17839	24.66785	25	21	Ss
-34.18353	24.68467	288	88	Ss	-34.18222	24.67607	36	23	Ss	-34.17984	24.67179	18	30	Ss	-34.17839	24.66785	355	60	Ss
-34.18353	24.68467	345	57	Ss	-34.18222	24.67607	132	75	Ss	-34.17984	24.67179	109	65	Ss	-34.17839	24.66785	96	67	Ss
-34.18353	24.68467	94	75	Ss	-34.18213	24.67653	50	24	Ss	-34.17984	24.67179	336	67	Ss	-34.17846	24.844	235	69	Ss
-34.18348	24.68387	327	87	Ss	-34.18213	24.67653	310	87	Ss	-34.17984	24.67179	114	60	Ss	-34.17846	24.844	170	70	Ss
-34.18348	24.68387	82	86	Ss	-34.18213	24.67653	350	60	Ss	-34.17974	24.6704	44	20	Ss	-34.17783	24.66656	22	20	Ss
-34.18347	24.68514	297	80	Ss	-34.18158	24.67531	12	55	Ss	-34.17974	24.6704	109	85	Ss	-34.17783	24.66656	336	62	Ss
-34.18347	24.68514	354	50	Ss	-34.18158	24.67531	117	86	Ss	-34.17974	24.6704	339	71	Ss	-34.17783	24.66656	123	55	Ss
-34.18347	24.68514	94	75	Ss	-34.18147	24.67965	84	67	Ss	-34.17974	24.6704	90	87	Ss	-34.17758	24.66605	52	12	Ss
-34.1834	24.67964	42	29	Ss	-34.18141	24.67545	343	70	Ss	-34.17994	24.84653	290	76	Ss	-34.17758	24.66605	102	70	Ss
-34.1834	24.67964	306	84	Ss	-34.18141	24.67545	94	83	Ss	-34.17994	24.84653	220	49	Ss	-34.17758	24.66605	304	80	Ss
-34.18337	24.67922	111	80	Ss	-34.18123	24.67489	50	14	Ss	-34.17958	24.67124	44	22	Ss	-34.17758	24.66605	336	69	Ss
-34.18333	24.67924	23	35	Ss	-34.18123	24.67489	301	87	Ss	-34.17958	24.67124	315	83	Ss	-34.17792	24.84284	155	66	Ss
-34.18333	24.67924	123	84	Ss	-34.18115	24.67867	123	78	Ss	-34.17958	24.67124	348	70	Ss	-34.17792	24.84284	236	40	Ss
-34.18333	24.67924	102	84	Ss	-34.18114	24.67508	122	56	Ss	-34.17958	24.67124	52	89	Ss	-34.17753	24.66517	33	12	Ss
-34.1833	24.68382	88	72	Ss	-34.18107	24.67521	22	30	Ss	-34.17961	24.84594	295	68	Ss	-34.17753	24.66517	106	62	Ss
-34.18305	24.67859	50	18	Ss	-34.18107	24.67521	300	85	Ss	-34.17961	24.84594	175	65	Ss	-34.17753	24.66517	286	80	Ss
-34.18305	24.67859	116	72	Ss	-34.18107	24.67521	149	71	Ss	-34.17961	24.84594	225	55	Ss	-34.17753	24.66517	322	80	Ss

APPENDIX B

Joint (Fracture) Readings

Latitude	Longitude	Azimuth	Dip	Strat
-34.17732	24.66601	150	75	Ss
-34.17719	24.66488	32	75	Ss
-34.17719	24.66488	302	72	Ss
-34.17719	24.66488	320	65	Ss
-34.17696	24.66426	55	32	Ss
-34.17696	24.66426	89	84	Ss
-34.17696	24.66426	292	86	Ss
-34.17696	24.66426	336	66	Ss
-34.17685	24.66506	20	25	Ss
-34.17685	24.66506	327	78	Ss
-34.17651	24.66344	26	33	Ss
-34.17651	24.66344	122	77	Ss
-34.17651	24.66344	313	86	Ss
-34.17651	24.66344	329	85	Ss
-34.17685	24.842	235	61	Ss
-34.17649	24.66394	28	22	Ss
-34.17649	24.66394	311	85	Ss
-34.17649	24.66394	335	65	Ss
-34.17634	24.66322	34	22	Ss
-34.17634	24.66322	124	86	Ss
-34.17664	24.84169	180	70	Ss
-34.17613	24.66277	38	34	Ss
-34.17613	24.66277	107	85	Ss
-34.17613	24.66277	139	83	Ss
-34.17613	24.66277	353	67	Ss
-34.17603	24.66228	336	22	Ss
-34.17603	24.66228	100	84	Ss
-34.17603	24.66228	286	90	Ss
-34.17603	24.66228	338	40	Ss
-34.17574	24.66169	20	9	Ss
-34.17574	24.66169	127	70	Ss
-34.17574	24.66169	116	82	Ss

Joint (Fracture) Readings

Latitude	Longitude	Azimuth	Dip	Strat
-34.17606	24.84106	215	49	Ss
-34.17606	24.84106	290	71	Ss

Fault Plane Readings

Latitude	Longitude	Azimuth	Dip
-34.21131	24.82749	18	90
-34.21096	24.8273	14	85
-34.21077	24.82677	35	72
-34.20841	24.82239	14	83
-34.20841	24.82175	24	80
-34.20738	24.81851	152	80
-34.19491	24.76004	97	62
-34.19067	24.74788	285	83
-34.19236	24.71015	313	78
-34.19215	24.70988	114	70
-34.18702	24.68961	11	89
-34.1871	24.68938	113	82
-34.18684	24.68809	120	74
-34.1871	24.68938	122	80
-34.19215	24.70988	114	60

Thrust Faults (Flats) Readings all taken in same area - one co-ords given for the general area where readings were taken

Latitude	Longitude	Azimuth	Dip
-34.18775	24.739361	220	7
-34.18775	24.739361	210	10
-34.18775	24.739361	190	13
-34.18775	24.739361	195	15
-34.18775	24.739361	203	20
-34.18775	24.739361	204	8
-34.18775	24.739361	204	10
-34.18775	24.739361	210	12
-34.18775	24.739361	225	16

Thrust Faults (Flats)

Latitude	Longitude	Azimuth	Dip
-34.18775	24.739361	203	15
-34.18775	24.739361	198	17
-34.18775	24.739361	195	18
-34.18775	24.739361	210	20
-34.18775	24.739361	208	8
-34.18775	24.739361	220	9
-34.18775	24.739361	225	10

Thrust Faults (Ramps)

Latitude	Longitude	Azimuth	Dip
-34.18775	24.739361	210	45
-34.18775	24.739361	202	46
-34.18775	24.739361	198	50
-34.18775	24.739361	220	33
-34.18775	24.739361	225	45
-34.18775	24.739361	190	40
-34.18775	24.739361	195	41
-34.18775	24.739361	201	45
-34.18775	24.739361	210	46
-34.18775	24.739361	210	41
-34.18775	24.739361	202	39
-34.18775	24.739361	203	40
-34.18775	24.739361	215	50
-34.18775	24.739361	216	55
-34.18775	24.739361	218	49
-34.18775	24.739361	220	33

Shale Cleavage

Latitude	Longitude	Azimuth	Dip
-34.192051	24.714436	50	45
-34.192096	24.714545	55	45
-34.192191	24.714504	51	46
-34.192169	24.71436	49	44
-34.192203	24.714264	55	43

Shale Cleavage

Latitude	Longitude	Azimuth	Dip
-34.192237	24.714264	53	44
-34.192344	24.714331	55	45
-34.192288	24.714427	54	48
-34.192282	24.714599	55	50
-34.192265	24.714702	47	43
-34.192259	24.71493	55	45
-34.192304	24.71473	58	48
-34.192396	24.714688	50	45
-34.192464	24.71423	54	42

Fold Axis Readings

Latitude	Longitude	Azimuth	Dip
-34.21275	24.83147	92	9
-34.21209	24.83143	52	13
-34.21115	24.82951	24	11
-34.21131	24.82749	56	30
-34.19646	24.77642	10	10
-34.19472	24.75981	18	5
-34.20116	24.80619	68	15
34.19831	24.79732	114	5
-34.19617	24.76691	10	18
-34.205472	24.813667	155	10

Appendix C1 — Borehole data

APPENDIX C1

Raubenheimer et al., 1988 borehole dataset

BH No.	Drill Angle	BH Incli-nation	Latitude	Longitude	BH Elev.	BH Depth	Vertical BH Depth	Depth to Bedrock / Overburden Thickness	Vertical Depth to Bedrock / Vertical Overburden Thickness	Bedrock Elev (m amsl)	Depth to Pebble Layer	Vertical depth to pebble layer	Pebble layer elevation (m amsl)	Bedrock Stratigraphy	First bedrock lithology intercepted in BHs as described in BH logs
BHDP1	65	112	-34.189181	24.706186	17.43	40.12	36.36	11.8	10.69	6.74	10	9.06	8.37	Skurweberg	Grey to darker grey quartzitic sandstone. Bedding well developed throughout the borehole
BHDP2	65	112	-34.188552	24.704343	20.74	45.35	41.1	18.1	16.4	4.34	N/A	N/A	N/A	Skurweberg	Grey to darker grey quartzitic sandstone. Some shaley beds from 19.5-19.8. Mica mineralization on the bedding planes. Bedding well developed.
BHDP3	65	112	-34.189671	24.707625	14.52	40.1	36.34	9	8.16	6.36	N/A	N/A	N/A	Skurweberg	Grey to darker grey quartzitic sandstone. Hard and massive.
BHDP4	65	112	-34.190292	24.709403	15.96	40.6	36.8	11	9.97	5.99	N/A	N/A	N/A	Skurweberg	Grey to darker grey quartzitic sandstone. Cross-bedding from 14-14.6m. Bedding not clear.
BHDP5	65	112	-34.190488	24.710012	14.19	40.5	36.71	11	9.97	4.22	N/A	N/A	N/A	Skurweberg	Dark to dark grey quartzitic sandstone with well developed bedding planes.
BHDP7	90	0	-34.190996	24.711741	10.78	30.17	30.17	5.5	5.5	5.28	N/A	N/A	N/A	Goudini	Dark-grey to black quartzitic sandstone with alternating shale bands. The quartzitic sandstone is very impure and possibly carbonaceous.
BHDP9	90	0	-34.190502	24.711749	12.02	30.35	30.35	7.2	7.2	4.82	N/A	N/A	N/A	Goudini	Lught-grey to grey quartzitic sandstone similar to Skurweberg Formation. This zone can be interpreted as a transition zone in to the Goudini Formation
BHDP11	90	0	-34.188862	24.707133	18.7	30.6	30.6	12	12	6.7	N/A	N/A	N/A	Goudini	Dark to very dark-grey "dirty" quartzitic sandstone, probably carbonaceous with a high percentage of clay minerals
BHDP12	90	0	-34.189774	24.706623	14.46	30.5	30.5	9.22	9.22	5.24	N/A	N/A	N/A	Skurweberg	Grey to dark-grey quartzitic sandstone. Very quartzitic and hard
BHPP1	90	0	-34.190964	24.711668	10.73	34	34	7.2	7.2	3.53	N/A	N/A	N/A	Goudini	Grey to dark-grey quartzitic sandstone. Very quartzitic and hard. Soft and shaley and weathered from 7.2 to 9m.
BHPP2	90	0	-34.191018	24.711651	10.72	32.83	32.83	5.2	5.2	5.52	N/A	N/A	N/A	Goudini	Grey to very-grey quartzitic sandstone. Weathered, stained and slightly clayey up tp 7.5m
BHPP3	90	0	-34.190957	24.71162	10.78	30	30	7.7	7.7	3.08	N/A	N/A	N/A	Goudini	Grey to dark grey quartzitic sandstone. Soft and slightly shalely
BHPP4	90	0	-34.190922	24.711688	10.8	30	30	8	8	2.8	6.8	6.8	4	Goudini	Green to dark grey quartzitic sandstone. Numerous weathered and stained zones occur up to 30m with a very shalely charater from 8-15m.
BHPP5	90	0	-34.191072	24.711659	10.74	30	30	6.5	6.5	4.24	N/A			Goudini	Grey and green to dark-grey quartzitic sandstone. Red iron staining occur indicating weathered fractures and joints.
BHPP6	90	0	-34.191015	24.711703	10.78	30	30	5.5	5.5	5.28	5	5	5.78	Goudini	Grey to dark grey quartzitic sandstone. Reddish and yellow staining occur frequently up to 30m indicating fractures and weathered joints
BHPP7	90	0	-34.190061	24.710586	12.1	9.5	9.5	8.57	8.57	3.53	N/A	N/A	N/A	Goudini	Quartzitic sandstone
BHPP8	90	0	-34.189035	24.707864	20.85	10.3	10.3	9.26	9.26	11.59	N/A	N/A	N/A	Goudini	Quartzitic sandstone
BHPP9	90	0	-34.191072	24.709751	11.01	36	36	6	6	5.01	N/A	N/A	N/A	Skurweberg	Very dark quartzitic sandstone. Probably in a transition zone to Goudini Formation
BHPP10	90	0	-34.191138	24.709743	10.63	36	36	6	6	4.63	N/A	N/A	N/A	Skurweberg	Dark grey to black quartzitic sndstone. Probably in the transition zone from Goudini to Skurweberg.
BHPP11	90	0	-34.191077	24.709688	10.62	36	36	6	6	4.62	N/A	N/A	N/A	Skurweberg	Dark grey quartzitic sandstone. Similar to the Goudini Formation. Probably represents a transition zone into the Goudini.
BHPP12	90	0	-34.19098	24.709763	11.47	36	36	7.8	7.8	3.67	N/A	N/A	N/A	Skurweberg	Very dark-grey colour. Quartzitic sandstone. Not typical Skurweberg Formation. Probably softer than usual.

APPENDIX C1

BH No.	Drill Angle	BH Incli-nation	Latitude	Longitude	BH Elev.	BH Depth	Vertical BH Depth	Depth to Bedrock / Overburden Thickness	Vertical Depth to Bedrock / Vertical Overburden Thickness	Bedrock Elev (m amsl)	Depth to Pebble Layer	Vertical depth to pebble layer	Pebble layer elevation (m amsl)	Bedrock Stratigraphy	First bedrock lithology intercepted in BHs as described in BH logs
BHPP13	90	0	-34.191122	24.709827	11.79	30	30	7	7	4.79	N/A	N/A	N/A	Skurweberg	Dark-grey quartzitic sandstone in the Skurweberg Formation transition zone. clayey from 7-9m.
Thyspunt BH3	90	0	-34.18735	24.704439	29.09	22.2	22.2	20.6	20.6	8.49	N/A	N/A	N/A	Goudini	A grey to dark-grey quartzitic sandstone. Dark colour possibly indicating a higher clay fraction or dark mineral content.
Thyspunt BH4	90	0	-34.187556	24.704355	26.97	21.1	21.1	N/A	N/A	N/A	18.9	18.9	8.07	N/A	N/A
Thyspunt BH5	90	0	-34.190099	24.710275	13.13	11.22	11.22	8.2	8.2	3.02	8	8	3.22	Goudini	Grey to dark-grey quartzitic sandstone
BHDB1	65	297	-34.188221	24.697525	10.62	35.35	32.04	10	9.06	1.56	N/A	N/A	N/A	Skurweberg	Alternating quartzitic sandstone and shale layers. shale bands vary from less than 1mm up to 50cm in thickness. The shale are sometimes a light-brown colour but mostly a dark-grey to black in colour and very carbonaceous. The quartzite is light to dark grey.
BHDB2	65	292	-34.187554	24.701279	21.93	45.2	40.97	13.59	12.32	9.61	13.09	11.86		Skurweberg	Grey to dark-grey quartzitic sandstone.
BHDB3	65	297	-34.187574	24.696015	17.28	50.5	45.77	18.9	17.13	0.15	10	9.06	8.22	Skurweberg	Grey to dark-grey quartzitic sandstone with grey-black carbonaceous shale.
BHDB4	90		-34.187117	24.69481	13.19	31.24	31.24	5.38	5.38	7.81	2.5	2.5	10.69	Skurweberg	Light to dark grey quartzitic sandstone.
BHDB5	65	292	-34.187867	24.702467	19.01	45.76	41.47	11	9.97	9.04	N/A	N/A	N/A	Skurweberg	Grey to dark grey quartzitic sandstone. The rock is massive and hard. Some thin shaley bands occur occasionally.
BHDB6	65	117	-34.186327	24.693089	19.05	44.85	40.65	11	9.97	9.08	N/A	N/A	N/A	Skurweberg	White to light-grey quartzitic sandstone up to 18m. The quartzitic sandstone is quite clean with a massive character.
BHDB7	90	0	-34.187997	24.69571	12.2	30.74	30.74	4.26	4.26	7.94	N/A	N/A	N/A	Skurweberg	Grey to dark grey quartzitic sandstone.
BHDB8	90	0	-34.187238	24.69629	14.54	48.7	48.7	10	10	4.54	N/A	N/A	N/A	Skurweberg	Grey to dark grey quartzitic sandstone. Rock is fractured with shale layers up to 19m.
BHDB9	90	0	-34.187523	24.697954	11.47	30.6	30.6	7.65	7.65	3.82	N/A	N/A	N/A	Skurweberg	Very dark quartzitic sandstone up to 12.3m. Weathered with kaolinitic fractures up to 9.2.
BHPB1	90	0	-34.188015	24.695608	12.15	50	50	3	3	9.15	N/A	N/A	N/A	Skurweberg	Grey to dark-grey quartzitic sandstone. Very sandy. Some reddish stained chips from 30-10.m indicating fractured and weathered zones.
BHPB2	90	0	-34.188148	24.695454	10.2	40	40	4	4	6.2	N/A	N/A	N/A	Skurweberg	Hard massive quartzitic sandstone. Light to dark grey colour with a red variatiion from 4-15m. The red colouring possibly indicates iron staining by water. The sandstone are very sandy and becomes lighter coloured from 11m onward. The red quartzite could also indicate fractures or joints.
BHPB3	90	0	-34.187986	24.695451	11.83	50	50	3	3	8.83	N/A	N/A	N/A	Skurweberg	White to grey quartzitic sandstone. Slightly wearthered from 3-4m. Very sandy. Weathered and stained quartzite chips occur frequently indicating fractures and joints. The red staining are probably iron. This grey-white, sandy quartzite occurs from 3-3.8m.
BHPB4	90	0	-34.18801	24.695543	12.01	45	45	4	4	8.01	N/A	N/A	N/A	Skurweberg	Light grey quartzitic sandstone up to 35m. Very sand and gre-white in powder form. Yellow and red stained quartzite chips occur frequently up to 24m which indicates iron staining in fractures and joints by weathering processes.
BHPB5	90	0	-34.186426	24.69518	22.73	15	15	14	14	8.73	N/A	N/A	N/A	Skurweberg	Quartzitic sandstone

APPENDIX C1

BH No.	Drill Angle	BH Incli-nation	Latitude	Longitude	BH Elev.	BH Depth	Vertical BH Depth	Depth to Bedrock / Overburden Thickness	Vertical Depth to Bedrock / Vertical Overburden Thickness	Bedrock Elev (m amsl)	Depth to Pebble Layer	Vertical depth to pebble layer	Pebble layer elevation (m amsl)	Bedrock Stratigraphy	First bedrock lithology intercepted in BHs as described in BH logs
Tony's Bay BH1	90	0	-34.186255	24.699332	26.97	16.03	16.03	13.78	13.78	13.19	N/A	N/A	N/A	Skurweberg	Grey to green-grey quartzite sandstone. Substaintial amount of darker minerals present. Some mica recognisable.
Tony's Bay BH2	90	0	-34.187144	24.698289	24.73	19.01	19.01	17.6	17.6	7.13	N/A	N/A	N/A	Skurweberg	Light grey, very quartzitic sandstone. A white quartz vein between 18.7 and 19m.
Tony's Bay BH3	90	0	-34.185948	24.694674	18.76	13	13	11.45	11.45	7.31	6.2	6.2	12.56	Skurweberg	Soft weathered, shaleyly sandstone with light-grey colour up to 11.7m. Very carbonaceous shale from 11.7m. Very carbonaceous shale from 11.7m (dark-grey to balck) grading into carbonaceous finr grained sandstone at 12.15m. Slightly graphitic at places and becoming less carbonaeous and more quartzitic deeper down.
Tony's Bay BH4	90	0	-34.186911	24.693484	14.93	8.9	8.9	6.7	6.7	8.23	N/A	N/A	N/A	Skurweberg	White to light-grey quartzitic sandstone. Very sndy and "sugary" from 7-8.9m. A kaolinitic or Talcic spot at 8.4m
Tony's Bay BH5	90	0	-34.186312	24.694198	20.97	16.44	16.44	14	14	6.97	13.5	13.5	7.47	Skurweberg	Wearthered, light-grey quartzitic sandstone up to 14.2m Soft, weathered, sandy and shalely material from 14.3 to 14.8m.
BHDH1	65	110	-34.199168	24.803664	6.65	28.83	26.13	4	3.63	3.02	3	2.72		Peninsula	White to light grey quartzitic sandstone. Quartz veining at 4.5m. Some bedding and quartz veining here. Fe-staining in fractures
BHDH2	55	110	-34.199768	24.805187	10.76	41.4	33.91	8.5	6.96	3.8	7.75	6.34	4.42	Peninsula	Grey to white, massive, quartzitic sandstone.
BHDH3	65	290	-34.200081	24.806374	13.64	36.1	32.72	8.5	7.7	5.94	8	7.25	6.39	Peninsula	White to light-grey quartzitic sandstone ("clean and massive"). Fe-staining in fractures
BHDH4	65	290	-34.200442	24.807773	22.1	45.67	41.39	9	8.16	13.94	N/A	N/A	N/A	Peninsula	White to light-grey quartzitic sandstone. Weathered and iron stained up to 13m.
BHDH5	65	290	-34.20095	24.807773	20.69	24.76	22.44	13.25	12.01	8.68	N/A	N/A	N/A	Peninsula	White to light-grey quartzitic sandstone. Weathered and iron stained from 13.25-14-18m.
BHDH6	64	110	-34.201278	24.810454	18.55	45.3	41.06	12.5	11.33	7.22	N/A	N/A	N/A	Peninsula	Pale-white to grey quartzitic sandstone.
BHDH7	55	200	-34.202294	24.809715	5.38	30.02	24.59	5.02	4.11	1.27	4.4	3.6	1.78	Peninsula	A "clean" pale-white quartzitic sandstone. sandy with a sugary texture up to 8.49m Some browish iron-stained surfaces (weathered).
BHDH8	90	0	-34.200618	24.810557	23.43	30.35	30.35	6.8	6.8	16.63	N/A	N/A	N/A	Peninsula	White to light-grey quartzitic sandstone. Weathered and stained up to 8m (in fractures)
BHDH9	90	0	-34.200228	24.807082	16.68	15.2	15.2	5	5	11.68	N/A	N/A	N/A	Peninsula	White to light-grey massive "clean" quartzitic sandstone. Sugary texture at places. Cross-bedding occur sporadically. Fe-staining in fractures.
BHDH11	90	0	-34.188862	24.707133	6.97	30.26	30.26	3.33	3.33	3.64	N/A	N/A	N/A	Peninsula	Grey to pale-white quartzitic sandstone. Contact with overlying sand very sharp. TMS very hard, fresh and massive. Some close to horizontal fractures and joints with brown stained weathering - probably Fe-staining
BHPH1	90	0	-34.200257	24.806097	6.96	35	35	5.5	5.5	1.46	4	4	2.96	Peninsula	Light and dark-grey quartzitic sandstone.
BHPH2	90	0	-34.200337	24.806048	6.43	35	35	5	5	1.43	3.5	3.5	2.93	Peninsula	Light-grey quartzitic sandstone chips quite sandy.
BHPH3	90	0	-34.200239	24.806056	6.96	33	33	8	8	-1.04	4	4	2.96	Peninsula	Grey to green powdery shale. Slightly clayey at places. Probably a shale layer in the Peninsula Formation.
BHPH4	90	0	-34.200215	24.806087	7.48	35	35	5	5	2.48	3.5	3.5	3.98	Peninsula	Light-grey quartzitic sandstone very sandy. clayey at top - possibly derived from cavinng in the boulders. More darker-grey deeper down. Weathered and stained chips occur frequently indicating fractures or open joints.
BHPH10	90	0	-34.191138	24.709743	24.27	7.6	7.6	7.2	7.2	17.07	N/A	N/A	N/A	Peninsula	Light-grey quartzitic sandstone.

APPENDIX C1

BH No.	Drill Angle	BH Incli-nation	Latitude	Longitude	BH Elev.	BH Depth	Vertical BH Depth	Depth to Bedrock / Overburden Thickness	Vertical Depth to Bedrock / Vertical Overburden Thickness	Bedrock Elev (m amsl)	Depth to Pebble Layer	Vertical depth to pebble layer	Pebble layer elevation (m amsl)	Bedrock Stratigraphy	First bedrock lithology intercepted in BHs as described in BH logs
BHPH12	90	0	-34.19098	24.709763	7.45	25	25	6.5	6.5	0.95	3	3	4.45	Peninsula	Very weathered quartzitic sandstone. Soft and sandy with a sugary texture. Mostly stained (red and yellow iron stains), indicating fractures and probably jointing
BHPH13	90	0	-34.191122	24.709827	26.77	11.45	11.45	11.45	11.45	15.32	N/A	N/A	N/A	Peninsula	Quartzitic sandstone.
De Hoek BH1	90	0	-34.201317	24.810163	18.01	13.63	13.63	11.75	11.75	1.88	N/A	N/A	N/A	Peninsula	A "clean" pale white and massive quartzitic sandstone. Sharp contact with overlaying sand. sandy at top and more quartzitic deepere down.
De Hoek BH2	90	0	-34.201946	24.809874	12.84	9.81	9.81	8.2	8.2	1.61	N/A	N/A	N/A	Peninsula	A "clean" and massive quartzitic sandstone with a "sugary" texture. Pale-white to grey colour.
De Hoek BH3	90	0	-34.199205	24.807638	28.37	13.12	13.12	11.15	11.15	17.22	N/A	N/A	N/A	Peninsula	Light-grey, massive quartzitic sandstone. sandy texture from 11.15-12m. Some granular areas deeper down with individual grains visisble in the quartzite. Sugary texture often visible.
De Hoek BH4	90	0	-34.200118	24.80722	19.27	8.15	8.15	6	6	13.27	N/A	N/A	N/A	Peninsula	Light-grey, massive quartzitic sandstone.
De Hoek BH5	90	0	-34.198184	24.803998	12.48	8.4	8.4	6	6	6.48	N/A	N/A	N/A	Peninsula	Grey to dark-grey quartzitic sandstone. A dark-green shale layer from 6.65-7m.
Rosewarne and Lomberg, 1989 borehole dataset															
BH4	90	0	-34.167393	24.820317	52	200	200	18.5	18.5	33.5	N/A	N/A	N/A	Skurweberg	Sandstone solid
BH6	90	0	-34.178828	24.837102	41	200	200	10	10	31	N/A	N/A	N/A	Skurweberg	Sandstone and clay
BH7a	90	0	-34.177872	24.821169	51	70.5	70.5	21	21	30	N/A	N/A	N/A	Goudini	Sandstone - grey black recrystalized
BH7b	90	0	-34.179159	24.818223	48	100	100	24	24	24	23	23	25	Goudini	Sandstone - light grey, recrystallised - weathered at fractures, otherwise hard
BH9	90	0	-34.184595	24.846675	25	82	82	8.5	8.5	16.5	N/A	N/A	N/A	Skurweberg	Sandstone -beige and white, hard
BH10	90	0	-34.176380	24.817682	62	86	86	26	26	36	25	25	37	Goudini	Sandstone - weathered and fractured. Becomes hard, recrystallised orthosandstone, light grey with heavy mineral speckles
BH11A	90	0	-34.173058	24.810572	63	108	108	22	22	41	N/A	N/A		Goudini	Sandstone - weathered and fractured, beige, medium grained, recrystallised hard
BH11B	90	0	-34.173560	24.808015	63	83	83	37	37	26	36	36	27	Goudini	Sandstone - grey/black, fine grained and recrystallised with pyrite
BH11C	90	0	-34.171866	24.804386	63	87	87	43	43	20	N/A	N/A	N/A	Goudini	Sandstone - dark grey recrystallised with vein quartz in numerous fractured
BH13A	90	0	-34.178184	24.827215	45	17	17	16	16	29	N/A	N/A	N/A	Goudini	Sandstone - grey, fine recrystallised - vein quartz
BH13B	90	0	-34.178134	24.827335	45	8.5	8.5	N/A	N/A	N/A	N/A	N/A	N/A	Goudini	N/A
Maclear, 2002, 2005,2006 borehole dataset															
SRK-1	90	0	-34.15375	24.819778	25	50	50	20	20	5	11 & 16	11 & 16	15 & 9	Bokkeveld	Sandstone, thin layer, yellow iron oxidation, medium to fine grained, hard
SRK-2	90	0	-34.155639	24.819611	25	25	25	17	17	8	12	12	13	Bokkeveld	Shale - Grey-black, fine, hard, interbedded (Bokkeveld Group)
SRK-3	90	0	-34.16275	24.812444	54	120	120	10	10	44	2	2	52	Skurweberg	Sandstone - brown-beige, fine to very fine, small amount of iron oxidation, clay lenses.
SRK-4	90	0	-34.153133	24.819378	17.55	21	21	19	19	-1.45	3 & 12	3 & 12	14.55 & 5.55	Bokkeveld	Black, fine grained Bokkeveld shale

APPENDIX C1

BH No.	Drill Angle	BH Incli-nation	Latitude	Longitude	BH Elev.	BH Depth	Vertical BH Depth	Depth to Bedrock / Overburden Thickness	Vertical Depth to Bedrock / Vertical Overburden Thickness	Bedrock Elev (m amsl)	Depth to Pebble Layer	Vertical depth to pebble layer	Pebble layer elevation (m amsl)	Bedrock Stratigraphy	First bedrock lithology intercepted in BHs as described in BH logs
SRK-5	90	0	-34.154644	24.819222	18.58	19.5	19.5	19	19	-0.42	16	16	2.58	Bokkeveld	Black fine grained Bokkeveld shale
SRK-6	90	0	-34.157367	24.819014	18.43	12	12	11	11	7.43	6	6	12.43	Bokkeveld	Brown, medium grained. Hard rock sandstone
SRK-7	90	0	-34.159131	24.818872	21.74	26	26	N/A	N/A	N/A	7, 10 & 14	7, 10 & 14	14.74, 11.74 & 7.74	N/A	N/A
SRK-8	90	0	-34.160067	24.81885	18.86	10.5	10.5	10	10	8.86	5	5	13.86	Bokkeveld	Sandstone
SRK-9	90	0	-34.161558	24.818817	19.97	8	8	7	7	12.97	5	5	14.97	Baviaanskloof	Grey sandstone (Table Mountain Group)
SRK-10	90	0	-34.155278	24.819175	18.6	20	20	19	19	-0.4	13	13	5.6	Bokkeveld	Dark grey, medium grained, Bokkeveld shale
SRK-11	90	0	34.15651	24.81758	25	29	29	21	21	4	N/A	N/A	N/A	Bokkeveld	Dark grey, fine grained shale with moderately sorted sand.
SRK-12	90	0	34.15543	24.81714	25	29	29	24	24	1	N/A	N/A	N/A	Bokkeveld	Dark grey, fine grained shale with moderately sorted sand.
SRK-13	90	0	34.15724	24.80239	45	13	13	12	12	33	N/A	N/A	N/A	Skurweberg	White, fresh, medium grained sandstone(bedrock).
SRK-14	90	0	34.1607	24.80247	50	16	16	15	15	35	N/A	N/A	N/A	Skurweberg	White, fresh, slightly fractured, fine grained sandstone.
SRK-15	90	0	34.15687	24.81013	30	13	13	12	12	18	N/A	N/A	N/A	Baviaanskloof	White, fine to medium grained, fresh, hard sandstone.
SRK-17	90	0	34.1546	24.81666	25	22	22	20	20	5	16	16	9	Bokkeveld	Dark grey, fine grained sands
Eskom, 2010 (a) borehole dataset															
THY-MR1	90	0	-34.17963	24.67646	29.1	12	12	N/A	N/A	N/A	N/A	N/A	N/A	N/A	N/A
THY-MR2	90	0	-34.17762	24.69187	51.6	42	42	N/A	N/A	N/A	N/A	N/A	N/A	N/A	N/A
THY-MR3	90	0	-34.17762	24.69922	76.9	55	55	N/A	N/A	N/A	N/A	N/A	N/A	N/A	N/A
THY-MR4	90	0	-34.18082	24.70482	44.8	35	35	N/A	N/A	N/A	N/A	N/A	N/A	N/A	N/A
THY-MR5	90	0	-34.1828	24.7072	42.9	38.25	38.25	38	38	4.9	N/A	N/A		Goudini	Dark grey, fine grained hard quartzitic sandstone bedrock
THY-MR6	90	0	-34.1839	24.71884	17.9	21	21	N/A	N/A	N/A	15	15	2.9	N/A	N/A
THY-MR7	90	0	-34.19027	24.71248	17.3	12.25	12.25	N/A	N/A	N/A	12	12	5.3	N/A	N/A
THY-MR8	90	0	-34.18931	24.79584	17.7	9.1	9.1	9	9	8.7	N/A	N/A	N/A	Peninsula	Quartzitic sandstone
THY-MR9	90	0	-34.18798	24.69711	11.7	8.2	8.2	8	8	0	N/A	N/A	N/A	Skurweberg	Quartzitic sandstone
THY-MR10	90	0	-34.18571	24.68718	7	2.2	2.2	2	2	5	N/A	N/A	N/A	Skurweberg	Quartzitic sandstone
THY-RP1	90	0	-34.14545	24.71139	141	133	133	1	1	140	N/A	N/A	N/A	Peninsula	Tan-beige fine-medium grained carbonaceous quartzitic sandstone
THY-RP1-M1	90	0	-34.14505	24.71138	145	61	61	0	0	145	N/A	N/A	N/A	Peninsula	Weathered red-brown-yellowish fine-medium grained quartzitic sandstone
THY-RP1-M2	90	0	-34.14569	24.71165	143	73	73	0	0	143	N/A	N/A	N/A	Peninsula	Yellow-orange-brown fine-medium grained quartzitic sandstone
THY-RP2	90	0	-34.16302	24.70771	87	79	79	19	19	68	18	18	69	Peninsula	Yellow-cream medium grained quartzitic sandstone, fractured/brecciated
THY-RP2-M1	90	0	-34.16309	24.70741	89	40	40	18	18	71	N/A	N/A	N/A	Peninsula	Yellow-beige weathered quartzitic sandstone fractured with angular pebbles and vein quartz at the top

APPENDIX C1

BH No.	Drill Angle	BH Incli-nation	Latitude	Longitude	BH Elev.	BH Depth	Vertical BH Depth	Depth to Bedrock / Overburden Thickness	Vertical Depth to Bedrock / Vertical Overburden Thickness	Bedrock Elev (m amsl)	Depth to Pebble Layer	Vertical depth to pebble layer	Pebble layer elevation (m amsl)	Bedrock Stratigraphy	First bedrock lithology intercepted in BHs as described in BH logs
THY-RP2-M2	90	0	-34.16274	24.70808	86	31	31	19	19	67	N/A	N/A	N/A	Peninsula	Cream-yellow fine-medium grained quartzitic sandstone
THY-RP5	90	0	-34.17867	24.68713	42.58	150	150	24	24	18.58	N/A	N/A	N/A	Goudini	Light-grey fine-medium grained quartzitic sandstone with minor siltstone interlayering, pebbles of quartzitic sandstone and siltstone at the top
THY-RP5-M1	90	0	-34.17869	24.68624	42.158	30	30	28	28	14.158	N/A	N/A	N/A	Goudini	Dark grey, very fine grained quartzitic sandstone
THY-RP5-M2	90	0	-34.17841	24.68795	46.22	42	42	28	28	18.22	N/A	N/A	N/A	Goudini	Weathered dark brown fine-medium grained quartzitic sandstone
THY-RP6	90	0	-34.18386	24.72052	18.472	49	49	23	23	-4.528	22	22	-3.528	Goudini	Black fine grained soft siltstone
THY-RP7	90	0	-34.18877	24.71278	18.72	31	31	23	23	-4.28	15	15	3.72	Goudini	Black muddy sandy siltstone, finely laminated
THY-RP8	90	0	-34.19125	24.71221	16	121	121	11	11	5	7	7	9	Skurweberg	Dark grey fine-medium grained hard quartzitic sandstone
THY-RP9	90	0	-34.19079	24.709	10.68	99	99	9	9	1.68	7	7	3.68	Skurweberg	Light grey fine grained hard quartzitic sandstone
THY-RP10	90	0	-34.18668	24.6925	15.067	98	98	6	6	9.067	N/A	N/A	N/A	Skurweberg	Light grey fine grained silty quartzitic sandstone
THY-RP10-M1	90	0	-34.18699	24.69291	13.32	50	50	6	6	7.32	3	3	10.32	Skurweberg	Light grey very fine grained, silty quartzitic sandstone
THY-RP11	90	0	-34.18735	24.71399	17.792	49	49	22	22	-4.208	20	20	2.208	Goudini	Dark grey fine grained siltstone finely laminated
THY-RP12	90	0	-34.18572	24.71803	14.16	49	49	19	19	-4.84	17	17	-2.84	Goudini	Dark-grey very fine grained quartzitic sandstone
THY-RP13	90	0	-34.18587	24.68782	7.82	39	39	8	8	-0.18	4	4	3.82	Skurweberg	Dark-grey very fine grained quartzitic sandstone
THY-RP14	90	0	-34.18781	24.69747	10.87	49	49	9	9	1.87	6	6	4.87	Skurweberg	Dark-grey very fine grained arenaceous siltstone
THY-RP15	90	0	-34.18373	24.71556	10.9	49	49	25	25	-14.1	21	21	-10.1	Goudini	Light-grey medium-course grained quartzitic sandstone interlayered with black siltstone
THY-RP16	90	0	-34.18382	24.71788	24.07	49	49	25	25	-0.93	23	23	1.07	Goudini	Dark grey to black fine grained siltstone
THY-MR11	90	0	-34.1839	24.71902	16	21	21	20	20	-4	19.1	19.1	-3.1	Goudini	Grey-black fine grained shale
THY-MR11-M1	90	0	-34.18385	24.71906	17.5	21	21	N/A	N/A	N/A	17.8	17.8	8.2	N/A	N/A
THY-MR11-M2	90	0	-34.18396	24.71908	12	21	21	19.1	19.1	-7.1	18.1	18.1	-6.1	Goudini	Grey-khaki fine grained shale

APPENDIX C1

BH No.	Drill Angle	BH Incli-nation	Latitude	Longitude	BH Elev.	BH Depth	Vertical BH Depth	Depth to Bedrock / Overburden Thickness	Vertical Depth to Bedrock / Vertical Overburden Thickness	Bedrock Elev (m amsl)	Depth to Pebble Layer	Vertical depth to pebble layer	Pebble layer elevation (m amsl)	Bedrock Stratigraphy	First bedrock lithology intercepted in BHs as described in BH logs
THY-MR11-M3	90	0	-34.18396	24.71905	8	24.1	24.1	23.5	23.5	-15.5	19.8	19.8	-11.8	Goudini	Grey fine-medium grained quartzitic sandstone hard rock
THY-MR12	90	0	-34.18392	24.72769	6	22	22	21	21	-15	N/A	N/A	N/A	Peninsula	Cream-tan to grey coloured fine-medium grained quartzitic sandstone, calcretised
THY-MR14	90	0	-34.17332	24.72916	67	24.3	24.3	24	24	43	N/A	N/A	N/A	Peninsula	White-grey to yellow-brown fine-medium grained quartzitic sandstone
THY-MR15	90	0	-34.1726	24.73443	95	24.5	24.5	24	24	71	N/A	N/A	N/A	Peninsula	Cream-white fine-medium grained quartzitic sandstone
Eskom, 2010 (b) borehole dataset															
NEW1	90	0	-34.181816	24.706315	48.006	49.62	49.62	40.85	40.85	7.156	37.55	37.55	10.456	Goudini	Grey, slightly weathered, thinly laminated, medium jointed, soft rock, sandstone.
NEW2	90	0	-34.182701	24.70627	45.174	56.8	56.8	46.34	46.34	-1.166	43.34	43.34	1.834	Goudini	Grey streaky dark grey, unweathered to slightly weathered, closely to medium jointed, cross bedded, water escape structures,soft rock to medium hard rock, quartzitic sandstone with occasional interbedded phyllite.
NEW3	90	0	-34.183460	24.705488	52.518	64.55	64.55	52.59	52.59	-0.072	51.12	51.12	1.398	Goudini	Grey, slightly weathered to moerately weathered, very closely jointed, very highly fractured, thinly laminated, very soft rock,phyllite.
NEW4b	90	0	-34.184513	24.704939	61.592	66	66	57.75	57.75	3.842	55.9	55.9	5.692	Goudini	Greenish khaki grey, slightly to moderately weathered, very closely jointed, finely laminated and iron-stained, micaceous, very soft rock, fine grained, quartzitic sandstone.
NEW5	90	0	-34.185298	24.707504	42.823	67.77	67.77	39.2	39.2	3.623	33.22	33.22	9.603	Goudini	Dark grey to black, moderately to highly weathered with occasional completely weathered, cross bedded with water escape structures, EW rock horisons (soil) at 46.62-46.77 and 46.86-48.27 and 49.77-49.97 m, very closely jointed, very soft rock, cabonaceous phyllite.
NEW6	90	0	-34.185298	24.708424	51.206	67.1	67.1	50.66	50.66	0.546	44.05	44.05	7.156	Goudini	Grey banded dark grey, slightly weathered to unweathered, very closely jointed, cross bedded with water escape structures, very soft rock to soft rock with minor zones of medium hard rock,interbedded phyllite/shale and quartzitic sandstone.
NEW7	90	0	-34.183397	24.708081	42	55.57	55.57	44.96	44.96	-2.96	39.07	39.07	2.93	Goudini	Dark grey, moderately weathered, very closely jointed, no internal structure visible, soft rock to medium hard rock, quartzitic sandstone.
NEW8	90	0	-34.182655	24.708442	40.294	51	51	37.5	37.5	2.794	34.44	34.44	5.854	Goudini	Grey to dark grey, slightly weathered, cross bedded, very closely to closely jointed, soft rock, quartzitic sandstone.
NEW9	90	0	-34.183302	24.710835	36.782	40.55	40.55	34.85	34.85	1.932	25	25	11.782	Goudini	Grey greenish towards top contact, moderately weathered, very closely jointed, cross bedded, very soft rock, fine grained,quartzitic sandstone.
NEW10	90	0	-34.184160	24.710307	48.567	60	60	51	51	-2.433	40.5 & 48.15	40.5 & 48.15	8.067 & 0.417	Goudini	Slightly greenish dark grey, slightly weathered, cross bedded and quartz veined, very closely spaced joints, soft rock with minor medium hard rock, fine grained, quartzitic sandstone.

APPENDIX C1

BH No.	Drill Angle	BH Incli-nation	Latitude	Longitude	BH Elev.	BH Depth	Vertical BH Depth	Depth to Bedrock / Overburden Thickness	Vertical Depth to Bedrock / Vertical Overburden Thickness	Bedrock Elev (m amsl)	Depth to Pebble Layer	Vertical depth to pebble layer	Pebble layer elevation (m amsl)	Bedrock Stratigraphy	First bedrock lithology intercepted in BHs as described in BH logs
NEW11b	90	0	-34.185106	24.709867	39.122	64.68	64.68	39.26	39.26	-0.138	34.68	34.68	4.442	Goudini	Dark grey, slightly to moderately weathered, very closely jointed (highly fractured and friable), very soft rock to soft rock, fine grained, quartzitic sandstone with interbedded phyllite bands.
NEW12	90	0	-34.185655	24.709013	26.718	49.95	49.95	25.95	25.95	0.768	18.45	18.45	8.268	Goudini	Dark grey, moderately to highly weathered, very closely jointed,highly fractured, friable, very soft rock, phyllite.
NEW13	90	0	-34.186467	24.71168	20.02	32.54	32.54	22.34	22.34	-2.32	18	18	2.02	Goudini	Grey banded dark grey, slightly weathered, closely to medium spaced, horizontal and cross bedding, soft rock, quartzitic sandstone with intercalated phyllite.
NEW14	90	0	-34.183701	24.715757	24.129	34.53	34.53	22.94	22.94	1.189	22.53	22.53	1.599	Goudini	Brownish grey, slightly weathered, very closely to closely jointed,quartz veined <5 mm thick, iron-stained joints, medium hard rock,quartzitic sandstone.
NEW15	90	0	-34.183693	24.716975	25.355	36	36	25.23	25.23	0.125	N/A	N/A	N/A	Goudini	Green to grey, slightly weathered, closely to medium jointed, cross bedded with occasional angular shale/phyllite clasts, soft rock,quartzitic sandstone.
NEW16	90	0	-34.183981	24.713073	33.255	45	45	34.56	34.56	-1.305	31.39	31.39	1.865	Goudini	Greenish grey, slightly weathered, very closely jointed, cross bedded, soft rock, quartzitic sandstone.
NEW17	90	0	-34.187438	24.713863	17.703	42.1	42.1	24.1	24.1	-6.397	17.26	17.26	0.443	Goudini	Dark grey, moderately weathered, closely spaced, very soft rock to soft rock, fine grained, quartzitic sandstone with interbedded (minor) phyllite.
NEW18	90	0	-34.186605	24.714271	24.75	38.36	38.36	28.34	28.34	-3.59	25.93	25.93	-1.18	Goudini	Dark grey, slightly weathered, medium to widely spaced (31.05-31.54 very closely spaced), cross bedded with minor water escape structures, soft rock, quartzitic sandstone.
NEW19	90	0	-34.183787	24.71841	19.578	31.05	31.05	20.73	20.73	-1.152	19.5	19.5	0.078	Goudini	Khaki green, slightly to moderately weathered, very closely jointed with occasional closely to medium jointed, 20.73-20.90m:extremely weathered rock mixed with pebbles and shell fragments, very soft rock to soft rock. rock. Quartzitic sandstone.
NEW20	90	0	-34.183896	24.719581	15.786	26.06	26.06	18.27	18.27	-2.484	17.01	17.01	-1.224	Goudini	Grey minor dark grey, moderately weathered, very closely jointed, thin phyliitic bands, very soft rock to soft rock. Quartzitic sandstone.
NEW21	90	0	-34.186373	24.717506	19.189	33.06	33.06	23.19	23.19	-4.001	21.13	21.13	-1.941	Goudini	Orange yellow, highly weathered to completely weathered, very closely to closely jointed, fissured, very soft rock to soft rock, quartzitic sandstone.
NEW22	90	0	-34.185212	24.718213	18.899	32.81	32.81	22.29	22.29	-3.391	21.39	21.39	-2.491	Goudini	Grey, unweathered, very closely to closely jointed, cross bedded, medium hard rock with very soft rock to soft rock zone at 22.29-22.51m, quartzitic sandstone.
NEW23	90	0	-34.183785	24.721653	17.119	39.27	39.27	23	23	-5.881	19.8	19.8	-2.681	Goudini	Grey, slightly to moerately weathered, very closely jointed, finely laminated, very soft rock, friable zones, phyllite.
NEW24	90	0	-34.180692	24.706748	42.647	49.5	49.5	37.42	37.42	5.227	37.27	37.27	5.377	Goudini	Grey occasionally streaky, slightly weathered to unweathered, very closely jointed, minor cross bedding, medium hard rock to hard rock with minor zones of soft rock, quartzitic sandstone.
NEW25	90	0	-34.180616	24.704154	39.683	42.55	42.55	30.51	30.51	9.173	N/A	N/A	N/A	Goudini	Brownish orange grey, slightly weathered, very closely to closelyjointed, cross bedded, soft rock to medium hard rock, quartzitic sandstone.

APPENDIX C1

BH No.	Drill Angle	BH Incli-nation	Latitude	Longitude	BH Elev.	BH Depth	Vertical BH Depth	Depth to Bedrock / Overburden Thickness	Vertical Depth to Bedrock / Vertical Overburden Thickness	Bedrock Elev (m amsl)	Depth to Pebble Layer	Vertical depth to pebble layer	Pebble layer elevation (m amsl)	Bedrock Stratigraphy	First bedrock lithology intercepted in BHs as described in BH logs
NEW26	90	0	-34.178326	24.70372	65.814	66	66	57.3	57.3	8.7	51.3	51.3	14.7	Goudini	Grey, slightly weathered, very closely to closely jointed, cross-bedded, soft rock to medium hard rock, quartzitic sandstone.
NEW27	90	0	-34.187324	24.711272	16	112.95	112.95	14.44	14.44	1.56	12.45	12.45	3.55	Goudini	Stained reddish, slightly greenish grey, moderately weathered, very closely jointed, horizontal lamination, soft rock to medium hard rock. Fine grained, micaceous quartzitic sandstone.
NEW28	90	0	-34.186479	24.706555	24	120.09	120.09	19.26	19.26	4.74	17.11	17.11	6.89	Goudini	Stained reddish, slightly greenish grey, moderately weathered, very closely jointed, horizontal lamination, soft rock to medium hard rock. Fine -grained micaceous quartzitic sandstone
NEW29	90	0	-34.188839	24.695324	3	102.07	102.07	0	0	3	N/A	N/A	N/A	Skurweberg	Grey, unweathered, close to medium jointed, cross-bedding, minor faulting, minor iron-staining, hard rock. Quartzitic sandstone.
NEW30	90	0	-34.186515	24.691042	12	108	108	7.35	7.35	4.65	N/A	N/A	N/A	Skurweberg	Dark grey mottled brown and light grey, unweathered, closely to medium jointed with occasional widely jointed, quartz veined (> 20mm thickness) healed fractures, open fractures with grey infill, very hard rock. Quartzitic sandstone.
TB1	90	0	-34.185148	24.686281	2.664	40.42	40.42	0	0	2.664	N/A	N/A	N/A	Skurweberg	Dark grey to grey, slightly weathered, closely to medium jointed,very hard rock, quartzitic sandstone.
TB2	90	0	-34.186408	24.687787	2.895	20.52	20.52	0	0	2.895	N/A	N/A	N/A	Skurweberg	Grey orange brown, slightly weathered, closely jointed, cross bedded, medium hard rock to hard rock, quartzitic sandstone.
TB3	90	0	-34.186794	24.69213	14.066	20.78	20.78	7.97	7.97	6.096	N/A	N/A	N/A	Skurweberg	Light grey, unweathered, medium or widely jointed, hard rock to very hard rock, quartzitic sandstone.
TB4	90	0	-34.188904	24.694369	2.25	20.2	20.2	0	0	2.25	N/A	N/A	N/A	Skurweberg	Grey to dark grey, slightly weathered, closely to medium jointed,cross bedded, very hard rock, quartzitic sandstone.
TB5	90	0	-34.188436	24.696807	11.948	20.51	20.51	10.52	10.52	1.428	N/A	N/A	N/A	Skurweberg	Grey, unweathered, closely jointed, quartz veined, hard rock,quartzitic sandstone.
TB6	90	0	-34.188789	24.698598	7.871	20.22	20.22	9	9	-1.129	6	6	1.871	Skurweberg	Dark grey patchy orange, slightly to moderately weathered,closely jointed, soft rock, interbedded sandstone and siltstone/shale.
TB7	90	0	-34.188646	24.703211	19.169	20.16	20.16	13.59	13.59	5.579	N/A	N/A	N/A	Skurweberg	Grey to dark grey, slightly to moderately weathered, closely to medium jointed, thinly laminated, very hard rock, siltstone.
TB8	90	0	-34.190023	24.704845	7	40.36	40.36	3.41	3.41	3.59	1.25	1.25	5.75	Skurweberg	Light grey, unweathered to slightly weathered, closely to medium jointed, vertical to subvertical quartz veining, very hard rock,
TB9	90	0	-34.191045	24.70876	7.284	30.6	30.6	4.5	4.5	2.784	0	0	7.284	Skurweberg	Grey to dark grey, slightly weathered, close to medium spaced, thin wavy laminations, hard rock, siltstone.
TB10	90	0	-34.192002	24.713726	2.075	40.33	40.33	0	0	2.075	N/A	N/A	N/A	Skurweberg	Sugary brown, slightly weathered, closely jointed, very hard rock,fine grained quartzitic sandstone.
TB11	90	0	-34.186998	24.715456	19.201	30.5	30.5	23.1	23.1	-3.899	22.35	22.35	-3.149	Goudini	Light and dark grey, moderately to highly weathered, thinly laminated, closely jointed, very soft rock to soft rock, siltstone.
TB12	90	0	-34.182745	24.706624	45.241	40.5	40.5	N/A	N/A	N/A	N/A	N/A	N/A	N/A	N/A
TB13	90	0	-34.185739	24.701949	42.743	28.5	28.5	N/A	N/A	N/A	N/A	N/A	N/A	N/A	N/A

APPENDIX C1

BH No.	Drill Angle	BH Incli-nation	Latitude	Longitude	BH Elev.	BH Depth	Vertical BH Depth	Depth to Bedrock / Overburden Thickness	Vertical Depth to Bedrock / Vertical Overburden Thickness	Bedrock Elev (m amsl)	Depth to Pebble Layer	Vertical depth to pebble layer	Pebble layer elevation (m amsl)	Bedrock Stratigraphy	First bedrock lithology intercepted in BHs as described in BH logs
TB14	90	0	-34.185947	24.694686	21.918	30.92	30.92	10.5	10.5	11.418	9.45	9.45	12.468	Skurweberg	Mottled dark grey, slightly weathered, closely to medium jointed, hard rock, quartzitic sandstone.
TB15	90	0	-34.188412	24.708227	21.15	30.1	30.1	15.55	15.55	5.6	N/A	N/A	N/A	Goudini	Grey banded reddish, moderately weathered, close to medium (minor) jointed, soft rock, horizontal and wavy sandstone and shale.
TB16	90	0	-34.186367	24.689462	9.338	30.6	30.6	6.36	6.36	2.978	N/A	N/A	N/A	Skurweberg	Light grey, moderately weathered, medium jointed, very hard rock,quartzitic sandstone.
TB17c	90	0	-34.187675	24.694135	14.333	30.52	30.52	5.91	5.91	8.423	N/A	N/A	N/A	Skurweberg	Streaky reddish orange grey, unweathered, closely to medium jointed, scross bedded, very hard rock, quartzitic sandstone.
TB18	90	0	-34.190389	24.707205	10.84	20.65	20.65	6.13	6.13	4.71	N/A	N/A	N/A	Skurweberg	Orange grey, slightly weathered, closely to medium jointed, hard rock, quartzitic sandstone.
TB19	90	0	-34.191861	24.711792	10.965	20.01	20.01	9.54	9.54	1.425	N/A	N/A	N/A	Skurweberg	Grey, slightly weathered, closely to medium jointed, very hard rock, cross beded, quartzitic sandstone.
TB21	90	0	-34.18605	24.692236	18.713	19.56	19.56	12.67	12.67	6.043	12.4	12.4	6.313	Skurweberg	Grey, unweathered, closely jointed, cross bedded, hard rock, quartzitic sandstone.
TB22	90	0	-34.187241	24.696661	18.784	28.5	28.5	17.78	17.78	1.004	12, 13.5 & 16.5	12, 13.5 & 16.5	6.784, 5.284 & 2.284	Skurweberg	Dark grey and black, slightly weathered to unweathered, closely jonted to very closely jointed, cross bedded, hard rock, quartzitic sandstone.
TB24	90	0	-34.187829	24.701137	18.934	30.58	30.58	11.72	11.72	7.214	N/A	N/A	N/A	Skurweberg	Grey to dark grey, slightly weathered, closely to medium jointed, wavy laminations, hard rock to very hard rock, siltstone with interbedded shale horizon.
TB26	90	0	-34.188734	24.701553	21.693	20.72	20.72	14.77	14.77	6.923	N/A	N/A	N/A	Skurweberg	Greenish grey, slightly weathered, very closely to closely jointed, cross bedded, very hard rock, quartzitic sandstone.
TB27	90	0	-34.190247	24.709902	14.031	20.1	20.1	9.63	9.63	4.401	9.18	9.18	4.851	Goudini	Spotty grey dark grey, slightly weathered, medium jointed, cross bedded, soft rock to hard rock, quartzitic sandstone.
TB29	90	0	-34.188484	24.701449	12.275	30.02	30.02	7.97	7.97	4.305	N/A	N/A	N/A	Skurweberg	Grey, slighty weathered, closely to medium jointed, cross bedded with minor quartz veining, very hard rock, quartzitic sandstone.
TB30	90	0	-34.186972	24.699411	23.233	30.01	30.01	14.11	14.11	9.123	13.7	13.7	9.533	Skurweberg	Grey, unweathered, closely to medium jointed, cross bedded, very hard rock, quartzitic sandstone.
TB31	90	0	-34.187263	24.703689	30.78	30	30	22.43	22.43	8.35	N/A	N/A	N/A	Skurweberg	Grey, unweathered, closely jointed, cross bedded, very hard rock, quartzitic sandstone
TB32	90	0	-34.190105	24.712511	16.874	30.1	30.1	14.05	14.05	2.824	N/A	N/A	N/A	Goudini	Grey to light grey, slightly weathered, closely jointed, minor horizontal laminations, hard rock to very hard rock, quartzitic sandstone.
TB34	90	0	-34.186593	24.701691	26.828	30.06	30.06	13.56	13.56	13.268	N/A	N/A	N/A	Skurweberg	Mottled greenish grey orange, slightly weathered, closely jointed, hard rock, quartzitic sandstone.
TB35	90	0	-34.185448	24.697433	46.119	33.03	33.03	30.9	30.9	15.219	N/A	N/A	N/A	Skurweberg	Dark grey to grey, slightly weathered, closely to medium jointed, profusely cross bedded, very hard rock, quartzitic sandstone.
TB36	90	0	-34.186024	24.699646	35.328	55.33	55.33	22.58	22.58	12.748	21.53	21.53	13.798	Skurweberg	Grey to dark grey banded reddish brown, unweathered, closely to medium jointed, minor cross bedding, very hard hard, quartzitic sandstone.
TB37	90	0	-34.186172	24.704124	25.592	54.51	54.51	15.43	15.43	10.162	14.01	14.01	11.582	Goudini	Banded light-dark grey and reddish brown, slightly weathered, closely to medium jointed, iron-stainedin bands, soft rock to hard rock, quartzitic sandstone.
TB38	90	0	-34.186945	24.706131	30.435	30.04	30.04	24.6	24.6	5.19	21.08	21.08	9.355	Goudini	Grey banded orange, slightly weathered, closely jointed, horizontally laminated, hard rock, quartzitic sandstone.

APPENDIX C1

BH No.	Drill Angle	BH Incli-nation	Latitude	Longitude	BH Elev.	BH Depth	Vertical BH Depth	Depth to Bedrock / Overburden Thickness	Vertical Depth to Bedrock / Vertical Overburden Thickness	Bedrock Elev (m amsl)	Depth to Pebble Layer	Vertical depth to pebble layer	Pebble layer elevation (m amsl)	Bedrock Stratigraphy	First bedrock lithology intercepted in BHs as described in BH logs
TB39	90	0	-34.18844	24.710719	20.6	30.15	30.15	15.41	15.41	5.19	15.15	15.15	5.45	Goudini	Brownish grey, slightly weathered, closely to medium jointed, cross bedded and iron-stained, hard rock, quartzitic sandstone
TB42	90	0	-34.186693	24.709144	21.544	30.05	30.05	18.08	18.08	3.464	14.83	14.83	6.714	Goudini	Banded dark grey-grey reddish brown, slightly to moderately weathered, very closely jointed, quartz veined, minor water escape structures, soft rock, quartzitic sandstone.
TB43	90	0	-34.18471	24.702561	66.311	49.99	49.99	N/A	N/A	N/A	N/A	N/A	N/A	N/A	N/A
TB44	90	0	-34.1851	24.699982	69.65	30.18	30.18	N/A	N/A	N/A	N/A	N/A	N/A	N/A	N/A
TB45	90	0	-34.185225	24.704599	49.244	40.78	40.78	N/A	N/A	N/A	N/A	N/A	N/A	N/A	N/A
TB45b	90	0	-34.18519	24.70461	49.833	52.8	52.8	42.56	42.56	7.273	39.5	39.5	10.333	Goudini	Banded dark grey and grey, unweathered, medium jointed (minor closely and widely jointed), cross bedded with water escape structures, soft rock, quartzitic sandstone.
TB46	90	0	-34.188231	24.713173	16.61	28.61	28.61	18.11	18.11	-1.5	14.77	14.77	1.84	Goudini	Dark grey, highly weathered to moderately weathered, very closely jointed, highly fractured, very soft rock to soft rock, intercalated shale and siltstone.
Hanson et al., 2012 borehole dataset															
CSF10	90	0	-34.193934	24.824805	41.6	55.18	55.18	51.04	51.04	-9.44	42.73	42.73	-1.13	Goudini	Highly fractured sandstone is very hard at the top of the run but gets softer and can be crushed as it gets deeper.MG - CG.SA-SR. Jointed at:51.51m ,51.51m, 51.66m, and 51.74m.within the joints, grey silt infills.
CSF13	90	0	-34.203459	24.82272	30.87	16.33	16.33	12.46	12.46	18.41	7.2	7.2	23.67	Peninsula	Minor (~5cm) SP @ top of run. Appears to be 'rubbish' material, a mix of SP, drilling fluids etc. Sstone is hard, MG, crystalline. Fairly structureless. Two minor qtz veins ≤ 1mm ~10cm from the base. One open fracture, competant.
CSF14	90	0	-34.19804	24.823889	39.01	57.18	57.18	50.53	50.53	-11.52	41.13	41.13	-2.12	Cedarberg	VFG.Black. Siltstone
CSF17	90	0	-34.199457	24.823594	38.12	43.6	43.6	39.35	39.35	-1.23	20.53	20.53	17.59	Peninsula	Sandstone rock with lenses of shale. Highly fractured and have a sharp joint that runs vertical the core and continues from the top, the joint shows some kind or mineralisation. Highly micaceous rock with pyrite at the bottom. Poor RQD=27%
CSF18	90	0	-34.201738	24.823101	32.92	19.6	19.6	15.28	15.28	17.64	11.7	11.7	21.22	Peninsula	The beginning of bedrock, quatzite with mud. The muddy layer from previous run ends at 15.45m,mixed with gravel pieces of bedrock material. The whole rock is highly fractured at weak points and filled with mud. Poor RQD=30%
TS-01	90	0	-34.180839	24.705247	44.06	39.95	39.95	36.15	36.15	7.91	N/A	N/A	N/A	Goudini	Sandstone: N7-N5, Highly jointed sandstone rock with lenses of black silt-stole.a bit fructured in places.Jointed at :36.30m; 36.94m, 37.15m, 36.6m, 37.70m, 37.78m, 38.25m,38.76m, 39.2m, 39.71m and 39.75m
TS-02	90	0	-34.179948	24.704887	47.05	42.27	42.27	39.25	39.25	7.8	39.17	39.17	7.88	Goudini	Mudrock: Greenish grey 5G 6/4, Very Well-sorted; Very fine-grained well rounded to sub-angular grains, Massive, Mostly clayey with trace medium to coarse grained heavy mineral grains.
TS-03	90	0	-34.179473	24.707163	44.1	39.84	39.84	36.87	36.87	7.23	35.11	35.11	8.99	Goudini	Sandstone: N7-N5, Highly jointed sandstone rock with lenses of black silt-stole.a bit fructured in places.Jointed at :36.30m; 36.94m, 37.15m, 36.6m, 37.70m, 37.78m, 38.25m,38.76m, 39.2m, 39.71m and 39.75m

APPENDIX C1

BH No.	Drill Angle	BH Incli-nation	Latitude	Longitude	BH Elev.	BH Depth	Vertical BH Depth	Depth to Bedrock / Overburden Thickness	Vertical Depth to Bedrock / Vertical Overburden	Bedrock Elev (m amsl)	Depth to Pebble Layer	Vertical depth to pebble layer	Pebble layer elevation (m amsl)	Bedrock Stratigraphy	First bedrock lithology intercepted in BHs as described in BH logs
TS-05	90	0	-34.178089	24.705665	59.4	63.25	63.25	60.92	60.92	-1.52	N/A	N/A	N/A	Goudini	Mudrock (clay AND SILT SIZE PARTICLES): 5GY 6/1-5GY 4/1, < than 1 mm thick flakes (wet weathered mudrock/shale)
TS-06	90	0	-34.178194	24.695744	59.93	62.7	62.7	56.1	56.1	3.83	44.57	44.57	15.36	Goudini	shale/mudrock: 5Y 4/1, 5Y GY 4/1, Sharp contact with pebbles above. shale/mudrock is weathered and had orange coloured staining in the fractures. High angle bedding is noted -rocks are tilted. Fractures have ~ 10cm spacing.
TS-07	90	0	-34.177574	24.691719	51.03	43.82	43.82	39.28	39.28	11.75	39	39	12.03	Goudini	Lean clay (CL): Black (N1), shale material, slightly weathered and breaks up easily(mechanically). Very fine-med grained, well sorted, SA-SR, rich micaceous minerals
TS-10	90	0	-34.178914	24.685565	42.32	25.93	25.93	21.9	21.9	20.42	21.19	21.19	21.13	Goudini	sandstone/clay: Medium gray N5, Fine grained sandstone with clay/mud at the bottom.sandstone (Fair=50.1%). Broken up along joints, with mud infill, highly weathered joints.Prominent bedding from 22.5m. clay/mud(micaceous rich), has 5-10% clay plasticity. Bedding shows alt of very shiny minerals (pyrite?) and mica. few mechanical breaks but all seem to have broken along weak joints. J1=22.08m aolng weak point, infill weathered. J2=22.18-22.33m mechanical break alon weak points. J3=22.67-22.93m highly weathered joint with mud.
TS-15	90	0	-34.177739	24.673099	37.43	22.65	22.65	17.97	17.97	19.46	N/A	N/A	N/A	Skurweberg	QUARTZOSE sandstone: N8 to 576/1 and N3-N4, fine to very FG quartzose sandstone.Mature to possibly supermature. Jointing running at 130 – 140 degrees to vertical. Massively bedded in upper 130cm. Some beds with iron staining (10YR4/6). Smooth to slightly rough joints. One with quartz infill at base. Joints at 18.10m, 18.74m, 19.10m, 19.18m and 19.27m. All between 40 and 50 degrees to vertical
TS-16	90	0	-34.178498	24.671824	23.36	12.18	12.18	7.19	7.19	16.17	6.23	6.23	17.13	Skurweberg	quartzite: Light gray N7-10 YR 5/4 medium yellowish brown, quartzite with multiple fractures and small quartz veins. Fractures have mud infills and highly weathered in places.Very poor RQD=0%. Mud infills are sandy and becomes white when dry. The light grey colour changes into a brown colour
TS-17	90	0	-34.176382	24.669548	49.41	29.03	29.03	25.43	25.43	23.98	N/A	N/A	N/A	Skurweberg	MetaAsandstone: 5Y4/1 TO 5Y4/2 AND N1 BANDS, bedrock quartzite. Bedding is seemingly at 45 degree angle to vertical and thinly bedded to thickly laminated and is a metamorphosed meta sandstone. Banding comes from highly micaceous horizons giving a bkackish (N1) striped appearance. Micaceous bands consist of quartz and biotite. The lighter bands have a higher proportion of quartz and some biotite. The micaceous bands are highly folidated. Quartz is round to subround. Biotite is oblate. Some recrustallisation of quartz. Possible heavy minerals black in colour. Relict undulatory continuous bedding and possible relict flaser bedding in last 30cm
TS-19	90	0	-34.183039	24.68152	12	7.77	7.77	4.45	4.45	7.55	3.83	3.83	8.17	Skurweberg	Quartzite: Light grey (N7), Clean qtzite, hard rock. sand matrix @ the top that was completely washed of by corewash/ fluid. Core has a lot of fractures, but is still intact. Looks like solution passed through cracks (black minerals visible) [Skurweberg Formation?]

APPENDIX C1

BH No.	Drill Angle	BH Incli-nation	Latitude	Longitude	BH Elev.	BH Depth	Vertical BH Depth	Depth to Bedrock / Overburden Thickness	Vertical Depth to Bedrock / Vertical Overburden Thickness	Bedrock Elev (m amsl)	Depth to Pebble Layer	Vertical depth to pebble layer	Pebble layer elevation (m amsl)	Bedrock Stratigraphy	First bedrock lithology intercepted in BHs as described in BH logs
TS-20	90	0	-34.187396	24.713902	17.66	26.8	26.8	22.47	22.47	-4.81	17.41	17.41	0.25	Goudini	Shale/mudrock: 5Y 4/4 (weathered mudrock/shale); N3 (unweathered mudrock/shale).,(19.72-19.88): Weathered (19.88-20.77): unweathered; Gradational contact between weathered and unweathered shale. Slightly [Goudini Formation]weathered zone at 20.67m.
TS-21	90	0	-34.186996	24.715454	19.08	23.37	23.37	20.07	20.07	-0.99	15.06	15.06	4.02	Goudini	LIGHT GREY quartzite (GP): 5B 7/11, FG-CG; WS-VWS, SR-SA, Slightly laminated,Jointed at 19.35, 19.38, 19.52 and 19.64m.gets gradually darker as we progress deeper. Might be a single boulder of > 0.5m in size.
TS-22	90	0	-34.18379	24.725615	19.91	27.1	27.1	24.04	24.04	-4.13	21.1	21.1	-1.19	Cedarberg	Shale / LAMINATED shale-siltstone: 5YR N2-3, dark greyish black siltstone or shale chips ground into a powder with some hard clasts of remnant shale. Interpreted as weathered regolith towards the beginning of bedrock. [Goudini Formation]
NEW Seismic A	90	0	-34.183844	24.714844	24.22	40.76	40.76	27.3	27.3	-3.08	24.28	24.28	-0.06	Goudini	Sandstone: Pale Olive (10Y 6/2), MS-WS, FG-MG, SR; Very thinly laminated, moderately hard, widely spaced fractures. SO (~45°). [Goudini Formation]
NEW Seismic B	90	0	-34.187007	24.715161	20.43	111.52	111.52	24.92	24.92	-4.49	N/A	N/A	N/A	Goudini	Quartzite: 10YR 6/6-quartzite, N6-clay, very fine grained; quartzite with clay at the bottom of the core
NEW Seismic C	90	0	-34.183708	24.71495	24.02	120	120	26.11	26.11	-2.09	N/A	N/A	N/A	Goudini	Sandstone AND shale STRINGERS AND/OR BLEBS: Sst: greenish grey (5GY 6/1)shale: dark grey (N3), 26.05-26.66m: MW sstone, MG, with minor = 1mm stringers. Fairly competant (some near horizontal fractures - may be unnatural and drilling induced). Moderately hard to soft. 26.66-26.80m: HW (?) sstone, very degraded. MG, with FG-VFG shale. Very soft blebs. Sstone is soft, no identifiable structure aside from JO at the bottom contact @26.80m - JO (~85°, smooth,planar). 26.80-27.15m same as 26.05-26.66m with blebs. All blebs = 3cm. Bottom contact JO(~45°, smooth, planar). Two joints spaced ~ 1cm apart at this point. Rest of the run is very broken (unnatural?). SO (?): ~45°.
Engelsman & Constable, 2012 borehole dataset															
New_D1	90	0	-34.188691	24.713051	18.724	79.9	79.9	19	19	-0.276	16	16	2.724	Goudini	Grey, moderately to highly weathered, very closely jointed, very soft rock to soft rock, Quartzitic sandstone and Mudstone.
New_E18	90	0	-34.187283	24.716332	22.566	87.09	87.09	25.5	25.5	-2.934	24.7	24.7	-2.134	Goudini	Light yellowish brown, moderately weathered, fine grained, very thinly banded, medium jointed and closely jointed (drilling induced), soft to medium hard rock. sandstone.
New_F1	90	0	-34.18375	24.720618	18.996	138.14	138.14	25	25	-6.004	21	21	-2.004	Goudini	Goudini Formation
New_G1	90	0	-34.181975	24.717087	23.006	84.36	84.36	24.59	24.59	-1.584	22.78	22.78	0.226	Cedarberg	Dark grey to black, very stiff, relic jointed, clayey SILT. RESIDUAL shale.

APPENDIX C1

BH No.	Drill Angle	BH Incli-nation	Latitude	Longitude	BH Elev.	BH Depth	Vertical BH Depth	Depth to Bedrock / Overburden Thickness	Vertical Depth to Bedrock / Vertical Overburden Thickness	Bedrock Elev (m amsl)	Depth to Pebble Layer	Vertical depth to pebble layer	Pebble layer elevation (m amsl)	Bedrock Stratigraphy	First bedrock lithology intercepted in BHs as described in BH logs
New_H1	90	0	-34.187995	24.7084	18.756	72.47	72.47	11.5	11.5	7.256	10	10	8.756	Goudini	Light grey banded black and reddish brown, unweathered to slightly weathered, closely to medium jointed but mainly widely jointed, slightly foliated, minor water seepage structures, soft rock to medium hard rock, Quartzitic sandstone/phyllite.
New_I1C	90	0	-34.186362	24.711714	22.812	140.5	140.5	24.47	24.47	-1.658	22.1	22.1	0.712	Goudini	Light grey banded dark grey, moderately to slightly weathered, medium to widely jointed, micaceous, occasionally thinlylaminated, soft rock, sandstone.
New_J1	90	0	-34.182003	24.709798	29.754	84	84	26.22	26.22	3.534	N/A	N/A		Goudini	Light grey, slightly weathered with moderately weathered zones, very fine to fine grained, very thinly banded, medium jointed, very soft to soft rock. siltstone / sandstone.
New_K1B	90	0	-34.177727	24.716201	57.25	90.67	90.67	33.5	33.5	23.75	N/A	N/A		Peninsula	Peninsula Formation
New_L1	90	0	-34.184361	24.70839	51.918	115.29	115.29	54.5	54.5	-2.582	51.58	51.58	0.338	Goudini	Goudini Formation
New_M1	90	0	-34.178795	24.710329	31.845	89.09	89.09	30	30	1.845	29.09	29.09	2.755	Cedarberg	Dark grey, moderately to highly weathered, occasionally completely weathered, very closely to closely jointed, intensely fractured, very thinly laminated, very soft rock, Graphitic shale.
New_N1	90	0	-34.186654	24.701874	27.349	131.36	131.36	19	19	8.349	N/A	N/A	N/A	Skurweberg	Orange brown and light grey, moderately to highly weathered, closely to medium jointed, soft rock to medium hard rock, sandstone/Quartzitic sandstone.
New_O1	90	0	-34.180592	24.704108	39.839	93	93	32.36	32.36	7.479	N/A	N/A	N/A	Goudini	Light greenish grey, unweathered, fine grained, very thinly banded, medium jointed, medium hard to hard rock.
New_P1	90	0	-34.179302	24.707529	38.949	140.03	140.03	36	36	2.949	30	30	8.949	Goudini	Grey, very intensely laminated silty fine sand with relict dark grey phylite laminations. Residual, Goudini Formation. Overall consistency likely to very dense.
New_Q1	90	0	-34.181585	24.719887	23.729	84.62	84.62	23	23	0.729	22.5	22.5	1.229	Cedarberg	Black, slightly weathered, very fine grained, very thinly laminated, closely jointed, very soft rock, shale
New_R1	90	0	-34.17815	24.70468	62.481	124.27	124.27	61	61	1.481	54.5	54.5	7.981	Goudini	Light greenish grey, moderately weathered, fine grained, medium to widely bedded, closely to medium jointed, very soft rock. sandstone.
New_S1	90	0	-34.186289	24.70411	25.758	78.5	78.5	16.5	16.5	9.258	16	16	9.758	Goudini	Yellowish brown, highly weathered, very closely to closely jointed soft rock quartzitic sandstone with occasional intensely bedded phyllite.
New_T1	90	0	-34.18312	24.705726	53.01	114	114	53.5	53.5	-0.49	50	50	3.01	Goudini	Dark grey, completely weathered very dense to very soft rock, micaceous, silty clay grading into phyllite.
New_U1	90	0	-34.184024	24.726247	20.202	84.62	84.62	24.5	24.5	4.298	22	22	-1.798	Cedarberg	Dark greyish black, highly to completely weathered, very closely jointed thinly laminated, intensely fractured (relic jointed) very soft rock, Graphitic shale.
New_V1	90	0	-34.178505	24.681899	45.079	87.74	87.74	28	28	17.079	N/A	N/A	N/A	Goudini	Light yellowish to greenish grey, moderately weathered, fine grained, closely jointed, hard rock.sandstone.
New_W1	90	0	-34.178301	24.696295	62.985	119.5	119.5	57.5	57.5	5.485	48.5	48.5	14.485	Goudini	Goudini Formation
New_X1	90	0	-34.181201	24.710137	39.786	81.72	81.72	36	36	3.786	33.72	33.72	6.066	Goudini	Light grey, moderately weathered, very closely to medium jointed, micaceous, highly fractured, soft rockto medium hard rock, sandstone layer.

APPENDIX C1

BH No.	Drill Angle	BH Incli-nation	Latitude	Longitude	BH Elev.	BH Depth	Vertical BH Depth	Depth to Bedrock / Overburden Thickness	Vertical Depth to Bedrock / Vertical Overburden Thickness	Bedrock Elev (m amsl)	Depth to Pebble Layer	Vertical depth to pebble layer	Pebble layer elevation (m amsl)	Bedrock Stratigraphy	First bedrock lithology intercepted in BHs as described in BH logs
New_Y1	90	0	-34.183702	24.715639	24.395	80.31	80.31	26	26	-1.605	24.5	24.5	-0.105	Goudini	Light greenish grey, moderately weathered, fine grained, medium bedded, widely jointed, soft to medium hard rock, sandstone . Notes:1. Very thinly laminated 27.79m-28.12m. Black shale/siltstone lamination @ 45° to core axis. 2. siltstone/shale stringent, typical 1mm thick.
New_Z1	90	0	-34.186522	24.718808	20.282	84.37	84.37	23.45	23.45	-3.168	21	21	-0.718	Goudini	Off-white and light grey, slightly to moderately weathered, closely to medium jointed, soft rock to medium hard rock, fine sandstone with very thin bedding lenses. Joints: Subhorizontal, smooth, moderately, narrow.

Appendix C2 – Borehole metadata

Ruabenheimer et al., (1988 a & b) Borehole Dataset

This borehole dataset is the oldest of 9 borehole datasets used in the construction of the geomodel. During the late 1980's AEC commissioned drilling at five locations along the south coast. These localities are, De Hoek, Thyspunt, Tony's Bay, Klippepunt and Morgan's Bay (Raubenheimer et al, 1988). The latter two localities fall outside the study area and were thus not used in the construction of the model. A total of 66 boreholes fall within the study area and are located in three localities, 19 boreholes at Tony's Bay, 25 boreholes at Thyspunt and 22 boreholes at De Hoek. Seventeen were inclined between 55-65° and were corrected to vertical. Borehole locations were surveyed and although no mention is made to its degree of inaccuracy, it is alleged to be small. Boreholes were surveyed in Cape Datum, Clarke 1880 spheroid, but were re-projected to Transverse Mercator, central medium 25° East, Hartebeesthoek94 datum (WGS84 Ellipsoid). Photo logs of the core were obtained, but were of a very poor quality and did not allow for further descriptions of lithology.

Rosewarne & Lomberg (1989) Borehole Dataset

Rosewarne and Lomberg (1989) completed a groundwater resource evaluation report of the St. Francis area in 1989. Their data set contained 19 vertical boreholes scattered around the southern Cape St. Francis and northern St. Francis areas. An initial assessment of the data set suggested that only 10 of the 19 boreholes could be used for the purposes of this study. Eight boreholes (BH1, BH2, BH3, BH5, BH8, BH12, BH14, and BH15) did not have a geological log. Borehole logs describe lithology, but not stratigraphy and little or no reference is made to the structure (bedding, possible offsets, faults or cleavage) of rocks. Boreholes positions were not surveyed and are considered approximate. Their positions were digitized off maps captured in Cape Datum, Clarke 1880 spheroid, but later re-projected to Transverse Mercator, central medium 25° East, Hartebeesthoek94 datum (WGS84 Ellipsoid). photo logs of the core could not be obtained.

Maclear (2002, 2005 & 2006) Borehole Database

During the construction of the St. Francis Golfing Estate, 3 hydrological investigations were conducted over a period of 4 years. The first phase of investigation (Maclear, 2002) included the drilling of 3 vertical boreholes, 2 shallow holes of 25 m (borehole SRK-2) and 46 m (borehole SRK-1) each and a 3rd considerably deeper 120 m borehole (SRK-3). The exploratory phase was followed, three years later by a development phase (Maclear, 2005) in which 7 vertical borehole were drilled (SRK-4 – SRK-10). In 2006 a last phase of drilling was undertaken were an additional 6 vertical boreholes were drilled to depths less than 29 m. Borehole positions and elevation was captured with a handheld GPS with an inaccuracy of ± 4 m radius in a WGS84 map datum (personal communication Riona Kruger, SRK) and re-projected to Transverse Mercator, central medium 25° East, Hartebeesthoek94 datum (WGS84 Ellipsoid). Lithological information is poorly described. Photo logs of the core could not be obtained.

Eskom (2010, a) Borehole Dataset

A total of 38 vertical boreholes were drilled in 2008 (Eskom, 2010b) as part of a hydrological investigation of the Thyspunt area. Borehole data was captured from a groundwater perspective (water strikes, yield and chemistry with little emphasis on geotechnical aspects. Lithological information is poorly described and no structural detail is noted. Five boreholes of more than a 100 m were drilled, the deepest of which reached 150 m. for borehole specific information. Average boreholes depths range in depth from 20-50 m. Seven boreholes (THY-MR1, THY-MR2, THY-MR3, THY-MR4, THY-MR6, THY-MR7 & THY-MR11-M2) did not reach bedrock. Boreholes positions were surveyed using the Transverse Mercator, central medium 25° East, Hartebeesthoek94 datum (WGS84 Ellipsoid) projection and their position and elevation is highly accurate (SURPLAN, 2012). Borehole lithology is poorly described, creating difficulty in assigning formation status in certain areas. Difficulty in identifying formation status was compounded by the fact that photo logs of the core could not be obtained.

Eskom (2010 b) Borehole Dataset

A total of 71 vertical boreholes were drilled within the Thyspunt site area in 2008 as part of a geotechnical study (Eskom, 2010b). Data was captured from a geotechnical perspective where emphasis is placed on identifying different lithologies. The dataset makes little reference to structural information; expect to mention joint characteristics such as spacing, and general inclination. Boreholes range in depth from 20 m (TB6) to 68 m (NEW5). The dataset contains 4 deep boreholes (NEW27, 28, 29, 30), each over a 100 meters in depth. Six boreholes (NEW4a, TB12, 13, 43, 44, and 45) did not reach bedrock. (See appendix B6 & C6 for more detail). Borehole NEW3, was logged to have a pebble elevation of 1.398 m amsl, which was subsequently changed during review of core at the CGS Core Library in 2011 to 7.468 m amsl (Hanson et al., 2012). Boreholes positions were surveyed using the Transverse Mercator, central medium 25° East, Hartebeesthoek94 datum (WGS84 Ellipsoid) projection. Borehole TB8 did not have an elevation reading, but its elevation (7 m) was determined by a calibrated handheld GPS.

Hanson et al., (2012) Borehole Dataset

Twenty two vertical boreholes were drilled at Thyspunt and Cape St. Francis as part of a marine terrace study during 2011-2012 (Hanson et al., 2012). All the boreholes were drilled vertical and all boreholes reached bedrock. Boreholes were drilled at least 3 m into bedrock (Hanson et al., 2012), expect 3 boreholes (New Seismic A, B and C) that were drilled to greater depths (maximum 120 m). Boreholes positions were surveyed using the Transverse Mercator, central medium 25° East, Hartebeesthoek94 datum (WGS84 Ellipsoid) projection and their position and elevation is highly accurate. The borehole lithology is general well described, however stratigraphy was not logged. The location and elevation of borehole TS-19, was not surveyed. The spatial position of the borehole was captured with a standard handheld GPS with a 4 m radius of inaccuracy. Stratigraphy was not assigned to borehole lithology,

however stratigraphy can be assigned based on the position of the borehole in relation to surrounding geological information and well described lithology descriptions within each borehole.

Engelsman & Constable (2012) Borehole Dataset

During 2012, 24 boreholes were drilled as part of a seismology study at Thyspunt (Engelsman & Constable, 2012). All boreholes were drilled vertical and all boreholes reached bedrock. Seven boreholes reached depths greater than 100m with borehole New P1 reaching a depth of 140 m. Lithology is well described, and bedrock stratigraphy is indicated. The dataset makes little reference to structural information; expect joint characteristics such as spacing, and joint surfaces. Boreholes positions were surveyed using the Transverse Mercator, central medium 25° East, Hartebeesthoek94 datum (WGS84 Ellipsoid) projection.

Appendix C3 – Borehole maps
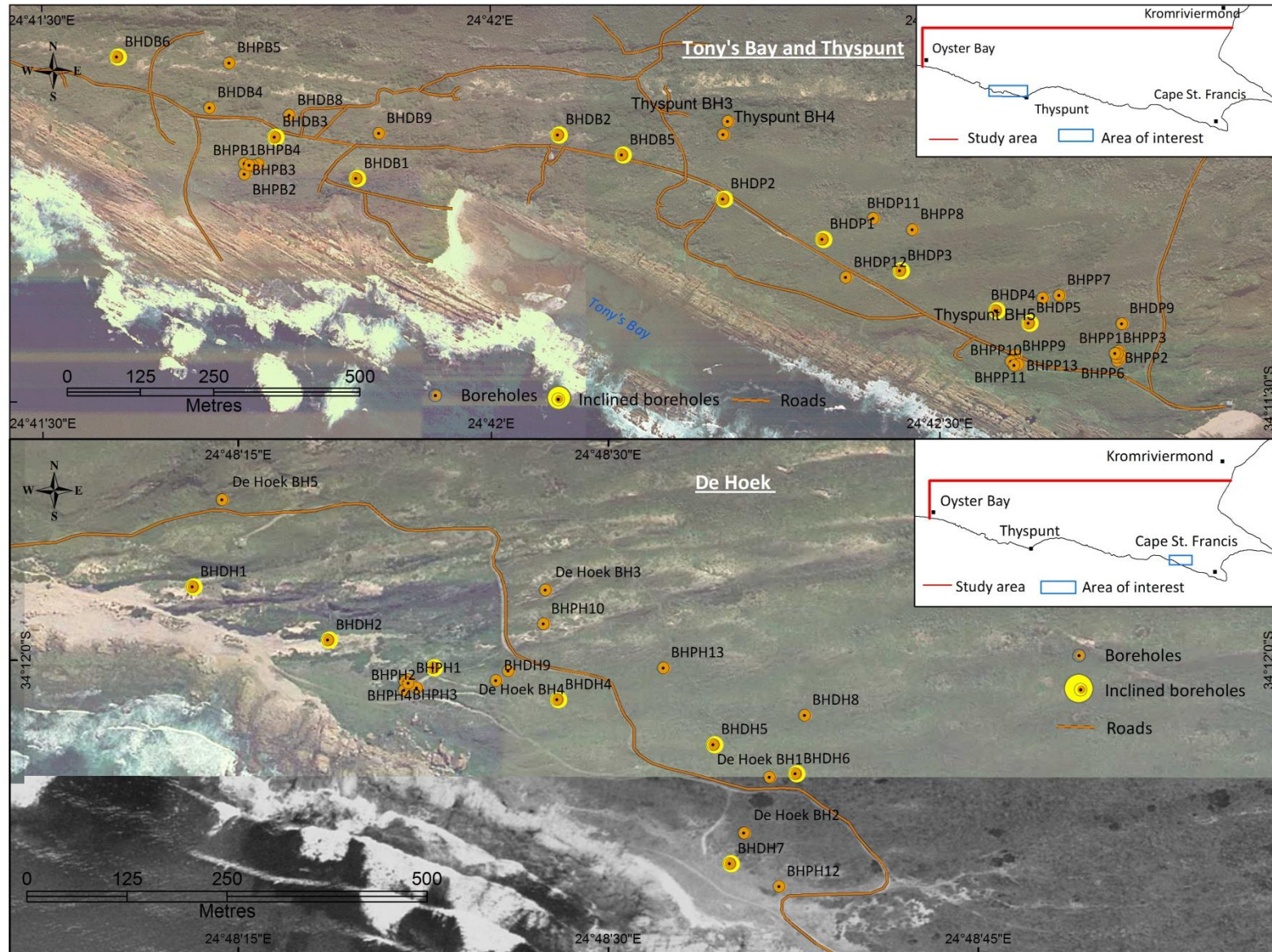
Figure 1: Borehole locations from the Raubenheimer et al., (1989 b) borehole dataset. Boreholes are located in two main areas, Thyspunt and Tony's Bay and De Hoek.
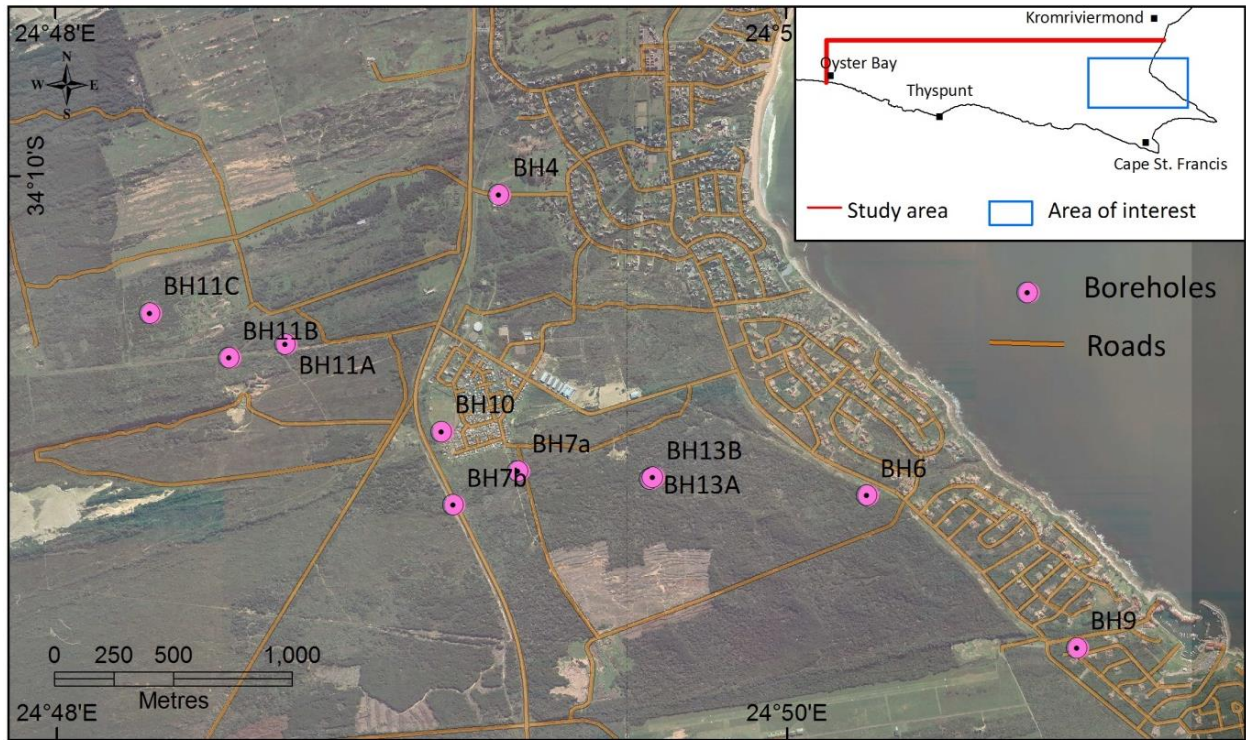
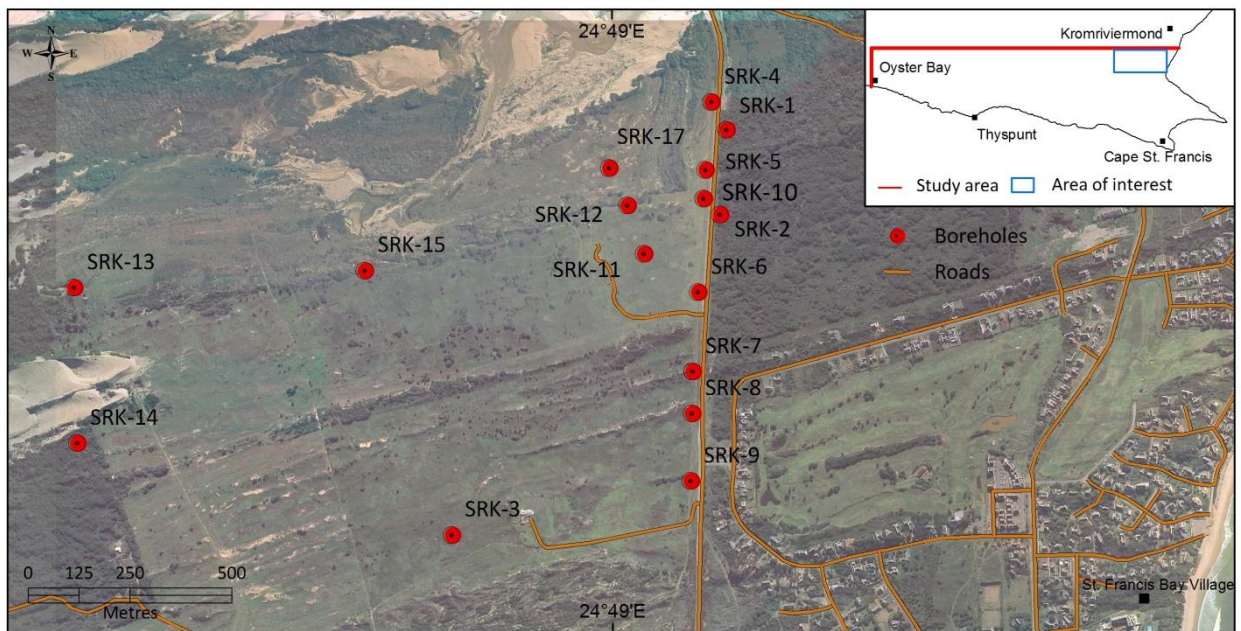*Figure 2: Borehole locations from the Rosewarne and Lomberg (1989) borehole dataset, near St. Francis.*

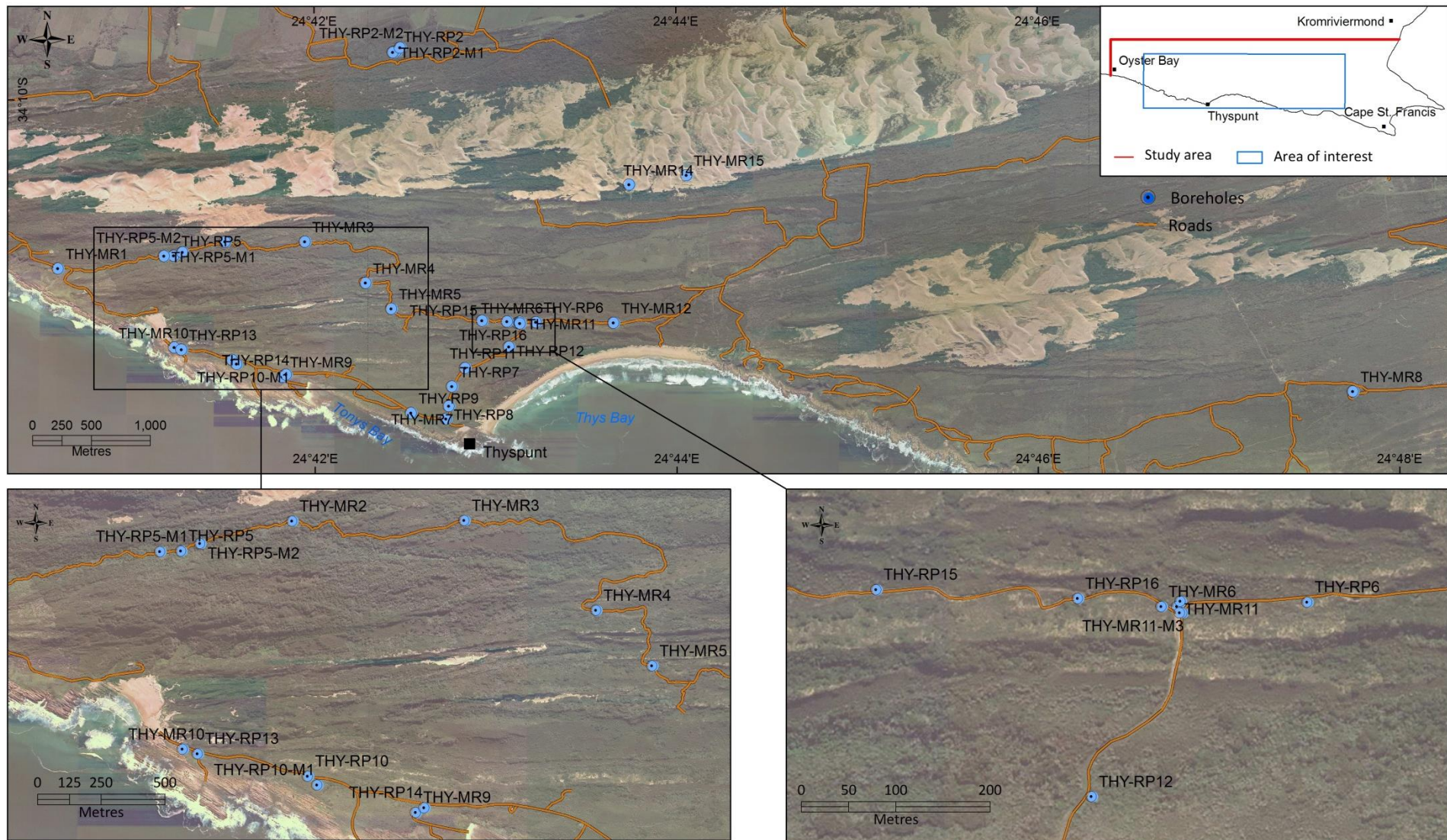*Figure 3: Borehole locations from the Maclear (2002; 2005; 2006) borehole datasets, near St. Francis.*

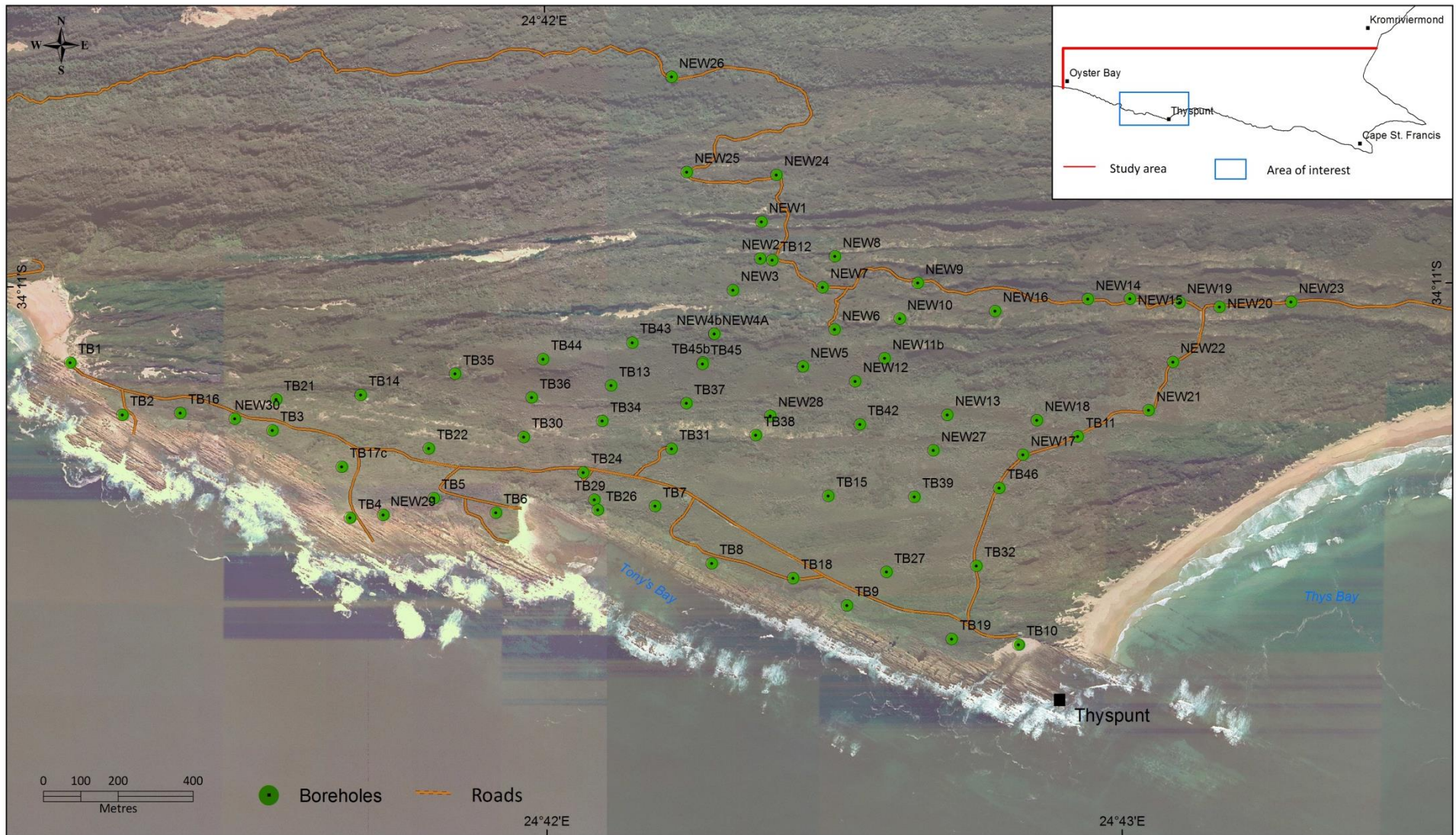*Figure 4: Borehole locations from the Eskom (2010 a) borehole dataset at Thyspunt.*

Figure 5: Borehole locations from the Eskom (2010 b) borehole dataset at Thyspunt.
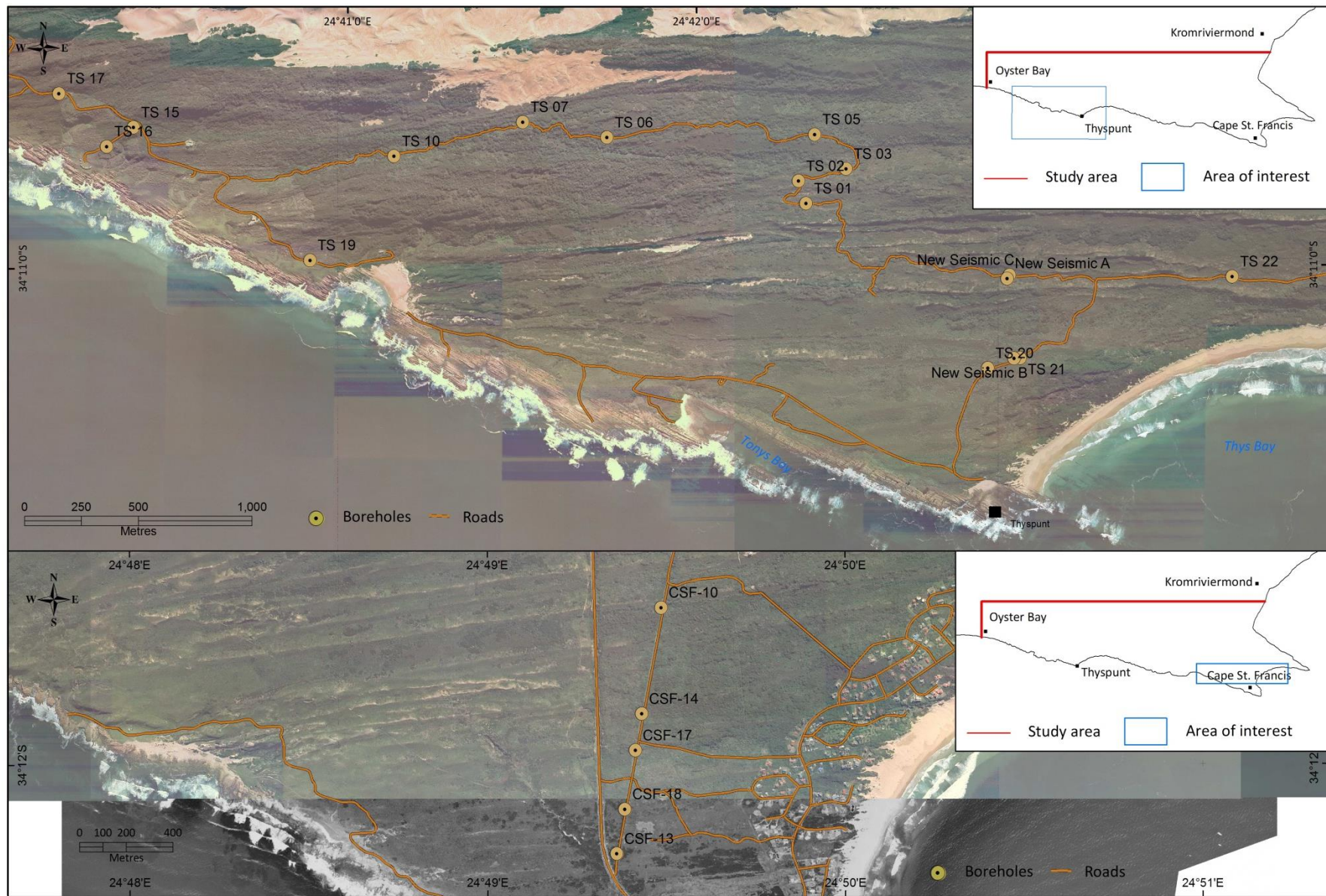
Figure 6: Borehole locations from the Hanson et al., (2012) borehole dataset.

Figure 7: Borehole locations from the Engelsman and Constable (2012) borehole dataset.

Appendix D – Geomodel files (Google Earth)